The WMO/IUGG
INTERNATIONAL AEROSOL PRECIPITATION SCIENCE ASSESSMENT GROUP
(IAPSAG)

Assessment of the effects of pollution on precipitation

Prof. Zev Levin, Chairman

Prof. William Cotton, Vice Chairman

Prof. Meinrat Andreae

Prof. Paulo Artaxo

Prof. Urs Baltensperger

Dr. Jean Louis Brenguier

Dr Roelof Bruintjes

Dr Graham Feingold

Prof. Roland List, IUGG Liaison

Prof. Zheng Guoguang

Prof. Peter Hobbs (deceased)

Prof. Ulrike Lohmann

Dr Yoram Kaufman

Dr J Marshall Shepherd

Dr Deon Terblanche

Dr Leonard Barrie, WMO Liaison

TABLE OF CONTENTS

PREFACE

Clouds are known to play a major role in climate through their direct interactions with solar radiation. In addition, precipitation from clouds is the only mechanism that replenishes ground water and completes the hydrological cycle. Changes in either the amounts and/or the spatial and temporal distribution of rainfall will have dramatic impacts on climate and on society. Increases or decreases in rainfall in one region could affect rainfall downwind. Similarly, changes in rainfall distribution will strongly affect semi arid regions that are of dire need of water.

Among the factors that could contribute to cloud and rain modification are the effects of air pollution from various sources such as urban air pollution and biomass burning. In 2003 the WMO and the IUGG recognized the potential danger from such effects and passed resolutions aimed at focusing attention to this issue. As a follow up to this resolution the WMO formed an international forum composed of a number of experts to review the state of the science and to identify areas that need further study.

Prof. Peter Hobbs from the University of Washington in Seattle was appointed as the chairman of this forum. Unfortunately, Prof. Hobbs passed away in mid 2005 and the responsibility for the report was transferred to Prof. Zev Levin (chairman) and William Cotton (Co-chairman). The organization of this report reflects in a large part, the layout that was set up by Prof. Hobbs.

Since the report is aimed to both the general public and to experts in the field, we took upon ourselves to include chapters that discuss in detail the scientific background and the most recent finding in this field. Each chapter was written by a number of people under the leadership of the lead author. Since the contributors to each chapter were numerous, we listed them at the beginning of the report. It should be noted that some of the contributors provided input to more than one chapter. We would like to thank all of them for their contribution.

Prof. Zev Levin
Department of Geophysics and
Planetary Science
Tel Aviv University
Israel

Prof. William Cotton
Department of Atmospheric Science
Colorado State University
Ft. Collins, CO
USA

IAPSAG -- EXECUTIVE SUMMARY

Lead Authors: IAPSAG lead authors

This report summarizes the state of knowledge of the field of aerosols-clouds-precipitation interactions. Although it is a comprehensive document, it could not have encompassed or covered this tremendously large field. The objective of the report is therefore, mainly to stress the potential importance to the hydrological cycle of the effects of pollution on clouds and precipitation.

It is important to emphasize that the global effects of pollution on rainfall amounts would probably be relatively small, because water molecules that are released into the atmosphere by evaporation have to eventually return to the surface (e.g. to soil, rivers, ocean etc). The predominant path by which these water molecules return to the surface is through precipitation. The lifetime of these water molecules in the atmosphere is therefore, of the order of a few days. It should therefore be clear that the potential effects of aerosols, be they from natural or anthropogenic sources, is to slightly modify the residence time of these molecules in the atmosphere. This is not a small matter, because even small changes in the residence time of the water vapor imply changes in the spatial and temporal distribution of precipitation. Such changes could have major consequences for the water supplies in some regions, especially arid and semi-arid areas, by affecting agriculture production and by modifying the water input into reservoirs.

In order to illustrate the connection between aerosols and precipitation we discuss in great length the characteristics of atmospheric aerosols, their sources and modification, their transport and their spatial distribution. We then describe the basic mechanism of cloud and precipitation formation and illustrate the potential effects of aerosols on them. We summarize the observations of the role of pollution in modifying clouds and precipitation and the numerical models that help us understand some of the observations. We subsequently describe some of the most modern instruments available for measuring aerosols, clouds and precipitation, both from the ground and from space. Finally we devote a chapter to the advertent attempts to modify precipitation amounts by injecting clouds with specific aerosols (cloud seeding).

The role of aerosols in clouds and precipitation is very complex because it is multi-dimensional. A small fraction of the atmospheric aerosols are responsible for the formation of drops and ice crystals (nucleation). The initial sizes and concentrations of these hydrometeors determine the efficiency with which the precipitation will be formed. Modifying the rate of growth of the precipitation may affect the dynamics of the clouds, thus modifying the shape (anvil) and size (horizontal and vertical) of the cloud. Furthermore, the clouds themselves affect the aerosols by modifying their composition and size through chemical reactions that take place in the hydrometeors. Since most clouds evaporate, they release these modified aerosols back into the atmosphere. The concentrations and composition of the aerosols vary due to the types of sources (e.g. natural sources such as dust and sea salt and anthropogenic sources such as vehicular emissions, industrial emissions and others) and sinks (e.g. scavenging by clouds and by precipitation, coagulation with other aerosol particles etc). Therefore, in order to better understand the role of the aerosols in cloud processes it is imperative to study the chemical nature of the aerosols, particularly their solubility, their size and composition, all as a function of time and space.

Ice nuclei are a very small sub-set of atmospheric aerosols. The techniques for measuring these particles have improved in recent years. However, measurements suggest that in many clouds there is very little correlation between the concentrations of ice nuclei in the atmosphere and the concentrations of ice crystals in the clouds. It has also been shown that in some cases, pollution tends to de-activate ice nuclei, thus possibly affecting ice formation in polluted clouds. These effects are not clear and require much more laboratory studies as well as field measurements in different environments.
The transport of pollution has also been identified as a major source of uncertainty. Therefore, models and measurements of aerosols under different meteorological conditions are needed.

From this review it becomes clear that over the past fifty years much work has been done on the role of aerosols in cloud formation. However, relatively little has been done on the last ring in the chain of events leading to precipitation. In other words, we seem to understand to some extend the modifications of the clouds by the aerosols, but we do not understand how these modifications affect precipitation on the ground. The reason for this deficiency is the difficulty in evaluating the observations in terms of the effects on precipitation. There have been many measurements of the aerosols ingested into clouds and their effects on the cloud

microphysics (size and concentrations of hydrometeors) but no simultaneous measurements of rainfall on the ground. Even if measurements of precipitation on the ground were available, it is difficult to conclude what the effects of the pollution are, since an identical cloud that is unaffected by pollution has to be measured simultaneously. In other words, in order to evaluate the role of pollution on precipitation similar methods used in cloud seeding experiments may be needed. Since the variations in cloud processes are so large, statistical approaches will have to be used.

Measurements will have to be evaluated over a long period of time. But even these types of studies suffer from the temporal variations of some of the parameters that control cloud and precipitation development. For example, urbanization has strong effects on aerosol emission as well as on the temperature of the boundary layer (urban heat island). Experiments that last a few years need to find a way to remove these changes from the evaluation.

Recent statistical studies over the upslope of orographic terrain show a decrease in precipitation downwind from urban centers, attributed to the effects of air pollution on cloud development. Similar results were suggested in measurements of snow on a mountain top. Namely, they reported that the decrease in cloud droplet size due to increase in aerosols, led to reduced snow crystal size and to lower falling snow mass. On the other hand, measurements downwind of paper mills suggest that precipitation actually increased. This increase was attributed to the effects of giant CCN, producing larger cloud drops that have a head start in the growth by collection. These analysis and conclusions, however, are based on relatively few measurements.

The use of satellites greatly improved our ability to look at cloud fields and not only at single clouds. However, the time and spatial resolutions are still not sufficient to be able to tell what happens in one cloud at a specific time. Plans are on the way to launch a number of new satellites that will complement each other and allow one to evaluate the characteristics of aerosols at relatively good temporal and spatial resolution, while at the same time also measure some cloud properties. Of course measuring cloud properties, such as effective radius, cannot provide information about the processes taking place deep in the cloud, in regions where precipitation is growing. In addition, if the effects of pollution on precipitation are of the order of a few percent or even a few tens of percent, the measurements from satellites cannot resolve such small changes. On the other hand, if other parameters (e.g. such

as cloud height) could be identified as good proxies for precipitation on the ground, the use of satellites for this purpose could be valuable.

In the conclusions of each chapter and in the summary and conclusion chapter of this report we list a number of suggestions that are important for resolving the potential effects of pollution on rainfall. These include suggestions of the types of measurements and modeling works that are needed to shed light on the processes involved. These should provide important data on aerosols, clouds and precipitation that could be applied to statistical evaluation as well as to help decipher the dominant processes involved in the interactions of aerosol-clouds and precipitation.

CHAPTER 1: THE HYDROLOGICAL CYCLE

Lead Authors: Peter V. Hobbs, Ulrike Lohmann, J. Marshall Shepherd,

William R. Cotton

We begin this Assessment with a brief description of the hydrological cycle, with emphasis on the role that aerosol particles play in the formation of clouds and precipitation. Several of the subjects touched upon here are discussed in more detail later in this report.

1.1 OVERVIEW

Earth is the only planet known in the solar system to support life. Life on Earth is critically dependent upon the cycling of water back and forth among the various reservoirs (ocean, land, atmosphere) in the Earth system, which is referred to as the *hydrological cycle*. Both natural and human-induced climate variations manifest themselves in the global water cycle [e.g., *Chahine*, 1992]. In fact, the most obvious signals to humans of climate change in the Earth system will likely manifest themselves in changes in the hydrological cycle, particularly regional precipitation regimes, and the exacerbation of extreme hydrologic events, such as floods, droughts and hurricanes. The hydrological cycle also affects and interacts with other components of the climate system. Consequently, any significant perturbations to the hydrological cycle, whether caused by aerosols or in other ways, are of paramount concern.

From an overall Earth Science perspective, the key questions are to what extent expected changes in climate (e.g., warming or changes in atmospheric aerosols) entail changes in the Earth's hydrological cycle, and what trends may be expected in the future. The hydrological cycle is driven by a multiplicity of complex processes and interactions, many of which are inadequately understood and poorly represented in climate models. The characterization of the hydrological cycle requires an understanding of moisture and energy storages and exchanges between and within the Earth's atmosphere, oceans, land, and biological systems over a wide range of space and time scales.

Figure 1-1 is a schematic of the hydrological cycle, which shows the amounts of water in the various reservoirs and the fluxes of water between them. The cycle is driven by evaporation of water from the oceans and the land, which adds water vapor to the atmosphere, and liquid water and ice in the form of clouds. Water in the atmosphere is returned to the Earth's surface by precipitation. The hydrological cycle is closely linked to the atmospheric circulation and to temperature, which determines the maximum amount of water vapor in the atmosphere. However, the hydrological cycle in turn affects other components of the climate system through complex feedback mechanisms. For example, latent heat released by the condensation of water to form clouds is an important part of the atmospheric heat balance.

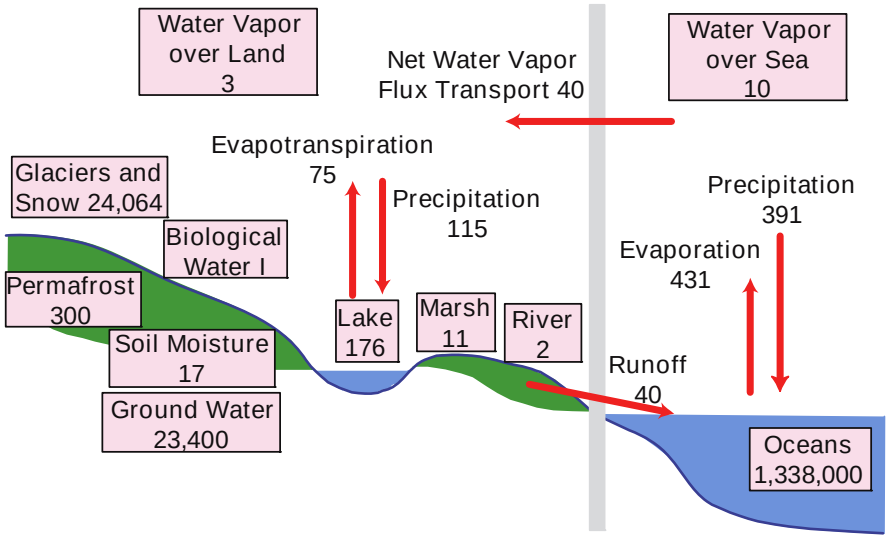

Figure 1-1. *A schematic diagram of the hydrological cycle. The numbers in the boxes are estimates of the total amounts of water in the various reservoirs in units of 10^{15} kg. The numbers alongside the arrows are estimates of average annual fluxes in units of 10^{15} kg/year. Adapted from Oki (1999).*

The atmosphere is by far the smallest reservoir of water: it accounts for only 0.3% by mass of the atmosphere itself. Nevertheless, clouds cover about 60% of the Earth's surface [*Rossow et al.*, 1993] and they play an important role in the radiative balance of the Earth, as well as forming a crucial component of the hydrological cycle. It can be seen from Figure 1-1 that evaporation from the oceans is 431×10^{15} kg/year compared to only 75×10^{15} kg/year from the land, and precipitation over the oceans is 391×10^{15} kg/year compared to 115 kg/year over land. There is a net flux of water vapor from over the oceans to over the land of 40 ×

10^{15} kg/year. If it is assumed that over a period of time the system is in steady state, then the flux of water into any of the reservoirs is equal to the flux of water out of that reservoir. Figure 1-1 is based on this assumption so, for example, averaged over the globe the fluxes of water vapor into the atmosphere due to evaporation over the oceans and evapotranspiration over the land are equal to the sum of the precipitation over the oceans and over the land. Any appreciable departure from the steady-state condition in the atmosphere would result in accumulation or depletion of water, which is not observed. However, in analyzing the atmospheric water balance for a limited region, the horizontal transport of water vapor by winds must also be considered. Thus, within the intratropical convergence zone (ITCZ), the rate of precipitation (P) is greater than the rate of evaporation (E); the excess precipitation is derived from an influx of water vapor carried by the converging trade winds. Conversely, in the region of the relatively dry, cloud-free sub-tropical anticyclones, E » P; the total excess water is carried toward the ITCZ on the equatorward side and toward the midlatitude storm tracks on the poleward side, by the diverging low-level winds. For the continents as a whole, P > E: the excess precipitation returns to the sea in rivers. For steady state it is required that for any land mass, the landward atmospheric flux of water vapor, integrated around the entire coastline, be equal to the total seaward flow across the coastline in rivers. Local evapotranspiration E accounts for an appreciable fraction of the moisture in summer rainfall P over the continents. Techniques for computing E–P include the use of rawinsonde data and the assimilation of observed moisture data into numerical models as part of four-dimensional data assimilation (4DDA).

The residence time of water in the atmosphere can be estimated by dividing the amount of water vapor in the atmosphere (13×10^{15} kg) by the total precipitation rate over the ocean and the land (506 kg/year), which gives a residence time of 0.03 years or about 9 days. This is by far the shortest residence time for water in any of its reservoirs. For example, the residence time of water in lakes and rivers is on the order of a year and the residence time of water in the Antarctic ice sheet is ~200,000 years. However, over a period of 10 days water vapor can be transported over thousands of kilometers before it condenses.

1.2 HOW MIGHT AEROSOLS AFFECT CLOUDS, PRECIPITATION AND THE HYDROLOGICAL CYCLE?

Precipitation (including rain, snow, and hail) is the primary mechanism for transporting water from the atmosphere back to the Earth's surface. It is also the key physical process that links aspects of climate, weather, and the global hydrological cycle. Moreover, precipitation is the parameter that has the most direct and significant influence on the quality of human lives in terms of the availability of drinking water and water for irrigation.

This Assessment is concerned with the possible effects of aerosols from natural and anthropogenic sources on clouds and precipitation. In subsequent chapters in this Assessment we discuss in some detail, the sources and nature of atmospheric aerosols, the dispersion, modification and sinks of aerosols in the atmosphere, the formation of clouds and precipitation, the effects of aerosols in general on clouds and precipitation, ground-based and airborne techniques for observing the effects of aerosols on clouds and precipitation, satellite measurements of aerosols, clouds and precipitation and deliberate attempts to modify clouds and precipitation by cloud seeding. Finally, in Chapter 9 we propose in the form of summary and conclusions some ways to increase knowledge of the effects of aerosols on clouds and precipitation. To set the scene for these discussions, we conclude this chapter with a brief review of ways in which aerosols might affect clouds, precipitation and hydrological cycle.*

1.2.1 Effects of Particles on Cloud Structures

Cloud droplets form on particles in the air, called *cloud condensation nuclei (CCN)*, by a process referred to as *heterogeneous nucleation*. As parcels of air rise in the atmosphere they cool by adiabatic expansion. As the air cools the relative humidity increases, eventually reaching 100%. However, slight supersaturations[1] on the order of 0.01–1%, are needed before the supersaturated vapor begins to condense onto some of the particles in the air. The supersaturation of the air continues to increase as the parcel is lifted, until the rate at which the supersaturation is increased due to cooling is equal to the rate at which the supersaturation is decreased by condensation. The peak value achieved by the supersaturation determines the

* These subjects are discussed in more detail in Chapter 4.

[1] The percentage supersaturation is defined as $\frac{e - e_s}{e_s}$ 100, where e is the water vapor pressure at the temperature T of the air, and e_s the saturated, or equilibrium, water vapor pressure over a plane surface of pure water at temperature T.

number of particles that are activated as CCN, and therefore the number concentration and size distribution of the cloud droplets that are formed in a rising air parcel.

If an air parcel contains numerous particles that are activated as CCN at relatively low supersaturations, a cloud that forms in the parcel will contain large numbers of small droplets. In such clouds, the formation of precipitation by the collision and coalescence of relatively large drops with numerous smaller droplets may be restricted due to the lack of sufficient numbers of larger drops. This is thought to be the situation over regions of the continents where CCN are numerous. Over the oceans, on the other hand, CCN are generally less numerous, and therefore cloud droplet concentrations are smaller, and precipitation is aided by a more efficient collision-coalescence process. This can aid the formation of precipitation.

The simple scenario outlined above provides explanations for some of the observed differences between continental and maritime clouds. For example, continental cumulus clouds tend to have more well defined ("harder looking") boundaries than maritime cumulus clouds. This is attributable to the greater concentrations of larger drops in maritime clouds, which can survive evaporation over greater distances as they venture out from the edges of a cloud into sub-saturated ambient air.

A striking demonstration of the effects of particles on cloud droplet size distributions is provided by the phenomenon of *ship tracks* (see Chapter 5 for a more detailed discussion). For some 40 years the effects of ships on stratiform clouds have been observed in visible satellite imagery [*Conover*, 1966]. The perturbations take the form of narrow, curvilinear regions of enhanced cloud reflectance. This is attributable to the large concentrations of particles emitted by some ships, which can increase the number concentration of cloud droplets in low-lying clouds, and therefore increase the amount of solar radiation that the clouds reflect back to space.

Once a few ice particles (~1 liter^{-1}) have formed in a cloud dominated by supercooled drops, they will grow relatively fast by condensation from the vapor phase, since the air will be at water saturation and therefore highly supersaturated with respect to ice. This is the so-called *ice particle method* for precipitation development in cold clouds.

At temperatures below 0ºC, ice particles can form in clouds, which affect cloud structures and can lead to additional pathways for the formation of precipitation. Above about -40ºC, ice particles in clouds are formed by heterogeneous nucleation on a subset of the atmospheric aerosol called *ice nuclei* (*IN*). Aerosols can act as IN by coming into contact with supercooled cloud droplets (*contact freezing*), or by initiating freezing from within a cloud droplet by *immersion* or *condensation freezing*, or by acting as *deposition nuclei* [*Rogers and Yau*, 1989]. Contact nucleation is usually the most efficient process at slight supercoolings, while at lower temperatures immersion freezing can be more prevalent. Unlike CCN, IN are generally insoluble particles, such as certain mineral dusts, soot, as well as some biological materials [*Schnell and Vali*, 1976a; *Levin and Yankofsky*, 1983; *Diehl et al.*, 2001; *Gorbunov et al.*, 2001]. Ice nuclei may lose their nucleability, if foreign gases, such as sulfur dioxide or ammonia, occupy their active sites [*Pruppacher and Klett*, 1997].

1.2.2 Effects of Particles on Increasing Precipitation

As mentioned in Section 1.2.1, clouds that form in air containing relatively low concentrations of CCN tend to have a broader droplet size distribution and a few large drops. Provided the latter drops are large enough (diameter $\gtrsim$ 40 μm) they can grow by collision-coalescence to form raindrops. It is for this reason that marine clouds tend to precipitate more efficiently than continental clouds. This is the theoretical basis for attempts to increase precipitation by seeding with large hygroscopic nuclei, which can provide the seeds upon which precipitable particles can grow (see Chapter 8).

Measurements of the concentrations of ice nuclei in the air suggest that they often fall below the concentration (~1 liter^{-1}) required for ice particles to grow efficiently to precipitable particles. This is the basis for the belief that seeding such clouds with artificial ice nuclei (e.g., silver iodide) might increase precipitation (see Chapter 8).

Effects of Particles on Suppressing Precipitation

In contrast to marine clouds that contain relatively few CCN, low droplet concentrations, and the development of precipitation by the collision-coalescence mechanism is relatively efficient, continental clouds have relatively high concentrations of CCN, which inhibit the development of precipitation by the collision-coalescence mechanism. These ideas have received support from studies of the effects on clouds and precipitation of smoke from

sugarcane and forest fires (see Chapter 5 for more detailed discussion). These smokes contain large concentrations of CCN, which increase cloud droplet concentrations, decrease cloud droplet sizes, and therefore tend to inhibit precipitation [*Warner and Twomey*, 1967; *Warner*, 1968; *Eagan et al.*, 1974b; *Reid et al.*, 1999; *Rosenfeld*, 1999; *Andrea et al.*, 2004]. However, there are also indications that with an appropriate mix of anthropogenic CCN with different activities, and/or giant or ultra-giant particles, augmented perhaps by emissions of heat and moisture, precipitation may be enhanced [*Hobbs et al.*, 1970; *Hindman et al.*, 1977a,b,c].

Andreae et al. [2004] observed that a reduction in cloud droplet sizes caused by biomass smoke in the Amazon Basin delayed the onset of precipitation from 1.5 km above cloud base in pristine clouds to more than 5 km in polluted clouds, and to more than 7 km in clouds spawned by biomass fires (so-called pyro-clouds). Although they did not obtain measurements aloft, they suggested that elevating the onset of precipitation released latent heat higher in the atmosphere, which could invigorate updrafts, causing intense thunderstorms and large hail. Several modeling studies reported in Chapter 6 support these ideas.

On a regional scale, *Rosenfeld* [1999, 2000] has provided some evidence that urban and industrial air pollution may shut off precipitation from clouds that have cloud top temperatures of about -10^{o}C. Satellite data revealed clouds downwind of industries that contained reduced droplet sizes, which suppressed precipitation, thereby confirming the earlier observations of *Hobbs et al.* [1970]. Furthermore, *Givati and Rosenfeld* [2004] showed a decrease in precipitation amounts in orographic clouds downwind of polluted regions as compared to similar adjacent regions that are unaffected by pollution.
However, precipitation from similar polluted clouds over the oceans may be less affected, possibly because large sea salt nuclei override the precipitation suppression effect of the large number of small pollution nuclei [*Johnson*, 1982; *Rosenfeld et al.*, 2002]. Here, large droplets initiated by large sea salt aerosols may grow by collecting small cloud droplets and grow to precipitation size, thereby cleansing the air.

Borys et al. [2003] show that the addition of anthropogenic sulfate aerosols to a clean background can reduce the orographic snowfall rate in the Colorado Rocky Mountains by up to 50%. *Borys et al.* suggested that this reduction is related to evidence that cloud droplet size distributions are strongly modified by the aerosols forcing smaller mean diameters when they

are present. They found also that smaller droplet sizes reduce their collection efficiency by falling snow crystals, thus inhibiting their growth by this process. They hypothesized that the amount of snowpack reduction varies in time both during and among different storms and is accomplished by as little as 1 μg m^{-3} of pollution sulfate in the air. Over the course of a winter season, 15% to 25% of the snowpack water content may be lost due to the aerosol effect.

1.2.4 Factors Explaining Variability in Aerosol-Precipitation Interactions

Uncertainties in the effects of urban aerosols on precipitation are clearly evident. In part, the variability in how aerosols affect precipitation is likely related to many factors including seasonality, aerosol type and source region, topography, land use, and complex dynamical responses of clouds to aerosols (Chapter 6). For example, ship track measurements have yielded hints, but not clear evidence, that drizzle reduced by exhaust from ships, due to the presence of smaller cloud droplets that reduce the efficiency of drop growth by collisions [*Ferek et al.*, 2000]. *Rosenfeld* [2000] demonstrated a widespread influence of aerosol pollution on continental precipitation due to reasons aforementioned. Figure 1-2 illustrates these processes schematically. A complicating factor is the possible role of giant soluble particles in the aerosols, which could act as CCN or "embryos" for large droplets and initiate the precipitation process. Giant soluble particles are used in some modern cloud seeding efforts, and there is evidence of aerosol-induced rainfall due to such particles (see Chapter 8).

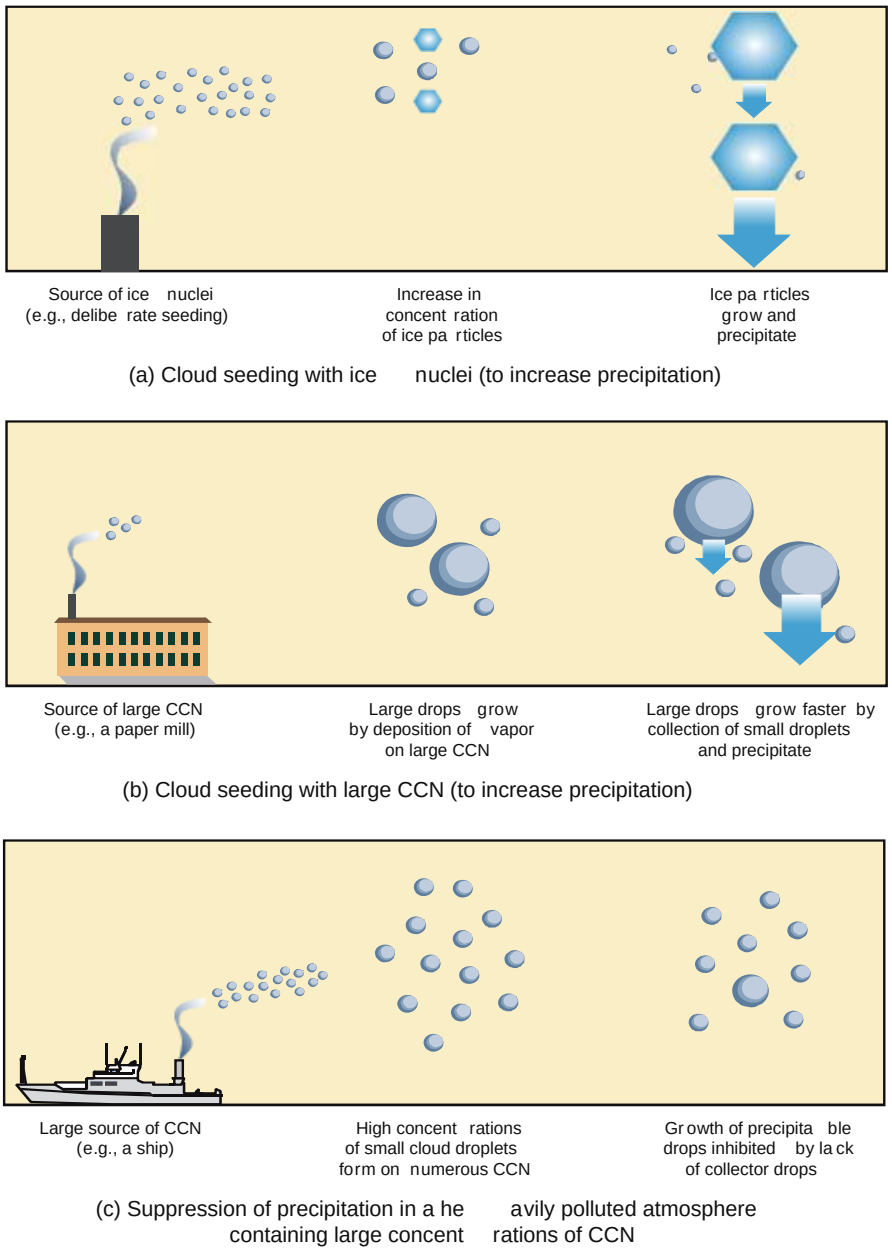

Figure 1-2. *Schematics of some effects of particles on cloud structures and formation of precipitation.*

It is shown in Chapter 6 that modeling studies suggest that once the precipitation process is modified, the resultant dynamical behavior of clouds can be altered in such a way that precipitation may increase or decrease. For example, the complex dynamical response of clouds to changing aerosol concentrations can lead to dynamical feedbacks through alteration of entrainment processes, through altering subcloud cold pool characteristics, or through

changes in surface temperatures, non of which can be guaranteed to increase or decrease precipitation overall.

Another complicating factor arises when the role of variable ice nuclei concentrations are considered. As discussed in Chapter 5 and 6, there is often a poor correlation between concentrations of IN and ice crystal concentrations. Since laboratory devices indicate the concentrations of ice crystals activated on IN increases with decreasing temperatures it is rather unsettling that some measurements in clouds [*Rangno and Hobbs*, 1994; *Korolev et al.*, 2003] suggest that there is a poor correlation between ice crystal concentrations and temperature in clouds. Furthermore, as discussed in Chapters 5, 6, and 8, we find that increased concentrations of ice crystals can sometime lead to increases in precipitation and sometimes to a decrease in precipitation.

1.3 POSSIBLE EFFECTS OF PARTICLES ON THE GLOBAL HYDROLOGICAL CYCLE

Another aspect of aerosol impacts on precipitation is the notion of shifting tropical rainfall patterns from regional to larger scales. Several general circulation modeling studies discussed in Chapter 6 suggest that direct and indirect aerosol effects can alter the general circulation patterns including shifts in the position of the intertropical convergence zone which can lead to major changes in rainfall patterns.

A potentially important link between aerosols and the global hydrological cycle is through the surface energy budget. As aerosol and cloud optical depths increase, less solar radiation reaches the surface. This must be balanced by decreased outgoing energy from the surface, either in the form of terrestrial longwave radiation or by reduced latent and sensible heat fluxes. As shown from coupled global climate model/mixed-layer ocean model simulations, the decrease in solar radiation seems to be more important in controlling the amount of evaporation in the global mean than the increase in surface temperature resulting from the increase in greenhouse gases [*Liepert et al.*, 2004]. Because evaporation has to equal precipitation in the global mean, precipitation over both ocean and land also decreases in the warmer and more moist present-day climate model simulations.

Therefore, if aerosols affect precipitation efficiency and alter ocean and land-surface heating and rate of latent heat release, they might have an impact on global circulations such as tropical Hadley and Walker Cells, and on middle latitude and high latitude ridge and trough patterns.

Since much of the precipitation worldwide originates via the ice phase ice nuclei from both natural and anthropogenic sources might affect precipitation. As discussed in Chapter 6, results of simulations by several cloud-resolving models and general circulation models suggest that changes in ice nuclei concentrations can have a major impact on both precipitation and on the surface energy budget, sometimes leading to surface warming and other times leading to surface cooling [*Carrio et al.*, 2005; *Lohmann*, 2002].

1.4 WHAT IS NEEDED TO ADDRESS AEROSOL-PRECIPITATION INTERACTIONS?

Anthropogenic and natural aerosols are strongly linked to the climate system and Earth's water cycle. Figure 1-3 illustrates global mean aerosol optical depths from the Terra spacecraft and the Georgia Tech/NASA Goddard Global Ozone Chemistry Aerosol Radiation Transport (GOCART) modeling system along with mean global precipitation rates from the Global Precipitation Climatology Project (GPCP). This figure is a manifestation of the emergence of new satellite systems, models, and programs that are uniquely suited for regional-global studies and inter-disciplinary interactions (e.g., aerosols, clouds, and precipitation).

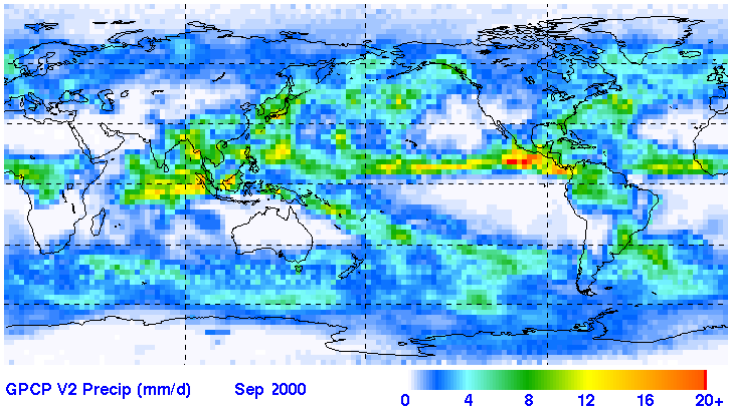

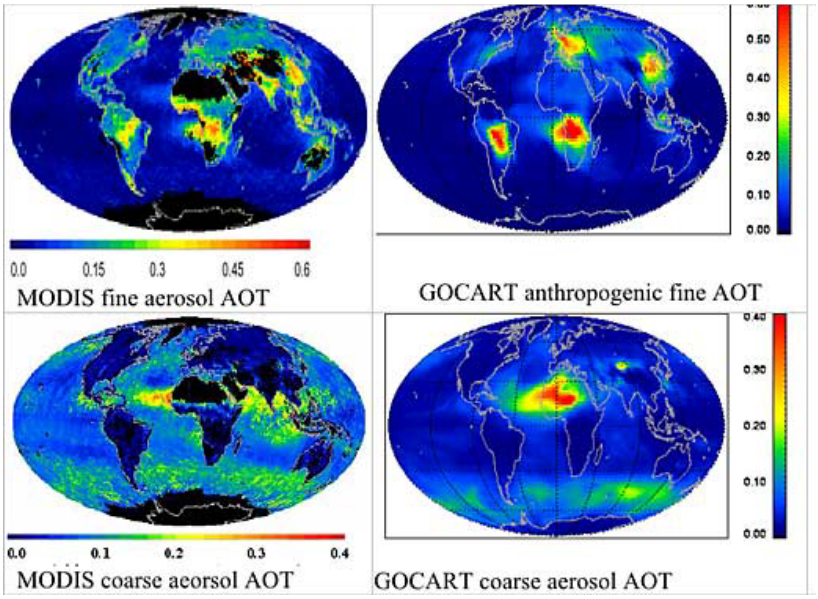

Figure 1-3. *Global mean precipitation for September 2000 from the Global Precipitation Climatology Project (GPCP and global analysis of fine and coarse aerosol optical thickness at 0.55 micron (AOT) derived from the MODerate resolution Imaging Spectroradiometer (MODIS) aboard NASA's Terra spacecraft. Model simulations from the Georgia Tech/ NASA Goddard Global Ozone Chemistry Aerosol Radiation Transport (GOCART) model are also included. Global analysis of the fine (top left) and coarse (bottom left) aerosol optical thickness at 0.55 μm (AOT) derived from data from the MODIS instrument on the Terra spacecraft, for September, 2000. On the right are the corresponding simulations by the GOCART model. Similar results are observed for dust in the tropics, pollution in North America and East Asia.*

To fully address the relationships and interactions between aerosols and precipitation, several things are required:

New satellite observing systems must be developed to monitor and track anthropogenic and natural aerosols,

New satellite and ground based observing systems that measure cloud microphysical and precipitation processes from evolution to fallout,

Modeling systems that explicitly resolve aerosols, cloud microphysics, and precipitation evolution so that a more conclusive understanding of the aerosol effect on precipitation and clouds can be attained,

Field studies to validate satellite observations and modeling simulations of cloud-aerosol-precipitation interactions and to extend basic understanding of the processes involved,

New global climate model simulations to understand the potential net impact of aerosols on the precipitation component of the water cycle under different aerosol scenarios.

In the following chapters the observations and modeling studies as well as the available and planned facilities that could help resolve the issue of the effects of aerosols on precipitation on the local and global scales discussed.

CHAPTER 2: SOURCES AND NATURE OF ATMOSPHERIC AEROSOLS

Lead Authors: Meinrat O. Andreae & Dean A. Hegg

Co-Authors: J. Feichter, S. Kloster, Z. Levin, C. Liousse, L. F. Radke, P. Stier

Contributors: L. A. Barrie, S. M. Kreidenweis, C. Textor, W. R. Cotton, U. Baltensperger

2.1 INTRODUCTION

In view of the nonlinear and spatiotemporally complex interactions between aerosols, clouds and precipitation, it is quite inadequate to represent aerosols by the conventional approach of atmospheric pollutant cycles, i.e., by specifying sources, burdens and sinks in terms of masses of particular aerosol components or "species". The basic information required for modeling the role of aerosols in cloud and precipitation processes is the 4-D distribution of the number concentration of particles that can be activated at the supersaturations occurring in clouds (Cloud Condensation Nuclei, CCN) or that can cause the formation of ice particles at temperatures above the level of homogeneous freezing of cloud droplets (Ice Nuclei, IN). This information is difficult or impossible to derive from conventional studies of aerosol cycles, such as those that formed the basis of the section on aerosol sources and burdens in the IPCC-TAR report [*Penner et al.*, 2001]. Several problems present themselves:

First, the very concept of "source strength" is difficult to define for some aerosol types, since the secondary aerosol species (e.g., sulfates, secondary organics) are not directly emitted, but are formed in the atmosphere from gaseous precursors. For these species, the "source" is a set of atmospheric reactions, not a surface emission process, and therefore the production rate depends sensitively on the efficiency of these reactions. These "sources" cannot be derived from measurements, but have to be inferred from measurements of the source strength of precursors, the (always incomplete) knowledge of atmospheric transformations, and a formal or informal inversion of measurements of atmospheric burdens. The source estimates for these aerosols therefore depend strongly on how the source processes are represented in the models.

Second, the conventional mass-based treatment of aerosol fluxes does not take into account the fact that the properties of aerosol particles can vary strongly with particle size, and that

the cloud-physical effects of aerosols depend on number concentrations, not mass concentrations. For example, the largest number concentration of cloud-active seasalt particles resides in the submicron size fraction, which represents only a very minor mass fraction of the seasalt aerosol. On the other hand, this fraction of the seasalt aerosol has quite different atmospheric sink mechanisms and lifetime than the coarse seasalt mode which dominates the mass source strength and burden of the aerosol component. Similar considerations apply to mineral dust and primary biogenic aerosols.

A third problem arises from the fact that aerosol species often combine to form mixed particles, with properties and atmospheric lifetimes different from those of their components. Even though the direct radiative effects of these "internal mixtures" may be substantially different from those of "external" mixtures [*Jacobson*, 2001; *Chung and Seinfeld*, 2002], this distinction has been ignored in many analyses of the global aerosol system. However, for the effects of aerosols on clouds, even relatively small amounts of soluble material in or on otherwise insoluble particles can cause large differences, and the mixing state of the aerosol cannot be ignored.

It follows from these considerations, that a meaningful analysis of the sources and burdens of cloud-active particles cannot be achieved through emission inventories, as it has been done typically for atmospheric trace gases. Rather, it must take the form of an atmospheric model that contains emissions of precursor gases and primary aerosol species, and accounts for transformations and sink terms of precursor species as well as the various aerosol components. The model must carry either explicitly or in parameterized form information about the number/size distribution of soluble and wettable materials, ice-nucleating ability, and the interactions between gas phase and various condensed phases. Fundamentally, therefore, the issue of aerosol sources cannot be separated from an analysis of transport and atmospheric processes and must be treated interactively within the framework of a numerical model that represents these processes. Unfortunately, this type of approach is still in its infancy. One of the most complete analyses (suitable for long-term climate simulations) to date is represented in the aerosol-climate model ECHAM5-HAM [*Stier et al.*, 2005a]. In this model, the major aerosol components sulfate, particulate organic matter (POM), black carbon (BC), seasalt, and mineral dust are determined through an aerosol module that is interactively connected to a climate model. In a somewhat complementary approach, the distributions of ammonium sulfate and nitrate aerosols have been modeled using prescribed meteorology and a detailed description of gas/aerosol partitioning [*Metzger et al.*, 2002a].

In the following sections, we will present an updated inventory of emission fluxes, production rates, and burdens for the major aerosol species, providing information about particle numbers (CN, CCN and IN) when possible. For selected aerosol types, we will provide spatial information in the form of 2D distribution maps. Ultimately, however, it must be acknowledged that this information just represents a convenient visualization of the spatiotemporally resolved distributions, which can be fully represented only in the form of aerosol modules in coupled aerosol-climate models. In addition, these data are results from one particular global aerosol model (ECHAM5-HAM) and do thus include the uncertainties connected to such simulations [*Textor et al.*, 2005].

2.2 NATURAL AND ANTHROPOGENIC SOURCES OF ATMOSPHERIC AEROSOLS

To structure the discussion, we group the aerosol sources into *primary* and *secondary* types. Primary aerosols are those that are emitted into the atmosphere directly as condensed solids or liquids, whereas secondary aerosols are formed within the atmosphere from gaseous precursors. Sea salt, mineral dust and soot particles are clearly primary particles, whereas organic particles from the oxidation of volatile organic compounds (VOC) and sulfates from the oxidation of SO_2 or other sulfur-containing gases are clearly secondary. There is a "grey zone" between primary and secondary in the case of some low-volatility organic compounds that condense onto aerosol near, but not directly within, emitting sources, such as some hydrocarbons in vehicular exhaust or condensable from biomass burning. We will discuss these materials together with the strictly primary emissions, taking into account that the definition of secondary aerosol formation involves chemical transformation from more volatile precursors [*Fuzzi et al.*, 2005a].

2.2.1 Primary Aerosols

2.2.1.1 Soil Dust

Soil or mineral dust is the most conspicuous aerosol component in satellite imagery of global aerosol distributions. Many estimates of source strength and burden have been published; much of the older work has been summarized by *Duce* [1995], while the more recent literature has been reviewed by *Tegen* [2003] and *Zender and Tegen* [2004]. The estimates of global annual source fluxes are in the range of 1000-2150 Tg a^{-1}, and have not changed much since the reviews of *Andreae* [1995] and *IPCC-TAR* [2001]. There has been tremendous

improvement, however, in the sophistication of the dust deflation and transport models used and in the techniques used for validation of the models, especially the use of remote sensing [*Israelevich et al.*, 2002; *Tegen et al.*, 2002; *Werner et al.*, 2002; *Luo et al.*, 2003; *Zender et al.*, 2003; *Miller et al.*, 2004; *Tegen et al.*, 2004]. The range of burdens predicted by these models, 8-36 Tg, remains still quite large, mostly due to differences in the way deposition processes are treated in the models.

There are major discrepancies in the size distributions of the mineral dust aerosol predicted by the models and observed by various techniques. Near the sources, the mass distribution peaks at large sizes, 10 μm or greater, in observation and models. At the source, about 10% of the dust is in the submicron fraction [*Tegen et al.*, 2002; *Luo et al.*, 2003]. More relevant at the regional and global scales is the size distribution in the atmospheric burden after some atmospheric transport and processing has taken place. In the models, mass median diameters are typically 2.5 μm or less. In a study using the NASA GISS atmospheric general circulation model (AGCM) with interactive treatment of dust flux and climate, Miller et al. [2004] obtain a substantially lower dust MMD (~1.6 μm) than in an off-line tracer model (~ 3 μm). Observations show at least twofold higher sizes, with some internal disagreement between different measurement approaches. Measurements of dust MMD by aerodynamic methods give a mean of 4.5±1.3 μm, in good agreement with the results from optical inversion methods (5±1.5 μm), but considerably below values obtained by optical counter methods [*Reid et al.*, 2003]. Since the current dust models are being constrained by data obtained by various combinations of these observational approaches, and in turn used to predict radiative forcing, substantial problems related to non-physical parameterizations may result.

Detailed analysis of dust source areas in recent years has shown that there are areas with particularly strong dust emission potential ("preferential source areas"), in particular dry lake beds in arid areas [*Israelevich et al.*, 2002; *Prospero et al.*, 2002; *Tegen et al.*, 2002; *Zender et al.*, 2003]. These regions are also of special relevance to the issue of aerosol/cloud effects, as they contain a high fraction of clay-size (1 μm or less) particles and therefore have the potential of releasing an over-proportionally high number fraction of particles compared to the coarser desert dust particles. They also include soluble residues from the evaporation of the lake water, which renders them highly suitable as CCN [*Formenti et al.*, 2003]. Clay minerals are also known to be effective ice nuclei.

Dust emission shows substantial variability at all time scales from the last glacial maximum to the anthropogenically influenced present and in simulations of the future. This variability is related to changes in vegetation cover, soil moisture, and anthropogenic disturbance of the soil and vegetation surface, as well as to changes in climatic parameters such as wind speed and precipitation [*Mahowald et al.*, 2002; *Tegen et al.*, 2002; *Werner et al.*, 2002; *Luo et al.*, 2003]. Variability at interannual to decadal time scales makes longer-term trends hard to discern. Earlier views that anthropogenic soil disturbance was responsible for as much as half of the present-day dust flux have been revised downward in the last few years, and the contribution of dust from agricultural activities is now estimated to be <10% [*Tegen et al.*, 2004]. Since dust affects precipitation both through radiative transfer and cloud microphysics, there is a feedback through soil moisture on dust emission. Dust exerts a negative forcing at the surface and positive one in the atmosphere. The magnitudes of these forcings are dependent on the optical properties (mineralogy) of dust, which are still poorly known. Model calculations by *Miller et al.* [2004] suggest that increased dust loadings results in more rain in the Sahara, thus producing a negative feedback. In their model, dust reduces global rainfall, thus lengthens the lifetime of aerosols, and increases the burden of dust and other aerosols.

Dust fluxes and burdens in future decades will depend strongly on changes in land cover and climate, but reliable estimates cannot be made at present. One estimate suggests that dust fluxes may decrease with future land use and climate change, that is, by 10-60% by 2100, [*Mahowald and Luo*, 2003], while another suggests smaller changes (10-25%), with increases or decreases possible depending on which climate/land-cover model is used [*Tegen et al.*, 2004]. Because of the strong dependence of dust mobilization on windspeed (increasing with a power of approximately 3-4), dust fluxes in future climates are highly sensitive to changes in the wind regimes in dust source areas.

For an analysis of the impact of dust aerosols on clouds and precipitation, the most important information would be the distribution of the number concentration of dust particles that can act as CCN, GCCN and IN. Unfortunately, the published studies on dust budgets do not provide this information. The issue is further complicated by the fact that dust particles may or may not contain soluble materials already at the time of emission, e.g., in the form of evaporation residues, or that they may become coated with sulfate, nitrate, or other soluble salts during atmospheric processing, especially in clouds [*Levin et al.*, 1996; *Yin et al.*, 2002;

Trochkine et al., 2003]. Most of the dust models carry information about number size distributions, explicitly or implicitly through specification of the modal or bin characteristics of the mass/size distributions. The number maxima of the dust modes are well below 1 μm diameter. For example, *Zender et al.* [2003] show the number maximum at 0.6 μm diameter. Given the relatively high contact angles between water and silicates [*Pruppacher and Klett*, 1997], we would expect that most of these particles would not be able to act as CCN at commonly found supersaturations, unless they were coated with soluble material. If they are not activated as cloud droplets, a substantial fraction of dust particles can remain as interstitial aerosol in convective clouds and reach the middle and upper troposphere, where they can act as IN. If, on the other hand, large dust particles are coated with soluble substances, they can play an important role as GCCN (see chapter 4). In summary, we find that the fluxes and burdens of dust aerosols, and the CCN- and IN-active fractions of this aerosol, depend strongly and interactively on atmospheric processes, especially on their behavior in clouds.

2.2.1.2 Sea Salt

Sea salt aerosols are generated by various physical processes, especially the bursting of air bubbles entrained during whitecap formation and the tearing of droplets from wave tops [*Schulz et al.*, 2004]. The rates of particle production by both mechanisms are strongly dependent on wind speed, with production of spume droplets from wave tops occurring only at wind speeds >9 m s^{-1}. Under moderate wind regimes, seasalt particle number concentrations are typically about 10 cm^{-3} or less, while under high wind conditions (>10 m s^{-1}), their concentration can rise to 50 cm^{-3} or more [*O'Dowd et al.*, 1997; *Shinozuka et al.*, 2004].

One of the few simultaneous measurements of the sizes of seasalt particles and their activity as CCN is that of *Hobbs* [1971]. He found that the concentrations of sodium-containing particles (SCP) over the ocean decreased sharply with increasing height. However, even at altitudes as low as ~17 m above the ocean surface, and over the surf zone, the concentrations of SCP were only a few percent of the concentrations of CCN at 0.5% supersaturation. Also, the average concentrations of CCN did not change significantly with altitude up to at least 3330 m. These measurements indicate that, in general, seasalt particles are not a major contributor to the CCN population. Under particular circumstances, however, at times and in

ocean regions where wind speeds are high and/or other aerosol sources are weak (such as the winter-time remote oceans of the Southern Hemisphere) seasalt may be the dominant contributor to CCN [*O'Dowd and Smith*, 1993; *Murphy et al.*, 1998a; *Quinn et al.*, 1998; *Gong et al.*, 2002; *Shinozuka et al.*, 2004].

Sea salt particles cover a wide size range (ca. 0.05-10 μm diameter), with most of their mass in the supermicron range. The highest number concentration of seasalt particles, however, is in the submicron range, with a pronounced number mode at ca. 500 nm, and significant number concentrations still present at 100 nm [*Campuzano-Jost et al.*, 2003]. Unfortunately, field observations of seasalt particles presently only reach down to ca. 100 nm [*O'Dowd et al.*, 1997; *Murphy et al.*, 1998a; *Campuzano-Jost et al.*, 2003], but laboratory studies of seasalt aerosol production by *Mårtensson et al.* [2003] indicate that the maximum of the number distribution is actually somewhat below 100 nm (~50-80 nm). Very small sea-salt particles, with a number maximum around 20-30 nm, were found to be produced by coastal breaking waves [*Clarke et al.*, 2003]. This is supported somewhat indirectly by measurements of particle flux from the sea surface [*Nilsson et al.*, 2001] that also yield a mode at or below 100 nm, but in this study the composition of these particles could not be identified as seasalt.

A substantial source of very small seasalt particles could be of importance to the marine CCN budget even if they are below the critical diameter for droplet activation at the low supersaturations in marine stratus clouds, because they can serve as nuclei for the growth of sulfate particles from the oxidation of dimethyl sulfide, DMS which is produced from ocean biota [*Charlson et al.*, 1987]. Direct production of sulfate particles by homogeneous nucleation is thought to be only rarely possible in the clean marine atmosphere [*Pirjola et al.*, 2000]. On the other hand, larger seasalt particles also serve as a sink for gaseous H_2SO_4 molecules, thereby reducing the amount of sulfate available for the formation of accumulation mode particles [*Gong and Barrie*, 2003]. More detailed studies on the size distribution, composition, and production rates of the submicron marine aerosol will be required to resolve these issues.

Several studies in the last few years have shown that the “seasalt” aerosol actually contains a substantial amount of organic matter, consisting both of insoluble material (biological debris,

microbes, etc.) and water soluble constituents [*Novakov et al.*, 1997; *Middlebrook et al.*, 1998; *Cavalli et al.*, 2004; *O'Dowd et al.*, 2004]. The fraction of organic components increases with decreasing particle size, and, in biologically active regions, may approach 90% in the size fraction around 100 nm [*Cavalli et al.*, 2004]. The chemical and isotopic composition of this organic matter suggests a marine biogenic source [*Turekian et al.*, 2003]. Organic materials and seasalt are present as internal mixtures, consistent with a production mechanism that involves fragmentation of organic-rich surface film layers during the bursting of air bubbles at the sea surface. Some evidence on dry particles suggests that the organics may be present as coatings on the surface of salt crystals [*Tervahattu et al.*, 2002b], but this finding may not be applicable to the more liquid-rich seasalt particles at ambient humidities.
Because sea salt particles are very efficient CCN, characterization of their surface production is of major importance for aerosol indirect effects. Estimates of the total sea salt flux from ocean to atmosphere vary over a wide range. The most recent estimate [*Schulz et al.*, 2004] is 2690 Tg a^{-1} in a mode centered at 2 μm diameter, plus 17,100 Tg a^{-1} in a mode at 11 μm diameter. At first glance, this appears considerably higher than most previous ones, e.g., 3300 Tg a^{-1} [*Houghton et al.*, 2001], 6500 Tg a^{-1} [*Grini et al.*, 2002], or 5900 Tg a^{-1} [*Tegen et al.*, 1997]. A large part of the differences, however, can be attributed to the choice of the upper size cut-off. With increasing cutoff size, a large mass flux of very coarse and therefore very short-lived salt particles is included in the estimate.

Because most of the seasalt mass is in the coarse mode, while most of the seasalt particle number is in one or more submicron modes, the conventional estimates for the mass source flux of seasalt are of little relevance anyway for the discussion of seasalt particles as CCN, and it is necessary to analyze their number production rates and atmospheric distribution in a size-resolved model. This applies both to the submicron fraction, where most of the seasalt-CCN are found, and to the coarse fraction, which contains the giant CCN (see chapter 4). There are several parameterizations available for the windspeed-dependent, size-resolved emission flux of particles from the sea surface, most of which have been summarized in Schulz et al. [2004]. The best match with the observed size distributions [*O'Dowd et al.*, 1997] is obtained using the *Vignati* and *Gong-Monahan* schemes [*Vignati et al.*, 2001; *Gong*, 2003], among which the Gong-Monahan scheme probably has the more faithful representation of the wind-speed dependence. Estimates of the number flux of seasalt particles have not been published so far, even though it must be assumed that they have been

calculated in the various aerosol models. Below (section 2.2.4) we are presenting an estimate that was retrieved from the model runs that formed the basis of the papers by *Stier et al.* [2005a; 2005b]. Because of the strong dependence of seasalt particle production on wind speeds, the role of these particles in cloud and precipitation processes is expected to change with anthropogenically induced climate change.

2.2.1.3 Primary Anthropogenic Aerosols (Industrial Dust, etc.)

This category includes aerosols from transportation (e.g., tire and brake detritus, road dust, etc.), coal combustion (fly ash, etc.), cement manufacturing, metallurgical industries, and waste incineration, but excludes carbonaceous aerosols to avoid double counting. Primary anthropogenic aerosols are prominent in uncontrolled emissions from old industrial and energy technology, but are now being controlled fairly tightly, especially in developed countries. Growing industrialization, especially in Asia, was expected to lead to significant increases of primary anthropogenic aerosols in some regions. On the other hand, increased awareness of the negative health impacts of aerosols in developing countries, coupled with readily available emission control technology, may lead to less significant growth in these emissions than had been previously anticipated [*Wolf and Hidy*, 1997]. To our knowledge, there are no recently updated global emission estimates for this aerosol type, so that the very rough estimates given in IPCC-TAR had to be reused in Table 2-1. Furthermore, no data are available on which a reliable estimate of the number source flux for this particle type could be based. The mass size distribution of these aerosols is dominated by the coarse mode, but a substantial submicron mode is also present, which contains significant amounts of soluble material [*Kleeman and Cass*, 1998]. Most of the primary particles from coal combustion are below 1 μm in diameter [*Chen et al.*, 2004]. (A fraction of these particles is carbonaceous, and therefore is represented in the category of primary carbonaceous aerosols below.) In Beijing, for example, primary aerosols have been estimated to account for more than half of PM2.5 [*Zhang et al.*, 2004b]. We conclude that primary anthropogenic particles could represent a significant source of CCN (and possibly IN), especially in polluted regions of the developing world.

Table 2-1. Primary particle emissions and burdens for the year 2000[a].

	Mass Emission	Low	High	Mass Burden	Number Prod.	Number Burden
	Tg a^{-1}			Tg	a^{-1}	
Carbonaceous aerosols						
Organic Matter (0-2 µm)	95	40	150	1.2	-	$310 \cdot 10^{24}$
Biomass burning	54	26	70	-	$7 \cdot 10^{27}$	-
Fossil fuel	4	3	9	-	-	-
Biogenic	35	15	70	0.2	-	-
Black Carbon (0-2 µm)	10	8	14	0.1	-	$270 \cdot 10^{24}$
Open burning & biofuel	6	5	7	-	-	-
Fossil fuel	4.5	3	6	-	-	-
Industrial Dust, etc.	100	40	130	1.1	-	-
Sea Salt						
d< 1 µm	180	60	500	3.5	$7.4 \cdot 10^{26}$	-
d=1-16 µm	9940	3000	20,000	12	$4.6 \cdot 10^{26}$	-
Total	10,130	3000	20,000	15	$1.2 \cdot 10^{27}$	$27 \cdot 10^{24}$
Mineral (Soil) Dust						
<1 µm	165	-	-	4.7	$4.1 \cdot 10^{25}$	-
1-2.5 µm	496	-	-	12.5	$9.6 \cdot 10^{25}$	-
2.5-10 µm	992	-	-	6	-	-
Total	1600	1000	2150	18±5	$1.4 \cdot 10^{26}$	$11 \cdot 10^{24}$

a) Range reflects estimates reported in the literature. The actual range of uncertainty may encompass values both larger and smaller than those reported here. Values are based on the following publications: [Andreae, 1995; Andreae and Merlet, 2001; Guelle et al., 2001; Penner et al., 2001; Gong et al., 2002; Luo et al., 2003; Bond et al., 2004; Liousse et al., 2004; Zender et al., 2004; Ito and Penner, 2005; Junker and Liousse, 2005; Stier et al., 2005a; Stier et al., 2005b].

2.2.1.4 Primary Biogenic Aerosols

Primary biogenic aerosol particles (PBAP) may enter the atmosphere from a number of sources. Plants shed various types of debris (cuticular waxes, leaf fragments, etc.), and soil deflation releases a mixture of humic matter, plant decomposition products, fungi and microbes. Atmospheric aerosols over land and oceans contain a large variety of microbial particles (bacteria, fungi, viruses, algae, pollen, spores, etc.). These particles cover a wide size range from tens of microns down to a few tenths of microns. Morphological studies using light and electron microscopy have shown that PBAP make up a large fraction of the aerosol down to ~0.2 μm at a variety of clean and polluted sites (e.g., the Amazon, Siberia, and even urban Central Europe [*Matthias-Maser and Jaenicke*, 1995; *Matthias-Maser et al.*, 2000; *Graham et al.*, 2003a; *Graham et al.*, 2003b; *Posfai et al.*, 2003]. Their number concentrations are in the range of tens to hundreds cm^{-3}. Unfortunately, it becomes quite difficult to unequivocally identify particles in the submicron range as primary biogenic, as they often have little or no diagnostic morphological or bulk chemical signatures. Chemical tracers studies suggest, however, that primary biogenic material contributes a large fraction of the pristine aerosol even in this size range [*Simoneit et al.*, 1990; *Graham et al.*, 2003b]. Very small PBAP (20-50 nm) may also play a role as growth nuclei for CCN-sized particles over the remote oceans, through condensational growth by deposition of sulfate derived from the oxidation of DMS [*Leck et al.*, 2002; *Leck et al.*, 2004].

There is considerable evidence that primary biogenic particles may be able to act both as CCN and IN [*Schnell and Vali*, 1976a; *Levin and Yankofsky*, 1983; *Diehl et al.*, 2001; *Bauer et al.*, 2003]. This is consistent with their often relatively large size and soluble matter content, but surface properties are also thought to play a significant role [*Bauer et al.*, 2003]. It is therefore likely, that PBAP represent a significant fraction of CCN and IN in the clean atmosphere, and therefore are of importance for the regulation of cloud microphysical properties under pristine or remote conditions, but not enough is known at this time to assess their role with any confidence. Since their atmospheric abundance may undergo large changes as a result of land use change, they deserve more scientific study.

Since many of these PBAP are of large size, they are of special interest because they can already be activated at very low supersaturations (<0.02%). Therefore, they will be the first to activate at cloudbase, and they can grow readily because of their large surface. They may

therefore represent a major source of GCCN. This enables them to play an important role in precipitation formation under circumstances when high concentrations of pollutant CCN otherwise would suppress warm rain production [*Yin et al.*, 2000a; *Rudich et al.*, 2002]. To date, there are no reliable estimates on the rates of PBAP emissions. The estimates given in Table 2-1 have been calculated based on the commonly observed mass concentrations of 1-2 μg m^{-3} over remote, vegetated continental regions and an estimated atmospheric lifetime of 2 days for these particles.

2.2.2 Carbonaceous Aerosols (Primary and Secondary)

Carbonaceous material, consisting of organic compounds and near-elemental, sub-graphitic material ("soot") represents an important fraction of the atmospheric aerosol. Only a minor part of this complex mixture, in the range 10 to 40%, has been identified at the molecular level [*Gelencsér*, 2004; *Decesari et al.*, 2005; *Kanakidou et al.*, 2005]. The carbonaceous aerosol contains a large fraction of oligomers and highly polymeric matter from various origins. This unique chemical complexity is the cause of much of the prevailing uncertainties regarding the sources and properties of carbonaceous aerosol.

Carbonaceous materials represent a continuum from semi-volatile organic species (SVOC), chemically-identified particulate organic carbon (POC), polymeric POC, to black carbon (BC) or elemental carbon (EC). The BC or EC component is operationally defined as light-absorbing ("black") or thermally refractory ("elemental") carbon, and is generally thought to consist of aggregates of 20-50 nm granules with a graphite-like crystal structure and near-elemental composition with some surface functionalities [*Smith et al.*, 1989]. Such particles are also called "soot" particles (which term often includes the organic coating that is usually associated with these particles), and originate from various types of combustion. Especially in biomass smoke, however, there are also other refractory organic compounds that operationally act like EC, and other light-absorbing organics that are determined as BC, so that at this time this aerosol component remains rather ill-defined. This is reflected in large discrepancies between the results of OC and BC/EC measurements from different laboratories (up to factors of 10 for BC/EC), even when identical samples and nominally identical analytical protocols are used [*Ten Brink et al.*, 2004]. The strong increase of the absorption with decreasing wavelength can sometimes be used to identify aerosols from biomass burning [*Kirchstetter et al.*, 2004; *Schmid et al.*, 2005].

As the most commonly used combustion-based chemical analyses provide carbon contents only, a conversion factor k is required to account for organic functional groups in particulate organic matter (POM = k x POC). The k factor varies with the origin and age of the particles over a wide range: 1.3 (close to sources) to >2.0 [*Putaud et al.*, 2000; *Turpin and Lim*, 2001; *Kiss et al.*, 2002; *Russell*, 2003].

In addition to primary carbonaceous aerosols there is a substantial amount of secondary organic aerosols (SOA) formed from a large variety of anthropogenic and biogenic gaseous precursors [*Seinfeld and Pankow*, 2003]. As a result, organic aerosols contain variable amounts of primary (PPOM/PPOC) and secondary (SOA) material. It has been shown that in source regions the formation of combustion-derived SOA occurs readily and could represent the same amount as PPOM [*Cooke et al.*, 1999]. Once formed, carbonaceous aerosols are subject to continuous chemical modification in the atmosphere by photochemical and multiphase reactions [*Maria et al.*, 2004]. This includes reactions with OH and other radicals from the gas phase [*Molina et al.*, 2004; *Zuberi et al.*, 2005], oligomerization with and without acid catalysis [*Claeys et al.*, 2004; *Gao et al.*, 2004; *Kalberer et al.*, 2004], and formation of humic-like substances (HULIS) by photochemical polymerization of biogenic precursors [*Gelencsér et al.*, 2002].

2.2.2.1 Sources of Carbonaceous Aerosol

Black carbon and a fraction of PPOM and SOA originate from combustion sources. Combustion sources using fossil fuel are found in industry, power generation, traffic and residential heating; they are found to about 90% in the Northern hemisphere [*Andres et al.*, 1996]. It has, however, been shown by carbon-14 analysis that even in cities the biogenic fraction may comprise about 60% of the carbonaceous aerosol, which in summer is mainly attributed to SOA from biogenic precursors, while in winter there is a substantial contribution from wood combustion [*Szidat et al.*, 2006]. In the intertropical zone, biomass burning (open savanna, forest and agricultural waste fires) and biofuel use form the main sources of anthropogenic carbonaceous aerosols. Biomass burning from natural fires provides a major source of carbonaceous aerosols mainly in the mid- to high latitudes of the northern hemisphere [e.g., *Lavoué et al.*, 2000]. SOA is also formed by the conversion of natural organic gases such as terpenes and, probably to a lesser extent, isoprene [*Claeys et al.*, 2004]. From both biomass burning and fossil fuel sources, POM (PPOM + SOA) is always the predominant fraction of the carbonaceous aerosol. However, the chemical composition of the

aerosol as represented by the BC/POM ratio is highly dependent on the type of sources: on average, the BC/POM ratio is higher for fossil fuel than for biomass burning sources. Also BC/POM ratio is linked to the type of burning: BC/POM is probably related to the temperature of the combustion process and thus for example higher for diesel emissions than for gasoline [*Bond et al.*, 2004]. Biomass combustion aerosols emitted under flaming conditions will have a higher BC/POM ratio than smoldering aerosols, which are almost entirely of organic nature [*Reid et al.*, 2005].

2.2.2.2 Emission Inventories for Carbonaceous Aerosols

At present, lack of adequate data for BC and PPOC concentrations precludes the use of inverse modeling. To estimate the emissions of combustion carbonaceous aerosols, the only suitable method is at present the bottom-up approach. Emission estimates are based on two different data sets: one is related to fuel consumption and another to particulate emission factors.

Spatial distributions of fuel consumption (fossil fuel and biofuel) may be obtained from data provided by a variety of national and international organizations. They are complemented by regional inventories that make special efforts to account for regional source characteristics and may provide more detailed consumption maps [*Streets et al.*, 2001; *Reddy and Venkataraman*, 2002; *Streets et al.*, 2003; *Schaap et al.*, 2004].

Mapping the amounts of burnt biomass is a difficult task. In previous studies [*Hao and Liu*, 1994; *Hao et al.*, 1996] estimates of burnt areas for savanna and forest fires were based on statistical data. For emissions related to agricultural practices, the FAO data are usually associated with assumptions of the burnt fraction [*Yevich and Logan*, 2003]. Qualitative improvements are now obtained from multi-year global distributions of fire pixel counts and burnt area given by satellite imagery (ATSR, AVHRR, MODIS and SPOT Vegetation), as these data allow taking into account the spatial and temporal variability of fires at different scales [*Kajii et al.*, 2002; *Generoso et al.*, 2003; *van der Werf et al.*, 2003; *Hoelzemann et al.*, 2004; *Ito and Penner*, 2004; *Liousse et al.*, 2004; *Michel et al.*, 2005]. The need to couple the two existing satellite tools (fire counts and burnt area) is illustrated by the work of *Michel et al.* [2005] on biomass burning inventory for Asia using SPOT imagery for burnt areas. The fire spatial and geographical distribution they obtain is totally different than that of *Streets et al.* [2003] derived from fire pixel count maps. Provided that current problems with detection

algorithms can be solved, the uncertainty of such products might be reduced to less than 15% for burnt areas. Uncertainty now resides primarily on the estimates of fire properties (biomass density and combustion efficiency) and further improvement will necessitate accounting for regional differences and relating in a common effort local measurements, remote sensing techniques and fuel models.

Emission factors for BC and PPOC (or PPOM) particles depend on the nature of the fuel used and on the physical conditions of the combustion processes. Thus for a given fuel, the type of use (industrial vs. domestic) and combustion technology will be of high importance. The level of development of each country and the regulating standards they apply are also crucial. For biomass burning, BC and PPOC emission factors have been reviewed based on a synthesis of the most recent experiments and existing papers [*Andreae and Merlet*, 2001].
For fossil fuels and biofuels, problems originate from the complexity, heterogeneity, and uneven coverage of available information. To cope with this difficulty, global inventories have been then constructed following a standard procedure that may apply to all activities in all countries and is flexible enough to be easily improved [*Cooke et al.*, 1999; *Junker and Liousse*, 2005]. The detailed sources were reduced to three main sectors of activities (traffic, industrial and domestic) and three levels of country developments (developed, semi-developed and developing) based on national gross income. This yields nine emission factors, each with a specific BC/PPOC ratio, for each fuel category for BC and primary POC. In an alternative approach, however, the exhaustive description of fuel combustion activities, technology divisions and emission controls (mostly for developed regions) has been preserved [*Bond et al.*, 2004]. But numerous assumptions had to be made for regions where combustion technologies and emission controls were poorly known.

The few existing BC and PPOC emission inventories show significantly different budgets and different regional partitioning of the emissions. Most of them do not account for all sources (industrial versus biomass burning) or are restricted to one component of the aerosols (BC or primary OC only). Furthermore, the use of either PPOC or POM (including the SOA fraction) is often confusing.

These disagreements persist in the recent existing comprehensive fossil fuel and biofuel (BC and PPOC) global emission inventories by *Bond et al.* [2004] (B04), *Liousse* and coworkers [*Liousse et al.*, 2004; *Junker and Liousse*, 2005] (L05) and *Ito and Penner* [2005] (I05)

(Table 2-2). We find that differences sometimes exceeding a factor of 2 exist between the various estimates. The B04 and I05 emissions are significantly lower than the L05 values, although new sources were added that had not been taken into account before (such as off-road vehicle emissions and waste combustion). An important source of disagreement between these two studies probably arises from the choice of significantly different emission factors (EFs) (Table 2-3). I05 in most cases used the B04 EFs, which also supports differences in EFs as the main cause of discrepancies.

Table 2-2. Global emission estimates for black carbon and primary particulate organic carbon (Primary POC) from fossil fuel, biofuel, and open biomass burning.

	Black Carbon Tg C a^{-1}			Primary POC Tg C a^{-1}		
	Fossil Fuel	Biofuel	Open Burning	Fossil Fuel	Biofuel	Open Burning
Liousse et al. [2004] *Juncker & Liousse* [2005]	5.9	2.9	4.3[1]	6.4	8.7	8.2[2]
Bond et al. [2004]	3.0	1.6	3.3	2.4	6.5	25
Ito & Penner [2005]	2.8	2.0	3.5	2.4[4]	7.3[4]	22[4]

[1)] *Including savanna, open agricultural fires and tropical fires [Liousse et al., 1996b] and extratropical fires [Lavoué et al., 2000].*

[2)] *Primary particulate organic carbon only, including savanna, open agricultural fires and tropical fires [Liousse et al., 1996b] and extratropical fires [Lavoué et al., 2000].*

[4)] *Using a conversion factor of 1.3 for PPOC=>PPOM.*

Table 2-3. Black carbon emission factors for the main fossil-fuel-related sources.

	Black Carbon Emission Factor [g C per kg fuel]	
	[Bond et al., 2004]	*[Junker and Liousse, 2005]*
Developed Countries	0.001-0.006	0.149
Industrial, Coal		
Industrial, Lignite	0.015-0.03	0.3
Traffic, Diesel	0.85	2
Traffic, Gasoline	0.04	0.03
Developing Countries		
Industrial Coal	0.28-4.5 (1.12)	1.10
Industrial Lignite	0.09	1.98
Traffic Diesel	2-7	10
Traffic Gasoline	0.14-0.6	0.15

To assess the role of the choice of EFs in the discrepancy, a calculation was conducted for the year 1996, with the B04 and L05 sets of EFs, but using the same UN fuel database and the same methodology with the 9 BC EFs per fuel. A comparison of the results shows about 10-fold larger emissions from lignite burning, 6-fold larger emissions from Diesel use, and about 25% greater emissions from hard coal burning when the L05 EFs are used instead of the B04 values. Recent combustion chamber experiments (not yet published) have shown that for Diesel emissions, the EF(BC) value of 2 for developed countries found in *Liousse* would be in the highest part of the acceptable range, whereas on the other hand for coal industrial combustion, Bond's EF(BC) value of 0.0024 would be too low. There is indeed a critical need for further targeted experiments and for an effort towards consistency between the authors of these two studies to avoid the numerous existing or forthcoming discrepancies.

A way to test the validity of these inventories is to apply them in a global model and to compare the modeled values with existing BC and POM measurements. Reasonable agreement can be obtained for surface BC and PPOM concentrations using the L05 emissions implemented in the TM-3 model. As the BC global burden estimated by B04 is almost half that of L05 it might be expected that comparisons between model and measurements would

be less satisfactory. At this point, a recommendation for global inventories for fossil fuel and biofuel combustion emissions of BC and PPOC would be to use the *Bond and Liousse* values respectively as the low and the high part of the range. Further improvements may come from simultaneous refinements in bottom-up estimates and combination with top-down approaches using distributions of emitted substances detected by remote sensing, such as in the recent study by *Ito and Penner* [2005].

2.2.2.3 Secondary Organic Aerosols

As mentioned before, organic aerosols are comprised of primary and secondary particles. The treatment of SOA in emission inventories of carbonaceous particles is still an open question. In the previous paragraphs, we have considered emission of primary particles (PPOC) only. There is no evidence for the direct formation of SOA particles by nucleation of organics from the gas phase in the present-day atmosphere. SOA-rich particles have been shown to form by condensation of organic gases with low vapor pressures on pre-existing particles, which may be as small as freshly nucleated sulfate particles in the ultrafine size class [*Kerminen et al.*, 2000; *Kulmala et al.*, 2000; *Kerminen*, 2001; *O'Dowd et al.*, 2002; *Lihavainen et al.*, 2003; *Maria et al.*, 2004; *Zhang et al.*, 2004a]. The resulting particle may consist almost completely of organic material, and the presence of the initial sulfate nucleus may not be readily detectable any more. This is most likely the case in environments such as the Amazon Basin, where nucleation events have never been observed in spite of high concentrations of VOC and high rates of photochemical oxidation [*Rissler et al.*, 2004]. Here, significant amounts of primary biogenic and other particles act as an efficient sink for condensable organics. On the other hand, in the presence of high concentrations of SO_2 and a high rate of H_2SO_4 production, new particle formation and growth by incorporation of organics occurs even at a high concentration of pre-existing aerosols, such as in the cities of Milan and Pittsburg [*Baltensperger et al.*, 2002; *Zhang et al.*, 2004a]. Once incorporated into the condensed phase, organics can be made less volatile by oxidation and polymerization reactions [*Gelencsér et al.*, 2002; *Limbeck et al.*, 2003; *Claeys et al.*, 2004; *Gao et al.*, 2004; *Kalberer et al.*, 2004].

A number of studies has been conducted in recent years to assess the magnitude of SOA formation from biogenic and anthropogenic precursors [*Liousse et al.*, 1996a; *Griffin et al.*, 1999; *Kanakidou et al.*, 2000; *Chung and Seinfeld*, 2002; *Kanakidou et al.*, 2005; *Tsigaridis et al.*, 2005]. In spite of these efforts, the range of estimates remains huge: 2.5-79 Tg yr^{-1} for

biogenic SOA and 0.05-2.6 Tg yr^{-1} for SOA from anthropogenic precursors. Ignoring the more extreme results of sensitivity studies, we can use the values from the review of *Kanakidou et al.* [2005] as a currently best guess: 19, 15, and 2 Tg yr^{-1} from terpenes, oxygenated VOC (OVOC) and anthropogenic VOC, respectively.

2.2.2.4 Organic Aerosols as CCN

Primary carbonaceous particles originating from fossil-fuel pollution may initially consist to a large extent of EC and water-insoluble substances (e.g., engine oil, etc.). They are at this stage probably not efficient CCN [*Hudson et al.*, 1991; *Weingartner et al.*, 1997; *Zuberi et al.*, 2005], but as they become partially oxidized and as soluble compounds (sulfates, nitrates, WSOC) deposit on them, they become CCN at realistic supersaturations [*Tsigaridis and Kanakidou*, 2003]. This process can occur on timescales of minutes to hours, depending on the circumstances. Primary particles from biomass burning (pyrogenic particles) are fairly efficient CCN already immediately over the fires, and become even more easily activated as they age and thereby increase in size and become more oxidized [*Warner and Twomey*, 1967; *Hobbs and Radke*, 1969; *Eagan et al.*, 1974b; *Hallett et al.*, 1989; *Radke et al.*, 1991; *Rogers et al.*, 1991; *Ross et al.*, 2003; *Andreae et al.*, 2004]. The SOA component can contribute to CCN activity by either forming new particles from the gas phase that consist exclusively or at least predominantly of SOA, or by condensation of SOA compounds on pre-existing aerosols, and thereby modifying their CCN properties.

Estimation of the source strength of the predominantly carbonaceous CCN from biomass and fossil fuel burning is in principle relatively straightforward, but still entails large uncertainties. In the case of biomass burning, the emission ratio of CN to CO is a relatively robust parameter, with a characteristic value of about 25±10 cm^{-3} ppb^{-1} [*Guyon et al.*, 2005], corresponding to about $2 \cdot 10^{13}$ particles emitted per gram CO. Of these particles, the fraction that can be activated at 1% SS (supersaturation) is very high, with most studies showing CCN/CN ratios of 60-100% for fresh or aged biomass smoke [*Radke et al.*, 1988; *Hudson et al.*, 1991; *Rogers et al.*, 1991; *Novakov and Corrigan*, 1996; *Ross et al.*, 2003]. Assuming an annual global emission of 700 Tg CO from biomass burning [*Andreae and Merlet*, 2001] and a $CCN_{1\%}$/CN ratio of 0.8 yields an estimate of $1.1 \cdot 10^{28}$ $CCN_{1\%}$ for the annual emission from biomass burning. It is encouraging that an alternative calculation, based on CCN (at 1% SS) with an emission factor of $2 \cdot \times 10^{15}$ per kg dry biomass, yields similar results.

Unfortunately, comparable emission factors are not available for fossil fuel combustion. *Bond et al.* [2002] have shown that residential coal burning produces $12 \cdot 10^{15}$ particles/kg for lignite (mostly >100 nm) and $14 \cdot 10^{15}$ for bituminous coal (mostly <100 nm). Given that residential burning tends to have considerably larger emission factors than industrial or power related combustion, the overall CCN emission factors for fossil fuel burning are likely to be considerably lower.

Carbonaceous aerosol emissions are projected to decline over the 21st century to about two-thirds of their present values by 2050, but most likely with a significant rise in the BC/OC ratio in industrialized regions [*Streets et al.*, 2004].

2.2.3 Primary Aerosol Number Fluxes

The calculation of the aerosol indirect effects and their interaction with the hydrological cycle requires size-resolved knowledge of the global distribution of aerosol number concentrations. Recently, the aerosol size distribution has been added to the prognostic parameter space of global microphysical aerosol models to account for these effects. In addition to the emission mass fluxes, these models require as input the primary aerosol number fluxes and therefore the knowledge of the emission size distribution.

Natural sea salt and mineral dust are predominantly emitted in the accumulation and coarse mode size range and their size distribution is mainly altered by size-dependent sink processes. A number of size-resolved emission parameterizations are available for sea salt and mineral dust (see above), and can be interactively calculated in numerical models. These parameterizations can also be used in future scenarios.

However, for primary emissions from combustion processes, the initial evolution of the size distribution is characterized by small-scale microphysical processes [*Jacobson and Seinfeld*, 2004] that cannot be resolved in regional and global aerosol models. Therefore, the sub-grid scale evolution of the size-distribution and mixing state shortly after emission should to be parameterized in a way that is appropriate to the model scale. Up to now, such parameterizations are not available and the emission size-distribution is generally estimated from measurements made on "slightly" aged plumes. For the AEROCOM aerosol model inter-comparison, an emission inventory has been provided [*Dentener et al.*, 2005], based on mass flux estimates by *Bond et al.* [2004] for carbonaceous aerosols from fossil- and bio-fuel use, by *Van der Werf et al.* [2003] for vegetation fires, and by *Cofala et al.* [2005] for

anthropogenic sulfur emissions (data and documentation available from ftp://ftp.ei.jrc.it/pub/Aerocom/). AEROCOM recommends 2.5% of the total SO_2 emissions to be emitted in the form of primary sulfate to account for sub-grid scale sulfate formation at the sources. In addition, source-specific size distributions are proposed (Table 2-4) for freshly emitted primary aerosols, which are then subject to further microphysical processing in global aerosol models. For comparison, the parameters of a log-normal fit [*Stier et al.*, 2005b] of natural sea-salt [*Schulz et al.*, 2004] and mineral dust [*Tegen et al.*, 2002; *Tegen et al.*, 2004] as used in the emission parameterizations, neglecting the super-coarse mode emissions are also given in Table 2-4.

The total emission number flux F_N of primary particles can be calculated from a given emission mass flux F_M and a log-normal emission size-distribution as follows:

$$F_N = F_M \frac{3}{4\pi\rho\left(r_{NMR}\exp(1.5\ln^2(\sigma))\right)^3}$$

where ρ is the density of the compound and r_{NMR} the number median radius and σ the standard deviation of the log-normal emission size-distribution.

Based on the AEROCOM anthropogenic emission inventory and the proposed emission size distributions, the total anthropogenic primary aerosol number flux can be estimated as listed in Table 2-4. This flux is highly dependent on the choice of the emission size distribution. For example, the usage of the same emission mass flux for primary sulfate, but with the significantly smaller emission size-distributions used by *Adams and Seinfeld* [2003] results in a $6x10^4$ larger number flux than using the large "fly ash" AEROCOM size distribution recommendation. This underlines the necessity of adequate emission size distributions and for careful adaptation to for the respective model scales.

Table 2-4. Global annual anthropogenic primary aerosol number fluxes as recommended by the AEROCOM emission inventory. For comparison, values for the natural emissions of sea salt [*Schulz et al.*, 2004] and mineral dust [*Tegen et al.*, 2002; *Tegen et al.*, 2004] are also given.

	Number Median Radius (μm)	Standard Deviation	Total Mass Flux (Tg a^{-1})	Total Primary Number Flux (a^{-1})
Fossil-Fuel Burning (BC+POM)	0.015	1.8	6.4[1]	4.8×10^{28}
Bio-Fuel Burning (BC+POM)	0.04	1.8	10.7[1]	4.2×10^{27}
Vegetation Fires (BC+POM)	0.04	1.8	37.7[2]	1.5×10^{28}
Primary Sulfate (H_2SO_4)	0.5	2.0	4.3[3]	5.1×10^{23}
Sea Salt (Accumulation Mode)	≈0.2 varying with wind-speed	1.6	54.1	7.4×10^{26}
Sea Salt (Coarse Mode)	≈2.2 varying with wind-speed	2.0	4955	4.6×10^{26}
Mineral Dust (Accumulation Mode)	0.2	1.6	7.5	4.1×10^{25}
Mineral Dust (Coarse Mode)	0.4	2.0	655	9.6×10^{25}

[1] *[Bond et al., 2004]*

[2] *[van der Werf et al., 2003]*

[3] *Industry, fossil- and bio-fuels from Cofala et al. [2005] and vegetation fires from van der Werf et al. [2003] with 2.5% of SO_2 emitted as primary sulfate.*

The primary number flux, however, is not a direct measure of CCN. Only a fraction of the particles emitted in the nucleation and Aitken size range will reach the CCN size range (usually larger than ca. 60 nm), non-linearly depending on the aerosol concentration, the

interaction with condensable vapors and secondary aerosols, and the atmospheric lifetime. As the growth processes are governed by microphysical interaction, a separate treatment of the different source types and components is not appropriate, and internal mixtures should be considered. Global microphysical aerosol models are required to globally predict the evolution of the size-distribution and the contribution of specific aerosol sources to the number of radiatively important aerosols and cloud condensation nuclei. In a study with the global microphysical aerosol-climate model ECHAM5-HAM, *Stier et al.* [2005b] demonstrated that the global CCN number concentration is non-linearly related to the emission mass flux. While primary carbonaceous aerosol emissions disproportionately contribute to the CCN number, anthropogenic SO_2 emissions less than proportionally contribute to the number of CCN, because a significant fraction of the produced sulfuric acid condenses on pre-existing aerosols. The co-emission of anthropogenic carbonaceous and sulfuric emissions produces generally less CCN in the vicinity of the source regions than the sum of the individual emissions. Therefore, in contrast to results from traditional bulk mass aerosol models, the sum of the change of CCN due to individual emission changes is different from the total CCN change due to several combined emission changes.

As a measure of the contribution of specific aerosol sources to the potentially CCN-relevant size range, one can define the difference in CCN due to omission of the specific aerosol source with respect to a simulation with the complete set of emission. In Figure 2-1 a) the annual zonal mean distribution of hygroscopic accumulation and coarse mode particles (an approximation of the CCN concentration) for the year 2000 is depicted, computed by the ECHAM5-HAM aerosol model [*Stier et al.*, 2005a]. Further shown are the differences with respect to this reference scenario due to the omission of b) carbonaceous emissions from fossil-fuel use and industry, of c) sulfur emission from fossil-fuel use, industry, and bio-fuels, and of d) total anthropogenic emissions.

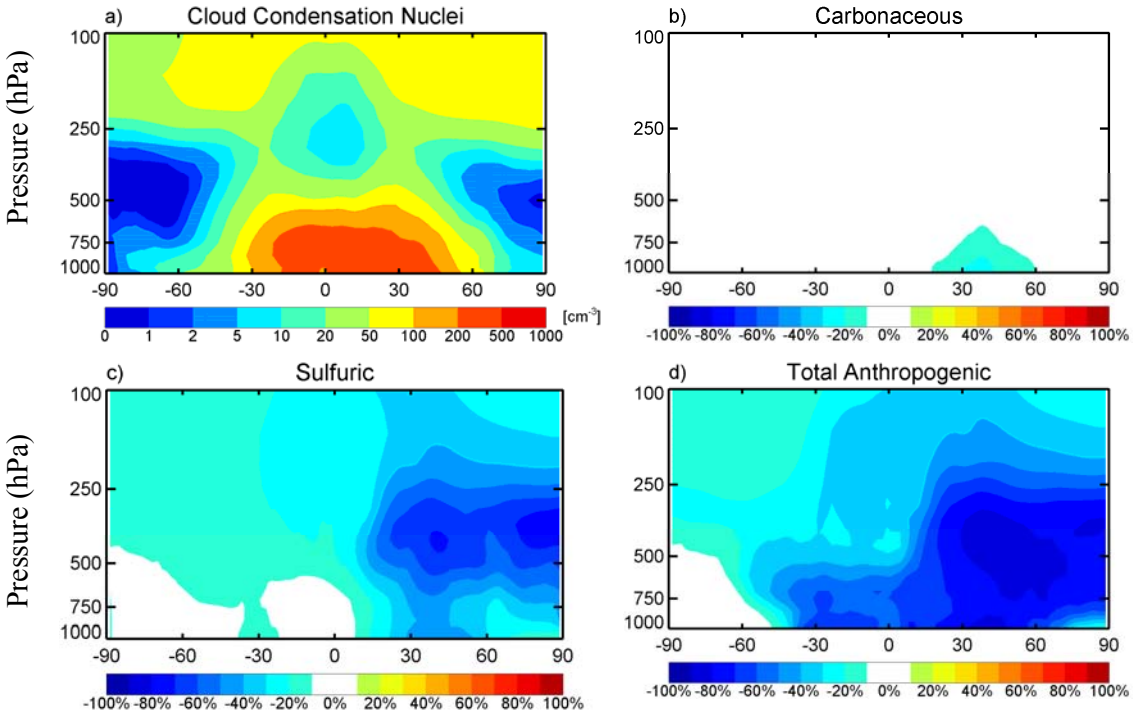

Figure 2-1. *a) Total zonal annual-mean cloud condensation nuclei (cm^{-3} STP{1013hPa, 273.15K}) as simulated by the ECHAM5-HAM aerosol model. CCN are defined here as hygroscopic accumulation and coarse mode aerosol particles. Change in CCN due to the omission of b) carbonaceous emissions from fossil-fuels and industry, c) sulfuric emission from fossil-fuels, industry, and bio-fuels, d) all anthropogenic emissions including fossil-fuels, industry, bio-fuels, and vegetation fires.*

The zonal mean distribution of CCN (a) shows a pronounced maximum in the lower to mid-troposphere (1000 hPa – 500 hPa) in the region of strongest anthropogenic emissions between 30°S and 50°N. The omission of carbonaceous emissions from fossil fuel use and industry (b) reduces the zonal mean number of CCN in the lower troposphere between 20°N and 60°N by up to 30 %. It has to be stressed that fossil-fuel use and industry contribute (with 6.4 Tg) only to 9.7% of the total carbonaceous mass emissions and a significantly smaller fraction of the total anthropogenic aerosol mass source. In the lower to mid-troposphere, sulfur emissions from fossil fuels, industry, and biofuels (c) contribute between 30% and 50% of the total number of CCN between 20°N and 60°N. In contrast, higher up in the NH mid-to-upper troposphere (750-250 hPa), they dominate the CCN numbers. The impact of anthropogenic sulfur emissions on southern hemispheric CCN in the lower troposphere is

negligible. Total anthropogenic emissions (d), including fossil-fuel use, industry, vegetation fires and bio-fuel use, largely control the low to mid-troposphere CCN numbers between 30°S and 70°N contributing to 50%-80% of total CCN numbers. Only the CCN at high southern latitudes are predominantly controlled by natural emissions.

2.2.4 Sulfates

Knowledge of the temporal and spatial details of anthropogenic and natural sulfur emissions is vital for estimating the atmospheric aerosol loadings of sulfate aerosols. The substantial growth of industrialization and energy production since the 1950s has resulted in increased burning of fossil fuels, causing extensive emissions of SO_2. Growing emissions are additionally driven by an increase in population. On the other hand local air quality concerns, structural change in energy supply and end-use, advanced technology and cleaning procedures have dramatically reduced air pollution, including SO_2 emissions, in some regions. Regional changes in emission pattern are additionally driven by a shift of strong polluting industry from the developed to the developing countries.

2.2.4.1 Sulfate Precursor Emissions

The most abundant sulfur gases in the atmosphere are carbonyl sulfide (OCS), DMS, sulfur dioxide (SO_2) and hydrogen sulfide (H_2S). They are all subject to oxidation by a variety of atmospheric species, including hydroxyl and nitrogen radicals, ozone, and excited oxygen atoms, and to photochemical decomposition [*Seinfeld and Pandis*, 1998]. The ultimate fate of these atmospheric sulfur compounds is the irreversible oxidation to sulfate (SO_4^{2-}), which forms particles mixed with water and ammonium (i.e., H_2SO_4, NH_4HSO_4, $(NH_4)_2SO_4$). A small fraction of DMS oxidizes to methanesulfonic acid (MSA), which condenses on existing particles. These atmospheric sulfur compounds have a variety of natural and anthropogenic sources, with anthropogenic fluxes dominating at present and into the foreseeable future [*Dentener et al.*, 2005]. The most important natural sources of DMS and SO_2 are the marine biosphere and exhalation from volcanoes, respectively. Intra-annual variability and climate induced changes of the source strength and distribution of natural sulfur sources are poorly known. *Gabric et al.* [2004] used simulations with the CSIRO GCM of the period of equivalent CO_2 tripling (2080) to derive the changes in oceanic DMS production and flux to the atmosphere. They predicted a globally integrated DMS flux increase of 14%. The greatest perturbation to DMS flux is simulated at high latitudes in both hemispheres, with little

change predicted in the tropics and sub-tropics. The largest change in annual integrated flux is simulated in the Southern Hemisphere between 50°S and 60°S. At this latitude, the DMS flux perturbation is most influenced by the GCM-simulated changes in the mixed layer depth. This indicates that future increases in stratification in the polar oceans will play a critical role in the DMS cycle and therefore the flux of sulfate aerosols in remote ocean regions.
Major uncertainties exist for the volcanic sulfur emissions and current estimates are probably too low [*Textor et al.*, 2004]. Volcanic emissions are however released at mountain peaks mostly above the planetary boundary layer where they have extended life times and disproportionate effects on cloud properties.

The major anthropogenic sulfur source is SO_2 emissions from the burning of sulfur-containing fuels, mainly coal. Metal smelting and other industrial processes also release significant quantities of SO_2. Global anthropogenic sulfur emissions are estimated to range between 65 and 90 Tg S in 1990 [*Houghton et al.*, 2001]. Reviews of most recent inventories indicate a most likely value of 75±10 Tg S in 1990 [*Smith et al.*, 2001], and 71 Tg S in the AEROCOM inventory for 2000 [*Dentener et al.*, 2005]. *Smith et al*. [2001] estimate that 56% of 1990 world sulfur emissions are from coal, 24% from oil, 15% from industrial processes and 3% from biomass burning. Emission from bunker fuel burned by the international cargo and passenger ship fleet represents a contribution of 4-7% to the global anthropogenic SO_2 emissions (3.0 Tg S in 1996 [*Endresen et al.*, 2003]; 3.7 in 2001 [*Endresen et al.*, 2005]. The majority of these ship emissions occur in the Northern Hemisphere.

Globally, emissions have been roughly constant from 1980 to the present. However, a significant shift has occurred in the spatial distribution of emissions. Many climate studies to date have used the emissions pattern from the GEIA inventory for 1985 and simply scaled these backwards and forwards in time. This is clearly an oversimplification, as the regional pattern of emissions has changed dramatically over the last 30 years [*Massie et al.*, 2004]. Different inventories are similar at the global-mean level, but show marked differences at the regional level.

While 60% of global emissions in 1980 were from around the North Atlantic basin, this region contributed less than 40% of the global total by 1995 and will contribute even less in the future [*Smith et al.*, 2001]. As a result of the implementation of international emissions agreements, SO_2 emissions decreased 32% from 1980 to 1990 in Europe, and 3% from 1980

to 1995 in North America. In 1990, the spatial pattern of emission shows that the US, the USSR, and China were the main sulfur dioxide emitters (i.e., approximately 50% of the total). Historical data for Asia are more problematic, but the trends are clearly in the other direction. The data indicate a roughly 60% increase in sulfur dioxide emissions from 1980 to 1990. The two main reasons for this are the region's rapid economic growth and its high dependence on coal. *Streets* and coworkers have estimated that China's SO_2 emissions grew 3.6% per year from 1985 through 1996, and India's SO_2 emissions grew at a rate of 4.9% per year during the 1990s [*Streets et al.*, 2000; *Streets and Waldhoff*, 2000]. This trend is confirmed by satellite data (TOMS) of aerosol optical depth (AOD). Large increases in AOD between 1979 and 2000 are evident over the China coastal plain and the Ganges River basin in India. For instance AOD increased by 17% per decade during winter over the China coastal plain [*Massie et al.*, 2004].

In contrast, *Carmichael et al.* [2002] report that since 1995 Asian SO_2 emissions have declined from 38.5 Tg in 1995 to 34.4 Tg in 2000, a decrease of 2.3% per year. This remarkable change is almost entirely due to a reduction in emissions in China, which emits about two-thirds of SO_2 from Asia. This has been brought about by several factors: a marked reduction in industrial coal use from the closure of small and inefficient plants, a slow-down in the Chinese economy, the improved efficiency of energy use, the closure of some high-sulfur coal mines, a general reform in industry and power generation, and a rising awareness of the dangers of air pollution.

2.2.4.2 Transformation and Sulfate Particle Formation

When emitted into the atmosphere, sulfur species undergo transport and chemical reactions to form compounds that condense on aerosol surfaces or nucleate. Wet deposition removes gases and particles in the atmosphere and deposits them on the Earth's surface by means of precipitation. With dry deposition, particles and gases reach land and water surfaces without precipitation. All the processes controlling dispersion, residence time in the atmosphere, aerosol load and composition vary with weather and climate. Since sulfur emissions themselves influence climate, and so change the transport and sink processes, one cannot accurately model the influences of anthropogenic emissions unless the climate influences are also modeled in a consistent way. While this clearly requires an appropriate coupled climate-sulfur-chemistry model, the primary driving force must be reliable, spatially-resolved SO_2 emissions [*Smith et al.*, 2001].

The percentage of SO_2 transformed into sulfate, according to simulations with global chemistry models, falls between 51 and 56% (four models) with one outlier calculating an efficiency of 83% (due to low dry deposition flux of sulfur dioxide) [*Berglen et al.*, 2004]. The COSAM model comparison [*Barrie et al.*, 2001; *Roelofs et al.*, 2001] reflecting the state of modeling in 1999 and the AEROCOM [*Kinne et al.*, 2005; *Textor et al.*, 2005] comparison performed in 2004 give a range of transformation rates between 45 and 67%, and between 50 and 81%, respectively. This transformation rate depends on transport, sink processes and chemical transformation. The latter will change due to changes in the emission of oxidants and oxidant precursors. Only gas phase oxidation by OH will lead to formation of new particles, whereas aqueous phase oxidation and catalytic oxidation by metals take place on existing particles, thereby changing their CCN properties. Gas phase sulfate formation contributes between 10 and 22% to the total oxidation of SO_2 in the COSAM comparison and between 14 and 42% in the more recent AEROCOM comparison.

In addition, a southward shift of the sulfur emissions toward regions with more incoming solar radiation and hence more OH would increase the fraction of SO_2 oxidized in the gaseous phase [*Berglen et al.*, 2004].

Secondary particle formation of sulfuric acid gas dominates the nucleation mode and contributes significantly to the particle number concentrations although contribution to total aerosol mass is small. Model calculations show that nucleation of sulfate particles is favored in regions with little available aerosol surface area, low temperatures, and high relative humidity. Thus, the maxima of the nucleation mode number concentration can be found in the upper tropical troposphere and in the remote regions of the Antarctic. The soluble Aitken mode numbers are dominated by particles growing from the nucleation in the Aitken size range. Accumulation mode soluble numbers are highest in the lower troposphere between 30^o S and 60^o N close to the sources from biomass burning and fossil fuel use. Increased levels can also be found in the upper troposphere, attributable to convective detrainment of particles and their precursors and evaporation of cloud droplets and ice crystals. Figure 2-1 shows the effect of the omission of SO_2 emissions from fossil fuel and biofuel use on the accumulation mode number concentration. Between 0^o and 60^oN sulfur dioxide from anthropogenic sources contributes about 25 to 30% of the total particle number burden.

Conventionally, additivity is assumed for aerosol emissions and for their climate impacts. However, due to the complex interactions between transport, aerosol and hydrological cycle, one cannot expect a linear relationship between emissions and aerosol load or aerosol effects. *Graf et al.* [1997] have shown that the efficiency by which sulfur precursors are transformed to sulfate depends on the source type. However, it depends additionally on the location and the season of the release. *Barth and Church* [1999] used the NCAR Community Climate Model (CCM3) to determine the contributions of southeast China to the global aerosol burden. Southeast China emitted 11.6% of the global anthropogenic sulfur emissions and contributed 9% to the global sulfate burden in their simulations, indicating a non-linear response between emission and burden. When anthropogenic sulfur emissions were doubled, the aerosol burden contributed by China increased by a factor of 2.2. Their simulations show a gas-phase oxidation rate from south-east-Asian emissions above average. Sulfate formed via this pathway is less susceptible to wet scavenging and thus contributes more efficiently to the atmospheric sulfate load than sulfate formed in clouds, which is already incorporated in cloud droplets and thus is more likely to undergo wet removal.

Stier et al. [2005b] analyzed the response of the global aerosol system to changes in anthropogenic sulfur emissions. In a scenario without anthropogenic sulfur emissions (corresponding to a reduction by 55%), the sulfate burden decreases globally by almost 50% and the accumulation mode number concentration by 21%. However, not only the sulfate budget is affected, but also annual global-mean life-times of black carbon, particulate organic matter, and dust increase by 8.9%, 2.5%, and 1.5%, microphysical aging times increase by 164%, 84%, and 66%, and annual zonal-mean column burdens in high northern latitudes increase by up to 70%, 20%, and 20%, respectively. This emphasizes that changes in one particular anthropogenic emission have impacts on the cycles of other aerosol components, resulting in changes of their life-times, column burdens, and microphysical aging times. These results suggest that the separate treatment of the different aerosol components and their precursors can lead to non-negligible errors in estimates of the aerosol climate effects.

2.2.4.3 Future Scenarios

Concerning future emissions of sulfur, the SRES scenarios portray similar emission dynamics – at various future dates (between 2020–2030 and 2070, depending on the scenario and its underlying storyline), global SO_2 emissions reach a maximum level and decline thereafter. By 2030 sulfur emissions range between 40 and 160 Tg S, by 2070 between 20 and 165 Tg S,

and by 2100 between 10 and 95 Tg S. Emission trajectories of the SRES scenarios reflect a combined impact of different scenario driving forces (local air quality concerns, structural change in energy supply and end-use, etc.), which lead to a gradual decline in sulfur emissions in the second half of the 21st century. Importantly, all SRES scenarios are sulfur-control scenarios only and do not assume any additional climate policy measures. There is, however, an indirect effect of GHG emission reduction from sulfur-control policies that result in energy conservation and inter-fuel substitution from high sulfur to low sulfur fuels (e.g., from coal to gas).

2.2.5 Nitrates

The production of secondary aerosol nitrate is closely tied to the relative abundances of ammonium and sulfate. If ammonia is available in excess of the amount required to neutralize the stronger acid H_2SO_4, gaseous HNO_3 and NH_3 can enter the condensed phase, and their subsequent dissociation yields nitrate (NO_3^-) and ammonium (NH_4^+) ions. Submicron particles containing nitrate are potentially efficient CCN [*Metzger et al.*, 2002a]. In the presence of acidic accumulation-mode sulfuric-acid containing aerosols, however, HNO_3 deposits on larger, alkaline mineral or salt particles [*Dentener et al.*, 1996; *Murphy and Thomson*, 1997; *Gard et al.*, 1998]. This deposition of soluble material on otherwise insoluble dust particles increases their CCN activity.

Until recently, nitrate has not been considered in assessments of the climatic effects of aerosols, and even current models often ignore the role of nitrate [e.g., *Stier et al.*, 2005a] or the sub-micron nitrate aerosol fraction [*Derwent et al.*, 2003]. *Andreae* [1995] estimated that the global burden of ammonium nitrate aerosol from natural and anthropogenic sources is 0.24 and 0.4 Tg (as NH_4NO_3), respectively, and that anthropogenic nitrates cause only 2% of the total direct forcing. *Adams et al.* [1999] obtained a value of only 0.17 Tg (as NO_3^-) for the global nitrate burden, which may be due to the fact that their model did not include nitrate deposition on sea salt aerosols. Their most recent estimate [*Adams et al.*, 2001], predicts a nitrate burden of 0.38 Tg in the form of secondary ammonium nitrate/sulfate particles.

The importance of aerosol nitrate is likely to increase substantially over the next century. For example, the SRES A2 emissions scenario projects that NO_x emissions will more than triple in that time period while SO_2 emissions decline slightly. Using this scenario, *Adams et al.*

[2001] predict a nitrate burden of 1.8 Tg for 2100, compared to a sulfate burden of 2.2 Tg for the same year. In their model run for 2100, the total anthropogenic forcing (direct and indirect) associated with nitrate actually exceeds that caused by sulfate.

2.3 PHYSICAL AND CHEMICAL NATURE OF ATMOSPHERIC AEROSOLS

2.3.1 Introduction and Methodology

Knowledge of the various primary and secondary aerosols sources, combined with the size and composition dependent aerosol sinks, in principle allows prediction of the chemical and physical nature of the atmospheric aerosol. In practice, such predictions are very difficult to make and we here summarize the phenomenology of the atmospheric aerosol. The most fundamental aspects of this phenomenology, and those most relevant to the impact of aerosols on precipitation, are the size distributions and compositions of atmospheric aerosols. These properties determine the nature and degree of interaction of the aerosol with water or, more specifically, their efficiency, or activity, as either CCN or IN. In light of this, the discussion here will center on both of the two fundamental aerosol properties, size distribution and composition, and the two derivative properties, CCN and IN activity. However, before delving into these aerosols attributes, a few methodological issues need discussion.

The first issue that arises is appropriate data selection. The atmosphere constitutes a very large 3-dimensional space, portions of which – such as the upper troposphere – are poorly sampled. Furthermore, aerosol properties vary widely over this potential sample volume, both vertically and horizontally. However, with respect to vertical variation, our focus on precipitation renders our task substantially easier. For warm precipitation processes, the aerosols that modulate the formation process are largely those in the lower troposphere. Hence, little is lost by concentrating on the aerosol properties in the lower troposphere, which are in any case the best known by far. With respect to cold precipitation formation, and thus ice nucleation, our sampling volume must be expanded in the vertical to address, for example, the role and characteristics of upper tropospheric IN in cirrus formation.

The second methodological issue is, in a sense, also related to spatial sampling issues, though this time more in the horizontal. Essentially, are there distinct aerosol regimes, likely related to sources, into which we can conveniently divide atmospheric aerosols? Of course, aerosol

properties are actually a continuum, as might be expected in a well mixed fluid. Nevertheless, some stratification into broad types would be useful to summarize aerosol interactions with precipitation. For purpose of discussion, we shall use a series of aerosol "regimes", as they may be found at various locales around the Earth: over the remote oceans and continents far from pollution sources ("remote marine" and "remote continental", respectively), over regions influenced by industrial pollution or biomass burning ("polluted continental" and "polluted marine"), and over areas dominated by mineral dust aerosols. Earlier classifications have attempted to separate the atmosphere into "marine" (equated with low pollutant levels and low CCN concentrations) and "continental" (high pollutant levels and high CCN concentrations) regimes. This view has been challenged, as it has become apparent that unpolluted continental regions may be just as clean, and have just as low CCN concentrations as remote marine areas [*Roberts et al.*, 2001; *Andreae et al.*, 2004]. Conversely, polluted marine areas have aerosol concentrations just as high as polluted continental regions [*Andreae et al.*, 2000; *Raes et al.*, 2000]. In this chapter, we will limit the discussion of the nature of aerosols to an analysis of generic properties within broad generic regimes; a further breakdown into regional characteristics is provided in chapter 3.

2.3.2 Size Distributions

The most fundamental property of atmospheric aerosol particles is their size distribution. While many different types of distribution functions have been utilized over the years to represent the atmospheric aerosol, the discussion here is in terms of the ubiquitous lognormal function introduced and popularized by *Junge* and later *Whitby* and his colleagues [cf, *Junge*, 1953; *Junge*, 1963; *Whitby et al.*, 1972; *Whitby*, 1978]. The distribution function itself can be expressed in terms of any of its moments, the most useful representation being dependent on the particular issue being addressed. For example, for exploring the dependence of cloud drop number concentration on aerosol concentration, the number size distribution has the most utility, whereas if one is considering the chemical nature of the aerosol, the mass distribution is commonly employed.

The simplest of the four categories into which we have subdivided the atmospheric aerosol, and a good choice to initiate discussion, is the *remote marine aerosol*. Note, that this category includes, but is not confined to, the seasalt aerosol, but that it contains in particular a large fraction of particles consisting of sulfate from the oxidation of biogenic DMS [*Raemdonck et*

al., 1986; *Charlson et al.*, 1987; *Andreae and Crutzen*, 1997; *Bates et al.*, 1998; *Andreae et al.*, 1999; *Bates et al.*, 2000; *Bates et al.*, 2001]. While there is, even within this aerosol type, substantial variability [cf, *Heintzenberg and Covert*, 2000], the most salient features are ubiquitous. Perhaps most characteristic, there is a prominent mode in the number distribution in the size range from about 0.1 to 0.2 μm diameter, which contains most of the DMS-derived non-seasalt sulfate. This mode corresponds to the accumulation mode and is virtually global in extent [e.g., *Kim et al.*, 1995; *Quinn et al.*, 1995; *Weber et al.*, 1998; *Bates et al.*, 2002]. *Hoppel* and his colleagues have argued persuasively that its location and prominence are attributable to cloud processing of aerosol [*Hoppel et al.*, 1986; *Hoppel et al.*, 1990; *Hoppel et al.*, 1994]. A second, smaller diameter, mode commonly occurs around 30-50 nm, particularly in the most remote locales. It has been variously referred to, most frequently as the *aged-nucleation* or *Aitken mode*, and is thought to arise from in-situ particle nucleation under conditions of low pre-existing aerosol surface area [*Wiedensohler and Covert*, 1996; *Brechtel et al.*, 1998; *Covert et al.*, 1998; *Collins et al.*, 2000]. The concentration of particles in these submicron modes ranges from a few tens per cm^3 to several hundred per cm^3 with concentrations in the northern hemispheric oceans generally (though not always) appreciably higher than those in the southern oceans. Finally, there is nearly always present a larger, or coarse, size mode in the size range from ~ 0.5 μm to perhaps 3 μm diameter, the so-called sea salt mode. While few in number, the contribution of this mode to particle mass – and thus the volume distribution – is always very substantial and commonly dominant. The particles in this mode are not strictly sea salt, however. It is well known that mineral dust can be transported over very long distances indeed and can have a decided presence even in remote marine air [e.g., *Andreae et al.*, 1986; e.g., *Arimoto et al.*, 1997]. It can make a very substantial contribution to the marine coarse volume distribution [*Bates et al.*, 2002; *Maring et al.*, 2003]. Non-seasalt sulfate is also always present in variable amounts in the coarse mode of the marine aerosol [*Andreae et al.*, 1999; *Andreae et al.*, 2000]. Furthermore, the impact of even small numbers of large particles to marine precipitation can be quite substantial [e.g., *Feingold et al.*, 1999]. Some representative size distributions, taken from *Bates et al.* [2002], are shown in Figure 2-2 and illustrate the features just discussed.

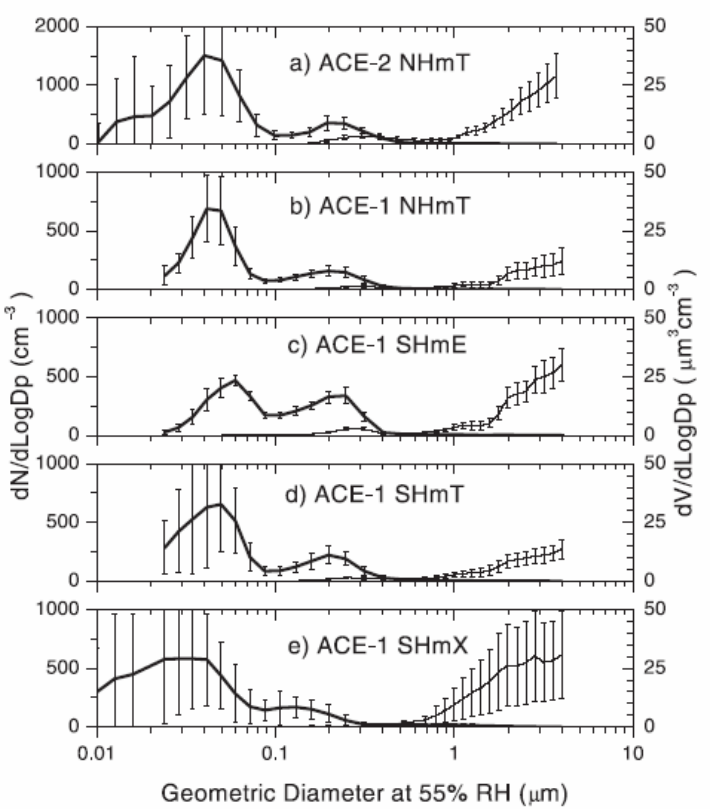

Figure 2-2. *Number (heavy line) and volume (light line) distributions at 55% RH for different air masses of origin during the first 2 ACE experiments. The vertical bars represent one standard deviation in mean number or volume in the size bin over the averaging period (23-114 hr). From Bates et al. [2002].*

Turning to *remote continental aerosol*, the essential issue is to what extent it differs from simply a dilute version of pollution aerosol. Because of the vast amounts of anthropogenic emissions of aerosol particles and their gaseous precursors, combined with efficient long range transport, it is nowadays very difficult to find areas of the Earth that are not measurably impacted by pollutant aerosols. This applies especially to the continental regions of the northern hemisphere, where most of the human activities are concentrated.

Aerosol particles have typical atmospheric lifetimes of 3-10 days, which implies that even after 10-30 days (3 lifetimes) about 5% of the initial burden is still left. Given that airmasses can easily travel several 1000 km in 15 days, and that, at least in the northern hemisphere, few places are more than a few 1000 km from major pollution sources, there are really no places where we can expect to find pristine conditions in the northern hemisphere. The remote continental aerosol nowadays consists of some natural material (dust, biogenic

materials, etc.), mixed with pollution aerosols at varying levels of dilution. For example, a study of the European aerosol climatology shows that the average PM2.5 concentration ranges from some 30 μg m^{-3} at urban sites to about 4 μg m^{-3} at the cleanest site, Sevettijärvi in northern Finland [*Putaud et al.*, 2004; *Van Dingenen et al.*, 2004]. The composition of the aerosol at this remote site is, however, very similar to that at urban and regionally polluted sites, with a large fraction of non-seasalt sulfate, and about 4% of the combustion tracer black carbon. Pollution aerosols dominate even in most continental areas in the Southern Hemisphere, especially in the dry seasons, when biomass burning is widespread [*Artaxo et al.*, 1988; *Artaxo et al.*, 1994; *Artaxo et al.*, 2002; *Sinha et al.*, 2003].

Only under relatively rare circumstances do aerosol concentrations over the remote continents approach pristine conditions. This usually occurs when clean marine airmasses are advected over practically uninhabited continental regions. Examples are the rainy season in central Amazonia, some of the desert regions in Australia and parts of the boreal regions in Eurasia and North America. Unfortunately, there are very few studies that document these conditions carefully enough to be useful for a assessment of what aerosol concentrations (and composition) would be like in the absence of anthropogenic emissions.

Size distributions from a variety of relatively unpolluted venues such as rural Canada [*Leaitch and Isaac*, 1991], the Southwestern U.S. and rural Midwestern U.S. [*Kim et al.*, 1993a], and the Amazon Basin [*Guyon et al.*, 2003a; *Rissler et al.*, 2004; *Krejci et al.*, 2005] and the high altitude site Jungfraujoch (3580 m asl) [*Weingartner et al.*, 1999] are differentiable from more strongly polluted air and share some common characteristics. The mass accumulation mode of the remote continental aerosol tends to center in the size range from 0.1 to 0.4 μm diameter, thus showing more size variability than the remote marine aerosol, particularly on the upper bound, though tending to a slightly smaller modal size. In number concentration, the remote continental aerosol also shows more variability, but with concentrations usually appreciably higher than those of its marine counterpart, typically from a few hundred to a few thousand particles per cm^3 [*Weingartner et al.*, 1999; *Putaud et al.*, 2004; *Van Dingenen et al.*, 2004]. This difference is the result of two factors – the presence of pollution aerosols and the frequent occurrence of large particle number concentrations in the nucleation and Aitken modes. In the few instances when nearly pristine conditions could be sampled, CN concentrations in the continental tropics [*Roberts et al.*, 2001; *Rissler et al.*,

2004; *Krejci et al.*, 2005] as well as in the lower free troposphere during winter [*Weingartner et al.*, 1999] were in the low hundreds, indistinguishable from marine values. In northern high latitudes, no published estimates of pristine levels exist, but concentrations are estimated to be in the tens to low hundreds per cm^3 (*M. Kulmala*, personal communication, 2005).

A separate Aitken or nucleation particle mode is frequently present, especially at times and in regions of unusually low particle surface area and in the presence of small, but significant concentrations of gaseous H_2SO_4 from SO_2 oxidation [*Kulmala et al.*, 2000; *Lihavainen et al.*, 2003]. Despite their high number concentrations, these particles are of little direct consequence for precipitation processes, as they do not have enough soluble mass to act as CCN. Only when they have grown to sizes approaching 100 nm, e.g., by condensation of terpene oxidation products [*Kerminen et al.*, 2000], are they able to nucleate cloud droplets.

The supermicron, or coarse mode, of the continental aerosol is commonly centered in the range from 2 to 5 µm diameter. The number concentration in this mode is more variable than its marine counterpart, but generally significantly lower, with typical concentrations in the range from 0.1 to 1 cm^{-3}, as compared to 1 to 10 cm^{-3} in marine air. It consists of mineral and soil dust and a variety of primary biogenic particles, and dominates the aerosol mass size distribution under the cleanest conditions [*Artaxo et al.*, 2002; *Guyon et al.*, 2003b].

The complex issue of the impact of pollution on remote aerosols must next be assessed. The complexity resides in the multiplicity of sources and even source types, and the variability in the transport between these sources and the remote locales. However, from the standpoint of their contribution to anthropogenic emissions and their overall impact on remote aerosol, two main emission types may be considered, biomass burning and industrial pollution. The former dominates anthropogenic aerosol in most regions of the Southern Hemisphere while the latter does so in the Northern Hemisphere [*Houghton et al.*, 2001]. While the differentiation between the impacts of these two source types resides primarily in their chemical composition (to be discussed in the next section), there are some modest differential size impacts as well. In this regard, differentiation between the *remote and pollution-impacted aerosol* is somewhat easier in the marine venue and we turn to it first.

Because of the contrast between the size distributions of continental and marine remote aerosols, it must be noted that even the simple advection of continental air into the marine

venue will alter the marine size distribution. Furthermore, while there may be a distinction in the chemical composition of remote continental and pollution aerosol, their impact on the marine size distribution is qualitatively similar though, quantitatively, the impact of pollution is of course much more substantial. This can be clearly seen in Figure 2-3, taken from *Covert et al.* [1998], which shows such impact for the Southern Ocean aerosol. For the submicron portion of the size distribution, the bi-modal structure characteristic of clean marine air has been subsumed, really overwhelmed, by a massive modal peak centered at 40-50 nm diameter. Similar changes have been reported for both the North and South Atlantic [*Hoppel et al.*, 1990; *Kim et al.*, 1995; *Bates et al.*, 2000; *Collins et al.*, 2000; *Johnson et al.*, 2000] and the Indian Ocean [*Cantrell et al.*, 2000], although in the latter case the modal peak was at ~ 150 nm – substantially higher. For the Pacific Ocean, *Moore et al*. [2003] have shown that some variability exists in the impact of pollution plumes, in some cases the pollution producing the subsuming just discussed while in others two distinct modes continue to exist though with the accumulation mode generally now the larger of the two and the dominant modal peak most frequently well above 100 nm diameter. In fact, *Bates et al.* [2002], in their survey of data from all of the major oceans, report a similar mixed result. Nevertheless, it is quite clear that the tendency of pollution in all cases is the imposition of a large monomodal structure on the submicron size range. For the coarse particle mode, advection of pollution generally (there are exceptions) has little effect unless soil dust is present [cf. *Li-Jones and Prospero*, 1998; cf. *Bates et al.*, 2002] though, once again, the impact will be dependent on the temporal and spatial scales of transport [*Maring et al.*, 2003; *Moore et al.*, 2003]. Coarse mode number concentrations may increase by factors of two or three during dust transport episodes (with still larger changes in coarse mode volume) but are generally smaller.

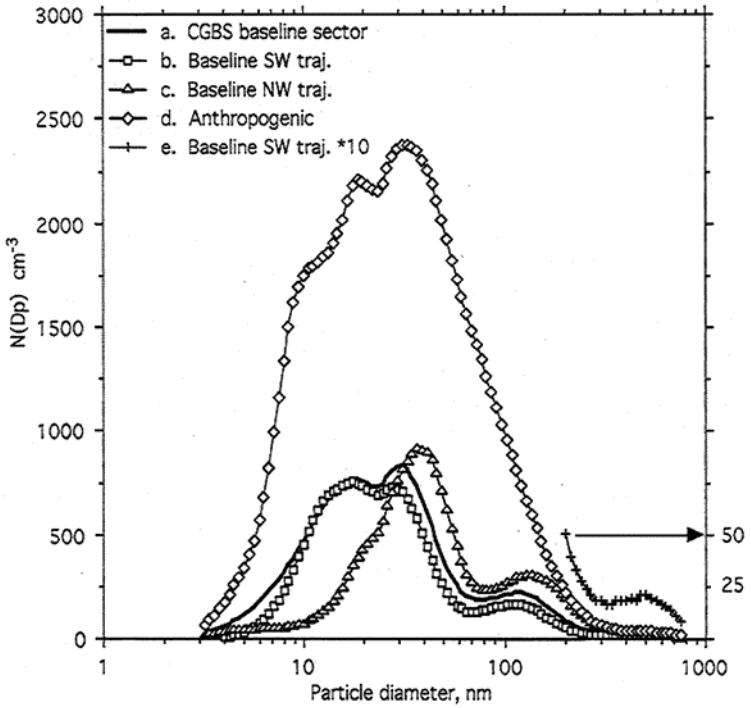

Figure 2-3. *Differential aerosol number size distributions from Cape Grim during ACE 1. CGBS in the legend refers to Cape Grim Baseline Station. Curve e is an expanded scale for curve b to show an additional mode above 200 nm. Taken from Covert et al. [1998].*

Finally, we address the *continental polluted aerosol*. Much of the early work on industrial air pollution was done in the highly polluted Los Angeles Basin. Studies there show a typically tri-modal aerosol with prominent nucleation, accumulation and coarse modes, and associated modal diameters of 0.01-0.02, 0.1 and 1.0 μm, respectively [e.g., *Heisler et al.*, 1973; *Sverdrup et al.*, 1975; *Whitby et al.*, 1975]. Later work has tended to confirm this basic structure but showed that the nucleation and accumulation modes are not always fully resolved [e.g., *John et al.*, 1990; *Hering et al.*, 1997; *Hughes et al.*, 1999]. Furthermore, both the bi-modal submicron structure and a prominent though variable coarse mode have been commonly found in European pollution [e.g., *Birmili et al.*, 2001; *Baltensperger et al.*, 2002; *Petzold et al.*, 2002]. Number concentrations, dominated of course by the submicron portion of the size distribution vary in the range from thousands to tens of thousands per cm^3. The partition in number concentration between the nucleation and accumulation modes is highly

variable with the larger concentration switching back and forth between the two as a function of time of day, as well as season and various other variables.

Biomass burning emissions, the other main pollution source on a global impact scale, comes largely from the tropical regions [*Crutzen and Andreae*, 1990], especially Brazil and Southern Africa, and our discussion will center on these two venues. *Andreae et al.* [1996], summarizing a number of studies in Africa, report a large accumulation (number) mode located at ~ 0.1 to 0.2 μm diameter for in-plume measurements. They also observed a biomass burning haze accumulation mode that is shifted to a slightly larger size, ~ 0.2 μm. There is also a coarse mode in both the plume and haze aerosol, but the number modal diameter is a bit unclear, in part because volume rather than number distributions are reported. Nevertheless, it would appear to be at least 1-2 μm in size. *Le Canut et al.* [1996] also report an accumulation mode centered at ~ 0.15 μm but a definite coarse mode centered at ~ 3 μm as well. More recently, from the SAFARI-2000 campaign, *Haywood et al.* [2003a; 2003b] have reported an accumulation mode at a slightly larger volume modal diameter of 0.25 μm with a coarse mode at ~ 10 μm. In none of these studies was a distinguishable Aitken or nucleation mode reported.

Data on Brazilian biomass burning aerosol has recently increased sharply as a result of the SCAR-A and SCAR-B studies [*Reid and Hobbs*, 1998; *Reid et al.*, 1998] and the LBA-SMOCC campaign [*Andreae et al.*, 2004; *Guyon et al.*, 2005]. *Reid et al.* [1998; 1998] have summarized work on both distinct fire plumes and the regional haze produced by such plumes. In distinct plumes, as in African emissions, there is no distinct nucleation mode but rather a single large accumulation number mode centered at 0.10-0.13 μm diameter, and a volume mode around 0.2-0.3 μm. In contrast, the regional haze associated with biomass burning shows an accumulation mode centered in the range 0.2-0.3 μm. In the fresh smoke, a coarse mode at ~ 3 μm was evident, while in the regional haze a significant coarse mode was not commonly present. Airborne measurements of fresh smoke from deforestation fires during the LBA-SMOCC campaign showed a single number mode near 0.10 μm, while in detrained smoke from pyrocumulus clouds the modal diameter had grown to about 0.13 μm [*Guyon et al.*, 2005]. At a ground site, where a mixture of fresh and aged smoke was present, the distribution was bimodal, with number modal diameters of 0.09±0.01 and 0.18±0.02 μm [*Rissler et al.*, 2005]. A nucleation mode with a diameter near 10 nm appeared sporadically.

Summarizing the biomass aerosol characteristics, irrespective of locale, the submicron aerosol is usually present as a large accumulation mode with number median diameters in the range of 0.1 to 0.2 μm and volume median diameters of 0.2-0.3 μm [*Reid et al.*, 2005], and with a distinct coarse mass mode centered around 4 μm diameter [e.g., *Radke et al.*, 1991]. After some appreciable aging, the number mode shifts up to 0.2-0.3 μm. A coarse mode is frequently, but not always seen, becoming less frequent in aging smoke and typically centered at or above a few μm in size. These characteristics contrast to some extent with the other major source of pollution, namely industrial emissions, where the accumulation mode and coarse mode are at somewhat smaller modal diameters and a distinct nucleation mode is frequently encountered.

2.3.3 Size-Dependent Chemical Composition and Solubility

The composition of marine aerosols, not surprisingly, varies substantially with geographic locale. The review by *Heintzenberg et al.* [2000] finds that anthropogenic pollution is commonplace globally and nearly ubiquitous over the oceans of the Northern Hemisphere. Therefore, the composition of the remote marine aerosol is most easily assessed in data from the Southern Hemisphere. Sea salt is naturally the single most common component of the aerosol with latitudinal maxima in both number concentration and mass in the mid-latitudes, were the strong winds associated with baroclinic systems predominate. The size distribution of the sea salt, once thought to be confined to super-micron sizes, has been more recently established to extend well down into the sub-micron range and indeed commonly peak there [e.g., *McInnes et al.*, 1997; *O'Dowd et al.*, 1997; *Kreidenweis et al.*, 1998; *Murphy et al.*, 1998a; *Campuzano-Jost et al.*, 2003]. Nevertheless, most sub-micron particles have long been thought to be primarily sulfate, derived from oxidation of DMS emitted from the ocean surface and SO_2 from long-range transport of continental sources and ship emissions [*Twomey*, 1971; *Charlson et al.*, 1987; *Andreae et al.*, 1988; *Andreae*, 1990; *McInnes et al.*, 1997; *Andreae et al.*, 2000]. However, numerous recent studies even in remote marine air have revealed a substantial organic presence [*Middlebrook et al.*, 1998; *Murphy et al.*, 1998b], both in coarse mode and accumulation mode particles [*McInnes et al.*, 1997; *Matthias-Maser et al.*, 1999; *Guazzotti et al.*, 2001; *Mayol-Bracero et al.*, 2001; *Cavalli et al.*, 2004]. The speciation of the organics, even in remote air, is still not entirely resolved but there are clearly substantial amounts of both soluble and insoluble carbon present.

While sea salt contributions to the marine aerosol mass are governed primarily by wind speed, the contribution of organics and inorganics such as sulfate and nitrate are strongly a function of geography, induced largely by anthropogenic emissions. Certainly the loadings of, for example, sulfate and carbon species increase dramatically in polluted marine air, particularly such obvious anthropogenic species as sulfate and elemental carbon [*Cachier et al.*, 1983; *Rau and Khalil*, 1993; *Andreae et al.*, 2000; *Heintzenberg and Covert*, 2000; *Putaud et al.*, 2000; *Guazzotti et al.*, 2001]. However, the relative rates of increase of the various pollutant species, not surprisingly, are dependent on the specific sources of the pollution. For example, pollution from either Europe or North America advected over the North Atlantic increases sulfate much more than the various carbon species, resulting in marked increase in the inorganic mass fraction [*Andreae et al.*, 2000; *Putaud et al.*, 2000]. On the other hand, pollution from India transported over the Indian Ocean results in a much higher percentage gain in both organics and elemental carbon, particularly the latter [*Cantrell et al.*, 2000; *Chowdhury et al.*, 2001; *Mayol-Bracero et al.*, 2002a]. Interestingly, while both the carbon and sulfate species are predominately sub-micron in size, the carbon tends to be disproportionately concentrated at the smallest sizes, particularly elemental and other insoluble carbon species [*Sicre et al.*, 1990; *Rivera-Carpio et al.*, 1996; *Neusüß et al.*, 2000]. This is of considerable interest since a number of these insoluble species act as surfactants, forming layers on the aerosol surface that might alter their CCN and IN properties [*Facchini et al.*, 2000; *Charlson et al.*, 2001; *Feingold and Chuang*, 2002]. Indeed, numerous surfactants and even surfactant layers have been found on marine aerosols [*Barger and Garrett*, 1976; *Gagosian et al.*, 1982; *Mochida et al.*, 2002; *Tervahattu et al.*, 2002a].

Remote continental aerosols have, of course, a considerable contribution from soil dust [e.g., *Jaenicke*, 1993; e.g., *Eleftheriadis and Colbeck*, 2001]. However, a substantial portion of the mass, particularly the sub-micron mass, is composed of sulfate and organic matter [*Malm et al.*, 1994; *Shrestha et al.*, 1997; *Andreae et al.*, 2002; *Henning et al.*, 2003; *Putaud et al.*, 2004]. While there are in fact land sources of natural sulfur compounds (e.g., volcanoes and terrestrial biota), their magnitude is rather small compared to anthropogenic sulfur emissions, and such anthropogenic emissions are well known to undergo long range transport [*Penner et al.*, 2001]. Similarly, small but significant amounts of nitrate are present even in remote locales, at least occasionally in excess of what would be expected from natural sources [*Talbot et al.*, 1988; *Talbot et al.*, 1990; *Malm et al.*, 1994; *Putaud et al.*, 2004]. Hence, it is likely that much of the sulfate found in remote continental aerosols is anthropogenic in

origin. The other major component of the remote continental aerosol is that of carbonaceous compounds, by far the largest portion of which is organic [e.g., *Artaxo et al.*, 1988; *Talbot et al.*, 1988; *Artaxo et al.*, 1990; *Talbot et al.*, 1990; e.g., *Malm et al.*, 1994; *Zappoli et al.*, 1999; *Krivacsy et al.*, 2001; *Artaxo et al.*, 2002; *Guyon et al.*, 2003b; *Putaud et al.*, 2004; *Kanakidou et al.*, 2005]. Indeed, in the most remote locales, the organic fraction can be as large or larger than that of sulfate [*Artaxo et al.*, 2002; *Graham et al.*, 2003a; *Graham et al.*, 2003b; *Guyon et al.*, 2003b]. It is also important to note that there is a definite trend towards a larger soluble organic fraction as the aerosol approaches pristine conditions [*Mazurek et al.*, 1997; *Zappoli et al.*, 1999; *Graham et al.*, 2003a]. While this might well be in part simply due to evolution of industrial pollution, several studies have shown that the natural organics are qualitatively different from polluted air [*Mazurek et al.*, 1997; *Graham et al.*, 2003a]. This aspect of remote aerosol composition is of considerable importance when considering CCN activity. The few existing studies show, that the aerosol from the least polluted sites in the Amazon Basin, for example, is very efficient at nucleating cloud droplets [*Roberts et al.*, 2001; *Andreae et al.*, 2004; *Rissler et al.*, 2004].

Continental polluted aerosols, the last aerosol type we shall examine, are by far the most widely studied. They are also, of course, by far the most variable and complex. Turning first to industrial pollution, the most clear-cut trend with higher pollution levels is the increase in elemental carbon, both in absolute terms and as a percentage of the overall mass [*Malm et al.*, 1994; *Zappoli et al.*, 1999; *Neusüß et al.*, 2002; *Putaud et al.*, 2004], although even here the tendency is not universal [*Molnar et al.*, 1999]. Organic carbon also increases substantially in absolute terms and commonly as a percentage contribution to the total aerosol mass but the latter trend is much less marked than for the elemental carbon. In part, this variability may be due to the fact that organic aerosol has a distinct biogenic source (primary particles and SOA) that produces a significant natural background, which is not the case for EC. The inorganic portion of the aerosol mass is dominated by sulfate and nitrate, accompanied by an extensive suite of metal cations [*Putaud et al.*, 2004].

The size distribution of the organics and inorganics is also of interest. In accord with the changes in the overall aerosol size distribution discussed in the previous section, most of the mass increase attributable to industrial pollution is confined to the sub-micron size range, for both organic and inorganic species. However, the carbon species, and particularly elemental carbon, tend to be disproportionately concentrated at the smaller sizes examined, especially

below approximately 0.1 μm diameter [*Hering et al.*, 1997; *Maenhaut et al.*, 2002; *Neusüß et al.*, 2002; *Jimenez et al.*, 2003]. Indeed, for the sub-micron range, the organic size distribution commonly appears slightly displaced to smaller sizes compared to the inorganic, although this can be misleading since most of the particles even in urban source areas are largely internally mixed [e.g., *Noble and Prather*, 1996]. Additionally, it should be noted that there is a tendency for the insoluble organics to be at smaller sizes than the soluble species [cf. *Neusüß et al.*, 2000].

Finally, the ratio of insoluble to soluble organics is generally higher in urban, industrial pollution than in background aerosols [e.g., *Zappoli et al.*, 1999], a characteristic attributable to the relatively reduced nature of industrial emissions compared to organics in more background settings [*Turpin and Lim*, 2001]. Once again, these characteristics of urban pollution may have implications for the formation of organic films on aerosols, with significant consequences for CCN properties. Surprisingly, however, there has been relatively little recent work on this compared to numerous studies on marine aerosols. An illustrative example of some of the composition variability that can be seen in transitioning from background to polluted venues can be seen in Figure 2-4.

For pollution arising from biomass burning, a somewhat different compositional picture arises. Much of the aerosol mass consists of carbonaceous species [*Andreae et al.*, 1996; *Cachier et al.*, 1996; *Mayol-Bracero et al.*, 2002b; *Sinha et al.*, 2003; *Decesari et al.*, 2005; *Fuzzi et al.*, 2005b; *Reid et al.*, 2005]. A sizable fraction of this is elemental carbon, somewhat higher than that in industrial pollution. A more significant difference from industrial emissions resides in the relatively high organic fraction of the emissions [*Andreae and Merlet*, 2001; *Sinha et al.*, 2003]. The actual speciated organic composition of the biomass smoke is quite distinct from that of industrial emissions, with a substantial component attributable to dehydrated sugars – essentially cellulose breakdown products such as levoglucosan [*Graham et al.*, 2002; *Mayol-Bracero et al.*, 2002b; *Gao et al.*, 2003; *Decesari et al.*, 2005]. However, from the standpoint of impact on precipitation, the key attribute of the biomass organic emissions is simply their relatively high solubility. The inorganic fraction of the biomass aerosol tends to be secondary, although it can become substantial with aging due, for example, to secondary sulfate production [*Reid et al.*, 1998].

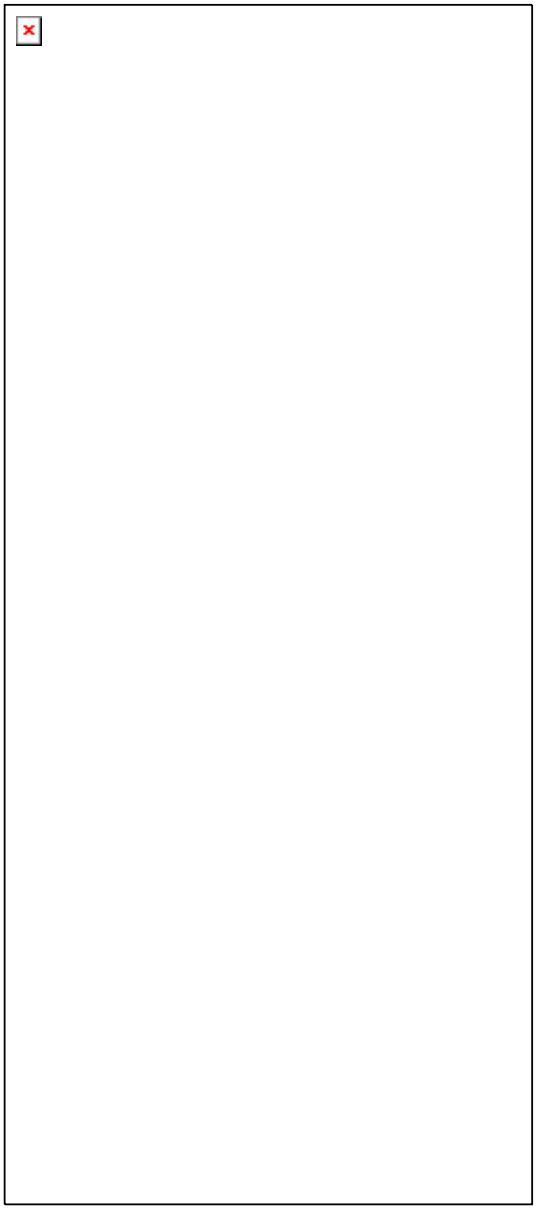

Figure 2-4. *Average mass balance at remote (a), rural (b) and polluted (c) venues in Western Europe. EC= elemental carbon, WINSOC= water soluble organic compounds, WINSIC= water insoluble inorganic carbon, WSOC=water soluble organic compounds, ND= not determined. (From Zappoli et al. [1999]).*

2.3.4 Hygroscopic Growth, CCN and IN Activity

All the interactions of aerosol particles with water, including hygroscopic growth at RH <100% as well as CCN and IN activity, are derivative from the aerosol composition and size, at least in principle. However, our theoretical understanding of this linkage, even for the long-studied CCN activity, is still not entirely satisfactory, and our understanding of the IN linkage is at present rudimentary [*Pruppacher and Klett*, 1997] (for more detail on ice processes see chapters 4 and 5). Nevertheless, it is useful to examine hygroscopic growth, and CCN and IN phenomenology within the context of our theoretical understanding. We turn first to the better understood issue of hygroscopic growth.

2.3.4.1 Hygroscopic Growth

At ambient humidity, water represents a significant component of most aerosol particles. The actual water content of a given particle is a function of its composition and size, and of the ambient relative humidity. Inorganic ionic components provide a large fraction of the soluble content of most aerosols, while the carbonaceous components include both water-soluble and insoluble species.

In most climate models, a fraction of emitted carbonaceous species, particularly the soot particles, is considered to be hydrophobic. These hydrophobic carbonaceous aerosols are then converted into hydrophilic aerosols by photochemical processes, condensation and coagulation, usually in a matter of hours to a day [*Riemer et al.*, 2004]. Once the carbonaceous aerosols are hydrophilic, they can act as CCN and IN, and thus are subject to in-cloud and below-cloud scavenging, whereas wet scavenging of hydrophobic carbonaceous aerosols is limited to below-cloud scavenging (see sub-section *3.4.2.1*). Likewise, hydrophilic carbonaceous aerosol particles have a larger dry deposition velocity than hydrophobic aerosols.

The equilibrium water contents of inorganic species as functions of ambient relative humidity (equivalent to water activity for bulk solutions) are well-known. Polynomial fits have been published for binary solutions [e.g., *Tang and Munkelwitz*, 1994] and models for rigorous calculations for multi-component mixtures are readily available [*Kim et al.*, 1993b; *Clegg et al.*, 1998; *Nenes et al.*, 1998; *Pilinis et al.*, 2000; *Clegg et al.*, 2001; *Metzger et al.*, 2002b]. If

particles composed of soluble inorganics are completely dried and then exposed to increasing RH, they take up no water until exposed to a relative humidity corresponding to the saturated-solution water activity, at which point a droplet of saturated solution forms. The water content progressively increases as RH is increased beyond this point. The wet-to-dry volume ratio at a particular RH can vary substantially with composition, with sulfuric acid (which is soluble in water in all proportions and thus has no deliquescence point) and sodium salts having relatively higher water contents than neutralized sulfates. As RH is increased, particles generally do not dry spontaneously at the deliquescence RH but rather retain water to a lower RH. This hysteresis implies that most particles in the atmosphere, having been exposed to relatively high RH at some time, contain at least some water and rarely exist in a completely dry state.

Much less is known about the hygroscopic behavior of individual organic species and their mixtures found in atmospheric aerosols. Most of the constituents of organic aerosol matter remain unidentified, and any single compound rarely accounts for a substantial fraction of the mass. Laboratory studies have measured equilibrium water contents for dicarboxylic acids, sugars, humic and fulvic acids, model polymers, and several other species [*Peng et al.*, 2001a; *Peng et al.*, 2001b; *Prenni et al.*, 2001; *Choi and Chan*, 2002; *Chan and Chan*, 2003; *Wise et al.*, 2003; *Brooks et al.*, 2004; *Hansen and Beyer*, 2004; *Mikhailov et al.*, 2004; *Chan et al.*, 2005; *Svenningsson et al.*, 2005]. The semivolatile nature of many organic aerosol species makes them more difficult to study in a controlled laboratory setting, and techniques that are readily applied to nonvolatile salts must be modified [e.g., *Choi and Chan*, 2002]. Furthermore, many relevant organic compounds are only sparingly soluble, and deliquesce at RH > 95%. It is difficult to control RH at these high values and thus laboratory water uptake experiments on such species are lacking, except for observations of their behavior at water supersaturations [e.g., *Cruz and Pandis*, 1997; *Corrigan and Novakov*, 1999; *Giebl et al.*, 2002; *Raymond and Pandis*, 2002; *Hori et al.*, 2003; *Kumar et al.*, 2003; *Raymond and Pandis*, 2003; e.g., *Bilde and Svenningsson*, 2004; *Broekhuizen et al.*, 2004].

It is generally adequate to model the density of multicomponent solutions assuming volume additivity [e.g., *Brechtel and Kreidenweis*, 2000a]. With respect to the water content of mixtures, the simplest treatment is the Zdanovskii-Stokes-Robinson (ZSR) assumption [*Seinfeld and Pandis*, 1998], which states that the total equilibrium water content at a specified relative humidity (RH) is the sum of the equilibrium water contents for each

individual species at the same RH. This approach can capture non-idealities that arise in individual binary solutions, but more sophisticated techniques are needed to represent solute-solute interaction effects. In other words, the ZSR approximation assumes that are no interactions between species that either enhance or diminish hygroscopic growth beyond that expected for each component. Although some counterexamples have been documented in the literature [*Tang*, 1997], the ZSR assumption appears to be adequate in many cases [*Malm and Kreidenweis*, 1997; *Prenni et al.*, 2003; *Brooks et al.*, 2004]. However, the deliquescence RH of a mixed salt is always lower than that of any of the components in the mixture [*Wexler and Seinfeld*, 1991], an effect that is not captured with the ZSR treatment. *Marcolli et al.* [2004] demonstrate that mixtures of organic species deliquesce at very low RH and thus atmospheric organic aerosols, which are known to be mixtures of many soluble and insoluble species, are expected to retain water to very low RH.

Recently, several workers [*Brechtel and Kreidenweis*, 2000a; *Brechtel and Kreidenweis*, 2000b; *Rissler et al.*, 2004; *Koehler et al.*, 2005; *Kreidenweis et al.*, 2005; *Rissler et al.*, 2005; *Svenningsson et al.*, 2005] have suggested that information on particle hygroscopic growth below 100% RH can be extrapolated to predict the critical supersaturations required for activation to cloud drops. This method involves using growth factors obtained from Humidified Tandem Differential Mobility Analyzers (HTDMA) and deducing composition-dependent water activities of aqueous solutions of pure materials or mixtures, or directly extrapolating HTDMA wet-to-dry volume ratios into the supersaturated regime. Thus far the methods have produced reasonable agreement with direct measurements of critical supersaturations for particles composed of inorganic [*Kreidenweis et al.*, 2005] and organic [*Koehler et al.*, 2005; *Svenningsson et al.*, 2005] compounds and with field measurements on ambient aerosols [*Rissler et al.*, 2004; *Rissler et al.*, 2005], generally within the uncertainties of CCN measurements. When used to predict nucleated drop numbers in an adiabatic parcel model, even the least accurate extrapolations predict drop numbers within the range of uncertainties of those predicted using the most accurate thermodynamic models [*Koehler et al.*, 2005].

2.3.4.2 CCN Activity

The classic description of the relationship between aerosol size, composition and CCN activity is the well-known Köhler theory. If this theory is indeed valid, then the CCN activity is specified by aerosol size and composition measurements, and direct measurement is

unnecessary. Such a situation would be a boon to large-scale modeling. This theory has been subject to numerous laboratory trials in which aerosols of various sizes and compositions have been subjected to supersaturated water environments and the size at which they activated measured. Much of the early such work, however, utilized inorganic salts and acids since these were thought to dominate ambient aerosol composition. While the experiments tended to nearly universally support the applicability of the theory [cf. *Fitzgerald*, 1973], more recent work on aerosol composition, which (as discussed above) attributes a very substantial role to carbonaceous species, has led to considerable theoretical questioning as to the prognostic power of the Köhler theory [e.g., *Shulman et al.*, 1996; *Facchini et al.*, 1999; *Charlson et al.*, 2001; *Anttila and Kerminen*, 2002]. Indeed, various modified forms of the theory have been proposed to take into account the sparing water solubility of many organics, their possible impact on haze particle surface tension, and even the influence of soluble gases that may co-condense with water during particle growth [*Laaksonen et al.*, 1998]. A further complication attributable to organics is the surfactant nature of many of them and the consequent possibility that they could form films that would hinder water condensation/evaporation (i.e., impose a kinetic limit to the thermodynamic Köhler theory) [*Gill et al.*, 1983; *Cruz and Pandis*, 1998]. However, laboratory experiments to quantitatively assess this phenomenon – and even some detailed theoretical assessments - have yielded mixed results. Most investigators have concluded that the sparing solubility and surface tension effects are quite small [*Cruz and Pandis*, 1998; *Hegg et al.*, 2001; *Anttila and Kerminen*, 2002; *Raymond and Pandis*, 2003; *Shantz et al.*, 2003; *Broekhuizen et al.*, 2004]. Indeed, the hygroscopic growth factors could well be reproduced at the high altitude site Jungfraujoch using the chemical composition of the mixed particles and the Zdanovskii-Stokes-Robinson (ZSR) relation [*Gysel et al.*, 2002; *Weingartner et al.*, 2002]. The temporal variability of hygroscopic growth factors was mainly a result of varying fractions of organic/inorganic mass, and the monomodal distribution of the hygroscopic growth factor confirmed the presence of an internally mixed aerosol.

Nevertheless, since there is some laboratory support for such limitation and evidence for organic films has indeed been found on ambient aerosols [*Mochida et al.*, 2002; *Tervahattu et al.*, 2002a], the possibility must be considered when analyzing atmospheric data.

The best methodology for investigating the CCN activity of ambient aerosols is the so-called CCN closure experiment [cf. *Covert et al.*, 1998; *Mircea et al.*, 2005; *Rissler et al.*, 2005]. In

such an experiment, the aerosol size distribution and chemical composition as a function of size are measured simultaneously with the CCN activity. The linkage between the variables is, of course, the Köhler theory, and the closure thus constitutes a test of the theory. However, the number of experiments in which all of the necessary variables are determined (in principle this would involve measurement of individual particle composition) is relatively small. Instead, there is a spectrum of closure experiments, with varying degrees of measurement completeness. Even some of the most rudimentary of these types of experiments have shed light on the CCN activity of atmospheric aerosols and it is therefore worthwhile to first look at a few of the simpler CCN activity measurements and proceed towards increasingly complete studies.

A good example of a "sparse study" is that of *Hoppel et al.* [1973], in which CCN and CN concentration were measured as a function of altitude in Arizona. Ratios of CCN active at various supersaturations to total CN were derived, although the authors themselves deal primarily with those active at 0.35%. Somewhat higher supersaturations are usually utilized and we note here that the ratio of CCN active at 0.7% supersaturation to the total particle concentration ranges from essentially 1.0 near the surface to 0.36 at the highest altitudes. *Hegg et al.* [1995] report data from the Arctic which show ratios of CCN active at 1% supersaturation to total particle concentration which range from 0.002 to 0.38, with a mean ratio of 0.15 – nearly exclusively lower than the Arizona measurements, despite the fact that the higher supersaturation would be expected to yield higher ratios. The authors attribute these low ratios to unusually small particles but cannot dismiss anomalous composition. Certainly a number of studies have attributed anomalously low CCN concentrations (based on Köhler theory) to concentration anomalies, specifically organics, though no actual compositional measurements were available [e.g., *Bigg*, 1986]. Observed systematic differences in the CCN efficiency (CCN to total particle concentration ratio) of atmospheric aerosol also suggest possible organic effects. For example, the study of *Hudson and Da* [*Hudson and Da*, 1996] contains data from five different locales measured with the same instrumentation. The aerosol CCN efficiency shows a tendency to decrease as the measurement venue becomes more polluted, again possibly associated with increasing levels of insoluble organics. On a slightly different note, work by *Matsumoto et al.* [1997] established statistical correlations between concentrations of CCN and several different aerosol chemical components, including soluble organics. However, actual closure was not attempted.

Turning to the more complete closure studies, *Novakov and Penner* [1993] and *Rivera-Carpio et al.* [1996] combined CCN spectral measurements with size resolved composition measurements and numerical inversion of the various species mass distributions to permit attribution of the CCN at various activation supersaturations to either sulfate or carbonaceous aerosols. Not surprisingly given the moderately polluted venue, both aerosol types contributed significantly to the CCN activity. Reasonable closure between the predicted CCN concentrations and measured concentrations was obtained. However, Köhler theory was not actually used to predict CCN activation diameters but rather each aerosol type concentration was summed and simply compared to the CCN concentration. Furthermore, one key assumption of this approach is that the various aerosol species are externally mixed. While some sensitivity studies suggested that this was not a critical assumption, latter studies, which have demonstrated the very high sensitivity of the activity of either organic aerosols or inorganic aerosols to trace quantities of each other, render this procedure questionable [*Roberts et al.*, 2002; *Bilde and Svenningsson*, 2004; *Broekhuizen et al.*, 2004].

Other closure studies have taken essentially three different approaches to the closure issue. In the first, the aerosol size distribution and CCN activation spectrum have been measured and a certain soluble inorganic composition (commonly ammonium sulfate) is assumed. Comparison of predicted (based on Köhler theory) and measured CCN concentrations then test this assumption [*Bigg*, 1986; *Liu et al.*, 1996; *Cantrell et al.*, 2000; *Snider and Brenguier*, 2000; *VanReken et al.*, 2003]. In some instances [e.g., *VanReken et al.*, 2003], reasonable closure has been achieved but in most instances, particularly in more polluted air, the predicted concentrations have substantially exceeded the measured CCN.

Another more constrained approach has been to measure simultaneously the CCN activation spectrum, the aerosol size distribution and the size dependent aerosol hygroscopicity. Theoretical justification for this approach is well established [cf. *Brechtel and Kreidenweis*, 2000]. Indeed, in a practical sense, it is a more complete approach even than utilizing size-dependent composition data since such data must then be coupled with characteristic thermodynamic data to essentially derive the activity of the aerosol chemical species. Nevertheless, several recent studies that have utilized this approach [*Covert et al.*, 1998; *Zhou et al.*, 2001; *Dusek et al.*, 2003; *Rissler et al.*, 2004] found modest discrepancies between predicted and measured CCN concentrations. While the differences were generally not significant, they were systematic with the predicted concentrations nearly always well in

excess of the measurements. Interestingly, the *Covert et al.* [1998] study showed that the percentage magnitude of the under prediction tends to vary directly with the extent of anthropogenic impact, consistent with the earlier work of *Hudson and Da* [1996] as discussed above.

The final type of closure study is that with particle size, size-resolved composition and CCN activity measurements. Examples of this are *Chuang et al.* [2000] and *Cantrell et al.* [2001]. In the latter, reasonable closure was achieved while in the former, the commonplace overprediction was found, this time by as much as an order of magnitude, in part no doubt because the CCN activity and compositional measurements were not co-located. In a comprehensive analysis of size-dependent chemical composition, hygroscopic growth, and CCN activity, *Mircea et al.* [2005] showed that knowledge of aerosol WCOC composition in terms of classes of compounds and of their molecular weights and acidic properties are sufficient to predict CCN activation.

In surveying the widely varying success of these closure experiments, we find that the ability of Köhler theory to predict CCN activity is best in instances where well-mixed aerosols with a high percentage of inorganics are present, or when detailed knowledge of soluble organics is available. It works significantly less well when unspecified organics, particularly insoluble organics, are present in significant amounts. As to the percentage of the total aerosol population that can act as CCN at typical atmospheric supersaturations, it can vary from a few percent to virtually all of the particles present. However, it is important to remember that much of the effective variance in the fraction of particles that are actually activated in clouds is in fact due to the variance associated with supersaturations encountered in the atmosphere.

2.3.4.3 IN Activity

If the situation with respect to CCN activity is not entirely satisfactory, the IN activity status is still worse. The situation circa 2000 has been well summarized in the latest IPCC report [*Houghton et al.*, 2001]. Such issues as the precise mode of action of aerosol acting as IN (e.g., contact, immersion, deposition, etc. nuclei), a lack of consistency in measurement techniques, in-situ modification of particle IN efficiency and secondary ice production all contribute to the lack of clarity regarding the IN activity of atmospheric aerosols. Nevertheless, a few facts have been ferreted out over the years. Firstly, there is no question that particles acting as IN are relatively rare. IN concentrations typically are measured at a

few per liter or less, thus constituting no more than a few tenths of a percent of the normal total aerosol population. In part this is no doubt due to the limited chemical compositions that are known to act as IN. Best known are crustally-derived minerals, for which there is a formidable and still growing body of corroborative data [*Kumai*, 1976; *Hagen et al.*, 1995; *Heintzenberg et al.*, 1996; *Castro et al.*, 1998; *Kreidenweis et al.*, 1998; *DeMott et al.*, 2003; *Cziczo et al.*, 2004]. There is also substantial field data supporting the IN activity of carbonaceous aerosols [e.g., *Karcher et al.*, 1996; *Petzold et al.*, 1998; *Strom and Ohlsson*, 1998] and of various biogenic particles [see the review by *Szyrmer and Zawadzki*, 1997]. Nevertheless, it is commonplace for the concentration of IN to be far below the concentration of particles containing any or all of these various favorable components. Differing degrees of IN deactivation due to pollutant deposition on IN surfaces have been invoked as an explanation for this phenomenon but clear evidence of this is wanting. Furthermore, it is also likely that deposition of favorable ice-forming substrates could be deposited as organic films on previously inactive particles. The mix of such in situ processes could well explain the long-puzzling variability in the IN fluxes from pollution sources [e.g., *Hobbs and Locatelli*, 1969; *Braham and Spyers-Duran*, 1974]. Once again, however, evidence of the impact of such secondary processes is sparse at best.

2.4 RECOMMENDATIONS FOR FUTURE OBSERVATIONS AND STUDIES

Emission inventories have been conventionally limited to estimates of mass emission fluxes for bulk aerosol components. To be useful in cloud and precipitation studies, size-resolved information about the numbers of particles emitted is required for the various primary aerosol sources, especially seasalt, mineral dust, pyrogenic aerosol and primary biogenic aerosol.

Emission information must be provided in forms that are suitable for dynamic emission inventories. It is much more useful to have emission algorithms that permit calculation of an emission flux from model variables than a static array of emissions valid for one particular time.

The ability of mineral dust particles to act as CCN, GCCN, and IN as a function of aerosol size, origin, and airmass history needs to be determined.

The abundance and rate of production of submicron seasalt particles is still under dispute. Since these particles can play a significant role in cloud microphysics and precipitation in

remote marine regions, observational constraints to their source parameterizations are urgently needed.

Primary biogenic aerosols probably play a significant role as cloud and ice nuclei at present in very remote regions, and must have been a key control on cloud processes in the pre-anthropogenic atmosphere. Their characteristics and rates of emission need to be investigated.

Due to the complexity of carbonaceous aerosol composition and emission processes, a critical concern is to define an adequate classification scheme for these aerosols based on observable characteristics.

Building a reliable inventory for carbonaceous aerosols (BC, PPOC and SOA) remains a challenge because of uncertainties in emission factors and activity estimates. Emission parameterizations must be provided that include size distributions and number fluxes.

The injection height of emissions also differs strongly from on aerosol source type to another, and even shows pronounced variability within some types of aerosol source. This applies especially to biomass burning and vegetation fires. Any changes in injection height due to shifts in agricultural or technical practices will have important consequences on the lifetime and fate of particles.

The rates of sulfate aerosol production are at least as dependent on the accurate representation of the processes leading from SO_2 to sulfate aerosol as they are on emission estimates of SO_2. Accurate knowledge of these processes and their correct parameterization in models is essential.

Aerosol nitrate is expected to increase in climatic importance in the 21st century. Accurate measurement techniques and reliable modeling approaches for this component must be established.

In order to assess the human impact on cloud physics, we need to know the aerosol and CCN and IN distributions in the pre-anthropogenic atmosphere. The sources, characteristics, and fluxes of natural aerosol types must be investigated by carefully conducted field and laboratory studies.

The ability of aerosol particles to act as CCN, GCCN and IN should be determined as a function of particle size, composition and supersaturation. Uncertainties are greatest for IN. These measurements should be conducted in the context of closure studies.

CHAPTER 3: THE DISTRIBUTION OF ATMOSPHERIC AEROSOLS: TRANSPORT, TRANSFORMATION AND REMOVAL

Lead Author: S.L. Gong & L. A. Barrie

Co-Authors: R. Arimoto, S. M. Kreidenweis, Z. Levin, S.M. Li, U. Lohmann, K. Strawbridge, N. Sugimoto, C. Textor, L.M. Zhang, Stefan Kinne, Sarah Guibert, Michael Schulz

3.1 INTRODUCTION

Because the time for air parcels to circle the Earth on winds in the troposphere is of the same order of magnitude as the residence time of atmospheric aerosols, there is no location on the globe that is not influenced by aerosol sources. Once released into the atmosphere from primary production or produced via gas-to-particle conversion (for source details, see Chapter 2), aerosols are subject to many processes that affect their global distribution, chemical and physical properties, and hence their influence on climate, weather, human health and ecosystems. They are dispersed in the atmosphere through processes of advection, convection and turbulence. They are also transformed and removed by physical and chemical processes involving clouds, precipitation as well as processes occurring in cloud-free air. During the life cycle of an aerosol in the atmosphere, gas to particle conversion and mixing of aerosols from different sources changes the chemical, physical and optical properties of the original aerosols.

3.2 GEOGRAPHICALLY DISTINCT AEROSOL REGIMES

Consider the global atmospheric aerosol distribution from the perspective of the distribution of mean annual aerosol optical depth (AOD) shown in Figure 3-1. It was determined from a combination of satellite and verified using surface-based observations (S. Kinne, personal communication). There are some biases in this distribution due to the dependence of satellite observations on sunlight. For instance, they cannot observe the polar regions in the dark winter half of the year, thus missing Arctic haze pollution [*Barrie and Barrie*, 1990], and they are unable to measure beneath clouds, thus possibly under-sampling the atmosphere where clouds are most frequent such as in the roaring forties of the southern ocean (see

Chapter 4) and are usually measured at a fixed time each day. Nevertheless, the geographical distribution in Figure 3-1 helps us to organize a description of the global aerosol and aids in understanding their influence on weather, climate, air quality and ecosystems.

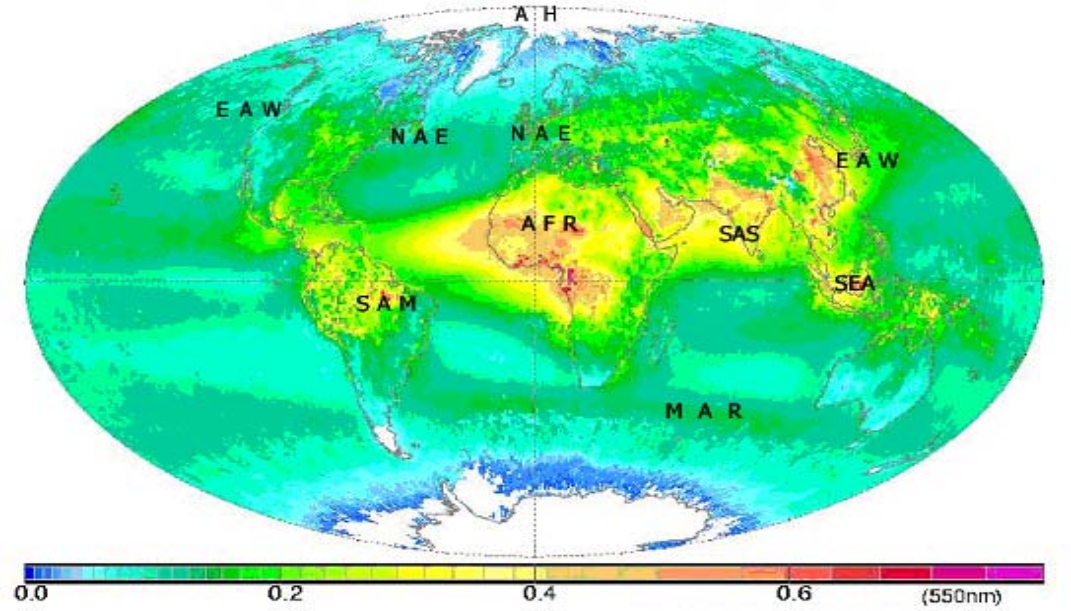

Figure 3-1. *A best estimate of the global distribution of annual average tropospheric aerosol optical depth (AOD) compiled by combining data from six satellites (operating for limited periods between 1979 and 2004). Observations for a region were selected using ground-based AOD observations as guidance (courtesy of S. Kinne MPI, Hamburg, Germany).*

There are 8 geographical aerosol regimes each involving particles of one or more aerosol types (e.g. sea salt, marine biogenic, soil dust, biomass burning, anthropogenic sulfates and organics).

3.2.1 Africa (AFR)

The aerosol regime in Africa is a good example of a primary (soil dust) aerosol mixing with primary and secondary biomass burning aerosols. The soil dust component covers the Saharan desert source region and extends thousands of kilometers downwind. It affects not only surrounding oceans but other continents such as the Americas, Europe, the Middle East and south Asia. Transport across the Atlantic can affect visibility and deposition of nutrients in the Caribbean. There are outstanding questions regarding its role in influencing hurricane development over the tropical Atlantic. For instance does it affect sea surface temperature which is one variable that is widely recognized as important to hurricane development? The effects of soil dust on cloud and precipitation formation processes are only beginning to be understood. There is evidence that a proper treatment of Saharan dust can improve winds

such as the easterly jet over West Africa in numerical weather predictions [*Tompkins et al.*, 2005].

Emissions from biomass burning sources in tropical and southern Africa drift over the tropical Atlantic into tropical South America as well as into the Indian Ocean off the southeast tip of Africa. A so-called "river of smoke", observed during the SAFARI 2000 field campaign flowed from northwest to southeast over the subcontinent, and caused heavy haze and reduced visibility over Botswana and South Africa [*Swap et al.*, 2003]. A satellite image (Figure 3-2) from *Kaufman et al.* [2005c] illustrates the difference between Saharan dust and bio-mass burning in central and west Africa. Contributions to the optical depth as a function of fine particle fractions were derived from the MODIS satellite observation, which semi-quantitatively separates the dust from bio-mass burning regimes. Superimposed on these major sources are lesser but still quite significant sources of fossil fuel aerosol resulting from human activities in the region.

The African monsoon occurs adjacent to Saharan soil dust sources and is co-located with biomass and air pollution sources. The role of aerosol radiative forcing in the dynamics of this monsoon is thought to be significant, but is only beginning to be investigated.

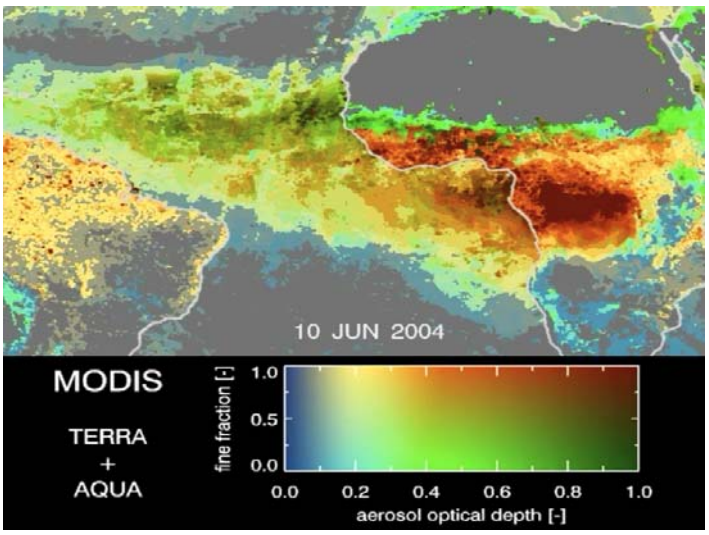

Figure 3-2. *MODIS aerosol composites for 10 June 2004. The color bar was constructed so that blue represents clean conditions, aerosol optical thickness <0.1, and green and red show higher optical thickness corresponding to the coarse (green) and fine (red) modes. The fine fraction (y axis) varies from green for fine fraction of zero to red for fine fraction of 1. Therefore pure dust is green, and pure smoke or pollution is red.*

3.2.2 Eastern North America, North Atlantic, Europe (NAE) and Arctic Haze (AH)

Widespread fossil fuel combustion in eastern North America leads to a North American plume that moves westwards across the North Atlantic where it mixes with sea salt (see below) and enters Europe receiving fresh fossil fuel combustion aerosols and precursors. Under the International Consortium for Atmospheric Research on Transport and Transformation (ICARTT) studies were conducted in 2004 to develop a better understanding of the factors that shape air quality in North America and Europe and the remote regions of the North Atlantic [e.g. *Methven et al.*, 2006]. Extensive field observations and modeling activities were carried out. Not evident in Figure 3-1 because of a blind spot of aerosol satellite observations in the polar troposphere is the reverse flow from Eurasia to North America over the Arctic from November to May that constitutes the Arctic haze [*Barrie*, 1986; *Barrie*, 1990; *Christensen*, 1997]. European pollution also drifts eastwards joining pollution from regions of the former Soviet Union and soil dust. The surface concentrations of aerosols in both North America and Europe from ground monitoring stations are discussed in Section 3.3.2.

3.2.3 South Asia (SAS) and Southeast Asia (SEA)

The aerosol regime in south Asia including the Arabian Peninsula and Indian Sub-continent is a result of soil dust, pollution and biomass burning aerosols. Saharan soil dust advected from the west affects the Indian Sub-continent, and this is combined with local sources of dust. In addition, the Indian sub-continent has pollution from fossil fuel and biomass burning that leads to a highly absorbing aerosol [*Ramanathan et al.*, 2005]. It is advected out of the region affecting clouds and precipitation in the Himalayas in summer and over the Indian Ocean in winter. There is even documented evidence of transport into the Mediterranean basin [*Lelieveld et al.*, 2002].

The presence of highly absorbing aerosol over the Indian Ocean was observed as far south as the Maldives in the Asian Brown Cloud (ABC) study. It had the effect of reducing solar radiation reaching the surface by as much as 20 W m^{-2} [*Ramanathan et al.*, 2005] and increasing the stability of the atmosphere through redistribution of solar energy from the surface to soot-bearing aerosols aloft. This affects the evaporative source of water vapor and hence the cloud regime. In addition, aerosol dust and pollution is thought to affect the Asian monsoon through direct radiative forcing of changes in regional circulation [*Lau et al.*, 2005] and indirectly through aerosol impacts on clouds and precipitation formation. The latter

which is the focus of this assessment, is the more difficult to quantify due to the non-linearity of processes involved (Chapter 5 and 6). In any case, there are documented changes in precipitation in India over the last half century that raises the issue of possible aerosol pollution effects as well as other changing climate that affects monsoon dynamics. For instance, river basins in central India (Sabarmati, Mahi, Narmada, Tapi, Godavari and Mahanadi) have been experiencing reduced rainfall from about the 1960s, while in others—Indus from 1954, Ganga from 1993, Brahmaputra from 1988, Krishna from 1953 and Cauvery from 1929—there has been an upward trend in rainfall. The recent trend in rainfall across India is believed to be due to global warming [*Singh et al.*, 2005]. Whether changing aerosol pollution in the region has played a role remains an open question.

Another aerosol source region that is prominent in Figure 3-1 is south-east Asia centered on Indonesia and Borneo. Biomass burning aerosols coupled with air pollution from mega-cities are the main components of this aerosol regime. During the 1997 forest fires in Indonesia, approximately 42 Tg of aerosol particles were emitted into the atmosphere, and resulted in a -0.32 Wm^{-2} forcing averaged over the 4 months of the fire season [*Davison et al.*, 2004]. There is some evidence that clouds and precipitation were affected [*Phillips et al.*, 2002]. This could be due to the large sulfur content in peat fire smoke stemming from sulfur deposited in previous volcanic eruptions in this region. This would possibly lead to a more hygroscopic smoke aerosol [*Langmann and Graf*, 2003].

3.2.4 Eastern Asia and Western North America (EAW)

Another major aerosol regime is located in eastern Asia, mainly including China, Korea and Japan and the downwind region of the north Pacific as far as western North America. Soil dust from the Gobi and Taklimakan deserts and anthropogenic pollution from industry and fossil fuel burning are the main aerosol types. The soil dust source is seasonal, peaking in February to May and originating from the western and northern parts of the region. The mineral dust advects in the northerly and westerly winds over populated areas, often mixing with pollution. It also is lofted by convection into strong westerly winds of the middle troposphere (2-7 km) that periodically transport it in a matter of 5 to 10 days to North America [*Jaffe et al.*, 1999] and even into the Arctic [*Sirois and Barrie*, 1999; *Welch et al.*, 1991]. Air pollution in the region is persistent throughout the year and has increased greatly in the latter half of the 20th century largely as a result of the economic growth in China. The southern part of this region is affected by monsoonal precipitation in summer and, as in

Africa and south Asia, the effects of aerosols are poorly understood. Observations have shown that regional precipitation has changed substantially in China between 1951 and 2000 [*Zhai et al.*, 2005]. Simultaneously, there is a decreasing trend in the total global radiation reaching the surface over most industrial regions [*Che et al.*, 2005] reflecting an increase in aerosol loadings (details in section 3.3.4). Whether these changes are linked remains an open question.

Natural biomass burning aerosols originating from fires ignited by lightning in the boreal region of Canada, Russia and Alaska cannot be neglected. They are highly seasonal but climatologically persistent. Occurring mostly in summer, the burning products sometimes loft to great heights and can even produce their own thunderstorm clouds into which pollution is mixed, scavenged and dispersed in the outflow regions. They can also drift long distances near the ground affecting air quality and human health. These aerosols appear most prominently in summer season AOD observations in the northern hemisphere. A good example was an event during the summer of 2002, over 360 fires occurred in the James Bay region of Canada. Sparked by a combination of lightning and dry conditions, these fires consumed hundreds of square kilometers of forest (8871 square kilometres) and created a huge plume of smoke (see Figure 3-3) that affected air quality in much of eastern Canada and, as far south as Washington, DC, in eastern United States.

Once airborne, boreal biomass burning aerosols can circle the hemisphere in 15- 20 days in the strong westerly winds of the middle to upper troposphere. They are much longer lived than lower tropospheric aerosols. Their radiative and microphysical effects on clouds are poorly understood. Since northern boreal regions tend to receive most precipitation in the summer period these aerosols are potentially very important.

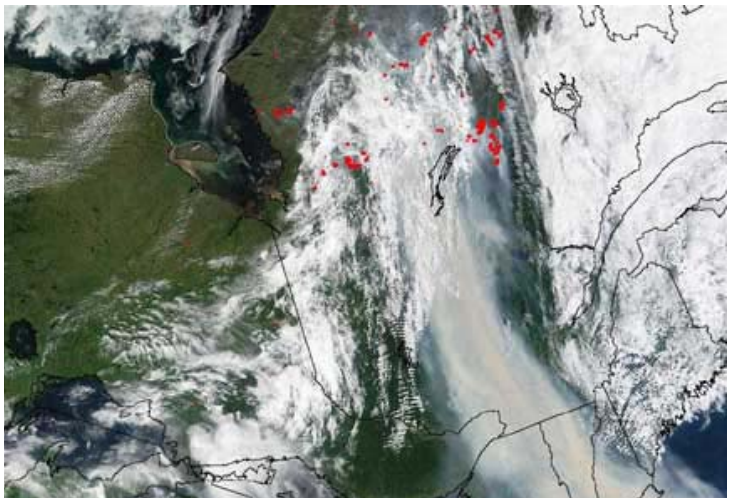

Figure 3-3. *In this satellite image taken on July 7, 2002, large fires in northern Quebec are identified as red spots, clouds are white and smoke has a brownish tint. MODIS image from NASA's Terra and Aqua satellites. Where the smoke plume enters the United States over the state lines of New York and Vermont, it measures almost 300 kilometres wide. The smoke affected air quality and visibility in major cities including Montreal, New York, Philadelphia, Baltimore and Washington, (D.C. Source: Canada Centre for Remote Sensing.)*

3.2.5 South America (SAM)

South American aerosols originate mainly from biomass burning in the Amazon and savannah regions as well as from pollution emitted from mega-cities. These aerosols, when released in the tropical Amazon basin, drift westwards towards the Andes. When released further south, they drift over the south Atlantic on westerly winds. Recently, the influence of smoke aerosols on the microphysical properties of clouds and convection has been extensively reported. One simulation result suggests that biomass burning aerosols, peaking shortly before the onset of the South American monsoon, may influence the development of the monsoon [*Liu et al.*, 2005b]. The monsoon precipitation is part of a complex climate system that affects large portions of southeastern South America. A second precipitation system further south tends to show an inverse relation with the core monsoon, so that an increase of precipitation in one implies a reduction of precipitation in the other. This out-of-phase variability or dipolar behavior has been observed for a broad range of frequencies, from daily to interannual time scales. The impact of the biomass burning aerosols on the precipitation has the potential impact on the dipolar structure.

3.2.6 Marine Aerosols (MAR)

Marine aerosols consisting of sea salt often mixed with marine biogenic sulfur are another prominent aerosol optical depth maximum (Figure 3-1) in the Earth's atmosphere particularly over the high wind "roaring 40's" belt between 40 and 60 S and in the north Pacific and north Atlantic in winter. The AOD-signal of marine aerosol is relatively weak in comparison to the marine aerosol mass present in this region since sea salt aerosols tend to be larger than pollution aerosols and less effective scatterers of light per mass unit. A global model of the distribution of the coarse and fine fraction of sea salt (Figure 3-4) shows clearly that they are prominent in and downwind of windy regions of the Earth's oceans [*Gong et al.*, 2002]. The fine particle distribution of sea salt (Figure 3-4b) shows that advection deep into continental regions can occur in some places. For instance, the penetration of marine aerosols into Amazonia is observed in precipitation 1000 km inland where it dominates the concentrations of major inorganic ions [*Andreae et al.*, 1990]. Coarse marine sea salt particles (Figure 3-3a) provide giant cloud condensation nuclei that can dramatically alter the effect of pollution aerosols on clouds. So it is important in studying the effects of aerosols on precipitation to take into account not only the main aerosol components but also minor aerosol components that can affect precipitation formation.

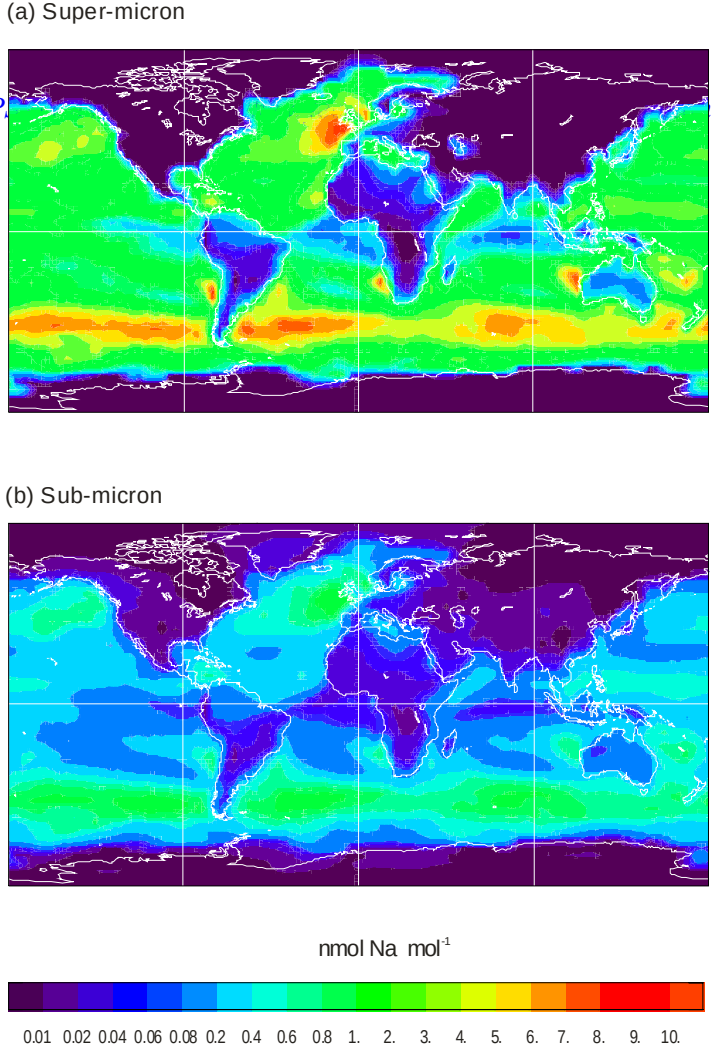

Figure 3-4. *Predicted global distributions of atmospheric sea-salt Na^+ mixing ratios in January in the atmospheric surface layer (0-50 m) for two size ranges: (a) Super-micron and (b) Sub-micron.*

3.3 AEROSOL SURFACE OBSERVATIONS AND REGIONAL CHARACTERISTICS

This section will review selected observational studies that characterize atmospheric aerosols and their chemical compositions in various regions. Chapter 7 covers additional aspects of in situ and satellite measurements of aerosols.

3.3.1 Global Monitoring Networks

The Global Atmospheric Watch (GAW) programme of the World Meteorological Organization consists of 24 Global observatories and approximately 200 Regional stations that measure the composition of the atmosphere including aerosols, their gaseous precursors and precipitation chemistry. Global observatories host facilities for a broad range of atmospheric observations and research and are often located in remote locations (Figure 3-5) and Regional stations measure at least one of the six GAW target variable groups and complete the global coverage. All observations are made according to GAW measurement guidelines [*GAW*, 2003]. Measurement of five core aerosol variables is recommended for all GAW stations: fine and coarse mass, fine and coarse aerosol composition, in situ aerosol scattering, in situ aerosol absorption and aerosol optical depth. In addition, a comprehensive list of optional observations is offered including LIDAR profiling, number size distributions, and cloud condensation nucleii. The GAW Global observatories Cape Grim, Australia and Mace Head, Ireland have unique long term records of cloud condensation nuclei which are directly related to cloud formation and initial cloud radiative properties.

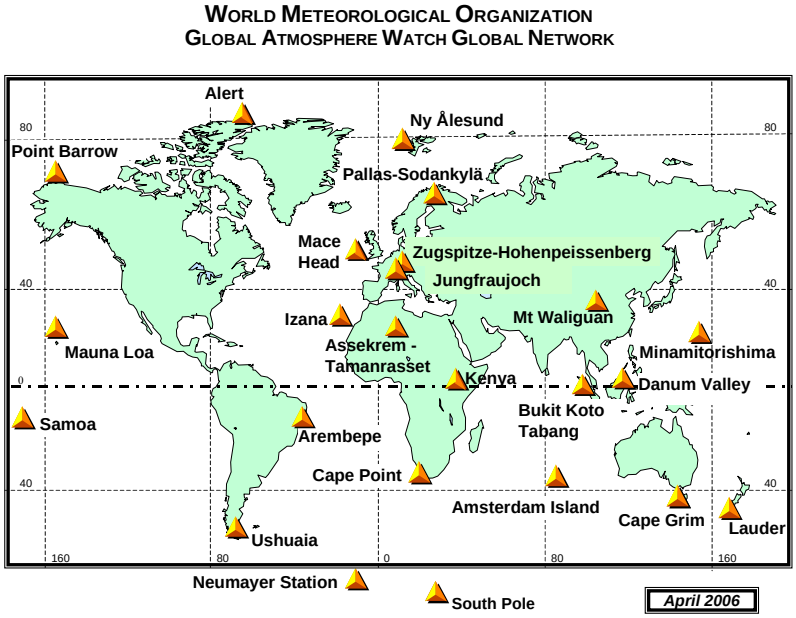

Figure 3-5. *The network of the WMO Global Atmosphere Watch (GAW) global observatories.*

Recently the GAW programme initiated an international effort to identify contributors to long term AOD observations globally and steps needed in quality assurance and coordination to merge them into a global AOD network [*GAW*, 2004]. Such observations will form the surface-based component of an integrated global aerosol system. With satellite observations they will yield global products such as the AOD map in Figure 3-1 and used in predictive weather and climate models. The surface AOD network in March 2004 [*GAW*, 2004] is comprised of approximately 90 stations operated by about five different networks (Figure 3-6).

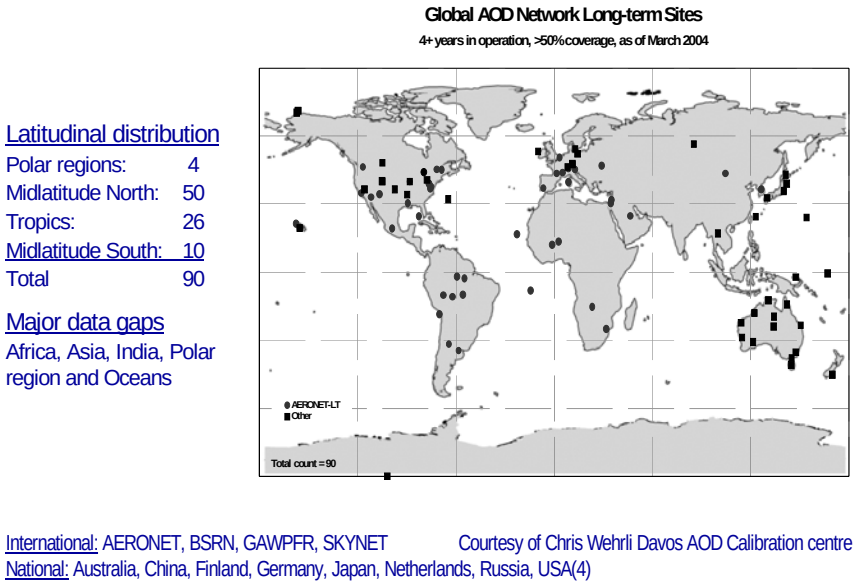

Figure 3-6. *The configuration of the long term surface-based aerosol optical depth network as of March 2004 [GAW, 2004] that will be an important component of an integrated global aerosol observation system. It is comprise of a large number of international and national networks.*

In North America, several networks have been operational since late seventies and early eighties. They were initiated mostly in response to acid deposition and visibility impairment problems. One of the goals of the Canadian Air and Precipitation Monitoring Network (CAPMoN) and the U.S. Clean Air Status and Trends Network (CASTnet) is a description of the aerosol chemical composition across North America. This is greatly augmented in the United States by the IMPROVE (Interagency Monitoring of Protected Visual Environments) network, which is operated by the U.S. Parks Service and the Environmental Protection Agency, It started with stations in most US National parks but later expanded into national

coverage including some urban areas. IMPROVE focuses on the monitoring of aerosol chemical properties and their relationship to visibility impairment [*Malm et al.*, 2002]. It has a comprehensive aerosol chemical characterization network.

Since 1977, the European Monitoring and Evaluation Programme (EMEP) has been routinely measuring the major ion composition of aerosols at stations mostly across western and northern Europe [*Kahnert and Tarrasón*, 2003; *Tørseth*, 2004; *Tørseth et al.*, 2002]. In addition, there is an extensive regulatory network for aerosol mass in Europe operated to monitor compliance with air quality standards. The stations tend to be in urban areas.

Aerosol mass and chemical composition monitoring networks have more recently been developed in Asia, including projects underway for the Air Pollution in the Mega-cities of Asia Program and Asiairnet (http://www.asiairnet.org/).

3.3.2 Observations In North America

Figure 3-7 shows the isopleths of the integrated aerosol mass for d<10 μm (PM_{10}) and for d< 2.5 μm ($PM_{2.5}$) over the three-year period from March 1996 through February 1999 from the IMPROVE network. Higher PM_{10} concentrations are found in the eastern United States. The highest concentrations (23 μg m^{-3}) were in Edwin B. Forsythe National Wildlife Refuge in New Jersey at 23 μg/m^3, followed by the Southeast region, Sequoia National Park, and the Mid South, which experienced concentrations >15 μg/m^3. Outside of southern California and the Northern Rockies the lowest PM_{10} concentrations occurred in the western United States where the concentration of PM_{10} was less than 8.0 μg m^{-3}. The spatial variations in $PM_{2.5}$ mimic those observed for PM_{10} (Figure 3-7b) although the spatial gradients tend to be smaller compared with PM_{10}; this trend is consistent with the known longer residence time of fine aerosol particles in the atmosphere.

(a)

(b)

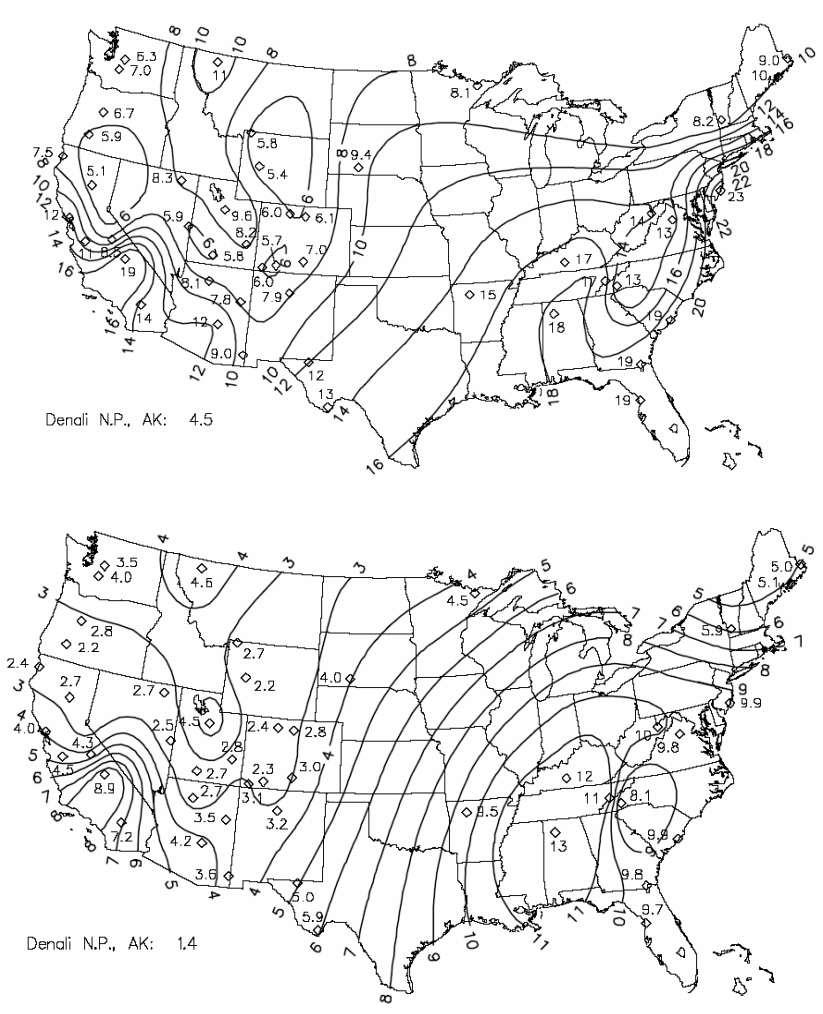

Figure 3-7. *Isopleths of the average mass concentrations (in μg m^{-3}) from the IMPROVE Network (a) PM_{10} and (b) $PM_{2.5}$*

IMPROVE has provided data for aerosol sulfate and nitrate, organic carbon (OC), light-absorbing black carbon (BC), and mineral dust; that is, all of the major aerosol components except sea salt, are measured [*Malm et al.*, 2004]. Results on fine aerosol (<2.5 um) sulfate from the U.S. are summarized by the isopleths plot in Figure 3-6. The average sulfate component of the fine aerosol measured over the three-year period March 1996 through February 1999 is shown. Since sulfate is a major component of fine aerosol mass, its spatial distribution and gradient across the United States is similar to that observed for total fine aerosol mass as shown in Figure 3-7b.

Sulfate concentrations (Figure 3-8) typically average ~5 μg m^{-3} over a broad region of the central eastern United States, amounting to 50 to 60% of the aerosol mass. Sulfate tends to peak in the summer, presumably due to photochemical processing of SO_2 from coal-burning sources. Sulfate decreases towards the west, both in terms of absolute concentration and the percent contribution to reconstructed fine mass (RCFM). Organic matter also exhibits its highest concentrations in the eastern U.S., averaging 2 to 3 μg m^{-3}, with some enhancements in the Southeast due to emissions from fires and secondary particles formed from volatile biogenic organic compounds. OC accounts for the highest percentage (40 to 50%) of the RCFM in the Northwest and 20 to 30% of the mass over much of the country, and the concentrations there are highest during April to September when fires are most common. Fine soil particles are highest in April, especially in the southwestern/south-central states, roughly from south-central Texas to northern Utah, where the concentrations are 0.5 to 2 μg m^{-3} and 30 to 50% of the RCFM. A secondary maximum in soil dust occurs in August in the western US. Regional and temporal patterns in dust loads suggest that large-scale transport may contribute, especially in the area around the Rocky Mountains.

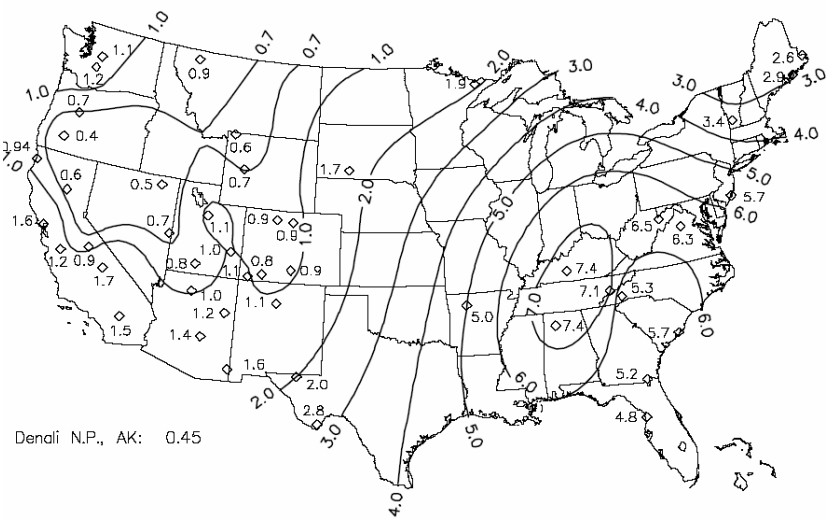

Figure 3-8. *Average fine sulfate aerosol concentrations (in μg/m^3) for each site in the IMPROVE Network, excluding Washington, D.C.*

High concentrations of fine particle nitrate (2 μg m^{-3}, 20% of the RCFM) were measured south of Lake Michigan, and similarly high concentrations were found in southern California, but there the percent fine nitrate was 20 to 40% of the RCFM due to the relatively low sulfate

and organics loadings. Nitrate is highest in the winter when conditions favor its formation. Low concentrations of nitrate are seen in the northwestern US. High proportions of OC to BC (OC/BC = 12) in the northwestern US suggest contributions from biomass burning, mainly from wood smoke and controlled burns. Lower OC/BC ratios over the northeast and southwest suggest little in the way of secondary organics or contributions from smoke. Other parts of the country have OC/BC ratios between 4 and 12, implying contributions from a mixture of sources.

Data for particulate matter in Canada have been compiled by Environment Canada into the National Chemical/Particulate Matter Database, with the purpose of investigating spatial and temporal trends in particulate matter, particular as PM relates to climate change, visibility, human health, and acid deposition. Data from the National Air Pollution Surveillance (NAPS) network in Canada are reported annually and they are periodically used to summarize trends, most recently from 1990 to 2001 (Environment Canada, 2004). Analyses of the NAPS data showed 89% of the PM_{10} and 72% of the $PM_{2.5}$ mass was from open sources, including forest fires, and several sources, i.e., agricultural tilling, wind erosion, construction, and road dusts, that involved the generation of mineral particles.

The highest $PM_{2.5}$ concentrations occurred in southern Ontario, and there the peak levels occurred in June. Prairie sites showed variable levels of $PM_{2.5}$, with peaks tending to occur in August, while in Vancouver, the $PM_{2.5}$ loadings were of the same magnitude but less variable than those over the prairies. PM_{10} concentrations were highest at the prairie sites, most likely due to the presence of mineral aerosol [*Brook et al.*, 1997]. The chemical composition also varies geographically in Canada (Figure 3-9); For example, the organic fraction in $PM_{2.5}$ decreases from 37.6% at Abbotsford on the west coast, to 25.8% at Egbert in Ontario, to 20.4% at St. Andrews in the east while the sulfate fraction increases from 16.9%, 25.6%, 27.0%, to 31.5%, respectively [*Vet et al.*, 2001]. This fractional difference is primarily due to higher $PM_{2.5}$ concentrations from higher emissions of NOx and SOx in the east and transports of PM and precursors from up-wind regions.

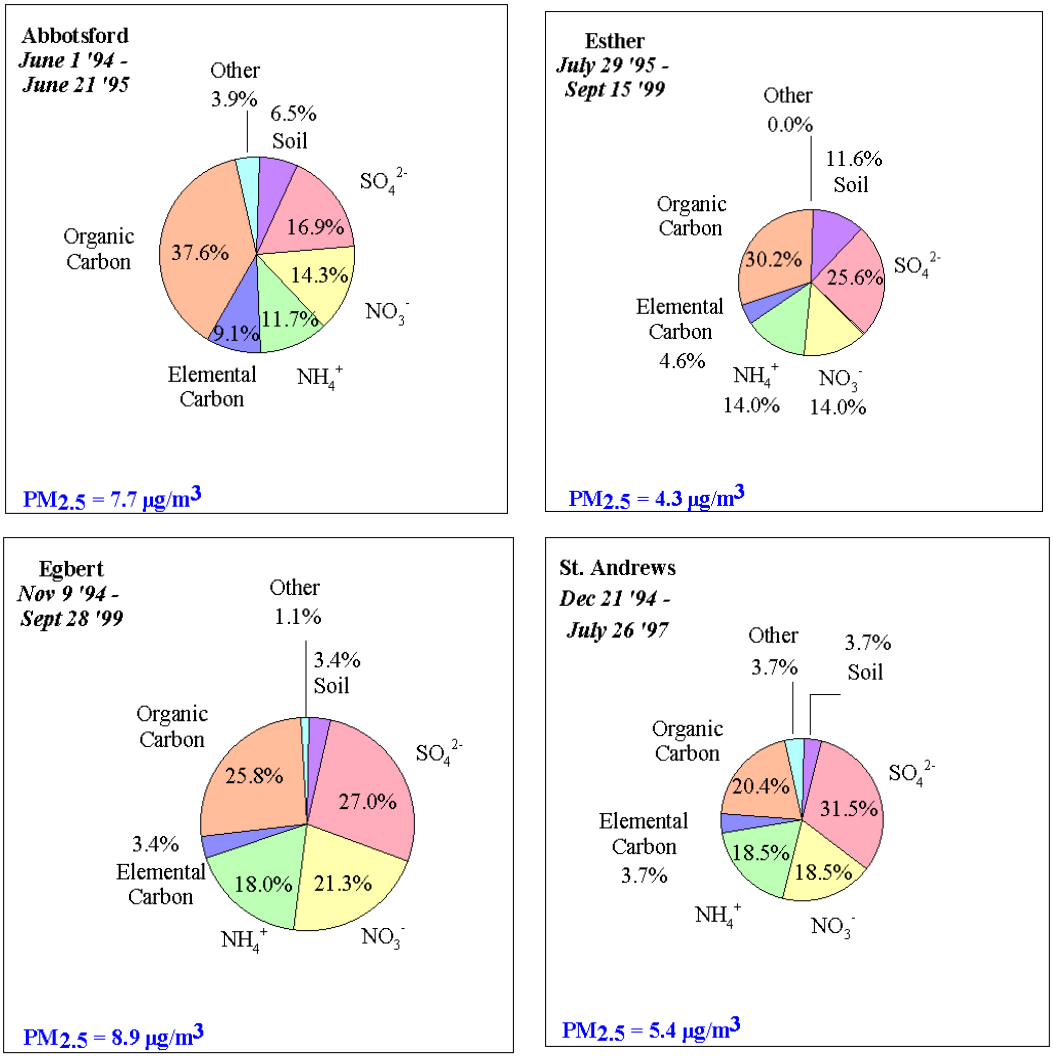

Figure 3-9. *Fractional composition of Rural $PM_{2.5}$ measured at Abbotsford (49.0° N, 122.3° W, BC), Ester (51.6° N, 110.2° W, AB), Egbert (44.2° N, 79.8° W, ON) and St. Andrews (45.9° N, 67.1° W, NB) of Canada. The size of the circle represents the magnitude of the total $PM_{2.5}$ concentration in that station.*

3.3.3 Observations In Europe

PM_{10} and $PM_{2.5}$ measurements of the EMEP Monitoring Network shown in Figure 3-10a indicate that the PM_{10} concentrations are the highest in Spain, where annual mean concentrations are typically above 20 µg m^{-3} but can be as high as >40 µg m^{-3}. Data from Switzerland and Germany indicate more moderate levels of PM_{10} between 10 and 20 µg m^{-3}. Data are lacking in large parts of Europe, in particular the eastern and southeastern parts of the continent. The geographical distribution of annual mean concentrations of $PM_{2.5}$ in 2002,

as measured at EMEP sites, is presented in Figure 3-10b [*Tørseth*, 2004]. Due to the limited number of monitoring stations, it is difficult to obtain a generalized spatial distribution pattern for the $PM_{2.5}$ mass. However, the available data indicate that $PM_{2.5}$ was generally between 5 to 15 µg m^{-3} in most of Spain, Switzerland, and Germany, with higher values observed in northern Italy and eastern Austria. Additional modelling work showed the highest $PM_{2.5}$ would be expected in the Netherlands [*Tørseth*, 2004].

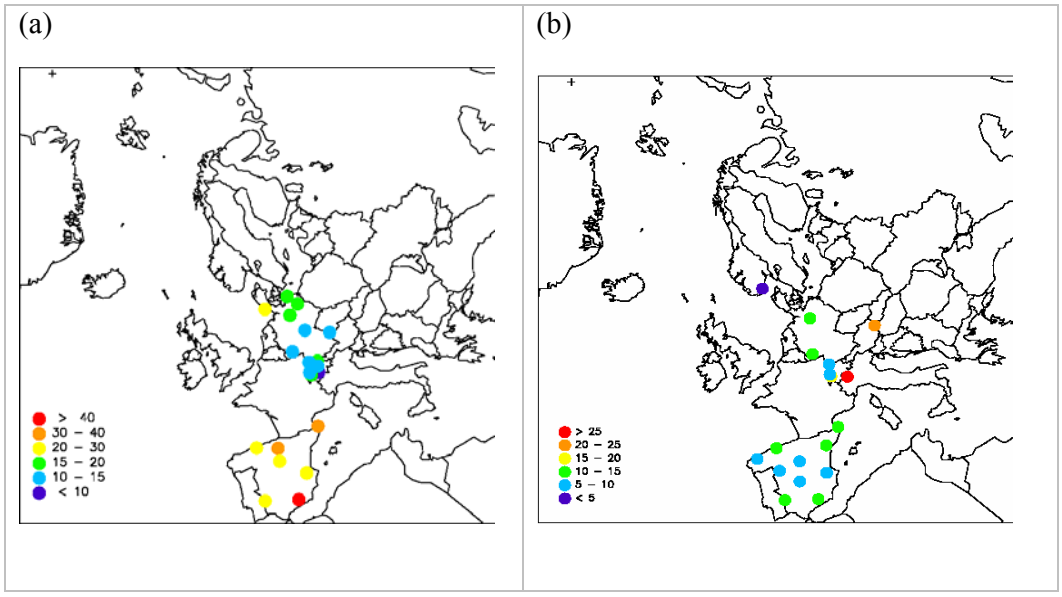

Figure 3-10. *(a) Annual averages of PM_{10} concentrations at EMEP sites in 2000 [Kahnert and Tarrasón, 2003] and (b) $PM_{2.5}$ in 2002 at selected monitoring stations in Europe.*

In future a growing network of continuous $PM_{2.5}$ observations generated by European air quality regulatory monitoring will provide valuable additions to the capability of studying links between aerosols and precipitation. In addition, a research project European Supersites for Atmospheric Aerosol Research (EUSAAR) will deliver through research from 2006 to 2011 a more comprehensive aerosol observational capability at approximately 20 observatories.

Measurement results of aerosol sulfate in Europe, from the EMEP particulate matter network, can be seen in Figure 3-11 [*Kahnert and Tarrasón*, 2003]. Similar to North America, aerosol sulfate concentrations in Europe coincide with anthropogenic SO_2 emissions, a consequence of coal as the primary energy source. Sulfate concentrations are highest in southern Europe, mostly at sites in Spain and Italy, and in central Europe, mostly in the eastern part of

Germany, Poland, Austria and Hungary, where they can be higher than 1.35 μg S m^{-3} (or 4.05 μg $SO_4^{=}$ m^{-3}) on an annual average (Figure 3-11). In Europe sulfur dioxide emissions increased from the post war years and peaked mainly in the 1960s and 1970s. Following emission control measures, gradual reductions took place in most countries and especially in Western Europe in the 1980s. From 2000 to 2001, the masses of ammonia and sulfate in aerosols changed little at several sites, however, a consistent increase in both was observed in The Netherlands. Also, there are clearly more stations at which an increase of sulfate concentrations has been observed compared with stations that have shown a decrease.

(a) (b)

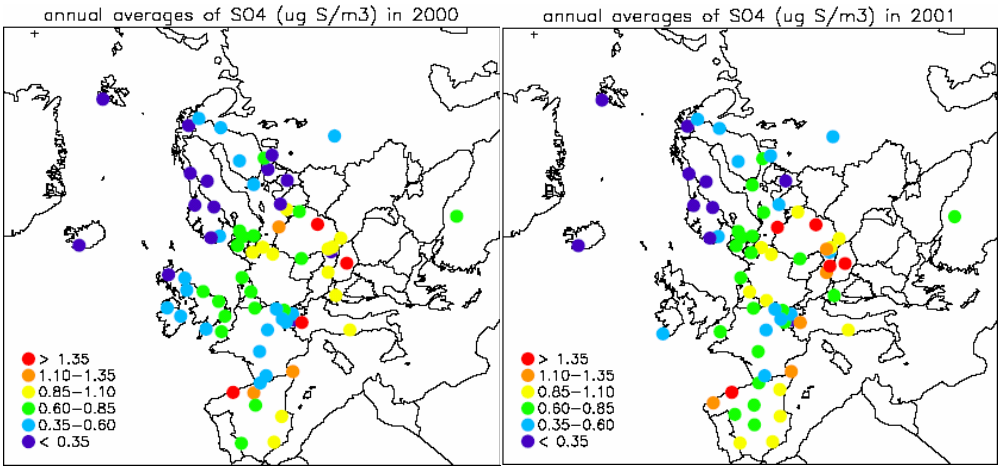

Figure 3-11. *The annual averages of sulfate mass (μg S m^{-3}) concentrations for 2000 (a) and 2001 (b) measured at EMEP sites.*

The regional characteristics of tropospheric aerosols in Europe are nicely represented by the EUROTRAC-2 (The Transport and Chemical Transformation of Environmentally Relevant Trace Constituents in the Troposphere over Europe; Second Phase) Program. The objectives of this program were to investigate the formation, transport, chemical transformation, deposition, and impacts of aerosols, photo-oxidants, acidifying substances, and various other atmospheric constituents through a set of subprograms.

The *Putaud et al.* [2003] compilation summarized data from thirty-four sites which were classified as follows: natural background, rural background, near city background, urban background, free troposphere and kerbside based on distances from large pollution sources,

vehicular traffic, etc. The background PM_{10} and $PM_{2.5}$ mass loadings at those sites averaged 7.0 ± 4.1 μg m^{-3} and 4.8 ± 2.4 μg m^{-3}, the latter being 5 to 10 times lower than the maximum $PM_{2.5}$. The persistent background was said to be a result of anthropogenic substances, such as black carbon, transported long distances in addition to particles originating from natural sources. The regional background was concluded to be a major influence on PM concentrations in cities, and this background was at least partially responsible for the observed variability in the PM masses within the various categories of sites. The PM mass data, which showed PM_{10} concentrations occasionally exceeding 40 μg m^{-3}, were consistent with measurements reported in EMP/CCC 5/2001 of PM_{10} reaching 50 μg m^{-3} in Western Europe and up to 70 μg m^{-3} in Eastern Europe (Figure 3-12). Interestingly, during polluted periods, the increases in aerosol mass were mainly due to $PM_{2.5}$.

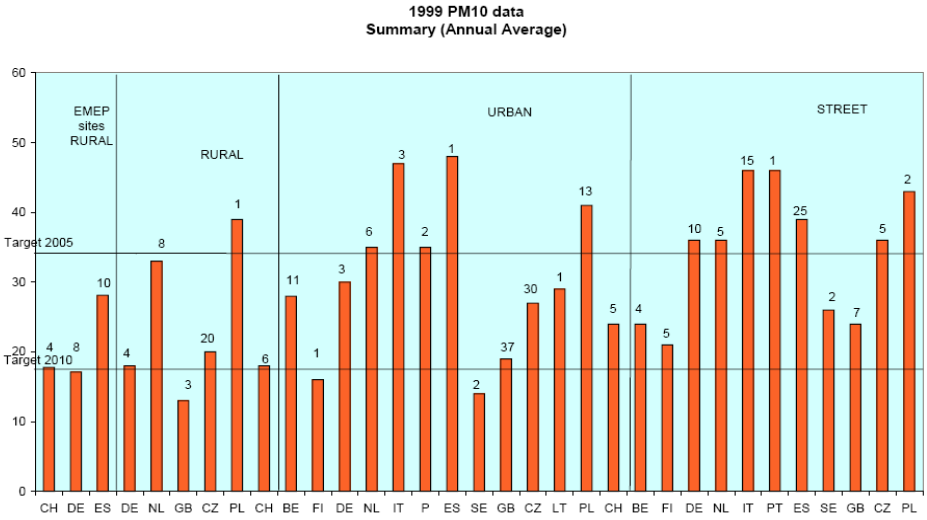

Figure 3-12. *Annual average PM_{10} concentrations in different European countries for various site types (units: μ g/m^3) during 1999, from EMEP/CCC-Report 5/2001.*

Indeed, the $PM_{2.5}$ masses at a subset of thirteen sites in the *Putaud* paper were found to be fairly similar, varying by roughly 3-fold, while in comparison, the particle number concentrations were more variable among that subset of data, differing by a factor of ten. The scales of these differences illustrate the limitations of mass-based data for problems more appropriately addressed by considering particle numbers as is the case for some issues concerning aerosol/cloud interactions. Particle size distributions reviewed by *Putaud et al.* showed diurnal influences from motor vehicle traffic and photochemistry, with influences

from the regional background on particles about 100 nm in size. These particle size data showed that even the clean sites were affected by pollution aerosol and that during transport particle numbers are reduced by dilution and coagulation, the latter process removing smaller particles from the aerosol population as they collide with large ones.

Further analyses presented in the *Putaud* compilation showed that the $PM_{2.5}$ masses were linearly related to particle number concentrations at the clean sites, suggesting that the small particles in clean air mostly originate from distant sources. This relationship did not hold at the more polluted sites, however, and consistent with what was noted above, the numbers of particles with diameters greater than 10 nm ($d > 10$ nm) tended to be more variable than $PM_{2.5}$ mass. Furthermore, 70 to 80% of the particles had $d < 100$ nm, and compositional analyses for size-separated samples indicated that these particles were mainly carbonaceous.

Seasonality was evident in the mass loadings at all but one of the polluted sites, that is, both PM fractions were highest in winter, but this trend was not seen at the natural or rural background sites. The elevated PM loadings in winter were thought to be driven primarily by meteorology, mainly large-scale stratification, but seasonality in emissions and long-range transport patterns and in the chemical processing of condensable species, such as ammonium nitrate and organics, at the lower winter temperatures were offered as additional explanations for the higher wintertime PM.

Chemical analyses showed that ~70% or more of the PM_{10} and $PM_{2.5}$ mass at the sites in the *Putaud* compilation could be accounted for by the chemical measurements and some simple assumptions relative to elements not measured, such as non-carbon atoms in organic compounds (Table 3-1). In comparison, a larger percentage of the mass, 28 to 46%, could not be identified in the coarse fraction (PM_{10} - $PM_{2.5}$). At a few sites, the PM_{10} and $PM_{2.5}$ fractions were similar in composition, but more often the two fractions differed chemically.

Table 3-1. *"Grand average" composition (%) of the annual mean contributions to PM_{10}, PM_{10}-$PM_{2.5}$ and $PM_{2.5}$. from EMEP/CCC-Report 5/2001.*

	PM10			PM2.5			PM10-PM2.5		
	Natural & Rural Background	Near-city & Urban Background	Kerbside	Natural & Rural Background	Near-City & Urban Background	Kerbside	Natural & Rural Background	Near-City & Urban Background	Kerbside
Black Carbon	6	5	13	8	8	**17**	4	3	7
Organic Matter	**16**	**20**	**22**	**23**	**22**	**29**	4	**8**	**10**
Nitrate	7	**15**	**10**	5	**17**	11	**8**	7	**8**
Ammonium	6	7	4	8	10	7	1	1	0
Sulfate	**19**	**13**	**10**	**29**	**17**	**13**	3	5	5
Sea salt	8	4	3	3	3	1	**20**	**9**	6
Mineral dust	**10**	9	**19**	5	7	8	**21**	**22**	**37**
Unknown (*)	*28*	*27*	*19*	*20*	*17*	*15*	*40*	*46*	*28*

(*) calculated only when all the main aerosol components were measured.

At most of the sites in the *Putaud et al.* review, sulfate and OC were the main components of $PM_{2.5}$. Sulfate mainly occurred in the $PM_{2.5}$ size fraction, as it often does elsewhere, accounting for 12 to 30% of the $PM_{2.5}$ mass. The EMEP/CCC-Report 5/2001 indicates that sulfate concentrations tend to be high in central and southern Europe, approaching 1 μg m^{-3}, with lower values ~0.4 μg m^{-3} in northern Europe and Scandinavia. Annex 4 of the *Putaud et al.* [2003] compilation shows non-seasalt sulfate concentrations of 5 to 6 μg m^{-3} in urban regions and 1 to 2 μg m^{-3} in natural and rural areas. In comparison with the IMPROVE values cited above, the percent contribution of sulfate to aerosol mass in Europe appears to be slightly less than for the eastern US and more comparable to mid-western and western states.

Carbonaceous particles were the most abundant component of $PM_{2.5}$ on a mass basis at the near-city and urban background and curbside sites in the *Putaud et al.* paper, reaching 5 to 10 μg m^{-3} at the most heavily impacted sites. With further reference to carbonaceous materials,

Noone et al. [2003] drew attention to the uncertainties in the composition and sources of organic compounds, and they noted that studies current at that time were beginning to show that aerosol organics might play a more important role in the multi-phase atmospheric system than previously thought. These authors highlighted the potential importance of water-soluble organic compounds (WSOC) for cloud formation and cloud properties, citing a study by *Saxena and Hildeman* [1996] showing that WSOC accounted for 20-70% of the total aerosol carbon.

Overall, mineral dust was the main contributor (20 to 40%) to the coarse particle fraction at all three general classes of the *Putaud* sites, with seasalt accounting for 5-20% of the coarse particles (Table 3-1). Nitrate and black carbon contributed roughly equal proportions to the PM_{10} and $PM_{2.5}$ fractions, and when the PM_{10} concentrations exceeded 50 μg m^{-3}, nitrate and organic matter were the main contributors to the aerosol mass.

In addition to the recognition of WSOC as a source of CCN, studies conducted for EUROTRAC -2 showed that road traffic is an important a source for nanometer-sized particles. Even though these particles are rapidly lost during transport, the processes involved became better understood as a result of research conducted for the program. Another general conclusion drawn from the EUROTRAC studies was that the algorithms for describing particle emissions from surface processes are not universal but rather there are differences between the situations in Europe compared with North America.

3.3.4 Observations In Asia

Asia is an immense and diverse source of aerosol particles and trace gases. Mineral dust particles mix with pollutants from various industrial and energy-related sources, biomass burning and transport exhaust to produce an extraordinarily complex regional aerosol mix. In the late winter and early spring of 2001, two major field campaigns were mounted to study the atmosphere over Asia and the western Pacific. A NASA sponsored program, TRACE-P (TRAnsport and Chemical Evolution over the Pacific) was conducted first, from February to April, and it was designed to determine the pathways for the outflow of chemically and radiatively important trace substances and to follow the chemical evolution of the Asian outflow over the western Pacific. From late March to May, an intensive observation campaign was made for ACE-Asia, the third in a series of Aerosol Characterization

Experiments (ACE). The ACE experiments were developed to investigate how atmospheric aerosol particles from different regions affect the Earth's climate system.

Several findings from these programs concerning Asian-aerosol outflow are directly relevant to this aerosol/cloud assessment. First, *Jordan et al.* [2003], *Seinfeld et al.* [2004], and others have presented data showing that gas-phase species mix with Asian dust particles, making the dust particles more hygroscopic, and presumably affecting the formation of clouds over regional scales. Data obtained with a single-particle mass spectrometer by K. Prather and colleagues aboard the research vessel Ronald H. Brown and reported in *Arimoto et al.* [submitted] indicate that the processes involved in the mixing of sulfate, nitrate, and chloride with dust are competitive or selective in nature. These uptake and mixing reactions not only affect the physical properties of the mineral dust but also affect the number and size distributions of the ensemble aerosol population, especially nitrate-containing but also sulfate-containing particles. In TRACE-P, *Kittaka et al.* [2004] showed that the mass of sulfate in ice clouds was much less than in liquid clouds and that sulfate particles could be released into the atmosphere following the oxidation of SO_2. Their study showed a close and direct linkage between meteorology and aerosols, that is, accurate predictions of clouds and precipitation were needed to successfully model the atmospheric sulfate budget.

ACE-Asia and TRACE-P also have provided information on new particle formation, particle distributions, Asia outflow, and how areas downstream could be affected by long range transport, all topics relevant to this assessment. For example, a study by *McNaughton et al.* [2004] showed evidence of secondary aerosol particle formation over synoptic scales. These particles formed heterogeneously in postfrontal air when dry continental air mixed with maritime air; that is, nucleation occurred when mixing led to supersaturations of condensable species. Comparisons of model results with aircraft observations showed that in areas where dust was concentrated, it composed up to 90% of the super-micrometer particles, and even though dust impacts sometimes extended above 6 km, the influences were strongest in the boundary layer [*Tsai et al.*, 2004]. These authors also showed correlations between submicron aerosol mass loadings and ethyne, an indicator of combustion sources, and from this they concluded that anthropogenic emissions were the major source for the submicron particles. Similar conclusions have been reached by many others; indeed *Clarke et al.* [2004] suggest that even though interactions sometimes do occur, the coarse mode and fine mode particles are for the most part independent phenomena. *Clarke et al.* also presented other data

that are highly relevant to aerosol/cloud processes; for example, coarse-mode dust was found to be nearly non-hygroscopic while the fine pollution aerosol was much more hygroscopic.

Aircraft studies for TRACE-P and ACE-Asia have shown that aerosol properties vary strongly with altitude, and comparisons with ground-based measurements show that boundary layer measurements generally are not good indicators of the aerosol properties above the surface. More specifically, the aerosol population in the boundary layer (below ~2000 m) is in many ways distinctly different from that in the free troposphere. Pollution aerosol is largely confined to the BL, while dust is distributed much more evenly throughout the column [*Clarke et al.*, 2004].

One drawback from the above analysis is that these campaigns were conducted over the marine atmosphere outside the mainland China downwind the major pollution sources. Within the mainland continent, observational data are very limited. Recently, monitoring stations have been established in China to quantify air pollution levels and to better define the problems. Data from the newly developed stations show elevated aerosol concentrations (X.Y. Zhang, Center for Atmosphere Watch and Services, CMA, personal communication). At Lin An station (30.3°N, 119.73°E) in eastern China, TSP ranges from 50 to70 μg m^{-3} while the sulfate is from 15 to 18 μg m^{-3}, nitrate from 2 to 4 μg m^{-3}, OC from 10 to 12 μg m^{-3} and black carbon around 2.0 μg m^{-3} for spring, summer and fall of 2004. This results in an organic carbon to black carbon (OC/BC) ratio of 5 to 6.

At Zhenbaitai in northwestern China (38.3°N, 109.7°E), the TSP ranges from 45-50 μg m^{-3} while the sulfate is from 4-9 μg m^{-3}, nitrate around 2 μg m^{-3}, OC from 9-17 μg m^{-3} and BC from 2-5 μg m^{-3} for winter, spring, summer and fall of 2003–2004 period. In eastern and northeastern China, *Zhang et al.* [2005] reported an analysis of bulk aerosol samples from two ground-based sites of Lian Yun Gang at a coastal site (LYG – 34.7°N,119.3°E) and Tong Liao (TL – 43.2°N, 122.2°E) in sandy land areas from June to December and summer of 2003, respectively. At LYG, the region-wide mean values for OC and EC in bulk aerosol particles during summer and autumn were similar, from 10 to 14 μg m^{-3} and 3.8 to 5.3 μg m^{-3}, respectively with an average TSP over 100 μg m^{-3}. The wintertime values were much higher with 24 μg OC m^{-3} and 11 μg EC m^{-3}, respectively. At TL TSP averaged about 78 μg m^{-3} in the summer, and the mean values of OC and EC were 7.3 μg OC m^{-3} and 2.0 μg EC m^{-3}

^{3}, which is lower than those at LYG, reflecting the weaker anthropogenic influences at the sandy land site.

Increased aerosol concentrations over China are reflected in long term decreases in the total global radiation reaching the surface [*Che et al.*, 2005]. Over the latter half of the 20th century, there have been significant decreases in global radiation (-4.5 W m^{-2} per decade), direct radiation (-6.6 W m^{-2} per decade), clearness index (-1.1% per decade), and the percentage of possible sunshine duration (-1.28% per decade). This is at least partially attributable to the increase in the aerosol loading in China. Changes in precipitation at the ground in China from 1951-2000 have been observed in the same areas where the total global radiation decreased [*Zhai et al.*, 2005]. Even though there is little trend in the country-wide precipitation for China, there are distinct regional and seasonal patterns. Annual total precipitation has significantly decreased over southern Northeast China, North China, and over the Sichuan Basin but significantly increased in western China, the Yangtze River valley and the southeastern coast. There are many factors influencing the precipitation variations. Nevertheless, coherent changes in the radiative fluxes and precipitation patterns no doubt contain valuable information on the link between the concentrations of aerosols and patterns of precipitation in China. This needs to be investigated in more detail using the extensive monitoring network observations and models of the China Meteorological Agency.

3.3.5 Southern Hemisphere Observations

PM_{10} and $PM_{2.5}$ have been determined gravimetrically, and more recently, with the use of TEOM monitors at a network of Australian monitoring stations that are mostly located near the major urban centers along the east and southeast coast. Annual median PM_{10} concentrations are typically 15 to 20 μg m^{-3} in coastal locations in New South Wales, Victoria, Queensland, and West Australia, but appear to be higher in Tasmania while the annual median of $PM_{2.5}$ concentrations range from 5-10 μg m^{-3} [*DEH*, 2004].

Hemispheric-scale differences in land area (39% of the northern hemisphere is covered by land vs. 19% in the southern hemisphere) and in human population have led to large inter-hemispheric differences in primary aerosol source strengths (Chapter 2). This involves both natural and anthropogenic aerosols, but the greatest differences are seen for fossil fuel and aircraft emissions. According to data summarized in Chapter 5 of the IPCC 2001 assessment report [*IPCC*, 2001], more than 90% of the aircraft emissions and ~99% of the fossil fuel

emissions are emitted into the atmosphere over the northern hemisphere. More than 80% of the mineral dust is produced in the northern hemisphere, according to *Jickells et al.* [2005], and less than 20% of the dust flux into the oceans occurs in the southern hemisphere. In contrast, biomass burning emissions are more evenly distributed between hemispheres, with a split of nearly 50%:50%. Sea salt is the only primary aerosol produced in greater quantities in the southern hemisphere (Chapter 2).

In terms of Earth systems, one might argue that the position of the inter-tropical convergence zone is a more meaningful boundary between hemispheres than the equator; and this would reduce the inter-hemispheric differences somewhat. Even so, the difference between hemispheres in the percent area covered by land also affects radiative fluxes and hence temperature, and because of this, the temperature ranges also differ, with the northern hemisphere not only warmer, but also exhibiting greater variability with season. This is important in the context of this assessment because inter-hemispheric differences in temperature as well as ocean currents, vegetation cover, conditions in the polar regions, the numbers of large urban areas, etc. all factor into how aerosols and clouds interact.

The weak sources for aerosols in the southern hemisphere are reflected in the extremely low aerosol concentrations that have been observed in some remote regions, especially over the oceans. This was seen at American Samoa, for example, where mineral dust concentrations were extremely low, of the order a few tens of nanograms per cubic meter [*Prospero et al.*, 1989]; these concentrations are comparable to what has been observed over Antarctica. *Quinn and Bates* [2005] recently compared regional aerosol properties based on data they obtained during a series of oceanographic cruises. That comparison included results from ACE-1, a program designed to characterize aerosol properties in the remote marine atmosphere south of Australia. Results of the comparison showed that the concentrations of NH_4^+ and nss SO_4^{2-} in submicron particles from ACE-1 (0.04 ± 0.01 and 0.16 ± 0.06 μg m^{-3}, respectively) were lower than any observed during the other sampling programs, which also included ACE-2; Aer99 Dust; Aer 99 Bio Burning; INDOEX; Arabia; INDOEX; India; ACE-Asia Polluted; ACE-Asia Polluted + Dust; NEAQS. Nitrate was below detection in the ACE-1 samples, but it was above detectable levels in all the other programs. The Quinn and Bates paper also showed that the concentrations of these species (except nss SO_4^{2-}) were low or below detectable levels in the supermicron fraction at the southern ocean site.

Arid and semi-arid regions in Africa make up the world's largest source for dust, producing 1700 Tg of dust per year [*Jickells et al.*, 2005], and even though two-thirds of this dust is produced in North Africa, significant plumes of African dust do spread over the Atlantic Ocean south of the equator. This is most evident during spring and summer when the dust flows southwest out of Africa [e.g., *Cakmur et al.*, 2001]. In one of the clearest cases of intercontinental transport, dust originating from the Sahara was shown to supply nutrients to the Amazon basin [*Swap et al.*, 1992]. Further studies [*Swap et al.*, 1996] show that in austral spring, dust from west Africa, which originates between 0° and 10° S, is transported into the central South Atlantic. African dust is transported westward to North America; eastward to the eastern Mediterranean, then to the Middle East; and northward over the Mediterranean and into Europe [*Goudie and N. J. Middleton*, 2001].

Relationships between African dust fluxes and climate variability are being investigated as a coupled atmosphere-land-ocean system for the African Monsoon Multidisciplinary Analysis (AMMA) program [*Marie and Prospero*, 2005]. Indeed the AMMA program is in part based on the assumption or expectation that the West African Monsoon and related features of the hydrological cycle and regional circulation impact other tropical and mid-latitude regions, including effects on atmospheric chemistry and aerosols.

In addition to the mineral dust exported out of Africa, large quantities of aerosols and trace gases, including ozone precursors, are emitted from Africa as a result of biomass burning [*Levine et al.*, 1995; *Andreae et al.*, 1996]. Particulate matter from prescribed fires in Africa that were studied during SAFARI-92 (Southern Africa Fire-Atmosphere Research Initiative) included not only biomass burning products, but also mineral dust, sulfate, and sea salt. The estimated production of black carbon from savanna fires was 10 to 26 Tg C yr^{-1}, of which more than 90% was thought to remain on the ground.

Compared with North America, Europe and Asia, there have been relatively few studies of aerosols over South America. An analysis of continental aerosols over the oceans based on satellite imagery (http://capita.wustl.edu/CAPITA/CapitaReports/_TropoAerosol/trop3.html) shows a narrow aerosol band oriented north-south off the coast of northwestern South America, near Peru. That analysis suggested that general absence of aerosol plumes over the oceans surrounding South America was conspicuous in light of the amount of biomass burned on that continent [e.g., *Levine et al.*, 1995].

Much of the aerosol research over South America has focused on the Amazon region and biomass burning during programs such as the Amazon Boundary Layer Experiments (ABLE-2b and 2b) and the Large-Scale Biosphere-Atmosphere Experiment in Amazonia (LBA-EUSTACH). As was the case for Africa, soil dust was found to be associated with the biomass burning activities, but the aerosols were predominantly carbonaceous, containing trace amounts of K, S, Ca, P, Cl, and Na. Studies conducted by *Guyon et al.* [2003; 2004] showed that the mass concentrations for particles < 2 μm diameter at a Brazilian rain forest averaged 2.2 and 33.5 μg m^{-3} for April/May and September/October, i.e., the respective wet and dry seasons. Those studies also uncovered seasonal differences in aerosol sources, with contributions from a natural biogenic component strongest in the wet season. Pyrogenic aerosols were dominant in the dry season, and soil dust, often was found to be internally mixed with the biomass burning products. As discussed elsewhere, the LBA-EUSTACH studies have shown that biomass-burning aerosols affect cloud properties in the Amazon Basin [*Roberts et al.*, 2003].

3.4 VERTICAL PROFILES

3.4.1 Vertical Profiles of Aerosols – Surface-based Network

Vertical profiles of atmospheric aerosols are an important property that determines the life time and long range transport potentials as well as the climatic impact. However, due to limitations in measuring equipment and technology, information on the vertical distribution of aerosols over the global is hardly available not to mention the lack of data on size distribution and chemical compositions in the vertical profiles. Currently, Lidar is the only surface-based tool for measuring vertical profiles of aerosol optical propreties [*Measures*, 1984]. There are three types of Lidar systems: Mie-scattering, Raman and high-spectral resolution (HSRL). Lidar is also used for measuring the distributions and characteristics of clouds. Mie Lidars are useful for detecting cloud-base height. Raman lidars and HSRLs are useful for measuring the extinction coefficient. Multi-field-of-view Lidars [*Bissonnette and Roy*, 2004], Liquid water (or ice) Raman Lidars [*Russo et al.*, 2004; *Wang and Overland*, 2004], and bistatic Lidars [*Sugimoto et al.*, 2001] can measure cloud particle size and cloud water content. Combinations of measurements made with Llidar and cloud profiling radar also provide insights into cloud microphysical parameters.

Ground-based Lidar networks for aerosols have been established in various locations (Figure 3-13). Currently, several Lidar networks are operated in the world which include the Micro-Pulse Lidar Network of NASA (MPLNET), the European Aerosol Research Lidar Network (EARLINET), the Commonwealth of Independent States Lidar Network (CIS-LiNet) and the Asian Dust Network (AD-Net). Since these networks are in an early stage of operational monitoring, a global data set for the vertical profiles of aerosols is not readily available. However, some regional characteristics of aerosol vertical profiles can be deduced from the networks.

EARLINET

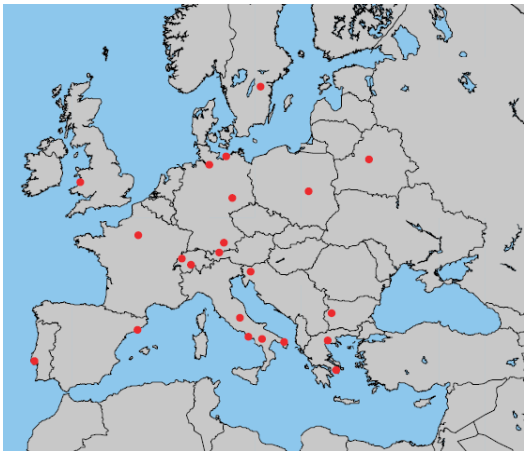

AD-Net

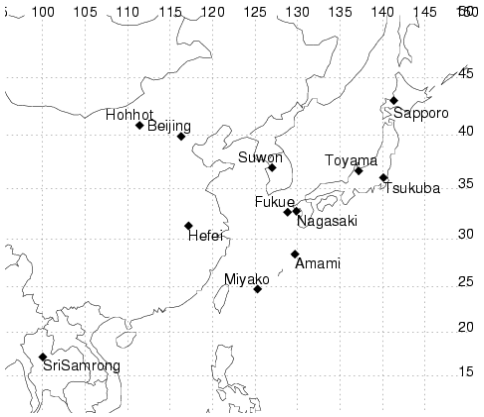

MPLNET

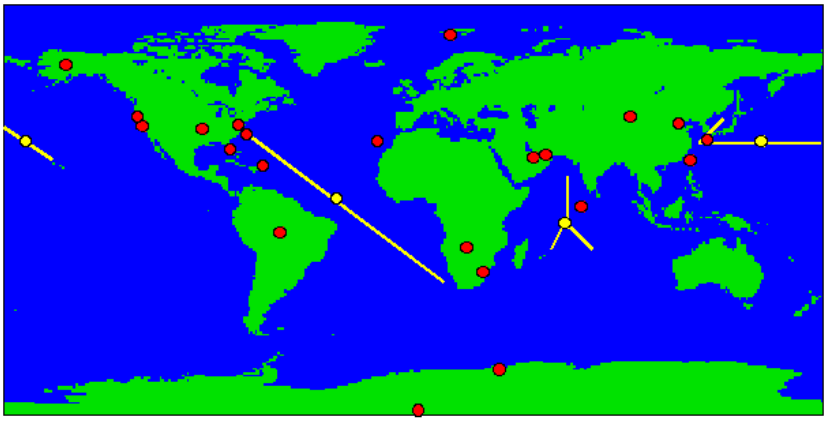

Figure 3-13. *Global lidar networks.*

EARLINET has provided information on the aerosol vertical distribution over Europe [*Matthias et al.*, 2004]. Figure 3-14 shows comparison of the mean aerosol extinction profiles from Lidar with outputs of the global aerosol models for northern and southern European stations in 2000 [*Matthias et al.*, 2004]. The model results are filtered for the observation period. The variability of the profile (16% and 84%) is shown. The result shows that aerosol layer height is higher for the southern stations and the aerosol concentration in the low altitude is higher in the northern stations and that the aerosol concentrations are higher at low altitudes in the northern stations. The model results agree reasonably well with observations. The contribution of dust is seen to be larger in the southern stations.

Figure 3-15 shows monthly mean extinction coefficient profiles observed at AD-Net lidar network site in Sri Samrong, Thailand (17.1° N, 100.0° E) during dry seasons in 2001-2004 [*Shimizu et al.*, 2005]. The boundary layer height increases from January to April, and the density of aerosols also increases. The marked increase of aerosol optical depth occurs from November to February. The source of the aerosols is considered to be mostly biomass burning. Year-to-year differences are seen in the aerosol density and seasonal variation. The aerosol density in 2003 was lower than other years. This result was consistent with the co-located skyradiometer data.

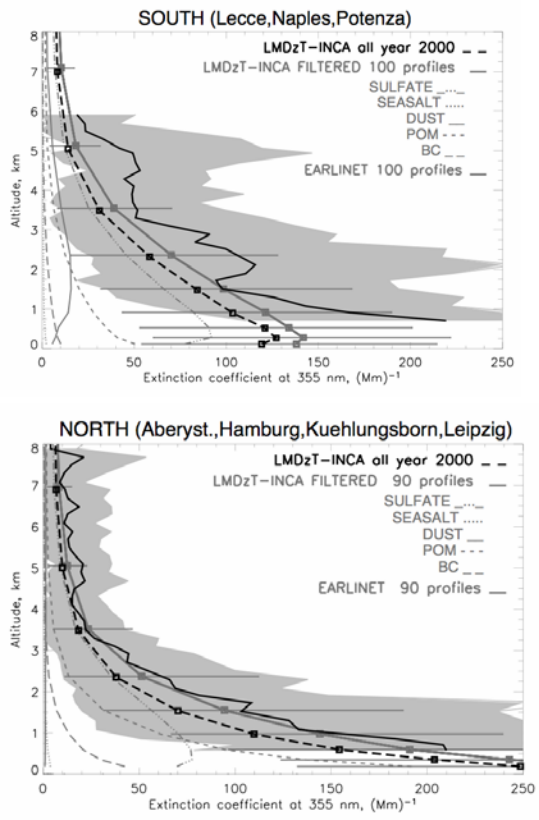

Figure 3-14. *Comparison of the mean aerosol extinction profiles from Lidar (at 355 nm) with the LMDzT INCA model for northern and southern EARLINET stations in 2000. The observed extinction profile is indicated by the solid black line with the 16–84% percentiles are shaded in gray. The all-year-average modeled profiles are plotted with a dashed black line. The vertical profiles filtered for the presence of measurements with indication of the 16–84% percentiles are plotted with the solid gray line. The squares in the latter two profiles indicated the model levels. The contributions from the individual species are shown as well in this figure, as indicated in the legend (adapted from Guibert et al. 2005).*

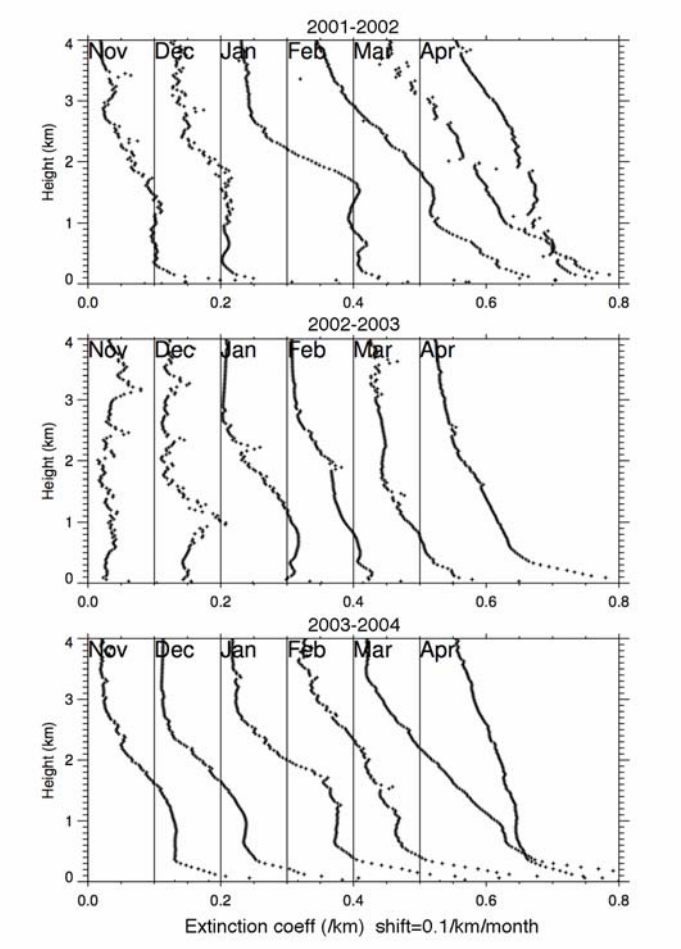

Figure 3-15. *Monthly mean extinction coefficient profiles in Sri Samrong, Thailand during dry seasons in 2001-2004 [Shimizu et al., 2005].*

One of the most useful applications of Lidar data is validation of aerosol transport models. For this purpose, event-to-event comparisons using a network of continuously operated Lidars is effective. Continuity of the observations and suitable locations of the observation sites (depending on the scale of phenomena) are very important. Aerosol type classification methods using depolarization ratio, wavelength dependence, and the Lidar ratio (if available) are useful for the comparison. Figure 3-16 shows an example of Asian dust transport captured by the Lidars in Beijing, Suwon (37.1° N, 127.0° E), Nagasaki (32.8° N, 129.9° E), and Tsukuba. Downwind of the dust source regions, measuring the clouds and aerosol

together using a polarization-lidar at Alaska, *Sassen* [2005] detected the long-range transported dust aerosols in 2004 spring; these particles served as ice nuclei (IN) in the atmosphere and caused ice clouds to form at modest super-saturations and temperatures, 4.5 and 6.5 km above sea level. The aerosol profiles peaked at a much higher height above the ground in Alaska compared than those observed at East Asian stations; these images show the evolution of dust long-range transport and the ability of dust to affect cloud formation and precipitation.

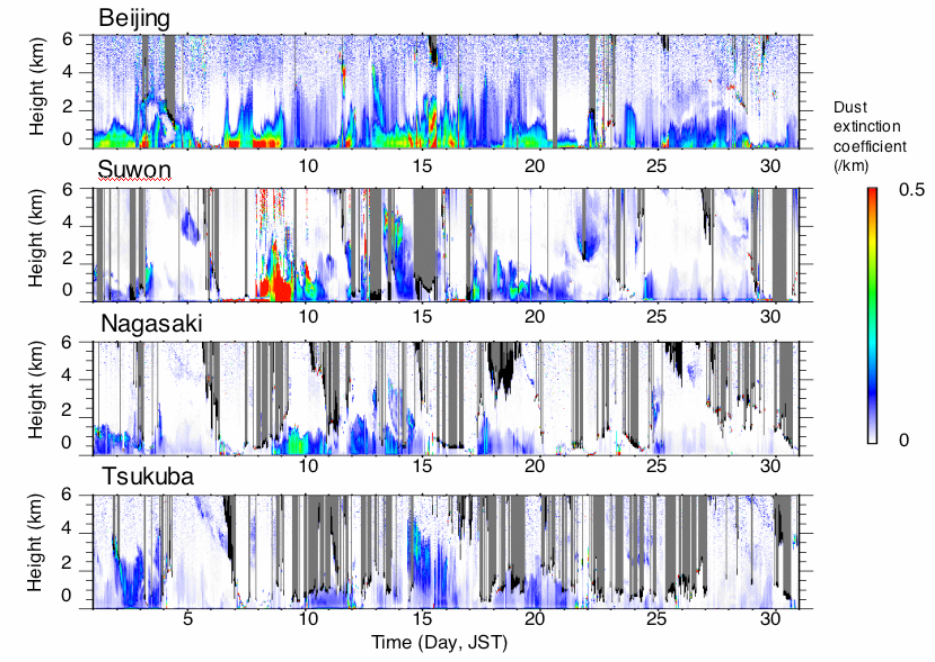

Figure 3-16. *Mie-lidar Dust Extinction Coefficient (S_1=50) at 4 locations in China and Japan, April 2002.*

Okamoto *et al.* [2002] studied the effects of aerosols on clouds in the marine boundary layer on stratocumulus cloud particle size using the combined Lidar and radar method. The experiment was performed on the Research Vessel Mirai in the northwest Pacific. Figure 3-17 shows the aerosol number density estimated from the two-wavelength Lidar using a forward data reduction method. The approach assumes that the aerosol size distribution is bimodal, and the cloud effective radius is derived from the combined method with the two-wavelength Lidar and the cloud profiling radar [*Okamoto et al.*, 2002]. The result shows the small cloud effective radius in clouds with high aerosol number concentration.

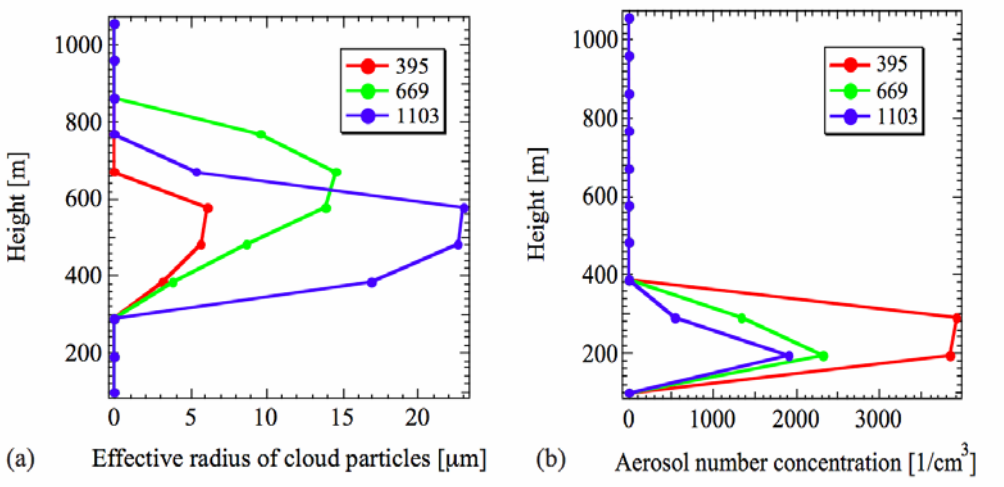

Figure 3-17. *Vertical profiles of (a) effective radius of water cloud, and (b) aerosol number density.*

3.4.2 Vertical Profiles of Aerosols – Space-borne

In contrast to individual or networked ground-based Lidars that profile the atmosphere above, at a single geographic location, or airborne Lidars that measure above and below aircrafts on regional scales, spaceborne Lidar allows the study of aerosol transport in regions that are difficult or impossible to explore by other means. The era of spaceborne backscatter Lidars was ushered in during September, 1994 with the successful launch of LITE (Lidar In-Space Technology Experiment), the primary payload, onboard the Space Shuttle Discovery. There were two purposes to the LITE mission: evaluate technological requirements of a spaceborne Lidar [*Couch et al.*, 1991] and evaluate the science capability [*McCormick et al.*, 1993]. LITE convincingly demonstrated the value of spaceborne lidar in retrieving the vertical structures of clouds [*Omar and Gardner*, 2001; *Winker and Trepte*, 1998] and aerosols on a global scale.

Several examples of the global transport of aerosols were evident from the LITE data. Aerosols from natural sources, such as Saharan dust was measured on several orbits by LITE. Although it has been known for quite some time that large quantities of Saharan dust are transported across the Atlantic towards the Caribbean, the unique capabilities of a spaceborne lidar proved ideal for tracking and quantifying the magnitude of these events [*Powell et al.*, 1996]. LITE showed these enormous plumes would stretch 100's of kilometres, reaching

altitudes of greater than 5 km (Figure 3-18). It is easy to imagine that if LITE had been a springtime mission, that Trans-Pacific transport of Asian dust would also have been observed and demonstrated the value of year round spaceborne lidar measurements.

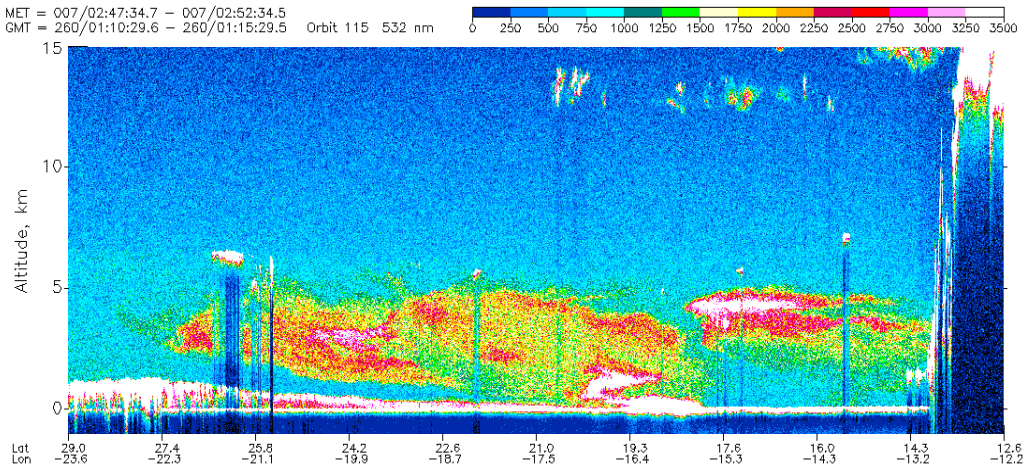

Figure 3-18. *LITE orbit showing Saharan dust plume over the Atlantic. Significant structure is shown within the plume as it reaches altitudes of 5 km (courtesy of NASA Langley Research Center).*

Aside from natural sources of tropospheric aerosols, the ever important role of anthropogenic emissions needs appropriate consideration. The contributions of tropospheric aerosols to the radiative budget are not well understood due to the lack of knowledge about their distribution, optical and chemical variability around the globe. LITE proved invaluable at pinpointing source regions of anthropogenic aerosols: from small local sources and combined net regional impacts, to large scale activity such as biomass burning. Observations from LITE showed biomass burning in South America extending hundreds of kilometres from the source region. The depth and complexity of these plumes are nicely captured by the Lidar making it possible to apportion their impact and quantify their contribution to long-range transport. Using multiple orbits as LITE precesses around the globe made possible the tracking of regional transport. A good example would be the measurement of anthropogenic aerosols leaving the Eastern United States and riding the "gulfstream highway" towards

Europe [*Hoff et al.*, 2001]. A clear advantage to spaceborne lidar is the ability to vertically profile the atmosphere in remote areas of the globe where ground-based or aircraft measurements are scarce and would be prohibitively expensive. Furthermore, some countries do not have lidar capability, yet make noteworthy contributions to the anthropogenic burden. As such spaceborne lidar results may be the only opportunity to capture measurements in those regions, essential in understanding the global transport perspective.

An example of a LITE validation track from the Canadian validation component is given in Figure 3-19. This represents an orbital overpass along the Californian coastline while aircraft measurements along the track were being made below. The most spectacular feature from the LITE data is the identification of the urban aerosol plumes from San Francisco and Los Angeles (the cities locations are obvious by the position of the plume origin) flowing out along the coastline for several hundred kilometres [*Strawbridge and Hoff*, 1996]. What is truly remarkable is the 60 s trip for a spaceborne lidar to go from San Francisco to Los Angeles. Other lidar data from various aircraft and ground sites provided validation of the measurements, thus increasing confidence in the LITE's performance.

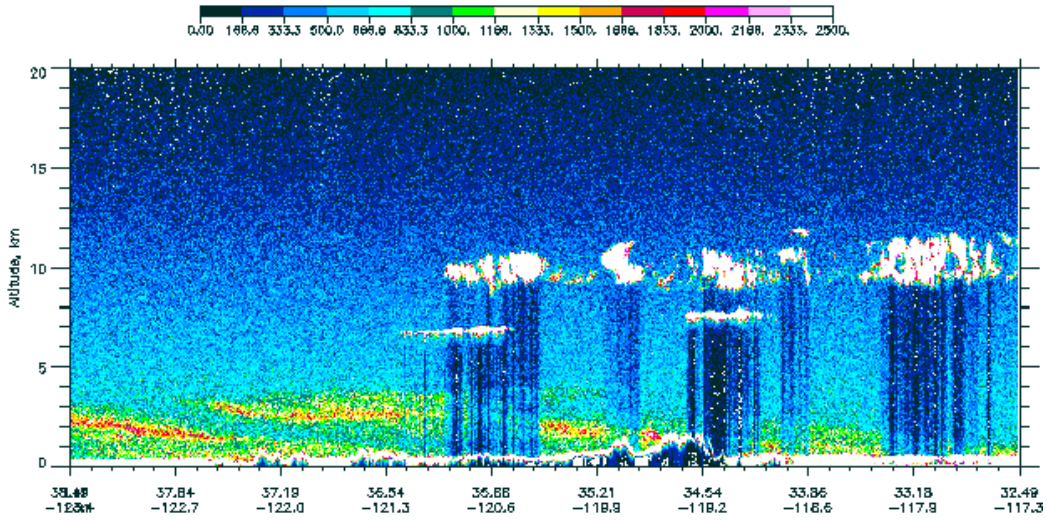

Figure 3-19. *A two minute snapshot from LITE along California's coast showing the long-range transport of pollutants from the Los Angeles and San Francisco areas (courtesy of NASA Langley Research Center).*

Among the most significant contributors to the radiative budget are the aerosols (and water vapor) found in the planetary boundary layer (PBL). Lidars have been used for several years

to determine PBL height [*Melfi et al.*, 1985; *Piironen and Eloranta*, 1995; *Strawbridge and Snyder*, 2004] because the large gradient in aerosol concentration that occurs between the top of the PBL and the free troposphere. Measuring the PBL for climate models in essential, since the PBL acts as the interface between the atmosphere and the Earth's surface, and the depth of the PBL controls the transfer of moisture and momentum between them. Current remote sensors cannot measure PBL characteristics. The extreme variability in the depth of the PBL, as seen in the LITE data, is a noteworthy contribution of spaceborne lidar to global measurements of PBL height: a vital parameter for model validation. One of the unique capabilities of LITE was to perform pitch and roll maneuvers, by maintaining the laser footprint at a constant position, allowing the variation in surface backscatter with angle of incidence to be observed. This variation is highly dependent on the surface wind speed and provides a potential means of monitoring surface wind speeds over the oceans [*Menzies et al.*, 1998].

The LITE technology provided the backbone for more recent satellite-based lidars; e.g. CALIPSO (Cloud-Aerosol Lidar and Infrared Pathfinder Satellite Observation) [*Winker et al.*, 2002] which will provide 3-D distributions of aerosol backscattering in the atmosphere after its launch in April 2006 (See Chapter 7 for more details).

3.5 NUMERICAL MODELING STUDIES

Numerical models have been effectively used to synthesize observations and current knowledge of aerosol processes and to provide more information on aerosol transport, transportation and global distributions. Various scales of models have been used to investigate the role of aerosols urban, regional and global issues ranging from air quality problems to climate change.

3.5.1 Transport of Atmospheric Aerosols

In climate models only advective transports are resolved while diffusion and convection are parameterized. The performance of these transport schemes can indirectly be evaluated by comparing the simulated aerosol fields far away from their source regions with observations. One such intercomparison was conducted by *Rasch et al*. [2000] who found that different models simulated observed sulfate surface concentrations mostly within a factor of 2, but that the simulated column burdens and vertical profiles were very different in different models. Comparisons of sulfate aerosols and precursor gases above the surface with observations

were revisited by *Barrie et al*. [2001], *Lohmann et al*. [2001] and *Roelofs et al*. [2001]. A general conclusion from these comparisons was that those models simulating the full oxidant chemistry tended to agree best with observations.

Long-range horizontal transport is important, for example, for dust aerosols being transported from Africa and Asia to North America [*Gong et al.*, 2003b; *Gong et al.*, 2006; *Husar et al.*, 2001; *Prospero*, 1999]. The spatial and vertical distribution of Asian aerosols was a main focus of the 2001 ACE-Asia study [*Huebert et al.*, 2003] as discussed in 3.2.2.3. In terms of aerosol-cloud interactions, long-range transport is important for the transformation of aerosols with consequences for their ability to act as CCN and IN [*Levin et al.*, 1996]. A study by *DeMott et al.* [2003] in which African dust aerosols were sampled in the east part of the US, concluded that these particles were very effective IN.

Pathways for trans-Pacific and trans-Atlantic transport differ in the following ways. For trans-Pacific transport, the highest concentrations in the outflow are in the boundary layer (0-2 km), but the strongest outflow fluxes are in the lower free troposphere (2-5 km) and reflect episodic lifting of pollution over central and eastern China ahead of eastward moving cold fronts. This frontal lifting, followed by westerly transport in the lower free troposphere, is the principal process responsible for export of both anthropogenic and biomass burning pollution from Asia [*Bey et al.*, 2001]. In contrast, trans-Atlantic transport of North American pollutants takes place in the lower troposphere year round, and transport in the middle and upper troposphere is also important in summer [*Li et al.*, 2002]. Compared to trans-Pacific transport of Asian pollution to North America, which takes place mainly in the free troposphere followed by subsidence [*Jacob et al.*, 1999; *Yienger et al.*, 2000], the relatively short distance between North America and Europe and the prevailing westerly flow extending down to the surface favor transport in the boundary layer. Over eastern Asia, in contrast, westerly winds do not extend down to the surface, so that lifting to the free troposphere is a prerequisite for trans-Pacific transport [*Bey et al.*, 2001].

Long-range transport to the Arctic is also of importance, because the background atmosphere, especially in summer, is very clean. *Girard and Curry* [2001] point out that the concentration of IN, aerosol number concentrations, the slope of the aerosol size distribution, and the aerosol solubility, may impact substantially the cloud phase and total water content. The liquid water path and ice water path can vary by as much as 100 g m^{-2} in the single column

model of the ARCSyM regional model as a result of the variations in these aerosol parameters. *Jiang et al*. [2001] used a large-eddy version of the Regional Atmospheric Modeling System (RAMS) with explicit representation of the CCN spectrum and cloud droplet spectrum to investigate aerosol/cloud interactions in the Arctic. Their results show that droplet concentrations increase about two-fold when the CCN concentration in the inversion increases from 30 cm^{-3} to 250 cm^{-3}, which are conditions representative of the long-range transport of aerosols and their precursors to the Arctic. Also, the cloud droplet effective radius decreased by 9–15% from cloud top to cloud base, liquid water content increased by 21%, and no drizzle reached the ground in comparison with results from the control run. A mesoscale model simulation by *Lohmann et al.* [2003] showed that the addition of anthropogenic aerosols to the background aerosol in the Arctic not only impacts liquid water clouds and drizzle, but can also alter snowfall rates. In this study, depending on the assumed snow crystal shape, which determines the accretion rate, the total amount of precipitation reaching the surface after 7 hours of simulation can be larger or smaller than the polluted case compared to the clean background.

The transport of atmospheric aerosols from their source regions is also complicated by the seasonal variation of transport patterns and removal processes [*Barrie*, 1990]. The strong seasonality of Arctic aerosols is a function with their lifetimes which are controlled by the variations in transport and removal processes [*Barrie*, 1986]. Because of stable thermal stratification in the atmospheric surface boundary layer and less than 10-mm liquid H_2O/month of frozen precipitation in the cold half of the year from October to May, aerosol residence times are much longer in winter (~3 to 7 weeks) than in summer (~3 to 7 days). Therefore, the seasonality of any aerosol species at Alert is more likely dominated by factors such meteorology, transport and removal processes specific to the major transport pathways and less to seasonal variations of emissions in the mid-latitude source regions of these species.

In addition, inter-continental transport is also modulated by climate fluctuations. By studying the transport of Asian dust to North America for the last 44 years, *Gong et al.* [2006] identified shifts in the inter-continental pathways for dust aerosols related to the El Niña Southern Oscillation. In that study, an analysis of the variability of the 44-year zonal transport flux, i.e. concentrations multiplied by westerly/easterly wind speeds, was conducted for eight typical El Niño and eight La Niña years. The zonal transport flux indicates the major

transport routes and direction of Asian dust across the Pacific. Most trans-Pacific transport of Asian dust aerosol occurs in the middle troposphere between 2 and 5 km [*Zhao et al.*, 2006]. Figure 3.20 shows the averaged dust transport flux (filled contours) for El Niño (Figure 3-20a and La Niña (Figure 3-20b years integrated from 3 to 10 km. On the same plot, eight year anomalies (dashed contour lines) from the 44 year averaged values are also superimposed.

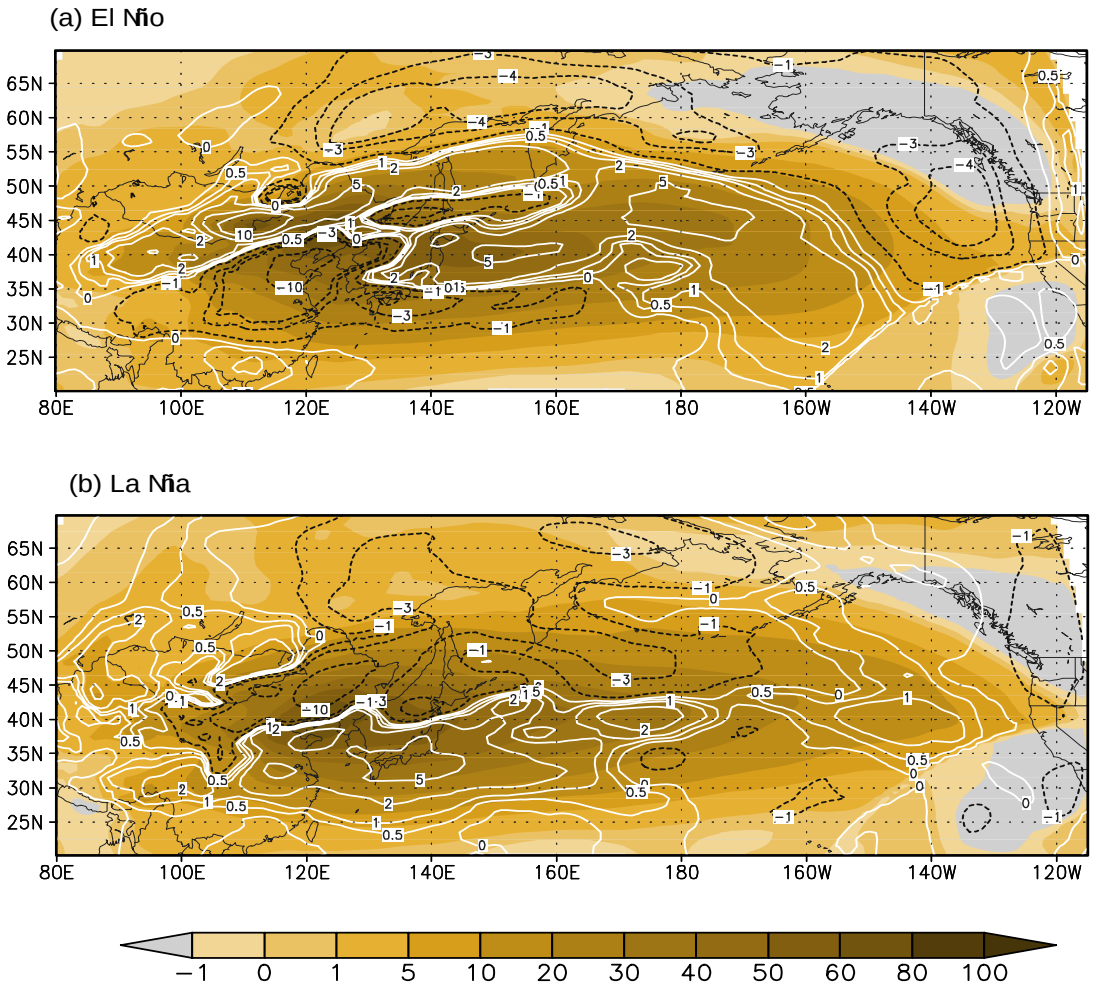

Figure 3-20. *The zonal transport fluxes ($\mu g.m^{-2}.s^{-1}$) of Asian dust in spring of (a) 8 El Niño years (1966, 73, 83 87, 87, 92, 98 and 2003) and (b) 8 La Niña years (1965, 71, 74, 76, 86, 89, 99 and 2000). The contour lines are for the anomalies relative to the 44-year mean of Asian dust aerosol in spring.*

A sharp difference between zonal transport during El Niño and La Niña years is most clearly seen in the centre of the transport path. During El Niño years, trans-Pacific transport is centred at 45° N while during La Niña years it is around 40° N. The zonal transport fluxes of Asian dust aerosol through 125° E in spring for the same El Niño and La Niña years indicate a shift of the main out-flow point in Asia from 45° N to 40° N during La Ninas. In contrast,

in the eastern Pacific (140^{o} W) where the outflow reaches the coast of North America, peak transport moves southward from 45° N to 40° N during El Nino years and to lower heights (5000 m during El Niño versus 6500 m during La Niña years).

Interannual variability of African dust transport over the north tropical Atlantic has been investigated by *Chiapello et al.* [2005] who analyzed in situ surface concentration data from Barbados beginning 1966, along with the Total Ozone Mapping Spectrometer (TOMS) and Meteosat dust optical thickness (DOT) records covering the last two decades. Their analysis shows a large regional impact of drought conditions in the Sahel on dust emissions and transport both in winter and in summer. Furthermore, the study showed that the influence of the NAO dominates the winter export and is more geographically limited to the eastern Atlantic north of 15° N, and possibly some localized source regions.

3.5.2 AEROCOM Results

AeroCom, (http://nansen.ipsl.jussieu.fr/AeroCom/AeroComhome.html), an initiative developed to compare global aerosol modules in global models, was started in 2003 to systematically identify and quantify uncertain elements in global aerosol simulations. AeroCom embarks on a two-fold strategy insofar as aerosol modules are both compared with each other and with observations. Five major aerosol types are normally considered: sulfate, black carbon, particulate organic matter, dust, and sea-salt. In an initial experiment (ExpA), modelers were asked to simulate aerosol properties for particular years in their usual configuration without any restriction to the aerosol emission data input. An analysis of the simulated aerosol life cycles shows large model diversities especially in spatial distributions, aerosol composition, and water uptake [*Textor et al.*, 2005]. Initial evaluations demonstrate the difficulty in identifying a 'best model', because model performances change by parameter, by season and by region [*Guibert et al.*, 2005; *Kinne et al.*, 2005] among the 16 international aerosol global modeling groups. Nevertheless, AeroCom provides ensemble features of global aerosol distributions derived from various models.

The zonally averaged vertical concentrations of the total (component-combined) aerosol mass for the AeroCom models are shown in Figure 3.21. The aerosol concentrations are dominated in mass by the natural aerosols: dust contributes 50% to 80% to mass in all models except two models where sea-salt is dominant. All models show two maxima, the one in the northern

hemisphere resulting from dust and that in the southern hemisphere from sea-salt in the 'roaring forties' of the South Pacific.

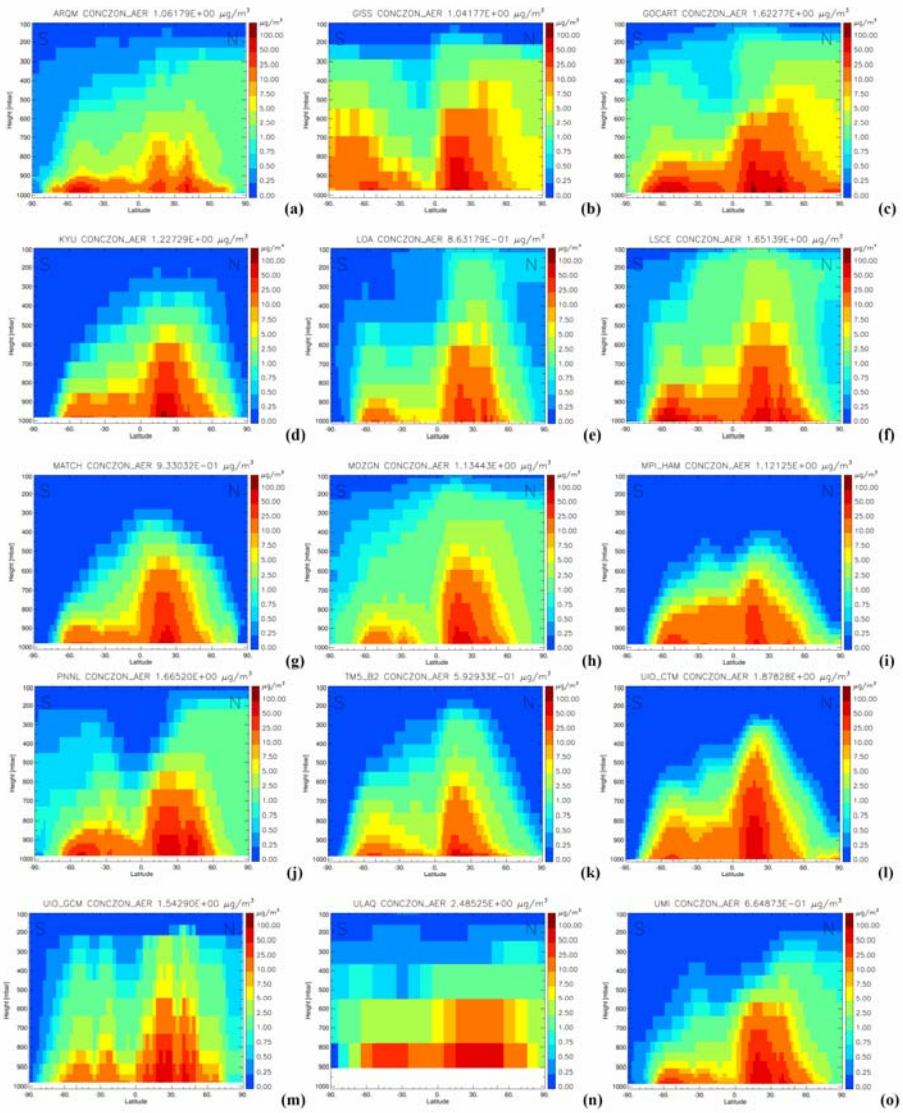

Figure 3-21. *Zonally and annually averaged concentration of total aerosol in [μg m^{-3}] Please note, we use a non-linear color scale. The white shading of lowest layer above ground in some models indicates that no data have been available in this layer.*

The highest model diversities among model results of vertical dispersivities are found for sea-salt, followed by dust, particulate organic matter, black carbon and sulfate. The ranges of vertical dispersivity, i.e., the differences for each model between the species with the largest and the smallest mass fractions above 5 km, respectively, are indicated by the gray shadings in Figure 3-22. These ranges, which indicate the degree of similarity of the vertical

dispersivity among the species within a given model, differ among the models; the all-models-average range is 25%, varying from 10% to 45%. Of the total aerosol mass, 14% is placed above 5 km height and this varies from 5% to 26%. The mass composition close to the surface, i.e., below1 km, is dominated by sea-salt in eight models and by dust in seven models. In this layer contributions to the total mass vary for sea-salt between 20% and 80% and for dust between 15% and 70%. All models have a dust mass maximum in the upper PBL between 1 and 2.5 km. Vertical dispersivity is relatively weak for the natural species. The sea-salt mass decreases strongest with height. The all-models-average mass fractions of sea-salt and dust above 5km are 9% (varying from 0.001% to 25%), and 14% (varying from 3% to 28%), respectively.

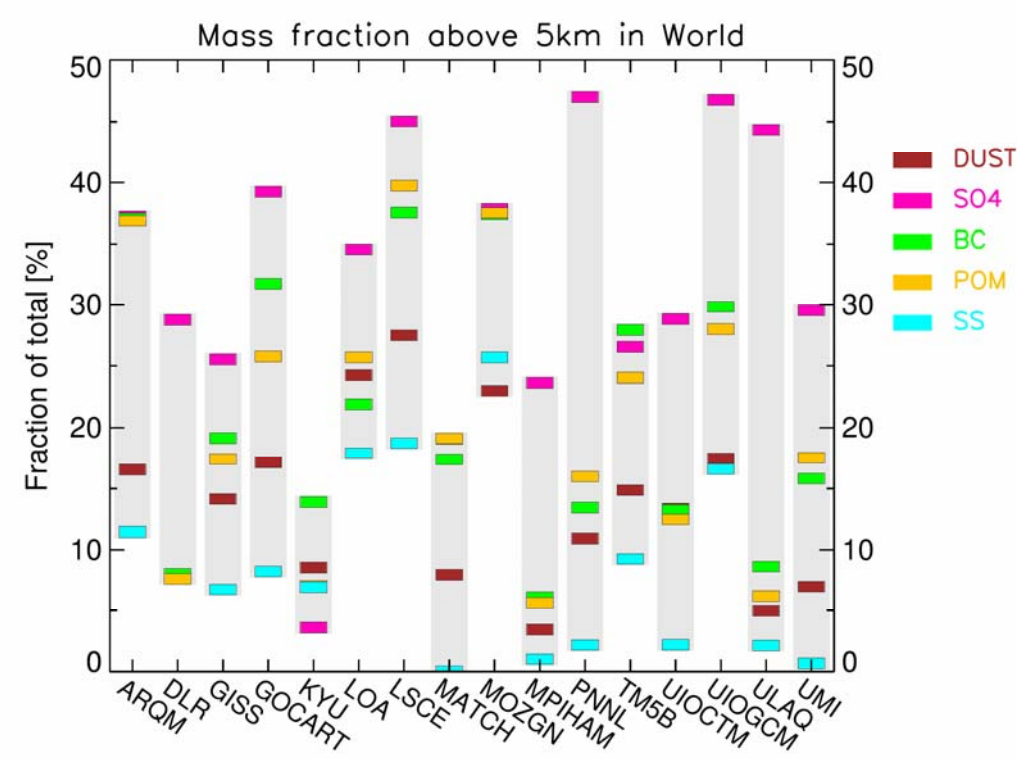

Figure 3-22. *Global, annual average mass fractions in [%] of total mass above 5 km altitude for the AeroCom models. The gray shadings frame the range for each model.*

The vertical distributions of black carbon and particulate organic matter are similar in most models. The two species are well dispersed in the vertical with the maximum situated in the upper PBL between 1 and 2.5 km in all models. The all-models-average mass fractions above 5 km are 22% (varying from 6% to 38%) and 21% (varying from 6% to 40%) for black carbon and particulate organic matter, respectively. In eight models, the vertical dispersivity

is stronger for black carbon than for particulate organic matter, in six models the situation is reversed, and in two models similar.

Sulfate is present at the highest altitudes of all species in most models. The all-models-average sulfate mass fraction above 5 km is 33% (varying from 4% to 47%). The main sulfate burden is situated in the upper PBL between 1-2.5 km in nine models, in the lower free troposphere between 2.5 and 5 km in three models, in the upper free troposphere between 5 and 10 km in one model, and above 10 km in the tropopause region in three models. In general, the sulfate-contribution to the total mass composition becomes increasingly important with height due to the removal of dust and sea-salt, and due to chemical sulfate-production at greater altitudes within the atmosphere. AeroCom predictions confirm the results of an extensive analysis of sulfur cycle simulations in large scale atmospheric models which was performed in the COSAM exercise [*Barrie et al.*, 2001; *Lohmann et al.*, 2001; *Roelofs et al.*, 2001]. The uncertainty in predicting the global sulfate distribution is related to vertical mixing of emitted sulfur species from the planetary boundary layer into the free troposphere. In addition, cloud physics and cloud distributions play a major role as they influence cloud-related processes, i.e., the aqueous oxidation of SO_2 and wet deposition. Furthermore, model agreement is low for the dry deposition of SO_2. The chemical production of sulfate at high altitudes explains why its mass fractions at higher altitudes are larger than those of dust, although these components have similar atmospheric residence times.

A similar diagnostic as for the vertical dispersivity can be performed for the horizontal distribution of aerosol. The mass fractions in Polar Regions can serve as an indicator for the horizontal dispersivity, i.e., for meridional long-range transport, because Polar Regions are far from the aerosol sources. We show the mass fractions of aerosols south of 80° S and north of 80° N, and the corresponding diversities of the model results in Figure 3-23.
The all-models-averages of the mass fractions at the poles in relation to global aerosol are 2.4% (varying from 0.3% to 8%) for total mass of five aerosol types, 6% (varying from 0.2% to 10%) for sulfate, 4.2% (varying from 0.4% to 10%) for black carbon, 3.3% (varying from 0.2% to 18%) for sea-salt, 3.3% (varying from 0.3% to 7%) for particulate organic matter, and 1.5% (varying from 0.03% to 4%) for dust, respectively. The AeroCom results show

major differences in aerosol transport and more observations especially in remote regions and vertical profiles are needed to constrain aerosol distributions.

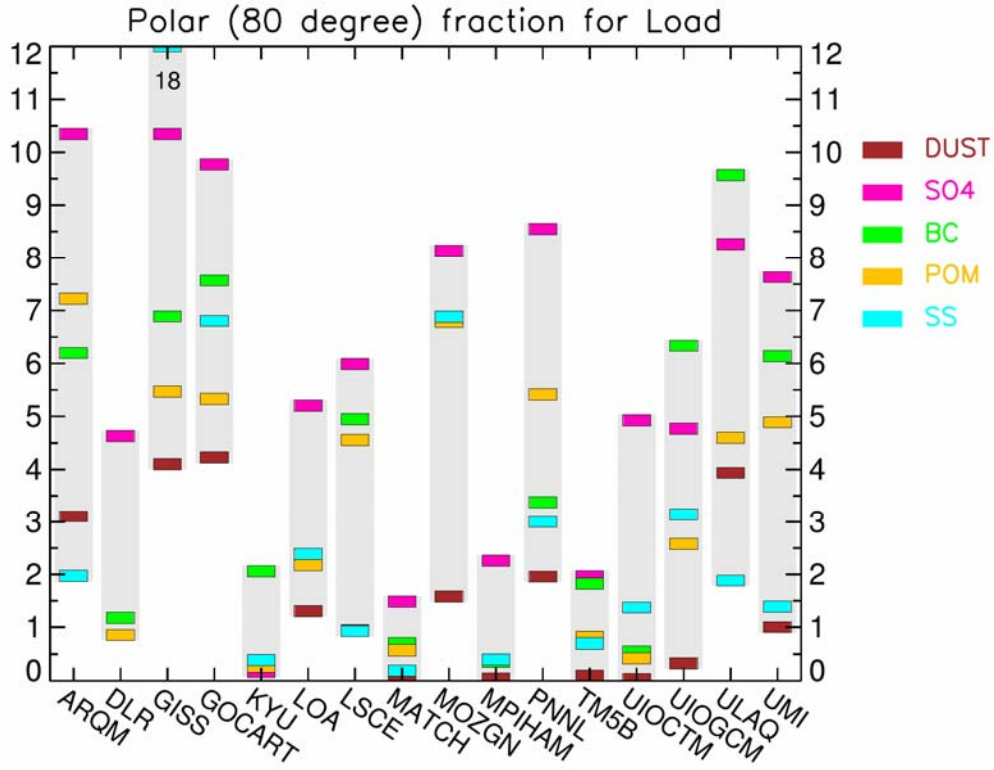

Figure 3-23. *Global, annual average mass fractions in [%] of total mass in polar regions (south of 80° S and north of 80° N) for all AeroCom models. The gray shadings frame the range for each model.*

3.6 PHYSICAL AND CHEMICAL TRANFORMATIONS

Even though there is increasing evidence that aerosol particles are predominantly a conglomerate of different internally mixed chemical substances [*Cziczo et al.*, 2004; *Kojima et al.*, 2004; *Murphy and Thomson*, 1997], most GCMs still treat aerosols as external mixtures in terms of their optical properties (e.g., [*Lohmann et al.*, 1999]). This is mainly because internal mixtures have more degrees of freedoms, are more complex, and therefore require an added computational burden. However, advanced aerosol modules in some GCMs have been expanded to include aerosol internal mixtures (e.g., [*Ghan et al.*, 2001; *Gong et al.*, 2003a]).

After aerosol particles are formed, they undergo chemical and physical transformations as they move through the atmosphere. Collision and coagulation due to Brownian motions is most important for the nucleation and Aitken-mode aerosol particles. Larger particles can collide if they have a substantial difference in gravitational settling velocity and phoretic forces. Also, vapors can condense on pre-existing aerosol particles, which is especially important for converting aerosol particles from being externally mixed (i.e., each particle is composed of only one chemical species) to being internally mixed (i.e., each particle is composed of more than one chemical species). Chemical transformation refers to chemical reactions on the surface or in the volume of aerosol particles that can increase aerosol mass, and/or change the ability of aerosols to act as CCN or IN. In-cloud oxidation and cloud processing can also produce aerosol mass. All these processes make aerosols more hygroscopic. This section reviews the processes modifying aerosols in the atmosphere and assesses their implications to the cloud and precipitation formations.

3.6.1 Aerosol Dynamics - Nucleation, Condensation and Coagulation

When condensable species such as H_2SO_4 (g) are formed in the gas phase by chemical reactions, they participate in two competing processes: nucleation and condensation on pre-existing particles depending on the particle size, vapor concentrations and source rates, and concentration, as well as relative humidity and temperature. In the atmosphere, "homogenous nucleation" is the formation of new particles from the direct aggregating or condensation of molecules in the gaseous phase without a seed, and a seed is anything that could provide a surface for the gases to condense onto during condensation or heterogeneous nucleation. The importance of a surface is that it alleviates the Kelvin effect that would increase the vapor pressure of very small drops and cause them to rapidly evaporate. Classical nucleation theory hypothesizes that pure water vapor will not homogeneously nucleate alone but will form new particles with sulfuric acid, H_2SO_4, as the mixture will have a lower equilibrium vapor pressure, and many studies have supported this idea. Still, some observations lead us to believe that a third component in the gaseous phase, such as ammonia or an ion, is necessary to induce nucleation [*Kulmala et al.*, 1998].

It is apparent that nucleation and condensation can occur at the same time. Condensation is responsible for the growth of atmospheric particles and for changing the aerosol chemical composition. When an aerosol exists in a supersaturated vapor environment, the vapor condenses on the particle population, resulting in a change of the particle size distribution.

The supersaturation is usually produced by cooling of saturated vapors via adiabatic expansion (atmospheric clouds) or by gas-phase chemical reactions yielding products of low vapor pressure (e.g., in photochemical smog or in oxidation of biogenic hydrocarbons). In the case of soluble particles, condensation can take place even in unsaturated conditions [*Hinds*, 1982]. On the other hand, higher saturation ratios may be needed for condensational growth of very small particles because the attractive forces between surface molecules are smaller due to sharply curved surface so that vapors more easily evaporate (Kelvin effect).

The condensational growth of aerosol particles is accompanied by simultaneous mass and energy transport. Analytical expressions for the condensational growth rate of a single particle have been presented by a number of researchers [*Mason*, 1971; *Kulmala et al.*, 1989; *Kulmala*, 1993]. Once the growth rate of a single particle is known, the change in particle size distribution can be obtained by solving the condensation equation [*Seinfeld and Pandis*, 1998; *Park and Lee*, 2000]. The condensational growth rate of a single particle is proportional to particle surface area (free-molecule regime) or to particle diameter (continuum regime). Its implication is that the particle size distribution becomes narrower as a result of condensational growth.

Nucleation events in a highly polluted region can produce CCN [*Laaksonen et al.*, 2005]. 2.5 years of continuous nucleation observations from San Pietro Capofiume, Italy (44°39′N, 11°37′W), showed that nucleation events occur frequently in the Po Valley region, even though the region is rather polluted with high pre-existing particle concentrations. The nucleation events are often very intensive, and the newly formed particles can grow to sizes as large as 100–200 nm in diameter within a few hours and thus constitute an important source of CCN.

Coagulation is a process whereby aerosol particles come into contact because of their relative motion then stick together to form larger particles. During coagulation process, the number of particles decreases and the average particle size increases while total mass of particles is conserved. High coagulation rates among disparate particles have another important implication, which is the change of mixing state of particles. Particles originated from different sources often have different size and chemical composition. Therefore, selected coagulation between unequal-sized particles will lead an externally mixed aerosol to

internally mixed state, which will results in changes of optical property and hygroscopic growth characteristics of the particles.

To calculate the change in particle size distribution due to simultaneous nucleation, coagulation and condensation, it is necessary to resort to numerical methods. During coagulation, however, the size distribution of particles changes by interaction of particles in so many size classes at each time step that the computing time becomes excessive for calculation of the change of concentration of particles in each size class. Considerable effort has been made to overcome this problem and to accelerate the computations [*Jacobson et al.*, 1994]. Among the most widely used numerical methods for aerosol dynamics are the modal dynamics method [*Whitby and McMurry*, 1997], which expresses the particle size distribution as a sum of two or three log-normal distribution functions, and the sectional method [*Gelbard et al.*, 1980], in which the entire particle size range is divided into a finite number of sections [*Gong et al.*, 2003a].

3.6.2 Chemical Modification by Heterogeneous Chemistry of Aerosols

In addition to the modification of atmospheric aerosols by nucleation, condensation and coagulation, there are two types of heterogeneous and chemical processes under cloud-free conditions that can take place in the atmosphere under cloud-free conditions, both leading to internally mixed aerosols and changes in hygroscopicity. These are reactive and non-reactive uptake of gases onto particles.

Non-reactive heterogeneous uptake. For the adsorption of semivolatile organics onto aerosols, particularly for persistent organic pollutants (POPs), the partitioning of the organics between the gas and aerosol phases is often modeled using the Junge-Pankow partitioning theory [*Junge*, 1977; *Pankow*, 1987; *Pankow*, 1994a; *Pankow*, 1994b] based on sub-cooled liquid vapor pressure p_{OL} (Pa). The Henry's law constants for a large number of compounds have been reported. These coefficients have been used to predict and model the gas-aerosol partitioning. Measurements of p_{OL} for many POPs have been conducted both in the laboratory and in the field, and they have been used in modeling of POP transport [*Hansen et al.*, 2005; *Malanichev et al.*, 2004; *Semeena and Lammel*, 2005]. The incorporation of organic species into the particle phase increases with pre-existing aerosol mass concentration, depending on the composition of the organic matrix, and is generally favoured at lower temperatures [*Pankow and Bidleman*, 1991]. This temperature dependency is likely a contributing factor to

the observed increase in the percentage of aerosol mass attributed to organic compounds with height in the troposphere [*Jaffe et al.*, 2005]. Recent measurements have also demonstrated that semivolatile species such as polycyclic aromatic hydrocarbons and pesticides can redistribute from submicron particles to be adsorbed onto supermicron dust particles during transport [*Falkovich et al.*, 2004].

Freshly emitted organic gases typically are fairly hydrophobic and only partly non-oxygenated. Their uptake onto the inorganic ionic sulphate- or nitrate-containing aerosols may lead to thin films on the surface of the particles. These films can significantly reduce the hygroscopicity of these inorganic ionic aerosols, altering their ability to take up water vapor, and making them less effective CCN.

The opposite effect can happen when uptake of fairly hydrophilic oxygenated organic compounds on hydrophobic particles, such as primary soot particles, occurs. Hydrophilic organic compounds are often formed in the atmosphere through gas phase photochemical oxidation of less hydrophilic precursors, for example, as hydrocarbons are oxidized to alcohols, ketones, aldehydes, and acids, as the oxidation progresses toward an eventually total breakdown of the entire molecule. Some of these oxygenated compounds can be directly emitted, particularly from biogenic sources. The end results are that the originally hydrophobic aerosols become more hygroscopic and more effective as CCNs.

3.6.3 Reactive uptake.

There has been a great deal of attention given recently to heterogeneous and multiphase reactions occurring on the surfaces and within tropospheric particles [*Ravishankara and Longfellow*, 1999]. For example, relative humidity enhances the reaction of $CaCO_3$ in dust with HNO_3 [*Goodman et al.*, 2000] and the reacted particles have been shown to be more hygroscopic than the un-reacted dust and are thus better CCN [*Krueger et al.*, 2003; *Laskin et al.*, 2005]. There is also evidence that SO_2 can be adsorbed onto mineral particles and oxidized to sulfate, creating mixed particles that may have complex hygroscopic behavior depending upon which cations are associated with the sulfate [*Usher et al.*, 2003]. Dust is also frequently associated with organic matter, although the mechanisms creating such mixtures and their effects on dust hygroscopicity are not well understood.

Deviations from model predictions by the Junge-Pankow partitioning theory based on equilibrium are often observed for organic gases and organic particulate matter in the

atmosphere [*Jang and Kamens*, 2001a; *Jang and Kamens*, 2001b]. The main reason for the deviation is that the absorbed product can further react within the host aerosols, thereby significantly increasing the capacity of the aerosols for continued uptake of the organic gases. In bulk solutions, many aldehydes form polymers under acid catalysis. Such polymerization has been proposed to occur in atmospheric aerosols [*Olson and Hoffmann*, 1989; *Tobias and P.J. Ziemann*, 2000; *Jang and Kamens*, 2001a; *Jang et al.*, 2003; *Noziere and Riemer*, 2003; *Gao*, 2004; *Kalberer et al.*, 2004]. Recent laboratory studies have shown that indeed for certain aldehydes, polymerization can occur at significant reaction rates [*Liggio et al.*, 2005a; *Liggio et al.*, 2005b]. *Liggio et al.* [2005b] observed the process of polymerization of glyoxal, a dialdehyde commonly encountered in the atmosphere from both anthropogenic and biogenic precursors, on a time scale of one to three hours in acidic aerosols and estimated that in a typical urban-suburban atmospheric environment, the glyoxal uptake alone would be sufficient to account for up to 10% of aerosol organic contents. Oligomers up to trimers were observed under conditions that can be directly applied to the atmosphere in less than one hour. This polymerization leads to a significant growth in the size and mass of the aerosols. It has been demonstrated that freshly-formed secondary organic aerosols from anthropogenic and biogenic precursors in a smog chamber continued to undergo oligomerization to higher-molecular-weight compounds over 28 h, and the particles exhibited increasing thermal stability with aging [*Baltensperger et al.*, 2005]. Interestingly, although the hygroscopicity of the particles (at 85%) increased during the first few hours, it remained virtually unchanged during the remainder of the experiment and was similar to that observed for humic-like substances (HULIs) that have been identified in atmospheric aerosols [*Brooks et al.*, 2004; *Baltensperger et al.*, 2005].

Arguably the most complex constituent of the tropospheric aerosol is the carbonaceous fraction, which includes both soot and myriad organic species. Many studies have shown that soot, although initially quite hydrophobic unless formed during combustion of high-S fuels [*Popovitcheva et al.*, 2001], becomes more hydrophilic as it ages through interaction with atmospheric gases such as SO_2, sulfuric acid, and nitric acid, and through oxidation [*Zuberi et al.*, 2005] in addition to the non-reactive uptake as discussed above. Chand *et al.* [2005] measured the hygroscopic growth of particles produced from burning of biomass in the laboratory, and noted that the growth was less than observed for aged smoke particles from similar origins. It has also been demonstrated that acidic particles catalyze the formation of secondary organic aerosol species from the gas phase on their surfaces [*Jang et al.*, 2002;

Gao, 2004], a mechanism whereby an acidic inorganic particle could become internally-mixed with organic species.

In summary, the chemical and physical aging of aerosols is generally considered to increase hygroscopicity of carbonaceous particles by mixing inorganic constituents into individual particles, and by modifying the composition of primary organic material through oxidation. The aging process is represented in many global-scale models as a simple shift from primarily hydrophobic to hydrophilic (i.e., subject to wet removal) character, occurring on a chosen e-folding time scale. *Liu et al.* [2005a] suggest, based on a modeling study that included representation of aerosol microphysics, that most carbonaceous aerosols in the troposphere are internally mixed with sulfate, nitrate, and secondary organics and are thus more hygroscopic and have significantly shorter lifetimes than predicted using typical hydrophobic-to-hydrophilic conversion rates. Clearly, more work is needed before atmospheric aerosol aging processes and their consequences for particle hygroscopicity and CCN activity are adequately represented in chemical cycle and climate models.

3.6.4 Aerosol Thermodynamics

Critical supersaturation for CCN activation depends not only on composition, but also on particle phases (e.g. crystalline vs. liquid) [*Broekhuizen et al.*, 2004]. *Nenes et al.* [1998] compared the equilibrium composition and partitioning of aerosol thermodynamic models – including their ISORROPIA, as well as the SCAPE model of *Kim et al.* [1993b] and SEQUILIB of *Pilinis and Seinfeld* [1987] – for representative urban, marine, remote continental, and non-urban continental mass loadings taken from *Heintzenberg* [1989] and *Fitzgerald* [1991]. These models consider the inorganic aerosol system of sulfate, nitrate, ammonium, chloride, sodium, potassium, calcium, magnesium, carbonate, and water. They generally agree within several percent except at high relative humidities, where differences in concentrations of particular ionic species differed by as much as 30%. The discrepancies in ionic content relate to the varying treatments especially of bisulfate, equilibrium constants, thermodynamic data, water content, and deliquescence. Using the coupled IMAGES-SCAPE2 model, Rodriguez and Dabdub [2004] found that nitrate concentrations predicted compare better with observations than those calculated with IMAGES alone. They also find that over polluted continental regions, the presence of sea-salt and dust aerosol potentially increases the formation of aerosol sulfate by 20–80%. Aerosol nitrate formation is enhanced by 14–60%, whereas ammonium formation is decreased by 20–60%. The AeroCom results

showed a global annually-averaged all-models-mean water mass fraction of 53% ranging from 9% to 99.9% [*Textor et al.*, 2005].

The partitioning and solubility of organic species is critically important to the resolution of questions surrounding the indirect effect of aerosols on clouds. Organic aerosols and condensable organic species are observed in all environments, and they are the dominant aerosol-phase species in some. Organic species also no doubt contribute to the composition of many primarily inorganic particles [*Abdul-Razzak and Ghan*, 2000]. However, the state of the science is such that the great majority of the organics present in aerosol are unidentified. For those that have been identified, the lack of measurements of solubilities and their dependence on inorganic solute concentration is imposing, not to mention the lack of a suitable unified thermodynamic formulation for mixed inorganic/organic aerosol [*Saxena et al.*, 1995; *Cruz and Pandis*, 1997; *Turpin et al.*, 2000; *Clegg and Seinfeld*, 2004]. The impact of the chemical compositions on aerosol activation is discussed in the following section.

3.6.5 Activation of Mixed Aerosols

Information on the spatial distributions of CCN and IN and how their numbers concentrations respond to changes in emissions of various particle types and particle precursors would be the key to understanding and predicting the effects of aerosol particles on clouds and precipitation. Unfortunately, information can generally only be generated by models because the methods for measuring CCN and IN remain complex and few extensive data sets exist. The most notable long-term studies of CCN have been made at Cape Grim, Tasmania [*Gras*, 1995] and Mace Head, Ireland [*Jennings et al.*, 1997], although a new CCN monitoring program is being established at Barrow, Alaska (R. Schnell, NOAA Earth System Research Laboratory, personal communication).

An increasing body of evidence suggests that the complexity of atmospheric aerosol may preclude realistic treatment of cloud formation using the levels of simplification incorporated into all large-scale models (and even most process-level descriptions). Thus, this sub-section will discuss the compositional complexity of atmospheric aerosol and the derived properties of their size and composition distributions that are thought to affect their ability to act as CCN. This has been thoroughly discussed in a recent review paper by *McFiggans et al.* [2005].

It is clear from all forms of the Köhler equation that any component of an activating particle, which can significantly alter the surface tension, may influence its activation behavior. All other things being equal, a reduction in surface tension will lead to a reduction in the Kelvin term, hence reducing the critical supersaturation and leading to possible effects on cloud formation [*Shulman et al.*, 1996; *Facchini et al.*, 1999; *Feingold and Chuang*, 2002; *Nenes et al.*, 2002; *Lohmann et al.*, 2004].

Broekhuizen et al. [2004], *Bilde and Svenningsson* [2004] and *Henning et al.* [2005] studied aspects of the effects of slightly soluble substances on CCN activation. All studies found that the initial particle phase played a significant role in the critical supersaturation of particles containing only slightly soluble substances. If the particle was initially totally liquid the critical supersaturation was found to be lower. *Bilde and Svenningsson* postulated that an increased critical supersaturation was due to an undissolved core forming an "activation barrier" when smaller than the fully dissolved wet size. Whilst the RH history (in terms of predicted deliquescence/ efflorescence relative humidities) of a particle in the atmosphere may be such that solid phases should exist for single organic components in solution, *Marcolli et al.* [2004] recently demonstrated that multicomponent organic solutions favored the liquid phase. For complex mixtures found in the atmosphere, it may be expected that aerosol comprising slightly soluble organics would be unlikely to contain undissolved material. Even relatively small amounts of ionic material can allow the activation of organic particles [*Lohmann et al.*, 2004; *Ervens et al.*, 2005], though the abundance and nature of organics will affect both equilibrium water content and droplet growth kinetics.

In contrast to the detailed studies discussed above, the treatment of aerosol activation in GCMs is much simpler. Most of the earlier studies concerned with the effect of aerosol particles on the climate system have taken sulfate particles as a surrogate for all anthropogenic aerosols [*Jones et al.*, 1994; *Boucher and Lohmann*, 1995]. Lately most major GCMs also include carbonaceous aerosols, dust and sea salt (Section 3.2.4.2).

The importance of mixed sea-salt/sulfate aerosols versus pure sulfate aerosols for predicting the cloud droplet number concentration (CDNC) in a GCM was discussed by *Gong and Barrie* [2003]. They found that the presence of sea-salt aerosol generally increases the mass mean diameter (MMD) of sulfate aerosols from 0.3 to 0.7 μm downwind of both polluted

North American and East Asian continents (Figure 3-24). Early reviews of atmospheric sulfate size distributions [*Whitby*, 1978; *Milford and Davidson*, 1987;] concluded that sulfate mass is present largely in the accumulation mode with a mass mean diameter of about 0.4-0.6 μm. Recent measurement during INDOEX [*Venkataraman et al.*, 2002] showed that sulfate aerosol over the coastal city Mumbai, India has a trimodal distribution with a dominant MMD of 0.6 μm. The simulated MMD of 0.7 μm in the *Gong and Barrie* study for mixed sea-salt and sulfate aerosols agrees with the observations better than sulfate-only MMD of 0.3 μm. Changes in the MMD will further alter the residence time, cloud formation and global distributions of sulfate aerosols. A reduction of 20–60% in the marine cloud droplet number concentrations was predicted because of the presence of sea salt, with greatest reductions in the roaring forties and in the northern hemisphere mid-latitudes where the sea salt concentrations were high. Similarly, along the equatorial regions some enhancement in CDNC was simulated because of the presence of sea-salt aerosols. Likewise the difference in treating sulfate and carbonaceous aerosols as an internal mixture rather than an external mixture in a GCM, reduces the total indirect aerosol effect from -1.5 W m^{-2} to -1.1 W m^{-2} [*Lohmann et al.*, 2000].

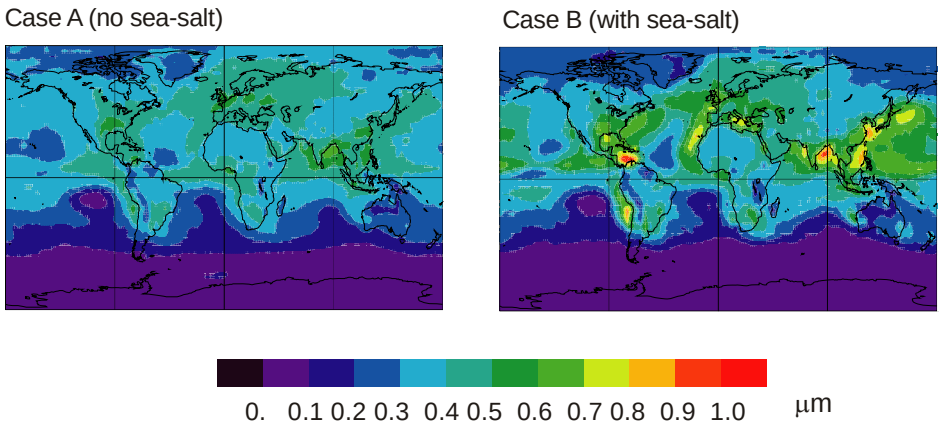

Figure 3-24. *The effect of sea salt aerosol on non-sea salt sulfate. Simulated sulfate mass mean diameters (MMD) in Spring (MAM) for two cases: (a) no sea salt present and (b) with sea salt present (Gong and Barrie, 2003).*

Cloud processes can also change the mixing status of aerosols. Particles that serve as CCN and are incorporated into fog and cloud water can become mixed in composition via

collision-coalescence [*Flossman et al.*, 1985; *Feingold et al.*, 1996] and through aqueous-phase chemical reactions that create nonvolatile species which remain in the particle phase if the drop evaporates before it is lost to precipitation [*Ervens et al.*, 2004]. *Levin et al.* [1996] suggested that cloud processing produced the sulfate coatings they observed on the surfaces of some desert dust particles. During stagnation events in California's Central Valley, the formation of extensive fog with high liquid water contents was associated with increases in both total aerosol mass concentrations and in the degree of internal mixing of species within individual particles [*Whiteaker et al.*, 2002].

Nucleation scavenging can also occur below the freezing level, when aerosols are scavenged by serving as IN. Knowledge on ice nucleation has been advanced considerably in the last decade, although major challenges still remain. A commonly used approach to heterogeneous freezing is an extension of the classical theory of homogeneous nucleation. The problem lies how one quantifies the reduction of the energy barrier between the supercooled liquid and the crystal because of the influence of a substrate. Several unsolved issues related to heterogeneous ice nucleation were recognized by *Cartrell and Heymfield* [2005]. These include properties of the heterogeneous nuclei, mechanism of contact nucleation, evaporation nucleation, and the role of organic compounds in ice nucleation.

3.7 REMOVAL OF ATMOSPHERIC AEROSOLS

Aerosols are removed from the atmosphere by dry and wet deposition, and the average residence times of atmospheric aerosols are of the order of a few days to a week. Clearly the residence times of any particular particle depends on its size and location. Larger aerosols settle out of the atmosphere very quickly under gravity, and some surfaces are more efficient at capturing aerosol than others. We will first examine some removal pathways before looking at how aerosol may be expected to change during the course of its atmospheric residence. Both removal processes need to be parameterized in global climate models and this results in rather large uncertainties in budgets.

3.7.1 Size-dependent Dry Deposition of Aerosols

Atmospheric aerosols can be removed from the atmosphere through dry deposition. They first have to be transported to the Earth surface where they are adsorbed by canopy external surface, leaf stomata, underlying soil, and any other kind surfaces such as water, ice and snow. Thus, the characteristics of the atmosphere, the nature of the surface, and the

physical/chemical properties of the atmospheric aerosols all affect the dry deposition [*Ruijgrok et al.*, 1995; *Zufall and Davidson*, 1998; *Wesely and Hicks*, 2000]. Although the dry deposition process is a slower process compared to wet deposition, it is a continuous event happening anytime over any surfaces. The accumulated amount of dry deposition can be much more important for some aerosol species/sizes [*Ginoux et al.*, 2001]. Carefully addressing dry deposition of particles in large-scale models is still a challenging task (see table 7 in *Textor et al.* 2005). However, considering the existing large uncertainties from different models [*Rasch et al.*, 2000]. This is especially important for the coarse aerosols types, sea salt and dust, where dry deposition contributes about 2/3 of the total deposition flux as shown for the AeroCom models [*Textor et al.*, 2005].

Most measurements on aerosol flux made between 1970-1990's are bulk sampling due to the limitations in aerosol measurement techniques [*Sehmel*, 1980; *Nicholson*, 1988; *Sievering*, 1989]. The development of more sophisticated measurement techniques in 1990's made it possible to measure size-resolved aerosol physical and chemical properties. The number of studies making direct aerosol fluxes using eddy correlation method also greatly increased [*Gallagher et al.*, 2002].

The process of particle dry deposition includes several mechanisms. Transported from the free atmosphere down to the viscous sublayer that envelops all surfaces is the first process. This happens due to passive transport within turbulent eddies, or for larger particles through sedimentation. They then are transported across the viscous sublayer by Brownian diffusion, phoretic effects, inertial impaction, interception or sedimentation. Brownian diffusion is the most important mechanism for very small particles (<0.1 μm) and its importance decreases rapidly as particle size increases. Gravitational setting dominates over other mechanisms for particles larger than 10 μm, although interception and impaction can be as important as gravitational setting under certain conditions (e.g., over forest). Impaction and interception are most important for particles of size 2-10 μm. None of the mechanisms is very effective in the deposition of particles of 0.1-2 μm.

Once across the viscous sublayer, particles will then interact with the surface, either sticking to the surface or bouncing off [*Ruijgrok et al.*, 1995]. A small fraction of very small particles may also diffuse into leaf stomata. After collected by leaf surface, water-soluble particles

may be gradually removed by wetting and insoluble particles may become embedded in epicuticular waxes. Both soluble and insoluble particles collected by surfaces may undergo chemical changes.

Deposition velocity generally increases with particle size for particles larger than 2 μm and increases again with the decrease of particle size for particles smaller than 0.1 μm. Available measurements show that deposition velocities of ultra-fine particles (< 0.01 μm) at field conditions can be higher than 5 cm s^{-1} [*Schery and Whittlestone*, 1995]. Particles larger than 2 μm tend to have a deposition velocity as high as a few cm s^{-1} over rough forests, (e.g., [*Hofschreuder et al.*, 1997]. Deposition velocities for particles in the size range of 0.1-2 μm can vary by several orders of magnitude.

Many earlier laboratory experiments suggest that deposition velocity for this size range particles should be of the order of 0.01 cm s^{-1} or less, over both smooth and rough surfaces [*Nicholson*, 1988]. Higher values have been obtained in many more recent field studies investigating some trace species which are usually considered to be representative of particles in this size range. Aerosol sulfate has been frequently used as a convenient marker, due to its ubiquitous nature and chemically conservative behavior. Field observations for sulfate and other sub-micron particles showed that the dry deposition velocities are one to two orders of magnitude higher than in some earlier studies [*Gallagher et al.*, 1997; *Gallagher et al.*, 2002], and references therein).

A review by *Nicholson* [1988] showed that some authors attempted to explain some of the higher dry deposition velocities by invoking meteorological factors and sampling errors. However, *Gallagher et al.* [1997] demonstrated that the recently observed higher deposition velocity values, typically 1 cm s^{-1} or more, for sub-micron aerosols deposition to a forest, are consistent across the aerosol size spectrum, despite the very different techniques involved. *Gallagher et al.* [1997] stated that previous model studies significantly underestimated dry deposition velocities, especially for sub-micron particles, over rough vegetated surfaces.

There are some models which calculate particle dry deposition velocity as a function of particle size [*Zhang et al.*, 2001; *Nho-Kim et al.*, 2004]. Some of the size-segregated dry deposition models apply only to one type of surface [e.g., *Davidson et al.*, 1982; *Williams*,

1982; *Peters and Eiden*, 1992]; others apply to any type of surface [e.g., *Giorgi*, 1986; *Zhang et al.*, 2001; *Nho-Kim et al.*, 2004]. Estimates from several models [*Ruijgrok et al.*, 1995] revealed that they differ from each other greatly and the largest uncertainty is for the 0.1-1.0 μm particle size range, which is not important for mass fluxes but is important in terms of number concentrations.

Field measurements of dry deposition fluxes for specific particle sizes over different natural surfaces (e.g., using eddy-correlation method above canopies rather than using surrogated surfaces) are needed in order to better understand this process and to improve existing models or develop new models. Meteorological conditions and surface characteristics need to be measured simultaneously in order to relate the dry deposition process to different controlling factors.

3.7.2 Wet Deposition

Wet deposition (or precipitation scavenging) is usually split into two categories, in-cloud and below-cloud scavenging. In-cloud scavenging includes contributions from both nucleation and impaction scavenging while below-cloud scavenging only includes contributions from impaction scavenging.

3.7.2.1 Below-cloud scavenging

Falling raindrops collide with aerosol and collect them within the swept volume that is proportional to the falling velocity and the particle sizes. This process is referred to as gravitational capture. For practical considerations, the below-cloud scavenging of aerosols is typically represented by a scavenging coefficient (S_c) in aerosol mass continuity equations in large scale models. Different approaches have been used to represent wet scavenging in current global models [*Textor et al.*, 2005]. Note that S_c for bulk number concentration and bulk mass concentration are expected to be different; however, they are the same for the number and mass concentrations for a specific aerosol size.

Whether or not aerosols within the swept volume are collected through below-cloud scavenging depends on the sizes of the drops and the particles and on their relative locations and is expressed in terms of the collection efficiency *Ec*. Usually, *Ec* is smaller than the theoretical value, because particles can follow the streamlines around the drop. It can however be much larger than one under certain conditions, e.g., for charged particles. For small aerosol particles with little inertia Brownian diffusion is important that can bring them

into contact with the drop thus increasing their collection efficiency. Apparently, the Brownian diffusion of particles decreases rapidly as particle size increases and this mechanism will be most important for particles having a diameter smaller than 0.1 μm. Large aerosols tend to experience inertial impaction because of their inertia which prevents them from following the rapidly curving streamlines around the falling droplets. Inertial impaction increases with the increase of particle size and is important for particles larger than 2 μm. Interception and inertial impaction are closely related, with interception occurring as a result of a particle's size irrespective of its mass while inertial impaction occurs due to its mass and not its size. For particles within the size range of 0.1-2 μm, commonly referred to as 'Greenfield gap' in the literature [*Greenfield*, 1957], neither the Brownian diffusion nor the inertial impaction plays an effective role. Thus the collection efficiency is smallest in this size range [*Slinn*, 1984; *Pruppacher and Klett*, 1997].

Collection of aerosols by snow crystals is more complicated than by liquid drops due to the irregular shape of ice elements. Large uncertainties exist in the collection efficiency between experimental result and theoretical predictions, especially for submicron particles. The differences between collection efficiencies by rimed and unrimed snow crystals seem to be small [*Murakami et al.*, 1985]; and references therein), although earlier laboratory studies showed an enhancement of collection by rimed snow crystals. Collection efficiencies depend on the shape of the particles and generally increase with the temperature. Charged snow crystals may also increase the collection efficiencies (see a review by [*Jennings*, 1998].

With the development of size-resolved aerosol modules within large-scale models, new parameterizations of S_c as a function of aerosol size need to be developed [e.g., *Jung et al.*, 2003]. Particles ranging from 0.001 to 20 μm have to be included in climate and air-quality models and S_c values for this size range can differ by three to five orders of magnitude. Other precipitation properties such as total droplet surface area may be needed in parameterizing S_c [*Zhang et al.*, 2004], especially under situations when the total aerosol number, not just aerosol mass, is a concern. This also further explains the large variation of S_c for sub-micron particles even under similar precipitation conditions.

3.7.2.2 In-cloud scavenging

In-cloud scavenging of atmospheric aerosols includes contributions from nucleation scavenging and impaction scavenging. Nucleation-scavenging almost completely removes all

aerosol mass within a cloud layer under usual atmospheric conditions [*Flossmann et al.*, 1985]. This is even true in stratiform clouds with very low supersaturations because a large fraction of aerosol mass is associated with a small amount of large aerosols which can be quickly activated. Impaction scavenging inside the cloud layer removes little aerosol mass; however, this process can remove substantial amount of small size aerosols if the clouds last for more than a few hours [*Zhang et al.*, 2004].

The mechanisms of impaction scavenging for in- and below-cloud scavenging are basically the same. The main difference is that cloud droplets inside the cloud-layer are generally much smaller than raindrops below the cloud. Thus, carefully parameterizing the collection efficiency of small size aerosols by small droplets is very important for in-cloud impaction scavenging if the interstitial aerosol number concentration inside the cloud-layer is a concern.

Residence Times of Various Aerosols

Some common features in deposition patterns have been found using global simulation results[*Ginoux et al.*, 2001; *Zhao et al.*, 2003; *Han et al.*, 2004; *Satake et al.*, 2004]. Large particles usually deposit rapidly close to their sources (e.g., within the continent). On the other hand, small particles, especially submicron particles, can be transported far away from their sources (e.g., Asia to North America, Africa to Atlantic Ocean).

The residence time τ cannot be measured globally, but has to be obtained from model simulations. It is independent of model differences in emissions strengths and reflects the integral of all simulated aerosol properties and processes. The residence time is controlled by the aerosol properties as it depends on particle size and solubility, but also the model-specific transports and parameterizations of aerosol processes. In addition it reflects the spatial distributions of aerosols, particularly as they relate to relative humidity, precipitation, and surface properties.

Figure 3-25 shows the simulated residence times from the AeroCom models [*Textor et al.*, 2005]. Sea salt has the shortest τ of about half a day, followed by sulfate and dust with about four days, and particulate organic matter and black carbon with about six and seven days, respectively. The largest model diversities in the residence times are found for the coarse aerosol types, in particular for sea salt.

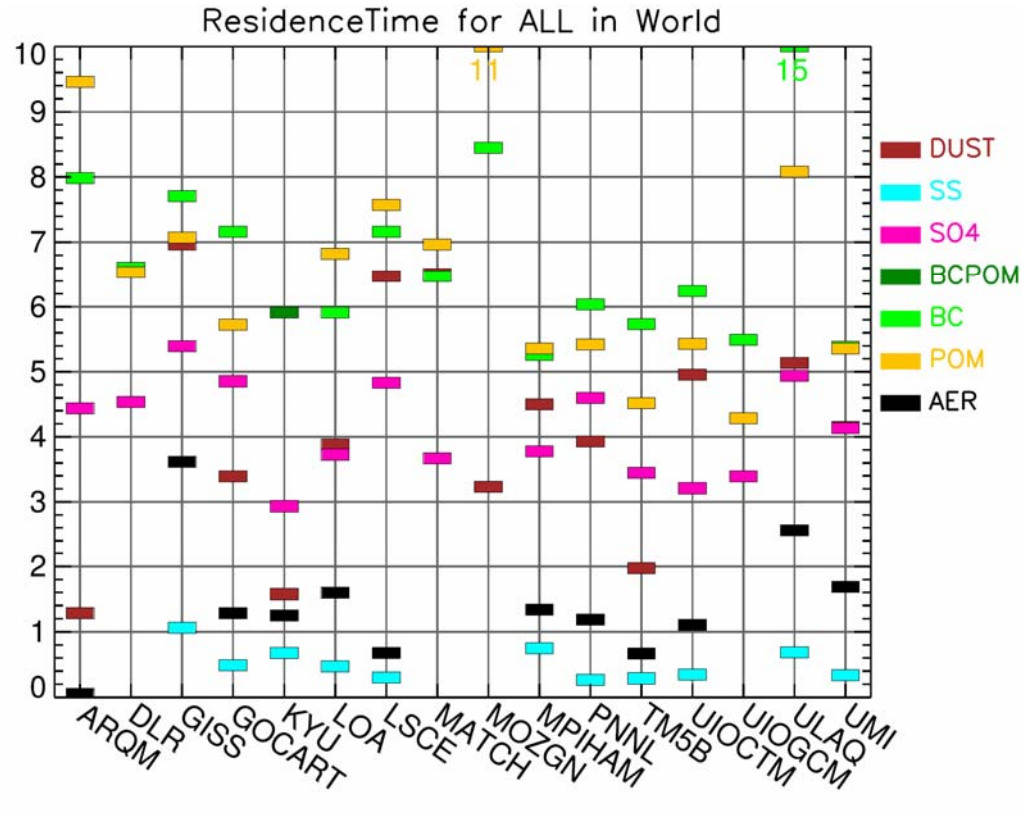

Figure 3-25. *Tropospheric residence times [days] in the AEROCOM models for different aerosol components.*

The residence time also varies with geographic locations. The size dependence of sea-salt residence time was investigated by *Gong et al.* [2002] for diameter ranges from 0.01 μm to 40.96 μm. For two size ranges of sea-salt aerosols, the residence time follows a similar pattern; that is, τ is larger on either side of the equator than at middle or high latitudes. There are two subtropical anticyclones in the Southern Hemisphere. One is in the Pacific Ocean and another in the Indian Ocean. Three climatologically persistent subtropical anticyclonic regions prevail in the Northern Hemisphere. Two are in the Pacific Ocean and one in the

Atlantic Ocean. These anticyclones are regions of long aerosol residence time. They are located on either side of the ITCZ where tropical cyclones with strong precipitation scavenging of aerosols are frequent. The removal of sea-salt is less in the anti-cyclonic regions resulting in a residence time peak.

3.8 RECOMMENDATIONS

To better understand aerosol impacts on surface precipitation the following activities are needed:

Systematic observational studies of aerosols and precipitation within the framework of a strategy that will better separate pollution aerosol effects on surface precipitation from other factors that influence precipitation (meteorological, natural aerosols, gaseous pollution etc).

Measurement of giant cloud condensation nucleii embedded in the strategy for the assessment of the impact on precipitation.

A review of the rationale and measurement strategy for systematic CCN observations including a program for validation and inter-comparison of CCN measurement methodologies.

Systematic global observations of aerosol number and composition size distributions in the lower to middle troposphere including vertical profiles.

Development of a suitable parameterization of aging and transformation processes and incorporation into weather and climate models to account for: (i) the secondary organic aerosol fraction, (ii) the hygroscopic nature of particles and (iii) modifications of aerosol optical properties by physical and chemical transformation processes.

Development of improved aerosol remote sensing techniques in the critical diameter range of cloud condensation nuclei formation (~80 to 100 nm).

Studies of cloud droplet activation as a function of chemical compositions of aerosols and cloud dynamics such as vertical velocity and turbulent mixing.

A global map of the conditional distribution of aerosols and aerosol-susceptible-precipitation.

CHAPTER 4: CLOUDS AND PRECIPITATION

Lead Author: Peter V. Hobbs, Sandra Yuter, William Cotton

Co-Authors: Z. Levin, M. Shepherd, J. Hallett

Contributors: U. Lohmann, G. Feingold

In this chapter we provide a detailed account of the basic physical processes responsible for the formation of clouds and precipitation. A number of important concepts are discussed and terms defined which will be used in later chapters.

4.1 FORMATION AND STRUCTURE OF CLOUDS

4.1.1 Dynamical Aspects of Cloud Formation

Clouds form in air that has become supersaturated with respect to liquid water or ice. By far the most common means by which air becomes supersaturated is through air ascending, which results in adiabatic expansion, cooling, and supersaturation. The principal types of ascent, each of which produces distinctive cloud forms, are:

Local ascent of warm, buoyant air parcels in a conditionally unstable environment which produces convective clouds. These clouds have diameters from about 0.1 to 10 km and air ascends in them with velocities of a few meters per second, although updraft speeds of several tens of meters per second can occur in large convective clouds. These lifting rates produce water (liquid and/or ice) contents of about 1 gram per cubic meter of air, although much higher values can occur in vigorous updrafts. The lifetimes of convective clouds range from minutes to several hours. However, from a precipitation point of view, cloud lifetime is not as important as the Lagrangian time scale (t_p), which is the time it takes a parcel of air to enter and exit a cloud. Ordinary cumulus clouds, for example, have typical depths of ~1500 m and characteristic updraft speeds of 3 m s^{-1}. Therefore, t_p = 1500 m/3 m s^{-1} = 500 s $\simeq$ 8 min. This represents the time available for initiation of precipitable particles. Once initiated, precipitation may continue over the remaining lifetime of the cloud. Ordinary thunderstorms, while having depths of ~10 km and updraft speeds of ~15 m s^{-1}, exhibit a Lagrangian time scale of t_p = 10,000 m/15 m s^{-1} $\simeq$ 660 sec $\simeq$ 11 mins, only slightly longer than cumulus clouds. The main advantage that an ordinary cumulonimbus cloud experiences over that of a

cumulus cloud in forming precipitable particles is associated with the greater amounts of condensate that is produced as moist air ascends through the depth of the troposphere. Because precipitation growth by collection is a non-linear function of the amount of condensate in a cloud [*Kessler*, 1969; *Manton and Cotton*, 1977], precipitation proceeds quite rapidly in cumulonimbus clouds relative to low liquid water content cumulus clouds. In spite of their relatively long lifetimes, due to their strong updrafts (~40 m s^{-1}), a 12,000 m deep supercell has a Lagrangian time scale of only t_p = 12,000 m/40 m s^{-1} = 300 s = 5 mins, which is shorter than that for cumulus clouds. This time scale is so short that in spite of the large amounts of condensate that they produce, a characteristic feature of supercell storms is the bounded weak echo region [*Browning and Ludlam*, 1962; *Marwitz*, 1972]. This is a region of the storm where updrafts are so strong that there is not sufficient time to produce radar-detectable precipitation elements.

Cloud top radiative cooling can lead to destabilization of cloudy layers. This is the main driving force for marine stratocumulus clouds, for example. It is also important in fogs, stratus clouds and cirrus clouds. Longwave radiative flux divergence at cloud top creates cooling of the air which, in turn, produces higher density air parcels that descend through the cloud layer causing vertical mixing. In the case of a marine stratocumulus layer in which the sea surface temperatures are slightly warmer than the overlying air, the descending cool air parcels can descend through most of the unstable sub-cloud layer, which enhances vertical mixing through the depth of the cloudy boundary layer. Typical lifetimes of stratus and stratocumulus clouds are long, being ~6 to 12 h. The parcel lifetimes for 1000 m deep clouds having vertical velocities of ~0.1 m s^{-1} is t_p = 1000 m/0.1 m s^{-1} = 10^4 s $\simeq$ 3 h. Thus, in spite of the fact that they have liquid water contents of only ~0.1 g kg^{-1}, the long Lagrangian time scales permit the formation of precipitation, in the form of drizzle, in stratus and stratocumulus clouds.

Forced lifting of stable air to produce layer or stratiform clouds. Such clouds can occur at altitudes from ground level to the tropopause and extend over hundreds of thousands of square kilometers. Lifting rates range from a few centimeters per second to ~10 cm s^{-1}. Layer clouds generally exist over periods of tens of hours, but their Lagrangian time scales are similar to that of stratocumuli being ~10^4 s. Again, due to their long Lagrangian time scales, precipitation is likely in these clouds in spite of their small water contents (~0.5 g kg^{-1}).

Forced lifting of air as it passes over hills or mountains to produce orographic clouds. Updraft velocities depend upon the speed and direction of the wind and the height of the barrier, but they can be several meters per second.Water contents are typically a few tenths of a gram per cubic meter of air. Orographic clouds may be quite transitory, but if winds are steady they may last for many hours. However, the relevant time scale that determines the time available for precipitation formation is not the time that it takes a parcel to ascend from cloud base to cloud top. Instead, it is the time that it takes a parcel to transect from the upwind lateral boundary to its downwind boundary, as shown in Figure 4-1. For example, for a 15 m s^{-1} wind speed and a cloud of 18,000 m lateral extent, t_p = 18,000 m/15 m s^{-1} = 1200 s = 20 min. This time scale is longer than that for cumulus clouds but considerably shorter than that for stratus clouds. Since the liquid water contents of stable, wintertime orographic clouds are low, production of precipitation requires either high precipitation efficiency such in shallow maritime clouds passing over mountains near shore or deeper ice-phase clouds with longer Lagrangian time scales.

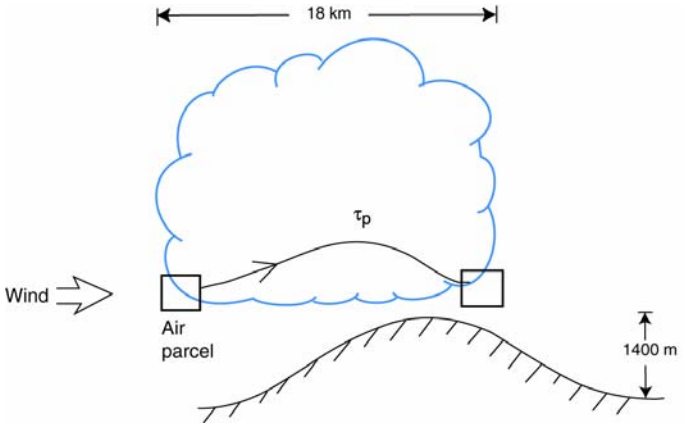

Figure 4-1. *Schematic of a stable orographic cloud indicating the trajectory of an air parcel through the cloud, which determines the Lagrangian time scale (t_p) for the development of precipitable particles.*

Keep in mind that the above concepts of a cloud are based on simple "back-of-the-envelope" calculations. In general clouds are very turbulent and thus the time-scales for precipitation formation can be much longer than simple Langrangian parcel estimates. Likewise the liquid water contents of clouds can be quite variable. In cumulus clouds it is not uncommon to find regions of high liquid water content, say 0.5 to 1.0 gram per cubic meter next to regions with hardly any condensate only tens of meters away. Often cumulus clouds exhibit considerable asymmetry is structure with upshear parts of the cloud experiencing little mixing and turbulence and downshear portions experiencing very large mixing and turbulence. In such a

cloud hydrometeors undergo growth on the upshear side and experience evaporation and turbulence on the downshear side (see discussion in *Cotton and Anthes*, 1989, Chapter 8).

4.1.2 Warm Clouds

If all portions of a cloud are warmer than 0ºC it is referred to as a *warm cloud*. Clearly, a warm cloud can contain only water droplets and no ice.*

4.1.2.1 Cloud Droplet Formation

Atmospheric aerosols make an important contribution to the heat balance of the Earth's atmosphere [*IPCC*, 2001]. However, another important effect of aerosols on climate and climate change is through their role in the formation of cloud particles and precipitation, which is the subject of this Assessment.

Kelvin [1870] derived an expression (called *Kelvin's Equation*) for the effect of the curvature of the surface of a small water droplet on the equilibrium water vapor pressure immediately above its surface. This equation can be used to determine the radius *r* of a droplet that is in (unstable) equilibrium with air with a given water vapor pressure (or equivalent relative humidity or supersaturation). This relation is shown plotted in Figure 4-2. It can be seen from this figure that a pure water droplet of radius 0.01 μm requires a relative humidity of ~112% (i.e., supersaturation of ~12%) to be in (unstable) equilibrium with its environment. A droplet of radius 1 μm requires a relative humidity of only 100.1% (i.e., supersaturation of 0.1%) to be in (unstable) equilibrium with its environment.

Since the supersaturations that develop in clouds due to the adiabatic expansion of air rarely exceed 1%, even embryonic droplets with radii as large as 0.01 μm, which might form by the chance collisions of water molecules (i.e., *homogeneous nucleation*), will be well below the size required for survival at 1% supersaturation. Consequently, droplets do not form in natural clouds by homogeneous nucleation. Instead they form by *heterogeneous nucleation* onto atmospheric aerosol.

* Regions of a cloud just below the melting level may contain ice remnants of ice from aloft, but these quickly melt.

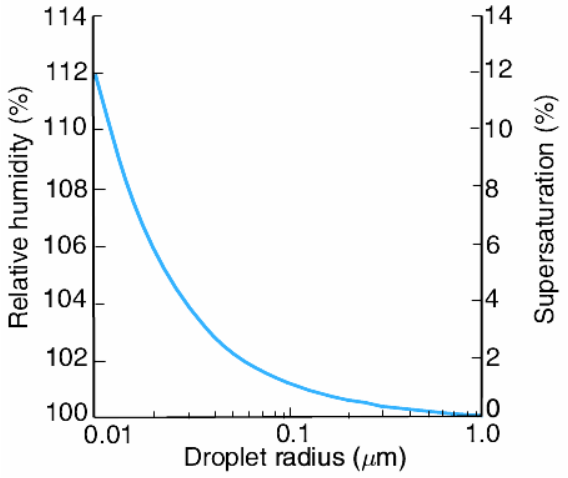

Figure 4-2. *The relative humidity and supersaturation (both with respect to a plane surface of pure water) with which pure water droplets are in (unstable) equilibrium at 5°C. From Wallace and Hobbs [2006].*

By combining Kelvin's equation with Raoult's Law for the effect of soluble materials on lowering the equilibrium vapor pressure above a solution droplet, *Köhler* [1926] determined the equilibrium vapor pressure above small solution droplets (Figure 4-3). It can be seen from the curves shown in Figure 4-3 that below a certain droplet size, the relative humidity of the air adjacent to a solution droplet is less than that which is in equilibrium with a plane surface of pure water at the same temperature (i.e., 100%). As a droplet increases in size, the lowering of the equilibrium vapor pressure above its surface due to the dissolved material becomes increasingly less and the Kelvin curvature effect becomes the dominant influence.

Suppose a particle of NaCl with mass 10^{-19} kg is placed in air with a water supersaturation of 0.4% (indicated by the dashed line in Figure 4-3). As can be seen from Figure 4-3, condensation would occur on this particle to form a solution droplet, and the droplet would grow along the red curve in Figure 4-3. As it does so, the supersaturation adjacent to the surface of this solution droplet will initially increase, but even at the peak in its Köhler curve the supersaturation adjacent to the droplet is less than the ambient supersaturation. Consequently, the droplet will grow over the peak in its Köhler curve and down the right-hand side of this curve to form a fog or cloud droplet. A droplet that has passed over the peak in its Köhler curve and continues to grow is said to be *activated*.

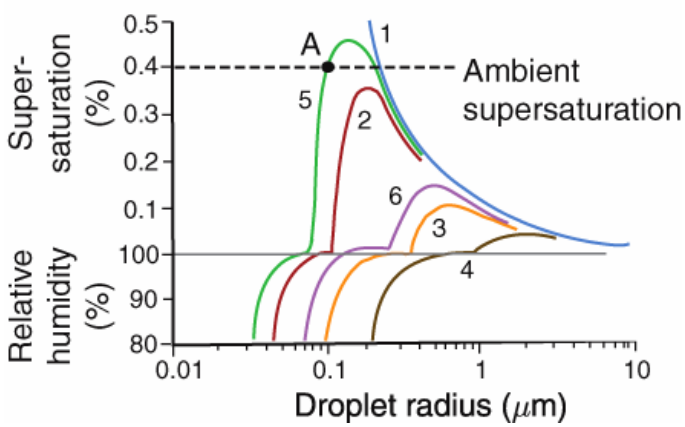

Figure 4-3. *Variations of the relative humidity and supersaturation adjacent to droplets of (1) pure water (blue), and adjacent to solution droplets containing the following fixed masses of salt: (2) 10^{-19} kg of NaCl (red), (3) 10^{-18} kg of NaCl (orange), (4) 10^{-17} kg of NaCl (brown), (5) 10^{-19} kg of $(NH_4)_2SO_4$ (green), and (6) 10^{-18} kg of $(NH_4)_2SO_4$ (violet). Note the discontinuity in the ordinate at 100% relative humidity. Adapted from Rasool [1973].*

Now consider a particle of $(NH_4)_2SO_4$ with mass 10^{-19} kg that is placed in the same ambient supersaturation of 0.4%. In this case, condensation will occur on the particle and it will grow as a solution droplet along its Köhler curve (the green curve in Figure 4-3) until it reaches point A. At point A the supersaturation adjacent to the droplet is equal to the ambient supersaturation. If the droplet at A should grow slightly, the supersaturation adjacent to it would increase above the ambient supersaturation, and therefore the droplet would evaporate back to point A. If the droplet at A should evaporate slightly, the supersaturation adjacent to it would decrease below the ambient supersaturation, and the droplet would grow by condensation back to A in Figure 4-3. Hence, in this case, the solution droplet at A is in stable equilibrium with the ambient supersaturation. If the ambient supersaturation were to change a little, the location of A in Figure 4-3 would shift and the equilibrium size of the droplet would change accordingly. Droplets in this state are said to be *unactivated* or *haze droplets*. Haze droplets in the atmosphere can considerably reduce visibility by scattering light.

The Köhler curves are computed assuming the aerosol particles are at the same temperature as the air. But, recent calculations by *Conant et al.* [2002] suggest that if the aerosol absorbs

sunlight effectively, for example, if it is carbonaceous, the effect of solar heating is to warm the aerosol and reduce its effectiveness as a CCN. Other effects that complicate the use of the Köhler curves in practice are discussed in Section 2.3.2.

4.1.2.2 Cloud Condensation Nuclei

A sub-set of the atmospheric aerosol discussed in Chapter 2 serves as particles upon which water vapor condenses to form droplets that are activated and grow by condensation to form cloud droplets at the supersaturations achieved in clouds (~0.1–1%). These particles are called *cloud condensation nuclei* (CCN). It follows from the discussion in Section 4.1.2.1 that the larger the size of a particle with a given chemical composition, the more readily it is wetted by water, and the greater its solubility, the lower will be the supersaturation at which the particle can serve as a CCN. For example, to serve as a CCN at 1% supersaturation, completely wettable but water insoluble particles need to be at least ~0.1 μm in radius, whereas soluble particles can serve as CCN at 1% supersaturation even if they are as small as ~0.01 μm in radius. Most CCN consist of a mixture of soluble and insoluble inorganic and organic components (called *internally-mixed nuclei*). The solubility of a particle has an important effect on its effectiveness as a CCN. For example, the initial minimum dry radius of a particle that is activated by a supersaturation of 0.1% is 0.075 μm if the particle is completely soluble. However, if the ratio of the soluble mass to the total mass of the particle is only 0.2, the particle would need to have a dry radius of 0.13 μm to be activated by a supersaturation of 0.1%.

Another aspect of CCN activity that is often overlooked is the wettability of the aerosol particle (i.e., the ability of water to spread out over the surface of the particle) as measured by the contact angle of water on the particle. It is generally assumed that particles are completely wettable. However, this is by no means always the case [e.g., *Knight*, 1971]. For example, in the atmosphere there are a number of organic materials that are not wettable. To the extent that a substance has a non-zero contact angle, its ability to serve as a CCN will be hindered.
The surface tension of the solution formed by condensation onto a soluble particle will also affect the subsequent growth of the solution droplet. This is because for the Kelvin effect the energy barrier that has to be overcome for a droplet to be activated varies as the third power of the surface tension [*Wallace and Hobbs*, 2006]. *Facchini et al.* [1999] measured the surface tension of partially evaporated cloud water samples collected over the polluted Po

Valley, Italy. The surface tensions were lower than that of pure water by up to one-third, which was attributed to dissolved organics. Such large surface tension changes, if they occur in cloud droplets near the critical size for nucleation, would lead to increases in cloud droplet concentrations. There is, however, a limit to the extent to which surface tension can be reduced close to saturation because of dilution [*Ervens et al.*, 2004]. The chemical components, concentrations, solubilities, and surface tensions of solution droplets that form in various environments are not well documented, and the effects of these parameters on droplet activation, individually and in combination are not well understood.

Because of the uncertainties in predicting the CCN nucleating ability of atmospheric particles, an empirical approach is generally taken by measuring the concentration of particles that serve as CCN at various prescribed supersaturations; this is called the *CCN supersaturation spectrum*. The concentrations of CCN active at various supersaturations can be measured with a thermal gradient diffusion chamber, or other devices based on similar principles. This device consists of a flat chamber in which the upper and lower horizontal plates are kept wet and maintained at different temperatures, the lower plate being several degrees colder than the upper plate. By varying the temperature difference between the plates, it is possible to produce maximum supersaturations in the chamber that range from a few tenths of 1% to a few percent, which are similar to the inferred supersaturations that activate droplets in clouds [*Wieland*, 1956]. Small water droplets form on those particles that act as CCN at the peak supersaturation in the chamber. The concentration of these droplets can be determined by photographing a known volume of the chamber and counting the number of droplets visible in the photograph, or by measuring the intensity of light scattered from the droplets [*Radke and Hobbs*, 1969]. By repeating the above procedure with different temperature gradients in the chamber, the CCN supersaturation spectrum can be determined. Some devices have been constructed that obtain a spectrum of simultaneous supersaturations from about 0.02 to several percent [*Hudson*, 1989]. Worldwide measurements of CCN concentrations have not revealed any systematic latitudinal or seasonal variations. At a given location, CCN vary by several orders of magnitude with time, depending on the proximity of sources, wind direction, air mass type, precipitation and cloudiness [e.g., *Twomey*, 1960; *Jiusto*, 1966; *Radke and Hobbs*, 1969]. Near the earth's surface continental air masses generally contain larger concentrations of CCN than clean marine air masses (Figure 4-4). For example, the concentration of CCN in the continental air mass over the Azores, depicted in Figure 4-4, is about ~300 cm^{-3} at 1% supersaturation, while in the marine air mass over

Florida it is ~100 cm^{-3}, and in clean Arctic air it is only ~30 cm^{-3}. The ratio of CCN (at 1% supersaturation) to the total number of particles in the air (CN) is ~0.2–0.6 in marine air; in continental air this ratio is generally less than ~0.01 but can rise to ~0.1. The very low ratio of CCN to CN in continental air is attributable to the large number of very small particles, which are not activated at low supersaturations. Concentrations of CCN over land decline by about a factor of five between the planetary boundary layer and the free troposphere [*Squires and Twomey*, 1966; *Hoppel et al.*, 1973; *Hobbs et al.*, 1985]. Over the same height interval, concentrations of CCN over the ocean remain fairly constant, or may even increase with height reaching a maximum concentration just above the mean cloud height [*Hoppel et al.*, 1973; *Hudson*, 1983; *Hegg et al.*, 1990]. Ground-based measurements indicate that there is a diurnal variation in CCN concentrations, with a minimum at about 6 a.m. and a maximum at about 6 p.m. [*Twomey and Davidson*, 1970, 1972].

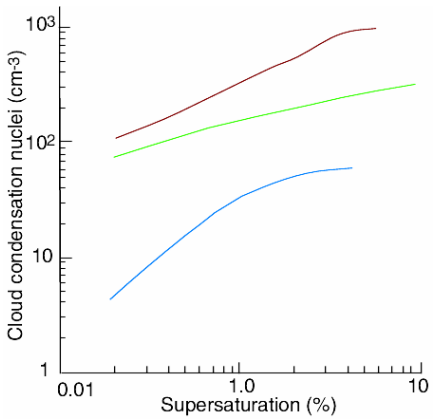

Figure 4-4. *Cloud condensation nucleus spectra in the boundary layer from measurements near the Azores in a polluted continental air mass (brown line), in Florida in a marine air mass (green line), and in clean air in the Arctic (blue line). Data from Hudson and Yum [2002].*

The observations described above provide clues as to the origins of natural CCN. First of all it appears that the land acts as a major source of CCN, because the concentrations of CCN are generally high over land and decrease with altitude. Some of the soil particles and dusts that enter the atmosphere probably serve as CCN, but they do not appear to be a dominant source. The rate of production of CCN (active at a supersaturation of 0.5%) from burning vegetable

matter is on the order of 10^{12}-10^{15} per kg of material consumed [*Eagan et al.*, 1974b]. Thus, forest fires are a prolific source of CCN [*Twomey*, 1960; *Twomey and Warner*, 1967; W*arner and Twomey*, 1967; *Warner*, 1968, *Hobbs and Radke*, 1969; *Woodcock and Jones*, 1970; *Stith et al.*, 1981]. Although sea-salt particles enter the air over the oceans, they do not appear to be a dominant source of CCN, even over the oceans [*Twomey*, 1968, 1971; *Radke and Hobbs*, 1969; *Dinger et al.*, 1970; *Hobbs*, 1971], although, because of their solubilities and large sizes, they may enhance precipitation by serving as giant CCN.

There appears to be a widespread and probably a fairly uniform source of CCN over both oceans and land, the nature of which has not been definitely established. A likely candidate is gas-to-particle conversion, which can produce particles up to a few tenths of a micrometer in diameter that can act as CCN if they are soluble and wettable. Gas-to-particle conversion mechanisms that require solar radiation might be responsible for the observed peak in CCN concentrations at ~6 p.m. Many CCN consist of sulfates. Over the oceans, organic sulfur from the ocean (in the form of the gases dimethylsulfide (DMS) and methane sulfonic acid (MSA)) provides a source of CCN, with the DMS and MSA being converted to sulfate in the atmosphere [*Charlson et al.*, 1987; *Hoppel*, 1987; *Luria et al.*, 1989; *Gras*, 1990; *Hegg et al.*, 1991a,b; *Ayers and Gras*, 1991; *Ayers et al.*, 1991; *Pandis et al.*, 1994]. Evaporating clouds also release sulfate particles that are somewhat larger than non-cloud processed aerosol because of the additional material deposited onto them in clouds [*Radke and Hobbs*, 1969; *Easter and Hobbs*, 1974; *Hegg et al.*, 1980; *Hegg and Hobbs*, 1981; *Hoppel et al.*, 1986; *Birmili et al.*, 1999; *Feingold and Kriedenweis*, 2002]. It has been estimated that ~80% of sulfate mass globally is formed in the aqueous phase, and the remainder from the gas phase. As expected from the Köhler curves, larger sulfate particles serve more efficiently as CCN [*Hegg*, 1985; *Leaitch et al.*, 1986; *Lelieveld et al.*, 1997]. The production of sulfates (and maybe other soluble materials), followed by the release of these particles when the droplets evaporate, is an important mechanism for increasing the efficiency of CCN [*Twomey and Wocjiechowski*, 1969; *Hobbs*, 1971; *Easter and Hobbs*, 1974]. There are also a number of anthropogenic sources of CCN, which are discussed in Chapters 2, 3 and 5.

4.1.2.3 Effects of CCN on the Microphysical Structures of Clouds

In a cloud we are concerned with the growth of a large number of droplets in a rising parcel of air. As the parcel rises it expands, cools adiabatically, and eventually reaches saturation with respect to liquid water. Further uplift produces supersaturations that initially increase at

a rate proportional to the updraft velocity. As the supersaturation rises CCN are activated, starting with the most efficient. When the rate at which water vapor in excess of saturation, made available by the adiabatic cooling, is equal to the rate at which water vapor condenses onto the CCN and droplets, the supersaturation in the cloud reaches a maximum value. The concentration of cloud droplets is determined at this stage (which generally occurs within 100 m or so of cloud base) and is equal to the concentration of CCN activated by the peak supersaturation that has been attained. Subsequently, the growing droplets consume water vapor faster than it is made available by the cooling of the air, so the supersaturation begins to decrease. The haze droplets then begin to evaporate while the activated droplets continue to grow by condensation. The rate of growth of a droplet by condensation is inversely proportional to its radius, therefore the radius of the smaller activated droplets grow faster than that of the larger droplets. Consequently, in this simplified model, the size distribution of the droplets in the cloud become increasingly narrower with time (that is, the droplets approach a *monodispersed* distribution). This sequence of events is illustrated by the results of theoretical calculations shown in Figure 4-5.

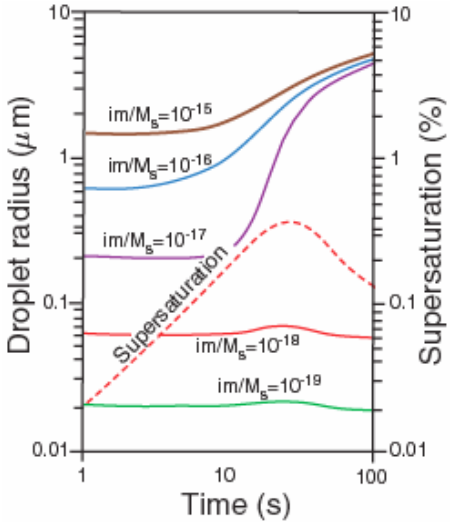

Figure 4-5. *Theoretical computations of the growth of cloud condensation nuclei by condensation in a parcel of air rising with a speed of 60 cm s^{-1}. A total of 500 CCN cm^{-1} was assumed with im/M_s values as indicated; m the mass of material dissolved in the droplet, M_s the molecular weight of the material, and i its van't Hoff factor (i.e., the number of ions produced by each molecule of the material when it dissolves). Thus, im/M_s is the effective number of kilomoles of the material is the dissolved droplet. Note how the droplets that have been activated (brown, blue and purple curves) approach a monodispersed size distribution after just 100 s. The variation with time of the supersaturation of the air parcel is also shown (dashed red line). From Wallace and Hobbs [2006], based on data from Howell [1949].*

Comparisons of cloud droplet size distributions measured a few hundred meters above the bases of non-precipitating warm cumulus clouds with droplet size distributions computed assuming growth by condensation for about 5 min show good agreement. The droplets produced by condensation during this time period extend only up to about 10 μm in radius. Moreover, as mentioned above, the rate of increase in the radius of a droplet growing by condensation is inversely proportional to the drop radius, therefore, the rate of growth decreases with time. It is clear, therefore, as first noted by *Reynolds* [1877], that growth by condensation alone in warm clouds is much too slow to produce raindrops with radii of several millimeters. Yet rain does form in clouds that contain only water drops. The enormous increases in size required to transform cloud droplets into raindrops is illustrated by the scaled diagram shown in Figure 4-6. For a cloud droplet 10 μm in radius to grow to a raindrop 1 mm in radius requires an increases in volume of one millionfold! However, only about one droplet in a million (about 1 liter^{-1}) in a cloud has to grow by this amount for the cloud to rain. The mechanism responsible for the selective growth of a few droplets into raindrops in warm clouds is discussed in Section 4.2.1.

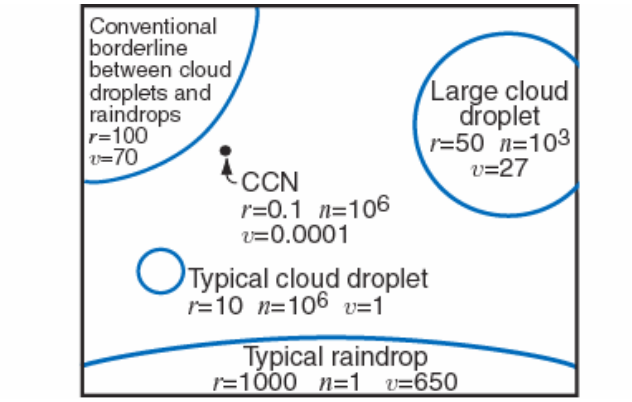

Figure 4-6. *Relative sizes of cloud droplets and raindrops; r is the radius in micrometers, n the number per liter of air, and v the terminal fall speed in centimeters per second. The circumference of the circles are drawn approximately to scale, but the black dot representing a typical CCN is twenty-five times larger than it should be relative to the other circles. From Wallace and Hobbs [2006],*

Since the concentration of CCN generally increases in passing from oceanic air sheds to continental air sheds to urban environments, the concentrations of cloud droplets likewise increase, the cloud droplet size distributions narrow, and the average size of the droplets decreases (Figures 4-7 to 4-9), at least for non-precipitating clouds [e.g., *Gerber*, 1996]. For example, droplet concentrations in non-polluted, non-precipitating marine cumulus clouds are

generally less than 100 cm^{-3} and droplet radii extend up to ~20 μm [e.g. *Squires*, 1958]. However, continental cumulus in clean regions precipitate readily and have much broader droplet size distributions than polluted cumulus clouds over the oceans. By contrast, in non-precipitating continental cumulus clouds the concentration of cloud droplets are several hundreds per cubic centimeter of air and droplet radii are below ~10 μm [*Squires*, 1958]. As we will see in Section 4.2.1, clouds with large concentrations of droplets and narrow droplet size distributions are more colloidally stable and less likely to precipitate than clouds with small concentrations of droplets and broad droplet size distributions.

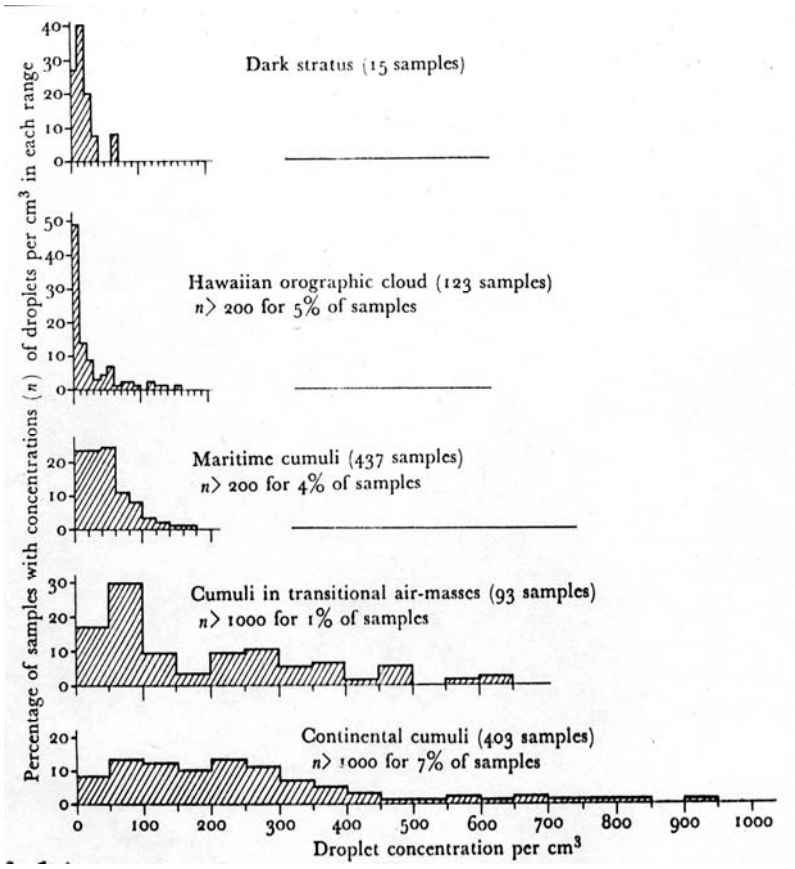

Figure 4-7. *Histograms of the percentages of samples taken in each of five cloud types for which the droplet concentrations fell in the ranges indicated by the horizontal axes. The scale of concentrations is common to the five histograms. From Squires [1958].*

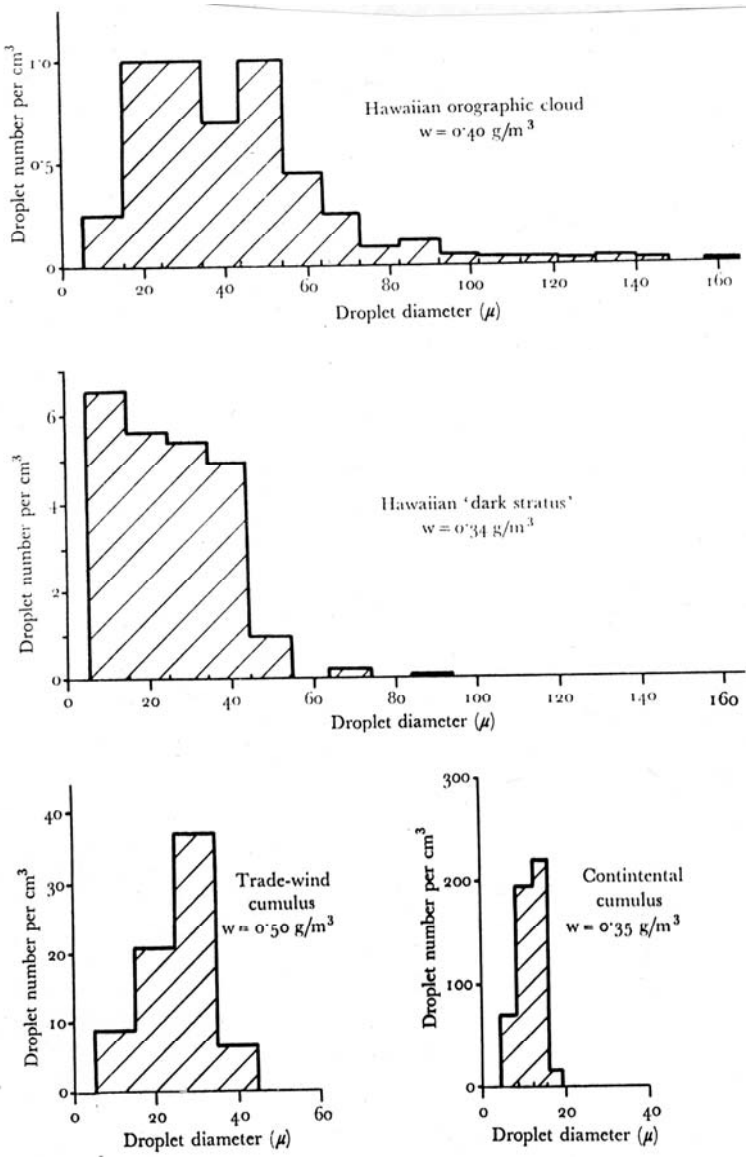

Figure 4-8. *Droplet spectra in clouds of various types, with liquid water contents w as shown. Cumulus samples were taken 2000 ft above cloud base, orographic and dark stratus values are average. Note change in ordinate scale from figure to figure. From Squires [1958].*

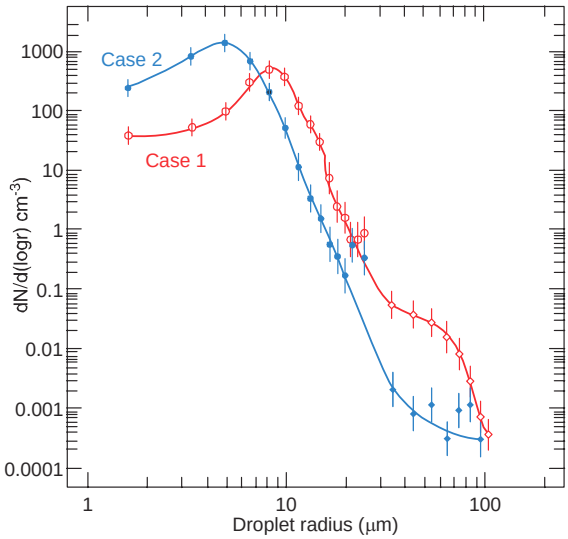

Figure 4-9. *Cloud droplet number distributions measured in stratocumulus clouds in the vicinity of the Azores by the FSSP-100 (circles) and PMS 1D (diamonds) cloud probes, averaged over 15 km of flight path for case 1—clean marine air (red symbols and curve), and averaged over 4 km of flight path for case 2—continentally influenced air (blue symbols and curve). The vertical bars are the geometric standard deviations of the droplet concentrations. From Garrett and Hobbs [1995].*

The effects of CCN from anthropogenic sources on cloud structures and precipitation is discussed in Chapter 5 and 6.

4.1.3 Cold Clouds

4.1.3.1 Nucleation of Ice; Ice Nuclei

If portions of a cloud are at temperatures below 0ºC (referred to as *cold clouds*), ice particles may be present. However, provided the temperature is not below about –40ºC, supercooled droplets may coexist with ice particles; the cloud is then referred to as a *mixed cloud*.

A supercooled droplet is in an unstable state. For freezing to occur, enough water molecules must come together within the droplet to form an embryo of ice large enough to survive and grow. If an ice embryo within a droplet exceeds a certain critical size, its growth will produce a decrease in the energy of the system. On the other hand, any increase in the size of an ice embryo smaller than the critical size causes an increase in total energy. In the latter case, from an energetic point of view, the embryo is likely to break up.

If a water droplet contains no foreign particles it can freeze only by *homogeneous nucleation*. Since the numbers and sizes of the ice embryos that form by chance aggregations increase with decreasing temperature, below a certain temperature (which depends on the volume of

water considered) freezing by homogeneous nucleation becomes a virtual certainty. Homogeneous nucleation occurs at about -41°C for droplets about 1 μm in diameter, and at about -35°C for drops 100 μm in diameter. Hence, in the atmosphere, homogeneous nucleation of freezing generally occurs only in high clouds or high latitudes.

If a droplet contains a rather special type of particle, called a *freezing nucleus*, it may freeze by a process known as *heterogeneous nucleation* in which water molecules in the droplet collect onto the surface of the particle to form an ice-like structure that may increase in size and cause the droplet to freeze. Since the formation of the ice structure is aided by the freezing nucleus, and the ice embryo also starts off with the dimensions of the freezing nucleus, heterogeneous nucleation can occur at much higher temperatures than homogeneous nucleation. The red symbols and line in Figure 4-10 show the results of laboratory experiments on the heterogeneous freezing of water droplets. The droplets consisted of distilled water from which most, but not all, of the foreign particles were removed. A large number of droplets of each of the sizes indicated in Figure 4-10 were cooled, and the temperature at which half of the droplets had frozen was noted. It can be seen that this median freezing temperature increases as the size of the droplet increases. The size dependence reflects the fact that a larger drop is more likely to contain a freezing nucleus capable of causing heterogeneous nucleation at a given temperature. Similarly if the water sample is subdivided sufficiently a droplet size is reached such that the droplet does not contain any nucleus and freezes homogeneously. For a solution droplet similar considerations apply with the homogeneous nucleation temperature reduced by the colligative freezing point depression; such depression goes away as the solution droplet dilutes during growth.

We have assumed above that the particle that initiates freezing is contained within the droplet, or what is called an immersion freezing nucleus. However, cloud droplets may also be frozen if a suitable particle in the air comes into contact with the droplet, in which case freezing is said to occur by *contact nucleation*, and the particle is referred to as a *contact nucleus*. Laboratory experiments suggest that some particles can cause a drop to freeze by contact nucleation at temperatures several degrees higher than if they were embedded in the drop [*Fletcher*, 1962; *Levkov*, 1971; *Gokhale and Spengler*, 1972; *Pitter and Pruppacher*, 1973].

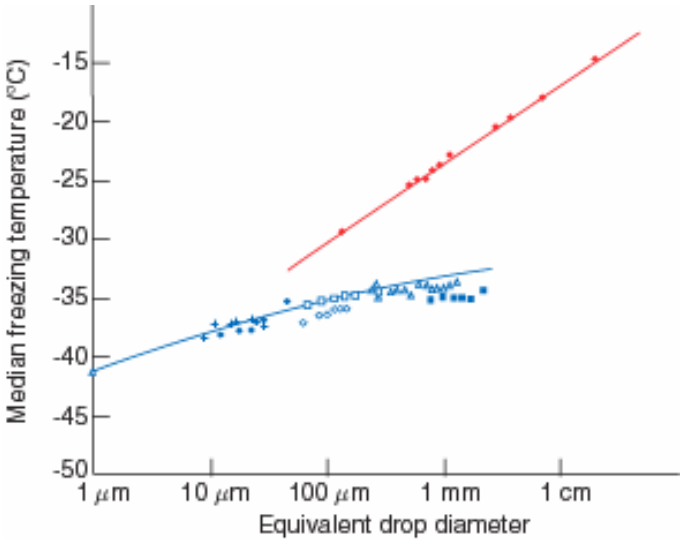

Figure 4-10. *Median freezing temperatures of water samples as a function of their equivalent drop diameter. The different symbols are results from different workers. The red symbols and red line represent heterogeneous freezing and the blue symbols and line represent homogeneous freezing. From Wallace and Hobbs [2006], adapted from Mason [1971].*

Recent laboratory experiments by *Durant and Shaw* [2005] suggest that contact nucleation may be just as effective from the inside-out as from the outside-in. They showed that as droplets evaporate, embedded aerosol particles become increasing likely to penetrate the air-water interface layer and promote what amounts to contact nucleation.

Certain *particles* in the air also serve as centers upon which ice can form directly from the vapor phase. These particles are referred to as *deposition nuclei*. Ice can form by deposition provided that the air is supersaturated with respect to ice and the temperature is low enough. If the air is supersaturated with respect to water, a suitable particle may serve either as a *condensation-freezing* nucleus (in which case liquid water first condenses onto the particle and subsequently freezes) or as a *deposition nucleus* (in which case there is no intermediate liquid phase, at least on the macroscopic scale). It is generally thought that condensation-freezing is preferred at smaller supercoolings and large supersaturations, while deposition is preferred at large supercoolings and small supersaturation. In practice, it is not easy to distinguish between deposition and condensation-freezing modes.

If we refer to an ice nucleating particle in general, without specifying its mode of action, we call it an *ice nucleus* (IN). However, it should be kept in mind that the temperature at which a particle can cause ice to form depends, in general, upon the mechanism by which the particle nucleates the ice as well as upon the previous history of the particle. The basic distinction that has to be made is whether nucleation is from the vapor or from the liquid phase [*Vali*, 1985]. *Deposition nucleation* refers to the formation of ice in an ice supersaturated environment. *Freezing nucleation* is the formation of ice in a liquid environment. *Condensation-freezing* is the sequence of events whereby a soluble component of the particle takes on water and initiates freezing of the condensate. These are most likely particles of internally mixed composition. *Contact freezing* is the nucleation of freezing by an aerosol particle coming into contact with a supercooled droplet. *Immersion freezing* is the nucleation of a supercooled droplet by a particle suspended in the body of the water.

Particles with molecular spacings and crystallographic arrangements similar to those of ice (which has a hexagonal structure) tend to be effective as ice nuclei, although this is neither a necessary nor sufficient condition for a good ice nucleus. Most effective ice nuclei are virtually insoluble in water. Some inorganic soil particles (mainly clays) can nucleate ice at fairly high temperatures (i.e., above -15°C), and they probably play an important role in nucleating ice in clouds. For example, in one study 87% of the snow crystals collected on the ground had clay mineral particles at their centers and more than half of these were kaolinite [*Kumai*, 1951]. Many organic materials are effective ice nucleators [*Schnell and Vali*, 1976a]. Decayed plant leaves contain copious ice nuclei, some active as high as -4°C. Ice nuclei active at -4°C have also been found in sea water rich in plankton. In addition, some plant pathogenic bacteria have also been found to be effective ice nuclei at temperatures as high as –2ºC [*Yankofsky et al.*, 1981; *Levin and Yankofsky*, 1984; *Levin et al.*, 1987].

The results of laboratory measurements on condensation-freezing and deposition shown in Figure 4-11 indicate that for a variety of materials the onset of ice nucleation occurs at higher temperatures under water supersaturated conditions (so that condensation-freezing is possible) than under water subsaturated conditions (when only ice deposition is possible). For example, kaolinite serves as an ice nucleus at -10.5°C at water saturation, but at 17% supersaturation with respect to ice (but subsaturation with respect to water) the temperature has to be about -20°C for kaolinite to act as a deposition nucleus. Anthropogenic sources of ice nuclei are discussed in Chapter 2 and 5.

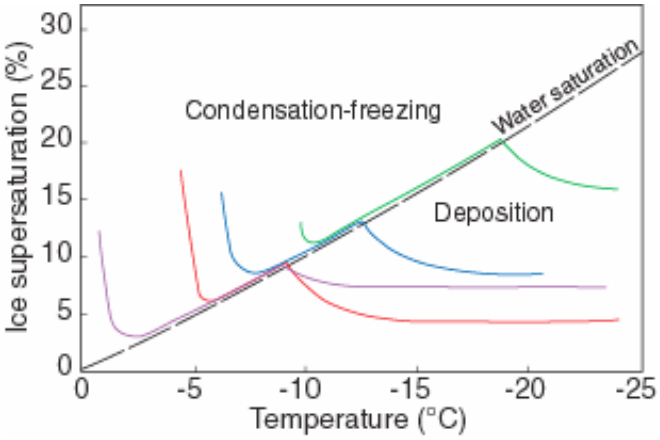

Figure 4-11. *Onset of ice nucleation as a function of temperature and supersaturation for various compounds. Conditions for condensation-freezing and ice deposition are indicated. Ice nucleation starts above the indicated lines. The materials are silver iodide (red), lead iodide (blue), methaldehyde (violet), and kaolinite (green). From Wallace and Hobbs [2006], adapted from Schaller and Fukuta [1979].*

In some cases, after a particle has served as an ice nucleus and all of the visible ice is then evaporated from it, but the particle is not warmed above -5°C or exposed to a relative humidity with respect to ice of less than 35%, it may subsequently serve as an ice nucleus at a temperature a few degrees higher than it did initially [*Roberts and Hallett*, 1968]. This is referred to as *preactivation*. Thus, for example, preactivated nuclei may be transferred between sequential wave clouds and act at higher temperature for the second and later clouds. However, preactivation is lost if the initially activated ice nucleus is either heated above at least –5ºC and/or is dehydrated to less than ~35% relative humidity with respect to ice. It is cautioned that preactivation can be lost if the particles are warmed or dehydrated prior to testing in an IN counter.

Worldwide measurements of ice nucleus concentrations as a function of temperature (Figure 4-12) indicate that concentrations of ice nuclei tend to be higher in the northern than in the southern hemisphere. It should be noted however that ice nucleus concentrations can sometimes vary by several orders of magnitude over several hours (see also Chapters 5 and 7). On average, the number N of ice nuclei per liter of air active at temperature T tends to follow the empirical relationship

(4.1) $$\ln N = a(T_1 - T)$$

where T_1 is the temperature at which one ice nucleus per liter is active (typically about -20°C) and a varies from about 0.3 to 0.8 [*Fletcher*, 1962]. For a = 0.6, eqn. (4.1) predicts that the concentration of ice nuclei increases by about a factor of 10 for every 4°C decrease in temperature. In urban air, the total concentration of aerosol is on the order of 10^8 liter^{-1} and only about one particle in 10^8 acts as an ice nucleus at -20°C!

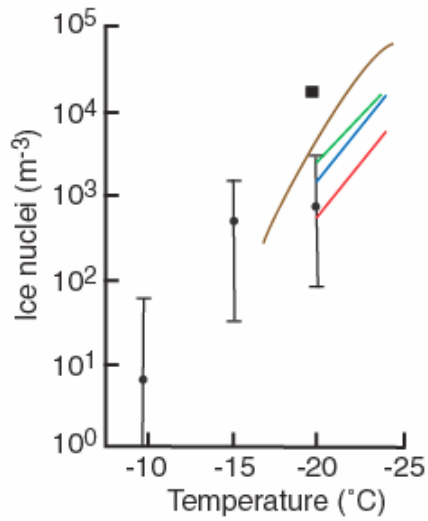

Figure 4-12. *Measurements of average ice nucleus concentrations at close to water saturation in the northern and southern hemispheres. Southern hemisphere, expansion chamber (red); southern hemisphere, mixing chamber (blue); northern hemisphere, expansion chamber (green); northern hemisphere, mixing chamber (black square); Antarctica, mixing chamber (brown). The vertical lines show the range and mean values (dots) of ice nucleus concentrations based on Millipore filter measurements in many locations around the world. From Wallace and Hobbs [2006].*

As we have seen, the activity of a particle as a freezing or a deposition nucleus depends not only on the temperature but also on the supersaturation of the ambient air. Supersaturation was not well controlled in many of the measurements shown in Figure 4-12, on which eqn. (4.1) is based. The effect of supersaturation on measurements of ice nucleus concentrations is shown in Figure 4-13, where it can be seen that at a constant temperature the greater the supersaturation with respect to ice the more particles serve as ice nuclei. The empirical equation to the best-fit line to these measurements (the red line in Figure 4-13) is

$$N = \exp\left\{a + b\left[100\left(S_i - 1\right)\right]\right\} \tag{4.2}$$

where N is the concentration of ice nuclei per liter, S_i the supersaturation with respect to ice, a = -0.639 and b = 0.1296 [*Meyers et al.*, 1992]. These measurements were obtained using a continuous flow diffusion chamber (CFDC), which tends to exhibit roughly a factor of ten

higher concentrations of IN than older devices such as the filter-processing systems. Measurements with the CFDC in a variety of field campaigns exhibit considerable variability and departure from that given by eqn. (4.2). Measurements in the Arctic boundary layer [*Rogers et al.*, 2001], for example, exhibited IN concentrations so small near the surface that they were below the detection limit of the CFDC, whereas above the capping inversion the IN concentrations were much higher but still well below those given by eqn. (4.2). On the other hand, measurements of IN concentrations over South Florida during a Saharan dust outbreak, reported by *DeMott et al.* [2003], were much higher than those given by eqn. (4.2); in fact, they were the highest ever measured with the CFDC.

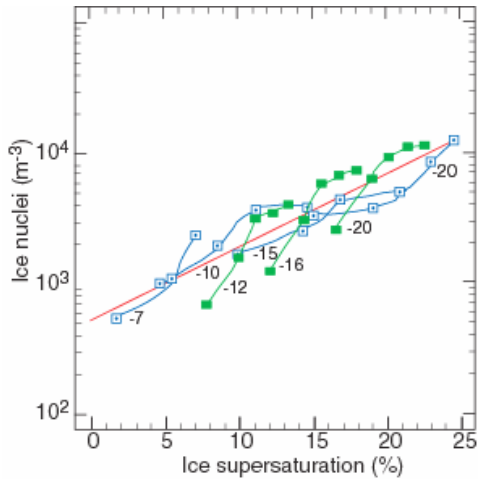

Figure 4-13. *Ice nucleus concentration measurements versus ice supersaturation; temperatures are noted alongside each line. The red line is eqn. (4.2). From Wallace and Hobbs [2006], data from D.C. Rogers, Atmos. Res., 29, 209 [1993]—blue squares, and R. Al-Naimi and C.P.R. Saunders, Atmos. Envir., 19, 1871 [1985]—green squares.*

In order to permit vertical and horizontal variations in IN concentrations *Cotton et al.* [2003] modified equation (4.2) to include the prognostic variable N_{IN}:

(4.3) $$Ni = NIN \exp [12.96 (Si - 1)],$$

where T < -5oC; rv > rsi (supersaturation with respect to ice), and T < -2^{o}C ; rv > rsl (supersaturation with respect to liquid). The variable NIN can be deduced from continuous flow diffusion chamber data and used in regional simulations [i.e. van den *Heever et al.*, 2004].

4.1.3.2 Concentrations of Ice Particles in Clouds; Ice Multiplication

The probability of ice particles being present in a cloud increases as the temperature decreases below 0°C, as illustrated in Figure 4-14. The results shown in this figure indicate that the probability of ice being present is 100% for cloud top temperature below about -13°C. At higher temperatures the probability of ice being present falls off sharply, but it is greater if the cloud contains drizzle or raindrops. Clouds with top temperatures between about 0 and -8°C generally contain copious supercooled droplets [e.g., *Mossop et al.*, 1967; *Koenig*, 1968; Hobbs, 1969; *Hobbs and Rangno*, 1985, 1998; *Rangno and Hobbs*, 1991, 1994, 2001; *Korolev et al.*, 2003].

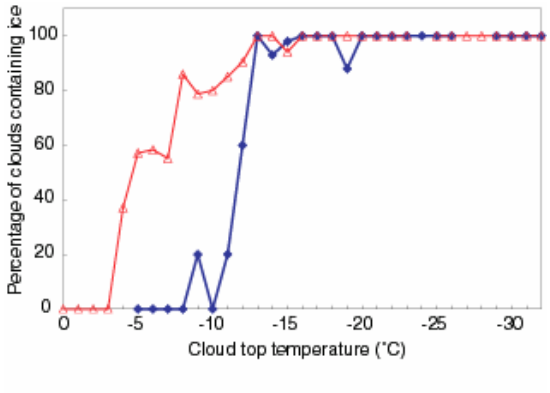

Figure 4-14. *Percentage of clouds containing ice particle concentrations greater than about 1 per liter as a function of cloud top temperature. Note that on the abscissa temperatures decrease to the right. Blue curve: continental cumuliform clouds with base temperatures of 8 to -18°C containing no drizzle or raindrops prior to the formation of ice; from Wallace and Hobbs [2006) using data from A.L. Rangno and P.V. Hobbs [1994]. Red curve: clean marine cumuliform clouds and clean arctic stratiform clouds with base temperatures from 25 to -3°C containing drizzle or raindrops prior to the formation of ice; from Wallace and Hobbs [2006], data from. Rangno and Hobbs, [1991], Hobbs and Rangno [1998], Rangno and Hobbs [2001], and Cloud and Aerosol Research Group, University of Washington, unpublished data.*

Shown in Figure 4-15 are measurements of the maximum concentrations of ice particles in clouds. Also shown are the concentrations of ice nuclei given by eqn. (4.1) with a = 0.6 and T_1=253°K (green line in Figure 4-15). It can be seen that eqn. (4.1) approximates the minimum values of the maximum concentrations of ice particles. However, on many occasions, ice particles are often present in concentrations several orders of magnitude greater than ice nucleus measurements. At temperatures above about -20°C, marine clouds

show a particular propensity for ice particle concentrations that are many orders of magnitude greater than ice nucleus measurements would suggest.

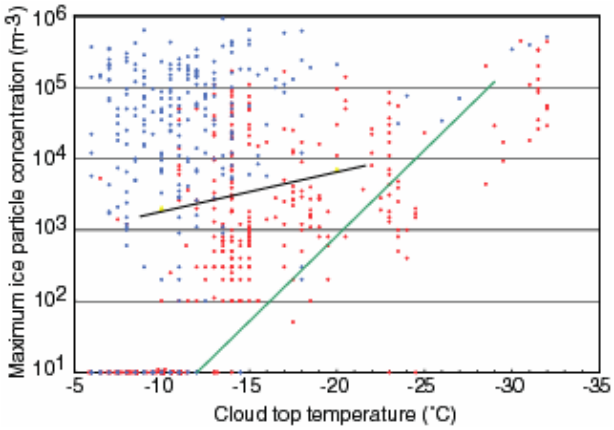

Figure 4-15. *Maximum concentrations of ice particles versus cloud top temperature in mature and aging marine cumuliform clouds (blue dots) and in continental cumuliform clouds (red dots). Note that on the abscissa temperatures decrease to the right. The symbols along the abscissa indicate ice concentrations* $\leq$*1 liter*$^{-1}$*, which was the lower limit of detection. Shown by the green line are the ice nucleus concentrations predicted by eqn. (4.1) with a = 0.6 and* T_1 *= 253 K. The black line shows the ice nucleus concentrations from eqn. (4.2) assuming water saturated conditions. From Wallace and Hobbs [2006], based on data from J. Atmos. Sci., 42, 2253 [1985], and Rangno and Hobbs [1991] and Rangno and Hobbs [1994]..*

Several explanations have been proposed to account for the high ice particle concentrations observed in some clouds. First, it is possible that current techniques for measuring ice nuclei do not provide reliable estimates of the concentrations of ice nuclei active in natural clouds under certain conditions. It is also possible that ice particles in clouds increase in number without the action of ice nuclei, by what are termed *secondary processes*, or alternatively *ice multiplication* or *ice enhancement*. For example, some ice crystals are quite fragile and may break up when they collide with other ice particles. However, the strongest contender for an ice enhancement process in clouds is one that involves water droplets freezing. When a supercooled droplet freezes in isolation (e.g., in free fall), or after it collides with an ice particle (the freezing of droplets onto an ice particle is called *riming*), it does so in two distinct stages. In the first stage, which occurs almost instantaneously, a fine mesh of ice shoots through the droplet and freezes just enough water to raise the temperature of the droplet to 0°C. The second stage of freezing is much slower and involves the transfer of heat from the partially frozen droplet to the colder ambient air. During the second stage of freezing an ice shell forms over the surface of the droplet and then thickens progressively

inward. As the ice shell advances inward, water is trapped in the interior of the droplet; as this water freezes it expands and sets up large stresses in the ice shell. These stresses may cause the ice shell to crack and even explode, throwing off numerous small ice particles or ice splinters.

Since an ice particle falling through a supercooled cloud will be impacted by thousands of droplets, each of which might shed numerous ice splinters as it freezes onto the ice particle, ice splinter production by riming is potentially much more important than ice splinter production during the freezing of isolated droplets. Laboratory experiments indicate that ice splinters are ejected during riming provided the, temperatures are between -2.5 and -8°C (with peak ice splinter production from -4 to -5°C), and the impact speed (determined in a cloud by the fall speed of the ice particle undergoing riming) is between ~0.2 and 5 m s^{-1} with peak splinter production at impact speeds of a few m s^{-1} [*Hallett and Mossop*, 1974]. *Mossop* [1978] also showed that the rate of production of splinters depends not only on concentrations of large drops (diameters $\geq$24 μm), but also upon the concentrations of small drops (diameters <13 μm). For example, laboratory measurements show that for a droplet spectrum characterized by 50 drops cm^{-3} with droplets ranging in diameter from ~5 to 35 μm, a LWC of 0.2 g m^{-3}, a temperature of -4.5°C, and an impact speed of 3.6 m s^{-1}, ~300 ice splinters are produced for every microgram of rime that is accumulated (for a spherical ice particle 1 mm in radius, 1 μg of accumulated rime corresponds to a layer of ice ~0.1 μm thick).

The high concentrations of ice particles (100 $liter^{-1}$ or more) observed in some clouds (see Figure 4-15) are associated primarily with older clouds. Young cumulus towers generally consist entirely of water droplets, and generally require about 10 min before showing signs of plentiful ice particles. It also appears from measurements in clouds that high ice particle concentrations occur after the formation of drops with diameters $\gtrsim$25 μm and when rimed ice particles appear. These observations are consistent with the hypothesis that the high ice particle concentrations are due to the ejection of ice splinters during riming. However, calculations based on the results of laboratory experiments on ice splinter production during riming, suggest that this process is too slow to explain the explosive formation of extremely high concentrations of ice particles observed in some clouds.

Laboratory experiments have indicated that some drops (>50 μm diameter) in certain circumstances can produce ice fragments while freezing in free fall [e.g., *Hobbs and Alkezweeny*, 1968]. It was hypothesized from these laboratory experiments that the tumbling of the drops as they froze in free fall resulted in a symmetric heat loss which allowed a shell of ice to enclose the liquid interior of the drop. The continued freezing and expansion of the liquid interior caused some drops to fragment and shed ice fragments.

Recently, support for individual drops fragmenting in free fall has been obtained by *Rangno and Hobbs* [2005] in field experiments. Two lines of evidence were obtained: they found images of millimeter-sized frozen drops with pieces missing, and large fragments of such drops; they also found a large number of ice fragments with maximum dimensions ~30–150 μm. The ice fragments outnumbered regular ice forms, such as needles, parts of needles, sheaths, or portions of sheaths, in the temperature range 0 to –10ºC in which they collected these data.

Stith et al. [2004], sampling in the same region as *Rangno and Hobbs*, found that cloud drops <50 μm diameter had frozen in updrafts at temperatures greater than –17ºC from as yet an unknown mechanism. The concentrations of the frozen drops in this moderate temperature ranged from 10–50 cm^{-3}, producing, therefore, probably the highest ice particle concentrations ever measured below cirrus levels.

There is numerous indirect or inferential evidence that evaporation enhances ice crystal concentrations. This evidence is perhaps more intriguing than it is compelling. Some field studies have related unusually high ice nuclei numbers or unusual increases in ice crystal numbers to circumstances in which clouds were evaporating. *Cooper* [1995], for example, found a 100-fold increase in ice crystal concentrations in the evaporation region of orographic layer clouds. The largest ice enhancements in the *Cooper* study were observed in clouds with temperatures approaching the onset temperature for homogeneous freezing. Smaller enhancements were found in warmer clouds and no enhancements were found warmer than about -20°C. Further evidence of the possible role of evaporation nucleation has been presented by *Field et al.* [2001] and *Cotton and Field* [2002]. They show observational evidence and supporting parcel modeling calculations from wave cloud studies that suggest ice had to form close to the downstream edge of wave cloud. Ice production coincident with

the start of the liquid cloud, or earlier, would have suppressed the observed liquid cloud. Some of the observations of rapid ice crystal concentration enhancement versus expected IN concentrations in cumulus cloud studies of *Hobbs and Rangno* [1985; 1990] and *Rangno and Hobbs* [1994] were also observed to originate in close proximity to regions of cloud evaporation. *Stith et al.* [1994] followed the development of ice in a cumulus turret near its top at -18°C. During the updraft stages, low ice concentrations were observed in the turret (similar to what would be expected from primary ice nucleation), but during the downdraft stages, the ice concentrations increased by an order of magnitude. This observation cannot be explained by rime splintering.

A possible mechanism for ice particle concentration enhancement in cumulus clouds comes from the laboratory studies by *Oraltay and Hallett* [1989]. They found that evaporating graupel particles produce copious numbers of ice bits which if entrained into an ice supersaturated region of a cloud could contribute to enhanced ice particle concentrations associated with an evaporated region of the cloud. Another possible mechanism is enhanced contact nucleation of nuclei embedded within supercooled drops that freeze more readily when contacting the droplet/air interface layer as the droplet evaporates [*Durant and Shaw*, 2005].

In summary, it is unlikely that all primary and secondary ice forming processes have been identified. As indicated schematically in Figure 4-16, an additional *"super" ice enhancement* mechanism may sometimes operate, but the exact nature of this mechanism remains a mystery.

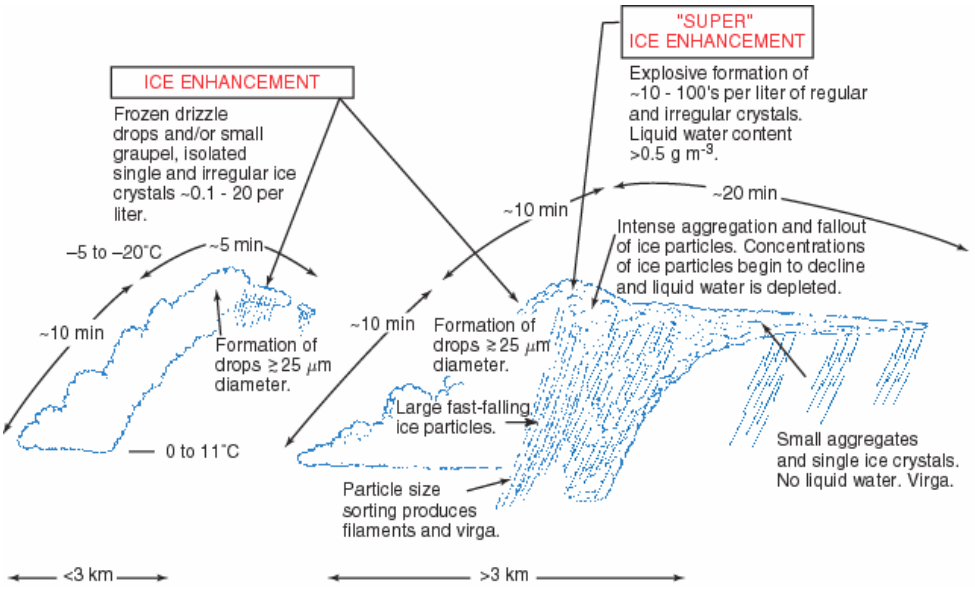

Figure 4-16. *Schematic of ice development in small cumuliform clouds. Adapted from Rangno and Hobbs [1991].*

4.2 FORMATION OF PRECIPITATION

Precipitation-sized particles can form by two mechanisms, known as the *collision-coalescence* and the *ice particle* mechanisms. The collision-coalescence mechanism can operate in clouds containing droplets, whether they are situated above or below (*warm clouds*) the 0ºC level. The ice particle mechanism can operate only in clouds with temperatures below 0ºC (*cold clouds*) and containing some ice particles.

4.2.1 The Collision-Coalescence Mechanism

This mechanism for rainfall production involves the initial formation of a few cloud drops with radii of about 20 μm by condensation onto CCN, followed by their rapid and substantial growth as they fall through the air and collide with smaller cloud droplets. If a drop increases in radius from 20 μm to a radius typical of raindrops, say 2 mm, its volume increases by a factor of one million. In other words, about one million cloud droplets have to combine to form one raindrop!

Due to the flow of air around a falling drop, a drop will not collect all of the droplets that lie in its path. Calculated values of the *collision efficiency*, defined as the ratio of the cross-sectional area over which droplets are collected to the geometric cross-sectional area of the collector drop, are shown in Figure 4-17. This figure shows that the collision efficiency is negligible (<0.1) until a collector drop attains a radius of about 20 µm. Hence the need for a few droplets to grow to 20 µm in radius by condensation if a cloud is to form raindrops by the collision-coalescence mechanism. The rate of increase in the radius of a droplet that is growing by condensation alone decreases as the droplet grows (Figure 4-18). In contrast, after a droplet has reached a radius of 20 µm its collision efficiency increases rapidly with increasing size (Figure 4-17), so the droplet grows increasingly fast by collision. Were it not for the fact that growth by collisions takes over as growth by condensation becomes negligible, many clouds would not rain.

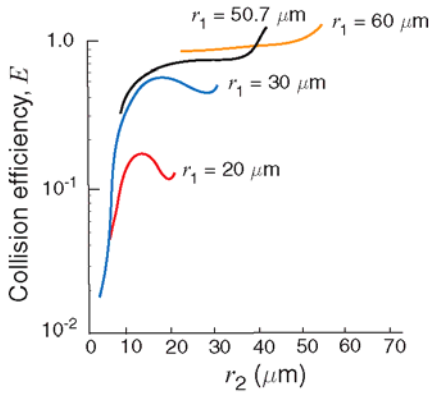

Figure 4-17. *Calculated values of the collision efficiency, E, for collector drops of radius r_1 with droplets of radius r_2. From Pruppacher and Klett [1997].*

The problem is how do drops grow to a radius of 20 µm or greater fast enough to allow precipitation growth during the lifetime of clouds? Four mechanisms have been hypothesized:

- Role of giant cloud condensation nuclei.
- Turbulence influences on condensation growth via fluctuating supersaturations.
- Turbulence influence on droplet collision and coalescence.
- Radiative broadening.

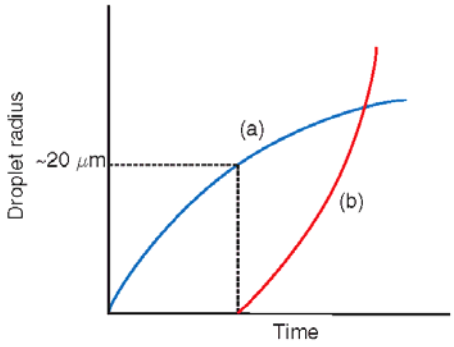

Figure 4-18. *Schematic curves of the growth of a drop (a) by condensation (blue curve) and (b) by collection of droplets (red curve).*

4.2.1.1 Role of Giant Cloud Condensation Nuclei (GCCN)

Observations reported by *Woodcock* [1953], *Nelson and Gokhale* [1968], *Hindman* [1975], *Johnson* [1976; 1982], and *Hobbs et al.* [1980] have shown the presence of potentially significant concentrations of aerosol particles of sizes as large as 100 μm. Their concentrations are ~10^{-3} cm^{-3} [*Woodcock*, 1953], that is, about one in 10^5 or 10^6 CCN are giant particles. Nevertheless, these particles can have a significant effect on the development of precipitation by serving as coalescence embryos [*Johnson*, 1982; *Feingold et al.*, 1999; *Yin et al.*, 2000a]. The droplet that forms is large enough for coalescence to start immediately even before the droplet reaches its critical size based on the Köhler equation. This can occur if the nuclei are completely soluble (e.g., sea-salt particles) or are mixed particles with a soluble coating [e.g., mineral dust with a coating of sulfate, *Levin et al.*, 1996] or are very large and wettable.

4.2.1.2 Turbulence influences on Condensation Growth via Fluctuating Supersaturations

Calculations of droplet growth by condensation in a smooth unmixed parcel of air show that the droplet spectrum narrows with time which is not conducive to initiating collision and coalescence Peak supersaturations in those calculations are generally less than 1%. It has been hypothesized that in a real cloud entrainment and mixing can lead to locally enhanced

supersaturations if the entrainment takes place inhomogeneously [*Baker et al.*, 1980]. One can view this as a two-stage process in which a tongue or stream of dry air penetrates into the interior of a cloud either from the top or the sides. During the first stage, the dry tongue and cloudy air remain distinctly separate. At the interface between the two streams, complete evaporation of all droplets occurs. At some distance, for example, greater than one meter, all cloud droplets will remain unaffected by the presence of the dry tongue. During the second stage, the interface breaks down and the two air masses intermingle. The final concentration of the new mixture will be reduced in magnitude from the unmixed cloudy air by an amount which is in proportion to the weighted mean of the values of cloud-free and cloudy air. Thus, finite blobs or streams of unsaturated air mix with nearly saturated blobs resulting in the complete evaporation of some droplets of all sizes; the main consequence of the inhomogeneous mixing process is that the overall concentration is reduced. As a result as air ascends and cools supersaturations rise to larger values than calculated in unmixed parcels of air and the largest drops grow much faster.

Shaw et al. [1998] proposed another mechanism of turbulence-induced condensation broadening in which cloud droplets are not randomly dispersed, but are concentrated in regions of low vorticity in turbulent flow. In regions of high vorticity the heavier droplets are centrifuged away from the vortex core, separating the droplets from lighter air. Thus in high strain regions of the turbulent flow, the concentration of droplets can be many times that found in the vortex cores. Thus if the turbulent eddies are embedded in generally rising air, the low concentration, high vorticity regions will experience high supersaturations while the high concentration, high strain regions will experience low supersaturations. Like the inhomogeneous mixing model, droplets in the low concentration regions will experience more rapid condensational growth, while those in the high concentration regions will experience less condensational growth. This should lead to large and small droplets coexisting which is essential for rapid growth by collision and coalescence.

4.2.1.3 Turbulence Influence on Droplet Collision and Coalescence

Turbulence can influence the collision and coalescence process in three ways:

- By enhancing collision efficiences.
- By enhancing the collection kernels.
- By producing inhomogeneities in droplet concentration.

The collision efficiencies we discussed earlier were calculated in laminar or stagnant flow. In turbulent flow droplets will be accelerating and thereby be able to cross streamlines more efficiently than in laminar flow resulting in enhanced collision efficiencies. Large droplets, having more inertia will be affected more by turbulence than smaller drops. Calculations by *Koziol and Leighton* [1996] suggest that this effect is small for droplets smaller than 20μm diameter.

But turbulence can also cause fluctuations on vertical fall speeds and horizontal motions, such that the collection kernel is enhanced [*Pinsky and Khain*, 1997; *Khain and Pinsky*, 1997], relative to that defined in laminar flow.

Because the collection rate is proportional to the square of droplet concentrations, inhomogeneities in droplet concentrations due to turbulence can produce enhanced regions of collection where the droplet concentrations are locally enhanced in, say regions of low vorticity [*Pinsky and Khain*, 1997].

4.2.1.4 Radiative Broadening

Consider a population of droplets that resides near cloud top for a sufficiently long time. Those droplets will emit radiation to space quite effectively if the atmosphere above is relatively dry and cloud free. As a result the droplets will be cooler than they would without considering radiative effects. This means that the saturation vapor pressure at the surface of the droplet will be lowered and the droplets will grow faster.

But radiation cooling is proportional to the cross sectional area of a droplet so that its effect is much greater on larger droplets than small ones [*Roach*, 1976; *Barkstrom*, 1978; *Guzzi and Rizzi*, 1980; *Austin et al.*, 1995]. In fact, *Harrington et al.* [2000] have shown that in a marine stratocumulus environment, when droplets are competing for a limited supply of water vapor, the larger droplets grow so rapidly by radiative enhancement that droplets smaller than 10μm in radius evaporate producing a bimodal size spectrum. This process is only effective in clouds where droplets reside near cloud top for time scales of 12 min. or longer such as fogs, stratus, and stratocumulus. Cumulus clouds with vigorous overturning “expose” droplets to space for too short a time.

Raindrops in excess of 8 mm in diameter, which grow by the condensation-coalescence mechanisms, have been observed in both clean and polluted environments [*Beard et al.*, 1986; *Hobbs and Rangno*, 2004]. This is despite the fact that the chance of a raindrop breaking up through collisions with other drops increases with increasing size [*Low and List*, 1982].

4.2.2 Ice Particle Mechanisms

Even though the temperature in a cloud may be below 0ºC, supercooled water droplets can still be present; such clouds may also contain ice particles. In Section 4.1.3 we discussed the nucleation of ice in clouds and ice multiplication mechanisms. Here we are concerned with the growth of ice particles to precipitable sizes in mixed clouds.

As early as 1789 *Benjamin Franklin* [1789] wrote "It is possible that, in summer, much of what is rain, when it arrives at the surface of the Earth, might have been snow, when it began its descent, but being thawed, in passing through the warm air near the surface, it is changed from snow to rain." This idea was not developed until the early twentieth century, when *Wegener* [1911] noted that ice particles will grow preferentially by deposition in a mixed cloud. Subsequently, *Bergeron* [1933] and *Findeisen* [1938] developed this idea in a more quantitative manner.

In a mixed cloud dominated by supercooled droplets, the air is close to saturation with respect to liquid water and is therefore supersaturated with respect to ice. For example, air saturated with respect to liquid water at –10ºC is supersaturated with respect to ice by 10%, and at –20ºC the air is supersaturated with respect to ice by 21%. These supersaturations with respect to ice are much greater than the supersaturations of cloudy air with respect to liquid water, which rarely exceed 1%. Consequently, in mixed clouds dominated by supercooled water droplets, ice particles will grow from the vapor phase much more rapidly than droplets. This can lead to a variety of ice crystal types, some of which may be large enough to precipitate. The optimum concentration of ice particles for the formation of precipitation is generally considered to be ~1 liter^{-1}. If ice particles significantly exceed this concentration, either naturally or by artificial seeding, the formation of precipitation may be reduced or not occur. If a cloud consists entirely of ice crystals it is said to be *glaciated*.

In a mixed cloud, ice particles can also grow by colliding with supercooled droplets, which then freeze onto them. This growth process, which is referred to as *riming*, can produce graupel particles and, if the cloud is deep enough and contains sufficient supercooled water, hailstones. Finally, ice particles in a cloud may collide and aggregate with each other, leading to larger particles.

The growth of ice particles, first by deposition of water vapor followed by riming and/or aggregation, can produce precipitation-sized particles. If temperatures at ground level are below 0ºC, these particles will reach the ground as snow; if the surface temperature is above 0ºC, the ice particles will partially melt, or melt completely, and reach the ground as wet snow or rain. An increase in the concentration of cloud droplets accompanied by decreases in the average size of the droplets (which can be caused by an increase in the concentration of CCN) may decrease growth by riming due to the lower collection efficiency of smaller droplets [*Borys et al.*, 2000, 2003; *Givati and Rosenfeld*, 2004].

4.3 PRECIPITATION EFFICIENCY

Precipitation efficiency is a measure of how effective a cloud, a rainband or a storm is in converting available water into precipitation. It is normally defined as [*Hobbs et al.*, 1980]:

$$\text{Precipitation Efficiency (PE)} = \frac{\text{total precipitation rate}}{\text{total condensation rate}}.$$

Instantaneous values of PE vary widely from near zero early in the lifetime of a cloud before precipitation has commenced to values exceeding 100% during the dissipation stages of a storm, when cloud-base moisture fluxes are near zero [*Market et al.*, 2003]. Thus, *Doswell et al.* [1996] suggest that PE is most meaningful when averaged over the storm lifetime. *Market et al.* [2003] propose that it is best to define a volume around a moving system and employ storm-relative winds in evaluating PE. In this way, storm-averaged PE can be obtained for a moving system. Such a procedure is similar to the floating target area basis for evaluation of the effectiveness of seeding Texas cumuli proposed by *Woodley and Rosenfeld* [2004]. *Woodley and Rosenfeld* used NEXRAD radars for their precipitation evaluations but more accurate radar estimates of precipitation can be obtained with polarization diversity radars [*Bringi and Chandrasekar*, 2001]. Such radars could provide useful statistics of storm-average PE's following radar identified floating storm targets.

Historically PE estimates are a mix of aircraft-derived measurements and radar estimates, with some providing storm-average values and others more point estimates, so care must be taken in interpreting these estimates [*Hobbs et al.*, 1980].

Braham [1952] estimated PE for ordinary thunderstorms using surface observations and soundings to calculate average moisture budgets. He estimated storm-averaged precipitation efficiencies of approximately 10%. Using aircraft and radar data, *Marwitz* [1972] inferred that PE varied inversely with windshear in U.S. High Plains thunderstorms (see Figure 4-19). *Marwitz* proposed that those storms in a strongly-sheared environment thrust more condensate into anvils. This is supported by PE estimates reported by *Heymsfield and Miller* [1988]. *Market et al.* [2003] however, found a weaker inverse dependence on vertical wind shear in their estimates of PE.

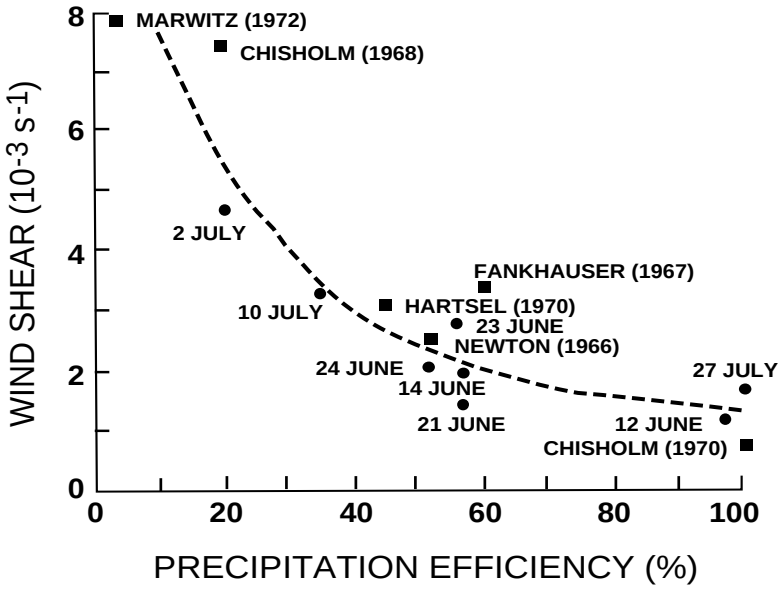

Figure 4-19. *Scatter diagram of wind shear versus precipitation efficiency for 14 thunderstorms that occurred on the High Plains of North America. From Marwitz [1972].*

Hobbs et al. [1980] concluded that rainbands in extratropical cyclones fall into two categories: those with PE's of ~100%, and those with precipitation efficiencies of ~50%. The former category includes warm-frontal, and some warm sector, and wide cold-frontal rainbands; the latter category includes narrow cold-frontal and some warm sector rainbands. Those rainbands exhibiting PE's of ~100% are characterized by a "seeder-feeder" mechanisms in which ice crystals from upper-level generating cells fall into lower-level

clouds where they grow by collecting water drops (referred to as *riming*) and ice crystals [*Bergeron*, 1950].

Fankhauser [1988] presented one of the most detailed studies of thunderstorm precipitation efficiency. Data were taken from seven storms during the Cooperative Convective Precipitation Experiment (CCOPE) using aircraft, rawinsondes, a surface mesonetwork and radar histories and calculated values ranging from 19% to 47%. Various environmental quantities, such as kinetic energy, cloud base area and height, and cloud base mixing ratio were found to be factors that had a strong positive correlation to PE levels. He found that variables such as the bulk Richardson number, the ratio of buoyant energy to the amount of wind sheer, and convective available potential energy (CAPE), a measure of potential updraft strength, did not correlate well with PE.

Table 4-1 summarizes some results from previous studies regarding lifetime-averaged PE values. As can be seen, there is a wide range of precipitation efficiencies, even among similar storm systems.

An alternate strategy for estimating precipitation efficiencies is to use drying ratio (DR) as proposed by *Smith et al.* [2003].
DR = total precipitation/vapor flux.
It encapsulates the moisture budget of the large scale air mass transformation. Because PE requires an estimate of vertical air velocity at cloud base, it is subject to rather large errors in those measurements. Since DR uses the ratio of precipitation to water vapor flux, it is easier to quantify. Moreover DR can be estimated using hydrogen and oxygen isotope analysis which permits evaluation using streamflow or sapwood collected near a stream.
Finally it is somewhat surprising that no one has made estimates of storm-averaged PE for storms developing in environment containing different cloud-nucleating aerosol concentrations. Perhaps the errors in estimating PE or DR are so great that the impact of aerosols cannot be extracted from the expected noise level.

Table 4-1. A sample of derived values of precipitation efficiency (PE) for various cloud systems. [From *Market et al.* [2003]].

AUTHOR	TYPE OF SYSTEM	PE (%)
Braham [1952]	Midlatitude thunderstorm	10
Newton [1966]	Midlatitude thunderstorm	50
Marwitz [1972]	Midlatitude hailstorm	15
Heymsfield and Schotz [1985]	Midlatitude squall line	25-40
Hobbs et al. [1980]	Rainbands in extratropical cyclones with a "seeder-feeder" mechanism	~50
Hobbs et al. [1980]	Other rainbands in extratropical cyclones	~20-50
Fankhauser [1988]	Midlatitude thunderstorm	19-47
Cotton et al. [1989]	Midlatitude Mesoscale convective complex (MCC)	49-113
Li et al. [2002]	Tropical convection	20-130
Market et al. [2003]	Midwestern (MCC)	4-48

4.4 MEASUREMENT OF PRECIPITATION

4.4.1 Introduction

Precipitation is a discontinuous geophysical field. It is raining on only ~4% of the earth's surface at any one time (*J. Kwaiatowski*, personal communication). An early description of rainfall measurement and its application to agriculture is from an Indian manuscript dated 400 B.C. [*Kautilya*, 1915], "In front of the storehouse, a bowl (Kunda) with its mouth as wide as an Aratni (18 inches) shall be set up as a raingauge (Varshanana)… Hence, i.e. according as the rainfall is more or less, the superintendent shall sow seeds which require either more or less water." Many current raingauges are based on the concept of catching rainfall in a bowl and measuring the contents at regular time intervals. Recent technological advances in rainfall measurement have focused on standardizing measurement in non-recording gauges, devising self-recording gauges [*Kurtyka*, 1953], and on remote sensing methods.

The spatial variability of precipitation and its intermittency in time make rainfall difficult to measure accurately. *Theissen* [1911] commented that:

"The fact that precipitation varies considerably over not only large but also quite limited areas is a matter of common observation. Many factors enter into the question as to why different amounts of precipitation are recorded at stations quite near one another, chief of which are the relation of stations to mountain ranges, their elevation, latitude, nearness to large bodies of water, and location in relation to the average tracks of storms. Any of these factors or any combination of them may cause a great difference between the rainfall in different sections of an area, as a State or large county."

The value of precipitation measurements depends on how well the measurement system is suited to the desired application. There is not a unique answer regarding the relative accuracy and precision of precipitation measurements since the magnitude of errors are dependent on the spatial and time scales of interest, the storm structure, and the instrument system making the measurement. There is also currently no consensus on how to report rainfall measurement uncertainties which makes comparison among different measurement systems and studies difficult.

A discussion of the different instruments for measuring precipitation can be found in Section 7.5. In it the various errors in the measurements are discussed, pointing to the difficulties of estimating the effects of pollution on precipitation. Section 7.5 also addresses the testability of the hypothesis that aerosols impact precipitation and provides an overview of the most common types of precipitation measurements and their associated uncertainties with an emphasis on empirical studies providing quantitative estimates of components of precipitation measurement uncertainty. A summary of the findings from that overview follows.

4.4.2 Summary

Uncertainties in precipitation measurement vary with the spatial scale, temporal scale, and storm type that are considered. For areal precipitation estimates derived from all types of sensors, storm total rainfall estimates from precipitating clouds covering larger areas with low spatial variability, of longer duration, and with moderate to heavy precipitation intensities generally have smaller uncertainties than estimates from short-lived, isolated

showers or light precipitation near the detection threshold of the measurement instrumentation. The few quantitative estimates of relative rainfall estimation error in the literature focus either on large areas and long time periods, such as a month or more, or on the subset of storms with moderate to heavy precipitation. These studies indicate that many of the independent sources of error have substantial biases and scatter. Representativeness error is estimated at 25-95% of hourly conditional mean rainfall and up to 50% for hourly areal average rainfall [*Tustison et al.*, 2001]. The daily radar/raingauge ratio for storms with at least 0.3 mm daily precipitation is only within a factor of 2 for 68% of summer days in Switzerland but these large daily uncertainties average to a summer seasonal bias of -11% [*Germann et al.*, 2006]. Comparison of radar derived rainfall over gauges (1 km^2) for storm totals with rainfall accumulations > 10 mm had root mean square errors from 10-40% when using the subset of gauges passing quality control, and up to 80% when all gauges in the network were used [*Steiner et al.*, 1999]. Errors for storms with lighter precipitation were not quantified but are expected to be higher. *Houze et al.* [2004] estimated ±50% uncertainties in radar-derived monthly areal average rainrates over 7 □ 10^4 km^2 tropical oceanic regions. Satellite temporal sampling errors, which are independent of the precipitation retrieval method, increase rapidly as temporal sampling decreases and range from 10% for 1 hourly sampling to 154% for 12 hourly sampling of daily areal average rainfall over a 100 km scale domain [*Steiner et al.*, 2003]. These values are from studies that have better control of error sources, such as calibration and instrument maintenance, than is typical worldwide and hence represent lower limits for rainfall measurement uncertainty. Uncertainties in snowfall measurement are larger than those for rain.

For long time scales, the impact of aerosols on precipitation is difficult to isolate from other sources of precipitation variability such as the location of storm tracks, urban boundary layer thermodynamics, and interannual cycles. Analysis of time scales of storm duration or shorter and spatial scales sufficiently small to distinguish regions under clearly observed aerosol plumes (≤ 50 km scale) would help to separate the impact of aerosols from other factors. At these short time and spatial scales, errors in precipitation measurement will typically be a factor of 2 or more. Given the large magnitude of these uncertainties, it will be difficult to discern the impact of aerosols that modify rainfall by less than a factor of 2!

4.5 GLOBAL DISTRIBUTION OF CLOUDS AND PRECIPITATION

The global distributions of clouds and precipitation are manifestations of three jointly interacting components of the Earth system— atmospheric circulations, the radiation balance, and the water cycle. At any given location, daily cloud and precipitation variability can be large since clear sky conditions can transition to overcast skies and rain within a few hours. When temporal averages of one month or more are calculated, climatological patterns of cloud and precipitation start to emerge. Large-scale atmospheric circulations yield regional differences in cloud and precipitation distributions, while the latent heat released as water vapor condenses into cloud droplets in turn helps drive the circulations. For a given region, the largest source of variability of clouds and precipitation is usually the seasonal cycle. Interannual variations in large-scale atmospheric oscillations such as El-Nino-Southern Oscillation (ENSO) and the North Atlantic Oscillation (NAO) are associated with interannual variability of global precipitation distribution.

4.5.1 Large-scale Atmospheric Circulations

The climatological mean surface wind field for an idealized ocean-covered Earth with the sun directly overhead at the equator is shown in Figure 4-20 [*Wallace and Hobbs*, 2006]. In middle and high latitudes, westerly wind belts centered at 45° N and 45° S dominate the circulation. The westerlies are perturbed by eastward migrating baroclinic waves which cause day-to-day weather at these latitudes. Low pressure centers formed in the middle latitudes migrate toward the poleward flank of the westerlies to form the subpolar low pressure belts. The tropical circulation is dominated by easterly trade winds in the northern hemisphere and southeasterly trade winds in the southern hemisphere. The trade winds are the surface manifestations of Hadley cells, meridional circulations which consist of equatorward flow in the boundary layer, rising motion near the equator, poleward return flow in the tropical upper troposphere, and subsidence in the subtropics. The middle latitude westerlies and lower latitude easterlies are separated by a sub-tropical high pressure belt centered on 30° latitude where surface winds tend to be weak. Jet streams at the tropopause level are located above the subtropical high pressure belts at the surface.

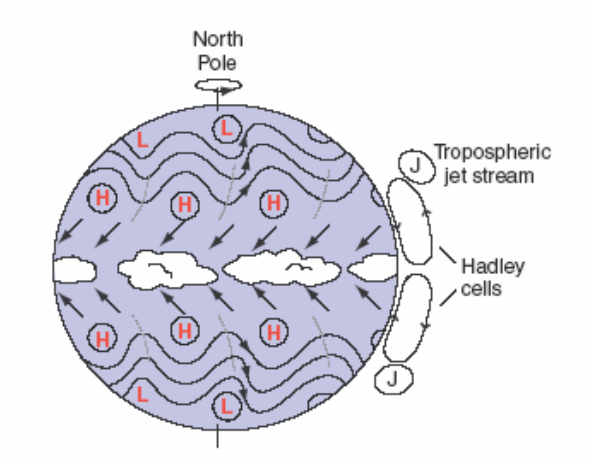

Figure 4-20. *Schematic description of sea-level pressure isobars and surface winds on an idealized ocean-covered Earth in perpetual solstice. The subtropical high pressure belts are indicated by the rows of H's while the subpolar low pressure belt is denoted by the rows of L's. Hadley cells and tropospheric jet streams are also indicated. From Wallace and Hobbs [2006].*

In the real world, surface winds tend to be stronger over oceans since there is less surface friction than over land. Compared to the idealized all-ocean Earth, the location of the intertropical convergence zone (ITCZ) is shifted northward to ~7° N and is associated with the influences of the land-sea geometry along the west coasts of the Americas and Africa and low cloud radiative forcing in the subtropics [*Philander et al.*, 1996]. The Asian monsoon circulation is driven by temperature contrasts between the tropical Indian Ocean and land surfaces in India and southeast Asia. Other large-scale circulations include the zonal overturning of the Pacific Walker circulation and Americas-Atlantic Walker circulation which have rising motion in the west and sinking motion in the east and circulations over Asia, the Middle East, North Africa and the Indian Ocean which have rising motion in the east and sinking toward the west. These zonal circulations exist year-round but vary considerably with the seasons. The longitudinal circulations have about a third of the mass flux of the peak Hadley cell, the latter occurring in early February and early August [*Trenberth et al.*, 2000].

4.5.2 Distribution of Clouds

Hartmann et al. [1992] used the International Satellite Cloud Climatology Project (ISSCP) cloud cover, cloud-top height and cloud-type datasets [*Rossow and Schiffer*, 1991] to yield

the global patterns of clouds subdivided by cloud type (Figures 4-21 to 4-23). High-cloud tops occur in regions with large scale ascent in the tropics and in midlatitude storm tracks associated with baroclinic waves. Optically thick high clouds occur where convection is most active and cover a smaller area of the globe than high, optically thin clouds. Low clouds are predominately oceanic and occur most frequently over the subtropical eastern ocean margins and over middle and high latitude oceans. The low clouds over the subtropical eastern oceans are associated with large scale subsidence (descending branch of the Hadley cell) and lower than average sea surface temperature which yield stratocumulus clouds trapped below an inversion. Low clouds over middle latitude oceans are usually stratus.

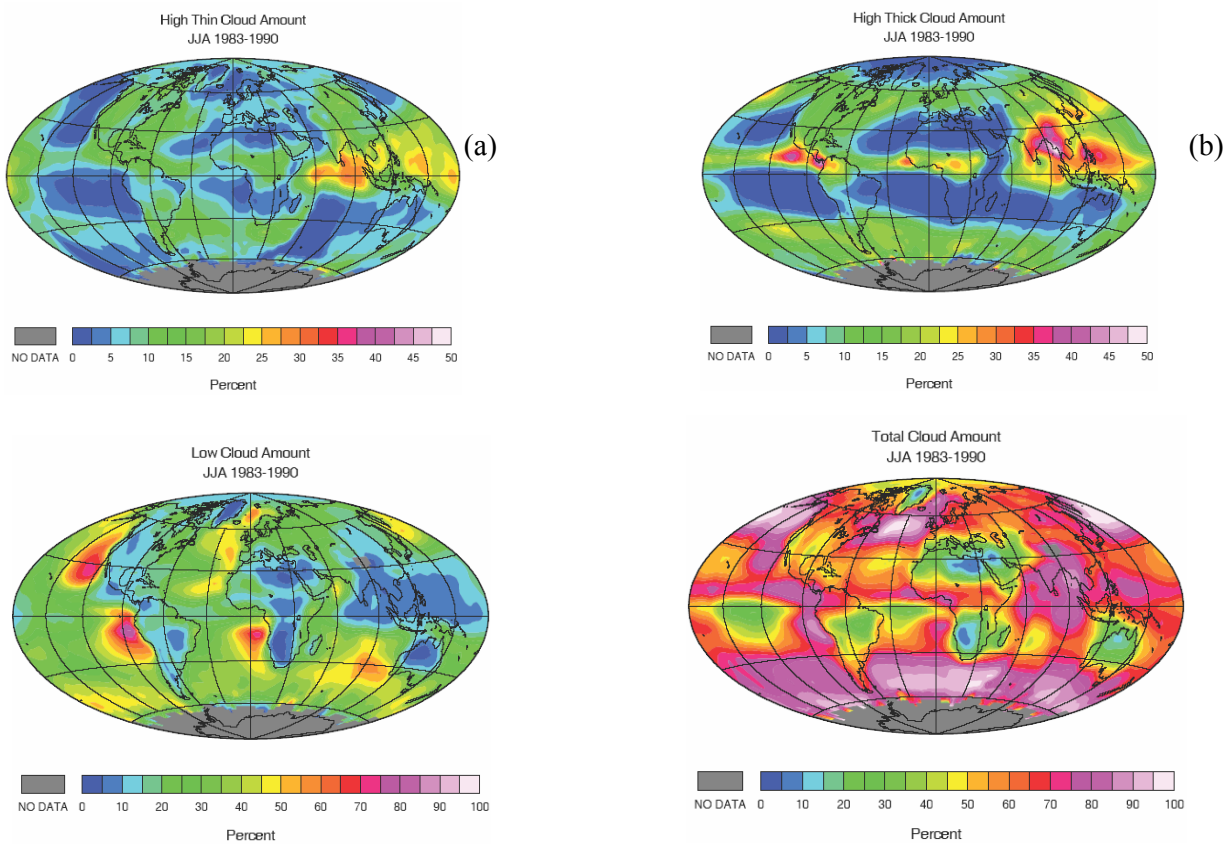

Figure 4-21. *Geographic distribution of cloud fractional coverage for June, July, August 1983-1990 for a) high thin cloud (cloud top height > 440 hPa and optical depth < 9.38), b) high thick cloud (cloud top height > 440 hPa and optical depth > 9.38), c) Low cloud (cloud top height < 440 hPa) and d) total cloud. Plots courtesy of D. L. Hartmann, University of Washington.*

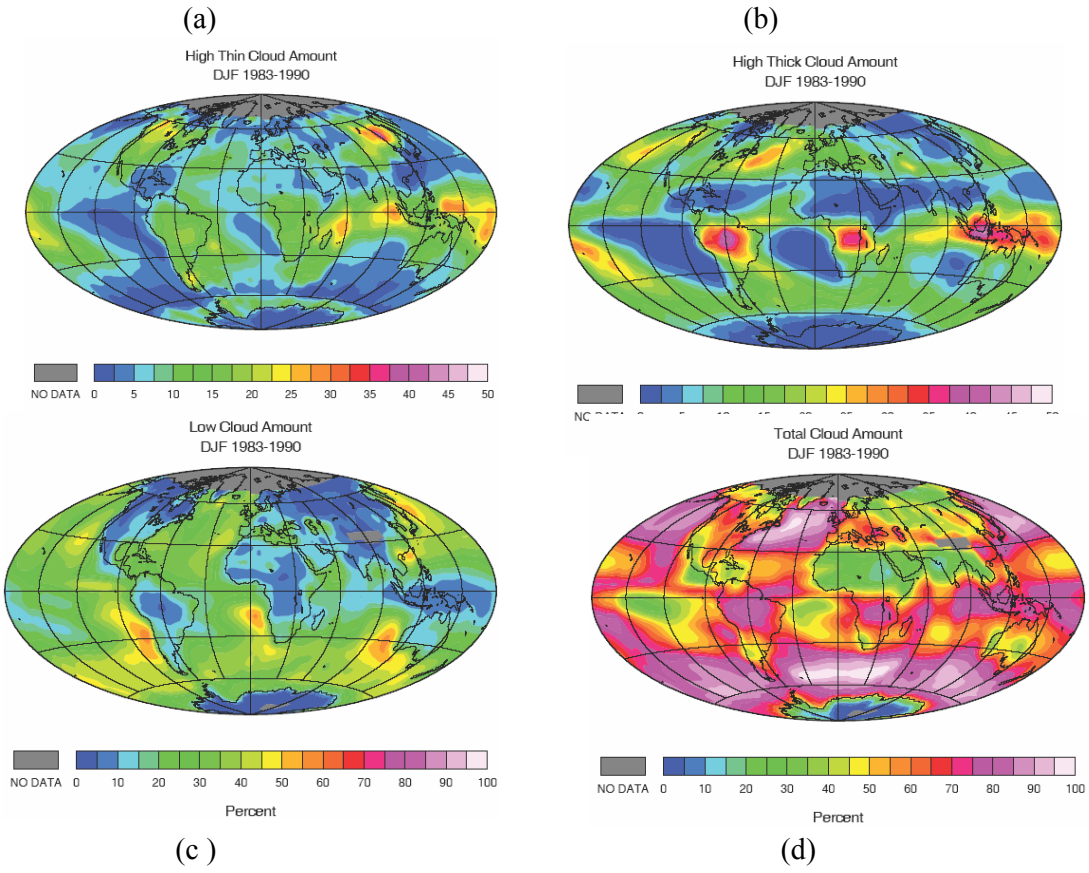

Figure 4-22. *As in Figure 4-21 except for December, January, February 1983-1990. Plots courtesy of D. L. Hartmann, University of Washington.*

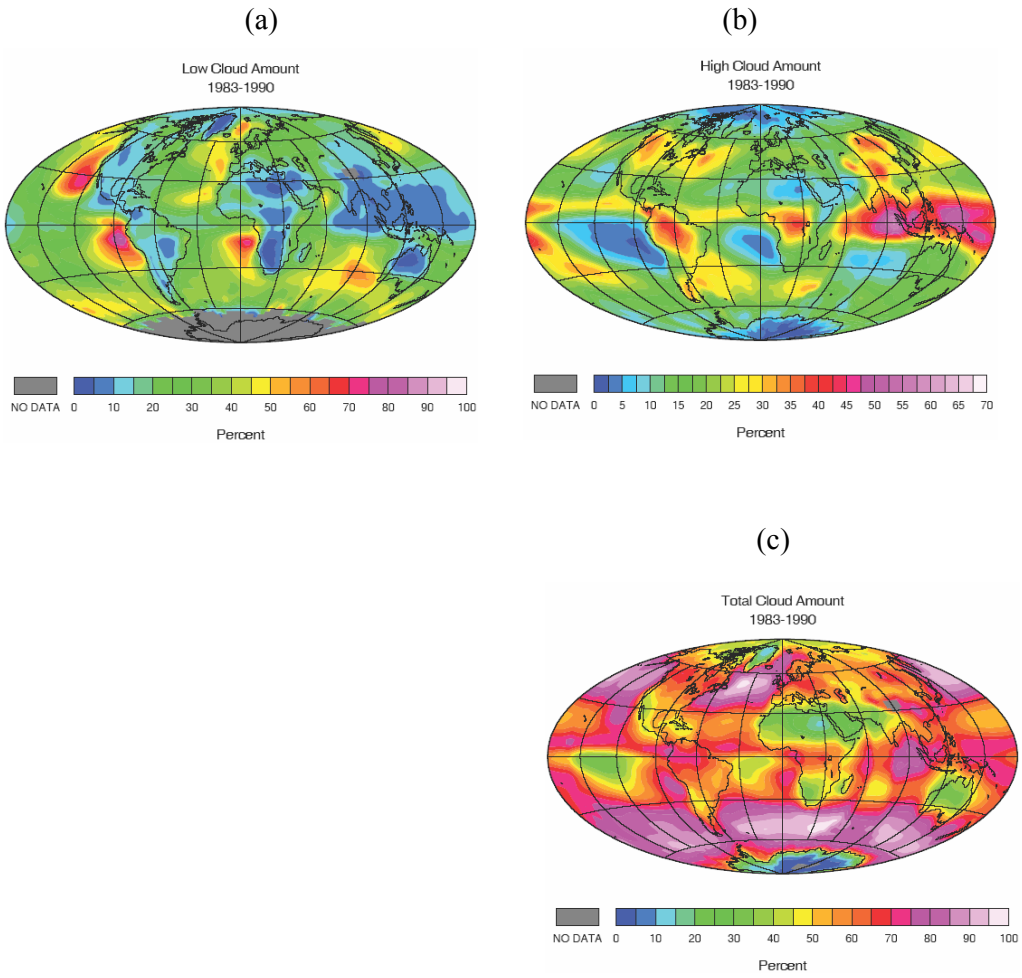

Figure 4-23. *Annual average cloud fractional coverage in percent estimated from ISSCP. (a) clouds with tops higher than 440 hPa, (b) clouds with tops lower than 680 hPa, (c) all clouds. Plots courtesy of D. L. Hartmann, University of Washington.*

Total cloud cover is greatest over middle latitude oceans in both the northern and southern hemispheres (Figure 4-23). Minima in cloud cover occur over subtropical desert regions but smaller cloud amounts also occur over the Caribbean Sea and the southern subtropical zones of the Pacific, Atlantic and Indian oceans [*Hartmann*, 1994]. Cloud cover has seasonal maxima in regions of intense tropical convection such as the Bay of Bengal in June-August (Figure 4-21) and over the Amazon and Indonesia in December-February (Figure 4-22).

4.5.3. Cloud Influence on Radiation Balance

In the global average, solar radiation reflected by clouds yields net radiative cooling which is compensated by the latent heat released in regions of precipitation and the conduction of sensible heat from the earth's surface. The albedo of clouds varies most

strongly with column-integrated water and ice contents but is also sensitive to droplet size, decreasing with increasing radius of cloud droplets [*Slingo and Schrecker* 1982]. Optically thick, high cloud tops have a larger contribution to net cooling *per unit area*, while the large areal extent of low clouds yield the largest contribution to net cooling *over the globe* [*Hartmann et al.* 1992]. Clouds with low cloud tops < 680 hPa have the largest impact on the net energy balance of the earth, providing about -16 W m^2 or 60% of net cloud forcing [*Hartmann et al.*, 1992]. High- and midlevel optically thick clouds each contribute about -7 W m^2. High and midlevel optically thin clouds make small positive contributions to global net cloud forcing since outgoing long wave radiation and absorbed solar radiation nearly compensate. Clouds are strong absorbers of long-wave radiation and are opaque to long-wave radiation for column-integrated liquid water paths ≥ 20 g m^{-2} [*Hartmann*, 1994].

4.5.4 Water Cycle

The water or hydrologic cycle describes the movement of H_2O as water vapor, liquid, and ice among reservoirs of water in the earth system including the atmosphere, fresh water lakes and rivers, ground water, alpine glaciers, the Greenland and Antarctic ice sheets, oceans, and the crust and mantle. Residence times for water in the atmosphere is on the order of days while residence times of water within lakes, rivers, ground water, and glaciers are days to years. For steady state conditions over a given area, areal average precipitation (P) equals evaporation (E) minus horizontal flux of water vapor out of the area. Within the ITCZ, the convergence of the trade winds provides an influx of water vapor and P >> E. For continents as a whole, P > E and the excess precipitation is transported to the ocean by rivers.

Precipitation cannot occur without clouds, so it is not surprising that the global distribution of precipitation (Figure 4-24) has many similarities to the global distribution of high clouds (Figure 4-6-23a). However, there are important differences between the cloud and precipitation maps related to the weak instantaneous correlations of cloud top properties and surface rainfall (see Chapter 7). Notably, the IR brightness temperatures of tropical oceanic mesoscale convective systems are poorly correlated to instantaneous surface rainfall rates [*Yuter and Houze*, 1998], and subtropical marine stratocumulus clouds typically yield more drizzle from regions with broken cloud compared to regions of unbroken clouds with higher areal average albedo [*Comstock et al.*, 2005, *Stevens et al.*, 2005]. The zonally averaged precipitation (Figure 4-25) is closely related to the global circulation pattern and cloud

pattern with peak values at the latitude of the ITCZ for the ocean, peak values over land associated with Amazonia and Indonesia, and secondary maxima at middle latitudes associated with the storm tracks of baroclinic disturbances. Global average precipitation is estimated to be between 2.6 to 3.1 mm day^{-1}, with higher average values over the ocean as compared to land (Table 4-2). On average, three quarters of the global precipitation falls over the world's oceans [*Adler et al.*, 2003].

Table 4-2. Global average precipitation in mm day^{-1} obtained using three methodologies: Global Precipitation Climatology Project (GPCP) Version 2 [*Adler et al.*, 2003], LW [*Legates and Willmott*, 1990] and JAE [*Jaeger*, 1976].

Surface	GPCP	LW	JAE
Ocean	2.84	3.50	2.89
Land	2.09	2.32	2.13
Total	2.61	3.13	2.65

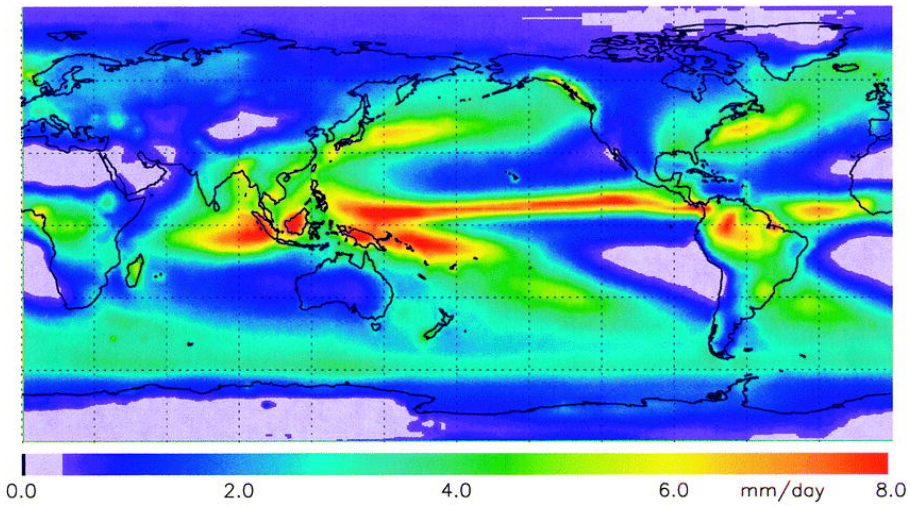

Figure 4-24. *The 23-year [1979-2001) annual mean precipitation (mm day^{-1}) based on GPCP Version 2. From Adler et al. [2003].*

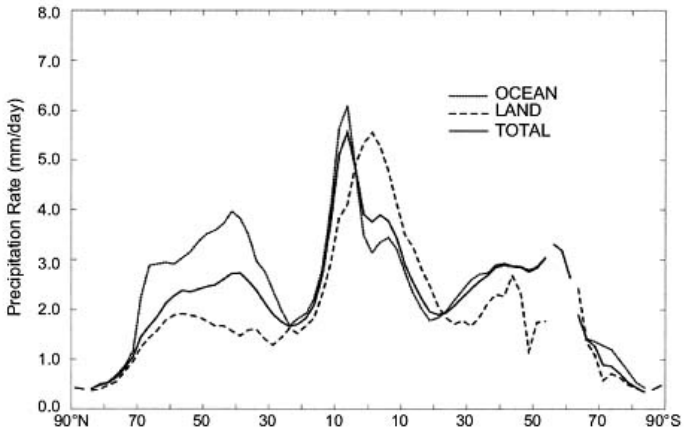

Figure 4-25. *Zonally averaged annual mean GPCP version 2 climatology (mm day^{-1}) calculated for 2.5° x 2.5° grid boxes. Total (solid line), ocean-only grid boxes (dotted line), Land-only grid boxes (dashed line) Gaps in high latitudes occur where there are no land or ocean grid boxes. From Adler et al. [2003].*

4.5.5 Variability and Trends in Global Precipitation

Global estimates of tropical precipitation between 30° N and 30° S have lower uncertainties as compared to middle latitude and polar precipitation estimates (Chapter 7.5), so we will focus our discussion of global precipitation variability to tropical areas. Figure 4-26 shows monthly global anomalies from a 23-yr tropical climatological mean value based on GPCP superimposed on 12-month running mean. Also overlaid are the Niño 3.4 SST index and months with significant volcanic eruptions. Monthly anomalies are typically smaller over ocean, usually < 0.4 mm day^{-1}, compared to larger variations occurring over land [*Adler et al.*, 2003, *Haddad et al.*, 2004].

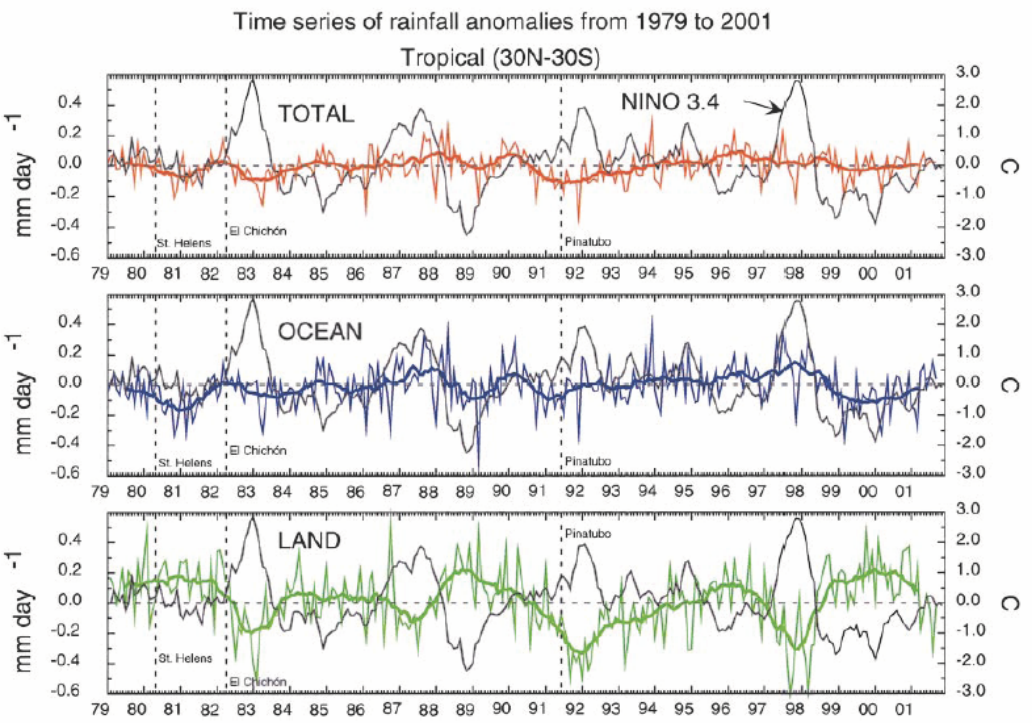

Figure 4-26. *Tropical (30° N to 30° S) averages of monthly precipitation anomalies (mm day^{-1}) for (top) total, (middle) ocean, and (bottom) land. Vertical dashed lines indicate months of significant volcanic eruptions. Black curves in all three panels indicate the Niño 3.4 SST index in °C. From Adler et al. [2003].*

Diverse studies have shown that the ENSO is a major factor in the interannual variability of sea surface temperatures, large-scale atmospheric circulations, and the global precipitation distribution [U.S. CLIVAR Pan American Implementation Panel, 2002]. Dry periods over the Maritime Continent, South America and Africa are associated with the warm phase of ENSO (Figure 4-27). These are some of the same regions where biomass burning is prevalent. The impact of major volcanic events on precipitation is difficult to isolate from that of ENSO [*Adler et al.*, 2003]. Removal of the ENSO signature on precipitation is a necessary step in assessing the long-term impact of aerosols on precipitation.

Although not as well documented in the current generation of satellite precipitation retrievals, the different phases of the NAO are associated with changes in the intensity and location of the North Atlantic jet stream and storm track [*Hurrell*, 1995], which in turn results in changes in precipitation patterns often extending from eastern North America to western and central Europe [*van Loon and Rogers*, 1978, *Rogers and van Loon*, 1979].

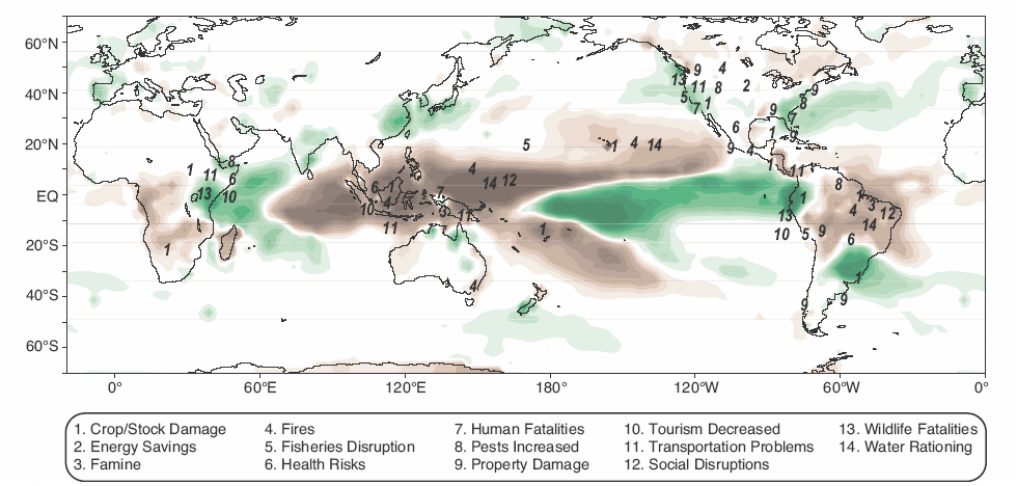

Figure 4-27. *Nature of global El Nino impacts during 1997-1998. Brown indicates dry regions while green indicates wet. From U.S. CLIVAR Pan American Implementation Panel [2002].*

In contrast to many climate predictions, the 23-year record examined by *Adler et al.* [2003] shows no noticeable trend in global or tropical precipitation. However, the size of the predicted precipitation increase associated with global warming is smaller in magnitude than the interannual variations associated with ENSO and is likely not detectable in such a short record.

CHAPTER 5: OBSERVATIONAL STUDIES OF THE EFFECTS OF AEROSOLS ON CLOUDS AND PRECIPITATION

Lead Authors: Zev Levin, Jean-Louis Brenguier, William Cotton,

Co-Authors: Graham Feingold, Yoram Kaufman, Marshall Shepherd

5.1 INTRODUCTION

The impact of aerosols on cloud macrophysical (cloud extent, cloud thickness and liquid water path), cloud microphysical (droplet and ice crystals concentrations and size distributions), and precipitation has received a great deal of attention for over 50 years. The pioneering work of *Gunn and Phillips* [1957], *Squires* [1958], *Squires and Twomey* [1961], *Warner* [1968] and *Warner and Twomey* [1967], to mention just a few, pointed out that high concentrations of CCN from anthropogenic sources, such as from industrial pollution and from burning of sugarcane, can increase cloud droplet concentration (CDNC), hence increasing cloud microphysical stability and potentially reducing precipitation efficiency. Although the connection between increased CCN and increased CDNC has been supported by many in situ observations, the impact of CCN on precipitation is less well established.

The main obstacle in assessing such a cause and effect relationship is the fact that different aerosol types generally correspond to different air masses, hence to different vertical profiles of moisture and stability. For example, in a subtropical boundary layer with a total water mixing ratio of 20 gm^{-3}, topped by a 200 m thick cloud, a 1 % decrease of the water mixing ratio corresponds to a decrease of the cloud layer thickness by a factor of 2, i.e. a factor of 4 decrease in LWP, which is likely to significantly reduce drizzle production. This impact is much stronger than what is expected to result from a CDNC doubling. Deeper clouds are less sensitive to small variations of the temperature and relative humidity, but they show a high sensitivity to the advection of moisture at cloud base and to the vertical profile of convective instability.

The following discussion illustrates how observational studies try to progressively overcome these obstacles by addressing each element of the long chain of physical processes connecting aerosols to precipitation.

5.2 WARM CLOUDS

5.2.1 What Kind of Aerosols Act as CCN

Beyond the ubiquitous sodium chloride and ammonium sulfate particles whose hygroscopic properties have been precisely characterized in the laboratory, field studies have shown that other aerosol types, either natural or anthropogenic may act as CCN [*Twomey and Wojciechowski*, 1969]. As an example of a specific anthropogenic source of CCN, *Hobbs et al.* [1970] measured the rate of production of CCN from large paper mills in Washington State to be as high as 10^{19} CCN per sec. *Eagan et al.* [1974a] identified plumes of CCN from paper mills up to 40 km downwind, and the concentrations of CCN in the plume exceeded those in the ambient air by a factor of ~4. The total particle count in the plume peaked after ~2 hr of travel time downwind.

5.2.1.1 Marine Aerosol and Seasonal CCN Variability

Oceans covering 2/3 of the Earth surface provide the major source of aerosol that is referred to as marine aerosol. It is composed of highly hygroscopic particles of sodium chloride and ammonium sulfate. The number concentration of CCN however is generally much lower than in natural continental or anthropogenic aerosols. Clouds growing in a marine aerosol background are therefore characterized by a low droplet concentration, between 10 and 100 cm^{-3}.

The CCN concentration in the marine aerosol is variable in space and time. In addition to the sea salt particles, the CCN concentration experiences significant changes driven by the temperature of the ocean, via the production of DMS. Atmospheric records taken at the Cape Grim Baseline Air Pollution Station (CGBAPS, 41° 25’ S, 141° 25’ E) over some 25 years have indicated that there are coherent seasonal cycles in the DMS flux, the concentration of CCN and its precursors [*Ayers and Gras*, 1991; *Ayers et al.*, 1991]. They also noted that, despite the absence of methane-sulphonate in winter (due to low DMS emission in winter), there is still a significant CCN concentration in the pristine atmosphere, which was therefore attributed to sea-salt particles.

Recent measurements in the northeast Atlantic marine air have shown that the organic fraction contributes ~15 – 63 % to the submicrometer aerosol mass [*O'Dowd et al.,* 2004], with peak values during summer when the biological activity is at its highest. The contribution of this component of marine aerosol to the CCN number concentration is still to be evaluated by field measurements.

5.2.1.2 Organic Compounds

The organic fraction of the fine aerosol mass is ~20-50% at continental mid-latitudes [*Saxena and Hildemann*, 1996; *Putaud et al.*, 2004] and up to 90% in tropical forested areas [*Talbot et al.*, 1990; *Andreae and Crutzen*, 1997; *Roberts et al.*, 2001]. An important part of this organic aerosol consists of water-soluble organic compounds (WSOC) [*Saxena and Hildemann,* 1996; *Kavouras et al.*, 1998; *Facchini et al.*, 1999a]. WSOC can influence the aerosol activation by increasing the amount of soluble material (thus making inefficient CCN into more efficient ones, although by replacing very effective material the reverse could happen), decreasing the surface tension as compared with the surface tension of pure water, modifying the wettability of the particle and affecting growth kinetics [*Shulmann et al.*, 1996; *Facchini et al.*, 1999b; *Raymond and Pandis*, 2002; *Kanakidou et al.*, 2005; *McFiggans et al.*, 2005]. Recently, considerable effort has been dedicated to the activation properties of WSOC in different parts of the world. Nevertheless, the activation behavior of WSOC is still not fully understood and quantified. This is mainly because of the multitude of organic species comprising the atmospheric aerosol and the lack of knowledge of their interactions and the interactions with the inorganic salts present in aerosols [*Kanakidou et al.*, 2005; *McFiggans et al.*, 2005]. However, advances have been made by investigating the activation of single organic compounds and by using simplified chemical compositions of aerosols, sometimes elaborated on the basis of laboratory analyses of atmospheric aerosol sampled in different environments [*Svenningsson et al.*, 2005].

Laboratory studies of activation of single-component aerosol particles at atmospherically relevant supersaturations have clearly shown that the solubility of the compounds is a key parameter for organic aerosol activation [*Novakov and Corrigan*, 1996; *Giebl et al.*,2002; *Raymond and Pandis*, 2002; *Hori et al.*, 2003; *Broekhuizen et al.*, 2004] and that the lowering of the surface tension can dramatically reduce the activation diameter of a moderately soluble organic particle [*Broekhuizen et al.*, 2004]. Moreover, it has been shown that the ability of organic particles to activate can be substantially enhanced by adding small amounts of soluble compounds as inorganic salts or surface-active species [*Hegg et al.*, 2001; *Bilde and*

Svenningsson 2004; *Broekhuizen et al.*, 2004]. Similar effects of the organic compounds were observed in laboratory experiments for mixtures of inorganic and organic compounds [*Svenningsson et al.*, 2005; *Henning et al.*, 2005].
Other measurements of the CCN properties of laboratory-generated SOA [*Van Reken et al.*, 2005; *Hartz et al.*, 2005] or combustion particles generated in a gas turbine combustor [*Pezold et al.*, 2005] also show the importance of organic compounds for mixtures similar to those existing in the atmospheric aerosol. Such studies are helpful for understanding the role of complex mixtures of compounds in the aerosol activation.

The influence of dynamical and thermodynamical processes on aerosol activation in the atmosphere makes it more difficult to assess the impact of organic compounds on clouds and precipitation. However, several studies based on field measurements have succeeded in showing the need to take into account the organic compounds, their solubility and surface tension for reproducing the observed concentrations of cloud condensation nuclei (CCN). *Lohmann and Leck* [2005] have shown the presence of surface-active particles from the ocean microlayer that account for an important fraction of CCN in a high Arctic aerosol. *Mircea et al.* [2005] showed that inorganic compounds by themselves cannot account for the CCN number concentration in the case of an Amazonian aerosol.

A recent modeling study by [*Ervens et al.*, 2005] noted that many studies have considered the important composition parameters of surface tension, solubility, molecular weight *(M_s)*, and van't Hoff factor independently. When considering the more realistic, simultaneous effects they noted that the negative relationship between surface tension and M_s [*Facchini et al.* 1999a] creates opposing trends so that increases in drop concentration due to lower surface tension (associated with higher molecular weight species) are countered by the decrease in drop concentration associated with higher M_s. Investigation of the simultaneous effects of solubility, surface tension and M_s suggested that for solubility greater than about 25 gL^{-1}, large reductions in drop number (relative to ammonium sulfate) are only expected at low updrafts (order 10 cms^{-1}), high aerosol concentrations (order 5000 cm^{-3}) and M_s greater than ~ 400 g mol^{-1}. Under many conditions, composition effects appear to be closer to ~ 15%. The authors attempted to reconcile their results with other laboratory and modeling studies. Some of the high (~100%) quoted differences in drop number due to composition effects appear to be associated with calculations that assume equilibrium droplet growth rather than a coupled model that simultaneously calculates the dynamical supersaturation field resulting from

expansion and cooling, and condensation growth. Thus it is important to note that composition effects on the aerosol activation diameter cannot be simply extrapolated to an effect on drop number concentration.

All these studies imply that more laboratory and field studies are needed to assess the role of organic compounds on aerosol activation in the atmosphere. Other processes such as primary and secondary aerosol formation and aerosol transformation are fundamental to characterize the organic aerosol and its interaction with water vapor.

5.2.1.3 Coated Mineral Dust Particles

Mineral dust particles are known to be efficient ice nuclei [*Pruppacher and Klett*, 1997] but not very efficient CCN. However, recent measurements of dust from the Sahara over the Mediterranean [*Levin et al.*, 1996], and of Asian dust over China and Japan during ACE-Asia [*Trochkine et al.*, 2003], show that dust particles can get covered by sulfate during their transport through the atmosphere, which may increase their effectiveness as CCN. More recently, *Levin et al.* [2005] showed that low-lying dust storms over the sea can lead to sea-salt coating on a large fraction of the dust particles. These types of coating could modify the particles into effective giant CCN as well as efficient ice nuclei. Sampling in clouds affected by particles coated with sulfate revealed the presence of relatively large drops close to cloud base (see Figure 5-1).

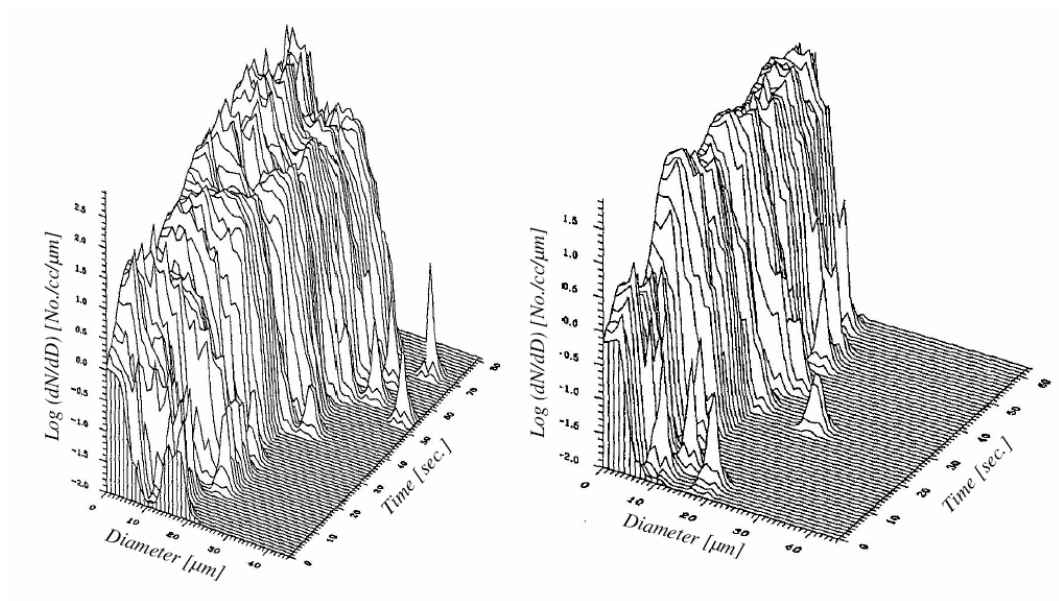

Figure 5-1. *Drop size spectra near the bases of clouds affected by large dust particles (left) as compared to the drop size spectra in cleaner clouds (right). The time axis represents the time of flight during the pass through the cloud. The airplane was flying at ~70 m s^{-1}.From Levin et al. (1996).*

Although the measurements described above suggest that the presence of larger drops at cloud base might increase rainfall, there are no in situ measurements that substantiate this hypothesis.

5.2.1.4 Biomass Burning

Warner and Twomey [1967] examined the production of CCN by sugar cane fires in Queensland. They also measured CCN production in a cloud chamber and found that burning sugar-cane leaf can produce about $8x10^{12}$ nuclei g^{-1}.

Eagan et al. [1974b] measured CCN from the burning of natural forest products. The CCN, active at 0.5% supersaturation, reached a peak value of 5000 cm^{-3} about 38 km downwind of the fire, compared to concentrations of 250–500 cm^{-3} upwind. It was estimated that 6×10^{10} CCN were produced per gram of wood consumed.

5.2.1.5 CCN Activation in Warm Clouds

The pioneering laboratory work of *Gunn and Phillips* [1957] demonstrated that increased pollution increases CDNC. Using their 3000 m^3 chamber they showed that average polluted air from the Gulf of Mexico produced stable laboratory clouds with over 3500 droplets cm^{-3}. As the air was slowly cleaned for 64 hours by high voltage precipitators, CDNC decreased to only about 10 cm^{-3}. *Radke and Hobbs* [1976] measured CCN concentrations of 1000–3500 cm^{-3} along the East Coast of the USA from Virginia to Long Island, compared to 100 cm^{-3} of CCN in clean maritime air and 300 cm^{-3} in continental air. They concluded that the global anthropogenic production rate of CCN may be comparable to the natural production rate.

At this point one may ask whether CDNC increases proportionally to the increase in CCN concentration. From collocated airborne measurements of both CCN and droplet concentrations, *Martin et al.* [1994], *Taylor and McHaffie* [1994], *Gultepe et al.* 1996, *Chuang et al.* [2000], *Snider and Brenguier* [2000], *Ramanathan et al.* [2001a] among others, have shown that regardless of location, increases in CCN lead to CDNC increases. However, these trends appear to taper off when the CCN concentration increases, as shown in the compilation of these diverse results [*Ramanathan et al.*, 2001b]. Indeed the proportion of available CCN actually activated in clouds depends on the peak supersaturation at cloud base (see Chapter 4) that is almost proportional to the intensity of the updraft. Stratocumulus clouds, with updraft speed of less than 1 ms^{-1} are not efficient at activating CCN particles (ASTEX and ACE-2 case studies in Figure 5-2), while deeper convective clouds can develop

updraft intensities of more than 10 ms^{-1}, hence activating most of the available CCN particles (North Atlantic case study in Figure 5-2).

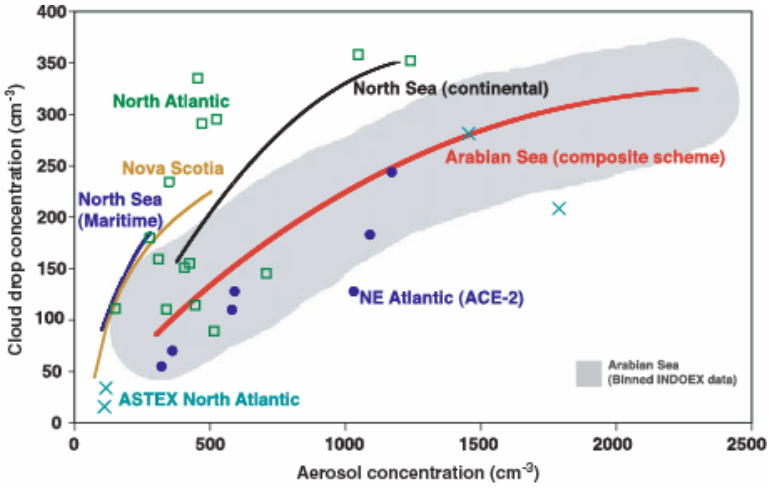

Figure 5-2. *Aircraft data illustrating the CDNC increase with the increase in aerosol number concentration. The thick red line is obtained from a composite theoretical parameterization that fits the INDOEX aircraft data for the Arabian Sea.*

Observational studies of the CCN activation process therefore require a comprehensive characterization of the particle size distribution, chemical composition, mixing state and surface coating (see Chapters 2 and 3 for more details), all contributing to the activation properties of the observed aerosols [*McFiggans et al.*, 2005]. The droplet concentration after activation and the vertical velocity at the activation level are also key parameters to document. The updraft intensity in a cloud field varies, as does the resulting CDNC. The droplet concentration is also reduced, after CCN activation, by other physical processes that are not directly linked to aerosol properties, such as entrainment-mixing, and coalescence and precipitation scavenging. *Pawlowska and Brenguier* [2000] characterized the probability distribution function, PDF, of the droplet concentration in 8 stratocumulus case studies of the ACE-2 CLOUDY-COLUMN experiment (see Figure 5-3).

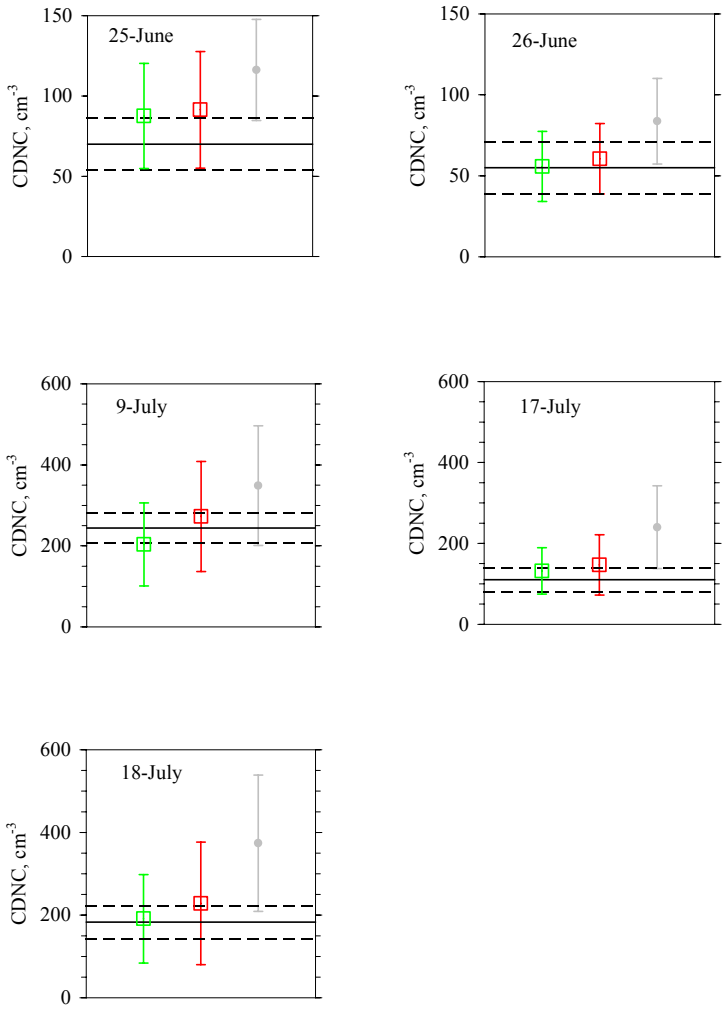

Figure 5-3. *CDNC values predicted by a CCN activation model for 5 ACE2 cases (colors correspond to different initialization modes). Error bars indicate the width (1 standard deviation) of the predicted CDNC probability distribution function corresponding to the measured frequency distribution of the vertical velocity at cloud base. Horizontal lines show the average and the average plus or minus 1 standard deviation of the conditionally sampled CDNC probability density function. From Snider et al. 2003.*

They showed that even after selection of the cloud samples that are not affected by entrainment-mixing nor by precipitation scavenging, CDNC varies from 0.5 to 1.5 of its mean value. These measured CDNC frequency distributions were further used to evaluate CCN activation predictions based on measured aerosol properties [*Guibert et al.*, 2003] and the measured frequency distribution of the vertical velocity at cloud base [*Snider et al.*, 2003].

5.2.2 Aerosol Impact on Cloud Microphysics

5.2.2.1 Deep Convective Clouds

Warner and Twomey [1967] and *Warner* [1968] reported that, through their activity as CCN, the release of smoke particles results in large CDNC increases, and consequent reduction in the sizes of cloud droplets (Figure 5-4), which may impede the coalescence process of rain formation.

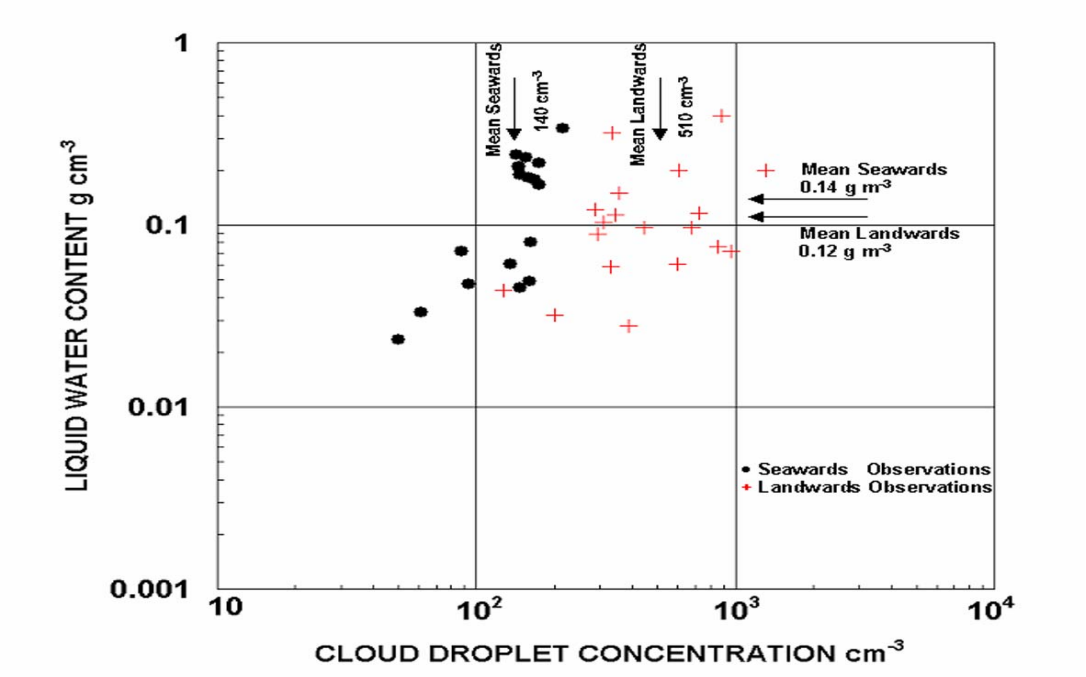

Figure 5-4. *Droplet concentration versus liquid water content of clouds affected by smoke from sugarcane fires in Australia. Note the CDNC increase from 140 to 510 cm^{-3} (red) and the slight decrease in liquid water content from 0.14 to 0.12 g m^{-3}, in the clouds affected by smoke compared to those affected by clean on-shore airflow (black). Adapted with modifications from Warner and Twomey (1967).*

Recently, *Andreae et al.*, [2004] reported on results from airborne and ground observations of cloud and precipitation development in the Amazon region. They divided their observations into four types of clouds. 1) Maritime shallow clouds over the ocean, which had low CCN concentrations and few cloud drops, including a few large ones, and rainfall from clouds that are not very deep. These were termed "Blue Clouds." 2) The name "Green Ocean" was given to clouds that developed in unpolluted conditions, mainly in the rainy season. These conditions were characterized by low CCN concentrations, due to washout by rain, and therefore resembled maritime clouds. 3) "Smoky Clouds" were those that were affected by high concentrations of CCN from smoke emitted from older fires. These particles remained in

the atmosphere for a long time due to the lack of rain in the dry season. They reported that the high concentrations of cloud drops reduce the efficiency for growth by collection. Therefore, these drops continued to grow by condensation and were surmised to reach higher altitudes and lower temperatures where ice can form. Since these clouds were deep they could produce lightning, hail and heavy rain. 4) "Pyro-Clouds" were clouds fed directly with smoke and heat from biomass fires. The high concentrations of CCN in the smoke produced large concentrations of small drops, thus limiting the warm rain production. On the other hand, some of the large ash particles in the smoke could produce large drops and enhance warm rain development. Figure 5-5 summarizes the drop size distributions in the four types of Amazonian clouds listed above.

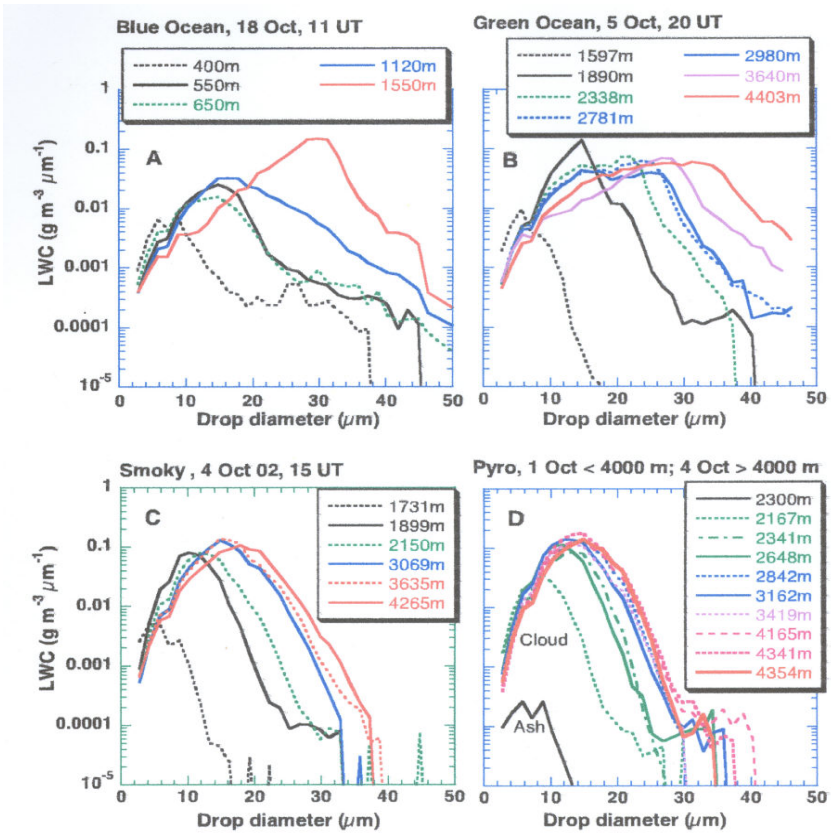

Figure 5-5. *The mass drop size distributions at different altitudes in a number of typical Amazonian clouds. Note the similarity and the wide drop size spectra in both the "blue" and "green ocean" clouds, compared to the narrow drop size spectra in the "smoky" clouds. Also note the large aerosol sizes in the ash and the resultant second peak in the drop size distribution in the "pyro-clouds." From Andreae et al. (2004).*

5.2.2.2 Boundary Layer Clouds

Garrett and Hobbs [1995] studied the effects of long-range transport of particles from polluted and unpolluted sources on the characteristics of shallow, non-raining stratus clouds around the Azores. The aerosols originating from continental sources (Europe) had a monomodal particle size distribution at about 0.05 μm, while the clean maritime air contained a bimodal particle size distribution with modes at 0.02 and 0.08 μm. The clouds affected by the polluted air had 160% higher concentrations of droplets, and a 27% smaller effective radius, than the clouds affected by the clean air (Figure 5-6).

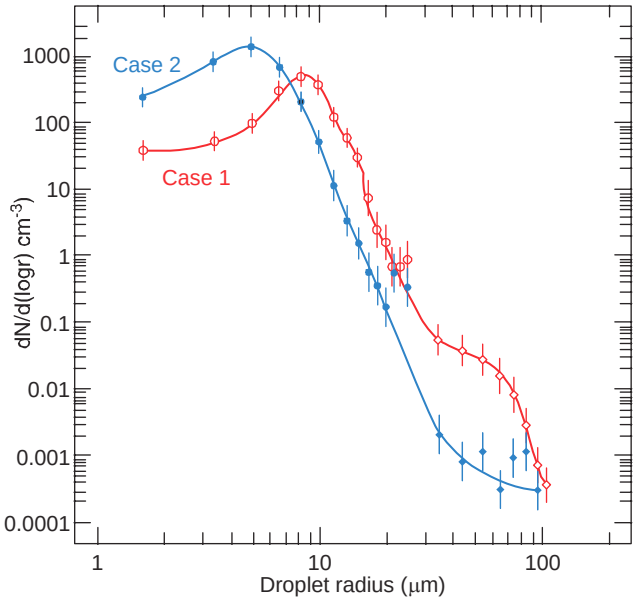

Figure 5-6. *Cloud droplet size distribution in clean (case 1) and polluted (case 2) warm clouds over the Azores Islands. Note the higher concentrations and the smaller sizes of the drops in the polluted clouds. Adapted from Garrett and Hobbs (1995).*

Relying on Cape Grimm observations of the CCN seasonal variability (see Sec. 5.2.1.1), the SOCEX experiment was designed to investigate whether these coherent seasonal cycles extend to the microphysical characteristics of the maritime cloudy boundary layer. The venue of the experiment was the atmosphere just west of Cape Grim, which is located at the northwestern tip of Tasmania, about 300 km south of the Australian continent. When the wind direction is from the southwest (*Baseline sector*, between 190^{o} and 280^{o}) the air stream has a typical fetch of 4000 to 5000 km over the Southern Ocean and is virtually devoid of anthropogenic influences.

Two experiments were carried out: SOCEX I, in July 1993 at the minimum of the seasonal cycles in DMS flux and CCN concentration; and SOCEX II in February 1995 at the maximum of the seasonal cycle. The results [*Boers et al.*, 1996; *Boers et al.*, 1998] from the experiments are summarized in Figure 5-7, that shows the average droplet concentration and the average effective radius as a function of pressure above cloud base, for the summer experiment (circles) and winter experiment (pluses). Only droplet properties (FSSP data) are shown, so the results exclude precipitation-size droplets. The seasonal differences are large and should be judged as a firm indication of the seasonality in the microphysical structure of clouds over the Southern Ocean. Near cloud base there is almost a factor of three differences in droplet concentration which ranges from 32 cm^{-3} in the winter to 94 cm^{-3} in the summer.

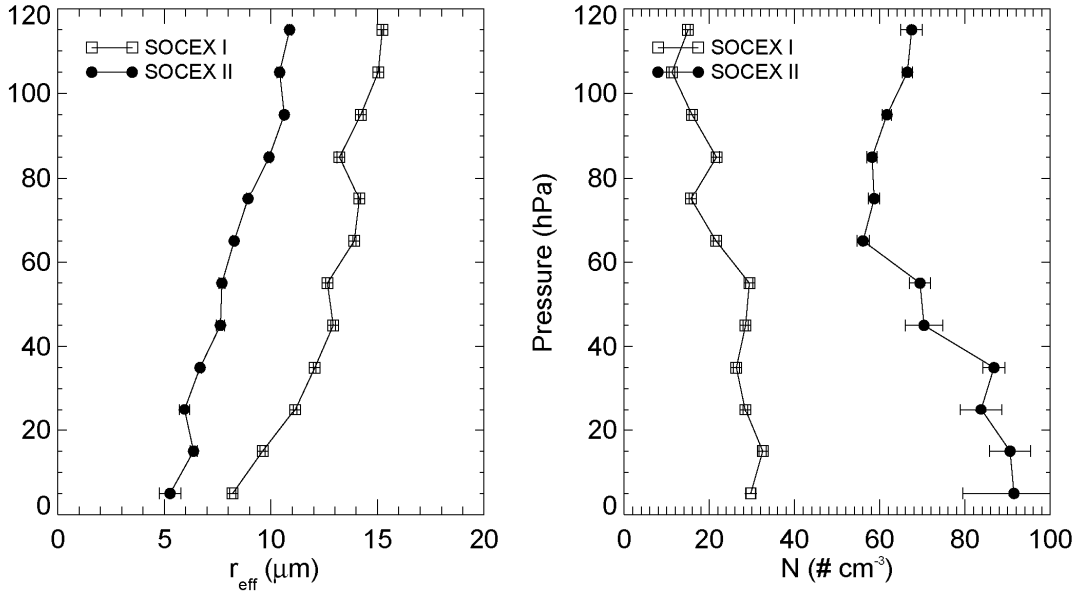

Figure 5-7. *In situ measured vertical profiles of droplet effective radius (left) and CDNC (right), for the SOCEX summer experiment (circles) and winter experiment (pluses).*

These results are almost identical to the predictions by *Boers et al.* [1994] who found, using a parcel model of adiabatic ascent, that the cloud base droplet concentration in unpolluted conditions over the Southern Ocean would range from 35 cm^{-3} in winter to 92 cm^{-3} in summer. Following *Twomey* [1977], the factor of three seasonal difference in droplet concentration implies a factor of 1.4 difference in cloud optical depth.

The ACE-2 CLOUDY-COLUMN experiment in 1997 provided a very comprehensive data set on the impact of anthropogenic aerosol on the microphysics of stratocumulus [*Brenguier*

et al., 2000a]. Figure 5-8 compares vertical profiles of CDNC, mean volume droplet radius and liquid water mixing ratio for the most pristine case (26 June, CDNC = 51 cm^{-3}), and the most polluted one (9 July, CDNC = 256 cm^{-3}). Frequency distributions of these parameters are based on more than 400 km sampling along a 60 km square track, and stratified over 30 m thick layers from cloud base to cloud top. The liquid water mixing ratio increases in average, as predicted by adiabatic convective models (Chapters 4 and 6). CDNC reaches its maximum value slightly above cloud base because in the first 30 to 80 meters, all CCN are not fully activated and some droplets are too small to be detected by the airborne droplet spectrometer. Close to cloud top CDNC is substantially reduced by cloud-top entrainment-mixing. The mean volume radius, that increases as predicted by the condensational growth theory (Chapter 4) up to cloud top, seems to be less affected by entrainment-mixing than CDNC. This feature is commonly referred to in the literature as inhomogeneous mixing [*Latham and Reed*, 1977; *Baker and Latham*, 1979; *Baker et al.*, 1980, *Burnet and Brenguier*, 2006).

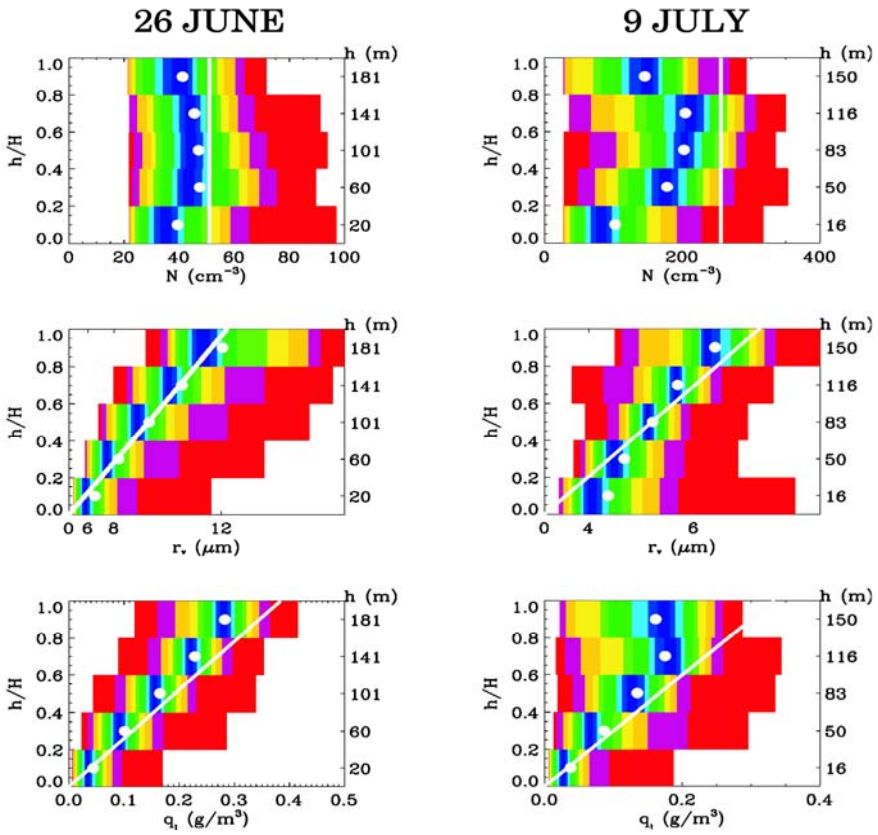

Figure 5-8. *Frequency distributions of N, r_v and q_l in five sub-layers, represented by their 5 % percentiles, for the 26 June and 9 July ACE-2 cases. Statistics limited to cloud samples ($N>20$ cm^{-3}). The mean value in each sub-layer is indicated by a white circle. The vertical line in the top row corresponds to the characteristic CDNC value N_{act} (51 cm^{-3} for 26 June, and 256 cm^{-3} for 9 July). In the next two rows the lines indicate the adiabatic droplet size prediction, with $N=N_{act}$, in the r_v distribution, and the adiabatic LWC in the q_l distribution. From Brenguier et al. (2003).*

5.2.3 Aerosol Impact on Cloud Radiative Properties

By modifying the microphysics of clouds, aerosols also affect their radiative properties hence allowing to detect their impact from satellite remote sensing measurements of the reflected solar and infrared emitted radiances. Most of the observational studies of the aerosol impact

on precipitation in fact rely on the interpretation of cloud radiative property changes that must therefore be precisely evaluated.

5.2.3.1 Ship Tracks

Ship tracks are narrow lines of perturbed regions in marine stratiform clouds caused by emissions from ships. Ship tracks appear brighter in satellite imagery, particularly at a wavelength of 3.7 μm [*Coakley et al.*, 1987]. Ship tracks (Figure 5-9) are often as long as 300 km or more and ~9 km wide [*Durkee et al.*, 2000, 2001]. They typically form in relatively shallow boundary layers between 300-750 m deep. They do not form in boundary layers >800 m [*Durkee et al.*, 2000]. Ship tracks are of considerable interest because they provide the most direct evidence that shallow, clean clouds can be modified by pollution sources that emit large concentrations of CCN.

Figure 5-9. *Ship tracks off France. From bands 1, 4 and 3 of MODIS on the Aqua Satellite. (Courtesy of NASA.)*

Hobbs and Garrett [2000] reported that various types of ships, burning both low-grade marine fuel oil (MFO) and U.S. Navy distillate fuel (NDF), emitted from ~4×10^{15} to 2×10^{16} total particles per kg of fuel burned (~4×10^{15} – 1.5×10^{16} particles per second). Diesel-powered ships burning MFO emitted particles with a larger mode radius (~0.03 – 0.05 μm) and larger maximum sizes than those powered by steam turbines using U.S. NDF. Consequently, for particles with similar chemical composition, those emitted by diesel ships burning MFO will serve as CCN at lower supersaturations, and will therefore be more likely

to produce ship tracks, than the particles emitted by ships powered by steam turbines using U.S. NDF.

The prevailing hypothesis is thus that the ship's trails appear brighter on satellite imagery because the effluent from the ships is rich in CCN particles. The more numerous CCN particles create larger concentrations of cloud droplets, which then reflect more solar energy than the surrounding clouds [*King et al.*, 1993]. Aircraft observations in ship tracks and surrounding clouds [*Radke et al.*, 1989, *Ferek et al.*, 1998] confirm that ship tracks exhibit higher droplet concentrations, smaller droplet sizes, and higher liquid water content than surrounding clouds. In some cases, ship tracks appear to be thicker than the ambient cloud [*Ackerman et al.*, 2000]. *Radke et al.* [1989] found that the concentration of drizzle drops (droplets of diameter ≥200 μm in ship tracks was only ~10% of that in surrounding clouds. This supports the laboratory results of *Gunn and Phillips* [1957] and *Albrecht's* [1989] hypothesis that a CDNC increase should reduce drizzle production. Another hypothesis is that the ship track clouds exhibit higher liquid water content because heat and moisture emissions from ships create deeper and wetter (hence brighter) clouds [*Porch et al.*, 1990]. This hypothesis is supported by the observation of ship tracks in an apparently cloud-free sky [*Conover*, 1966]. *Porch et al.* examined this hypothesis and showed that ship tracks are not only characterized by greater brightness but also by clear bands on the edges of the cloud tracks. They speculated, and provided some modeling evidence, that the heat and moisture fluxes from ship effluents excite a dynamic mode of instability which, in some marine stratocumulus, leads to enhanced upward and downward motions associated with the cloud circulations. However, measurements during the Monterey Area Ship track Experiment (MAST) suggest that heat and moisture emissions from ships are much too small to have any impact on clouds [*Hobbs et al.*, 2000]. An alternate explanation for the formation of deeper and wetter clouds in ship tracks, and perhaps clearing to the sides of ship tracks, is that when drizzle is suppressed, cloud top radiative cooling is enhanced. The enhanced cloud top cooling destabilizes the cloud layer, which results in strong ascending motions in the clouds that transports more moisture aloft making the clouds wetter and deeper. In addition, in compensation for the enhanced upward motions, sinking motions surrounding the regions of enhanced ascent could cause clearing just outside of ship tracks.

An extensive series of papers on ship tracks can be found in a special issue of the *Journal of the Atmospheric Sciences* (volume 57, 15 August 2000) devoted to the MAST.

Ship tracks nicely illustrate the complexity of the aerosol effects on clouds by showing that impacts on precipitation formation can hardly be examined independently of concurrent dynamical and radiative feedback processes. Note however that ship tracks are an extreme realization of the aerosol impact on clouds because of the amount of CCN released and their narrow spatial extent that may facilitate the development of very specific dynamical modes that are not representative of extended boundary layer clouds. Their narrow extent also facilitates detection through the radiance contrast with the surrounding cloud.

5.2.3.2 Extended Cloud Systems

During ACE2 CLOUDYCOLUMN, the aerosol properties and cloud microphysical properties discussed above in Sec. 5.2.1.5 and 5.2.2.2, were measured by two instrumented aircraft flying below and inside the stratocumulus, respectively. Cloud radiative properties were measured simultaneously by a third aircraft equipped with a nadir pointing multispectral radiometer, flying above the cloud layer, and following the same track as the in situ aircraft. Figure 5-10 shows the vertical profiles of the mean volume droplet radius measured in situ, and the conditional frequency distributions of the remotely sensed visible (VIS) versus Near IR (NIR) reflectances for the 26 June and 9 July ACE2 cases. The grids on the background reproduce radiative transfer simulations in adiabatic clouds for various values of CDNC and of the geometrical thickness [*Schüller et al.* 2003]. They corroborate the *Twomey* hypothesis that polluted clouds have a higher reflectance than pristine clouds at constant liquid water path and that the optical thickness scales as $LWP^{5/6}N^{-1/3}$ [*Brenguier et al.* 2000b].

While the impact of aerosols on cloud microphysics has been clearly established since the sixties, the ACE2 closure experiment, relying on collocated and independent measurements of aerosol properties, cloud microphysics and cloud radiative properties, provided compelling observational evidence of the link between these microphysical changes and radiation at the scale of a cloud system, i.e. at a much larger scale than the ship tracks. This quantitative assessment of the link between cloud microphysics and radiation is a crucial step because retrievals of cloud properties from ground or satellite remote sensing instruments that are discussed in the next sections and in more detail in Chapter 7 rely on similar measurements of cloud radiative properties.

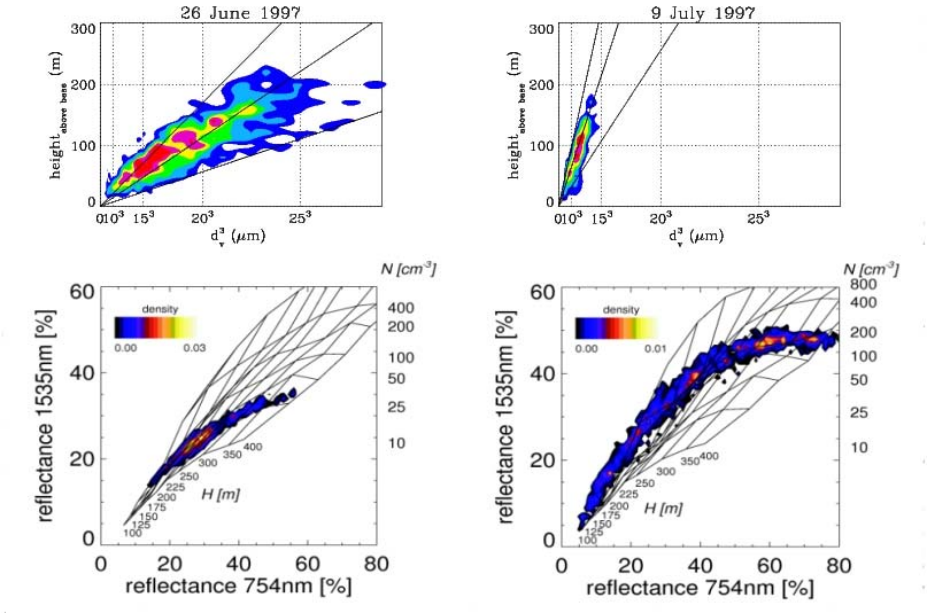

Figure 5-10. *Vertical profiles of the droplet mean volume diameter (top) and conditional frequency distributions of the remotely measured VIS versus NIR reflectances above the same cloud layer (bottom) for the ACE2 26 June pristine case (left) and 9 July polluted case (right). From Pawlowska and Brenguier, 2000 (top) and Schüller et al., 2003 (bottom).*

5.2.4 Satellite Monitoring of Aerosol and Cloud Properties

Field experiments are designed to address specific questions and test hypotheses in detail by focusing a comprehensive suite of in situ and remote sensing instruments on a selected atmospheric phenomenon. But they are limited in time and spatial coverage and only provide a few case studies. Long term observations of clouds in contrast rely on remote sensing that can be operated continuously from the ground or on board satellites. Clouds vary widely in space and time due to variation of atmospheric conditions. The aerosol effect can be only a small perturbation on the large natural variability. The wide spatial scale of satellite data can provide the large statistics necessary to separate the aerosol forcing on cloud properties from natural variability. With the advancement in remote sensing techniques, it is now possible to estimate the effects of the aerosol on clouds over much greater spatial and temporal extents. Of course, due to their larger field of view and coarser spatial resolution, satellite

measurements cannot resolve aerosol effects on as small scales as in situ measurement can (e.g., due to issues related to cloud contamination at the scale of individual clouds).

Because of the link between cloud microphysics and radiation, remote sensing techniques can be used to retrieve cloud microphysical properties and further establish statistical correlations with collocated aerosol properties. The response of remote sensing instruments depends on the technique: for active remote sensing instruments, LIDAR backscattering is sensitive to the second moment of the cloud particle size distribution while radar backscattering is rather proportional to the 6^{th} moment. For passive remote sensing instruments, the reflected radiance in the visible range depends on the cloud optical thickness, while in the near-infrared range it is sensitive to the particle effective radius (the ratio of the third to the second moment) and microwave radiation emitted by warm clouds is proportional to the liquid water path. Consequently, the retrieval of cloud microphysical properties from satellite often involves a combination of passive and active instruments operating at different wavelengths (see Chapter 7).

5.2.4.1 Aerosol Properties

In Chapter 7 we discuss the development of remote sensing capabilities over the course of 20 years, using a single or dual wavelength and single angle of observations 20 years ago that were not designed for aerosol measurements (e.g. the AVHRR, TOMS, METEOSAT, and GOES satellite instruments) to the newer instruments using wide multi spectral (MODIS), multi angular (MISR), polarization sensitive (POLDER) and mixed spectral-angular instruments (ATSR) that were specifically designed for aerosol measurements. Although these new generation instruments provide the most detailed information on the column aerosol concentration and properties, the older instrument (AVHRR, TOMS, GOES) have the longest record and provide the best chance to observe long term regional and global systematic variation in the aerosol burden and effects on clouds and precipitation.

Long term records of aerosol concentrations were obtained from TOMS and AVHRR that showed a systematic increase in the aerosol concentration in the developing world; e.g. 10% a year increase was reported for India [*Massie et al.* 2004]. Global observations by TOMS and AVHRR show the impacts of volcanic eruptions and seasonal variability but no clear global trend [*Torres et al.*, 2002; *Geogdzhayev et al.*, 2005]. The AVHRR study also showed evidence of reduction in the aerosol emissions in the former Soviet Union. AVHRR and

Meteosat observations were used to track emission of dust from Africa [*Carlson and Prospero*, 1971; *Moulin*, 1997] and correlate them with changes in the air circulation,

These satellite observations used mainly the aerosol optical thickness (AOT) as a measure of the aerosol column concentration. There is an issue with that approach when applied to aerosol interaction with clouds. For fine aerosol the AOT is proportional to the aerosol volume concentration while for coarse aerosol it is proportional to the cross section concentration. Therefore on the global scale the correlation of AOT with CCN or aerosol number concentration may be low, because the ability of aerosols to be efficient CCN depends on their size and composition while the AOT depends on the aerosol extinction. *Nakajima et al.*, [2001] used the product of AOT with a measure of the aerosol size – the Angstrom exponent to represent better the spatial variation of column CCN concentration. The usefulness of the aerosol index as a CCN proxy has recently been evaluated using in-situ data by *Kapustin et al.* [2006], who pointed out that aerosol humidification may be a significant compounding factor.

Data from the new era satellites can be better linked to CCN and cloud processes, by reporting not only the AOT but also separating it into fine and coarse aerosols. MODIS does the separation using spectral properties [*Tanré et al.*, 1997], MISR using the angular properties [*Kahn*, 2001] and POLDER using the strong polarization of the fine aerosols [*Breon et al.*, 2002]. The ability to separate fine from coarse aerosol from space enables an estimate of the anthropogenic contribution to the global aerosol system. It is estimated that 20% of the aerosol AOT over the ocean is of anthropogenic origin [*Kaufman et al.*, 2005a]. Advance analysis of a combination of POLDER data from the PARASOL mission, together with the wide spectral MODIS data shows the potential to retrieve not only higher accuracy optical thickness of the fine and coarse aerosols but also to estimate the size of the fine aerosol, needed for precise conversion into number of particles and estimate of a CCN proxy [*Gerard et al.*, 2005]. These methods are yet to be applied to study aerosol-cloud interaction.

5.2.4.2 Cloud Optical Thickness and Droplet Effective Radius

The *Twomey and Cocks* [1989] and *Nakajima and King* [1990] technique described in Chapter 7 has been extensively used to retrieve cloud optical thickness and droplet effective radius from satellite multispectral radiances and to examine the aerosol impact on clouds. *Kaufman and Nakajima* [1993] used AVHRR 1 km resolution data to study well-developed

clouds in the Amazon region during the dry-burning season. An increase in the smoke optical thickness (measured at a wavelength of 0.55 μm) from an average background value of 0.2 to 1.0 in very hazy conditions decreased the effective cloud droplet radius from 15 to 8 μm. Though the absolute droplet size is difficult to measure from satellites, the decrease in cloud droplet size by 40% with five-fold increase in aerosol concentration (represented by the aerosol optical thickness measured in clear pixels) is a good indication of the overall effect of the aerosols on clouds. The increase in the smoke optical thickness and the corresponding decrease in the average drop size were associated with a decrease in the cloud reflectance from 0.71 to 0.68. This may be due to absorption of sunlight by black carbon in the smoke, which reduces cloud brightness. This may also lead to a warming of the atmosphere and a cooling of the surface, thus tending to reduce the strength of convection.

To detect if the aerosol affects cloud brightening due to increases in CCN in more susceptible (less reflective clouds), *Kaufman and Fraser* [1997] used a different cloud selection technique to highlight less developed clouds. The results showed that smoke increases cloud reflectance from 0.35 to 0.45, while reducing droplet size from 14 to 9 μm. However, *Kaufman and Fraser* found that the smoke effect varies systematically with the location of the measurements: in the moist tropical forest in the north of Brazil, the smoke had a maximum effect on clouds, while in the drier Cerrado in the south of Brazil the effects were minimal.

Further analysis of two years data over the Amazon region by *Feingold et al.* [2001] confirmed the latitudinal dependence of the effect of smoke on clouds, although they showed that it was unrelated to the humidity gradient. They also found a substantial difference between the two years they analyzed [1987 and 1995]. Saturation of the response of cloud droplet size to aerosol occurred at an aerosol optical depth of 0.8 in 1987 and 0.4 in 1995.
Han et al. [1994] examined ISCCP data and found "the expected systematic decreases of the droplet effective radius over land compared with over ocean and in the Northern Hemisphere compared with the Southern Hemisphere", but not the corresponding expected cloud albedo increase. *Han et al.* [1998] extended the statistical approach to the seasonal and geographic variability of cloud albedo and droplet effective radius, in relation with the LWP variability. They concluded "that cloud albedo increases with decreasing droplet size for most clouds over continental areas and for all optically thicker clouds, but that cloud albedo decreases with decreasing droplet size for optically thinner clouds over most oceans and the tropical

forest". Observations using AVHRR satellite data over the oceans by *Nakajima et al.* [2001] however, do not show any systematic trend of liquid water path (derived from cloud optical depth and drop size) on column aerosol number concentration over the full range of column aerosol number concentrations.

Wetzel and Stowe [1999] used NOAA PATMOS data to evaluate the relationship between aerosol optical depth and cloud droplet size. POLDER satellite data were used by *Breon et al.* [2002] to derive aerosol concentrations and cloud droplet effective radii from 8 months of spaceborne measurements, and to explore the aerosol effect on cloud microphysics. It was found that the cloud droplet size decreased with increasing aerosol index (a measure of the aerosol column number concentration), showing that the effect of aerosols on cloud microphysics occurs on a global scale. However, the extent of the drop-size response to changes in aerosol was much lower than expected from theory.

Similar cloud optical thickness and droplet effective radius retrievals were examined against sulfate burden simulated with a chemical transport and transformation model [*Harsvardhan et al.*, 2002; *Schwartz et al.*, 2002]. The analysis of two episodes of substantial influx of sulfate aerosol from industrial regions of Europe and North America to remote areas of the North Atlantic revealed "a decrease of the droplet effective radius concomitant with the increase in modeled sulfate burden", while "cloud optical thickness and albedo exhibit little evident systematic trend over the episodes". *Han et al.* [1998], *Harsvardhan et al.* [2002], and *Schwartz et al.* [2002] speculated that the variability of LWP was the most likely reason for this puzzling observation, but these studies were missing the independent LWP measurements required to corroborate their hypothesis.

These contradictory observations reflect the fact that cloud radiative properties are primarily determined by the cloud macrophysical properties, such as LWP. CDNC only modulates the optical thickness. Indeed, within the idealized framework of the *Twomey* hypothesis, the cloud optical thickness increases as $N^{1/3}LWP^{5/6}$. The two radiative parameters that are measured from satellite, optical thickness and droplet effective radius, are therefore not sufficient to distinguish between changes in the cloud macrostructure and possible impacts of aerosols on cloud microphysics and precipitation. To overcome the ambiguity due to the natural variability of LWP, two different approaches have been developed.

Liquid Water Path and Droplet Concentration

If the observed cloud field contains non-precipitating convective cells, optical thickness and droplet effective radius can be combined to derive information on CDNC and the cloud geometrical thickness or LWP. *Brenguier et al.* [2000b] developed the technique using a vertically stratified adiabatic cloud model to build up the neural network training data base necessary for the processing of the measured radiances (see Chapter 7). In this scheme, LWP is proportional to H^2. The technique was validated [*Schüller et al.* 2003] against the ACE2 data set, where cloud geometrical thickness and CDNC were directly measured in situ. Figure 5-11 shows the comparison between retrieved and in situ measured values of these two parameters. The CDNC differences between pristine (blue and purple) and polluted (yellow orange and red) are precisely captured. The cloud geometrical thickness, hence LWP however are always overestimated. The origin of this bias, which is connected to the current overestimation of the droplet effective radius in most radiance retrieval techniques, has not yet been identified.

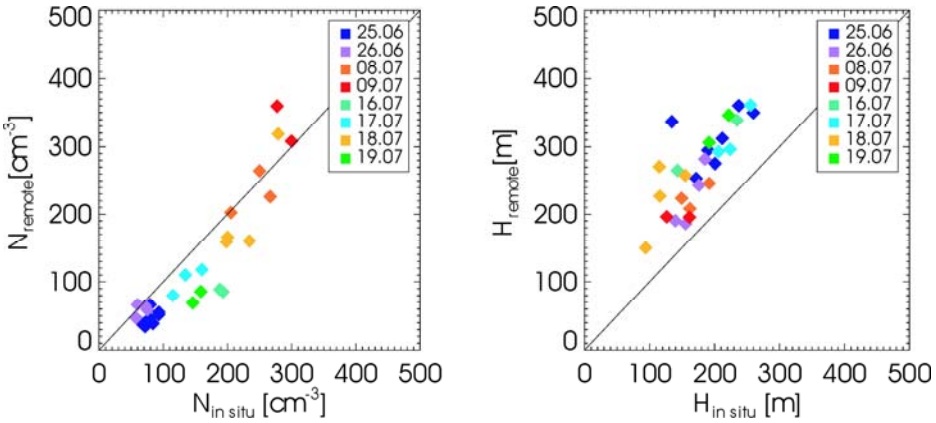

Figure 5-11. *Comparison between retrieved and in situ measured values of CDNC and cloud geometrical thickness in non-precipitating stratocumulus*

The technique has been extended to the retrieval of LWP (or cloud geometrical thickness) and CDNC from MODIS radiances (*Schüller et al.*, 2005).

Recently *Boers et al.* (submitted to JGR) have improved the technique by taking into account sub-adiabatic LWC values in the cloud layer and tested it against long term observations of the seasonal CCN variations recorded at Cape Grimm. Over the four years, the retrieved

CDNC closely follows the seasonal variations of the CCN concentration at the ground (Figure 5-12).

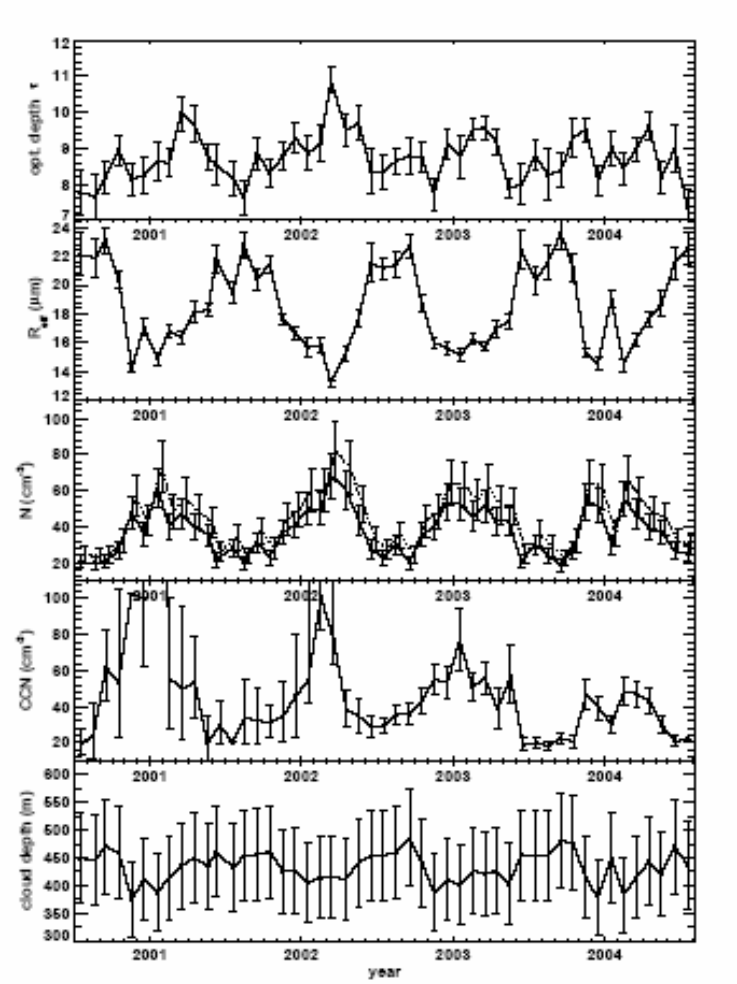

Figure 5-12. *Time series of MODIS-derived cloud optical depth and effective radius (first two panels), retrieved cloud droplet concentration (third panel), CCN concentration at Cape Grim (fourth panel) and retrieved cloud depth (fifth panel).*

Using this technique thus allows discriminating among the observed variations of the cloud albedo, the respective contributions of the LWP natural variability (which is related to cloud depth, especially under adiabatic conditions) and of CDNC that reflects the impact of the aerosol.

Note however that the technique is only applicable to quasi adiabatic cloud layers, i.e. to non precipitating clouds that are not significantly affected by mixing with the environmental air. When mixing is prevalent, especially at the top of stratocumulus clouds, its impact on the droplet size distribution, hence on cloud radiative properties depend on the thermodynamic

conditions at the mixing level. Either the droplet concentration is preserved while droplet sizes decrease (homogeneous mixing), or their concentration decreases while their sizes remain unchanged (heterogeneous mixing) [*Latham and Reed,* 1977; *Baker and Latham,* 1979; *Baker et al.*, 1980, *Burnet and Brenguier*, 2006]. When mixing is of the inhomogeneous type, the retrieved droplet concentration may be significantly underestimated and polluted clouds can be interpreted as pristine [*Chosson et al.* 2006].

5.2.4.4 Droplet Effective Radius Vertical Profile

Rosenfeld and Lensky [1998] applied a method based on retrieval of the droplet effective radius at cloud top from satellite observations. The method assumes that all the clouds in the field of view of the satellite behave the same way, namely, that they all have the same base altitude and the same droplet growth history. By looking at different cloud tops and their temperatures, they build profiles of effective radius and show that the effective radius increases as cloud depth increases. However, in continental clouds, the growth of the particles is slower than in maritime clouds. As a result, in continental clouds, drops commonly grow beyond an effective radius of 14 μm (assumed to represent the demarcation between clouds that may precipitate and those that do not) at much higher altitudes than in maritime clouds. In addition, the appearance of ice in the clouds appears as a sharp increase in effective radius with altitude. *Rosenfeld and Lensky* concluded that drops remain liquid to much higher altitudes in continental clouds, and hence ice forms at much higher altitudes. A problem with this method is that satellite observations can only penetrate a few hundred meters below cloud top. Precipitation formation that takes place below cloud top, as it normally does, cannot be detected by this method.

5.2.5 Aerosol Impact on Precipitation Efficiency

Since the sixties, in-cloud measurements have clearly established that aerosols impact cloud microphysics. The overall feature is that increased CCN concentration leads to increased CDNC, although, as mentioned previously, the relationship also depends on vertical velocity at cloud base and on how CCN are distributed in size, among the Aitken,

the accumulation and the coarse modes. Field studies have also revealed that the increased CDNC and decreased droplet sizes have an impact on the formation of precipitation embryos by droplet collection. For example, *Boers et al.* [1998], analyzing the SOCEX data set, found that the fraction of LWC contained in drizzle drops sharply increases, when the droplet effective radius increases above 12 μm (see Figure 5-13).

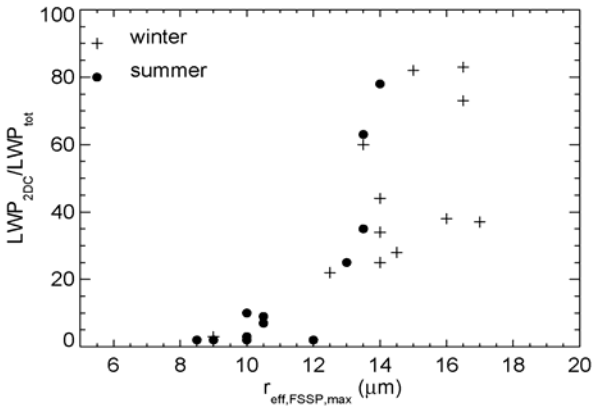

Figure 5-13. *Drizzle liquid water path fraction as a function of the maximum average effective radius observed in the case study profiles. Each data point is representative of individual stacks that were flown during the research flights. All winter and summer data have been included, except the 19 July 1993 (from Boers et al., 1998).*

Similarly, *Pawlowska and Brenguier* [2003] showed (see Figure 5-14) that, for the 8 case studies of the ACE-2 experiment, the averaged precipitation rate R, normalized by the cloud geometrical thickness H, scales with H^3/N, a feature that may be useful for parameterizing precipitation in general circulation models.

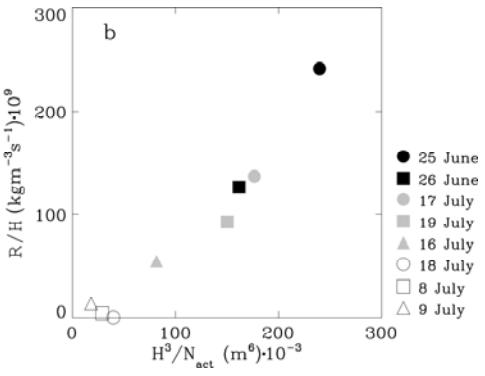

Figure 5-14. *Normalized precipitation rate versus H^3/N.*

Rosenfeld [2000] used both satellite remote sensing in the visible and IR, and measurements from the radar aboard the TRMM satellite, to examine how urban and industrial pollution

might inhibit precipitation development. Figure 5-15a shows an image taken from AVHRR over Australia in which a pollution plume affects clouds over a large distance. In Figure 5-15b the TRMM radar measurements show that the region affected by the polluting aerosols had a much lower radar reflectivity, suggesting lower rain mixing ratios. Figure 5-15c shows the effective drop radii at cloud tops in three regions (1, 2 and 3). The effective radius in region 2 never exceeded 14 μm.

(a)

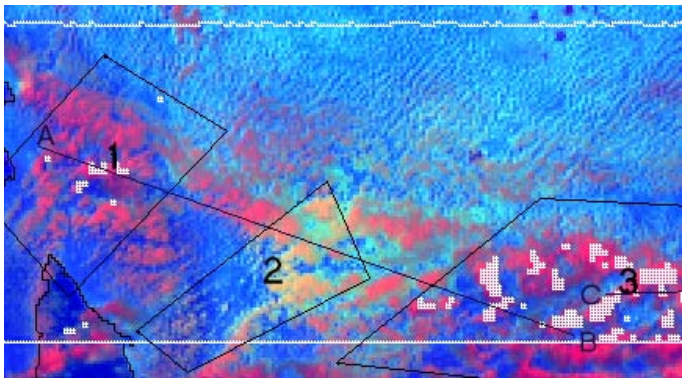

(b)

(C)

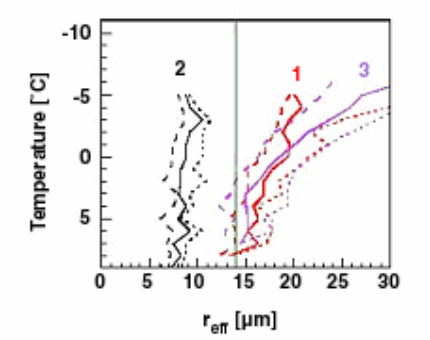

Figure 5-15. *(a) Pollution tracks (yellow) detected by AVHRR satellite imagery in clouds over South Australia. The higher reflectivity is due to reduced droplets sizes. (b) Radar shows precipitation as white patches outside pollution tracks, although these clouds have the same depth as adjacent non-polluted clouds. (c) Average effective radius of particles (probably water drops) at cloud tops in these regions (1, 2, and 3). The dashed lines represent standard deviations from the averages. From Rosenfeld (2000).*

Rosenfeld [2000] illustrated that similar pollution tracks can be found in the Middle East, in Canada, and South Australia. He inferred that the pollution tracks were clouds composed of numerous small droplets that inhibit precipitation formation. It is interesting to note that this

effect is not limited to warm clouds. Some of the clouds exhibiting pollution tracks were in Canada, where ice precipitation processes are prevalent. Perhaps most significant in *Rosenfeld's* analysis is the conspicuous absence of pollution tracks over the United States and Western Europe. The implication is that these regions are so heavily polluted that clouds affected by local sources cannot be distinguished from the widespread pollution-induced narrow cloud droplet spectra in surrounding regions. Subsequent work by *Rosenfeld et al.* [2001] suggests that dust storms may also tend to reduce precipitation from convective clouds, but to a lesser extent than if the clouds ingested pollution.

In addition to its impact on droplet concentration, the aerosol also impacts radiative transfer through clouds via absorption of solar light (semi-direct effect), which may accelerate cloud dissipation (cloud burning effect). Using satellite observations, *Koren et al.* [2004] reported that smoke reduced cloud cover over the Amazon forest, from 38% in clean conditions to 0% in heavy smoke (optical thickness of 1.3). This response reverses the regional smoke instantaneous forcing of climate from –28 W m^{-2}, when only the direct effect is taken into consideration, to +8 W m^{-2}, when the dissipation in cloud cover is accounted for Figure 5-16. MODIS aerosol data over the ocean [*Tanre et al.*, 1997; *Remer et al.*, 2002], and cloud data from *King et al.* [2003] and *Platnick et al.* [2003] from the Terra satellite, have also been used for evaluating aerosol-cloud interactions for shallow, stratiform and trade-wind cumulus clouds and for convective clouds over the Atlantic Ocean. *Kaufman et al.* [2005b] show that each of four aerosol types covering the Atlantic Ocean during June through August (maritime aerosol from 30°S -20°S; smoke from 20°S-5°N; dust from 5°N-30°N; and, pollution aerosols from North America and Europe from 30°N-60°N) are correlated to a 20-40 % cloud coverage variability of shallow stratiform and trade-wind cumulus clouds. Using co-variability analysis they suggest that the aerosol particles might be responsible for ~40-100% of observed increases in cloud coverage. Although a direct proof is still not available, the increase in cloud cover due to aerosol is consistent with *Albrecht's* [1989] hypothesis that enhanced CCN concentrations suppresses precipitation and thus increases cloud lifetimes.

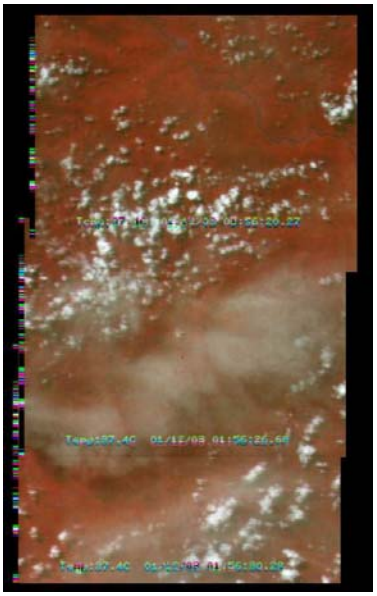

Figure 5-16. *Reduction of cloud cover due to absorption of solar radiation by particles from biomass burning in Brazil. Photograph taken from the NASA Columbia shuttle STS-107 tragic flight on January 2003.*

Analysis of convective clouds by *Koren et al.* [2005] show systematic effects of pollution, desert dust and biomass burning aerosols on the development and coverage of convective clouds over the Atlantic. As expected, cloud droplet sizes are decreased by ~20% in high aerosol concentrations. This change has been accompanied by an increase in the coverage of convective and high clouds from ~30% for low aerosol concentrations to ~60% in hazy atmospheres. This sharp increase in cloud cover is associated with an aerosol-induced increase in cloud top altitude by as much as 1500 m, apparently through inhibition of early precipitation and the resultant strengthening of updrafts.

In most of the papers discussed thus far the effects of aerosol on clouds have been confined to warm non- or slightly raining clouds, and in a few cases to convective clouds that may have contained ice. Satellite monitoring of aerosol and cloud properties thus provides evidence of correlations between aerosol optical thickness and cloud macrophysical properties (cloud fraction, cloud extend, liquid water path). However, progressing from statistical correlations to cause and effect relationships remain a challenge. Satellite measurements of cloud optical thickness, as a proxy of CCN number concentration, does not allow discriminating between aerosol layers that may interact with clouds and those that do not interact because they are located higher up. Saharan dust for example is often exported towards the North-East Atlantic

ocean in the free troposphere, i.e. at an altitude much higher than the boundary layer where clouds develop. Such mineral dust is unlikely to interact with cloud microphysics but it may affect clouds in other ways. For example, a high dust layer may slightly decrease the incoming solar radiation, heat the atmospheric layer above the clouds and consequently increase the cloud cover of stratiform clouds [*Johnson*, 2004] as measured off the coast of Africa [*Kaufman et al.*, 2005b]. Additionally, falling dust particles from above may nucleate ice particles near cloud top, thus modifying the development of precipitation via the ice phase. Quantifying the contribution of the meteorological circulation to cloud variability is also a serious obstacle because of the sensitivity of the liquid water path to presently undetectable changes of the temperature and humidity in the boundary layer. Statistical analysis of the respective contributions of the aerosol and meteorology to cloud variability thus remains questionable because there are presently no robust meteorological predictors of shallow cloud cover.

The ACE2 CLOUDYCOLUMN data base illustrates the paradox. Figure 5-17 shows the cloud geometrical thickness H and optical thickness τ, droplet mean volume radius r_v and number concentration N. Pristine cases are in blue, polluted cases in red, and intermediate cases in green. If only pristine and intermediate cases are considered, Figure 5-17 corroborates the expected increase of optical thickness with decreasing droplet radius. Figure 5-17 -a however reveals that the three polluted cases are thinner than the 5 other cloud systems. Back trajectory and meteorological analysis showed that the reduced thickness of these polluted cases was not due to their increased aerosol content, but only to the fact that these air masses were transported over the European continent for a few days before entering the maritime area of the experiment, north of Tenerife. As a consequence, the liquid water path, hence the optical thickness, of the polluted cloud systems sampled during ACE2 was lower than the ones of the pristine or intermediate cases. This field campaign thus illustrates correlations between aerosol, liquid water path and cloud radiative properties, that contradict satellite statistics, because in this case, aerosol is not the cause of the cloud variability, both being determined, rather, by the mesoscale circulation.

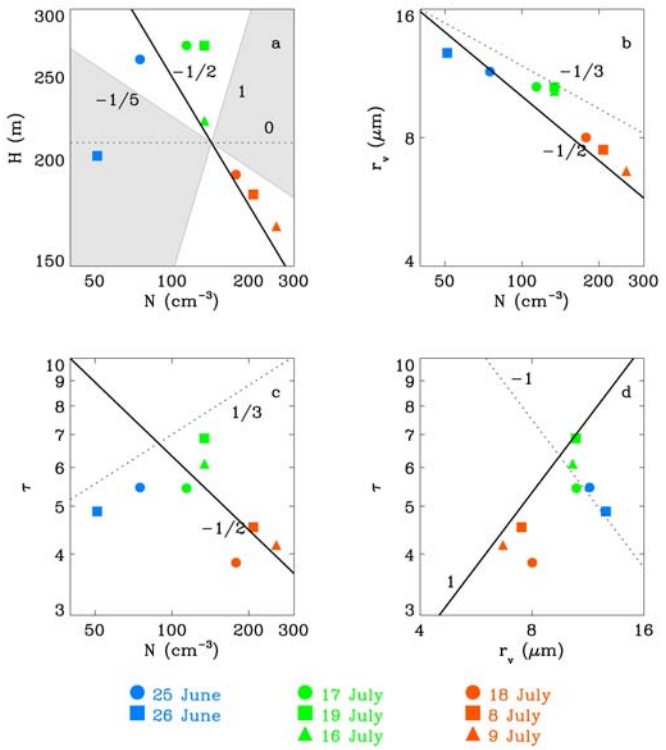

Figure 5-17. *Summary of the ACE2 CLOUDYCOLUMN 8 case studies; a) cloud geometrical thickness H function of droplet number concentration N; (b) droplet mean volume radius function of CDNC; (c) cloud optical thickness τ function of CDNC; and (d) optical thickness function of r_v.*

To overcome the limitations of satellite observations, surface-based remote sensing data sets have been recently used to examine aerosol effects on clouds. Although these methods can only be applied at a limited number of locations, they yield high temporal resolution data. They offer some interesting insights, and are complementary to the global satellite view. *Feingold et al.* [2003] used data collected at the ARM site to allow simultaneous retrieval of aerosol and cloud properties, with the combination of a Doppler cloud radar and a microwave radiometer to retrieve cloud drop effective radius r_e profiles in non-precipitating (radar reflectivity Z < -17 dBZ), ice-free clouds. Simultaneously, sub-cloud aerosol extinction profiles were measured with a LIDAR to quantify the response of drop sizes to changes in aerosol properties. The microwave radiometer made it possible to sort the cloud data according to LWP, consistent with *Twomey's* [1977] conceptual view of the first aerosol indirect effect. With high temporal/spatial resolution data (of the order of 20 s or 100's of

meters) realizations of aerosol-cloud interactions at the large eddy scale were obtained. Moreover, by examining updrafts only (using the radar Doppler signal), the role of updrafts in determining the response of r_e to changes in aerosol (via changes in drop number concentration N_d) was examined. *Feingold et al.* [2003] defined the magnitude of the first aerosol indirect effect as

$$IE = -d \ln r_e / d \ln \sigma_e,$$

Where σ_e is the sub-cloud aerosol extinction and a positive value of IE indicates a relative decrease in r_e resulting from a relative increase in σ_e. This formulation is convenient because values of IE can be related to basic cloud physics theory, and because a measurement of IE does not require a calibrated r_e or σ_e. Analysis of data on 7 days showed a positive correlation between IE and cloud turbulence as expected for clouds in relatively polluted conditions.

In addition to radar/microwave radiometer retrievals of σ_e, surface based radiometers such as the Multifilter Rotating Shadow-band Radiometer [MFRSR – *Michalsky et al.*, 2001] have been used in combination with a microwave radiometer to measure an average value of r_e during daylight when the solar elevation angle is sufficiently high [*Min and Harrison*, 1996]. Using this retrieval, *Kim et al.* [2003] performed analyses of the r_e response to changes in aerosol at the same continental site, and instead of using extinction as a proxy for CCN, they used a surface measurement of the aerosol scattering coefficient σ_s. Their analysis spanned much longer time periods and their data included a range of different aerosol conditions. A similar study was conducted by *Garrett et al.* [2004] at a location in the Arctic. The advantage of the MFRSR/microwave radiometer combination is that it derives r_e from cloud optical depth and LWP and it is not sensitive to large drops as the radar is. Its drawback is that it can only be applied to clouds with extensive horizontal cover during daylight hours. It should be emphasized that none of these methods can directly address the effects of aerosols on precipitation.

5.2.6 Aerosol Impact on Rainfall

Jin et al. [2005] investigated how urban aerosols vary with clouds and precipitation in New York and Houston. In their analysis, virtually no seasonality is observed for rainfall over Houston and New York City, suggesting that aerosols affect rainfall less than clouds. Around Houston, the Tropical Rainfall Measuring Mission (TRMM) satellite-based accumulated rainfall data show that the maxima monthly mean rainfall occurred in October 2000, May

2001, and September 2002. This is consistent with the transition between seasons in this region. In general, New York's rainfall had less month-to-month variation than Houston, with a maximum slightly above 200 mm/month in October 2002.The effective radius for water clouds was lower in New York City than in Houston, suggesting either more aerosols in New York City than Houston, or thinner clouds. Jin et al. hypothesized that the increase in the effective radius of drops in water clouds was associated with increases in rainfall. Similarly, for ice clouds, there was little relationship between cloud drop effective radius and accumulated rainfall. Analysis of monthly mean aerosol optical thickness and rainfall did not show strong relationships between aerosol and rainfall in a climatological sense. Understanding the mechanism responsible for rainfall anomalies is essential to simulating them in numerical models. The less direct relationship between rainfall and aerosol optical thickness implies that urban rainfall anomalies are not fully related to changes in aerosol. This observation is consistent with the earlier conclusions from METROMEX (*Ackerman et al.* [1978] and the recent hypothesis of *Shepherd and Burian* [2003]) that dynamic processes, such as surface convergence and boundary destabilization, are more dominant than aerosols in modifying urban-induced convective clouds.

5.3 FIELD STUDIES OF THE EFFECTS OF ICE NUCLEI ON CLOUDS AND PRECIPITATION

5.3.1 Ice Nucleation and Ice Nuclei

Ice crystals may form in clouds whenever a cloud reaches altitudes where the temperature falls far below 0ºC. However, at temperatures above –40ºC, ice principally forms by what is called *heterogeneous nucleation* on particles that are effective as ice nuclei (IN), although homogeneous freezing of large drops could take place at temperatures as high as -34 ºC. In spite of the large body of literature that deals with measurements and theory of ice formation in clouds, it is still one of the major missing links in our understanding of cloud and precipitation processes.

As discussed in Section 4.1.3.1, IN have four basic modes of action: deposition, condensation-freezing, immersion-freezing, and contact-freezing. A number of studies have tried to combine various measurements to better formulate the effectiveness of each of these nucleation mechanism. *Meyers et al.* [1992] synthesized measurements of contact nuclei

concentrations using electrostatic precipitators [*Vali*, 1985], phoretic forcing [*Deshler*, 1982], and measurements by *Cooper* [1980]. The results suggest that contact nuclei concentrations increase exponentially with the degree of supercooling and that deposition/condensation-freezing is far more effective in initiating ice than contact nucleation. This is consistent with the theoretical findings of *Baker* [1991]. On the other hand, laboratory results of *Levin and Yankofsky* [1981] and *Diehl et al.* [2002] reported that biological nuclei such as pollen and bacteria are more efficient as contact nuclei. Of course, a major uncertainty still remains as to how representative the laboratory results are in replicating ice nucleation in the atmosphere and how much time and spatial variability there is in IN concentrations.

Shown in Figure 5-18 are the variations in average IN concentrations measured at a number of locations around the world. This figure suggests that IN concentrations are similar around the globe. However, for a particular temperature IN concentrations can vary by up to an order of magnitude. Figure 5-19 shows another set of similar measurements from *Bigg and Stevenson* [1970] that indicates also that at each location, the average IN concentration at a particular temperature has a large standard deviation. Day-to-day variations in the IN concentration have been observed at a variety of locations. Such variations are shown in Figure 5-20. These variations in IN number concentration were measured in Antarctica, a very remote location indeed. Similar variations have been measured in other geographical locations.

Various explanations for such rapid variations in IN concentrations have been proposed. One suggestion is that folding of IN-rich lower stratospheric air into the troposphere in the vicinity of jet streams might transport high concentrations of IN to lower altitudes. The IN concentrations are than mixed into the lower troposphere and eventually to the surface. Large-scale advection of IN from varying sources, such as volcanic eruptions and dust storms, that occur on large scales in N. China, Mongolia, and the Sahara Desert, transport IN over large distances [e.g. *DeMott et al.*, 2003] has also been suggested. It has also been shown that evaporation of cloud and precipitation particles release insoluble particles into the atmosphere, which may act as IN. Decomposed leaves from plants [*Schnell and Vali*, 1976a] and active ice nucleating bacteria on plants [e.g., *Levin and Yankofsky*, 1988] are very efficient freezing nuclei that are dispersed into the atmosphere by winds. However, the concentrations of these latter biological particles in the atmosphere and their effects on clouds and precipitation have not yet been established.

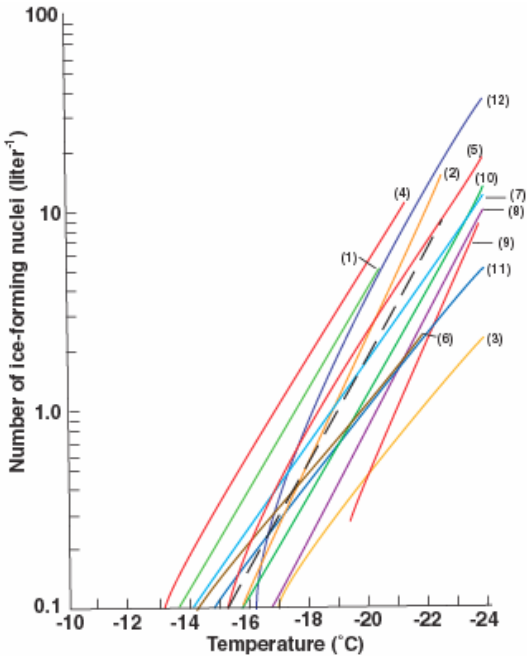

Figure 5-18. *Variation of the average or median number concentration of IN with temperature and geographic location. (1) Bracknell, England (51° N, 0° W); (2) Clermont-Ferrand, France (46° N, 3° E); (3) Corvallis, Oregon, USA (44° N, 123° W); (4) Tokyo, Japan (36° N, 140° E); (5) Tucson, Arizona, USA (32° N, 111° W); (6) Jerusalem, Israel (32° N, 35° E); (7) Palmbeach, Florida, USA (27° N, 80°W); (8) Hawaii, USA (20° N, 158° W); (9) Swakopmund, S. Africa (34° S, 14° E); (10) Sydney, Australia (34° S, 151° E); Tasmania, Australia (43° S, 147° E); and (12)Antarctica (78° S, 166° E). The dashed line represents IN = 10^{-5} exp(0.6□T). Data from Heffernan and Bracewell, 1959; Isono et al., 1959a; Carte and Mossop, 1960; Bigg and Hopwood, 1963; Kline, 1963; Soulage, 1964; Bigg, 1964; Drossler and Hefferman, 1965; Stevenson, 1968; Gagin, 1965; and, Mossop, 1970.*

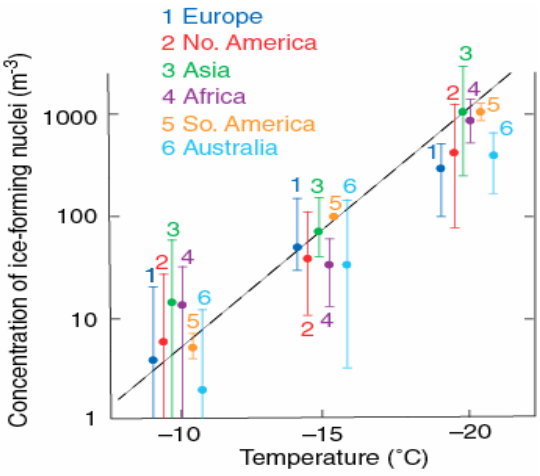

Figure 5-19. *Range of median number concentrations of ice nuclei as a function of temperatures for various geographical locations. The dashed line represents* $N_{IN}=10^{-5}$ *exp(0.6 □T). From Bigg and Stevenson (1970).*

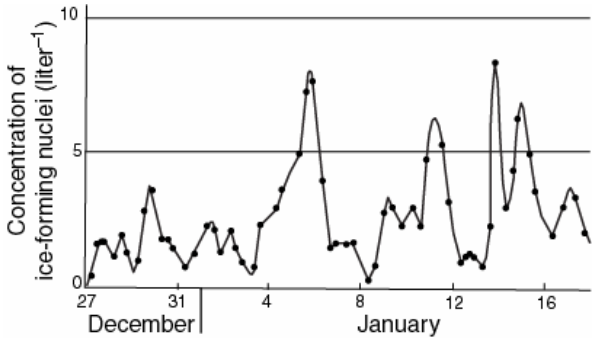

Figure 5-20. *Variations in the daily number concentrations of ice-forming nuclei at –20ºC measured during December 1961 and January 1962 in Antarctica. From Bigg and Hopwood (1963).*

Bigg [1973] reported on large concentrations of ice active nuclei from marine sources. Analysis of this data by *Schnell and Vali* [1976a] shows that the high IN concentrations correspond to regions of upwelling, suggesting that IN from biological sources may play a very important role in these regions.

5.3.2 Vertical Variation in Ice Nuclei

In chapter 2 and 3 we showed that total aerosol concentrations typically decrease with altitude. Ice nucleus concentrations also generally decrease with altitude. However, few studies have found a relationship between total aerosol concentration and IN concentration.

Some studies have suggested a correlation between IN concentrations and the concentrations in the large mode of the total aerosol size distribution [*Georgii and Kleinjung*, 1967; *DeMott et al.*, 1994]. In general, the large aerosol mode exhibits a nearly linear decrease in height.

IN concentrations, however, do not always decrease with height. There are a number of observations that show high IN concentrations above inversion layers. Figure 5-21 shows the results of measurements taken over the Arctic ice sheet during the 1998 FIRE/SHEBA field campaign. The IN concentrations were at the measurement detection level in the sub-cloud layer, while concentrations up to nearly 20 per liter were found above a boundary-layer capping inversion. It is hypothesized that these aerosols were advected over long distances above the boundary layer, possibly from anthropogenic sources over lower latitudes. Since dust particles are known to be effective IN, and it is often observed that dust storms are transported at high levels, it is conceivable that many of the natural IN at high levels, at least in mid-latitudes, originate from deserts. This conclusion is corroborated by recent measurements in Florida during Crystal Face experiment [*DeMott et al*, 2003]. It is also in agreement with *Fridlind et al.* [2004] who concluded that higher IN concentrations at higher altitudes are responsible for the ice crystals observed in some thunderclouds.

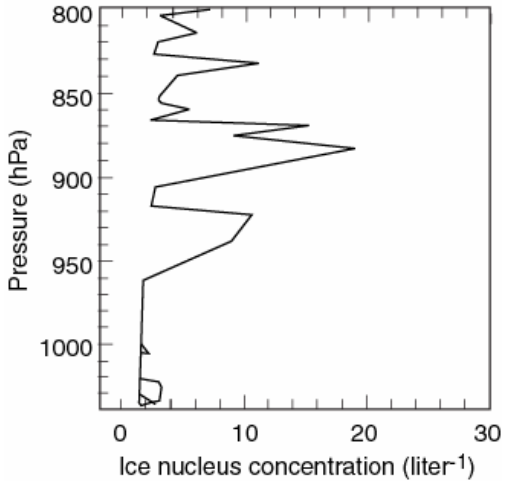

Figure 5-21. *A vertical profile of ice forming nuclei measured over the Arctic ice sheet in 1998. The inversion level was at 960 hPa (530 m). From Jiang et al. (2001).*

Our understanding of the processes of ice formation in clouds become even less clear following the report of *Korolev et al*. [2003] who showed that the average ice crystal concentration between about -10C and -30C in many stratiform clouds associated with frontal systems is almost constant

(between about 2 to 5 cm-3). The relatively constant concentrations with height that are also much higher than those predicted by the parameterizations of *Fletcher* [1962] and *Meyers et al.* [1992], suggest that processes other than nucleation by IN must play an important role in ice crystal formation in clouds. In the same study *Korolev et al.* [2003] also observed that the effective diameter of the ice crystals was about 14 mm, much smaller than most commonly used instruments can identify as ice crystals, thus suggesting the need to develop new instrumentation that can detect and identify small ice crystals.

5.3.3 Sources of Ice Nuclei

In many studies, silicate particles have been found to be the dominant IN particles. This suggests that deserts and arid regions are major sources of IN. Laboratory measurements have confirmed the nucleating ability of clays (e.g. *Grosch and Georgii*, 1976 and *Kumai and Francis*, 1962, *Demott et al.*, 2003). Normally clay particles such as kaolinite, anauxite, illite and metabentonite nucleate ice crystals at temperatures between -10 and -20 C at water saturation (see *Szyrmer and Zawadzki*, 1997 for a review of the subject)

Another source of IN comes from volcanic eruptions *Isono et al.* [1959b] and *Hobbs et al.* [1971]. However, not all volcanoes are sources of IN, for example, Pacific volcanoes do not contain suitable particles in their eruptions to nucleate ice, *Schnell and Delany* [1976]. Pacific volcanoes emit molten lava, and not silicate particles. Emissions from a Japanese volcano indicate an increase of more than an order of magnitude above the average background IN concentrations (see Figure 5-22).

Other sources of IN are combustion products (e.g., forest fires, burning of sugar cane fields, etc. *Hobbs and Locatelli*, 1969; *Pueschel and Langer*, 1973) and industrial processes (e.g., steel mills, aluminum works, sulfide works, power plants). Many of these are sources of metal oxides, which are good IN. Decaying leaves [*Schnell and Vali*,1976 a and b]; and, bacteria [e.g., *Levin and Yankofsky*, 1988] have also been found to be good IN sources.

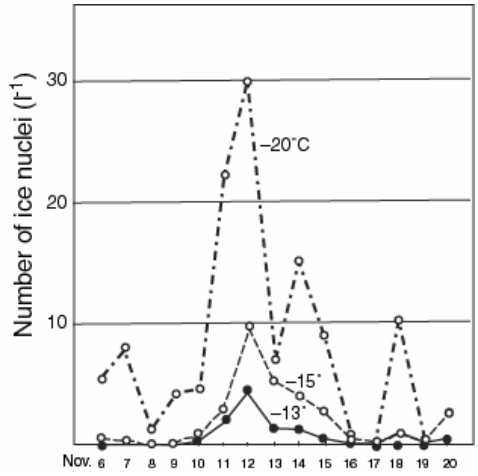

Figure 5-22. *Effect of the eruption of the volcano Asama in Japan on November 10, 1958 on the concentration of IN. From Pruppacher and Klett (1997).*

In general, anthropogenic emissions from urban complexes are not good IN [*Borys and Duce*,1979]; In fact, IN may be *de-activated* when they are exposed to atmospheres with high concentrations of gases such as SO_2, NH_3, and NO_2, or high concentrations of Aitken nuclei produced by industrial processes. *Georgii and Kaller* [1970] showed that in polluted air with Aitken concentrations of $10^6 - 10^7$ cm^{-3}, IN may be deactivated in 12 to 72 hours. If the IN are only partially deactivated, they may serve as IN at lower temperatures than they would otherwise.

Exceptions are heavy metal industries, such as steel mills and smelter plants. *Schaefer* [1948] observed very high concentrations of IN downwind of steel plants near Buffalo, New York. In general, salt particles and sulfates over the oceans are not good IN, since they are very soluble. In fact, in oceanic locations there often exists a negative correlation between CCN and IN concentrations (Figure 5-23).

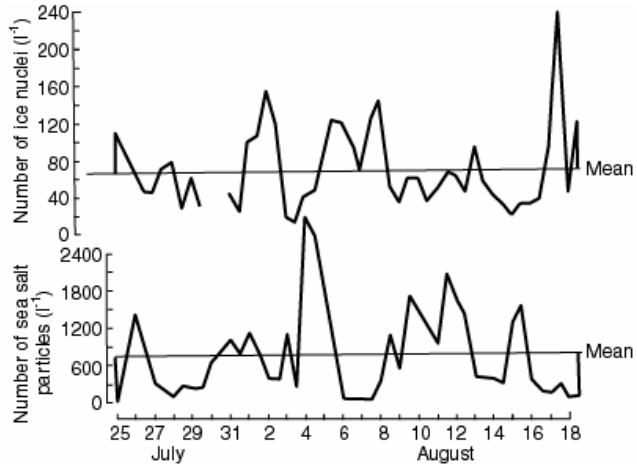

Figure 5-23. *Correlation between number concentrations of ice-forming nuclei (0 to –30ºC) and sea-salt particle concentrations on the island of Valencia during July and August, 1958. From Pruppacher and Klett (1997).*

5.3.4 Requirements for Ice Nuclei

Pruppacher and Klett [1997] summarized the observations and laboratory experiments in a list of requirements for aerosols to be effective IN:

Insolubility: in general, IN must be very insoluble

Size: IN must have a size comparable to, or larger than, that of a critical ice embryo. Generally speaking, the radius of the IN must be >0.1 μm. At sizes less than this critical radius the nucleating ability of the particle decreases rapidly and becomes increasingly more temperature dependent [*Georgii and Kleinjung*, 1967].

Chemical Bond: The type and strength of the chemical bonds at the IN surface, affect nucleation. Since an ice crystal lattice is held together by hydrogen bonds it is reasonable to assume that an IN must have similar hydrogen bonds at its surface for nucleation to occur.

In view of the chemical bond requirement, certain complex organic molecules exhibit good ice nucleating abilities. Examples of organics that nucleate ice at just a few degrees below 0ºC are cholesterol, metaldehyde, phloroglucinol.

Crystallography: Ice nucleating ability generally increases as the lattice structure approaches that of ice, since this provides increasingly good molecular matching between the molecules

of ice and the substrate. Crystallographic matching reduces the "misfit"' and *elastic strain in the ice.*

Active Sites: Laboratory studies indicate that ice nucleation is preferred on those substrates that have pits and steps on their surfaces, where ice nucleation can be initiated.

Certain types of plant pathogens can serve as efficient IN, active at temperature as high as -2–5ºC. The mechanism which makes these bacteria active IN is not yet fully understood. It has been demonstrated however, that some protein on the inner membrane of these bacteria is responsible for the nucleation of ice. Whether these organisms are found in high concentrations in the atmosphere has not yet been demonstrated.

5.3.6 Ice Multiplication

The concentrations of ice particles in clouds are not always represented by the concentrations of IN measured or expected to be activated in such environments. This is referred to as *ice multiplication* or *ice enhancement*. In particular, at temperatures higher than –10ºC, the concentration of ice particles can exceed the concentration of IN activated at cloud top temperature by as much as three or four orders of magnitude [e.g. *Koenig*, 1963; *Braham*, 1964; *Mossop*, 1970; *Mossop et al.*, 1967, 1968, 1972; *Auer et al.*, 1969; *Hobbs*, 1974;]. The effect is greatest in clouds with broad drop-size distributions [*Koenig*, 1963; *Mossop et al.*, 1968, 1972; *Hobbs*, 1974]. In contrast, there are a number of reported measurements that show some agreement between IN concentrations and ice crystal concentrations [*Gagin*,1971]. But even these measurements have been challenged, showing that for these types of convective clouds the ice crystal concentration can often increase by about two orders of magnitude over the average IN concentrations [*Levin et al.*, 1996]. In contrast, *Heymsfield* [1972] and *Heymsfield and Knollenberg* [1972] observed concentrations of about 50 ice crystals per liter in cirrus clouds at temperatures of -30^0C at which the expected IN concentration should be about 10^3 per liter, namely, considerably lower concentrations of ice crystals than IN. Clearly, these and other measurements suggest that IN are not reliable predictors of ice particle concentrations in many clouds.

A number of hypotheses have been proposed to explain the discrepancies between IN concentrations and the concentration of ice particles in clouds. Some of the hypotheses are: (i) fragmentation of large drops during freezing [*Mason and Maybank*, 1960; *Korolev et al.*, 2004; *Stith et al.*, 2004; *Rangno and Hobbs*, 2005). *Dye and Hobbs* [1966, 1968] showed that

the number of splinters depends, among other things, on CO_2 concentrations in the air. Subsequent studies indicate that each drop-freezing event produces, on average, <2 ice splinters [e.g. *Brownscombe and Thorndyke*, 1968; *Pruppacher and Schlamp*, 1975]. (ii) Mechanical fracture of fragile ice crystals (i.e., dendrites and needles) caused by collision of these crystals with graupel and other ice particles [e.g. *Hobbs and Farber*, 1973]. (iii) Splinter formation during riming of ice crystals [e.g *Hobbs and Burrows*, 1966; *Afdermauer and Johnson*, 1972]. These studies produced conflicting results in regard to the quantity of secondary ice particle produced during riming. *Hallett and Mossop* [1974] and *Mossop and Hallett* [1974], showed that copious quantities of secondary ice particles (often referred to as ice splinters) are produced during the riming of ice particles under selective conditions. The main conditions are: temperature in the range of –3 to –8ºC; and, a substantial concentration of large (D > 24μm) cloud droplets. Under these conditions, laboratory studies indicate an optimum average ice splinter production rate of 1 for 250 large droplet collisions. (iv) Oraltay and *Hallett* [1989] and *Dong et al.* [1994] examined the generation of secondary particles during the evaporation of ice particles. At relative humidity below 70%, as many as 30 pieces per crystal formed. However, this did not occur with columns or solid plates. Under certain conditions, evaporation of simulated graupel particles of a few millimeters produced several hundred ice particles. This process has not been further quantified in the laboratory or been inserted into cloud models to examine its potential importance.

5.3.6 Observations of Very High Ice Particle Concentrations

Hobbs and Rangno [1985, 1990, 1998] and *Rangno and Hobbs* [1988, 1991, 1994, 2005] discussed ice particle initiation and multiplication in maritime and continental cumulus clouds in a number of geographic locations. They showed that the ice particles originate in two-stages. During stage 1, initial ice particles seem to originate through the freezing of larger cloud droplets in concentrations comparable to that estimated with the formula of *Meyers et al.* [1992] derived from IN measurements. During stage 2, however, ice particle concentrations of 10's to 1000's per liter form in less than ten minutes at temperatures as high as –13ºC. Such high concentrations appear coincident with or soon after the formation of graupel particles. Supercooled raindrops or drizzle drops need not be present. In some cases, the time-scales for the formation of high ice particle concentrations are too short for the riming-splintering process to account for the observations.

Although the effects of ice particles in clouds on the formulation of precipitation are in principle understood, the quantitative contributions of IN and ice particles to precipitation development and precipitation amounts are still unclear. Therefore, the contribution of pollution to precipitation through the increase in aerosol concentrations, and especially to the concentration of IN, is also poorly understood. One element that seems to emerge from the body of literature on IN is that small drops tend to freeze at lower temperatures. If this is correct, then increases in pollution which, as we have seen, can lead to smaller drops in clouds, should result in freezing at lower temperatures. However, if the pollution contains some particles that are effective IN, the formation of ice should start at higher temperatures. Similarly, if among the pollution particles large and giant CCN are present, large drops could be formed and some ice could appear at warmer temperatures and lower altitudes. The presence of such ice crystals in regions with high liquid water content would expedite the process of riming and the formation of graupel particles.

5.3.7 Effects of Air Pollution on Clouds and Rain From Orographic Clouds

Borys et al. [2000] and *Borys et al.* [2003] provided some evidence that pollution can suppress precipitation in winter orographic clouds in the Rocky Mountains. Their analysis shows that pollution increases the concentration of CCN and therefore cloud drops, leading to the formation of smaller cloud drops. The reduced drop size leads to less efficient riming and therefore to smaller ice crystals (see Figure 5-24), smaller fall velocities, and less snowfall.

Borys et al.'s observation was supported by *Givati and Rosenfeld* [2004] who analyzed about 100 years of precipitation records in regions downwind of pollution sources and compared them to precipitation in regions unaffected by these sources. Two geographical areas were chosen for this study: California and Israel. The topography in both regions is similar, although the mountains in Israel are much lower than the Sierra Nevada. The statistical results for both locations show that downwind of pollution sources, on the upslope of mountains and mountain tops, precipitation is reduced by ~20% and ~7%, respectively (Figure 5-25). It was hypothesized that this decrease is due to an increase in droplet concentrations and a decrease in droplet size. Farther downwind on the lee side of mountains, the amount of precipitation is increased by ~14%. The authors postulate that this increase is due to smaller cloud particles taking longer time to grow, allowing the winds aloft to carry

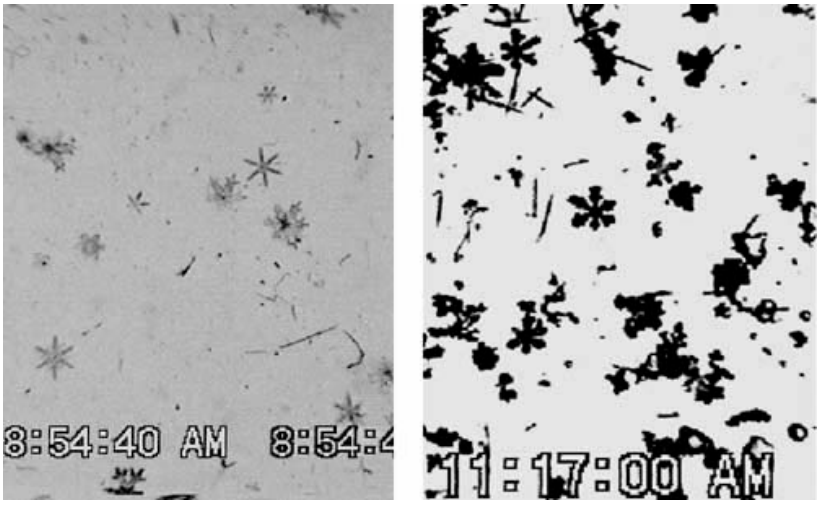

Figure 5-24. *Light riming of ice crystals in clouds affected by pollution (left) compared to heavier riming in non-polluted clouds (right). From Borys et al. (2003).*

them over the mountain top (see earlier study of similar effects, produced by deliberate over seeding with ice-producing particles, by *Hobbs*, 1975). However, the integrated rainfall amount over the whole mountain range appeared to be reduced by the pollution. Although this study is among the few that comprehensively connects between increases in pollution and precipitation on the ground, it lacks the direct measurements of aerosols and possible effects of moisture and low level winds.

In contrast to the above observations, *Diem and Brown* [2003] partially attributed downwind precipitation enhancement in Phoenix to increased pollution-derived CCN, although they acknowledged that increased humidity from irrigation projects, and urban land-use induced surface convergence, were likely the dominant factors.

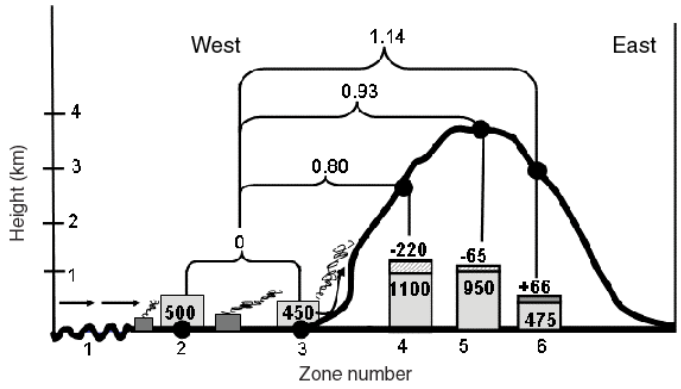

Figure 5-25. *The effects of pollution on rainfall in the Sierra Nevada Mountains in California and in Israel. The figure is a schematic topographic cross section showing the effects of urban air pollution on precipitation as the clouds move from west to east from the coast to the Sierra Nevada and to the eastern slopes. The boxes show the amount of the annual precipitation (mm yr^{-1}) in each topographic location, and the numbers above them show the loss or gain of precipitation (mm yr^{-1}) at each site. Maritime air (zone 1) is polluted over coastal urban areas (zones 2, 3), with no decrease in precipitation. The polluted air rises over mountains downwind and forms new polluted clouds (zone 4), with decreases of ~15%–20% (losses of 220 mm yr^{-1}) in the ratio between the western slopes and the coastal and plain areas (appears as 0.80 above the line connecting zones 4 and zones 2-3). The clouds reach to the high mountains in zone 5. All of the precipitation is snow, with a slight decrease of ~5%–7% (loss of 65 mm yr^{-1}) in the ratio between the summits and the plain areas (appears as 0.93). The clouds move to the high eastern slopes of the range (zone 6), with an increase of ~14% (gain of 66 mm yr^{-1}) in the ratio between the eastern slopes and the plain (appears as 1.14). From Givati and Rosenfeld (2004).*

5.4 SUMMARY

Except for a very few papers, most studies to date have dealt with the effects of anthropogenic aerosol on shallow warm non- or slightly precipitating clouds. Since the sixties, it has become more obvious that an increase of the CCN concentration results in an increase of the droplet concentration, although the relationship between aerosol physico-chemical properties, updraft intensity at cloud base, and the resulting concentration of

activated nuclei (i.e. the concentration of cloud droplets at cloud base) still needs to be improved for accurate evaluation of the aerosol impacts on clouds.

In situ observations also corroborate the predictions of cloud microphysics theory, namely that polluted clouds with more numerous, and hence smaller cloud droplets produce fewer precipitation embryos, than pristine clouds with a similar liquid water path.
Global monitoring of these effects from satellite is less convincing because of the present uncertainty in remote sensing measurements of the liquid water path that are required to stratify the observed data sets and separate the aerosol impact from the natural LWP variability.

Beyond the LWP variability, there are also additional cloud features that may significantly affect the retrieval of cloud microphysical properties from satellite, namely their spatial heterogeneity and the variability of the impacts of the mixing processes on cloud microphysics, especially in the upper part of the cloud layer that mainly determine its radiative properties.

There are recent remote sensing observations showing that the increase in drop concentrations leads to larger cloud fraction and deeper clouds. Similar results have been reported from numerical model simulations of deep mixed phase clouds.
However, there are some remote sensing observations of small warm clouds that suggest that the effect of increased aerosol loading is to reduce cloud fraction. Understanding the relative effects of aerosol and meteorology is key to our understanding the relative role of aerosols on precipitation.

In spite of the numerous publications about the effects of pollution on clouds, there are only very few that deal with the effects on precipitation on the ground.
Observations of snowfall from cold orographic clouds show that increased pollution leads to smaller cloud drops and reduced riming. This reduction in ice crystal growth leads to reduced snowfall.

Statistical analysis of orographic rainfall upwind and downwind of large urban centers suggests that the net effect of pollution on rainfall on the regional scale is to reduce the total rainfall amount. However, more simultaneous measurements of aerosol characteristics

coupled with measurements of meteorological parameters are needed to establish the validity of this conclusion.

A few measurements suggest that in the presence of a few large or giant CCN a few large drops can be formed in the early development of the clouds. Numerical models show that the total amount of rainfall on the ground should be increased when a few GCCN are added to the background aerosols. GCCN occur in very small concentrations (order 1 per liter) and measurement of GCCN is very difficult. The effects of such GCCN are difficult to observe by remote sensing from space since they mostly occur deep in the clouds and far away from cloud tops, where the measurements are taken. The role of GCCN in precipitation development needs more observational support.

A reduction of the precipitation efficiency in a single cloud due to increase in aerosols however, does not necessarily imply a reduction in total rainfall from a cloud system, because changes in dynamics in one cloud could lead to enhancement of precipitation development in neighboring clouds.

Total rainfall from a cloud system mainly depends on cloud dynamics. Aerosols do not only interact with clouds via their CCN and IN properties, but also via their effects on the dynamics of the cloud through changes in the temporal and spatial release of latent heat and redistribution of hydrometeors. Also light absorption properties that may strongly modify the heating of the cloud layer in the day and the IR cooling at night may affect convection and rainfall. In some cases, these absorption effects may largely counteract or enhance the microphysical impacts (cloud burning).

Land-use also plays an important role in cloud and precipitation formation (e.g., Jacob et al. 2005). Changes in surface albedo, soil moisture and surface temperature are all important in determining the strength of the convection and the resulting precipitation. At the same time land-use is strongly affected by the amount and temporal distribution of the precipitation. Aerosol effects on clouds need to be considered within the context of this tightly coupled system.

The mechanisms responsible for ice formation in clouds are still not understood. Since in many cases, ice plays an important role in precipitation development, it is essential that this void in our understanding be resolved.

To reach firmer conclusions on these effects, further observational studies and new techniques are needed on the following issues:

- For each aerosol type always characterize their CCN, IN and light absorption properties (single scattering albedo).
- Measure the vertical profile of the aerosol layers with respect to the cloud layers to determine if the aerosol directly interacts with cloud microphysics.
- Evaluate the role of GCCN in the precipitation development.
- Improve the satellite retrieval techniques of the liquid water path, accounting for the cloud spatial heterogeneity and the mixing process biases.
- Better quantify the uncertainty in the characterization of the meteorological conditions that generate clouds and derive the resulting uncertainty on the predicted liquid water path.
- Improve measurements of the rainfall amount at the ground at the scale of the pollution plumes.
- Evaluate by carefully designed statistical analyses, the hypothesis that precipitation at the ground can be altered by anthropogenic sources of aerosols.

CHAPTER 6: NUMERICAL MODELING STUDIES OF THE EFFECTS OF AEROSOLS ON CLOUDS AND PRECIPITATION

Lead authors: William Cotton, Graham Feingold, Ulrike Lohmann, Zev Levin

6.1 INTRODUCTION

The history of numerical modeling of the effect of aerosols on clouds dates back at least 50 years to the work of *Howell* [1949] and *Mordy* [1959] who considered the growth of a population of aerosol particles in a rising parcel of air. Models such as these addressed the effects of both aerosol and dynamical parameters (i.e., updraft velocity) on the number and size distribution of cloud droplets. To this day similar models are in wide use to examine the effects of aerosol composition and atmospheric trace gases on droplet activation (e.g., [*Kulmala et al.*, 1993; *Ghan et al*., 1997; *Feingold and Chuang*, 2002; *Nenes et al*., 2002a]).

From the early roots of cloud parcel models, simulating droplet growth by condensation, there have been two parallel and complementary foci (Figure 6-1). The cloud physics community has pursued the modeling of precipitation formation in a variety of modeling frameworks, ranging from parcel models to 1-D, 2-D and 3-D models of both warm and cold clouds. Simultaneously, the aerosol and chemistry communities have developed models that have placed more emphasis on the effect of aerosol composition on cloud microphysics, as well as on the role of clouds as processors of aerosol (e.g., via aqueous-phase chemistry). Although these efforts are depicted as parallel in Figure 6-1, there has been some communication between the two communities with the result that the more recent modeling efforts include representation of the coupled aerosol-cloud-chemistry system (e.g., [*Barth et al*., 1992; *Respondek et al.*, 1995; *Feingold and Kreidenweis*, 2002; *Yin et al*., 2005]). The representation of all these components is required to model the effect of aerosols on precipitation because of the myriad feedbacks that can occur in the system. For example, aerosols that are modified by cloud processes, and are then released back into the atmosphere after cloud evaporation (most clouds evaporate and do not precipitate) could affect other clouds [*Scott and Hobbs*, 1967; *Radke and Hobbs*, 1969, 1991; *Easter and Hobbs*, 1974; *Hegg and Hobbs*, 1978, 1979, 1981, 1982, 1986, 1987, 1988; *Hegg et al.*, 1980, 1984a,b,

1986, 1989, 1991, 1996; *Hegg*, 1990, 1991; *Hegg and Larson*, 1990; *Barth et al.*, 1992; *Hobbs*, 1993; *Perry and Hobbs*, 1994, 1996; *Wurzler et al.*, 2000; *Garrett et al.*, 2002; *Tabazadeh et al.*, 2004). Therefore, not only must the effects of aerosols on clouds and precipitation be considered but also the effect of clouds and precipitation on aerosols. These processes could be simulated in detail or be parameterized to account for the impact of chemistry on the number, size and composition of the aerosols, without going into detailed chemistry.

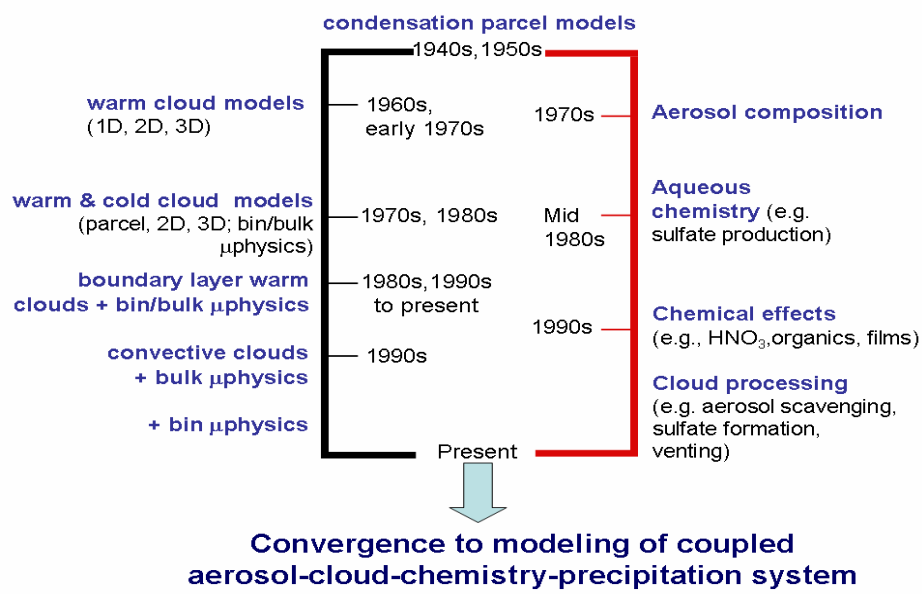

Figure 6-1. *Brief summary of parallel efforts in aerosol-cloud-precipitation studies over the past six decades. The left branch has focused on precipitation development, while the right branch has been concerned with aerosol composition and aqueous chemistry. Communication between these efforts over the past decade has stressed the importance of considering the aerosol-cloud-chemistry-precipitation system in a coupled manner.*

The challenge to the cloud modeler is to represent the numerous, and sometimes poorly understood cloud processes depicted in Figure 6-2 in a dynamical framework, and preferably in three dimensions (3-D). The lifetime of an individual cloud cell is on the order of an hour but, when considering precipitating cloud systems, multi-hour simulations need to be performed, with the result that computational costs quickly become prohibitive. The challenges therefore include adequate representation of (i) physics, (ii) chemistry, (iii) numerical methods for solving the equations, and (iv) consideration of the most important processes.

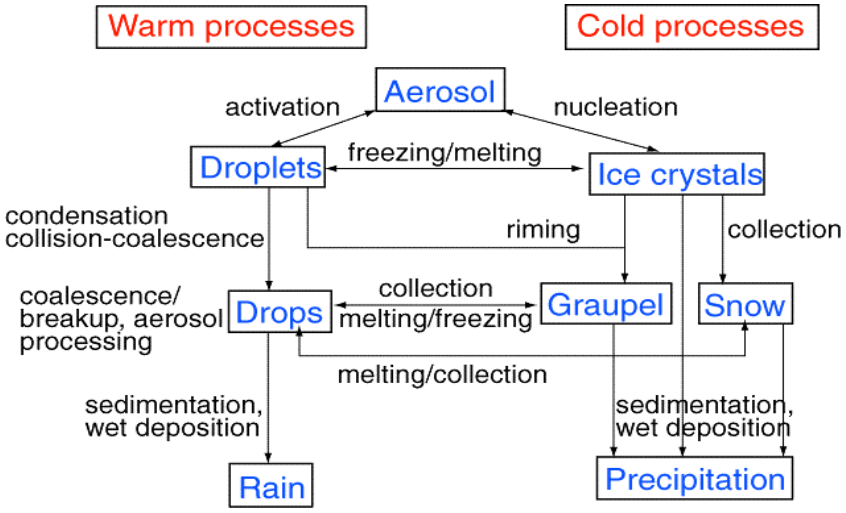

Figure 6-2. *Simplified schematic of warm and cold microphysical interactions and some of the processes that are represented in models. The multiple pathways shown illustrate the complexity of the system and the importance of correct decision-making when designing cloud models.*

Below we describe some of the modeling techniques that have been used to represent precipitation, and parallel efforts at improving numerical methods, as well as the representation of the physical processes themselves. We then give examples of key results pertaining to aerosol-cloud-precipitation interactions. Finally, we discuss some of the challenges in quantifying aerosol effects on clouds and precipitation.

6.2 NUMERICAL METHODS FOR MODELING CLOUD MICROPHYSICS

Cloud modeling requires a recognition that the aerosol cloud system comprises coupled components of dynamics, aerosol and cloud microphysics, radiation and even chemistry (Figure 6-3), and that depending on the system being modeled, neglect of some of the components may have important consequences. The correct approach to modeling the effects of aerosol on precipitation requires an appropriate balance of treatment of these components. Earlier modeling efforts tended to focus on just parts of the system (e.g., the effect of aerosol size and composition on the drop size distribution [*Mordy*, 1959], or the formation of precipitation in a 1-D model using simple representations of microphysics, frequently with little representation of aerosol [*Silverman and Glass*, 1973]. To this day, cloud models are often used to focus on just one aspect of the system because the neglect of other components simplifies investigations and serves to elucidate specific processes. However, with the

increase in computing power, and the evolution of numerical methods, the community has slowly moved towards representing both microphysics and dynamics with varying degrees of sophistication.

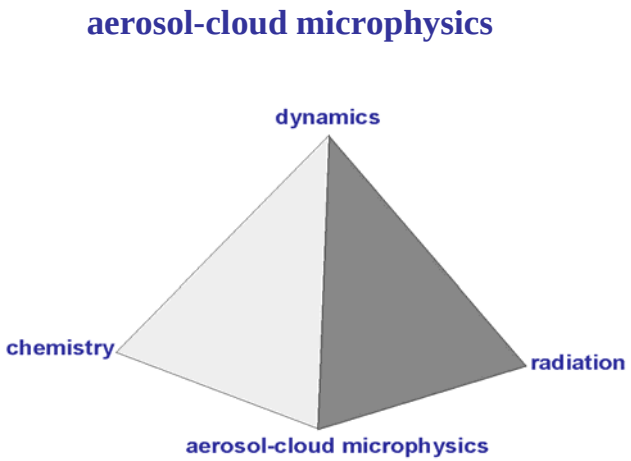

Figure 6-3. *Schematic indicating the coupled nature of the microphysics involving clouds and precipitation. Although great gains in knowledge have been acquired through consideration of individual pairs of components in this figure, an appropriate balance between these components must be considered when modeling aerosol-cloud-precipitation interactions.*

6.2.1 Bulk Microphysics

When considering cloud microphysical processes, earlier models, and many current models, use a "bulk" representation of microphysics that represents a size distribution of hydrometeors by one or more of its moments (e.g., mass mixing ratio, number mixing ratio, surface area, radar reflectivity). In one approach drops and ice particles are represented by a simple exponential function (with fixed pre-exponent) and a single-moment of the hydrometeor spectra is predicted [*Kessler*, 1969]. In this case self-collection among cloud droplets is parameterized using an autoconversion formulation, and large hydrometeors such as raindrops are assumed to collect smaller drops and ice by continuous accretion. Moreover, all classes of large hydrometeors are assumed to fall with a constant fall speed, usually a water content-weighted fall speed. The autoconversion formulations have been either ad hoc (e.g., [*Kessler*, 1969; *Manton and Cotton*, 1977; *Cotton et al*., 1986]) or derived from parcel or box detailed bin-microphysics simulations (e.g., [*Berry*, 1967; *Berry and Reinhardt*, 1974; *Beheng*, 1994]). A number of investigators have extended Kessler's approach to consider

more general functions, such as gamma or log-normal, and to predicting two moments of the spectra [*Nickerson et al*., 1986; *Ferrier*, 1994; *Meyers et al*., 1997; *Reisner et al*., 1998; *Seifert et al*., 2005a,b]. This approach has also been extended to predicting three moments of the basis functions such as the concentration and mass of particles, and radar reflectivity (e.g., [*Milbrandt and Yau*, 2005a,b]).

The two-moment scheme by *Seifert and Beheng* [2005a,b] predicts the evolution of mass as well as number densities of the five hydrometeor types cloud droplets, raindrops, cloud ice, snow and graupel. It includes novel parameterizations of autoconversion, accretion and self-collection of water drops that have been derived by *Seifert and Beheng* [2001] directly from the stochastic collection equation. In contrast to most other schemes, the new autoconversion parameterization further considers aging of the cloud droplet size distribution with time by relying on a dynamic similarity theory.

Multi-moment bulk schemes typically prescribe basic functions for the drop size distributions, such as gamma or log-normal distributions [*Clark*, 1976; *Clark and Hall*, 1983], and then explicitly predict the evolution of those basic functions (in terms of their moments) by vapor deposition/evaporation, stochastic coalescence, and sedimentation. The advantage of these multimoment schemes is that they predict number concentration, mass mixing ratio (and sometimes higher order moments) and therefore are able to derive the broad features of the drop size distribution. In so doing they improve the representation of growth processes and precipitation formation. Multimoment bulk methods have also been applied to representation of aerosol growth processes (e.g., [*McGraw*, 1997]).

An example of a multi-moment scheme implemented in a large scale model is that which is implemented in RAMS (Regional Atmospheric Modeling System, *Pielke et al.*, 1992 and *Cotton et al.*, 2001). The evolution of this modeling approach can be found in *Verlinde et al*. [1990], *Walko et al.* [1995], *Meyers et al.* [1997], *Feingold et al.* [1998], and *Saleeby and Cotton* [2004]. Instead of using continuous accretion approximations, which has been common in cloud parameterizations, *Feingold et al.* [1998] showed that full stochastic collection solutions for self-collection among cloud droplets and for rain (drizzle) drop collection of cloud droplets can be obtained for realistic collection kernels by making use of look-up tables. This approach has been extended to all hydrometeor class interactions by collection, including the growth of graupel and hail by riming. The philosophy of bin

representation of collection has been extended to calculations of drop sedimentation [*Feingold et al.*, 1998]. Bin sedimentation is simulated by dividing the basis function into discrete bins and then building look-up tables to calculate how much mass and number in a given grid cell fall into each cell beneath a given level in a given time step. *Saleeby and Cotton* [2004] refined this approach by the addition of a large cloud droplet mode from 40-80 μm diameter, and by predicting the number concentration of cloud droplets through explicit activation of CCN and giant-CCN. The large cloud droplet mode provides a better depiction of self-collection of cloud droplets (or autoconversion) and permits simulation of drizzle from fogs and marine stratocumulus clouds. The activation of CCN is parameterized through the use of a Lagrangian parcel model that considers ambient cloud conditions for the nucleation of cloud droplets from aerosol.

6.2.2 Size-resolved Microphysics

Size-resolved or explicit bin microphysical methods have been developed with the recognition that many cloud growth processes are highly sensitive to drop size. The first such class is the Lagrangian method, which represents particles at discrete sizes and allows each particle to grow on a moving mass grid. This approach eliminates numerical diffusion and allows for a smooth transition from aerosol to haze to cloud droplets without artificial distinctions between these classes. The cloud supersaturation is calculated based on source (cooling, which is related to updraft velocity) and sink (condensation) terms, enabling accurate determination of the number of activated droplets. These models typically focus on the initial growth phases from haze to droplet and include detailed representation of aerosol sizes and compositions [*Mordy*, 1959; *Fitzgerald*, 1974; *Facchini et al.*, 1999; *Feingold and Kreidenweis*, 2000; *Feingold and Chuang*, 2002; *Lohmann et al.*, 2004]. They frequently also consider the effect of trace gases on activation [*Kulmala et al.*, 1993]. Aqueous production of sulfate has also been represented in studies that examine the effects of cloud processing on the aerosol size distribution [*Hegg et al.*, 1991; *Bower and Choularton*, 1993; *Feingold and Kreidenweis*, 2000]. The Lagrangian method is used almost exclusively in kinematic cloud parcel models, where a parcel of air is moved either adiabatically or according to some known trajectory through a cloud. It is not easily adapted to the study of growth by processes such as collision-coalescence, and it is not suitable for general application in Eulerian dynamical models.

Fixed bin, or Eulerian (in size space), microphysical models have been developed to fill this need. Supersaturation calculations also follow from a balance equation for cooling (dynamical tendency) and condensation but accuracy depends on the grid resolution [*Clark* 1973, 1974]. Activation is not represented as accurately because the Eulerian framework does not represent the transition from dry particle to haze to droplet as in the Lagrangian framework. Condensation growth is also subject to numerical diffusion associated with the mass-grid resolution (This also feeds back to the accuracy of the supersaturation calculation). The bin framework is most useful for collision-coalescence calculations. Early efforts by *Telford* [1955], *Berry* [1967], *Berry and Reinhardt* [1974], *Kovetz and Olund* [1969], and *Bleck* [1970] showed that great care must be taken in representing collision-coalescence to avoid numerical diffusion in the mass-transfer equations and rapid (spurious) acceleration of growth to precipitation-sized particles. More recent bin models, such as those used by *Tzivion et al.* [1987], *Hounslow et al.* [1988], and *Chen and Lamb* [1994], use a multi-moment representation of the cloud microphysics in each individual drop bin; this significantly reduces numerical diffusion and has the added benefit of conserving more than one moment of the size distribution. This has led to development of numerical methods that include a bin representation of aerosol in each individual hydrometeor size-bin [*Bott et al.*, 1990; *Chen and Lamb* 1994; *Kerkweg et al.*, 2003]. Such methods are very accurate but still too computationally intensive to be included in 3-D models. Simpler methods that track dissolved aerosol within each hydrometeor bin are more commonly used [*Flossman et al.*, 1985; *Respondek et al.*, 1995; *Toon et al.*, 1988; *Feingold et al.*, 1996; *Yin et al.*, 2005].

While the focus here has been on numerical methods for solving microphysical interactions, it is important to consider numerical issues related to the dynamical aspects of cloud modeling. The advection equation is also susceptible to numerical diffusion (and dispersion). Modeling of the dynamical equations for hydrometeor species requires "positive-definiteness" for mass conservation. Numerical diffusion on the spatial grid has to be considered along with numerical diffusion on the mass grid; again, an appropriate level of balance is important [*Clark*, 1973, 1974].

6.3 REPRESENTATION OF PYSICAL PROCESSES

The importance of numerical techniques that minimize spurious particle growth must be considered hand-in-hand with the representation of the physics inherent to cloud

microphysical and dynamical processes. For example, the kernel function for collision and coalescence between different types of hydrometeors is based on both theory and laboratory experiments, in which the outcome of the interactions between pairs of hydrometeors of different sizes is calculated or measured. These are then parameterized into more general functions that can be embedded in the microphysical equations. Accurate parameterization of these processes is as important as consideration of numerical methods in determining our confidence in representing microphysical processes in cloud models. For example, the growth of drops and of ice particles by collection strongly depends on the collision and coalescence efficiencies. There is a good database of the efficiencies of drop collisions [*Beard and Ochs*, 1993] but somewhat poorer knowledge of the coalescence efficiencies [*Whelpdale and List*, 1971; *Levin et al.*, 1973; *Beard and Ochs*, 1993; Ochs et al., 1995]. The efficiency of riming of cloud droplets with ice particles and aggregation efficiencies/kernels is even more poorly documented. Therefore, different parameterizations of these data lead to different model results. It should be noted also that laboratory measurements have generally been made under non-turbulent conditions. (See Chapter 4 for a discussion of the effects of turbulence on collision-coalescence.)

6.4 MODELING AEROSOL-CLOUD-PRECIPITATION INTERACTIONS

6.4.1 Warm Clouds: Aerosol Effects on Drizzle in Stratocumulus Clouds

Stratocumulus clouds have been the focus of numerous intensive field campaigns as well as detailed modeling efforts, primarily because of their importance to the Earth's radiation budget rather than because they produce precipitation in significant quantities. Their importance derives largely from their frequency of occurrence and extensive spatial coverage, as well as their high reflective contrast with the underlying surface (particularly over oceans). Over land and ocean, stratocumulus clouds have an annually averaged coverage of ~18% and 34%, respectively [*Warren et al.*, 1986a,b]. Stratocumulus clouds frequently produce drizzle (e.g., [*Paluch and Lenschow*, 1991; *Stevens et al.*, 2003] and the initiation of drizzle has been the focus of much modeling effort. Modeling of aerosol-cloud interactions in stratocumulus clouds received attention in the early 1990s with the development of 1-D turbulence closure models coupled to bin microphysical models [*Ackerman et al.*, 1995; *Bott et al.*, 1996], and modeling at the large eddy scale in 2-D and 3-D simulations [*Kogan et al.*, 1994; *Liu et al.*, 2000; *Feingold et al.*, 1994, 1996, 1997; *Stevens et al.*, 1996, 1998; *Khairoutdinov and Kogan*, 2000; *Feingold and Kreidenweis*, 2002; *Jiang et al.*, 2002].

Ackerman et al. [1995] used a 1-D turbulence closure model coupled to an aerosol and cloud particle size-resolved model to show that progressive aerosol scavenging by drop collisions and drizzle in a stratocumulus cloud can reduce the cloud liquid water path (LWP) and optical depth to a point where there is insufficient cloud-top cooling to maintain the cloud. Under such conditions the cloud collapses into a fog layer. These authors suggested that coalescence scavenging and drizzle could limit the lifetime of stratocumulus clouds. They contrasted this phenomenon with the more common hypothesis that increases in aerosol concentrations suppress drizzle and help to sustain clouds with higher LWPs [*Albrecht*, 1989]. *Bott et al.* [1996] used a similar 1-D model to examine dynamical-microphysical-radiation feedbacks. Recognizing the importance of better representation of boundary layer dynamics, *Feingold et al.* [1994] and *Kogan et al.* [1994] coupled similar bin microphysical models to 2-D and 3-D Eulerian models with grid sizes on the order of 50 m–100 m. *Kogan et al.* [1995] demonstrated the importance of microphysical-dynamic coupling, particularly through the supersaturation field. *Feingold et al.* [1996] showed that in-cloud residence time is an important factor in determining precipitation development in stratocumulus. *Stevens et al.* [1996] pointed out that air parcels that spend significant time at cloud top, where LWC is highest, are more likely to produce drizzle drops.

Feingold et al. [1997] showed that broadening of drop spectra via collision-coalescence tends to increase cloud susceptibility (as defined by *Twomey* [1991]). *Khairoutdinov and Kogan* [1999] compared their LES model with bin microphysics to measurements from field experiments and showed generally good agreement in the dynamical and microphysical fields. Driven by the large computational expense of resolving drop size distributions in LES, *Feingold et al.* [1998] and *Khairoutdinov and Kogan* [2000] studied drizzle formation in stratocumulus using both bin and bulk (2 moment) schemes and showed that bulk schemes can reproduce many of the features of drizzle formation. *Liu et al.* [2000] studied ship tracks using LES and demonstrated the effects of boundary layer stability on both inclusion of the stack effluent into the clouds as well as maintenance of the ship track. Decoupling of the boundary layer suppresses transport of the effluent into cloud. Because boundary layer stability has a diurnal cycle, which modifies both cloud LWC and the amount of aerosol affecting the cloud, persistence of ship tracks is not easily predicted.

The LES/bin-microphysics simulations performed by *Stevens et al.* [1998] illustrate the importance of drizzle to the cloudy marine boundary layer. For strongly drizzling cases where

the drizzle reaches the surface, evaporation results in cooling of the surface and stabilization of the sub-cloud layer [*Paluch and Lenschow*, 1991]. As a result, the cloud structure changes to a cumulus-under-stratus regime, which has very different optical properties than a solid stratocumulus field. However, in *Jiang et al's.* [2002] weakly drizzling LES model simulations, the response was quite different. The small amount of drizzle that was produced evaporated just below the cloud base, and had a destabilizing effect on the cloud layer. Addition of higher concentrations of aerosol suppressed this drizzle and consequently, the destabilization. This resulted in weaker penetrating cumulus and an overall reduction in the LWC and LWP of the clouds.

Other aspects of the effect of aerosol on cloud liquid water path (LWP) were considered by *Ackerman et al.* [2004]. They also showed that increases in aerosol do not necessarily result in increases in LWP in stratocumulus clouds, as proposed by *Albrecht* [1989]. A primary factor affecting the LWP response to aerosol changes appears to be the profile of humidity above the inversion. Only when the humidity above the inversion was high did increases in aerosol result in an increase in LWP. When dry air overlies the inversion, increases in aerosol tend to decrease LWP because of enhanced entrainment drying. Similar results were obtained by *Lu and Seinfeld* [2005]. In large eddy simulations of marine trade cumulus clouds, *Xue and Feingold* [2006] showed that although aerosol has a strong effect on precipitation, aerosol effects on cloud LWP and cloud fraction are relatively small compared to the dynamical variability of the clouds at given aerosol concentrations. In fact their simulations showed a decrease in cloud fraction with increasing aerosol, apparently due to stronger evaporation of the smaller cloud droplets, and an evaporation-entrainment feedback that reduced cloud size. Note that this result is for small cumulus clouds (order few 100 meters) and that the result is contrary to the *Albrecht* hypothesis and the satellite-measured increase in cloud fraction with increasing aerosol for larger clouds [*Kaufman et al.* 2005b]. The small aerosol effects on LWP in warm cumulus have also been modeled by *Grabowski* [2006] based on very long simulations (100s of days) with a two-dimensional cloud model and bulk microphysics.

6.4.2 Role of Giant Cloud Condensation Nuclei

An early hypothesis for droplet spectral broadening and the development of precipitation in warm clouds is that aerosols contain giant cloud condensation nuclei (GCCN) and/or

ultragiant aerosol particles that can act as the embryos for initiating coalescence growth (Chapter 4). *Johnson* [1979, 1982] using a parcel model representing droplet growth on a population of aerosol particles via condensation and coalescence calculated that the addition of GCCN at concentrations on the order of 1 per liter (i.e., about 1 particle in 10^5 or 10^6; typical measured concentrations) can account for rapid development of precipitation-sized particles, even in colloidally stable, continental clouds. *Woodcock et al.* [1971] and *Takahashi* [1976] found that giant salt nuclei do not contribute substantially to warm rain initiation in maritime cumulus clouds because drizzle is active anyway under clean conditions. *Feingold et al.* [1999] used several models, including parcel models and 3-D large eddy simulations of marine stratocumulus clouds with detailed two-moment bin-resolving microphysics, to study the effect of GCCN on drizzle formation in stratocumulus. They found that observed GCCN concentrations of 10^{-4} cm^{-3} to 10^{-2} cm^{-3} were sufficient to transform a non-precipitating stratocumulus into a precipitating one when CCN concentrations were in the range 50– 250 cm^{-3}. At lower CCN concentrations, addition of GCCN has little impact on drizzle formation, in agreement with earlier work in clean cumulus clouds.

Similar results were obtained by *Yin et al.* [2000a] for warm convective clouds (using a 2-D slab symmetric cloud model). *Yin et al.* found the intriguing result that a polluted cloud with CCN concentrations of ~ 1700 cm^{-3} and GCCN of 0.02 cm^{-3} can precipitate more readily than a cleaner cloud (~ 1000 cm^{-3} CCN) with no GCCN. This modeling result is supported by the observations of *Eagan et al.* [1974a, b] and *Hindman et al.* [1977] on the effects of effluents from paper mills on cloud micro-structures and of *Rudich et al.* [2002] on the effects of salt on polluted clouds near the Aral Sea. *Wurzler et al.* [2000] showed that cloud-processed dust particles coated with a soluble material can enhance precipitation. *Rosenfeld et al.* [2002] suggested that GCCN could be an effective mechanism for controlling precipitation, in agreement with earlier studies. The relative sensitivity of a cloud to GCCN has to be considered in the context of the non-linear response of the collision-coalescence process to cloud liquid water content, the sensitivity to cloud drop concentration, and the time available for collection. Quantification of precipitation in terms of GCCN alone is therefore not feasible; no study to date has quantified the effect of GCCN in terms of all the pertinent parameters.

The importance of GCCN requires consideration of the body of modeling studies of hygroscopic seeding that consider the addition of giant salt particles into clouds as a means of

artificially enhancing precipitation (e.g., [*Hindman et al.*, 1977; *Cooper et al.*, 1997]). The study of *Cooper et al.* [1997] and *Yin et al*. [2000b] are of special interest because they elucidate the role not only of the giant seeded particles, but also of the other hygroscopic particles present in flares that have been used for artificial seeding. (See Chapter 8 for a more detailed discussion of deliberate cloud seeding.)

6.4.3 Cloud Processing

The recognition that aerosols not only affect clouds but that clouds affect aerosols (e.g., [*Easter and Hobbs*, 1974; *Hegg et al.*, 1980]) provided challenges to the modeling community by requiring that CCN be treated as size-resolved prognostic species and be tracked as soluble material inside drops [*Flossmann et al.*, 1985; *Bott et al.*, 1990; *Chen and Lamb*, 1994; *Feingold et al.*, 1996]. Modeling of aqueous sulfate production, and the resultant modification of the aerosol size distribution, has most often been simulated in Lagrangian parcel models (e.g., [*Easter and Hobbs*, 1974; *Hegg and Larson*, 1990; *Bower and Choularton*, 1993; *Wurzler et al.*, 2000]). These models have reproduced the creation of a bimodal aerosol size distribution as observed by *Hoppel et al.* [1990]. The implications of this processing range from increases in light scattering [*Hegg et al.*, 1996] to effects on CCN and drop number concentration [*Bower and Choularton*, 1993; *Feingold and Kreidenweis*, 2000; *Yin et al*, 2002]. Eulerian models have also been used to study cloud processing. *Bott* [2000] used a 1-D model, with a very detailed 2-D representation of the joint aerosol-drop distribution function, to study the modification of aerosol size distributions by aqueous chemistry for a range of aerosol and gas phase conditions. *Feingold et al.* [1996] incorporated bin microphysics for aerosols and drops in 2-D simulations of stratocumulus and studied the rate of aerosol scavenging via drop collection. Drop collection reduces the total drop number concentration, so that on subsequent evaporation the available solute mass is redistributed among fewer, and therefore larger, particles. These authors compared their results to aqueous chemistry processing and suggested that at high LWC, coalescence processing of aerosol would likely dominate aqueous chemistry processing. Similar inferences were made by *Hatzianastassiou et al*. [1998] and *Wurzler et al.* [2000]. *Feingold and Kreidenweis* [2002] used a 3-D LES model with size-resolved aerosol and cloud drops, as well as aqueous sulfate production. They showed that the addition of sulfate mass could increase or decrease drizzle formation in stratocumulus depending on the size distribution of the background aerosol. When mass addition occurred at sizes significantly larger than the background CCN, drizzle

was increased; conversely, when mass addition occurred close to the mode of the background CCN, drizzle was reduced.

In precipitating clouds, the most direct form of cloud processing of aerosol is through wet deposition to the surface. *Respondek et al.* [1995] used a 2-D slab-symmetric model with bin microphysics to simulate the uptake, redistribution, and wet removal of aerosol by a mixed-phase convective cloud. Their model, which included tracking of dissolved aerosol inside hydrometeors, was one of the first to couple the effects of aerosol and precipitation in mixed phase clouds. They showed that the simulated scavenging efficiency was very similar to the precipitation efficiency (~ 10%). *Yin et al.* [2005] performed similar simulations, using a detailed bin microphysical model as well as aqueous sulfate production. Their simulations showed that the addition of sulfate mass had an insignificant effect on cloud evolution, even for polluted conditions (10 ppbv SO_2 and 1 ppbv H_2O_2).

Convective clouds also act to transport boundary layer aerosol to the middle and upper troposphere (e.g., [*Cotton et al.*, 1995, *Flossmann and Wobrock*, 1996]). This can have important implications for precipitation as well as for upper tropospheric heterogeneous reactions and the life cycle of aerosols [*Clarke et al.*, 1999]. Additionally, *Teller and Levin* [2006] showed that polluted clouds containing high concentrations of CCN not only lead to reduced precipitation but also leave much more water vapor from the evaporation of cloud drops and ice crystals at higher altitudes after precipitation stops. This could affect radiation transfer as well as various chemical reactions.

6.4.4 Mixed-phase Clouds: Effects of Aerosols on Precipitation

Reisin et al. [1996a,b] studied the effects of changes in CCN on precipitation in an axisymmetric cloud model with a comprehensive bin microphysical representation of water and ice hydrometeors. They showed that a simulation with relatively low CCN (100 cm^{-3} at 1% supersaturation) produced precipitation efficiently through the freezing of large droplets interacting with ice crystals. With increasing CCN concentrations and decreasing drop sizes, graupel growth was suppressed and the precipitation efficiency decreased (for CCN=900 cm^{-3}, precipitation was reduced by 85%). This study also showed that for the sounding considered, increases in ice nucleus (IN) concentrations tended to produce higher precipitation amounts but the changes were very small for a three order of magnitude change

in IN in a moderately polluted cloud (CCN=600 cm^{-3} at 1% supersaturation). They found a greater sensitivity to IN concentrations when CCN concentrations (1100 cm^{-3}) were high.
A number of earlier studies have shown that the speed of glaciation of a cloud is highly dependent on the presence of large supercooled raindrops or on the concentrations of CCN [*Cotton*, 1972; *Koenig and Murray*, 1976; *Scott and Hobbs*, 1977]. When CCN concentrations are high, warm-cloud collection processes are suppressed and supercooled raindrops are few in number, small ice crystals must first grow to several hundred micrometers in diameter before they begin collecting cloud droplets. Then the riming process proceeds slowly until the ice particles have grown to millimeter-size. Furthermore, since riming is suppressed in clouds forming in air masses with high CCN concentrations, secondary ice particle production by the riming-splintering process [*Hallett and Mossop*, 1974; *Mossopp and Hallett*, 1974] is suppressed as well.

Khain et al. [1999] used a 2-D (slab-symmetric) model with bin microphysics to simulate aerosol effects on precipitation in an Eastern Mediterranean coastal setting. They too found that warm rain was significantly reduced by an increase in the aerosol concentrations. However, they noted that in the case of polluted clouds, the lofting and downwind transport of smaller precipitation particles could produce more rain a few tens of kilometers from the convective region than was produced by the cleaner clouds with their efficient warm rain process. The result points to the importance of both dynamics and microphysics through particle "size sorting" and spatial redistribution of ice and water phases in the spatial domain.
Khain et al. [2001] simulated the effect of varying the concentration of CCN on ice-crystal concentrations in deep convective clouds. Clean clouds (CCN ~ 100 cm^{-3}) produced large drops and rapid freezing at ~ -15ºC, resulting in significant depletion of cloud water. In a polluted cloud, (CCN =1260 cm^{-3}), freezing was delayed until much lower temperatures (~ -35ºC) because the small drop sizes rendered mechanisms that convert water droplets to ice inefficient, until the level of homogeneous freezing was reached. These simulations compare well with in-situ measurements exhibiting high LWC at temperatures as low as -38ºC under polluted conditions [*Rosenfeld and Woodley*, 2000]. Precipitation amounts were about half of those in the clean case. *Khain et al.* suggested that the general assumption that droplet-graupel collision efficiencies are equal to droplet-droplet collision efficiencies strongly overestimates the rate of collection of small droplets by small graupel; a sensitivity test showed that cloud LWC is depleted at much higher temperatures if this assumption is made.

This result points to the importance of quantifying collision efficiencies and the importance of commensurate efforts in both modeling methodology and laboratory studies.

The importance of treating aerosol and cloud microphysics as a coupled system has been highlighted in recent papers by *Fridlind et al.* [2004] and *Yin et al.* [2005]. The former combined measurements from Florida cumulonimbus with 3-D modeling (with bin-microphysics for aerosol and hydrometeors) to infer that most anvil ice-crystals form on mid-tropospheric aerosol and not boundary layer aerosol. Lateral entrainment incorporates these particles into the updrafts where they are exposed to supersaturations and activated. Similar conclusions were drawn by *Yin et al.* [2005] with a 2-D axisymmetrical model employing bin microphysics for aerosol and cloud microphysics, as well as aqueous sulfate chemistry. They showed that aerosol regeneration, which returns aerosol to the mid-troposphere upon evaporation of hydrometeors, has a significant effect on microphysical pathways; when this process was neglected, graupel concentrations were nearly doubled and surface precipitation increased by ~50%.

In simulations of entrainment of Saharan dust into Florida thunderstorms, *Van den Heever et al.* [2004] found that dust not only impacts cloud microphysical processes but also the dynamical characteristics of convective storms. Dust may serve as CCN, GCCN, and IN. The effect of dust on cloud microstructure and storm dynamics in turn alters the accumulated surface precipitation and the radiative properties of anvils. These results suggest that the dynamic structure of the storms is influenced by varying dust concentrations. In particular, the updrafts are consistently stronger and more numerous when Saharan dust is present compared with a clean airmass. This suggests that the clouds respond to dust in a similar manner to that envisaged in “dynamic seeding.” That is, dust results in enhanced glaciation of convective clouds, which then leads to dynamical invigoration of the clouds, larger amounts of processed water, and thereby enhanced rainfall at the ground [*Simpson et al.*, 1967; *Rosenfeld and Woodley*, 1989, 1993]. However, *Van den Heever et al.'s* simulations suggested that rainfall is enhanced by dust ingestion during the first two hours of the formation of deep convective cells, but it is reduced on the ground later in the day. Thus the clean aerosol simulations produced the largest surface rain volume at the end of the day. This is a result of complex dynamical interactions of clouds to aerosol changes via cold pool variations beneath the clouds and to scavenging of dust, so that few GCCN and IN remained late in the day.

In their simulations of the effects of smoke-enhanced CCN concentrations, *Khain et al.* [2004] also found that smaller cloud droplets reduce the production of drizzle drops. When these droplets froze, the associated latent heat release resulted in more vigorous convection. In a clean cloud, on the other hand, drizzle depleted the cloud liquid water so that less latent heat was released when the cloud glaciated, resulting in less vigorous convection. Thus, they found that a squall line did not form under clean conditions, whereas a squall line developed under continental aerosol conditions and produced more precipitation after two hours. *Zhang et al.* [2005] came to similar conclusions in their model simulations for different three-week periods over the ARM site in Oklahoma.

Seifert and Beheng [2005b] showed that the effect of changes in CCN on mixed phase convective clouds is quite dependent on cloud type. They found that for small convective storms, an increase in CCN decreases precipitation and the maximum updraft velocities. For multicellular storms, the increase in CCN has the opposite effect – namely, promoting secondary convection, and increasing maximum updrafts and total precipitation. Supercell storms were the least sensitive to CCN. Their study also showed that the most important pathway for feedbacks from microphysics to dynamics is via the release of latent heat of freezing.

Cloud-resolving simulations of Arctic boundary layer clouds were carried out for a particular day [*Carrió et al.*, 2005a] and for an entire spring season [*Carrió et al.*, 2005b]. The model was initialized with either clean sub-cloud aerosol concentrations throughout the boundary layer or with observed polluted aerosol concentrations above the inversion and clean below. During the spring season simulations were performed with the model coupled to a sea-ice model. The multi-month simulations were performed using 2-3 daily soundings nudged into the cloud-resolving model to represent daily variations in the synoptic atmosphere. Mixed-phase clouds prevailed during the first two months of simulation, while predominately liquid clouds were simulated during the last month. The effects of IN entrainment in the presence of mixed-phase clouds decreased LWC while ice water paths increased. Even though IN concentrations above the inversion were much lower than estimates from mid-latitudes using the *Meyers et al.* [1992] formula, the clouds were essentially over-seeded. As a result crystal fall speeds were reduced, as were precipitation rates. This resulted in longer residence times of the ice particles and increased total condensate paths. This produced enhanced downward longwave radiation. Enhanced albedo associated with enhanced CCN concentrations (hence

droplet concentrations) also occurred, but net surface radiation was still higher. As a consequence, sea-ice melting rates were greater. Changes in surface fluxes of the opposite sign were simulated for short time periods when predominately liquid clouds were present, and during the last month. The effect on melting rates associated with the presence of enhanced CCN concentrations above the boundary layer is opposite although less important than that of IN entrainment. Overall these model simulations suggest that the entrainment of a polluted layer of air overriding an inversion enhances sea-ice melting rates. Melting rates were approximately 4% higher when the air above the boundary layer was polluted than when the entire layer was composed of clean sub-cloud air.

Saleeby and Cotton [2005] examined the influence of varying concentrations of CCN and GCCN on simulated wintertime orographic clouds and precipitation over the Park Range of Colorado. They found that higher CCN concentrations lead to the formation of smaller, more numerous droplets and reduced riming consistent with the observations by *Borys et al*. [2000, 2003] as discussed in Chapter 5. Total precipitation on the ground was therefore reduced. Higher concentrations of GCCN resulted in enhanced surface precipitation when CCN concentrations were high. When CCN concentrations were low, however, higher GCCN concentrations caused greater vapor competition for ice particle and droplet nucleation and vapor deposition growth, which led to a reduction in surface precipitation. Those simulations were performed using the *Meyers et al* [1992] formula for IN activation. Observations of IN concentrations over the Park Range using a continuous flow diffusion chamber by *Demott et al.* [2005, personal communication] suggest that the Meyers formula overestimates IN concentrations. Using the lower IN concentrations produced very small changes in cloud mixing ratios, but lowered ice water contents, and reduced surface precipitation.

6.4.5 Semi-direct aerosol effects

Heating of the air by absorbing aerosols can result in stabilization of a moist moderately stable layer and weaken convection and precipitation. This could have important climatic implications through the hydrological cycle. In regions where there is not sufficient moisture or instability to support deep convection, aerosol impacts should be less. This effect of aerosols has been termed the *semi-direc*t effect [*Grassl*, 1975; *Hansen et al.*, 1997]. The reduction in cloud cover associated with this effect can alter the surface energy budget significantly. If the aerosol contains a large fraction of soot, such as the south Asian haze,

then warming of the aerosol layer can nearly totally desiccate stratocumulus cloud layers and alter the properties of the trade-wind cumulus layer [*Ackerman et al.*, 2000]. The influence of black carbon dominates via its absorption of solar radiation within the atmosphere, which leads to lower surface temperatures [*Ramanathan et al.*, 2001; *Lohmann and Feichter*, 2001]. General circulation model simulations by *Menon et al.* [2002b] suggest that black carbon emissions over China may be producing changes in the general circulation, which contribute to the observed increases in summer flooding in south China and drought in north China. Thus, in spite of the fact that anthropogenic aerosol emissions are regionally concentrated, their potential for global impacts is great. *Wang* [2004] studied the radiative effects of black carbon in a coupled aerosol-climate model and also showed that black carbon modifies precipitation patterns. Interestingly, the model shows an increase in low clouds and a decrease in mid level clouds as a result of black carbon.

Johnson et al. [2004] conducted large eddy simulations (with bulk microphysics) of stratocumulus clouds and imposed a range of heating rate profiles. They found that the location of the absorbing aerosol was important in determining cloud response. When the absorbing aerosol was located within the well mixed boundary layer, cloud LWP and cloud fraction was reduced. However, when the absorbing aerosol resided above the cloud layer, LWP was increased due to a strengthening of the inversion and reduction in entrainment of dry air. In response to *Koren et al.'s* [2004] observations that smoke in biomass burning regions significantly reduces cloud fraction, *Feingold et al.* [2005] modeled the semi-direct effect using a LES model with bin microphysics for aerosol and cloud drops. Predictive equations for aerosol allowed heating rates to evolve with the boundary layer and cloud fields. Through a series of numerical experiments, they established that in addition to the importance of the location of the smoke, the reduction in net surface radiation, and therefore land-surface latent and sensible heat fluxes associated with the smoke was likely the most important factor in suppressing cloud formation. This reduction in surface fluxes was also a robust feature in *Wang* [2004]. Note that the fact that the presence of aerosol, and particularly absorbing aerosol, modifies the sensible and latent heat fluxes is of great importance since it points to possible non-monotonic responses of LWP to aerosol. As aerosol increases, it may act to increase LWP and suppress precipitation, but with increasing aerosol loading a point may be reached where the associated reduction in surface fluxes will act to suppress convection and therefore reduce LWP [*Jiang and Feingold*, 2006]. This result can be broadened to stress the importance of land-surface characteristics and land management for

cloud development. For example, as large tracts of forest are converted to pasture in the Amazon, clouds and precipitation are expected to be modified [*Fisch et al.*, 2004].

Another facet of aerosol direct and semi-direct effects is on the nucleation of cloud droplets and thus the concentration of droplets in clouds. *Conant et al.* [2004] computed the effects of carbon black aerosols on cloud droplet nucleation. Figure 6-4 illustrates the equilibrium supersaturation over solution drops containing carbon black aerosols. The peak in the curves, called Köhler curves, represents the supersaturation that must be attained in a cloud to form growing cloud droplets. If the cooling rate in clouds, which is normally proportional to updraft velocity, is not large enough to exceed the peak values in the curves, then the aerosol particle of the size indicated cannot form a cloud droplet (see also Chapter 4 for more details). Their calculations showed that since carbonaceous particles are strongly absorbing of solar radiation, the warming of these particles elevates the peak supersaturation. Thus, for example, if many aerosols are 0.1 μm in diameter, and peak supersaturations are less 0.01%, these particles will not be activated to form cloud droplets due to the absorption of solar radiation. This effect is most pronounced at low supersaturation clouds, such as in fogs. Moreover, the effect is most pronounced for larger aerosol particles, since the absorption cross section is proportional to the area of the particle. Its main impact is on giant CCN [*Nenes et al.*, 2002b], which can initiate or accelerate the collision-coalescence process. Thus, if the carbonaceous particles absorb solar radiation they may not become large enough to initiate collision-coalescence which, in turn, may suppress precipitation. This process is probably important only for optically thin clouds or clouds over high albedo surfaces.

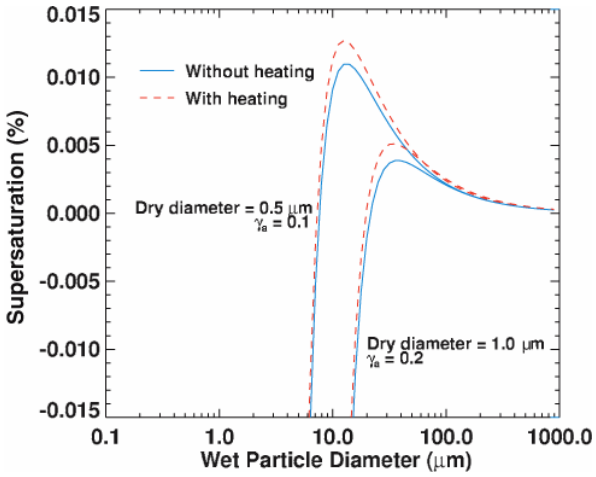

Figure 6-4. *Effect of droplet heating on the Köhler curves of particles with dry diameters of 0.5 μm and 1.0 μm. Heating parameters of 0.1 and 0.2 were used for the two droplet sizes, respectively. Particles were assumed to have the hygroscope properties of sulfate. From Conant et al., 2002.*

6.5 AEROSOL EFFECTS ON PRECIPITATION AND THE HYDROLOGICAL CYCLE FROM A GCM PERSPECTIVE

General circulation models (GCMs) represent the primary tool for prediction of climate change but moreover, they could also play an important role in evaluating the regional effects of pollution on modifying precipitation distribution and amounts. By integrating atmospheric, radiative, oceanic, and land-surface processes on the global scale they provide an indication of expected changes in the coupled system, including possible consequences of greenhouse gas warming and aerosol on the climate system.

GCMs have been used to examine the influence on global climate of widespread sources of CCN. First it must be recognized that GCMs have grid spacings of 150 km to 250 km and that clouds often cover a small fraction of the grid-cell area of a GCM, and the average vertical velocities in a grid cell are very small (~0.01 m s^{-1}) whereas actual cloud-scale vertical velocities are ~1 m s^{-1} or greater. The poor representation of convection is likely a major source of the disparity in model-predicted LWP amongst GCMs (Figure 6-5). Space-

based measurement of LWP is also difficult, although uncertainties in observations are smaller than the inter-model differences in Figure 6-5; nevertheless, models are not well constrained by observations. Model predictions of total precipitation show less variability reflecting the fact that models are heavily tuned to observations [*Stephens et al.*, 2002] and because the global annual mean amount of precipitation is constrained by the global mean evaporation. The problem of prediction of condensate is not limited to GCMs: Comparisons between total liquid water content (ice plus water) generated by three different cloud schemes in a forecast model show very large variability amongst themselves, and as compared to in-situ aircraft data [*Guan et al.*, 2002]. Similar discrepancies in condensate between single column models (SCMs) were obtained by *Menon et al.* [2003] in their simulations of clouds observed during the ACE-2 campaign.

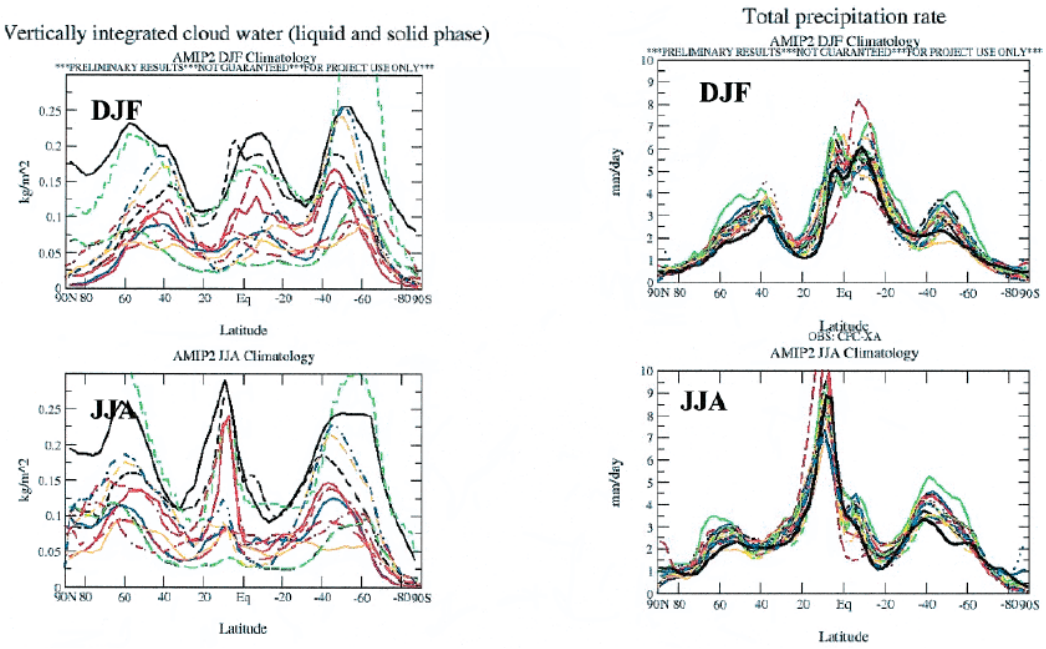

Figure 6-5. *GCM calculations of (left panel) LWP (liquid and solid) and (right panel) total precipitation rate from a variety of model simulations as part of the AMIP project. Figure from Stephens et al. (2002)*

Cloud-scale velocities generate the peak supersaturations in clouds, which together with the number of CCN available determine the number of activated drops. It is therefore necessary to estimate cloud-scale vertical velocities to predict cloud drop concentrations. Some

modelers have assumed an empirical relationship between predicted sulfate mass concentrations and droplet concentrations [*Martin et al.*, 1994; *Boucher and Lohmann*, 1995; *Kiehl et al„* 2000], but that is equivalent to assuming there is only a single-value of cloud updraft velocity for all clouds in the model. Others have estimated vertical velocity based on predicted turbulent kinetic energy from boundary layer models [*Lohmann et al.*, 1999]. This is a step in the right direction, but it does not take into account the fact that cloudy updrafts are at the tail of the probability density function (PDF) of vertical velocity. *Ghan et al.* [1997] and *Chuang et al*. [1997] assumed a normal distribution of vertical velocity with a mean value given by the GCM grid point mean. They then determined the velocity-weighted mean droplet concentration that takes into account the tails of their assumed PDF of vertical velocity. However, observed PDF's of vertical velocity in clouds in the boundary layer are multimodal and are better represented by double-Gaussian PDF's [*Larson et al.*, 2001] with a mean that is a function of the RMS vertical velocity rather than a GCM grid point mean. Moreover, the complications of precipitation or drizzle processes on cloud lifetime, cloud water contents, and cloud radiative properties discussed above cannot be simulated well in GCM cloud parameterization schemes. For example, precipitation processes are non-linear functions of total condensate water contents. As a result, the mean LWC from a GCM model grid-box is essentially meaningless for the representation of precipitation production [*Stevens et al.*, 1998; *Pincus and Klein*, 2000]. A PDF approach to subgrid modeling may be the optimum approach to resolving these deficiencies [*Larson et al.*, 2004]. Another option, though considerably more computationally expensive, is to use what has been called "super-parameterizations" in which cloud resolving models are activated at model grid points [*Grabowski et al.*, 1999; *Randall et al.*, 2003]. These models have the capability of predicting cloud-scale vertical velocities and LWC and thus explicitly representing precipitation processes but have yet to be applied to aerosol effects on precipitation. If the representation of aerosol and clouds in such models, or others using new and innovative techniques for representing subgrid processes can be improved, they should improve predictions of the role of aerosols in changing clouds and precipitation spatial distribution and amounts as well as climate. With these caveats in mind, we will now describe some of the results of GCM simulations of the effects of aerosol on clouds and precipitation.

6.5.1 Aerosol Impacts on Clouds; the Twomey and Cloud Lifetime Effect in GCMs

Aerosol-cloud interactions in GCMs are usually divided into the first indirect effect, or the albedo effect, and the second indirect effect, or "lifetime effect". The cloud lifetime effect is based on *Albrecht's* [1989] hypothesis that higher concentrations of cloud droplets resulting from higher concentrations of CCN will decrease droplet size, suppress drizzle, and increase liquid water contents and thereby result in clouds with greater lifetimes. As noted above, however, there is recent evidence from large eddy simulations that under certain conditions higher concentrations of cloud droplets can result in lower liquid water content clouds and reduced cloud liquid water path. It is also noted that there are only few studies (cloud-scale modeling or observational) of cloud lifetime and that the spatial/temporal resolution of GCMs makes them ill-suited to calculation of cloud lifetime.

There is considerable difference in predicted forcing due to the albedo effect, and even more significant disagreement in the lifetime effect. The global mean magnitude of the cloud albedo effect since pre-industrial times is estimated to be between -0.5 and -1.9 W/m^2 from different climate models and the cloud lifetime effect to be between -0.3 and -1.4 W/m^2 (Figure 6-6 and *Lohmann and Feichter*, 2005). The total aerosol effect is restricted to warm clouds except for the simulations by *Lohmann and Diehl* [2006] who are the only ones to include the glaciation indirect effects on stratiform mixed-phase clouds [*Lohmann*, 2002]. Models do not even agree about the relative importance of the albedo and lifetime effects. Differences are likely related to the range of treatments of droplet activation, assumptions of what constitutes the background aerosol, as well as differences in autoconversion parameterizations.

6.5.2 Aerosol Influences on Precipitation in GCMs

Several studies have considered the response of a GCM with a mixed-layer ocean to indirect aerosol effects [*Rotstayn et al.*, 2000; *Williams et al.*, 2001; *Rotstayn and Lohmann*, 2002] or to a combination of direct and indirect aerosol effects [*Feichter et al.*, 2004; *Takemura et al.*, 2005; *Kristjansson et al.*, 2005]. All of these found a substantial cooling that was strongest in the Northern Hemisphere, with a consequent southward shift of the Intertropical Convergence Zone (ITCZ) and the associated tropical rainfall belt. *Rotstayn and Lohmann* [2002] went on to suggest that aerosol effects might have contributed to the Sahelian droughts of the 1970s and 1980s. The southward shift of the ITCZ was less pronounced in the *Feichter et al.* [2004]

study than in the other studies, perhaps due to their more complex treatment of cloud droplet nucleation, which tends to give less weight to the effects of sulfate than simpler schemes do. In contrast, *Chung and Seinfeld* [2005] considered the response of a GCM to direct forcing by black carbon aerosols, and found a northward shift of the ITCZ due to enhanced warming of the Northern Hemisphere.

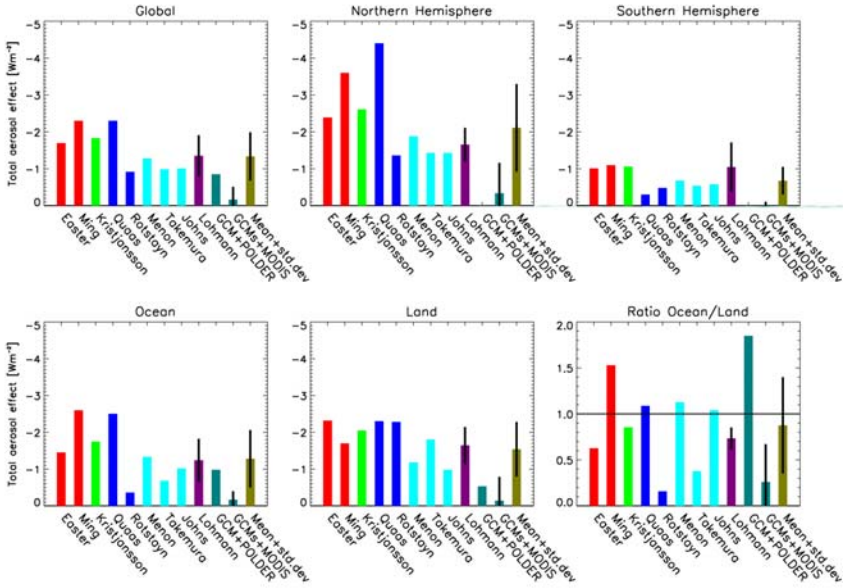

Figure 6-6. *Global mean total anthropogenic aerosol effect (direct, semi-direct and indirect cloud albedo and lifetime effects) defined as the response in net radiation at the top-of-the-atmosphere from pre-industrial times to present-day and its contribution over the Northern Hemisphere (NH), Southern Hemisphere (SH), over oceans and over land, and the ratio over oceans/land. Red bars refer to anthropogenic sulphate (Easter et al., 2004; Ming et al., 2005[+]), green bars refer to anthropogenic sulphate and black carbon (Kristjánsson, 2002[*,+]), blue bars to anthropogenic sulphate and organic carbon (Quaas et al., 2004[*,+]; Rotstayn and Liu, 2005[+]), turquoise bars to anthropogenic sulphate, black, and organic carbon (Menon and Del Genio, 2005; Takemura et al., 2005; Johns et al., 2006), dark purple bars to the mean and standard deviations of anthropogenic sulphate, black, and organic carbon effects on water and ice clouds (Lohmann and Diehl, 2006), teal bars refer to a combination of GCM and satellite results (ECHAM+POLDER, Lohmann and Lesins, 2002; LMDZ/ECHAM+MODIS, Quaas et al., 2005) and olive bars to the mean plus standard deviation from all simulations.*

*****refers to estimates of the aerosol effect deduced from the shortwave radiative flux only*

[+] *refers to estimates solely from the indirect effects*

Global climate model estimates of the change in global mean precipitation due to the total aerosol effects are summarized in Figure 6-7. Consistent with the conflicting results from

detailed cloud system studies, the change in global mean precipitation vary between +0.005 mm day^{-1} and -0.13 mm day^{-1}. These differences are amplified over land, ranging from –0.17 mm day^{-1} to 0.02 mm day^{-1}. The decreases in precipitation are larger, when the atmospheric GCMs are coupled to mixed-layer ocean models (green bars), where the sea surface temperature and, hence, evaporation is allowed to vary.

Observations by *Borys et al.* [2003] in midlatitude orographic clouds show that for a given supercooled liquid water content, both the riming and the snowfall rates are reduced if the supercooled cloud has more cloud droplets (see also Chapter 5). Examination of this effect in global climate model simulations with pre-industrial and present-day aerosol concentrations showed that while the riming rate in stratiform clouds has indeed decreased due to the smaller cloud droplets in polluted clouds, the snowfall rate has actually increased because of feedbacks within the climate system. The pollution induced increase in aerosol and cloud optical thickness reduces the solar radiation at the surface and causes a cooling that favors precipitation formation via the ice phase [*Lohmann*, 2004].

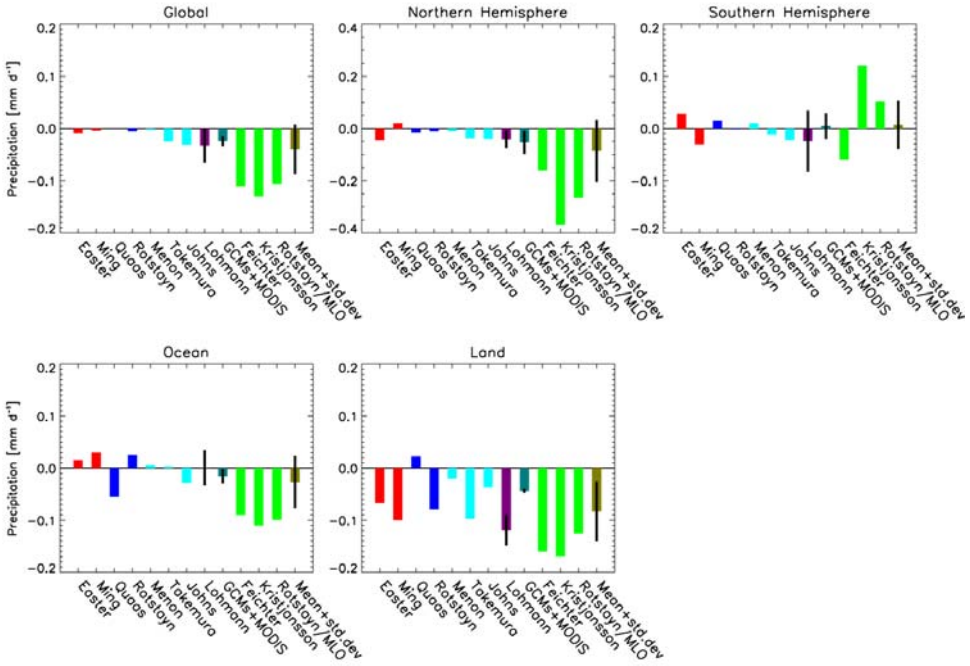

Figure 6-7. *Global mean change in precipitation due to the total anthropogenic aerosol effect (direct, semi-direct and indirect cloud albedo and lifetime effects) from pre-industrial times to present-day and its contribution over the Northern Hemisphere (NH), Southern Hemisphere (SH) and over oceans and over land. Red bars refer to anthropogenic sulphate (Easter et al., 2004; Ming et al., 2005*[+]*), blue bars to anthropogenic sulphate and organic carbon (Quaas et al., 2004*[+]*; Rotstayn and Liu, 2005*[+]*), turquoise bars to anthropogenic sulphate, black, and organic carbon (Menon and Del Genio, 2005; Takemura et al., 2005; Johns et al., 2006), dark purple bars to the mean and standard deviations of anthropogenic sulphate, black, and organic carbon effects on water and ice clouds (Lohmann and Diehl, 2006), teal bars refer to a combination of GCM and satellite results (LMDZ/ECHAM+MODIS, Quaas et al., 2005), green bars refer to results from coupled atmosphere/mixed-layer ocean (MLO) experiments (Feichter et al., 2004 - sulphate, black, and organic carbon; Kristjansson et al., 2005 - sulphate and black carbon; Rotstayn and Lohmann, 2002*[+] *- sulphate only) and olive bars to the mean plus standard deviation from all simulations.*

[+] *refers to estimates solely from the indirect effects*

6.5.3 Coupling of the Hydrological Cycle and Greenhouse Gas Warming

Greenhouse warming, as a result of enhanced CO_2 concentrations, is amplified when the global hydrological cycle is enhanced and greater amounts of water vapor are evaporated into the air principally over the oceans but also over land. This is because water vapor is a much

more powerful greenhouse gas than CO_2. The increased amounts of water vapor in the air, in turn, results in a strong positive feedback to CO_2 warming. Recent GCM simulations of greenhouse warming and direct and indirect aerosol effects [*Liepert et al.*, 2004] show that in accord with the discussion in 6.4.4, the indirect and direct cooling effects of aerosols reduce surface latent and sensible heat transfer (Figure 6-8) and, as a consequence, act to spin-down the hydrological cycle and thereby substantially weaken greenhouse gas warming. This is important since most investigators compare top of the atmosphere radiative differences for greenhouse gas warming and aerosol direct and indirect effects separately. Since greenhouse warming depends on a spin-up of the hydrological cycle, and aerosol direct and indirect cooling counteracts the spin-up, the potential influence of aerosols on climate could be far more significant than previously thought. The decrease in global mean precipitation from pre-industrial times to the present may, however, reverse into an increase of about 1% in 2031–2050 as compared to 1981–2000, because the increased warming due to black carbon and greenhouse gases then dominates over the sulfate cooling [*Roeckner et al.*, 2006].

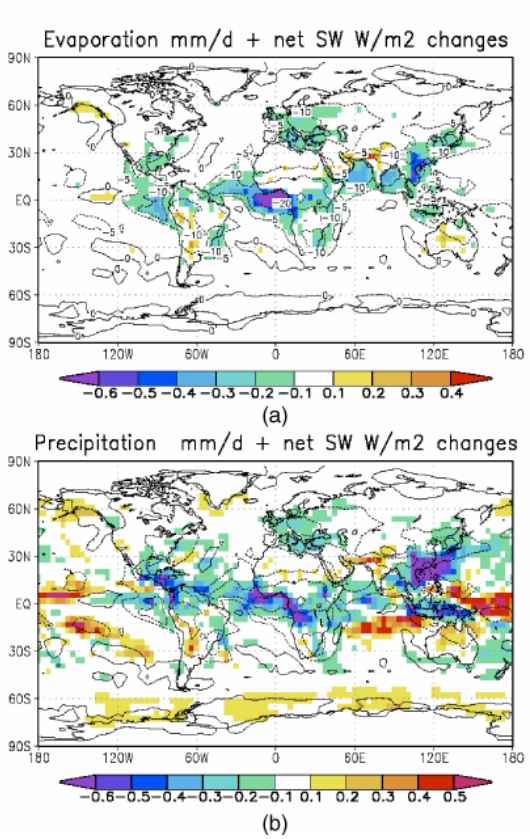

Figure 6-8. *Simulated changes in (a) evaporation (colors) and net surface solar radiation (contours) and (b) precipitation (colors) and net surface solar radiation (contours). Model results are differences of present-day minus pre-industrial climate simulations with modified anthropogenic aerosol and greenhouse gas concentrations. [from Liepert et al., 2004]*

We summarize by stressing that the results of these GCM simulations should not be viewed as quantitative forecasts of the effects of aerosols on patterns and amounts of regional precipitation. As noted previously, there are many uncertainties in the distribution and concentrations of aerosols and condensate. In addition, there are many simplifications in the models that limit their ability to realistically simulate the indirect effects of aerosols. However, these model simulations demonstrate the potential effects of direct and indirect aerosol forcing on clouds and precipitation in a coupled global system.

6.6 RECOMMENDATIONS FOR FUTURE OBSERVATIONS AND STUDIES

To place our understanding of aerosol-precipitation interactions on a firmer footing, we recommend the following for future modeling efforts.

1. Improve model physics

There is a strong need for an improvement in the representation of cloud microphysical processes in models. This includes both the representation of the physics of hydrometeor behavior, hydrometeor interactions (e.g., laboratory studies of collision and coalescence efficiencies for various combinations of hydrometeor types), the parameterization of these processes so that they can be applied in numerical algorithms, and numerical methods. Although there has been much progress in development of new bin and bulk microphysical methods, advances in representation of hydrometeor collection kernels have lagged. In spite of the sophisticated numerical methods that are now in use, the computational demands of high resolution studies of aerosol-precipitation interactions are such that this is likely to remain an active research area. Much progress has been made in the understanding of aerosol-precipitation interactions at small scales and for individual clouds, but to obtain a more robust and broader perspective, simulations of these interactions should be extended to larger scales (and in 3-D) without significantly compromising the temporal/spatial resolution (see below).

Simulations of aerosol-cloud interactions should be done at the appropriate scale so that the development of cloud supersaturations, droplet activation, and growth processes are resolved. This will yield greater confidence in the model's ability to represent actual cloud responses to variable aerosol inputs. Because of the potential for dynamical feedbacks, aerosol effects on

clouds should be considered in domains large enough to include multiple clouds and for simulations long enough that results can be considered statistically robust.

Land surface characteristics determine the surface latent and sensible heat fluxes and drive boundary layer and cloud development. Current and future changes in vegetation and soil moisture are therefore an important consideration. Moreover, because the presence of atmospheric aerosol (particularly absorbing aerosol) modifies the surface radiation budget, it also changes the surface fluxes, and these changes are likely to differ from one land-surface regime to another. Consideration of the coupled aerosol-cloud-land-surface system is therefore of great importance.

Improve techniques for representing cloud-aerosol-precipitation processes in GCMs

Because of the coarse grid spacing of GCMs, clouds and cloud properties essentially have to be parameterized as sub-grid-scale processes. The challenge is to parameterize aerosol activation, the influence of aerosols on precipitation processes, the precipitation processes and their feedbacks on cloud and storm dynamics, and cloud processing of aerosols all in sub-grid-scale parameterizations.

Approaches that offer some promise include *super-parameterization* in which cloud-resolving models are run on GCM grid points, the *PDF-based approach* to single-column higher-order closure models where PDFs of subgrid quantities, such as vertical velocity and LWP, are determined from prescribed basis functions in which various moments of the basis functions are predicted in the models [*Pincus and Klein*, 2000*; Golaz et al.*, 2002a,b; *Larson et al.*, 2004].

Neither GCMs nor regional-scale models resolve topography sufficiently well to depict cloud-scale vertical motions responsible for the nucleation of aerosol and the formation of precipitation. Solving this problem goes beyond traditional thinking for cloud parameterization schemes.

2. Need for model input data

To model aerosol-cloud-precipitation interactions, either with cloud-resolving models or GCMs, input data on aerosol that have the potential to act as CCN, GCCN, and IN is needed. Ideally these data should include not only surface measurements but also vertical profiles. They should include measurements or diagnosis of aerosol source functions, especially those aerosol that serve as CCN, GCCN and IN. One of the greatest challenges faced by modelers of aerosol-cloud interactions is to acquire data that represents long term trends in cloud nucleating aerosol concentrations. For the most part, all that is available are data from a few

intensive field campaigns. Long-term baseline measurements of CCN, GCCN and IN concentrations should be made at a number of locations throughout the world. Where possible, CCN proxies such as accumulation mode aerosol concentration together with composition information should be considered.

Ice nucleation deserves specific mention. New methods of measuring ice nuclei and analyzing their composition need to be developed [e.g., *Cziczo et al.*, 2004]. The representation of ice formation in cloud models is still rudimentary and relies on a very limited number of measurements and parameterizations [e.g. *Meyers et al*., 1992 and *Hallett and Mossop*, 1974], all of which show strong dependence of ice concentration on temperature and supersaturation. However, some measurements in clouds [*Rangno and Hobbs*, 1994; *Korolev et al.*, 2003] suggest that there is a poor correlation between ice crystal concentrations and temperature in clouds. It is therefore clear that much more work is required to better understand the role of ice nuclei and of ice crystals in the development of precipitation.

The absorbing properties of aerosol need to be characterized. As described above, aerosol absorption has important implications for clouds because it modifies atmospheric stability and reduces surface fluxes. This may have consequences at both the cloud and regional scales.

Aerosol effects on clouds must be considered within the appropriate dynamical and meteorological context. It is quite possible that the response of clouds to aerosol may vary depending on input thermodynamic sounding, surface fluxes, subsidence, large-scale advective tendencies, etc.

Satellite data can provide valuable constraints on aerosol effects on clouds and precipitation. This may require combination of passive radiometry to characterize aerosol and cloud drop sizes, and radar to characterize precipitation. The launch of CLOUDSAT and CALIPSO later this year as part of the A-Train (see Chapter 7 for more details) promises to provide important data on aerosol, clouds, and precipitation [*Stephens et al.*, 2002].

Cause-and-Effect

Assessment, attribution of cause-and-effect

Models are particularly useful for providing quantified estimates of parameters such as precipitation amounts for a given simulation. However, the skill level of models in so doing should be quantified statistically. Models should be used to isolate the role of aerosols from the influence of the meteorology and to quantify the relative importance of each process.

Use models to quantify precipitation efficiency. Precipitation efficiency is the ratio of observed rainfall to the (computed) condensed water. Other proxies such as the drying ratio (total precipitation/vapor influx; *Smith et al.*, 2003) may be more easily derived from observations. Measures such as these would provide quantification of aerosol effects on precipitation.

Models should consider the role of clouds as aerosol scavengers and the scavenging efficiency of clouds and rain. Cloud scavenging, both through coalescence scavenging (6.4.1) and precipitation washout are important aerosol sinks. Consideration of these processes should be included in clouds of all scales.

Identify *cause-and-effect.* Models are very effective tools for isolating cause-and-effect in a physical system. The process of evaluating models versus observations is an important confidence building step. It is important to correctly ascribe the reasons for agreement or disagreement with observations. As models become more complex, it becomes increasingly difficult to isolate causal relations. Effort should be put into applying existing and new methodologies for quantifying the sensitivity of a given parameter to a change in an input parameter or change in a combination of inputs. Methods such as the factor separation [*Stein and Alpert*, 1993] could be used to resolve such effects.

CHAPTER 7: IN SITU AND REMOTE SENSING TECHNIQUES FOR MEASURING AEROSOLS, CLOUDS AND PRECIPITATION

Lead authors: Yoram Kaufman, Paulo Artaxo, Zev Levin, Sandra Yuter

Co-authors: Urs Baltensperger, Larry Radke, Marshall Shepherd
Contributors: Eyal Amitai, Ali Tokay

7.0 INTRODUCTION

In this chapter we review the methods presently available and expected in the near future to measure the effect of aerosols on clouds and precipitation, and the reasons why it is difficult to assess this connection.

The short lifetime of clouds and aerosols, the large variability of cloud properties, and the variability in the aerosol chemical and physical properties, makes it difficult to decipher the impact of aerosols on cloud properties and on the onset of precipitation. An array of satellite instruments, and surface networks that routinely measure aerosol, clouds and precipitation are designed to overcome some of these obstacles by generating large statistics of precipitation, cloud properties and the nearby aerosols. The aerosol properties include measures of the column concentrations (expressed by the aerosol optical thickness) and size (given by distribution of the aerosol in 2 to 3 size modes or measurement of the angstrom coefficient). A major remaining obstacle that is still hard to overcome relates to the precise measurement of precipitation and its collocation with cloud and aerosol measurements.

The measurement tools of aerosols and precipitation, therefore, include in situ measurements from the ground or from the air, remote sensing from the surface or from space and indirect assessments using other attributes. The use of measurements to deduce the effect of aerosols on precipitation includes the following groups: Long term statistics of precipitation with assessment of aerosol based on location and time of the measurements [*Warner*, 1968; *Givati and Rosenfeld*, 2004]; Individual case studies, usually in extreme conditions of precipitation from TRMM involving qualitative assessment of the presence of aerosols based on location downwind of cities or power plant [*Rosenfeld,* 2000].

7.1 MEASURING AEROSOL PROPERTIES FROM THE GROUND

It is not easy to collect and analyze atmospheric aerosols with high precision and with high reproducibility and specificity [*McMurry*, 2000]. A number of factors make this task difficult. The dynamic range of aerosol particles in the atmosphere is ~1 nm to 100 µm, and they occur in large variety of shapes and different chemical compounds. In particular our knowledge of the composition of organic compounds is rudimentary and a significant fraction of the aerosol mass is semi-volatile. In this section issues of aerosol sampling, followed by the physical and chemical characterization of aerosols are discussed. We will focus on the properties that are relevant to aerosol-cloud interactions. More information is found in the GAW Measurement Guide compiled by the WMO/GAW Scientific Advisory Group for Aerosols [*WMO*, 2003].

7.1.1 Ground Based Aerosol Sampling and Mass Analysis

Particle mass is one of the most commonly measured parameters regarding aerosol properties. Sampling artifacts are of concern for some chemical species, particularly those exhibiting evaporative losses of semi-volatile organic compounds [*Baltensperger et al.*, 2001]. The very broad range of particle sizes makes unbiased sampling and analysis of aerosol properties difficult. Aerosol particles may be divided into three general size ranges: PM_{10} (particles smaller than 10 µm aerodynamic diameter), $PM_{2.5}$ (<2.5 µ m aerodynamic diameter), and $PM_{1.0}$ (<1 µm). The ideal aerosol sampling inlet would draw in 100% of the particles in a specified size range and transport them all without modification to a detector or collector. A broad range of instruments has been developed over the past 10 years to measure aerosol mass concentration in certain size ranges [*Artaxo*, 2002]. The *gravimetric method* is the most common, in which a filter (Teflon, Nuclepore, quartz fiber, nylon, etc.) is exposed to a flow of air loaded with particles from ~1 to 24 hours, after conditioning the aerosol sample in a temperature and humidity controlled environment, and the mass of aerosol deposited onto the filter is weighed using a microbalance. This method provides high accuracy, but is very labor intensive and cannot be done in real time. Sampling artifacts can affect aerosol concentrations in special situations were semi-volatile compounds are present in significant amounts, either increasing the collected aerosol mass or decreasing the mass of already collected aerosol particles. New real time PM_{10}, $PM_{2.5}$ or $PM_{1.0}$ instruments, such as the Tapered Element

Oscillating Microbalance (TEOM) instrument measures the gravimetric mass of the particles with high time resolution (<30 minutes) are now widely used in air pollution monitoring networks. In its original configuration the air had to be heated to 50ºC or more, which resulted in some loss of semi-volatile organic and inorganic compounds. New versions of this instrument correct for the particle losses in real time, and provide gravimetric mass with good accuracy.

Aerosol monitors using beta attenuation (also called beta gauges) are widely used for real time aerosol mass measurements in urban areas, although they can have large errors due to the different beta radiation attenuation coefficients needed for different aerosol elemental composition and size. New instruments derive PM_{10} or $PM_{2.5}$ using light scattering from small lasers, but they requires careful calibration and are prone to errors when aerosol types or size distributions change. Some aerosol samplers, such as the Dichotomous Partisol-Plus (Model 2025 Sequential Air Sampler; *Patashnick et al.*, 2001), collect aerosols in two size ranges: $PM_{2.5}$ and PM_{10} ($2.5<d_p<10$ µm) on two Teflon filters that are suitable for gravimetric, ionic and trace element analysis. Stacked Filter Units (SFU) collect aerosols in the same two size ranges on sequential Nuclepore filters for subsequent gravimetric and elemental analysis [*Hopke et al.*, 1997]. High volume samplers can also be used to collect large amounts of PM_{10} and $PM_{2,5}$ for analysis of various organic and inorganic compounds when large amounts of material is required [*Artaxo*, 2002].

7.1.2 Aerosol Size Distributions and Particle Counting

Measurement of aerosol size distribution for the whole size range (from 1-2 nanometers to several hundred micrometers) requires different approaches and different instruments. Cascade impactors separate particles in several size ranges for subsequent analysis. For example, the MOUDI (Microorifice Uniform Deposit Impactor) cascade impactor acts as a 12-stage impactor when the inlet stage and final filter are included, with the stages having 50% cut-points ranging from 0.056 to 18 µm in aerodynamic diameter [*Marple et al.*, 1991]. New versions, such as nano-MOUDI, can size and collect particles down to 10 nm. Many other types of cascade impactors, such as the Berner impactor, are widely used to collect aerosols. Condensation particle counters (CPC) detects particles optically, allowing them to

grow in a highly supersaturated atmosphere. Particles down to 3 nm can be detected and counted, and very low particle number concentrations can be measured. There are CPCs that use Butanol as the saturator vapor and some new instruments are water-based. However, size distributions measurements are not possible using a CPC alone. Particle number size distributions can be measured with a scanning mobility particle spectrometer (SMPS), which is an adaptation of the differential mobility particle sizer (DMPS). Both methods can measure aerosol size distributions from 3–800 nm with a time resolution of a few minutes. They include a differential mobility analyzer (DMA) to separate particles according to their size and a condensation particle counter (CPC) to count them. Coarse mode particles can be sized optically with the Aerodynamic Particle Sizer (APS) spectrometer or with single particle optical particle counters (OPC). The latter instrument measures the intensity of light scattered by individual particles as they traverse a tightly focused beam of light.

At relative humidity >70–80%, water could comprise a large fraction of the fine particle mass. Water uptake capacity of aerosol particles is critically important in determining the CCN activities and optical properties. The water uptake capacity can be measured with instruments such as the Humidified Tandem Differential Mobility Analyzer (HTDMA), which measures the hygroscopic diameter growth of aerosol particles of 100 nm at different RH [*McMurry and Stolzenburg*, 1989]. The HTDMA works with two DMA working in tandem, where the first selects a particular narrow size range in a dry air flow that is then conditioned to a certain relative humidity, while the second scan the size range to analyze the growth factor of the particles. In general HTDMA can measure growth rates for relative humidity up to 80%, but new methods can measure the growth factor up to 97% relative humidity. These instruments can separate hygroscopic from hydrophobic particles based on their water affinity, a critical property for determining their ability to act as Cloud Condensation Nuclei (CCN).

7.1.3 Individual Particle Analysis

Particles collected on filters can be analyzed by scanning electron microscopy (SEM), to provide size, morphology and elemental composition. Basically, a finely focused high energy electron beam scans the particle and secondary electrons from the

sampled particle are collected to form an image of the particle [*Van Grieken et al.*, 1991]. X-rays emitted by the interaction between the high energy electron beam and the sample are analyzed by a Si(Li) X-ray detector and elemental composition information is obtained [*Artaxo et al.*, 1992]. Scanning electron microscopy can be used to measure particles >0.1 μm in diameter, with a mass detection limit for elements of ~0.5%. The measurement and quantification of the elemental mass is complicated by particle matrix effects. Environmental SEMs allow analysis of particles under low vacuum and different humidity and temperature conditions, thus also allowing the determination of volatile particles. Automated SEM can measure and quantify thousands of particles on a filter in a few hours. Transmission electron microscopy is used to observe particles less than 0.1 μm diameter. Optical microscopy can be used to observe and count large particles (larger than 0.5 μm). Laser Microprobe Mass Analysis (LAMMA) measures organic and inorganic ions by the use of a laser beam to vaporize particles that are then analyzed in a time of flight mass spectrometer. Measurement of the elemental composition of individual particles is a valuable addition to bulk measurements, especially when the effects of aerosols on clouds are of interest, because of the potential to measure the internal versus external mixture of the particles [*Van Grieken et al.*, 1991]. This is because the presence of internally mixed particles, containing some soluble material in them, can change CCN efficiencies in the atmosphere. For example, dust particles that are normally not efficient CCN can become good CCN if some soluble material accumulates on their surfaces [*Levin et al.*, 1996].

7.1.4 Measurements of Optical Properties of Aerosols - Light Absorption and Scattering

Light scattering and absorption is critically important to assess the climatic impacts of aerosols [e.g., *Ogren*, 1995, *Ramanathan et al.*, 2001]. The aerosol single scattering albedo (ω_0) is a critically important aerosol parameter that expresses the ratio between absorption and extinction of radiation and can be derived from simultaneous measurements of scattering and absorption coefficients. To measure light scattering, integrating nephelometers measure the total amount of light scattered by a sample volume of air loaded with particles. Nephelometers of various types are used, some with a single wavelength (generally 500–550 nm), while others use three wavelengths

that can provide useful information on aerosol size distributions and the Angstrom coefficient with high time resolution and sensitivity. Instruments are available that measure both forward and backward scattering coefficients.

Measurements of light absorption are notoriously difficult. Several instruments are available to measure the light absorption coefficient, which is related to the so-called “black carbon" or the incorrectly called "elemental carbon”. The Aethalometer and the Particle Soot Photometer (PSAP) are two widely used instruments that measure aerosol absorption on a filter. New versions, operating at several wavelengths, allow measurement of the absorption coefficient as a function of wavelength. These instruments suffer from multiple scattering processes in the filter substrate, resulting in high uncertainty of the data. The Multi Angle Absorption Photometer (MAAP) uses transmitted as well as scattered light for the quantification of the absorption coefficient, resulting in a more accurate reading [*Petzold and Schönlinner*, 2004]. Absorption coefficients are most commonly determined from measurements of particles collected on filters using integrating spheres or photometers. Photoacoustic spectroscopy measures the absorption coefficients of suspended particles in real time, and can obtain a reliable measurement of aerosol absorption; however, their sensitivity still needs to be improved. Individual light-absorbing particles can also be measured by incandescence [*Baumgardner et al.*, 2004]. Aerosol absorption coefficients can be inferred from measurements of elemental carbon concentrations and mass measurements, using real time elemental carbon measurements that can nominally separate the “organic” from the “elemental” carbon component using a temperature profile. The method is problematic because it is difficult to distinguish unambiguously between elemental, black or organic carbon based only on the temperature profile, because the elemental composition affects this separation. Commercially available quasi-real time organic and elemental carbon monitors are available, but the methods are far from being widely accepted, and intercomparison between measurements is problematic. This area requires important advances in terms of measurement methods and instrumentation.

7.1.5 Elemental Composition of Aerosol Particles

A variety of techniques are used for the determination of chemical composition of bulk or size-segregated samples. In particular aerosol source apportionment methods uses the elemental composition information to infer and quantify aerosol sources [*Artaxo*, 2002]. The use of factor analysis and chemical mass balance methods requires the knowledge of the elemental composition of aerosols with as much detail as possible [*Artaxo et al.*, 1999]. X-Ray Fluorescence (XRF) uses an X-ray beam to provide information on aerosol elemental composition. The newest instruments use polarized X-rays for excellent detection limits. Detection of light elements ($Z<20$) requires analysis in vacuum. About 15-20 elements can be routinely measured by XRF in a non-destructive analysis lasting about 5 minutes. Synchrotron radiation sources provide the best detection limits, but are a rather expensive analysis [*Bukowiecki et al.*, 2005]. Particle induced X-ray emission (PIXE) uses a beam of protons with energy between 2 and 3 MeV and X-ray spectrometry to measure routinely the concentration of trace elements such as Na, Mg, Al, Si, P, S, Cl, K, Ca, Ti, V, Cr, Mn, Fe, Ni, Cu, Zn, Ga, Sr, Pb, As, Se, Br, Zr, Rb, and others [*Artaxo et al.*, 1993]. The detection limits are ~0.1–10 ppm or a few ng/m³. For optimum results using PIXE analysis, samples should be collected on the thinnest possible backing materials composed exclusively from low atomic number elements, such as carbon, hydrogen, oxygen or nitrogen. Polycarbonate Track Etched (PCTE) and Teflon filters are often used, as are impaction surfaces such as Kapton and Mylar [*Johansson and Campbell*, 1988]. Blank values should be carefully taken into account for reliable measurements of trace elements.

Multi-element analysis by means of inductively coupled plasma-mass spectrometry (ICP-MS) provides excellent detection limits, in the range of parts per trillion (ppt). The aerosol sample is extracted from filters and mixed with water and nitric acid and is injected into the plasma torch via a nebulizer. The dissociated elements are detected by mass spectrometry for a very fast and precise quantitative determination. In INAA (Instrumental Neutron Activation Analysis) spectrometry a flux of neutrons in a nuclear reactor is used to produce unstable nuclei and gamma-ray spectrometry to measure trace elements with high accuracy and very low detection limits. Ion chromatography (IC) is commonly used to measure nitrate, sulfate and a broad range

of ionic compounds, including organic components. Ion chromatography has also recently been adapted for semi-continuous measurements of particulate and gaseous species on commercial instruments. Detection limits and precision are excellent, but calibration and blank control must be followed closely.

Real time sulfate and nitrate measurements are now possible with commercial instruments. Flame photometric detectors (FPD) measure sulfates by detecting 394 nm light produced by excited-state S_2 molecules formed when sulfur compounds are burned in a hydrogen-rich flame. A few minutes time resolution is possible, with 1 $\mu g/m^3$ detection limit for sulfate. Particulate nitrate concentrations can be measured with a single stage impactor that is 95% efficient for particles >0.1 µm aerodynamic diameter and the collected particles are analyzed by flash vaporization using a chemilluminescent NO_x analyzer.

7.1.6 Real-Time Aerosol Mass Spectrometry

Recently a number of different approaches have been developed to measured aerosol composition in real time, either in single particles or bulk composition (see review by *Sullivan and Prather*, 2005). Particle analysis by laser mass spectrometry (PALMS and similar instruments) makes it possible to determine the ionic compositions of single particles [e.g. *Prather et al.*, 1994, *Hinz et al.*, 1996, *Noble and Prather*, 2000, *Schneider et al.*, 2004]. Aerosol particles are drawn by vacuum into the instrument. A fraction of these particles are detected by a visible light laser (532 nm), the scattered light from which triggers an excimer laser (193 nm) that ablates and ionizes individual particles. A complete positive or negative mass spectrum is obtained on particles by using a time-of-flight mass spectrometer. A different approach to mass spectrometry was adopted in the Aerodyne Aerosol Mass Spectrometer (AMS) which measures properties of an ensemble of particles. The AMS electron impact ionization (EI) and quadrupole mass spectrometry (QMS) applies thermal desorption for aerosol characterization. The AMS consists of three main parts: an aerosol inlet, a particle sizing chamber, and a particle composition detection section. The different sections are separated by small apertures and are differentially pumped. The aerosols are sampled through an inlet that focuses them into a narrow beam. Size-dependent particle velocities created by expansion into vacuum are used to determine particle

size through a particle time-of-flight measurement. The focused particle beam is modulated by a rotating wheel chopper. Time-resolved particle detection, after a known flight distance, gives the particle velocity from which the particle aerodynamic diameter is obtained. Detection is performed by directing the particle beam onto a resistively heated, roughened surface under high vacuum (~10^{-7} Torr). Upon impact, the volatile and semi-volatile components in/on the particles flash vaporize. The vaporization source is integrally coupled to an electron impact ionizer at the entrance of a quadrupole mass spectrometer. When the quadrupole is tuned to a representative mass, bursts of ions are produced that are averaged to give a size-resolved mass distribution [e.g., *Jayne et al.*, 2000, *Jimenez et al.*, 2003].

7.1.7 The Counterflow Virtual Impactor (CVI)

The counterflow virtual impactor (CVI) has been utilized both in aircraft experiments and on the ground to study aerosol/cloud interactions, cloud physics, and cloud impacts on climate [*Ogren et al.*, 1985; *Noone et al.*, 1988]. The CVI separates interstitial aerosol particles from cloud or ice droplets. At the CVI inlet tip, cloud droplets or ice crystals larger than a minimum aerodynamic diameter are separated from the smaller interstitial aerosol and impacted into a dry carrier gas. This separation is possible via a counterflow stream of nitrogen out the CVI tip, which assures that only larger particles (cloud droplets or ice crystals) are sampled. The non-volatile residual nuclei remaining after droplet evaporation and water vapor are sampled downstream of the inlet with selected instruments. These may include a condensation particle counter, an optical particle counter, and various chemical techniques.

7.1.8 Cloud Condensation Nucleus Measurements

A fraction of the particles in the atmosphere can serve as cloud condensation nuclei (CCN) for cloud droplet formation. The fraction depends on the size, composition and surface properties of the particles, and on the water supersaturation of the air [*Roberts and Nenes*, 2005]. CCN are linked to cloud microstructures and precipitation formation although this last link in the chain is still under discussion and is the main aim of this assessment. In addition, the role of the CCN in climate feedback remains largely unknown. Measurements of CCN are very challenging [e.g., *Twomey*, 1963]

because they depend on supersaturation which is a function of both size and chemical composition, although recent measurements in Germany by *Dusek et al.* [2006] show that size is the most important parameter in determining CCN efficiency. Significant improvements in measurement techniques are needed in this area, and even basic concepts needs improvements.

A few instruments are available for measuring the CCN number concentration (or *activation spectrum*), including those based on the static thermal gradient diffusion cloud chamber (SDCC), continuous flows spectrometers (CFC), and other principles [*Nenes et al.*, 2001]. The SDCC consists of two parallel plates, held at different temperatures with their facing surfaces wetted; the lower plate being several degrees colder than the upper plate. By varying the temperature difference between the plates, it is possible to produce maximum supersaturations in the chamber that range from a few tenths of 1% to a few percent, which are similar to the inferred supersaturations that activate droplets in clouds [*Wieland*, 1956]. Small water droplets form on those particles that act as CCN at the peak supersaturation in the chamber. The concentration of these droplets can be determined by photographing a known volume of the chamber and counting the number of droplets visible in the photograph, or by measuring the intensity of light scattered from the droplets [*Radke and Hobbs*, 1969]. By repeating the above procedure with different temperature gradients in the chamber, the CCN activation as a function of supersaturation can be determined. Figure 7-1 shows the CCN Spectra for different types of aerosol particles in Amazonia, expressed as CCN efficiency defined as the ratio of

CCN to CN (condensation nuclei) the total particles. Green ocean measurements (see Chapter 5 for more details) refer to natural biogenic conditions during the wet season. Most of the CCN are biogenic particles in the wet season in Amazonia. Fresh and aged smoke refers to conditions during heavy biomass burning emissions.

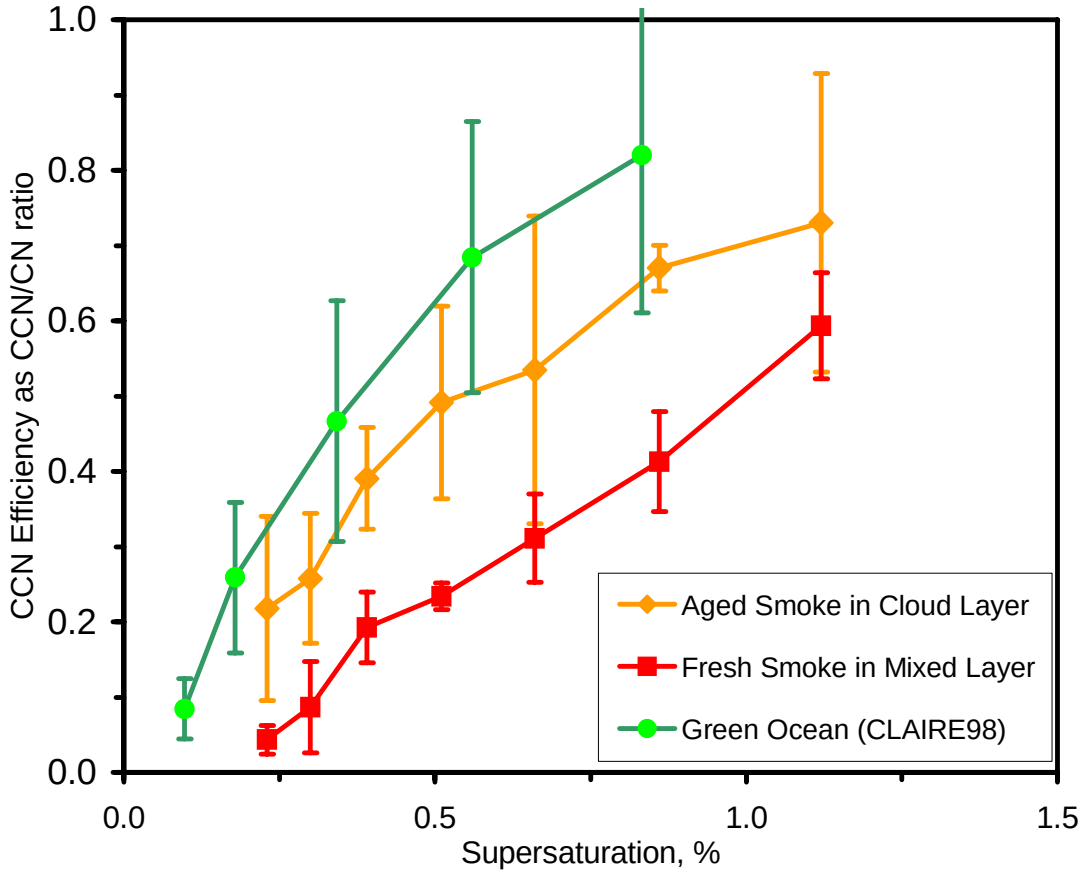

Figure 7-1. *CCN Spectra for different types of aerosol particles in Amazonia. Green ocean measurements refer to natural biogenic conditions during the wet season. Most of the CCN are biogenic particles in the wet season in Amazonia. Fresh and aged smoke refers to conditions during heavy biomass burning emissions.*

Recently, a commercially available cylindrical continuous flow thermal gradient diffusion chamber has been built [*Roberts and Nenes*, 2005] employing a novel technique of generating a supersaturation: by establishing a constant streamwise temperature gradient so that the difference in water vapor and thermal diffusivity yields a quasi-uniform centerline supersaturation. The droplet spectrum at the outlet of the growth column is detected using a standard optical particle counter (OPC). This design allows for atmospheric CCN measurements with high time resolution for

supersaturations in the range from ~0.07-3% achieved by varying the flow rates and temperature gradient along the growth column.

In the dynamic CCN spectrometer, the aerosol sample is exposed to a varying supersaturation field and the CCN spectra is obtained by analyzing the outlet droplet size distribution. Time resolution for CCN spectrometers can vary from 1–30 s. Although these two types of counters provide some measure of the CCN concentrations and their dependence on supersaturation, they both suffer from deficiencies, among which is the inability to correctly measure giant CCN. These particles fall out in the chambers before they can be measured. Although these particles are generally present in small concentrations, their effect on cloud droplet spectra can be critical.

Giant CCN (GCCN) is wettable particles greater than about 5 μm in diameter that can initiate collision and coalescence in a very efficient way and thus efficiently produce precipitation embryos. Due to their large size, and low statistics, it is difficult to measure GCCN. Giant aerosol particles can be measured with relatively low efficiency from aircraft by optical scattering sensors (PMS FSSP, PCASP) in the size range up to about 25 micrometers, because their sample volumes are very small (about 1 m^3 in 12h of flight). Since typical concentrations of these particles are a few hundreds per cubic meter, the sampling statistics by these probes is poor. Another method of sampling GCCN is to sample air by an inlet tube into an aircraft using a low turbulence intake [*Hubert et al.*, 2000]. This approach is good for particles up to 7 μm in diameter so many ultra-giant particles are not sampled. A third method of sampling GCCN is to sample them by impaction on a glass slide. With slide sample areas of 1 cm^2, 1 m^3 of air can be sampled in 1-2minutes of aircraft time [*Levin et al.*, 2005]. The disadvantage of this approach is that tedious, labor intensive microscopic analysis of each slide. However, new methods that use computer-controlled counting systems can automatically size the particles. It is also possible to set up the system in a humidity-controlled environment which will permit dry particle sensing as well as allow growth of hygroscopic particles.

7.1.9 Ice Nucleus Measurements

A significant fraction of supercooled clouds contain ice crystals, while some clouds (e.g., cirrus) are generally completely glaciated. The presence of ice in clouds is very important for the development of precipitation; it is also an important component of the aerosol indirect effect on climate. At temperatures warmer than about -40C, ice can form by heterogeneous nucleation on particles called *ice nuclei* (IN) (see Chapters 4 and 5). For clouds with temperatures below about –40ºC, ice can form both by heterogeneous nucleation on insoluble particles and by homogeneous (spontaneous) nucleation. In spite of the importance of IN in clouds, there is a great deal of uncertainty in measurements of their concentrations and even in their characterization. Heterogeneous ice nucleation can take place via a number of processes (see Chapter 4): *immersion freezing*, *contact*, *condensation-freezing* and *deposition*. In many of the instruments that measure IN activity or spectrum, ice may be formed by one or more of these processes, some of which depend on the supersaturation of the air as well as on temperature, without being able to differentiate between them. For example, in expansion chambers cooling is produced by compressing the air and then suddenly expanding it. In case of mixing chambers cooling is produced by refrigeration. Moist air is then introduced into a cloud but the amount of supersaturation is not well controlled.

The traditional way of measuring IN activity is to collect aerosols from air samples of about 300 liter on Nuclepore filters. The filters are then inserted into an IN chamber made up of two parallel plates held at different temperatures below the 0^0 C. Supersaturation with respect to ice is reached just above the sample. The concentration of ice crystals formed at each temperature is recorded through a downward looking microscope or a video camera. The number of crystals detected as a function of temperature is then plotted and a best fit curve is obtained [e.g., *Gagin*, 1975].

Another method measuring the IN activity spectrum is via drop freezing measurements. This uses an insulated chamber, the lower horizontal plate of which is temperature controlled. Aerosol samples collected on a filter and washed into a beaker with a known quantity of water. About 100 drops from this water are placed on the

cold stage. The number of drops that freeze at each temperature as the plate is cooled down, is recorded. Knowing the volume of air sampled and the amount of water used in the washing process, a qualitative estimate of immersion freezing spectra can be obtained [e.g., *Vali*, 1971]. A more recent development is the continuous-flow diffusion chamber (CFDC), which measures ice nucleation by aerosol particles under defined temperature (between -5^0 and –80ºC) and humidity conditions [*Rogers et al.*, 2001]. The instrument focuses on an aerosol particle stream in the central portion (approximately 10% of volume) of a vertically downward-oriented laminar flow between two ice-coated cylindrical walls held at different temperatures. The inter-wall temperature gradient and vapor field expose the aerosol stream to constant temperature and relative humidity conditions for a period (5–7 s), enough to initiate ice nucleation and growth to occur. A hydrophobic material replaces ice on the warmer wall in the lower one third of the CFDC, which helps to evaporate liquid particles, including cloud droplets, leaving the ice crystals to pass through. The ice crystals that grow in the CFDC are detected and counted optically. By changing the supersaturation conditions, different modes of ice nucleation (e.g., deposition, condensation-freezing, immersion- freezing and homogeneous-freezing) can be detected [*DeMott et al.*, 2003]. It should be noted that none of these techniques simulate contact nucleation since the droplets must remain in the chamber for a long enough time to scavenge the aerosol particles acting as IN. A few prototype devices have been built to simulate contact nucleation [*Meyers et al.*, 1992] but none have been implemented for field measurements.

7.2 AIRBORNE INSTRUMENTATION FOR CHARACTERIZING AEROSOLS AND CLOUDS

7.2.1 Introduction

In situ measurements of aerosol vertical profiles necessitate the use of airborne platforms with instrumentation suitable to fast and accurate analysis. Isokinetic inlets are required when using airplanes to correctly represent the natural conditions in still atmosphere, isokinetic inlets are required. The adequacy of the inlet and the necessary high time resolution make measurements of aerosol from aircraft particularly challenging. Aircraft used for atmospheric measurements typically fly at speeds from ~40–200 m s^{-1}, while the flow speed through filter samplers or aerosol counting/sizing

instrumentation is typically less than 3 m s^{-1}. Variations in pitch, roll and yaw, together with turbulence generated at high aircraft speeds, make the conditions for isokinetic sampling very difficult and with large associated uncertainties, especially for sampling of particles >0.5 μm [*Huebert et al.*, 1990].

Instruments capable of conducting real time measurements with time resolution better than a few minutes are desirable. In addition, many airplanes are pressurized and sampling of aerosols inside the cabin requires special care to prevent cabin air from contaminating the samples. In spite of these constrains, a large number of airborne campaigns have obtained critically important data on atmospheric aerosol. Aerosol mass spectrometers, nephelometers, CPCs (Condensation Particle Counters), SMPS (Scanning Mobility Particle Sizer), DMPS (Differential Mobility Particle Sizer), OPCs (Optical Particle Counter), and high time resolution instruments have provided critically important information in recent experiments. Bulk aerosol composition is still a challenge in aerosol aircraft measurements, since large samples require high volume pumping over long time periods, something that is not always feasible aboard aircraft. The aerosols samples collected on board the airplane are then analyzed by one of the techniques mentioned in Section 7.1.

Distortion of airflow caused by the aircraft itself can enhance or deplete certain sizes of particles, generating errors that may be larger than those inherent in the measurement sensor itself [*King*, 1984; *Twohy and Rogers*, 1993]. However, instruments located on aircraft wings can measure particle size distributions in real time. The PMS FSSP-100 (for measuring particles 0.3 to 47 μm aerodynamic diameter) and the PMS-PCASP-100 (for 0.15 to 3 μm) are examples of such instruments. Cloud droplets and ice particles can also be collected, counted, sized and identified using airborne platforms.

7.2.2 Cloud Physics Aircraft Instrumentation

A set of excellent aerosol and cloud droplets probes were developed using small lasers and photo detector arrays. Particle Measuring Systems (PMS), have manufactured a large fraction of the instruments based on single droplet light scattering and linear array cloud particle shadow imaging [*Knollenberg*, 1981]. These

instruments came to dominate airborne cloud microphysics observations for more than two decades. However, these instruments are no longer manufactured by, or supported by PMS. The major instruments developed and still used today are the PMS PCASP-100X (Aerosol sizes 0.1 - 3.0 μm), PMS FSSP-100 (Cloud particle sizes 2 – 47 μm) , PMS OAP-2D2-C (Cloud and drizzle particle sizes 25 – 800 μm) and the PMS OAP-2D2-P (Precipitation particle sizes 200 – 6400 μm).

New products from Particle Droplet Measurement Technologies (DMT) such as the Cloud Droplet Probe (CDP) measures the light scattered when a particle passes through a laser beam. The CDP can measure cloud particles in the range of 1–50μm. The Cloud and Aerosol Spectrometer (CAS) provides a large number of particle measurements, including cloud droplet and particle aerosol (0.5μm to 1μm) diameters. The **CAS** instrument relies on particle light scattering to determine particle size. A major feature of this new probe is the addition of the backscatter block to measure the scattered light in the backwards direction. For spherical particles, this allows determination of the real component of a particle's refractive index. It also makes use of the fact that aspherical particles scatter significantly more light in the backward direction than do spherical particles, while near-forward scattered light is less affected. The ability to discriminate between spherical and non-spherical cloud particles can be particularly useful in mixed phase clouds. *Cober et al.* [2001] have shown that simple light scattering instruments like the FSSP can be subject to complex errors in mixed phase clouds. Consequently, a signal indicating the presence of spherical particles is very useful.

7.2.3 Liquid water meters

Cloud liquid water is a very fundamental property of clouds. It can be measured in flight by the Johnson and Williams (JW) and King liquid water probes. The DMT Liquid Water Content Sensor (LWC-100) is a strut-mounted sensor. The temperature of the sensor is maintained via a digitally controlled variable-duty-cycle current pulse. Operationally the more liquid water present, the greater the current required to maintain the fixed 125ºC temperature. Liquid water content at 100Hz is then determined as a function of current through the probe and the true air speed. The range of measurements is 0–3 g m^{-3} at 5–50μm droplet diameter. This instrument has

been at least partially eclipsed by the very fast responding and versatile Gerber Scientific optical cloud water sensor (the Particulate Volume Monitor PVM-100). The Gerber et al. (1994) PVM-100 is an optical cloud microphysics probe designed to characterize the liquid water content (LWC), droplet surface area (PSA), and droplet effective radius (Re) of the smallest droplets in a cloud. The PVM makes these measurements optically on a cloud volume of ~10 cm^{-3}, such that the measurements are independent of air speed. The accuracy of the PVM is estimated to be better than 10% for droplet spectra with volume medium diameter (VMD) smaller than 30 μm, with a precision on the order of 0.002 g m^{-3} [*Gerber et al.*, 1996].

7.2.4 Cloud Particle Shapes

Some instruments can measure cloud particle shape in real time, and these instruments are called 2D probes. The cloud particles enter a sensitive volume where they occult a laser beam casting a shadow on a photodiode array. Because the size range of cloud particles is several orders of magnitude, and the size of the arrays in the early 1980's was rather small, several 2D instruments had to be flown to sample the full range of cloud particles likely present in precipitating clouds. These digital images provided a substantial quantitative advance, especially as recognition analysis allowed separation of the images by crystal habit and particle dimensions. However, the limited number of pixels in the array detector limited the resolution of these devices. It was not always possible to decide whether the imaged particle was liquid or frozen. The cloud imaging probe (CIP from DMT) is a new design based on older optical imaging probes. Improvements include a solid-state diode laser, on-board pitot tube, an on-board Digital Signal Processor, and a synchronous RS-422 data channel providing statistics and compression of image data. The Stratton Park Engineering Company (SPEC) Cloud Particle Imager (CPI) produces digital, near photographic quality, images of the cloud particle at aircraft speeds.

7.2.5 Conclusions

There are important weakness and technical difficulties in measuring aerosols and cloud properties in airborne platforms. Despite attempts at instrument de-icing, this can still be a problem in supercooled clouds even light icing will distort the sample flow, resulting in particle size sorting and shadowing. Additionally, several

droplet instruments have significant "dead time" after a particle is observed, before it is ready to measure the next particles. At high droplet concentrations this can result in significant errors. Light scattering instruments are calibrated with spherical non-absorbing particles. Hence, the calibration is not strictly valid for absorbing and non-spherical particles. The airflow surrounding any instrument attached to the exterior surfaces of an aircraft will be changed as the aircraft maneuvers. Therefore, mounting locations should be selected to minimize these effects.

Despite satisfaction with recent instrument developments, our routing toward the next generation of airborne instruments remains uncertain. However, we must now consider measuring clouds ranging from the local to the global scale. For example, on the smallest scales the interplay between aerosols, water vapor supersaturation, and condensation on CCN, turbulence, coalescence, electrical charge separation and the production of precipitation remains observationally shrouded. To address such complex systems it will be necessary to observe down to the inter-droplet spacing. While in cloud measurements of temperature and humidity using radiation transfer and tunable diode laser technology show promise, much more work is needed in this arena. Tomorrow's instrumented research aircraft will need, in addition, to *in situ* instruments a compliment of remote sensing tools that permit a 3-D perspective of cloud structures and motions. Elegant microwave imager's, such as NCAR's ELDORA Doppler radar, proportioned to much shorter wavelengths, is a powerfully research tool. Such miniaturized 3-D imagers can then be used in real time to depict the optimal locations to employ *in situ* observing tools. Characterizing the 3-D nature of clouds is particularly critical in radiation transfer calculations [e.g., *Kasyanov*, 1999].

7.3 SURFACE-BASED REMOTE SENSING OF AEROSOLS AND CLOUDS

7.3.1 Measurement of Aerosol Optical Depth

Aerosol optical depth (AOD) is a quantitative measure of the extinction of solar radiation by aerosol scattering and absorption between the point of observation and the top of the atmosphere. It is a measure of the integrated columnar aerosol load and an important parameter for evaluating direct radiative forcing. AOD can be determined from the ground through measurements of the spectral transmission of solar radiation through the atmosphere using rather simple and relatively inexpensive

instruments pointed directly at the sun called sun photometers or filter radiometers. Routine ground-based AOD observations are of utmost importance for the calibration and validation of AOD retrievals from satellites. In addition, they are necessary to correct for aerosol effects in the retrieval of other satellite products. The Ångström exponent, which gives an indication of the column integrated aerosol size distribution, can be derived from simultaneous AOD measurements at several wavelengths.

AOD is not directly measured, but is retrieved from observations of atmospheric spectral transmission. The solar irradiance I at a given wavelength can be expressed as $I=I_0 \exp(-m\tau)$ with I_0 the extraterrestrial (top-of-the-atmosphere) irradiance of the sun, m the air mass and τ the total optical depth. The air mass equals 1 for a vertical path and is roughly proportional to $1/\cos z$ with z the zenith angle of the sun during the observation. The total optical depth τ at a given wavelength is composed of several components such as scattering by gas molecules, τ_R (Rayleigh scattering), extinction by aerosol particles, τ_A, absorption of trace gases, τ_G, like ozone, and possible cloud contamination. Thus, the AOD can be obtained from the total optical depth by subtracting modeled estimates of the other components $\tau_A=\tau-\tau_R-\tau_G$. Because AOD is essentially a difference between two larger numbers, it is very sensitive to small calibration errors and to a minor degree also to the methods chosen to model the other components [*WMO* 2003].

The current state of long-term observational networks for AOD was reviewed by a group of international experts gathered at a meeting in Davos, Switzerland in March 2004 [*WMO*, 2005]. There are a number of international and national networks that have a continuous record of AOD measurements. The international networks are AERONET (including AEROCAN, PHOTONS, AEROSIBNET), BSRN, GAW-PFR, and SKYNET. The national networks include Australia (Bureau of Meteorology), China, Finland (Finnish Meteorological Institute), Germany (DWD, the German Weather Service), Japan (JMA), Netherlands (KNMI, including Surinam), Russia (Sibrad), and USA (networks including ARM, SURFRAD, CMDL, USDA). Figure 7-2 presents the Global AOD network of long-term sites. These comprise 90 stations with a continuous record for the past 4 years and temporal data coverage of 50% (this should not be confused with the fact that in any given year many more stations may be operating if short term campaign observations are taken

into account. For instance, AERONET reported 110 stations operating during 50% of 2003). Half of the stations fall within the AERONET project, while the other half is maintained mainly by WMO Members and SKYNET. Hemispheric coverage corresponds roughly to the landmass distribution, (⅓SH, ⅔NH), with Australia, Europe and North America accounting for more than 50% of stations. Major gaps exist in Africa, India, Latin America and the Polar Regions.

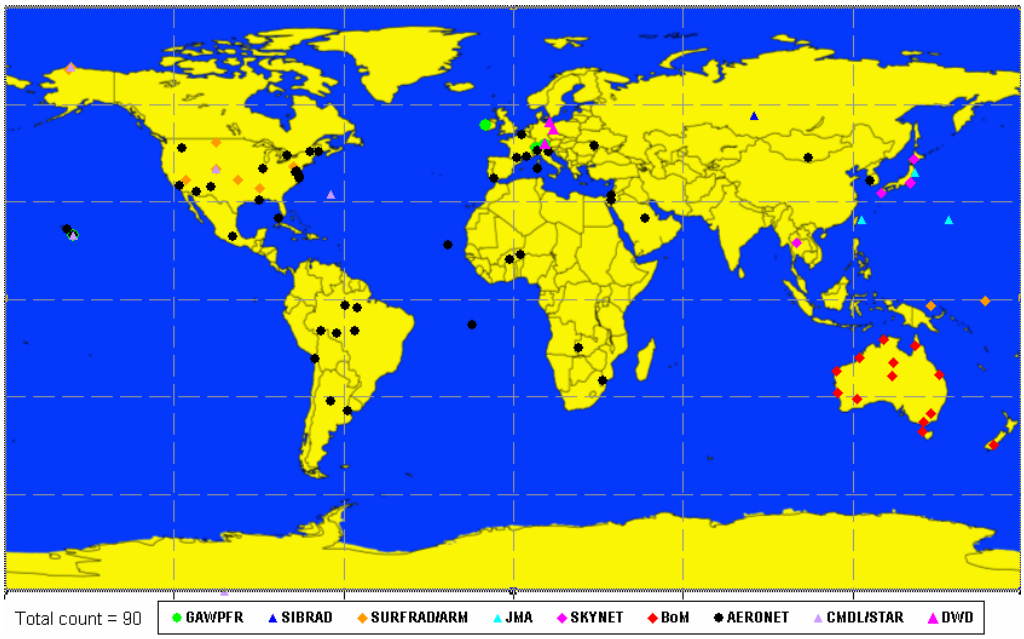

Figure 7-2. *Global AOD network of long-term sites, i.e., with a continuous record for the past 4 years and temporal data coverage of more than 50%.*

The AERONET and the GAW-PFR network play a special role, as AERONET is by far the largest network, and the GAW-PFR network was assigned a special role in the harmonization of worldwide AOD data during the AOD workshop in Davos [*WMO*, 2005], in the process of forming a federation of diverse networks, coordinated under the WMO/GAW umbrella. These two networks will therefore be described in some more detail below.

7.3.1.1. The AERONET Network for Monitoring Aerosol and Cloud Properties

The AERONET network of ~200 well calibrated sunphotometers and sky radiance radiometers distributed around the world [*Holben et al.*, 1998, 2001], measures the aerosol optical properties in key locations that are representative of a

wide diversity of aerosol conditions. Both direct sun and diffuse sky directional radiance measurements taken throughout the daylight hours are utilized to characterize total column integrated aerosol optical properties. The spectral aerosol optical depths are measured from 340 to 1020 nm in 7 wavelengths for the standard CIMEL sun/sky radiometer and also to 1640 nm in the extended wavelength CIMELs. Additionally, radiatively effective column integrated size distributions, complex refractive indices, and single scattering albedo are retrieved from these measurements [*Dubovik et al.*, 2002]. The AERONET spectral aerosol optical depth (AOD) measurements are highly accurate (~0.015 uncertainty; *Eck et al.*, 1999) and are used to validate satellite retrievals of AOD from all the current satellite sensor systems, including MODIS, TOMS, SeaWiFS, MISR, and AVHRR [*Remer et al.*, 2002a; *Chu et al.*, 2002; *Hsu et al.*, 2002*; Diner et al.*, 2002; *Torres et al.*, 2002, *Zhou et al.*, 2002]. In addition to validation, the aerosol size distributions and single scattering albedo retrievals from AERONET are utilized in algorithm development for some of these sensors, such as MODIS and TOMS [*Remer et al.*, 2002b].

The CIMEL sky radiance almucantar measurements at 440, 675, 870, and 1020 nm in conjunction with the direct sun measured τ_a at these same wavelengths are used to retrieve aerosol size distributions following the methodology of *Dubovik and King* [2000]. Almucantar sky radiance measurements are made at optical airmasses of 4, 3, and 2 in the morning and afternoon, and once per hour in between. The option of either spherical or spheroid particle shape may be assumed in the retrievals, depending on whether coarse mode dust aerosol is present in the aerosol mixtures [*Dubovik et al.*, 2002]. Sensitivity studies performed by *Dubovik et al.* [2000] were used to analyze the perturbations of the inversion resulting from random errors, possible instrument offsets and known uncertainties in the atmospheric radiation model. Simultaneous retrievals of aerosol single scattering albedo are also made with this algorithm and the sensitivity analysis shows that these retrievals have an uncertainty of ~0.03 for both desert dust and biomass burning aerosols when $\tau_{a440} \geq 0.5$ [*Dubovik et al.*, 2000].

The use of the AERONET network of ground-based radiometers to obtain average size distribution integrated over the whole atmosphere has been proven to be highly

effective. Figure 7-3 taken from *Dubovik et al*. [2002] is an example of the averaged optical properties of different types of tropospheric aerosol. Urban/industrial, biomass burning and desert dust aerosols are shown for $t_{ext}(440) = 0.7$. Oceanic aerosol is shown for $t_{ext}(440) = 0.15$ since oceanic background aerosol loading does not often exceed 0.15. The figure shows the single scattering albedo (top), the size distribution (bottom) and values of the real refractive index (n) and the Angstrom exponent (a), estimated using optical thickness at two wavelengths 440 and 870 nm.

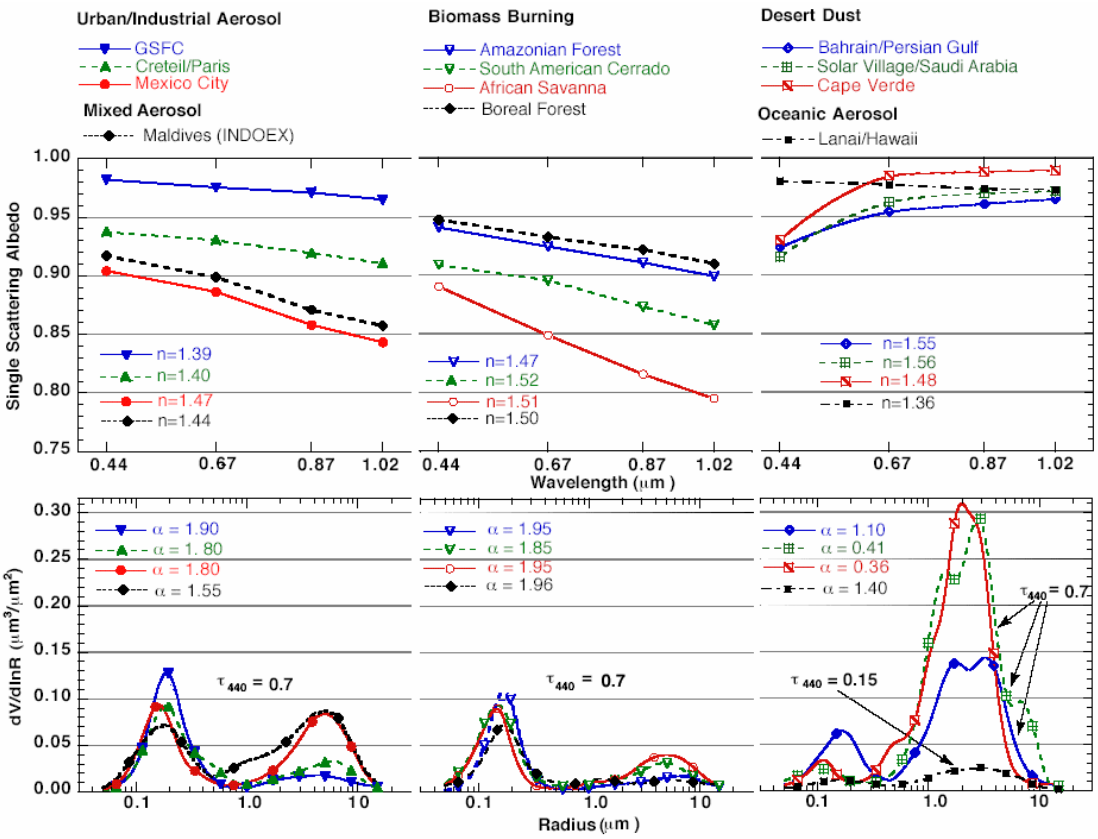

Figure 7-3. *The averaged optical properties of different types of tropospheric aerosol retrieved from the worldwide- multi-year AERONET network of ground-based radiometers. Urban/industrial, biomass burning and desert dust aerosols are shown for $t_{ext}(440) = 0.7$. Oceanic aerosol is shown for $t_{ext}(440) = 0.15$ since oceanic background aerosol loading does not often exceed 0.15. The figure shows the single scattering albedo (top), the size distribution (bottom) and values of the real refractive index (n) and the ¸Angstrom exponent (a), estimated using optical thickness at two wavelengths 440 and 870 nm. After Dubovik et al., [2002].*

The aerosol size distributions from all of the biomass burning sites are dominated by accumulation mode particles, however the sub-micron particle size is somewhat smaller in the savanna and cerrado sites due perhaps to the phase of combustion, but

also possibly due to differences in aerosol aging, fire intensity, and ambient relative humidity and temperature.

AERONET's distribution across the globe with standardized instrumentation and processing algorithms provides similar characterizations, aerosol climatologies and aerosol models for marine, urban/industrial, aeolian dust, biogenic, arctic and mixtures of these aerosol types. Current polarization observation capabilities along with non-spherical modeling of scattering, show great progress for more universal characterization of aerosols. AERONET data co-located with other web-based data sets such as back trajectories, lidar profiles, satellite and chemical transport and global climate models facilitates synergism to address issues of radiative forcing, public health and long term environmental impacts.

7.3.1.2. The GAW Precision Filter Radiometer (PFR) Network

A new generation of sunphotometers called 'Precision Filter Radiometers' (PFR) was designed at the World Optical Depth Research and Calibration Center (WORCC) in Davos with emphasis on instrumental stability and ruggedness in field use. A series of 34 instruments were built by PMOD/WRC for deployment in the trial network and for use as traveling standards. The remaining instruments were sold to different research groups and national weather services; PFR instruments are now in operation at 19 stations ranging from the tropics to beyond the polar circle and from sea level to sites above 3,500 m. The PFR instrument is presently not available commercially. Measurements are taken continuously at 1-minute intervals during 1.5 seconds and stored locally, together with simultaneous readings of the atmospheric pressure, for later retrieval to a personal computer via a serial link. Level-2 files are produced at the stations by standardized software, which extracts measurements from data logger files (Level-1) and combines them with meta data from a station parameter file. These Level-2 files are self-contained ASCII datasets, suitable for further evaluation into AOD results or Langley calibration runs either at the stations or at a centralized data center. During the trial phase, data are transmitted monthly to WORCC for evaluation, quality control and archiving. Instantaneous values of multi spectral AOD are calculated using exoatmospheric calibration coefficients and individual air masses for Rayleigh scattering, ozone absorption and aerosol

components. Ångström exponents α are calculated by log-log regression of AOD from 368 to 862nm.

In the GAW-PFR network, a new calibration method was tested as a possible alternative to classic Langley extrapolations at high altitude stations. A reference instrument has obtained its exoatmospheric values in October 1998 during a stratospheric balloon flight at 40km height, and its radiometric stability has been monitored since then by repeated spectral comparisons with a silicon trap detector that is traceable to the Physikalisch-Technische Bundesanstalt in Berlin [*Wehrli*, 2000]. Additional reference instruments were calibrated by Langley extrapolations at Jungfraujoch and Mauna Loa. All field PFR radiometers are calibrated at WORCC by comparison with 1 or 2 reference instruments before deployment in the trial network. In-situ Langley calibrations are routinely made at the high altitude or arid sites; for other sites, parallel measurements with a traveling standard, exchange of instruments or re-calibration at Davos were used.

GAW-PFR stations are co-located with other networks at several sites. A first comparison during 2000 at Mauna Loa with AERONET individual AOD results showed excellent agreement within 0.005 OD. In 2001, the PFR at Bratt's Lake participated in a 3-month, multi-network comparison [*McArthur et al.*, 2003] where average differences smaller than 0.01 OD per observation were found for direct-pointing instruments at most wavelengths.

7.3.2. Aerosol vertical profiles retrieved by Lidar

Lidars are useful tools for measuring vertical profiles of aerosols. There are various lidar techniques for measuring aerosols, air pollutants, water vapor, temperature, wind velocity, etc. The lidar methods used for aerosol observations are Mie-scattering lidar, Raman lidar, and high-spectral resolution lidar (HSRL). Mie scattering lidar is the simplest lidar technique, which detects elastic backscattering from aerosols. Mie lidars, however, have limitation in quantitative measurement because the lidar equation cannot be solved without an assumption on aerosol optical characteristics or some additional constraint such as independent optical depth measurement, for example, with a sunphotometer. Usually, the lidar equation is

solved with an assumption on the extinction-to-backscatter ratio, or lidar ratio (or S1). An additional feature of Mie scattering lidar is the depolarization ratio measurement, which detects polarization components parallel and perpendicular to the polarization direction of the transmitted laser. The depolarization ratio is a good index of non-sphericity of the scatterers. It is useful for detecting mineral dust particles and distinguishing water and ice clouds. Mie lidar measurements at multiple wavelengths also provide useful information for characterizing (or classifying types of) aerosols.

Raman lidars and HSRL can measure extinction coefficient and backscattering coefficients independently. Consequently, the profile of the lidar ratio is also obtained with these methods. Raman lidars for aerosol measurements utilize Raman scattering of atmospheric molecules such as nitrogen. Because the profile of atmospheric molecules is known from radiosonde observations and models, the extinction coefficient profile of aerosols is derived from the Raman scattering signals. Using the Mie-scattering signals simultaneously measured with the Raman signals, the backscattering coefficient is also determined [*Whiteman et al.*, 2003]. Raman lidars can be extended for multi-wavelength measurements and for water vapor profile measurement. It is also possible to have rotational Raman channels for measuring temperature profiles. A weak point of Raman lidar method is the low sensitivity. Raman lidars, generally, require larger laser pulse energy and larger telescope size. HSRLs use a similar method but utilize Rayleigh scattering of atmospheric molecules [*Liu et al.*, 1999]. HSRLs have a higher sensitivity, because Rayleigh scattering cross sections of molecules are much larger than Raman scattering cross section. HSRLs are technically more difficult, because they need very high-resolution filters for separating spectra of Mie scattering and Rayleigh scattering.

Networks of ground-based lidars are effective for observing three-dimensional distribution of aerosols and their optical characteristics. Currently, several lidar networks are operated in the world, which are described shortly in the following (see Chapter 3 for more details). The Micro-Pulse Lidar Network (MPLNET) operated by NASA is the network of the micro-pulse lidar (MPL) co-located with the sun/sky photometer sites in the NASA Aerosol Robotic Network (AERONET). MPL is a single-wavelength (523 nm) eye-safe lidar capable of unattended operation. At present, MPLs are operated at 22 sites around the world. The combined lidar and

sunphotometer measurements are able to produce quantitative aerosol and cloud products, such as optical depth, sky radiance, vertical structure, and extinction profiles (http://mplnet.gsfc.nasa.gov/).

The European Aerosol Research Lidar Network, EARLINET established in 2000 is highly instrumented lidar network (http://www.earlinet.org/). The primary purpose of EARLINET is to build a quantitative comprehensive statistical database of the horizontal, vertical, and temporal distribution of aerosols on a continental scale. Also, additional measurements are performed to address important processes, for example, dust events, forest fire events, and volcanic eruptions.

The Commonwealth of Independent States Lidar Network (CIS-LiNet) established in December 2004 is the lidar network in CIS regions (http://www.cis-linet.basnet.by). The basic concept of the network is similar to EARLINET.

The Asian Dust Network (AD-Net) (http://www-lidar.nies.go.jp/AD-Net/index.html) is a voluntary network of lidar researchers in the East Asia region for exchanging data and information. Various groups with various instrumentations are involved in AD-Net. There are multi-wavelength Raman lidars in Tokyo and Gwangju, Korea, and a high-spectral-resolution lidar in Tsukuba, Japan. The NIES Lidar Network (http://www-lidar.nies.go.jp/), which is a part of AD-net, is a somewhat operational network of automated two-wavelength polarization lidars (backscattering at 1064 nm and 532 nm, and depolarization at 532 nm). Currently, 13 lidars (Japan (8), Korea (1), China (1), and Thailand (1)) including those of cooperative sites, are operated continuously, year-round. Many of the lidars are co-located with the Skyradiometer Network (SKYNET) (http://atmos.cr.chiba-u.ac.jp/)

The Regional East Atmospheric Lidar Mesonet (REALM) is the network of lidar research groups on the east coast of the United States (http://alg.umbc.edu/REALM/).

Figure 7-4 shows a comparison of the mean lidar extinction profiles with the global aerosol models for northern and southern European stations in 2000 [*Matthias*, 2004]. The model results are filtered for the observation period. The variability of the profile (16% and 84%) is shown.

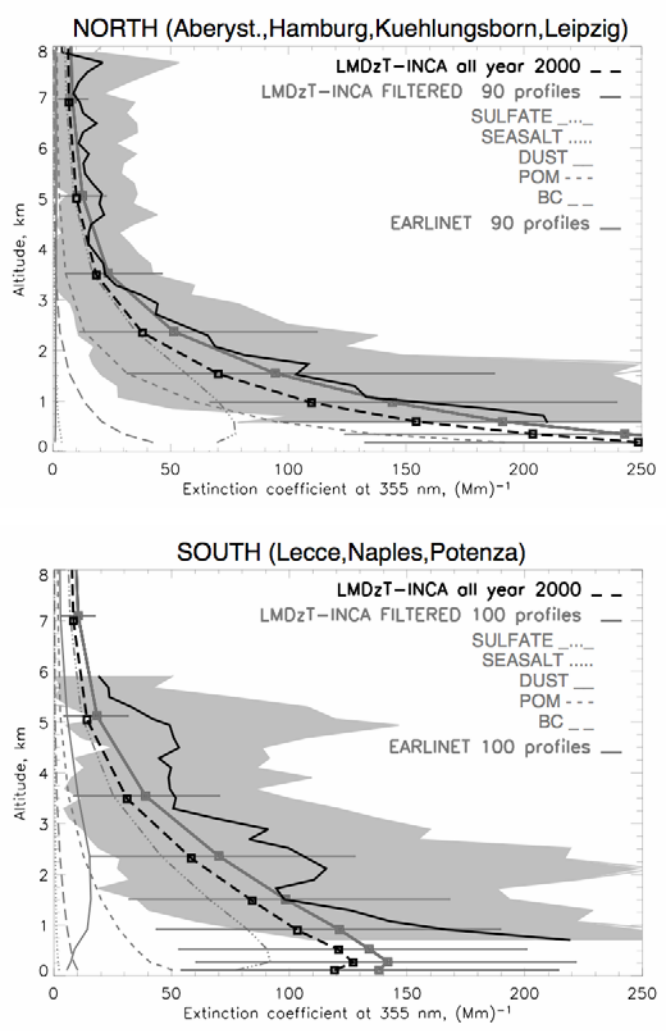

Figure 3-4. *Comparison of the mean lidar extinction profiles (at 355 nm) with the models for northern and southern EARLINET stations in 2000 [Matthias et al., 2004]. The variability (16% and 84% percentiles) of the mean profile is shown with the gray area.*

7.3.3. Surface Based Remote Sensing of Clouds

AERONET also measures the cloud optical thickness, the most important of all cloud optical properties and vital for any cloud-radiation parameterization. Its impact on radiative fluxes and therefore climate is matched only by cloud fraction. Cloud optical thickness is also the most fundamental optical variable in any cloud-resolving model.

Progress on cloud-radiation parameterization may halt because without good optical depths, the radiation calculations could be wrong.

There are also lots of ambiguities in definitions of cloud fraction. Visual cloud fraction is a nice thing to know but climate models need a *radiative* cloud fraction, and not a visual quantity. By radiatively effective cloud fraction we mean the one that forces plane-parallel radiative transfer calculations to give the same radiation as the measured ones. *Stephens* [1978] showed that radiatively effective cloud fraction is the cloud property actually required in GCM cloud parameterizations and it is always different from a simple visual one. In addition to aerosol, the AERONET network has begun monitoring *cloud* optical properties, such as cloud optical thickness and (effective) cloud fraction, using AERONET "idle time" inappropriate for aerosol study. When the sun is blocked by clouds, a radiometer instead of going "to sleep" is forced to look straight up and measure zenith radiance. We call this new feature the AERONET "cloud mode." Several radiometers have now been equipped with this mode.

There have been two major problems with inferring cloud optical thickness from measurements of zenith radiance: (i) lack of a unique relationship to determine cloud optical thickness; and (ii) a strong influence of 3D cloud structure on measured radiance. To solve these problems, a new method that exploits the huge jump in vegetated surface reflectance across 700 nm wavelength has been proposed. The idea was to use zenith radiance measurements in two narrow spectral bands on each side of the jump. In the RED spectral region (~670 nm), the chlorophyll in green leaf absorbs 90-95% of solar radiation; thus, the vegetation albedo is low. In contrast, in the NIR spectral region (~870 nm), a green leaf reflects 90% of incident radiation; thus its albedo is high at this wavelength. If AERONET measurements are combined with surface reflectance properties, then zenith radiances at RED and NIR wavelengths can be used to determine the overlying cloud properties. This is illustrated in Figure 7-5 using surface data from Terra's MODIS. The left panel shows a calculated set of curves for one particular choice of RED and NIR surface reflectances, and for a range of possible cloud optical thicknesses □ and cloud fractions N_c. Also plotted are three groups of 10 data-points measured by an AERONET radiometer on July 28, 2002 at the DOE/ARM site in Oklahoma at three different times. The plot shows that the 3

clusters of AERONET measurements correspond to three different pairs of cloud properties – (N_c = 0.9; □= 28), (N_c = 0.8; □= 22), and (N_c = 0.4; □= 12). The right panel shows an image from DOE/ARM's "all sky camera." Note that N_c = 0.8 is not a horizontal cloud fraction that would be seen in the surface camera, or the satellite image, but a "radiatively effective" fraction that accounts for the horizontal inhomogeneity of the clouds. For details, see *Marshak et al.* [2004].

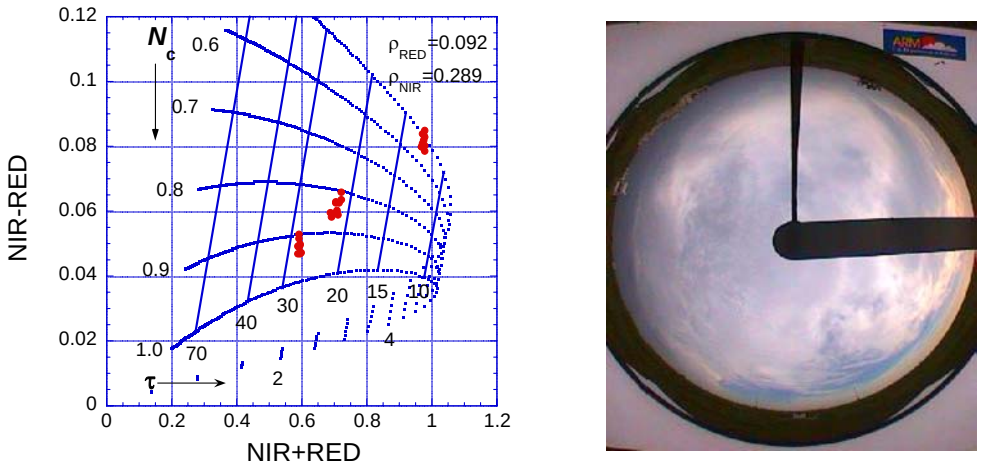

Figure 7-5. *Left panel: DISORT calculated values of RED and NIR radiances for a wide range of optical depth τ and cloud fraction N_c for SZA =62°±3°, surface albedos ρ_{RED}=0.092 and ρ_{NIR}=0.289. When N_c is constant and τ is varying, the set of calculated values define the cloud fraction isolines. When τ is constant and A_c is varying, the set of values define the optical depth isolines. Values RED and NIR are from AERONET measurements at the ARM site on July 28, 2002. Measurements were taken around 13:45, 13:58, and 14:11 UT, respectively. Right panel: Total Sky Image taken at 14:00 UT with SZA=62.75^0.*

Recently, surface-based remote sensors have been used to examine aerosol effects on clouds. Although these methods can only be applied at a limited number of locations, they yield high temporal resolution data. They offer some interesting insights, and are complementary to the global satellite view. Satellite-borne probes measure cloud properties in cloudy pixels and aerosol properties in adjacent, cloud-free pixels, with the implicit assumption that these aerosols are representative of the aerosols entering cloud base.

7.4 SATELLITE MEASUREMENTS OF AEROSOL AND CLOUDS

7.4.1 The Large Scale Picture of Aerosol Distribution

Radiant energy reflected and emitted by the Earth's surface and atmosphere, carries with it a signature of the atmospheric and surface properties. By measuring the reflected light's spectral, angular and/or polarization properties, satellite sensors can quantify several atmospheric and surface properties (polarization is the degree of organization of the electric field of the scattered solar radiation into a given direction). By measuring sunlight transmitted directly or diffusively to the surface through the aerosol and cloud layers, surface based networks of radiometers can also derive aerosol and cloud properties.

To get a perspective on our remote sensing capability from satellites and surface radiometers, we start with our experience with the human eye. Our eye is sensitive to a narrow spectral range of the solar spectrum, with spectral receptors in the blue, green, and red. We get depth perception using the eyes' slightly different angles of observation. By analogy, aerosol remote sensing started using a single wavelength and single angle of observation [*Fraser et al.*, 1984; *Husar et al.*, 1997], corresponding to the viewing ability of a color blind person using a single eye (e.g. METEOSAT, and GOES). The TOMS instruments, flown since 1978 have two channels sensitive to ultraviolet (UV) light that were discovered to be excellent for observations [*J. Herman et al.*, 1997] of elevated smoke or dust layers above scattering atmosphere. A two-channel technique was used for the AVHRR with simultaneous analysis of aerosol and clouds [*Nakajima et al.*, 2001; *Sekiguchi et al.*, 2003; *Mishchenko et al.*, 2003]. These instruments supply a long term series of aerosol and clouds properties, currently 20 year long – see Figure 7-6 [*Torres et al.*, 2002], that can be used to assess regional changes in the aerosol concentration; but calibration and characterization of the instrument performance is difficult [*Vermote et al.*, 1995], and the TOMS analysis requires an assumption of the height of the aerosol layer [*Torres et al.*, 2002]. Note that the geostationary satellites, METEOSAT and GOES have an advantage over the AVHRR and TOMS of being able to generate long term series with the full diurnal cycle, albeit at a single wavelength. This approach has not yet been completely explored.

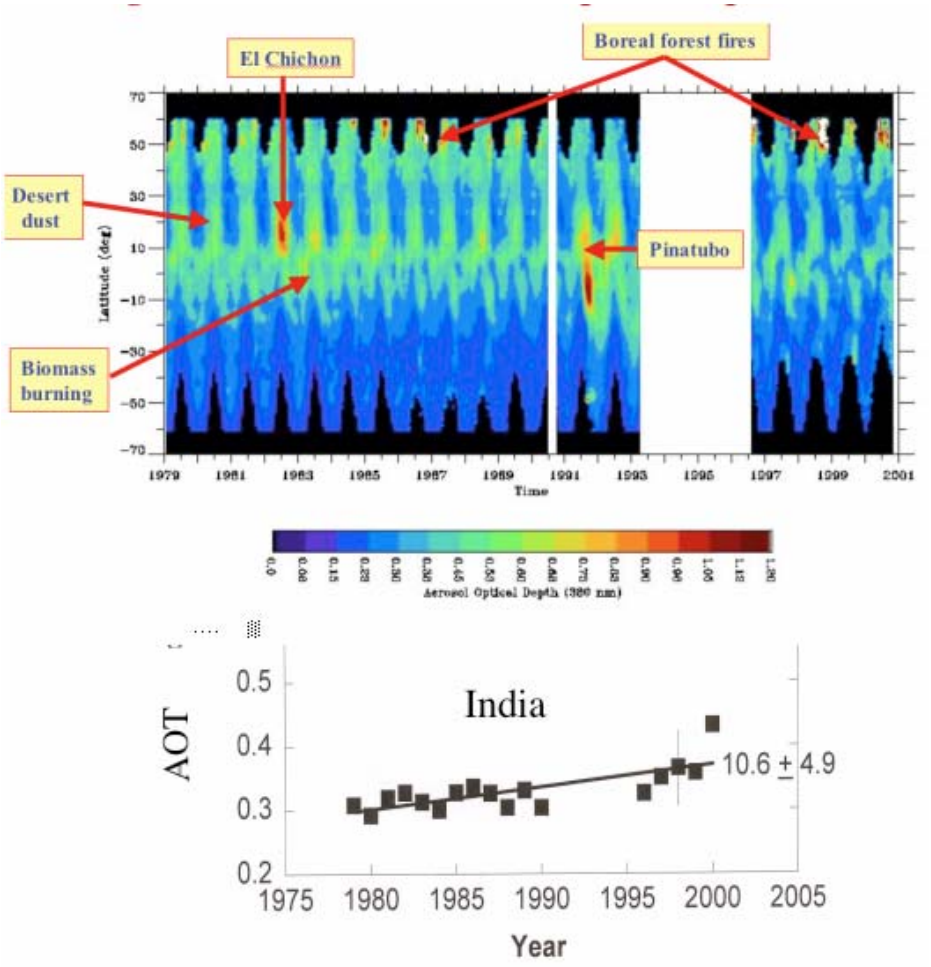

Figure 7-6. *20 year time series of aerosol optical thickness from the TOMS satellite UV measurements. Top: for the globe as a function of latitude [Torres et al., 2002], Bottom time series for India [Massie et al., JGR, 2004]*

The first remote sensing instrument designed for aerosol measurements, POLDER (Polarization and Directionality of the Earth Reflectances, [*M. Herman et al.*, 1997]), uses a combination of spectral channels in a range wider than the human vision (0.44-0.91 μm). The instrument is a wide-angle camera that observes the same target on the Earth at 14 different angles. POLDER also measures light polarization (that we cannot see) to detect fine aerosols over land, taking advantage of the small, fairly constant and difference between the spectrally neutral polarized light reflected from the Earth's surface and the spectrally decreasing polarized light reflected by fine aerosols.

Two instruments, MODIS (MODerate resolution Imaging Spectroradiometer) and MISR (Multi-angle Imaging SpectroRadiometer), on the Terra satellite [*King et al.*, 1999] have been measuring global aerosol distributions and properties since 2000. Over the ocean, MODIS uses the aerosol spectral signature in a wide range (0.47 to 2.1 μm) to distinguish small particles, which in high concentrations are typically associated with anthropogenic pollution or smoke, from coarse particles usually identified as natural sea-salt or dust [*Tanré et al.*, 1997; *Kaufman et al.*, 2002]. This information is used to derive the fraction of aerosol optical thickness that is due to anthropogenic sources (21±7% over the oceans) [*Kaufman et al.*, 2005]. Over land, MODIS uses the 2.1 μm channel to observe the surface cover properties, to estimate surface reflectance at visible wavelengths, and to derive the aerosol optical thickness [*Kaufman et al.*, 1997; *Remer et al.*, 2005] from the residual reflectance at the top of the atmosphere.

The brightness of the earth-atmosphere system at the top of the atmosphere is affected by the angle at which the light is reflected by the surface and atmosphere. MISR [*Diner et al.*, 1998] takes advantage of this fact by detecting the reflected light at different viewing angles (nadir to 70° forward and backward) along the satellite's track in a narrower spectral range (0.44-0.86 μm), thus being able to separate the aerosol signal from that of the surface, and to derive information about particle size and shape [*Martonchik et al.*, 1998; *Kahn et al.*, 2001]. A mixed approach using two view directions but a wider spectral range (0.55-1.65 μm) is used by ATSR [*Veefkind et al.*, 1998] to derive the aerosol concentration and type. These instruments, POLDER, MODIS, MISR and ATSR have controlled calibration and characterization that results in known and smaller errors than the previous generation of instruments [*King et al.*, 1999].

The realization that aerosols affect surface temperature, Earth's radiation budget and precipitation patterns, creates a demand for more informative spaceborne observations. This will hopefully be achieved with the completion of the so-called A-Train (see Figure 7-7) that is designed to measure aerosol, clouds and precipitation, with PARASOL (Polarization and Anisotropy of Reflectances for Atmospheric Sciences coupled with Observations from a Lidar [POLDER-like instrument launched Dec. 2004]) and MODIS for passive aerosol and cloud observations in the visible to

IR, the OMI instrument for aerosol observations in the UV to visible, the CALIPSO lidar for aerosol profiling in two spectral channels and cloud top height detection, and CloudSat radar for profiling cloud liquid water and structure.

Figure 7-7. *The A train – a constellation of satellites that jointly will measure aerosol, clouds and precipitation properties.*

In parallel with the development of aerosol and cloud measurements, the Tropical Rainfall Measuring Mission (TRMM) [*Kummerow et al.*, 2000] was launched in 1997 to measure tropical-subtropical rainfall and in so doing, acquiring the first accurate, representative, and consistent ocean climatology of precipitation. TRMM carries the first spaceborne precipitation radar (PR) producing new measurements of precipitation's vertical structure (~250 m resolution) and several additional instruments to conduct new observations of the Earth's assortment of convection, frontal zones, precipitating storms, and tropical cyclones.

The set of measurements described above covers information from aerosol distribution and properties to cloud properties and precipitation. The satellite data are evaluated and complemented by ground-based remote sensing of aerosols (e.g., AERONET and MPL networks – *Holben et al.*, 1998), aerosol effects on clouds (at

the ARM sites – *Feingold et al.*, 2003; *Kim et al.*, 2003; *Garrett et al.,* 2004) and precipitation [*Kummerow et al.*, 2000]. The data are used to evaluate aerosol transport models [e.g. *Chin et al.*, 2002] and as input to climate models that study the effects of aerosol on clouds and precipitation [e.g. *Menon et al.*, 2002b]. Statistics have been acquired of the aerosol effect on cloud microphysics and albedo [*Kaufman and Nakajima*, 1993, *Kaufman and Fraser* 1997, *Nakajima et al.*, 2001; *Bréon et al.*, 2002; *Sekiguchi et al.*, 2003; *Matsui et al.*, 2004], but it has been recognized that the clouds being studied depend on the sensor resolution and method of investigation; which in turn affects the strength of the aerosol impact on clouds [*Rosenfeld and Feingold*, 2003].

The accuracy of satellite retrievals is higher over the dark ocean surface than over the variable land albedo. Densely vegetated land areas, e.g., the Amazon Forest, are dark and uniform and therefore some of the best targets for measurements of the aerosol impacts over the land. Surface conditions affect both the aerosol and cloud retrievals and the measurements of liquid water content from TRMM. Therefore, the statistical analysis of aerosol-cloud interaction can be done globally over the oceans and over some continental regions, in particular the dark forests. The increase in cloud fraction and cloud development with increase in aerosol loading is in agreement with the notion that increase in CCN loading modifies cloud microphysics and inhibits precipitation (see chapter 5 for more details), although the changes in cloud microphysics due to increase in aerosol on inhibition of precipitation has not yet been statistically established. New instruments are being designed or proposed for future launches with several critical innovations:

- Spaceborne instruments that combine a wide spectral range with a wide viewing angle range and with polarization [e.g., the Glory mission, *Mishchenko et al.*, 1997; Advanced PARASOL, (Tanré, private communication); Next-generation MISR (Diner, private communication)]. Such instruments are expected to improve derivation of fine and coarse aerosol concentrations, their sizes and refractive index. Refractive index, an optical property, is sensitive to the aerosol composition and water uptake [*Chowdhary et al.*, 2002].

- Derivation of aerosol absorption over the land [*Kaufman et al.*, 2001] and over the oceans by measuring the aerosol spectral attenuation of the bright glint [*Kaufman et al.*, 2002].
- Measuring the vertical distribution of cloud microphysics using slant angle spectroradiometers [*Martins et al.*, private communication].
- New strategies and instruments to measure precipitation from space [*Smith et al.*, 2003].

It is recognized that there is a need for coordination of the aerosol, clouds and precipitation measurements and coordination with in situ and network measurements as well as development of models that can integrate large data sets [*Diner et al.*, 2004; *Seinfeld et al.*, 2004].

In the last decade we have witnessed a quantum leap in the amount and quality of satellite and surface-based remotely sensed data of aerosol, clouds, and precipitation. We are probably at the peak of research benefits from this new array of satellite and surface measurements; however specific plans for the next 2 decades are presently limited in scope. There are specific plans to launch the NPOESS system, having similar capabilities to those we anticipate from the A-train and the Glory mission. More attention is needed to ensure that the degree of sophistication in the aerosol, clouds, and precipitation measurements and the degree of coordination among them continues to increase.

In the following we describe in more detail some of the instruments used to measure the effect of aerosol on clouds and precipitation. One of the advantages of the multi-instrument system to measure clouds and aerosol is the ability to intercompare the results. Figure 7-8 shows an example of such intercomparison for 4 satellite observation of the pollution over the Indian subcontinent.

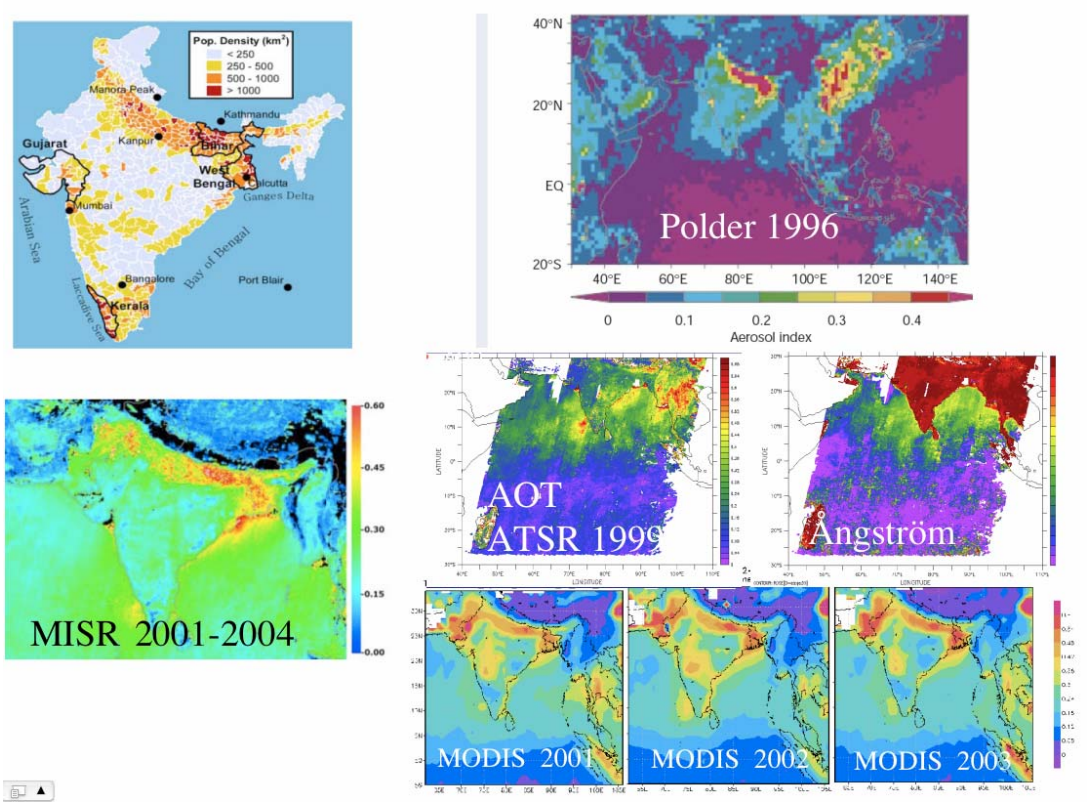

Figure 7-8. *Intercomparison for 4 satellite observation (MODIS, Polder, ATSR and MISR) of the pollution over the Indian subcontinent. Top left - population density per km2, top right - POLDER measurements of the Aerosol index that is similar to the fine aerosol optical depth, center right -ATSR optical thickness and Angstrom exponent for 1999, bottom right - MODIS aerosol optical thickness for 2001 through 2003, left bottom - MISR optical depth averaged over 2001-2004.*

7.4.2 Measurement of Aerosols Using the POLDER Instrument

The POLDER instrument [*Deschamps et al.*, 1994] measures the solar radiance reflected by the Earth's surface and atmosphere in the visible and near infrared (440 to 910 nm). The two main characteristics of POLDER are the ability to measure the linear polarization of the radiance in three spectral bands, and to acquire the directional variation of the reflected radiance: the instrument concept is based on a

wide field of view lens and a bi-dimensional CCD that provides an instantaneous field of view of ±43° along-track and ±51° cross-track. As the instrument flies over the target, up to fourteen views are acquired; these can be composited to infer the directional signature of the reflectance. This signature provides information on the surface, aerosol, and cloud characteristics. A limitation of POLDER is the rather coarse spatial resolution of about 6 km, which affects the ability to account for scene heterogeneity.

The POLDER instrument flew onboard the ADEOS 1 and 2 platforms in 1996-1997 and 2003, respectively. Unfortunately, due to the failure of the satellite solar panels, the measurement time series are limited to respectively 8 and 7 months. Another very similar instrument was launched in December 2004 onboard the microsatellite PARASOL to be part of the A-train.

As for all Earth observing radiometers that operate in the visible spectral range, the measurements can be interpreted in terms of aerosol and cloud optical thickness. Algorithms have been developed to process the measurements in terms of aerosols [*Deuzé et al.*, 2001; *Herman et al.*, 2005] and cloud characteristics [*Buriez et al.*, 1997, *Parol et al.*, 1999]. These algorithms have been applied to the full dataset and are available from the POLDER web site [*CNES*, 2004]. We now discuss in more detail how the specific characteristics of POLDER have been used to measure aerosols and clouds and assess aerosol-cloud interactions.

7.4.2.1 Derivation of Aerosol Properties Over the Oceans

Although the spectral range of POLDER measurements is limited compared to that of other spaceborne instruments such as MODIS, the combination of spectral-directional and polarized signature provide a very strong constraint to invert the aerosol optical thickness and characteristics. The present algorithm [*Herman et al.*, 2005] assumes spherical or non-spherical particles, non-absorbing particles and the size distribution follows a combination of two log-normal aerosol size distributions in the accumulation and coarse modes respectively. As a first step, the retrieval of optical thickness and size distribution is achieved using radiance measurements in two aerosol channels, 670 and 865 nm. When the geometrical conditions are optimal, i.e., when the scattering angle coverage is larger than 125°-155°, the shape (spherical or not) of the particles is derived. As a second step, the refractive index retrieval is

attempted from the polarization measurements. The real part of the refractive index of the coarse mode is retrieved when spherical particles are present but the derivation of the refractive index of the accumulation mode is very tentative and is still under investigation. The results demonstrate that a large fraction of the aerosol concentration downwind of the continents, in particular from dry areas, is composed of non-spherical particles, with scattering properties that differ from their spherical counterparts.

Comparisons with ground based AERONET measurements show excellent agreement, with typical RMS errors on the order of 0.05, including errors due to cloud cover, with no significant bias. The fine-mode optical thickness can also be compared to AERONET measurements, albeit with some uncertainty in the aerosol radius cutoff. Statistical results indicate a low bias of 0.02 with a standard deviation of 0.02.

The combination of spectral, directional and polarization information has been used to attempt a retrieval of the aerosol real refractive index over the oceans. The results indicate that when the coarse mode is spherical, the refractive index is close to that of water (1.35), indicating hydrated particles. When the coarse mode is mostly non-spherical, however, the retrieval is found to be inconclusive. As for the fine mode, the inverted refractive index is generally found to be between 1.40 and 1.45, with no clear spatial preference.

7.4.2.2 Derivation of Aerosol Properties Over Land

The retrieval of aerosol properties over land surfaces is based on polarized reflectance measurements. When the surface reflectance is generally larger than that generated by aerosols, which makes their quantification difficult from radiance measurements alone, the polarized reflectance of land surfaces is small and fairly constant, although it does have a very strong directional signature [*Nadal and Bréon*, 1999]. On the other hand, scattering by submicron aerosol particles generates highly polarized radiance [*Deuzé et al.*, 2001], which makes it possible to estimate the corresponding aerosol optical thickness – a measure of the column concentration. Nevertheless, larger aerosol particles, such as desert dust, do not polarize sunlight and are therefore not amenable to a quantitative inversion from POLDER measurements. The retrievals from POLDER measurements show that submicron particles are dominant in regions of biomass burning as well as over highly polluted areas [*Goloub and Arino*, 2000;

Tanré et al., 2001]. Early results of the optical thickness of the accumulation mode are reported on Figure 7-9 for May 2003. The continuity at the land/sea boundaries is observed in most regions, which gives us good confidence in the quality of the inversions.

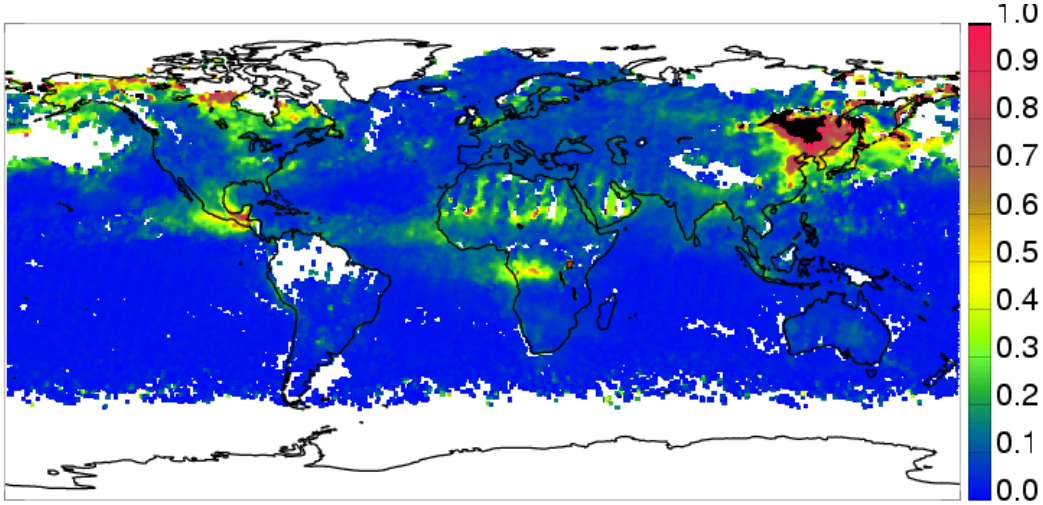

Figure 7-9. *POLDER aerosol monthly optical thickness of the accumulation mode for May 2003. The continuity at the land/sea boundaries is observed in most regions, which gives us good confidence in the quality of the inversions. Methods aim at quantifying roughly the accumulation fraction of the aerosol loading with different methods over land and ocean. Note the aerosol emitted from Central America, Equatorial Africa and Asia.*

Over land, the evaluation of POLDER retrievals is made against the fine mode optical thickness derived from AERONET measurements. The results show no significant bias and an RMS error on the order of 0.04 when dust-loaded atmospheres are excluded (i.e., a validation in regions affected by biomass burning or pollution aerosols).

7.4.2.3 Derivation of Cloud Droplet Radius from Satellite Sensors

The classical method of evaluating cloud droplet radius (CDR) from satellite measurements is based on the spectral signature of cloud reflectance between the visible and near-IR spectral ranges [*Nakajima and King*, 1990]. POLDER provides an alternative method, based on the analysis of cloud bows (Figure 7-10) that can be observed in the polarized radiance measurements [*Bréon and Goloub*, 1998]. Although this method is very precise with no known causes for error or biases, it is

applicable only in very specific conditions, i.e., extended cloud fields (150 x 150 km^2) with narrow size distributions at cloud top. As a consequence, the method does not apply to all cloud types. The requirements are most often fulfilled over stratocumulus cloud fields on the Eastern part of oceanic basins, as well as over the Antarctic Ocean [*Bréon and Colzy*, 2000]. A comparison with MODIS estimates of cloud droplet radius show a high correlation over the oceans, but poor correlation over land surfaces. There is a bias in the two estimates that is not understood [*Bréon and Doutriaux-Boucher*, 2005]. The CDR from POLDER has been used together with aerosol estimates to assess their effect on cloud microphysics [*Bréon et al.*, 2003]. Very precise CDR values are derived with an error of <0.3 µm.

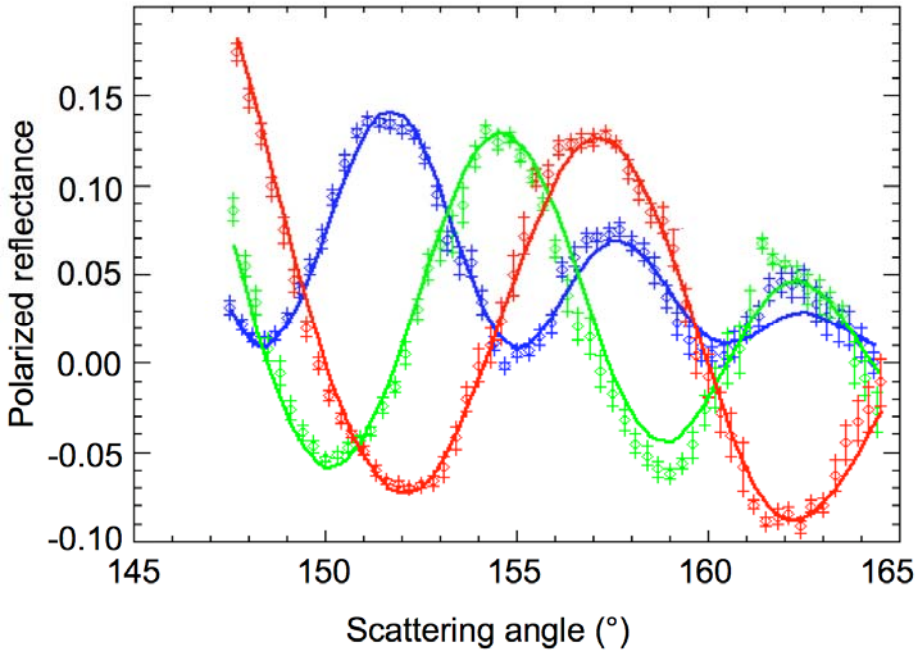

Figure 7-10. *Polarized reflectance from a cloud field as a function of the scattering angle in the three polarized channels of POLDER (blue - 443, green - 665 and red - 865 nm). The measurements over a 150x150 km^2 area have been averaged in 0.3 scattering angle bins. The figure shows the average (diamond) and the standard deviation (crosses) together with the result of a best fit (line). In this case, the best fit indicates a droplet effective radius of 8 µm.*

The polarization capabilities of POLDER also permit an unambiguous identification of the cloud top phase, from the presence or absence of a "cloud bow" for a scattering angle of 140° [*Riédi et al.*, 2000]. There are no validation data available to evaluate the POLDER cloud radius product. The consistency of the results in the three bands

and the excellent fit between the measured and modeled polarized reflectances indicate a retrieval precision better than 0.5 μm. However, comparisons with the MODIS product have shown significant discrepancies, with a bias of 2 μm and a standard deviation of 2 μm. The discrepancies may be explained by a combination of differences in the vertical weighting of the cloud, since POLDER measures the very top of cloud while the standard method that is based on the cloud spectral signature, senses deeper into the cloud [*Bréon and Doutriaux-Boucher*, 2005]; due to the larger sensitivity of the MODIS algorithm to deviations from the plane parallel assumption; and due to the need of the POLDER algorithm, to view horizontally uniform clouds [*Rosenfeld and Feingold*, 2003].

7.4.2.4 Determination of Cloud Top Pressure

The POLDER characteristics provide two means of evaluating the cloud top pressure. One method is based on the measurement of the polarized radiance generated by molecular scattering in the atmosphere. The presence of a cloud layer reduces and scatters the light reflected by air molecules below. As a result, the polarized reflectance in the blue part of the spectrum (where molecular scattering is very efficient) is decreased as a function of the cloud top pressure. A combination of several spectral bands can be used to make out the cloud and molecular contributions to the polarized reflectance and then to provide an accurate estimate of the cloud top pressure. The comparison to ARM lidar/radar measurements indicates that the POLDER cloud pressure is close to the middle of the cloud. The statistics show a negligible bias and a standard deviation of 65 hPa.

The other method is based on the ratio of two radiance measurements centered on the oxygen A-band at 763 nm [*Vanbauce et al.*, 1998]. One channel is 10 nm wide while the other is 40 nm wide with the same central wavelength. As a consequence, the ratio of the narrow and wide channels provides an indication of the oxygen absorption between the reflector and the satellite, which is a direct proxy of the reflector pressure. A comparison with lidar measurements of cloud profiles has checked the validity of the two methods [*Vanbauce et al.*, 2003].

7.4.3 Remote Sensing of Aerosols by MODIS

The MODerate resolution Imaging Spectroradiometer (MODIS) began collecting data in February 2000 from the Terra (10:30 am and 10:30 pm equatorial crossing time) spacecraft and June 2002 from the Aqua spacecraft (1:30 pm and 1:30 am equatorial

crossing time). Special emphasis is given to on-board calibration facilities, lunar observations, and detailed analysis of the calibration time series on the ground [*Barnes et al.*, 1998]. MODIS provides measurements of the spectral radiances from 0.41 to 14 μm in 36 spectral bands daily over most of the globe. MODIS measurements are used to characterize the global aerosol, clouds, water vapor, fires, vegetation, sea surface temperature, and ocean color. The aerosol characteristics are derived over the oceans [*Tanré et al.*, 1997] and land [*Kaufman et al.*, 1997] using independent algorithms.

7.4.3.1 The MODIS Aerosol Algorithm

Over oceans, the MODIS aerosol algorithm uses the measured 500 m resolution radiance from six MODIS bands (550-2100 nm) to retrieve aerosol information. Specifically, in cloud-free, glint-free ocean scenes [*Martins et al.*, 2002], MODIS retrieves at a 10 km resolution: the aerosol optical thickness at 550 nm, τ_{550}, the fraction of τ contributed by the fine (sub-micron size) mode aerosol, f, and the effective radius of the aerosol, r_{eff} [*Tanré et al.*, 1997]. Over land the 2.1 μm channel is used to estimate the surface properties [*Remer et al.*, 2005] and the 0.47 and 0.66 μm channels are used to derive f and τ. Aggregation of the MODIS aerosol information from the 500 m pixels to the 10 km product allows for rigorous cloud screening, avoiding data gaps, and still generates large enough statistics for a stable and accurate product. The MODIS-derived aerosol properties have been validated [*Remer et al.*, 2005]. In agreement with theoretical error analysis [*Tanré et al.*, 1997; *Kaufman et al.*, 1997], the aerosol optical thickness is derived with an error of $\Delta\tau_{550} = \pm 0.03 \pm 0.05\tau$ over the oceans and $\Delta\tau_{550} = \pm 0.05 \pm 0.15\ \tau$ over the land. Over the oceans the errors were found to be mostly random with very little bias remaining for large statistics of data. For aerosol dominated by dust, a bias of about +10% was observed. Figures 7-11 - 7-12 show examples of the MODIS observations over the globe. [MODIS monthly data can be accessed interactively from http://lake.nascom.nasa.gov/movas/. Information and images on the MODIS atmospheric products can be found at http://modis-atmos.gsfc.nasa.gov/.

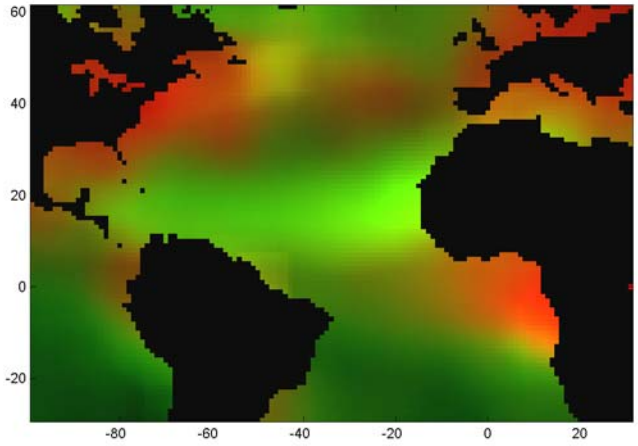

Figure 7-11. *MODIS aerosol observations over the ocean. MODIS measurement of the aerosol optical thickness and the ratio of fine to coarse particles were used to construct this image over the Atlantic ocean, averaged over June through Aug. 2002. The optical thickness is represented by the brightness of the image, the contribution of fine particles to the optical thickness by the color, red - dominance by submicron particles - smoke from central Africa and pollution from Europe and North America, and green – dominance by dust from Africa or sea salt in regions with high winds.*

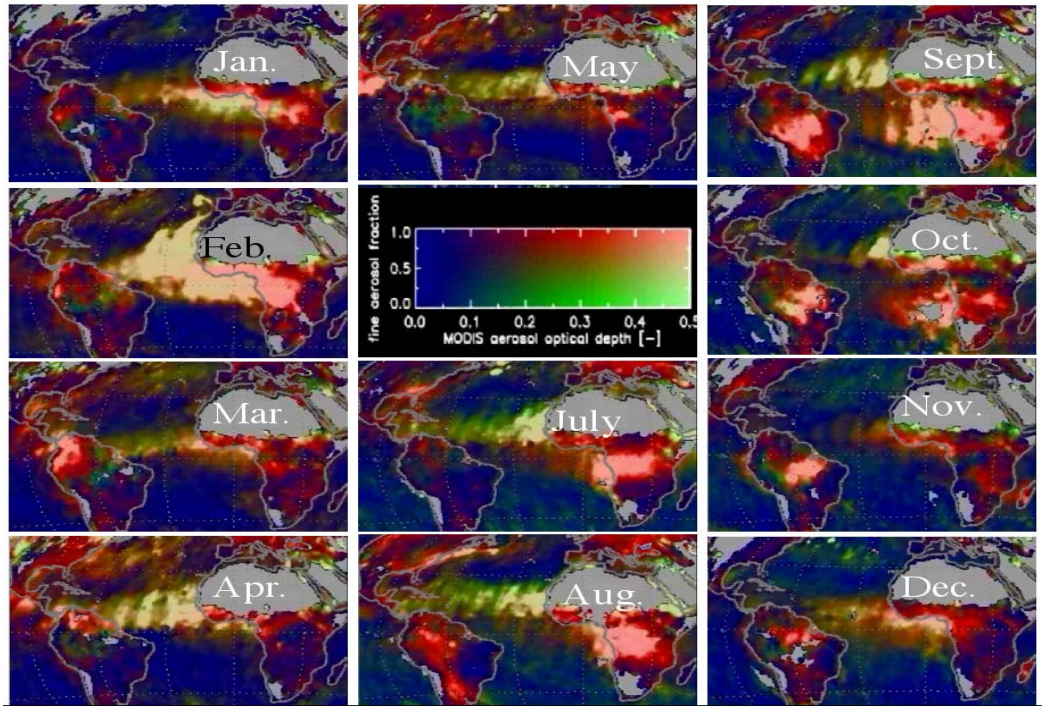

Figure 7-12. *MODIS aerosol monthly composites for 2001. Each composite is for the 15th of each month ± 5 days to find enough cloud free regions. Data for June are not shown since no MODIS data were available during the middle of the month. The color bar is located instead. The color bar was constructed so that blue represents clean conditions, aerosol optical thickness <0.1, green and red show higher optical thickness corresponding to the coarse (green) and fine (red) modes. Therefore pure dust is shown as green and pure smoke or pollution red. Note that the color of the aerosol emitted from Africa changes from mixed red and green in January through April, to green in July-August. Biomass burning occurs in the Sahel during January-March, and moves to Southern Africa for July-August, when it is separated from the dust flow.*

7.4.3. 2 Remote Sensing Measurements of Cloud Properties

The MODIS cloud product [*Platnick et al.*, 2003; *King et al.*, 2003] combines infrared and visible techniques to determine the physical, radiative, and microphysical properties of clouds. Cloud optical thickness and effective radius are derived globally using six visible and near-infrared bands at 1-km spatial resolution. Cloud-top properties, including cloud-top temperature, cloud-top pressure, and effective

emissivity, are derived using the infrared split window and longwave CO_2 absorption bands (both day and night) at 5-km spatial resolution. Cloud thermodynamic phase is computed at 5-km resolution using a two-band algorithm that includes an additional thermal band at 8.55 μm, and also at 1-km resolution using a different technique based on results from the cloud mask tests followed by a bispectral threshold test, shortwave infrared tests, and finally cloud top temperature [*King et al.*, 2004]. Finally, the cloud product contains a cirrus reflectance product at a visible wavelength for use in removing cirrus scattering effects from the land surface, and it utilizes an additional band at 1.38 μm. Hence, the cloud product contains many different cloud properties derived from 14 bands in total, and the file size is different during the night (only cloud-top properties and thermodynamic phase at 5-km resolution) than during the day (when additional 1-km resolution products are included).

Figure 7-13 shows an example of the cloud optical thickness, cloud top pressure, and effective radius for a daytime granule of Terra-MODIS data over the Western Pacific Ocean near the Kamchatka Peninsula on August 10, 2001 at 0025 UTC. The true color image in Figure 7-13 (a) shows extensive cloud cover over the Sea of Okhotsk, including mid-level and upper-level ice clouds, whereas the Bering Sea to the east of the Peninsula contains extensive marine stratocumulus clouds with numerous ship tracks in the southeastern portion of the image. Figure 7-13(b) shows cloud optical thickness, Figure 7-13(c) shows cloud-top pressure, and Figure 7-13 (d) shows cloud effective radius, where a different color scale for water and ice clouds were used in Figure 7-13(b) and (d). The optically thick marine stratocumulus to the east of the peninsula is identified as water clouds with optical thicknesses (0.65 μm) up to 25. The optically thick ice clouds over the Sea of Okhotsk and around the southern portion of the Kamchatka Peninsula have cloud optical thicknesses approaching 40. The ship tracks are not easily identified in the cloud optical thickness image shown here, but they result in reduced effective radii in the microphysical retrievals shown in Figure 7-13(d). For this scene, the thermal infrared and decision tree algorithms for deriving cloud thermodynamic phase, discussed by Platnick et al. [2003], are in quite good agreement. Finally, the cloud-top pressure for the cloud-filled pixels, shown in Figure 7-13(c), clearly show that the water clouds lie predominantly between 700 and

850 hPa, whereas the optically thick ice clouds over the Sea of Okhotsk lie at altitudes above the 500 hPa level.

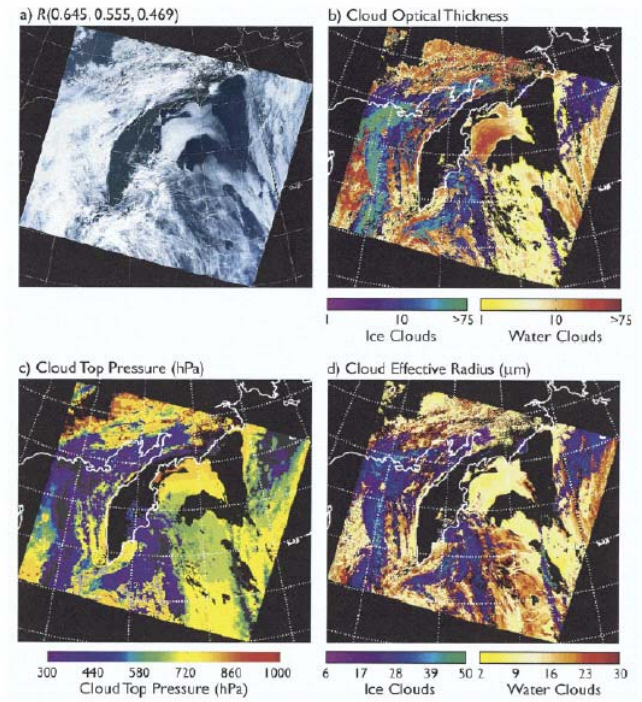

Figure 7-13. *Cloud properties over the western Pacific Ocean off the Kamchatka Peninsula on August 10, 2001. Panel (a) is a true color composite of one MODIS granule, showing marine stratocumulus clouds with ship tracks as well as upper level ice clouds. Panels (b) and (d) show the cloud optical thickness and effective radius derived from all cloudy pixels, where we have used a separate color bar to denote clouds processed as ice and water clouds. Panel (c) shows the cloud-top pressure for all clouds in this scene.*

7.4.4 Measuring Aerosols With the Multi-angle Imaging Spectro Radiometer (MISR)

The Multi-angle Imaging SpectroRadiometer (MISR) instrument on Terra [*Diner et al.*, 2002] observes the Earth globally at nine different angles, ranging from 70° forward to 70° backward along the spacecraft track. MISR aerosol, cloud, and surface products are available through the NASA Langley Atmospheric Sciences Data Center (http://eosweb.larc.nasa.gov); further information about the MISR Mission can be found at http://www-misr.jpl.nasa.gov.

Images are obtained in four spectral bands (446, 558, 672, and 866 nm) with a ground spatial sampling of 275 m - 1.1 km. Such data offers several advantages for aerosol

retrieval. Oblique viewing provides high sensitivity to aerosol optical thickness. Over major aerosol source regions such as deserts and urban areas, where the high surface reflectance presents a challenge, MISR algorithms make use of the systematically changing ratio of surface to atmospheric radiance with view angle to separate the surface from atmospheric signals [*Martonchik et al.*, 1998; 2002]. The resulting optical thicknesses show good agreement with values derived from AERONET [*Kahn et al.*, 2005; *Abdou et al.*, 2005; *Martonchik et al.*, 2004; *Diner et al.*, 2001].

Over water, MISR's scattering angle coverage (~ 60°-160° in mid-latitudes) helps distinguish particle size and shape. Three-to-five particle size groupings between about 0.1 and 2.5 microns are identified in the data [*Kahn et al.*, 2001; 2005], and recent work indicates that MISR is able to separate different mineral dust shape classes [*Kalashnikova et al.*, 2005]. Although such detailed validation opportunities are rare, retrievals from MISR data acquired during the CRYSTAL-FACE campaign identified three distinct aerosol modes within the column: maritime-type particles, cirrus, and Saharan dust, in proportions that agree with independent data to within about 20% [*Kahn et al.*, 2001]. On another occasion, retrievals over Galveston Bay, near Houston, TX, distinguished two aerosol modes, one with an effective radius near 0.1 μm and the other with an effective radius near 0.6 μm, showing sensitivity to differences between >~0.95 and <~0.88 in aerosol single scattering albedo, in agreement with field measured upwind of the city, and consistent with pre-launch sensitivity expectations.

MISR routinely obtains the heights of reflecting surfaces such as cloud tops stereoscopically, provided there is some spatial contrast so image pattern matching can be performed. This is often the case for aerosols near volcanic, forest fire, and dust source regions, where distinct plume features are present. The technique retrieves the altitude at which the contrast is most visible, which is typically the top of the plume. MISR algorithms perform pattern-matching globally in an automated manner [*Moroney et al.*, 2002], with 1.1 km horizontal resolution and about 0.5 km sensitivity in the vertical. An example for a wildfire is shown in Figure 7-14. The stereo retrieval is successful in distinguishing the heights of two separate plumes associated with the fire complex.

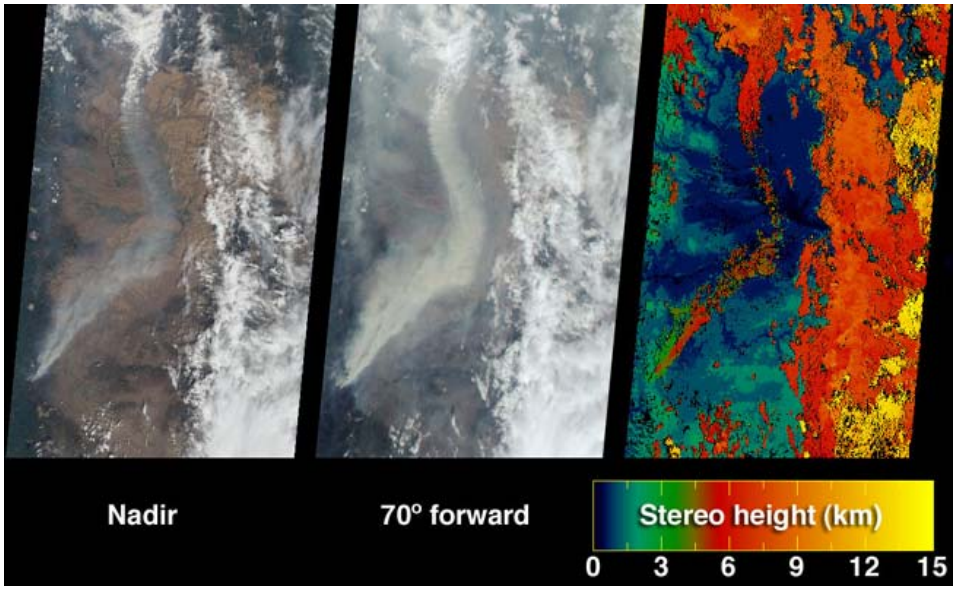

Figure 7-14. *MISR nadir camera image (left), 70□-camera image (middle), and standard stereo height retrieval product (right) for the B&B fire complex in Oregon, acquired September 4, 2003. The smoke snakes northward from several blazes located near the lower left.*

7.4.5 Meteosat Second Generation – MSG

The Meteosat series of geostationary satellites, at 0° longitude, are ideally located to follow the export of dust from the Saharan and Sahel dry areas and the biomass burning activity in Sahel and central Africa, two major sources of aerosols to the atmosphere. This opportunity has been exploited since the early 1990s to quantify the export of dust over the Atlantic and the Mediterranean [*Jankoviak and Tanré*, 1992; *Dulac et al.*, 1992; *Moulin et al.*, 1997]. Likewise, the thermal infrared channel of Meteosat was used to locate the main source areas of dust in Northern Africa through their impact on the apparent temperature at midday during dust storms and a corresponding Infrared Difference Dust Index (IDDI) has been defined [*Legrand et al.*, 2001].

The first generation of Meteosat satellites carried only three wide spectral bands respectively in the visible band [0.45 to 1.0 μm], in the water vapor absorption band [5.7 to 7.1 μm] and in the thermal infrared (window) band [10.5 to 12.5 μm], so it is not possible, for instance, to distinguish between aerosol types like dust or biomass burning aerosols over ocean. This limitation does not apply to the Meteosat Second Generation (MSG) that carries three channels in the solar spectral range, from 0.6 to

1.6 μm, and two in the thermal infrared (window) band, 10.8 and 12.0 μm. It is expected that this operational satellite will permit an excellent monitoring of the aerosol sources and transport over the African continent. One major advantage of the geostationary satellites, compared to the polar orbiters, is their ability to provide images of a given area with high temporal sampling, every 15 min for MSG, which permits the monitoring of aerosol transport and impact on clouds and precipitation in different parts of the diurnal cycle.

7.4.6 Multi-angle, Multi-spectral Polarimetric Remote Sensing (The NASA Glory Mission)

Remote sensing of clouds and aerosols from satellite is a major component of current attempts to map the characteristics of clouds worldwide and evaluate the effects of aerosols on their properties. The aerosol effect on the cloud albedo can be detected and quantified from space by means of long-term global measurements of the change in the number concentration of aerosol particles acting as cloud condensation nuclei (CCN) and the associated change in the cloud albedo and lifetime. Other measurable manifestations of the indirect effect include modifications to the cloud droplet size distribution and number concentration and changing liquid water path [*King et al.*, 1995; *Schwartz et al.*, 1995, *Brenguier et al.*, 2000a, 2003].

Since the efficiency of droplet nucleation by aerosols depends on the latter's size and hygroscopicity, the measurement of the aerosol number concentration must be accompanied by the determination of the aerosol size spectra and chemical composition with sufficient accuracy to provide a useful estimate of the number of cloud condensation nuclei (CCN) that are present [*Mishchenko et al.*, 1997]. Although the chemical composition of aerosols cannot be determined directly from remote sensing measurements, the spectral refractive index and shape of aerosols can and this information provides strong constraints on aerosol composition.

Existing satellite instruments provide estimates of column optical thickness, the Ångström exponent, fine mode fraction, and an effective particle size of aerosols and the optical depth and effective radius of cloud droplets. However, radiance-only measurements cannot constrain the width of aerosol and cloud size distributions nor can they accurately determine aerosol composition and shape. Moreover, errors in

assumed size distribution width and aerosol composition cause increased uncertainties in the quantities that can be retrieved using radiance only measurements [*Mishchenko and Travis*, 1997]. In order to reduce these uncertainties the National Aeronautics and Space Administration (NASA) Glory mission will therefore deploy a high precision multi-spectral photopolarimeter called the Aerosol Polarimetry Sensor (APS) that will scan along the spacecraft ground track in order to provide multi-angle views of each scene [*Mishchenko et al.*, 2004].

Polarimetric measu rements such as those made by the planned APS sensor can be used to provide extremely accurate estimates of aerosol optical depth (with accuracy of ±0.02) together with aerosol effective radius, effective variance, spectral real refractive index (with accuracy ±0.02) and single scattering albedo (with accuracy ±0.03) of a bimodal aerosol model [*Mishchenko et al.*, 2004], though with a foot print of 10 km. Two examples of the fidelity of the aerosol optical depth and size distribution estimated from this type of remote sensing measurement are shown in Figure 7-15(a). In this figure spectral optical depths measured by sun photometers are compared with those retrieved using polarimetric measurements [*Chowdhary et al.*, 2001]. The fact that the entire spectral range is well fitted in cases with both strong and weak spectral slopes is indicative of the reliability of the size distribution estimate for both small and large particles. Comparisons have also been made between in situ and retrieved size distributions and have also been found to agree extremely well (difference in effective radius of less than 0.04 μm, *Chowdhary et al.*, 2004). The single scattering albedo of aerosols can also be estimated from polarimetric measurements because of the differing sensitivity of polarized reflectance and unpolarized reflectance to aerosol absorption. In Figure 7-15(b) we show a comparison of the estimated single scattering albedo derived from polarimetric remote sensing measurements with *in situ* [*Magi et al.*, 2004] and with estimates from ground based sky radiance [*Dubovik et al.*, 2000] measurements. The discrepancy between these estimates may be related to the loss of particles in the sampling system for in situ measurements, humidification of the *in situ* extinction coefficients but not the absorption coefficients and uncertainties in the retrieval of single scattering albedo ϖ from AERONET data that may be caused by the considerable horizontal variability in the aerosol burden [*Magi et al.*, 2005]. Nonetheless the polarimetric estimate of single

scattering albedo is consistent with the other measurements given their inherent uncertainties.

In determining the effect of aerosols on clouds it is essential that the cloud properties that are used do not have biases that depend on the type of cloud, or season. Existing methods for remotely determining the size of cloud droplets use the fact that the efficiency of liquid and ice absorption depends on particle size [*Nakajima & King*, 1990; *Minnis et al.*, 1998; *King et al.*, 2004], or that the rainbow and glory features of radiation scattered by spherical particles are sensitive to particle size [*Bréon and Goloub*, 1998; *Mayer et al.*, 2004]. Methods using the efficiency of liquid and ice absorption must assume an effective variance of the droplet size distribution in their

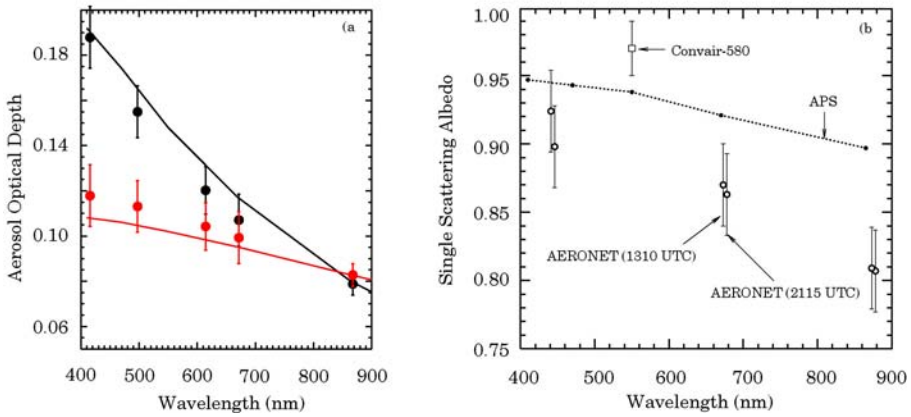

Figure 7-15. (*a) Optical depth comparison. Sun photometer measurements for 14 October 1999 are shown as black filled circles and for 31 March 2000 as red filled circles. Spectral dependence of aerosol optical depth inferred from polarimetry measurements on these two days are shown by solid curved. Error bars are only shown for the Sun photometer measurements. b) Single scattering albedo as a function of wavelength. The dotted lines are best estimate values retrieved from RSP data. Also included are the estimates from data collected during Convair-580 flight 1874 and from the AERONET sky radiance measurements.*

retrievals, which can cause biases in the estimated effective radius if incorrect [*Nakajima & King*, 1990]. Existing analyses of the rainbow and glory features in the radiation scattered by liquid water droplets are limited to very narrow size distribution widths for which these features have a large magnitude. This may cause serious sampling biases when trying to evaluate the effect of aerosols on clouds. The APS sensor makes measurements that allow both methods to be combined and reduces

their limitations. Polarized reflectance measurements are sensitive to the droplet size distribution (effective radius and effective variance) in the top layer of the cloud (optical depth less than three) while the reflectance measurements in spectral bands where ice and water absorb (1.6 and 2.2 μm) are sensitive to a weighted integral through the depth of the cloud [*Platnick*, 2000]. The type of measurements made by the APS therefore requires a cloud model with two vertical layers. This allows the complete set of measurements to be matched with the additional benefit of providing sensitivity to the vertical profile of droplet size and consequently reducing any biases in the estimated liquid water path and number density of droplets. In addition, the polarized reflectance at scattering angles well separated from the rainbow and glory can be used to determine cloud top height [*Goloub et al.*, 1994] and the optical properties of haze above cloud top. An example of the fit that can be obtained between model and measurements at a pair of wavelengths (0.865 and 2.25 μm) is shown in Figure 7-16. It is clear that not only is the cloud droplet effective radius accurately estimated, but also the effective variance of the droplet size distribution. Although the effective variance is a secondary variable in determining the radiative properties of clouds, it is necessary to have accurate estimates of the effective variance in order to determine the concentration of cloud drops [*Mishchenko et al.*, 1997, 2004]. The effective variance of the cloud droplet size distribution is also a diagnostic measure of the relative contributions of dynamics, thermodynamics, and aerosols to the cloud formation process [*Hudson & Yum*, 1997; *Khvorostyanov & Curry*, 1999].

Although there have so far been limited attempts to evaluate the effect of aerosols on ice clouds, recent results suggests aerosols may play a significant role in determining ice particle sizes [*Reisin et al.*, 1996; *Yin et al*., 2000a; *Khain et al.*, 2001; *Fridlind et al.*, 2004; *Koren et al.*, 2005] and consequently in determining precipitation rates. It will therefore become more important in the future to have accurate global estimates of ice particle sizes. A common problem in the current remote sensing of ice clouds is that the shape of the crystals is unknown and any errors in the assumed shape can propagate into errors in the estimated particle size and optical depth [*Rolland et al.*, 2000]. The multi-angle measurements made by the APS sensor can reduce these biases since the measurements allow a plausible shape distribution of particles to be determined.

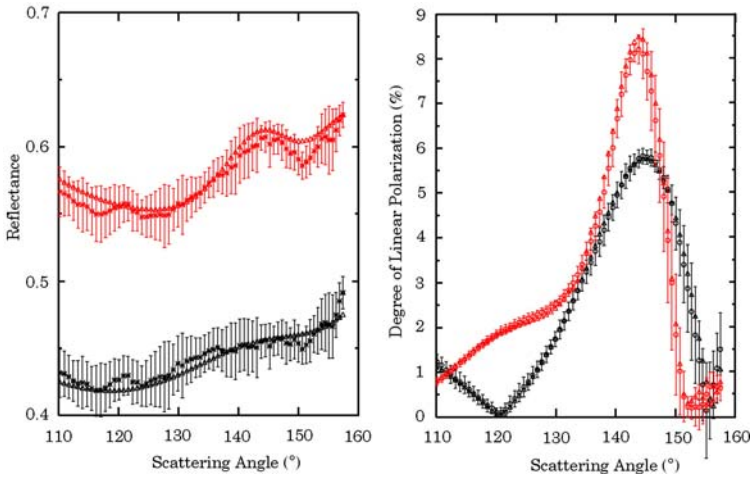

Figure 7-16. *Comparison of model calculations (triangular symbols) and measurements (circular symbols with error bars) of reflectance and degree of linear polarization at 0.865 and 2.25 µm for a best fit two layer cloud model. Measurements were obtained with an aircraft instrument [the Research Scanning Polarimeter (RSP), Cairns et al., 1997] with a pixel size of 40 m. Analysis is for a ten pixel average and the error bars are primarily a result of cloud variability over this 400 m strip.*

An example is shown in Figure 7-16 where multi-angle polarized reflectance measurements are compared against several shape distributions. Only a shape distribution that included small (5 µm) spheroids was acceptable for this cold cloud (200 K) case and this assignment was borne out by *in situ* size distribution measurements and images from a cloud particle imager. The estimated optical depth of this thin cirrus cloud (0.1) is also in agreement with Cloud Polarization Lidar (CPL) measurements indicating the capability of the planned APS polarimetric measurements to identify particle shape and derive realistic cloud ice particle sizes and optical depths. These measurements are of interest to a global understanding of clouds since existing size and shape distribution measurements tend to be biased towards warmer mid-latitude cirrus clouds than the example presented here. These cold sub-tropical clouds appear to have smaller particles [*Garrett et al.*, 2003] and have significant quantities of spheroidal particles and small irregular particles that are not assumed to be present in current retrieval methods [*Rolland et al.*, 2000]. Since these small particles may be affected by pollution in unexpected ways [*Fridlind et al.*, 2004] and can have a noticeable effect on the radiative properties of cirrus clouds

[*Garrett et al.*, 2003], it would appear that the capability to measure them is of considerable value in determining the effect of aerosols on clouds.

In summary, the APS measurements will allow aerosol and cloud remote sensing retrievals with a hitherto unavailable level of accuracy and detail. Although these measurements will only be available along the spacecraft ground track, they will provide a detailed estimate of aerosol and cloud properties in which context the type of correlative studies currently being used to investigate the effect of aerosols on clouds can be better understood and evaluated.

7.4.7 National Polar-orbiting Operational Environmental Satellite System (NPOESS)

The NPOESS satellite system is planned for long term monitoring of the Earth and atmosphere, therefore its aerosol and cloud measurements from the Visible/Infrared Imager/Radiometer Suite, VIIRS (a multi-spectral imager somewhat similar to MODIS) and APS (polarimeter similar to Glory) instruments will be used to monitor regional and global change, difficult with present short duration systems. The operational aerosol products from APS on NPOESS will thus begin the routine, long-term monitoring of global aerosol conditions. Because the APS scans its IFOV along the spacecraft ground track to obtain multiple viewing angles for each scene in order to maximize its capability for aerosol retrieval, it necessarily is subject to the limitation that it does not provide the spatial coverage of an imager. However, all of the NPOESS satellites will carry the VIIRS. Using the detailed aerosol properties within a narrow swath along the ground track provided by APS, one can constrain and calibrate the VIIRS retrieval algorithm and thus expect to obtain improved aerosol retrievals over at least a portion of the wide swath of the imager. Development and demonstration of this APS and VIIRS synergy will be a goal of the Glory Mission, implemented by having the Glory spacecraft fly in formation with the NPOESS Preparatory Project (NPP) platform, which will include VIIRS.

7.4.8 Advanced PARASOL mission

The next generation observing system will learn the lessons from the POLDER and MODIS experiments. The MODIS concept is based on a moderate spatial resolution and a wide spectral range covering the visible, shortwave infrared and the thermal

infrared spectra. The moderate resolution improves dramatically the screening between aerosol plumes and clouds. The POLDER experiment clearly demonstrates that the measurement of the polarized state of the top-of-the-atmosphere upwelling radiances in several directions provides essential information on the Earth-Atmosphere system. However POLDER suffers because of a crude spatial resolution and a limited spectral range. Improvement of this concept will be devoted to the increase of the spatial resolution and the extension of the spectral range from the ultraviolet to the shortwave infrared. The expected benefits in the study of aerosols and clouds and of their interactions are given below.

7.4.8.1 Polarization in the SWIR and Aerosol Over Land

Evaluation of the aerosol load and properties over land requires an estimate of the contribution of the surface. As the atmosphere becomes more transparent at 2.1 µm, the surface reflectance can be estimated at this wavelength. As most of the polarized properties of continental surfaces do not change with wavelength this is a fairly direct and accurate estimate of the surface contribution that will be used in the inversion of aerosol properties (Figure 7-17).

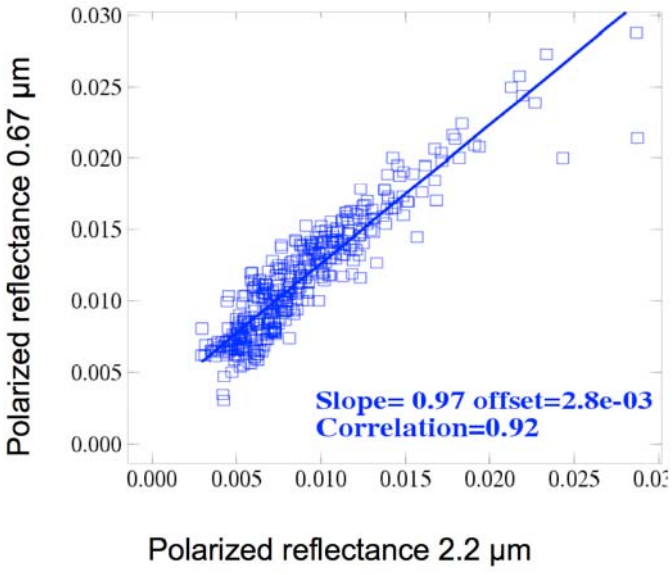

Figure 7-17. *Relationship between the polarization by surface at 2.2 µm and 670 µm for a rural area in the North of France.*

7.4.8.2 Aerosol Type

The refractive index is an intrinsic parameter related to the chemical composition of the aerosols and its degree of humidification and thus it is related to the ability of the aerosols to be efficient CCN. The real part of the aerosol refractive index strongly influences the polarization radiances, especially for aerosol belonging to the accumulation mode. This parameter can be retrieved from space if the aerosol size distribution is also accurately determined. Additional wavelengths at 1.6 and 2.1 µm enable the evaluation of the size distribution as demonstrated by the MODIS experiment. So the advanced POLDER will provide unprecedented information on the aerosol refractive index and type. This is of importance to understand the different type of aerosols that play a role in modifying cloud microphysics.

7.4.8.3 The Ice Phase and the Aerosols

Observation of the polarization induced by clouds is extremely efficient at detecting the phase of the cloud and for separating ice and liquid water phases. An additional channel in the SWIR (1.6 µm) will be used to provide a detailed description of the microphysics of the ice cloud. Thanks to an increase in the spatial resolution and a wider spectral range, it will be possible to also obtain the aerosol properties around the cloud fields. The aerosol vertical distribution is also required to understand their impact on high-level clouds. Lidar systems are the most adapted to retrieval of the aerosol and cloud altitude. Further developments using the oxygen A-band differential absorption technique are also required as this technique is promising for the retrieval of the aerosol and cloud altitude [*Vanbauce et al.*, 2003].

7.4.8.4 Cloud Droplet Size

The droplet radius of water cloud can be evaluated from the POLDER polarized measurements. This parameter can also be retrieved using the MODIS VIS and SWIR channels. The comparison of both retrievals exhibits significant differences that are not yet explained. Measuring the polarization in the VIS and the SWIR will enable a comprehensive understanding of the microphysical properties of water clouds and so enhance our capacity to understand how the aerosol can impact the cloud microphysics.

7.4.9 Aerosol and Clouds Profiling From Space

7.4.9.1 The GLAS Lidar Mission

The Geoscience Laser Altimeter System (GLAS) was launched in 2003. It is the sole scientific instrument on the Ice, Cloud, and land Elevation Satellite (ICESat). GLAS combines a precision surface lidar with a sensitive dual wavelength cloud and aerosol lidar. GLAS has 3 lasers, operating one at a time, that emit infrared and visible laser pulses at 1064 and 532 nm wavelengths. On orbit, GLAS continuously emits laser pulses at a rate of 40 per second from the Earthfacing (nadir) side of ICESat. GLAS measures precisely how long it takes for photons in a laser pulse to pass through the atmosphere to the Earth, reflect, and travel back to GLAS. Halving the total travel time, and applying corrections for the speed of light through the atmosphere, the distance from ICESat to the laser footprint on Earth can be calculated. ICESat will collect data for calculating its position in space by using onboard GPS (Global Positioning System) receivers augmented by a network of ground GPS receivers and satellite laser ranging stations. The angle of the laser beam relative to stars is measured precisely by GLAS with star-tracking cameras on the zenith side of ICESat. As ICESat orbits, GLAS takes data along ground tracks defined by the sequence of laser spots. GLAS produces a series of approximately 70 m (230 ft) diameter spots that are separated by nearly 170 m (560 ft) along track. These ground tracks will be repeated every 8 days during the commissioning phase of the mission and then every 183 days during the main portion of ICESat's multi-year mission. Though ICESat main mission is to measure polar ice, it will also provide detailed information on the vertical distribution of clouds and aerosols illuminated by its laser spots (Figure 7-18).

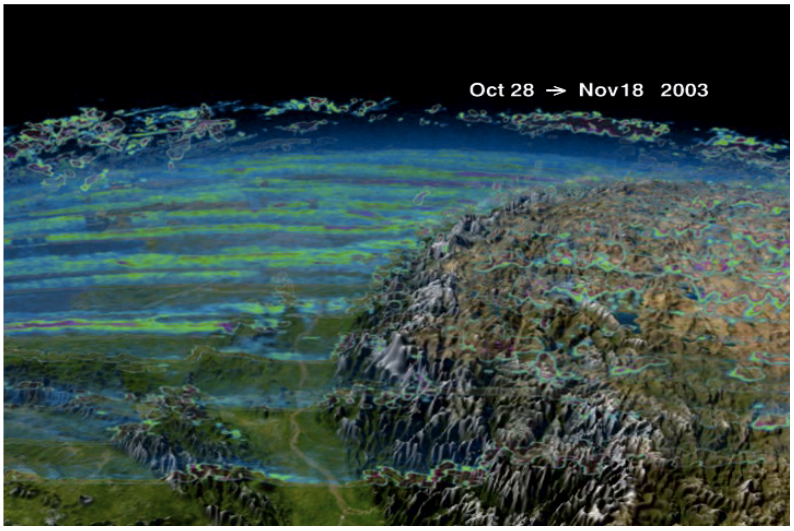

Figure 7-18. *GLAS profiles of aerosols on the region of the Himalayas. Image at (**http://icesat.gsfc.nasa.gov/images/movies/india_noclouds_dates.mpeg**).*

7.4.9.2. The Calipso Satellite Mission

The Cloud-Aerosol Lidar and Infrared Pathfinder Satellite Observation (CALIPSO) satellite, scheduled to be launched in 2006, will provide vertical distribution of aerosols and clouds (Winker et al 2003). It will continue the GLAS aerosol and cloud measurements but with emphasis on the atmospheric studies and in coordination with other measurements on the A-train set of satellites. CALIPSO will combine an active lidar instrument with passive infrared and visible imagers to probe the vertical structure and properties of thin clouds and aerosols over the globe. CALIPSO is a joint U.S. (NASA) and French (Centre National d'Etudes Spatiales/CNES) satellite mission that will fly as part of the A-train with an expected 3 year lifetime.

Retrieving the spatial and optical properties of clouds and aerosols from the CALIPSO lidar backscatter data will be confronted by a number of difficulties that are not faced in the analysis of ground-based lidars. Among these are the very large distance from the target, the high speed at which the satellite traverses the ground track, and the resulting low signal-to-noise ratios [*Winker et al.*, 2004]. To retrieve the aerosol extinction profile, the appropriate lidar ratio needs to be used in the optical

analyses of aerosol layers. Field measurements of aerosol lidar ratios show large variability from 15 sr to 120 sr and cannot be derived from the backscatter lidar. Lidar-only measurements of lidar ratios require a Raman lidar or a high spectral resolution lidar (HSRL). CALIPSO therefore determines the lidar ratios using a model-matching scheme, with the help of geophysical (e.g., latitude, longitude), and temporal (season) information. Six aerosol types are used, four of these (polluted continental, biomass burning, desert dust, and polluted dust) are derived from a comprehensive cluster analysis applied to AERONET data gathered from numerous sites from around the globe [*Winker et al.*, 2004].

Alternatively the MODIS measurements can be used to constrain the inversion of the lidar data [*Kaufman et al.*, 2003]. The combined lidar and spectral measurements can be used to sense the vertical distributions of aerosol concentrations and properties. Figure 7-19 shows the results of inversions of combined aircraft lidar and MODIS data to study the properties of smoke off the southwest coast of Southern Africa. The inversion derives profiles of the aerosol extinction due to fine and coarse particles. Comparisons with three sets of airborne in situ measurements show excellent agreement of the aerosol extinction profiles; however the lidar inversion derives smaller spectral dependence of the extinction than the in situ measurements.

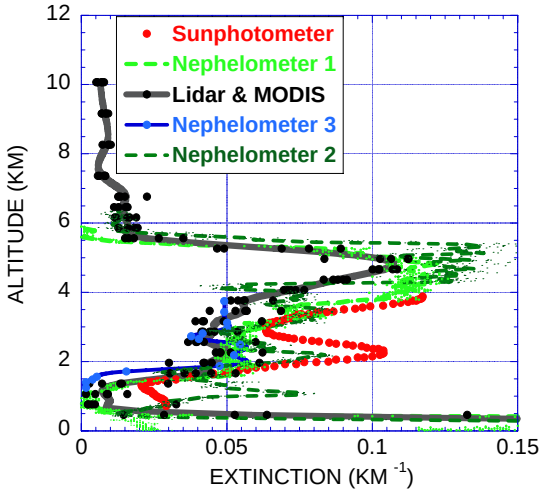

Figure 7-19. *Extinction profiles derived from the lidar & MODIS data (black), in situ nephelometer measurements (blue, light and dark green) converted to ambient extinction, airborne sunphotometer measured extinction profile (red), all for wavelength of 0.55 μm. The corrected in situ data reveal the smoke and boundary layer marine aerosol, shown in the inverted lidar-MODIS data.*

7.5 IN-SITU AND REMOTE SENSING OF PRECIPITATION

7.5.1 In-Situ Point Measurements of Precipitation

Raingauge measurements are usually underestimates of the true precipitation at the location of the instrument [*Groisman and Legates*, 1994]. Wetting on the internal walls of the gauge and evaporation of liquid within the gauge decrease measured precipitation. Wind-related undercatch is usually the largest individual error source and is particularly large for snow. For objects such as precipitation gauges mounted above the surface, wind deviates around the object yielding a pattern of turbulence and accelerated and decelerated flow [*Oke*, 1987]. The divergence of flow acts to divert lighter particles such as small drops and snow, away from the top orifice of the gauge, which decreases the precipitation falling on the gauge in comparison with what it would be at the surface if the instrument was not present [*Folland*, 1988; *Nešpor and Sevruk*, 1999]. For a given particle size, undercatch increases with increasing wind speed [*Sevruk*, 1982]. Wind effects can be lessened by applying a wind correction based on the rain rate and wind speed [e.g., *Servuk*, 1982; *Hasse et al.*, 1998], by deploying a wind shield around the instrument, by modifying the shape of the instrument [*Folland*, 1988], and by placing the instrument in an area of low wind. Wind undercatch can be eliminated by placing the instrument in a pit so that the gauge orifice is at the ground surface. For typical rainfall events in the central plains of the USA, undercatch by above-ground tipping bucket and weighing gauges compared to a pit gauge is 4-5% [*Duchon and Essenberg*, 2001]. For an extreme event in the same region with very heavy rain (200 mm/hr) and high winds (12.5 m s^{-1}) undercatch was 15% [*Duchon and Essenberg*, 2001]. A separate study intercomparing measurements among above-ground gauges found that losses related to wind, wetting, and the common practice of counting trace precipitation (<0.127 mm) as 0 mm lead to average underestimates in rainfall of 20% for Barrow, Alaska [*Yang et al.*, 1998].

The uncertainty in estimation of liquid water equivalent of snowfall is a function of wind speed, air temperature, whether a wind shield is present, and the type of wind shield and gauge [*Goodison*, 1978; *Groisman et al.*, 1991]. Errors have been estimated to be as low as 10% at wind speeds ≤ 5.5 m s^{-1} for Canadian Nipher

shielded snow gauges [*Goodison*, 1978] to several hundred percent for unshielded 8" non-recording gauges historically used by the US weather service [*Yang et al.*, 1998].

In situ rainfall measurements at sea vary in quality as a function of wind speed, instrument type and exposure, and to what degree the ship or buoy distorts the wind flow in addition to the distortion created by the instrument itself [*Yuter and Parker*, 2001].

7.5.1.1 Basic Types of In Situ Rain Instruments

Non-recording or manual rain gauges based on the bowl concept have hundreds of different designs and are still in widespread use. These instruments catch precipitation for recording by hand at regular time intervals. Measurement is performed either with the liquid in place or by pouring the contents of the gauge into a graduated cylinder. These methods yield slightly different estimates for the same catch. Depending on the length of time and the ambient environment, precipitation can be lost to evaporation before it is measured.

Different types of self-recording *in situ* rain instruments measure rainfall by myriad methods. Instruments that catch rainfall and direct it to a measuring mechanism employ a bucket on a pivot that tips when it is full (tipping bucket), the weight of collected water, the capacitance of the water within a container, and the conversion of collected water back into drops of fixed size and the counting of the formed drops [*Strangeways*, 1996]. Raindrop-induced optical scintillation is also used to estimate rain rate [*Wang et al.*, 1979]. Hot-plate sensors estimate rain and snow rates using cooling due to melting and evaporation of precipitation [*Rasmussen et al*. 2005].

Disdrometers measure precipitation droplets size distributions by counting the number of drops within each of several size categories over a time interval. Disdrometers are a ground-based analog to aircraft precipitation particle probes (Section 7.2.2) since both yield size distributions of liquid and snow particles large enough to fall ($\geq$ ~0.2 mm diameter). The size distributions are used to estimate bulk properties of the raindrop distribution including median diameter, rain rate, liquid water content, and equivalent radar reflectivity. Some disdrometers use the kinetic energy of a raindrop impact to count natural drops in specified size ranges [*Joss and Waldvogel*, 1967]. Other

disdrometers use optical methods including occultation and image processing [*Löffler-Mang and Joss*, 2000; *Fiser et al.*, 2002; *Kruger and Krajewski*, 2002; *Barthazy et al.*, 2004]. Some optical disdrometers can measure particle size and velocity simultaneously and have the capability of distinguishing among particle types in mixed rain and snow [*Löffler-Mang and Joss*, 2000; *Kruger and Krajewski*, 2002].

Self-recording precipitation measurement instruments can be ranked by their precision and latency. The smaller the detectable accumulation of rainfall, the better the instrument is at sensing low rain rates and the start and end of rainfall events. Latency is the time delay between when the rain passes through the plane of the sensing orifice and when it is registered by the instrument. Instruments such as impact or optical sensors have latency equal to their measurement time interval. Instruments with funnels to direct rainfall into the measuring mechanism have latency greater than or equal to their measurement time interval. For instruments with funnels, the percentage of rainfall lost to instrument wetting and the latency increases with decreasing rain rate. At low rain rates it may take minutes to hours for sufficient rain to accumulate and be detected by an instrument with coarse precision. The impact of precision and latency on rainfall measurement is illustrated in Figure 7-20 which shows 1 min rainfall data collected by an impact disdrometer [*Joss and Waldvogel*, 1967] with precision < 0.01 mm, a drop-forming raingauge [*Hasse et al.*, 1998] with precision of 0.1 mm, and two tipping bucket raingauges with a precision of 0.254 mm. While all four time series show the same general temporal variation in precipitation, the 1 min rain rates, storm accumulations, and storm durations differ among the instruments. The highest precision instrument yields the highest accumulation and the longest storm duration, while the coarser precision instruments yield smaller accumulations and shorter storm durations. The latency at low rain rates is visible as gaps in the tipping bucket data, and to a lesser degree the drop-forming gauge data, when the disdrometer shows light rainfall. Relative errors between raingauges and remote sensing estimates are addressed later under remote sensing systems.

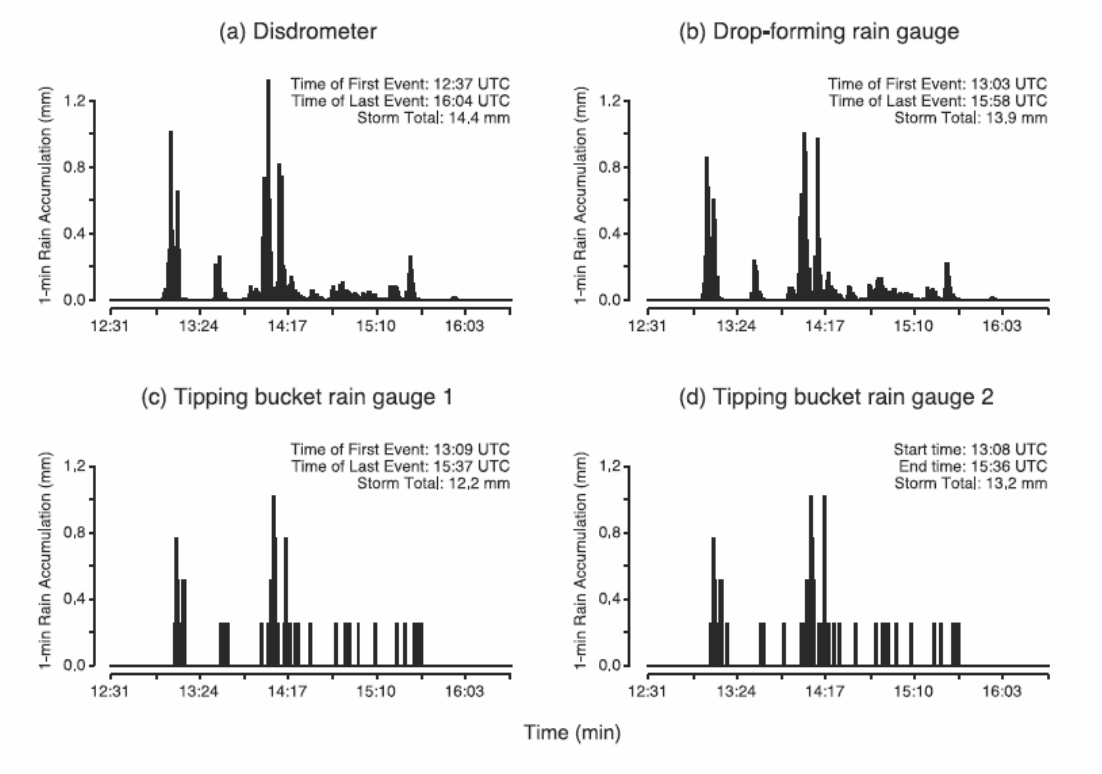

Figure 7-20. *Time series of recorded 1-min rain rates obtained from 1230-1630 UTC on 27 August 2003 from four instruments within 10 m of each other on Kwajalein Island in the Republic of the Marshall Islands. Instruments are (a) Distromet Inc. RD-69/ADA-90 impact disdrometer, (b) Eigenbrodt Inc. SRM-450 drop-form rain gauge, and (c)-(d) Qualimetrics Inc. 6011-A series 0.254 mm tipping bucket rain gauges.*

7.5.1.2 Tipping Bucket Raingauge Networks

Tipping buckets raingauges are one of the least expensive automated gauges available, and are often deployed in operational raingauge networks. These instruments have sampling limitations related to their coarse precision (0.1 mm to 0.254 mm increments of rainfall). *Habib et al.*, [2001] characterized sampling errors in 0.254 mm (0.01 in) tipping bucket gauges commonly used in the USA. They simulated tipping bucket data from a high resolution data sample obtained during summer in Iowa. Their sample was dominated by intense convective storms, typically with significant temporal variability and intermittency, and had few stratiform events. The simulation of the tipping bucket data permitted isolation of the sampling error from other instrumentation errors such as calibration and malfunctions. Sampling errors decreased with increasing time scales and were primarily related to difficulty in

capturing small temporal features of the rainfall time series. For measurements at individual tipping bucket raingauges, sampling errors were ~50% for 1 min., 30% for 5 min. and 15% for 15 min. time scales.

Additionally, tipping bucket gauges are often badly sited relative to obstructions and poorly maintained [*Strangeways*, 1996]. *Steiner et al.* [1999] highlighted problems in operational tipping bucket raingauge networks by comparing nearby gauges to each other and to a radar-derived rainfall map. Over a two year study period, *Steiner et al.* [1999] reported that none of the 30 gauges in the network covering an area of 21.4 km^2 worked 100% of the time, but that for 80% of the storms investigated ~70% of the gauges worked reasonably well. Tipping bucket raingauges were prone to malfunction due to mineral particulate and biological detritus accumulation such as dust, blown grass, pine needles, spider webs, dead insects, and bird droppings. Detritus malfunctions include partial or complete blockage of the gauge funnel leading to underestimates of rainfall.

7.5.1.3 Point to Point Spatial Variations of Precipitation

Huff and Shipp [1969] used statistical correlation methods to describe spatial variability and to define sampling requirements for raingauge networks based on data obtained during four summer seasons. Spatial correlations decay with distance at rates that vary with rain type and synoptic pattern. Spatial correlations at a given scale decrease with increasing spatial variability. For thunderstorms, they found r^2=0.98 at 1.6 km distance and 0.88 at 9.7 km distance compared to r^2=1.00 at 1.6 km and 0.98 at 9.7 km during passage of low pressure centers [*Huff and Ship*, 1969]. Spatial correlation increased for increasing storm durations up to 12 hr and then decreased [*Huff and Shipp,* 1969]. *Morin et al.* [2003] obtained similar results based on analysis of 15 summer airmass thunderstorms observed in southeastern Arizona. To measure at least 75% of explained variance between sampling points within summer storms, *Huff and Shipp's* recommended rain gauge separations of 0.5 km for 1 min rain rates and 12 km for storm totals. In comparison, typical rain gauge densities in operational networks, such as the one in California, have gauge separations of ~10 km near population centers and ~20 km in rural areas. The Global Precipitation Climatology Project of the World Climate Research Program has estimated that between 5-20 rain gauges are required per 2.5° latitude box to meet a 10% criterion for relative sampling error for monthly precipitation [*Rudolf et al.*, 1994]. This recommended rain gauge

density is met in most industrialized areas but is not met over the majority of the earth's land surface.

7.5.1.4 Point to Point Temporal Variation

The intermittence of rainfall describes its temporal variation between two points and provides information on the frequency of high spatial variability rainfall. *Krajewski et al.*, [2003] examined the probability of the concurrent occurrence of rainfall accumulation and rainy time fraction for rainy periods exceeding 0.5 mm/hr at two points separated by 1 km distance for five regions: central Florida, Oklahoma, and Iowa City, Iowa in the United States, the Island of Rota (near Guam in the west Pacific), and Ji Paraná, Rondonia, in Brazil. The fraction of total time raining was small, less than 3% in Florida, Oklahoma, Iowa, and the West Pacific, and less than 6% in Brazil. The joint occurrence of rainfall accumulations 1 km apart greater than or equal to 0.5 mm/hr for 5 min was lowest in the west Pacific location near Guam (79%) and slightly higher in Brazil (85%) and Florida (85%). Widespread precipitating clouds were more common in the mid-latitude locations resulting in higher joint probabilities in Iowa (89%) and Oklahoma (89%) compared to the tropical sites. Joint occurrence of precipitation at gauges 1 km apart increased with increasing time interval.

7.5.1.5 Representativeness Error in Areal Precipitation Estimates

A good estimate of local precipitation (± 10%) can be made at the location of a gauge when it is properly sited, calibrated, and maintained. However, most applications of rainfall mapping require areal estimates of precipitation, frequently at a basin-wide scale. The transformation of a point measurement or set of point measurements into an areal estimate requires taking into account the time and spatial variability of precipitation. Multi-gauge and gauge-radar studies of populations of storms can provide information on the typical distribution of time and spatial variability characteristics. Usually, the actual variability of rainfall around a gauge is unknown and yields an error source associated with transforming between spatial scales that is independent of the errors associated with the instrument itself.

Representativeness error occurs when observations at the native scale of the sensor are used to represent data at a different spatial scale [*Tustison et al.*, 2001]. For example, use of raingauge data, a measurement made at a scale less than 1 m^2, to

represent areal average rainfall for an area >> 1 m^2 introduces a representativeness error. Analogously, use of satellite data with a sensor spatial resolution of 20 km □30 km to represent rainfall at 5 km × 5 km scale also introduces a representativeness error. Representativeness error is independent of measurement errors at the native scale such as calibration errors. Representativeness error between gauge measurements and areal estimates is dependent on the difference in spatial scales, the smoothness of the actual rainfall field, raingauge spacing, and the method used to transform between the scales. A numerical experiment designed to isolate representativeness errors from other error sources found that representativeness error ranged from 25% to 95% of the hourly conditional mean rainfall and up to 50% of the hourly areal average rainfall for scales between 5 to 50 km [*Tustison et al.*, 2001].

7.5.2 Radar Estimation of Surface Rainfall

Weather radar [*Battan*, 1973; *Doviak and Zrnic*, 1993; *Meischner*, 2004] can provide estimates of precipitating storm location, size, and intensity over large areas and at higher spatial resolutions and time resolutions than operational raingauge networks. Ground-based scanning precipitation radars are used in short-term weather and flood forecasting, and to estimate the distribution and amount of cumulative rainfall over a region. The weather services of many countries have networks of operational radars that monitor precipitation near population centers, as well as in remote areas.

7.5.2.1 Methods and Sources of Error

Currently, radar reflectivity is the primary input to algorithms used to estimate surface rain rates. Both radar reflectivity (Z) and rain rate (R) are moments of the raindrop size distribution and can be related by a power-law of the form $Z=aR^b$ called the Z-R relation. Sources of error in radar-derived estimates of rainfall [*Austin*, 1987; *Joss et al.*, 1998; *Krajewski and Smith*, 2002; *Yuter*, 2002] include: non-meteorological echoes such as ground clutter, sea clutter, insects, birds, and anomalous propagation; instrument noise, absolute calibration, beam blockage, changes in the vertical profile of precipitation from the height of the radar beam to the surface, signal enhancement by melting particles or hail, attenuation, presence of downdrafts, and variations in the drop size distributions (manifested as variations in the Z-R relation). Different operational and research radar groups producing rain maps have different methods to mitigate these errors. Most apply some method of quality control to remove non-

meteorological echo as an initial step. Some rain-map products use a mean field bias adjustment [*Amitai et al.*, 2002, *Gjertsen et al.*, 2004] to address multiple error sources simultaneously while others address individual sources of error independently [*Joss et al.*, 1998; *Zawadzki and Bellon*, 2003; *Houze et al.*, 2004]. The use of polarimetric radar variables for quantitative rainfall estimation mitigates some error sources such as attenuation and the presence of hail. Hybrid methods using a combination of reflectivity and polarimetric variables as input are being developed and evaluated [e.g., *Bringi and Chandrasekar*, 2001; *Illingworth*, 2004] and are planned for operational deployment in several countries later this decade.

7.5.2.2 Quantification of Errors in Radar-Rainfall Estimates

The weather service of Switzerland, MeteoSwiss, has a comprehensive program to quantify errors in surface precipitation estimates and, based on those empirical results, to refine quantitative rainfall products from their radar network [*Joss et al.*, 1998; *Germann and Joss*, 2004]. Precipitation estimation in mountainous terrain has additional challenges compared to flat terrain. Gauge observations in mountains have large uncertainties associated with wind, snow-drift, and small-scale spatial variability. Radar observations are prone to both strong ground clutter and beam shielding by mountains. The historical data analysis and algorithm refinements by MeteoSwiss (Table 7-1) illustrate several important points. A particular algorithm refinement may improve some statistics but degrade others. To improve the statistics across the board, a combination of refinements was needed including: rigorous elimination of clutter, correction for the vertical profile of precipitation between the altitude of radar measurement and the ground surface, hardware calibration to insure reproducibility of measurements, and long-term adjustment to independent data to minimize bias. These data also provide information on the residual relative error for daily rainfall between raingauge and the average of nine 1 km^2 radar pixels centered over the gauge when primary sources of error in radar rainfall mapping have been minimized. For 2004 storms with daily rainfall > 0.3 mm, probability of detection is 0.89 and false alarm rate is 0.14. For 2004 storms with daily gauge rainfall≥ 0.3 mm, average bias for over all of Switzerland (41,290 km^2) is -11% and scatter is 3 dB(R). The scatter refers to the spread of daily radar/gauge ratios when pooling all rainy days and gauge stations over all of Switzerland together. For example, 3.0 dB(R) scatter in summer 2004 means that the radar-derived estimate of daily precipitation at a gauge

location is within a factor of 2 of the gauge estimate for 68% of the rainy days, for the remaining 32% theuncertainty is larger. Uncertainties decrease closer to the radar. Within 70 km from a radar, scatter decreases to a factor of 1.4. For winter of 2004, average bias over Switzerland is -3% and scatter is 3.9 dB(R) or a factor of 2.5. These relative errors are a result of the superposition of gauge and radar uncertainties and hence the values in Table 7.5.1 are overestimates of the true uncertainty of the radar estimates [*Germann et al.*, 2006].

Table 7-1. *Relative errors between MeteoSwiss RAIN product for daily radar-derived rainfall and daily raingauge totals for summer season in Switzerland. The radar data are averaged over nine 1 km^2 pixels centered on 58 gauge locations including 19 gauges used for long-term adjustment. Bias and scatter statistics based on events with daily gauge rainfall ≥ 0.3 mm. Probability of Detection (POD, perfect score = 1) and False Alarm Rate (FAR, perfect score = 0) based on events with daily rainfall > 0.3 mm. Adapted from Germann et al. (2006).*

Year	Bias (dB)	Bias (%)	Scatter (dB)	Scatter (factor)	POD	FAR
1997	-2.4	-43	4.0	2.5	0.84	0.34
1998	-1.2	-23	4.0	2.5	0.87	0.30
Changes in operational clutter elimination						
1999	-4.2	62	4.8	3.0	0.73	0.08
2000	-3.2	52	4.4	2.8	0.74	0.11
Introduction of profile correction						
2001	-4.1	61	3.0	2.0	0.75	0.08
Long-term adjustment and modification of profile correction						
2003	0.2	5	3.4	2.2	0.89	0.18
Long-termadjustment modification						
2004	-0.5	-11	3.0	2.0	0.89	0.14

Steiner et al., [1999] examined relative errors of 1 km^2 radar-derived rainfall compared to tipping bucket raingauges within a network of 30 raingauges within the Goodwin Creek watershed (21.4 km^2) in Mississippi, USA. For heavy rain events with rainfall accumulations >10 mm, the root mean square errors of storm total rainfall between radar and raingauges were 10% to 40% when using the subset of

raingauges passing quality control and up to 80% when all gauges in the network were included. For storms with rainfall accumulations <10 mm, uncertainties are expected to be higher.

Amitai et al. [2002] found average relative errors of 20% between monthly tipping bucket rain gauge accumulations and 4 km^2 radar-derived rainfall accumulations over the gauge locations for August-September 1998 in Melbourne, FL. The 15 gauges were part of a dense rain gauge network of 10 km^2 area within 35 km range of the radar. They found that the average difference between the radar estimate over the gauge and the gauge accumulation was the same order as the differences between point rainfall measurements within the same 4 km^2 radar pixel.

Houze et al. [2004] used data from two rainy seasons at Kwajalein Atoll, Republic of the Marshall Islands, to estimate the magnitude of several independent components of radar-derived rain-map uncertainty under tropical oceanic conditions. Underlying assumptions regarding radar calibration, vertical profile correction, the Z-R relation, and missing data were varied within empirically determined bounds and their impact was assessed on the resulting monthly areal mean rainfall accumulation based on 4 km^2 pixels averaged over a ~7 x 10^4 km^2 area (between 17 km and 150 km range from the radar). The largest individual source of uncertainty was the absolute calibration of the radar, which was estimated at ±30% based on the practical limit of ±2dB(Z) on reflectivity calibration using several methods in the Kwajalein setting. The next largest source of uncertainty (±10 - 15%) was associated with the correction for the vertical profile of precipitation from the altitude of the radar beam to surface. Since the radar beam altitude varies with range, this correction is largest for pixels at farthest ranges. Uncertainties in the Z-R relation based on disdrometer data accounted for only ±5% uncertainty and small number of data gaps when the radar was not operational had associated uncertainty of < ±2%. A total uncertainty in monthly areal average mean rainfall of 50% was estimated by adding the individual error sources.

7.5.3 Satellite Estimation of Surface Rainfall

Weather satellites in geosynchronous orbit (36,000 km altitude) and low earth orbit (typically 250-1000 km altitude) use remote sensing measurements to estimate

precipitation at the earth's surface. The primary methods are infra-red (IR), passive microwave, and radar (active microwave). None of these methods measure rain rates directly. Rather, the satellite observed physical characteristics of precipitating clouds are used as inputs to algorithms of varying complexity to retrieve surface rainfall.

7.5.3.1 Satellite Precipitation Retrieval Algorithms

Methods to estimate precipitation from geosynchronous IR satellite data are based on empirical relations between area fraction of cold cloudiness and areal average rainfall. These methods decompose the areal average rainfall into a rainfall area estimated by satellite and a mean conditional rain rate estimated by independent measurements. In a series of studies [*Arkin*, 1979; *Richards and Arkin*, 1981; *Arkin and Meisner*, 1987], *Arkin* and his collaborators refined empirical relations between IR cloud temperatures and areal-average surface rainfall accumulation estimated from an array of four shipborne radars using data sets collected in the eastern tropical Atlantic. The best correlations (r^2=0.8) were found for the largest spatial scale (2.5° ×2.5°) and temporal scale (1 day) they examined. Correlations between rainfall area and IR cold cloudiness are very poor (r^2=0.05) for instantaneous data at 240 km scale [*Yuter and Houze*, 1998]. The GOES Precipitation Index (GPI) algorithm [*Arkin and Meisner*, 1987] defines areal average precipitation as the product of the mean fractional cloudiness in a 2.5° x 2.5° box lower than an IR temperature threshold, the time interval in hours, and a mean conditional rain rate in mm/hr. Based on data from the tropical eastern Atlantic and South America, they recommended a temperature threshold of 235K, and a mean conditional rain rate of 3 mm/hr for the tropics. A temperature threshold of 220K was recommended for the extratropics based on comparisons over the continental USA. Comparisons between GPI estimates and independent estimates over land using raingauges and radar show that GPI reproduces the occurrence of deep convective rainfall well but is less successful at estimating the intensity of rainfall [*Arkin and Meisner*, 1987; *Janowiak*, 1992].

Multispectral rainfall algorithms designed for geosynchronous satellites [e.g. *Ba and Gruber*, 2001] often follow a similar methodology to GPI by decomposing rainfall into the probability of detectable rain and a mean rainfall rate but utilize IR as well as visible, near infrared, and water vapor channels. Multispectral methods exhibit improved detection of rainfall from lower altitude (higher temperature) cloud tops as

compared to IR-only methods. A limitation of these algorithms is that the visible channel is available only during the day.

Satellite passive microwave precipitation estimation techniques utilize the modification of surface upwelling radiation by precipitation [*Spencer et al.*, 1983, *Wilheit*, 1986]. Microwave brightness temperatures are the result of the column scattering and absorption properties of precipitation, cloud, and water vapor. Observed brightness temperatures are dependent on the particular hydrometeor types and their mixing ratios within the column and the frequency of the sensor. Between 22 and 60 GHz both scattering and absorption are important and either may dominate depending on the specific situation. Below 22 GHz, absorption, primarily by liquid water, dominates. Above 60 GHz, ice scattering dominates. Scattering by precipitation is detectable over both water and land. Surface water has low emissivity at microwave frequencies and thus presents a cold background, which makes the small increase in brightness temperature associated with absorption by precipitation detectable. Land has larger and variable emissivities and presents a much warmer background against which the absorption signal is difficult to detect unambiguously [*Wilheit*, 1986]. As a result, passive microwave precipitation retrievals weight the input frequency channels differently over oceans and land.

Passive microwave algorithms address the problem of relating brightness temperatures (column measurements) to surface rainfall (the flux at the bottom of the column) using some combination of "empirical" and "physically-based" methodologies [*Smith et al.*, 1998]. Empirical algorithms [e.g., *Liu and Curry*, 1992; *Ferriday and Avery*, 1994] derive a statistical regression between measured brightness temperatures at several frequencies and ground-based measurements of rainfall (radar and/or raingauge network). Physically-based algorithms [e.g., *Kummerow*, 1998; *Bauer*, 2001] use cloud models to simulate the three-dimensional water vapor, cloud, and precipitation properties of storms, which are in turn used as input to forward radiative transfer calculations to estimate brightness temperatures. The cloud model and radiative transfer calculations yield a database associating sets of brightness temperatures with different precipitation structures and surface rainfall rates.

Error sources in both empirical and physically-based passive microwave estimates [*Tesmer and Wilheit*, 1998; *Bauer et al.*, 1999; Harris *and Foufoula-Georgiou*, 2001; *Olson et al.*, 2001] are related to the three-dimensional precipitation structure and include uncertainties in the depth of the rain layer, mixing ratio profiles of cloud water, water vapor, and super-cooled precipitable water, the radiative characteristics of mixed phase layers such as wet aggregates in the melting layer, the natural variability of the profile of particle size distributions, and inhomogeneities of the rainfall pattern at scales smaller than the sensor field of view.

Intercomparison of different passive microwave precipitation retrieval algorithms using the same input data set revealed a bias uncertainty between estimates of ±30% [*Smith et al.*, 1998]. Differences among algorithms were partitioned into those associated with rainfall detection (rain area) and those associated with the conversion from brightness temperature to rain rate (rain intensity). For oceanic regions, detection differences mainly affected light rainfall regions that did not contribute significantly to area average rain rates. Over the ocean, the largest contribution to relative error among algorithms was the weighting of the input frequency channels which impacts how intense rain rates were calculated and the maximum allowable rain rate. In contrast, over land rainfall detection was the dominant factor in producing differences among the algorithms.

The Tropical Rainfall Measuring Mission (TRMM) satellite, a successful collaborative effort between the U. S. and Japanese space agencies, has as one of its sensors the first spaceborne precipitation radar (PR) [*Kummerow et al.*, 1998]. The PR operates at K_u-band (2.3 cm) and yields reflectivity profiles at satellite-relative orientations from nadir (0°) to ±17°, yielding earth-relative vertical resolutions of 250 m to 1500 m. Unlike operational weather radars operating at S-band (10 cm) and C-band (5 cm), the K_u-band signal is strongly attenuated by rainfall. The signal attenuation is cumulative downward and is largest near the earth's surface. An attenuation correction must be applied to the near-surface reflectivity (Z) values before a meaningful transformation to surface rainfall (R) can be made. There are currently several methods to estimate total path-integrated attenuation and to distribute the attenuation correction in the vertical [*Meneghini and Kozu*, 1990; *Iguchi*

et al., 2000]. Independent evaluation and error diagnosis of attenuation correction methods applied to satellite radar data has proven to be difficult. Error sources in the estimation of surface precipitation from an attenuated reflectivity profile include many of the same error sources in passive microwave algorithms. The set of passive microwave sensors on the TRMM satellite are referred to as the TRMM Microwave Imager (TMI). Zonal averages of areal average precipitation derived from TRMM TMI and PR at native sensor resolution exhibit relative differences of 20-40% [*Kummerow et al.*, 2000].

Multi-satellite products attempt to combine the strengths of different types of satellite sensors to mitigate their individual weaknesses. Several multi-satellite products use variations of the GPI algorithm [*Janowiak and Xie*, 1999; *Huffman et al.*, 2001; *Kuligowski*, 2002. IR cloud top temperatures from geosynchronous satellites are used to determine rain areas at high temporal resolution. The IR temperature threshold and average conditional rain rate are adjusted for designated time and spatial scales using some combination of global passive microwave data and raingauge data over land. Comparisons between dense gauge networks over land to these types of multi-satellite products show similar results to those products using IR data alone, they perform better in deep convection typical of the warm season than in shallower convection typical of the cool season, and tend to perform poorly over complex terrain regardless of season [*Arkin and Meisner*, 1987; *Huffman et al.*, 2001].

Global satellite observations, raingauge areal estimates, and numerical model outputs are merged to create monthly analyses as part of the Global Precipitation Climatology Project [*Huffman et al.*, 1997, *Adler et al.*, 2003) and the Climate Predication Center Merged Analysis of Precipitation [*Xie and Arkin*, 1997]. The value of merged products is based on the assumption that the combination of several estimates with unknown errors is closer to the truth than any single estimate. Analogous to ensemble numerical forecast modeling, this assumption holds if the individual estimates are distributed around the true value.

7.5.3.2 Uncertainties Associated With Satellite Temporal Sampling

Common to all satellite precipitation estimates are uncertainties related to estimating temporal average precipitation (e.g., daily, 5-day, monthly) from the nearly instantaneous samples for a given area obtained by satellite. Depending on storm

duration, structure, and stage of evolution, a single snapshot of a storm has varying value as a representative sample of the storm temporal and spatial average. *Steiner et al.* [2003] utilized a set of operational radar network composites over the United States central plains during summer as a baseline data set to investigate errors associated with different satellite temporal sampling schemes. The radar composite had a spatial resolution of 2 km and a temporal resolution of 15 min. These data were subsampled at 1-, 3-, 6-, 8-, and 12-h intervals and averaged over 100-, 200-, and 500-km spatial scale domains. The uncertainty associated with discrete temporal sampling varies directly with sampling time interval and inversely with rainfall rate and space and time domain size.

Although summer-time rainfall in the United States central plains has different characteristics than rainfall in other seasons and at other locations, the uncertainty values in the *Steiner et al.* [2003] study provide guidance on the magnitude of errors due only to satellite temporal sampling. Based on *Steiner et al.'s* calculations for a 100 km scale domain with areal average rainfall of 0.1 mm hr^{-1}, median rainfall sampling uncertainty for daily rainfall is 10% for 1 hour, 43% for 3 hour, 92% for 6 hour, and 154% for 12 hour sampling time intervals. The uncertainties decrease for 500 km scale to 3% for 1 hour, 11% for 3 hour, 31% for 6 hour and 61% for 12 hour. Current geosynchronous satellites sample IR full-disk images at 1 to 3 hour intervals. The temporal sampling of individual low-earth orbit satellites such as TRMM is dependent on the details of the orbit and latitude. TRMM Precipitation Radar revisit times over an area of 120 km radius vary from 78 hours at the equator to 17 hours at 35 deg latitude. A set of low-earth orbit satellites with similar passive microwave sensors can be utilized as a group to obtain temporal sampling intervals of ~6 hour in the tropics (30°S to 30°N) decreasing to ~3 hour at latitudes above 60° [*Turk et al.*, 2003].

Since satellite algorithm retrieval errors are strongly dependent on the details of the three-dimensional precipitation structure, these errors vary with regional and seasonal changes in precipitation structure. It would be useful to isolate errors in the satellite retrieval algorithm from errors related to temporal sampling, differences in spatial scale, and differences in minimum detectable rain rate that are a function of the sensitivity of the sensor. In practice, this is difficult since the different types of

sensors on the current generation of satellites were not designed to have matching spatial resolutions or sensitivity.

7.5.3.3 Future Satellite Precipitation Measurements

The proposed joint US and Japanese space agency Global Precipitation Measurement (GPM) Mission builds on the success of TRMM to address the critical need for a more comprehensive global precipitation measuring program. The GPM Mission consists of a Core satellite similar to TRMM and a constellation of internationally contributed multichannel passive microwave satellites. The GPM Core satellite will be used as a calibration reference for moderate to heavy rainfall for the constellation satellites. Additionally, the replacement of the single frequency Ku radar used on TRMM with a dual frequency radar (Ku/Ka) with improved sensitivity on the GPM Core satellite provides the ability to estimate bulk properties of the rain drop size distribution and to improve the attenuation-corrected vertical profile of reflectivity and rain rate using differential attenuation methods. An additional satellite, EGPM, proposed to the European space agency will carry a multichannel radiometer and Ka-band radar. The higher sensitivity of the Ka-band radar on EGPM (~5 dBZ) compared to the GPM Core satellite Ka radar (~12 dBZ) and higher orbit inclination for EGPM (90 deg) versus GPM (65 deg) are designed to optimize observations of light rainfall and light to moderate snowfall. Analogous to GPM Core satellite, the EGPM satellite will be used as a calibration reference for light rainfall and snow for the passive microwave constellation satellites. The full set of satellites associated with the GPM mission--GPM core, EGPM, and the constellation satellites will be used together to improve the frequency and quality of global precipitation estimates (Figure 7-21).

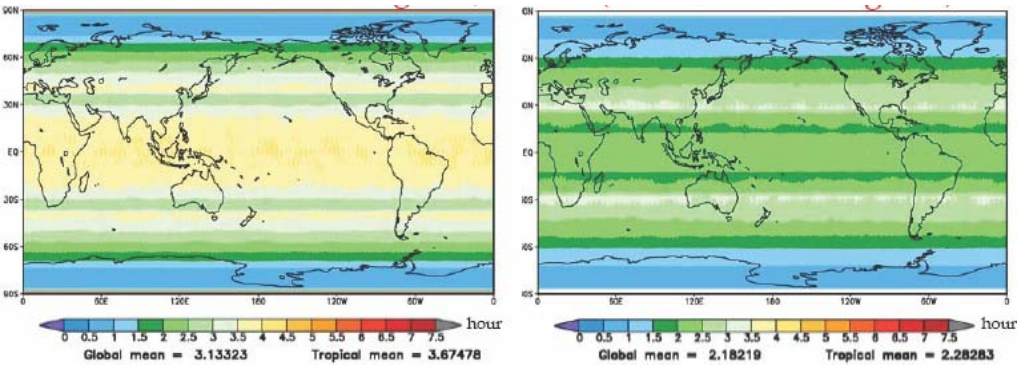

Figure 7-21. *Revisit times of satellite passive microwave radiometers. (left) Current sampling by TRMM, Aqua, and DMSP F13, F14 and F15 satellites yields < 3h sampling over 35% of the globe and < 4 h sampling over 57% of the globe. (right) Best-case scenario sampling in GPM-era based on planned orbits of GPM-core, NASA-90°, GCOM-W, EGPM, and 3 NPOESS satellites would yield < 3 hr sampling over 96% of the globe. (NASA, Goddard Space Flight Center).*

7.5.4 Discrepancies Among Different Methodologies

One of the most extensively analyzed data sets of recent years is from the Tropical Ocean Global Atmosphere Coupled Ocean Atmosphere Response Experiment (TOGA COARE) [*Webster and Lukas*, 1992], which took place in the western Pacific warm pool region from November 1992 to February 1993. The TOGA COARE intensive flux array (IFA) had an area of ~2.25 □ 10^5 km^2. Areal average daily rainfall estimates for the IFA (Table 7-2) were obtained using many different methods for estimating surface rainfall [*Johnson and Ciesielski*, 2000; *Weller et al.*, 2004]. Values varied from 5.4 mm/day for the shipborne radars to 9.3 mm/day for a merged gauge/satellite method. Discrepancies are a function of differences in subregion examined, temporal sampling, and spatial resolution of the rainfall estimates [*Weller et al.*, 2004]. These differences make it difficult to isolate errors associated with specific techniques or to determine the best estimate. For example, *Johnson and Ciesielski* [2000] showed that part of the reason the ship radar data estimate was lower than the other estimates was that the ships were not present for some of the heavier precipitation events during the study period, and that one of the two radar ships was stationed in a precipitation minimum.

Table 7-2. *TOGA COARE intensive flux array intensive observation period estimates of areal average daily rainfall using different techniques. "Sat/mixed" (Curry et al., 1999) utilized a combination of passive microwave brightness temperatures and visible and IR radiances from geosynchronous and low-earth orbiting satellites. "CMAP" refers to the CPC Merged Analysis of Precipitation of raingauge, IR and microwave satellite estimates (Xie and Arkin, 1997). Adapted from Johnson and Ciesielski (2000) and Weller et al. (2004).*

Method	Rainfall estimate (mm/day)	Citation
Atmospheric moisture budget-multiquadratic technique	8.2	*Johnson and Ciesielski (2000)*
Atmospheric moisture budget-Barnes scheme	5.6	*Johnson and Ciesielski (2000)*
Ocean freshwater budget (near ship)	8.0	*Feng et al. (2000)*
Shipborne radar (2 km resolution within 145 km of ships)	5.4	*Short et al. (1997)*
Sat/Mixed	8.3	*Curry et al. (1999)*
CMAP	9.3	*Johnson and Ciesielski (2000)*
NCEP T62 reanalysis (210 km resolution)	8.4	*Johnson and Ciesielski (2000)*
ECMWF T106 reanalysis (125 km resolution)	6.7	*Johnson and Ciesielski (2000)*

Attempts to intercompare monthly global estimates of precipitation [e.g., *Adler et al.*, 2001] have suffered similar problems to the TOGA COARE rainfall comparisons. The impacts of differences in temporal sampling and spatial scales of the input sensor data are not usually removed. As a result, the factor of 2 to 3 differences among different satellite retrievals and ground-based observations [*Adler et al.*, 2001] are difficult to diagnose in terms of specific algorithm or measurement system deficiencies. Estimates tend to cluster based on input data type and hence similar temporal and spatial sampling [*Ebert et al.*, 1996]. Inclusion of all available operational data sets into blended or merged products limits opportunities for comparison to truly independent estimates.

The International Precipitation Working Group (IPWG) was established in 2001 as a permanent working group of the Coordination Group for Meteorological Satellites (CGMS) and is co-sponsored by CGMS and the WMO. The IPWG validation/intercomparison project provides standardized web-accessible

intercomparisons over Australia, the continental US and Europe between daily precipitation estimates from rain gauge and radar networks and a variety of operational and semi-operational satellite algorithms and numerical weather prediction models [*Ebert*, 2004, *Ebert et al.*, 2006]. Example daily statistics aggregated over two 3 month periods between the 0.25° operational rain gauge analysis for Australia [*Weymouth et al.*, 1999] and a GPI algorithm, a merged multi-satellite algorithm, and the ECMWF forecast are shown in Table 7-3. Performance of both satellite algorithms is better during the December-February period corresponding to the wet season in tropical northern Australia as compared to the dryer June-August period. No one method performs best across all statistics for both the dry and wet seasons.

Table 7-3. *Aggregate daily statistics from IPWG intercomparison from 1 Dec 2003 – 29 Feb 2004 and 1 June 2004-31 August 2004. Statistics shown were compiled over land areas based on estimates of the daily accumulation from a GPI algorithm, a NASA TRMM 1 hourly multi-satellite product (3B41RT, Huffman et al. 2003), and the ECMWF 36 hour forecast for 24 hr precipitation accumulation compared to the Australian national rain gauge network. Spatial scale of intercomparison is 0.25° for all products. Data courtesy of E. Ebert.*

	GPI	TRMM Multi-sat	ECMWF forecast	GPI	TRMM Multi-sat	ECMWF forecast
	Dec – Feb	Dec – Feb	Dec – Feb	June – August	June-August	June-August
Ratio of Estimated to Observed Average Volume	1.18	1.08	0.74	0.38	0.55	0.75
Bias Score	0.97	0.69	0.91	0.22	0.31	0.80
POD	0.71	0.56	0.73	0.13	0.16	0.69
FAR	0.26	0.19	0.19	0.41	0.49	0.13
Mean Absolute Error (mm/d)	4.0	3.9	2.8	0.66	0.89	0.39
RMS Error (mm/d)	9.0	10.7	7.5	2.6	4.0	1.4

7.6 CONCLUSIONS

Even though we clearly see in measurements and in simulations the strong effect that aerosol particles have in cloud microphysics and development, we are not sure what is the magnitude or direction of the aerosol impact on precipitation and how it varies with meteorological conditions. The reasons behind this difficulty are the result of:

- The limited accuracy of the measurements:

Quantitative radar measurements of precipitation can be off by up to a factor of 2 for daily rainfall and spatial scales ≤ 50 km.

Measurements of the cloud droplet size from satellites are biased by up to 30% for convective clouds, due to departure of the clouds from the plane parallel model. However we can still measure the relative change of cloud properties with change in aerosol concentrations.

Aerosol column optical thickness measured from satellites is not accurate enough: accuracy is ±20% over the oceans, less accurate over vegetated land, deserts or urban areas. Ground based remote sensing of aerosol can have a high precision of ±0.02 in units of aerosol optical depth.

Translation of the optical thickness into the column aerosol concentration and into CCN is difficult due to variation in the aerosol size distribution and chemical composition and the vertical distribution of the aerosols and thermodynamic conditions.

In situ measurements from aircraft may influence the aerosol and cloud properties, and have limitations in correctly sampling all aerosol and cloud droplets sizes. Surface based measurements may not always represent the total column or at the cloud altitudes.

- Small spatial and temporal coverage for highly variable parameters:

High spatial and temporal variability of precipitation and aerosols makes it difficult to measure coincidental aerosol, clouds and precipitation. Therefore we are not aware of studies that include direct statistical correlations of aerosol and precipitation.

Cloud properties have a diurnal cycle not well represented by satellite observations. Geostationary satellite measure the diurnal cycle but with limited ability to derive the cloud droplet size.

- Cause and effect:

Once a statistical connection is established between the aerosol concentration, the cloud properties and precipitation, it is still difficult to assess whether the changes in the precipitation patterns are a result of the aerosol impact or whether it is changing of the local meteorological conditions that affect the aerosol properties and the precipitation. Therefore, it is clear that even the most informative measurements so far on the effect of aerosols on precipitation do not include simultaneous quantitative measurements of aerosols, precipitation and meteorological parameters.

CHAPTER 8: DELIBERATE CLOUD SEEDING EXPERIMENTS AND MODELING STUDIES

Lead Authors: William Cotton, Roelof T. Bruintjes,

Co-authors: Deon Terblanche, Peter V. Hobbs, Arthur L. Rangno, Zev Levin

8.1 INTRODUCTION

It is beyond the scope of this report to carryout a comprehensive assessment of attempts to modify precipitation by deliberate cloud seeding. However, such experiments, in which specific types of particles are injected into clouds generally with the goal of increasing precipitation, can shed light on important aspects of the modification of precipitation by particles. Therefore, we provide here a brief assessment of the current status of experiments to modify precipitation by deliberate cloud seeding. Deliberate cloud seeding experiments can be divided into two broad categories: *glaciogenic seeding*, in which ice-producing materials (e.g., dry ice [solid CO_2], silver iodide, liquid propane, etc.) are injected into a supercooled cloud for the purpose of stimulating precipitation by the ice particle mechanism (see Section 4.2.2). The underlying hypothesis for glaciogenic seeding is that there is commonly a deficiency of natural ice nuclei and therefore insufficient ice particles (~1/liter at –20ºC) for the cloud to produce precipitation with maximum efficiency by the ice particle mechanism.

The second category of artificial seeding experiments is referred to as *hygroscopic seeding*. In the past this type of seeding was usually used for rain enhancement from warm clouds. However, more recently, and as will be discussed later, this type of seeding has been applied to mixed phase clouds as well. The goal of this type of seeding is to increase the concentration of *collector drops* (again to ~1/liter) that can grow efficiently into raindrops by collecting smaller droplets and by enhancing the formation of frozen raindrops and graupel particles. This is done by injecting into a cloud (generally at cloud base) large or giant hygroscopic particles (e.g., salt powders) that can grow rapidly by the condensation of water vapour to produce collector drops (see Section 4.2.1).

8.2 STATIC GLACIOGENIC SEEDING EXPERIMENTS

Static cloud seeding experiments refer to the use of glaciogenic materials to modify the microstructures of supercooled clouds and precipitation. Many hundreds of such experiments have been carried over the past 50 years or so. However, most of these experiments need not concern us here since they have provided little useful information, because of poor design, inadequate supporting measurements, and/or poor post analysis. For example, operational cloud seeding experiments (many of which are still being carried out around the world) rarely provide sufficient information to decide whether or not they modified either clouds or precipitation. At the other end of the scale, well designed scientific experiments provide extensive measurements that can be analyzed to determine if artificial seeding modified cloud structures and, if the seeding was randomized, the effects of the seeding on precipitation can be analyzed statistically with a quantitative level of significance assigned to any changes in precipitation attributed to the seeding. To attain a level of significance (p^*) large enough to be reasonably assured that the seeding affected precipitation (say, $p > 0.05$), many years of experimentation may be necessary. For firm "proof"[see NRC, 2003; *Garstang et al.*, 2005] that seeding affects precipitation, *both* strong physical evidence of appropriate modifications to cloud structures and highly significant statistical evidence is required. Until recently it has generally been agreed that only a few cloud seeding experiments have satisfied these criteria: for example, the Climax Experiments carried out in Colorado by scientists from Colorado State University (CSU), and the Israeli Experiments carried out by scientists from the Hebrew University of Jerusalem (HUJ).

8.2.1 Winter Orographic Randomized Cloud Seeding Experiments

A series of three important and apparently successful randomized cloud seeding experiments took place at Climax, near Fremont Pass, Colorado (referred to as *Climax I* and *Climax II*), Colorado, during the 1960s. The investigators reported stunning results: increases in precipitation of 50% and more were reported on favorable days [e.g. *Grant and Mielke*, 1967; *Mielke et al.*, 1970, 1971], and the results were widely viewed as demonstrating the efficacy of cloud seeding (e.g., National Academy of

[*] A p value of >0.05 indicates that the odds are better than 20 to 1 against the increase in precipitation occurring in the absence of artificial seeding.

Sciences, 1973; *Sax et al.*, 1975; *Tukey et al.*, 1978a,b; American Meteorological Society, 1984), even by those most skeptical of cloud seeding claims (e.g., *Mason*, 1980, 1982).

Lending credibility to the statistical results the Colorado Investigators proposed plausible physical conceptual models of why seeding should increase snowfall. Nonetheless, *Hobbs and Rangno* [1979], *Rangno and Hobbs* [1987; 1993] question both the randomization techniques and the quality of data collected during those experiments and conclude that the Climax II experiment failed to confirm that precipitation can be increased by cloud seeding in the Colorado Rockies. Even so, *Rangno and Hobbs* [1987] did show that precipitation may have been increased by about 10% in the combined Climax I and II experiments. This should be compared, however, to the original analyses by *Grant et al.* [1967], *Grant and Kahan* [1974], *Grant and Elliott* [1974], *Mielke et al.* [1971], *Mielke et al.* [1976] and *Mielke et al.* [1981] which indicated greater than 100% increase in precipitation on seeded days for Climax I and 24% for Climax II. Subsequently, *Mielke* [1995] responded and explained a number of the criticisms made by *Rangno and Hobbs* in regard to the statistical design of the experiments, in particular the randomization procedures, the quality and selection of target and control data and the use of 500 mb temperature as a partitioning criteria as part of the statistical evaluation. It is clear that the design, implementation, and analysis of this experiment were a learning process not only for meteorologists but statisticians as well.

The results of the many re-analyses of the Climax I and II experiments have clearly "watered down' the overall magnitude of the possible increases in precipitation in wintertime orographic clouds. Furthermore, they have revealed that many of the concepts that were the basis of the experiments are far too simplified compared to what we know today. Furthermore, many of the cloud systems seeded were not simple 'blanket-type orographic clouds" but were part of major wintertime cyclonic storms that pass through the region. As such, there was a greater opportunity for ice multiplication processes and riming processes to operate in those storms, making them less susceptible to cloud seeding.

Two other randomized orographic cloud seeing experiments, the Lake Almanor Experiment [*Mooney and Lunn*, 1969] and the Bridger Range Experiment (BRE) as reported by *Super and Heimbach* [1983] and *Super* [1986] suggested positive results. However, these particular experiments used high elevation AgI generators, which increase the chance that the AgI plumes get into the supercooled clouds. Moreover, both experiments provided physical measurements that support the statistical results [*Super and Heimbach*, 1983;1988]. Using trace chemistry analysis of snowfall for the Lake Almanor project, *Warburton et al.* [1995a] found particularly good agreement with earlier statistical suggestions of seeding-induced snowfall enhancement with cold westerly flow. They concluded that failure to produce positive statistical results with southerly flow cases was likely related to miss-targeting of the seeded material. Targeting of seeding material with ground-based seeding of winter orographic clouds depends on boundary layer transport and dispersion of the seeding material [*Bruintjes et al.*, 1995]. Strong inversions can trap the seeding material (especially with valley based generators) in the valleys preventing it from becoming entrained into the clouds in the higher terrain. Chemical analysis of chemical tracers in snow that are concurrently released with the seeding material [*Warburton et al.*, 1995] have revealed that most of the precipitation falling in the targets during seeded periods does not contain seeding material. These two randomized experiments strongly "suggest" that higher elevation seeding of orographic clouds in mountainous terrain can produce meaningful seasonal snowfall increases.

There have been a few attempts to use mesoscale models to evaluate cloud seeding programs. Recently, *Cotton et al.* [2006] applied the Colorado State University Regional Atmospheric Modeling System (RAMS) to the simulation of operational cloud seeding in the central Colorado mountains in the 2003-2004 winter season. RAMS was run with 3km grid spacing covering all the target area and much of the surrounding mountainous terrain. The model included explicit representation of surface generator production of AgI at the locations, burn rates, and times supplied by the seeding operator. Moreover, the model explicitly represented the transport and diffusion of the seeding material, its activation, growth of ice crystals and snow, and precipitation to the surface. Detailed evaluation of model forecast orographic precipitation was performed for 30 selected operational seeding days. It was shown that the model can be a useful forecasting aid in support of the seeding operations.

But, the model over-predicted natural precipitation, particularly on moist southwest flow days. The model also exhibited virtually no enhancement in precipitation due to glaciogenic seeding. There are a number of possible causes for the lack of response to seeding, such as over prediction of natural precipitation, which prevented the effects of seeding from being seen. In addition, the background CCN and IN concentrations are unknown, therefore selecting low CCN concentrations would make the clouds more efficient rain producer, thus interfering with the seeding from taking effect. However, this paper demonstrates that potential benefits that could emerge from the use of such models in rain enhancement experiments and operations.

In summary, while not meeting the full criteria of scientific "proof", there are strong indications that seeding of wintertime orographic clouds can enhance precipitation, at least in some locations and under certain weather regimes.

8.2.2 Israeli Randomized Cloud Seeding Experiments

At about the same time as the Climax experiments were reported, in the late 1960s and early 1970s, two landmark experiments (Israeli I and Israeli II), carried out in Israel, were described in the peer-reviewed literature. The experiments were carried out by researchers at the Hebrew University of Jerusalem (HUJ), hereafter the experimenters. For many years these two experiments were the foundation for the widespread belief that under appropriate conditions, cloud seeding could increase precipitation (e.g., National Academy of Sciences, 1973, *Sax et al.*, 1975; *Tukey et al.*, 1978a,b; *Simpson*, 1979; *Dennis*, 1980; *Mason*, 1980, 1982; *Kerr*, 1982; *Silverman*, 1986; *Braham*, 1986; *Cotton*, 1986a,b; World Meteorological Organization, 1992; *Cotton and Pielke*, 1992, 1995; *Young*, 1993).

In the Israeli randomized experiments, carried out from 1961 to 1975, the clouds that were seeded were mainly cumulus and cumulonimbus clouds. These clouds form due to the advection of cold air from the European continent to the warm Mediterranean waters, which accompanies transient upper-level troughs in the region [e.g., *Gagin and Neumann*, 1974; *Hobbs et al.*, 1995a]. Under these conditions cloud bases are typically between 5 and 10°C. They can occur in clusters, bands and in isolation as orchestrated by the upper level dynamics and the length of fetch over the

Mediterranean Sea. Showery spells often last for several days at a time in Israel. Each of the two Israeli experiments had two target areas: one randomly designated in advance to be seeded, and the other a control for each day during the Israeli rainy season, which runs from about the middle of October through about the middle of April. This type of experiment design has been referred to as a *crossover* experiment, in which the results of seeding are combined from two target areas. In this type of design, the experimental data builds up at twice the rate of single target designs.
In Israeli I and II, the two target areas were separated by a small "buffer zone," which was to be left unseeded. In Israeli I, the two targets were referred to as "North" and "Center"; in Israeli II, the two targets were referred to as "North" and "South". The "South" target area in Israeli II was much larger than the "Center" target area in Israeli I.

Israeli I lasted six and a half rainy seasons. Evaluations of seeding indicated that statistically significant increases in rainfall amounting to ~15% had occurred when the data from *both* targets were combined [e.g., *Gabriel,* 1967a,b; *Gabriel and Feder*, 1969; *Gabriel and Baras*, 1970; *Wurtele*, 1971; *Gagin and Neumann*, 1974]. The seeding effects were reported to be larger in the Center target area than in the North target area, and they were larger still farther inland from the coastline [*Gagin and Neumann*, 1974].

The main conundrum in Israeli I was that the greatest effect of cloud seeding appeared to be in the small "buffer zone," between the North and Center targets, where seeding should not have occurred [*Wurtele*, 1971; *Gagin and Neumann*, 1974]. The HUJ Investigators themselves were intrigued and puzzled by this discrepancy, but ultimately attributed the anomaly in the buffer zone to an unintended effect of seeding [*Gagin and Neumann*, 1974].

In addition to *Wurtele's* independent review of the Israeli I experiment, *Brier et al.*, [1973] examined the rainfall in Lebanon and Jordan. Although this analysis supported the seeding effects reported by the HUJ Investigators, they also found that increases in rainfall, similar to those attributed to seeding, extended into downwind regions in Jordan, and into other regions that could hardly have been seeded at all [cf., *Rangno and Hobbs*, 1995a].

Israeli II was carried out in the rainy seasons of 1969–70 to 1974–75. The North Target Area was shifted inland from Israeli I [e.g., *Gagin and Neumann*, 1974, 1981]. This created a new Control region to the west; in the region of the Carmel Mt. between the Sea and the seeding line. The South Target Area was expanded over that of the Center target area in Israeli I: it included the "Center" Target Area of Israeli I as well as an area to the drier south [*Gagin and Neumann*, 1974; *Gabriel and Rosenfeld*, 1990].

The Israeli II experiment can be evaluated in four ways: 1) Using the crossover design that combines data from both targets, as in Israeli I. 2) Using rainfall in the non-seeded target area as a control for the seeded target area. 3) The evaluation of each target area individually as a "stand alone" randomized experiment with no controls. 4) And, using a target/control evaluation, which allows the assessment of seeding effects in the North Target Area alone. The HUJ Investigators felt that since seeding material was released just offshore from the South Target Area, coastal stations in the South Target Area might have been "contaminated" and therefore should not be used as controls. The HUJ Investigators [e.g., *Gagin and Neumann*, 1974] declared their intention to evaluate Israeli II using rainfall in the non-seeded target area as a control for the seeded target area. They noted the North Target Area, after just two seasons of seeding, indicated in preliminary evaluations a statistically significant increase in rainfall of ~12%, while the South target was a non-significant increase of ~1%.

In 1976, following the conclusion of Israeli II, the HUJ Investigators reported that the results of Israeli II confirmed those of Israeli I in the North Target Area, but that results for the South Target Area were "inconclusive" [*Gagin and Neumann*, 1976]. Important additional support for the efficacy of seeding in the north-target area in Israeli II was provided through stratification of the random seeding results by temperatures. The temperatures at the tops of radar echoes on the subset of days with median echoes located at temperatures between –12 and –21°C contained virtually all of the apparent increases in rainfall due to seeding [e.g., *Gagin and Neumann*, 1981]. This range of echo top temperatures corresponded to earlier aircraft and later radar studies that indicated that clouds over Israel contained few ice crystals at temperatures above –21ºC [e. g., *Gagin and Neumann*, 1974; *Gagin*, 1975, 1980).

With the success of cloud seeding in increasing rainfall in the North Target Area apparently confirmed by Israeli II, a third randomized experiment, referred to as Israeli III and starting in the winter of 1975–76, was conducted solely in the South Target Area [*Rosenfeld*, 1998].

As unlikely as it might seem at first glance, the microstructure of the cumuliform clouds of Israel was reported being a mirror image of the cloud microstructure of wintertime stratiform clouds in the Colorado Rockies [cf., *Grant*, 1968; *Gagin* ,1975]. Importantly, "ice multiplication" was reported as not occurring in Israel [*Gagin*, 1971, 1975, 1986]. The reason cited for this result was the lack of cloud droplets >23 μm diameter at temperatures between–2.5° to –8°C, which is a requirement for ice multiplication by riming [e.g., *Mossop*, 1985]. It was also reported that precipitation-sized drops, also an important accelerator of ice formation, were completely absent in clouds over Israel [*Gagin*, 1986]. Instead, ice particle concentrations as a function of temperature in the clouds of Israel were reported to be similar to those given by *Fletcher's* [1962] summary of ice nucleus concentrations in the atmosphere [e.g., *Gagin*, 1975]. However, *Rangno* [1988] showed that rain could form in clouds in Israel with tops warmer than -10^{o}C.

Finally, it is interesting to note that in both the Israeli and Colorado experiments the effects of artificial seeding with silver iodide appeared to be an increase in the duration of precipitation, with little if any effect on the intensity of precipitation [e.g., *Chappell et al.*, 1971; *Gagin*, 1986; *Gagin and Gabriel*, 1987], a finding compatible with the "static" seeding hypothesis.

As in the case of the Climax experiments, an erosion of confidence in the positive results of the highly acclaimed Israeli cloud seeding experiments has occurred over the past 15 years. *Rangno and Hobbs* [1995a] concluded from their re-analysis of both the Israel I and II experiments that the appearance of seeding-caused increases in rainfall in the Israel I experiment was due to "lucky draws" or a Type I statistical error. Furthermore, they argued that during Israel II naturally heavy rainfall over a wide region encompassing the north target area gave the appearance that seeding caused increases in rainfall over the north target area. At the same time, lower natural

rainfall in the region encompassing the south target area gave the appearance that seeding decreased rainfall over that target area. In addition, *Levin et al.* [1997] in model simulations of the release and targeting of seeding as used in the Israeli programs indicated that only a fraction of the seeding material would reach their intended target.

Rosenfeld and Farbstein [1992] and *Rosenfeld and Nirel* [1996], however, suggested that the differences in seeding effects between the north and south target areas during Israel II is the result of the incursion of desert dust into the cloud systems. They argue that the desert dust contains more active natural ice nuclei and that they can also serve as coalescence embryos enhancing collision and coalescence among droplets. Together, the dust can make the clouds more efficient rain-producers and less amenable to cloud seeding.

Rangno and Hobbs [1995a] also reported on observations of clouds over Israel containing large supercooled droplets and quite high ice crystal concentrations at relatively warm temperatures. In addition, *Levin et al.* [1996] presented evidence that the winter clouds are less continental in nature, with droplet concentrations of 300-450 cm^{-3} and high ice concentrations suggesting active ice multiplication processes in Israeli clouds. This further erodes the perception that the clouds over Israel were as susceptible to seeding as originally thought. Naturally, the *Rangno and Hobbs* [1995] paper generated quite a large reaction in the weather modification community. The March issue of the Journal of Applied Meteorology contained a series of comments and replies related to their paper [*Rosenfeld*, 1997; *Rangno and Hobbs*, 1997a; *Dennis and Orville*, 1997; *Rangno and Hobbs*, 1997b; *Woodley*, 1997; *Rangno and Hobbs*, 1997c; *Ben-Zvi*, 1997; *Rangno and Hobbs*, 1997d, e]. These comments and responses clarify many of the issues raised by *Rangno and Hobbs* [1995a].

Nonetheless, the image of what was originally thought of as the best example of the potential for precipitation enhancement of cumulus clouds by static seeding has become somewhat tarnished.

8.2.3 U.S. HIPLEX Experiments and Australian Experiments

In the High Plains Experiment (HIPLEX-1) the static seeding hypothesis was tested [*Smith et al.*, 1984] in a well-designed field program. These studies revealed the important result that after just 5 min, there was no statistically significant difference in the precipitation between seeded and non-seeded clouds, [*Mielke et al.*, 1984]. *Cooper and Lawson* [1984] found that while high ice crystals concentrations were produced in the clouds by seeding, the cloud droplet region where the crystals formed evaporated too quickly for the incipient artificially produced ice crystals to grow to appreciable sizes. Instead they formed low density, unrimed aggregates having the water equivalent of only drizzle drops, which were too small to reach the ground before evaporating. *Schemenauer and Tsonis* [1985] affirmed the findings of *Cooper and Lawson* in a reanalysis of the HIPLEX data emphasizing their own earlier findings [*Schemenauer and Isaac*, 1984] that cloud top lifetimes were too short in the HIPLEX domain for seeding to have been effective in the clouds targeted for seeding (i.e., those with tops warmer than –12ºC). Although the experiment failed to demonstrate statistically all the hypothesized steps, the problems could be traced to the physical short lifetimes of the clouds [*Cooper and Lawson*, 1984; *Schemenauer and Tsonis*, 1985]. This in itself is a significant result that shows the ability of physical measurements and studies to provide an understanding of the underlying processes in each experiment. The results suggested that a more limited window of opportunity exists for precipitation enhancement than was thought previously. *Cotton and Pielke* [1995] summarized this window of opportunity as being limited to:

Clouds that are relatively cold-based and continental;

Clouds with top temperatures in the range –10 ^{o}C to –25 ^{o}C, and

a timescale confined to the availability of significant supercooled water before depletion by entrainment and natural precipitation processes.

Today, this window would even be viewed too large, since many cold based continental clouds with tops >–25ºC have copious ice particle concentrations [e.g., *Hobbs and Rangno*, 1985; *Rangno and Hobbs*, 1988]. The HIPLEX results also indicated that small clouds make little contribution to rainfall.

Finally, *Ryan and King* [1997] reviewed over 14 cloud seeding experiments covering much of southeastern, western, and central Australia as well as the island of

Tasmania. They concluded that static seeding over the plains of Australia is not effective. They argue that for orographic stratiform clouds, there is strong statistical evidence that cloud seeding increased rainfall, perhaps by as much as 30% over Tasmania when cloud top temperatures are between -10 and -12 C in southwesterly airflow. The evidence that cloud seeding had similar effects in orographic clouds over the mainland of southeastern Australia is much weaker. If the results of the Tasmanian experiments are real, benefit/cost analyses suggests that seeding has a gain of about 13/1. This is viewed as a real gain to hydrologic energy production.

8.2.4 Overseeding of Layer and Orographic Clouds

If a cloud consists mainly of ice particles it is said to be *glaciated*. Under these conditions the growth of ice particles by the Bergeron process is restricted (i) because this requires supersaturations with respect to ice, which are generally produced by the co-existence of ice particles among many more supercooled droplets (see Chapter 4), and (ii) because the available water vapor has to be shared among copious ice particles. Consequently, glaciated clouds often consist of numerous small ice particles, with relatively few particles large enough to fall out and survive complete evaporation before reaching the ground unless they are relatively low and the terrain is high.

The first field trials using Dry Ice as a glaciogenic seeding agent were carried out in the USA in November 1946 when ~1–5 kg of crushed Dry Ice were dropped along a line ~5 km long into a layer of supercooled altocumulus cloud (Figure 8-1). The cloud along the seeded path was quickly converted into numerous small ice crystals, leaving a cloud-free region. Snow was observed to fall from the base of the seeded cloud for a distance of ~0.5 km before it evaporated. Since then this technique has been used at a number of airports worldwide for making temporary holes in supercooled clouds through which aircraft may pass.

Figure 8-1. *First cloud seeding experiments in 1946 glaciating a supercooled altostratus cloud layer by seeding with Dry Ice pellets.* *Don't have a reference for it)*

A series of cloud seeding experiments, utilizing the ability of Dry Ice to glaciate clouds, was carried out in the Cascade Mountains of the USA in the 1970s (the *Cascade Project*). In winter, orographic clouds form in moist westerly airstreams over the Cascade Mountains, and ice particles grow over the windward slopes primarily by *riming* (i.e., by collecting supercooled droplets). Since rimed ice particles have relatively large fall speeds (~1 m s^{-1}), they follow fairly steep trajectories as they fall to the ground. Consequently, most rimed particles reach the ground on the windward slopes, and runoff of the snowmelt in summer is to the west [*Hobbs*, 1975a]. If the clouds on the windward side are overseeded with Dry Ice, the supercooled droplets can be virtually eliminated and growth by riming significantly reduced. In the absence of riming, the ice particles grow by deposition of vapor and their fall speeds are reduced to ~0.5 m s^{-1}, so that they are carried farther to the east by the winds and are deposited on the normally drier leeward slopes. A series of such seeding experiments carried out in the Cascade Project provided strong evidence for the sequence of

physical events outlined above [*Hobbs and Radke*, 1973, 1975; *Hobbs*, 1975b]. However, since randomized statistical experiments were not carried out, the amounts of snow diverted across the mountain crest by overseeding was not quantified. It was hypothesized that if the concentration of ice particles in an orographic cloud is increased too much, aggregation of the ice particles will be enhanced, which will increase the fall speeds of the ice particles and tend to reduce diversion of the snow across a mountain crest. This hypothesis has not been confirmed by models or by observations.

8.2.5 Some Conclusions Concerning Static Cloud Seeding Experiments

The most surprising conclusion concerning the many static cloud seeding experiments that have been carried out over the past half century or so is that very little has been proven unambiguously. In particular, it has not been unambiguously proven that precipitation on the ground can be significantly modified even by deliberate cloud seeding with particles that are known to modify (in some cases drastically) cloud structures. *Silverman* [2001] lists a number of possible reasons for this:

Adequate measurements to provide an understanding of the basic physical process leading to the formation of precipitation have often been lacking in cloud seeding experiments.

High concentrations of ice particles occur naturally in some cumulus clouds at temperatures as warm as –5ºC. Therefore, the window of opportunity for enhancing rainfall from a given cloud (or cloud) system is limited.

Seeding may both enhance and reduce precipitation.

Results based on small clouds might not be transferable to dynamically more vigorous and larger cloud complexes.

Perhaps, however, the most challenging obstacle to evaluating cloud seeding experiments to enhance precipitation, is the inherent natural variability of precipitation in space and time, and the inability to increase precipitation amounts to better than ~10%.

8.3 DYNAMIC GLACIOGENIC SEEDING EXPERIMENTS

So far we have considered only *static seeding experiments*, in which the principle thrust is to modify the microstructures of clouds generally for the purpose of

enhancing precipitation. There is, however, another glaciogenic seeding hypothesis in which the cloud-scale dynamics of a cloud is enhanced by stimulating buoyancy and upward motions of air. This is referred to as *dynamic cloud seeding*. In principal, this can be done by glaciating convective clouds so that large quantities of latent heat are released by the freezing of copious liquid water, to invigorate updrafts in the cloud.[2] This can be particularly effective if prior to seeding, the tops of the clouds are restricted by a stable layer produced by a temperature inversion. In this case, the sudden release of a large quantity of latent heat might provide enough buoyancy to push the top of the cloud through the stable layer and into a region where the air is naturally unstable. The cloud might then rise to much greater heights than it would have done naturally.

The possibility of dynamic seeding was first suggested by *Krauss and Squires* [1947]. These investigators seeded large, supercooled cumulus clouds with Dry Ice in Australia. They reported that 6 out of 8 clouds gave radar echoes after seeding, and in 4 of these, heavy rain reached the ground. In a spectacular case, a cloud with base at 11,000 ft, the 0ºC level at 18,000 ft, and cloud tops at 23,000 ft was seeded with 150 lbs of Dry Ice, whereupon the cloud tops increased to 40,000 ft in 13 min; a radar echo appeared within 5 min of seeding, and after 21 min heavy rain exited cloud base. No other radar echoes were observed within a range of 100 miles.[*]

In a series of randomized experiments carried out in Florida in 1968 and 1970–1973 (called the Florida Area Cumulus Experiment or FACE), it was found that precipitation (measured by radar) from isolated cumulus clouds ~5 km in diameter, which were artificially seeded to induce explosive growth, was about twice that from the unseeded control clouds [e.g., *Simpson and Woodley*, 1975; *Woodley et al.*, 1982]. The seeded clouds rained more than the control clouds because they were bigger and lasted longer, rather than their rainfall rates being significantly greater.

In FACE II, the attempt was made to confirm and replicate the results of FACE I by going the additional step of specifying the manner in which clouds would respond to

[2] Later, the focus and description of dynamic seeding was changed to emphasize seeding to enhance downdrafts not buoyancy.

[*] Interestingly, Krauss subsequently was of the opinion that these results were fortuitous and neither he nor Squires participated in any further cloud seeding experiments.

seeding based on what was understood to have been the response in FACE I. While there were several suggestions of seeding effects on some clouds and some days [e.g., *Woodley et al.*, 1983], the overall experiment officially failed to confirm the results of FACE I [*Flueck et al.*, 1981; *Nickerson*, 1979, 1981]. One of the problems that impacted the experiment was a large outlier natural rainfall day fell on a day that was randomly selected as a non-seeded one. However, the authors pointed out that "even if the far-out day had never existed, the P-value support for a seeding effect would still not be strong." The authors noted also that one of the impediments to FACE II was an incomplete understanding of the cloud-to-precipitation processes in clouds, a problem that is still with us today, even with our much improved understanding. Lacking in the dynamic seeding research is an identification of

The hypothesized chain of physical processes that lead to enhanced rainfall on the ground over a target region. Observations in clouds seeded for dynamic effects showed that seeding did indeed glaciate the clouds (convert the cloud from liquid to primarily ice) [*Sax et al.*, 1979]. The one-dimensional models clearly predict that artificial glaciation of a cloud should result in increased vertical development of the cloud. Those one-dimensional models, however, cannot simulate the consequences of increased vertical growth. A chain of physical responses to dynamic seeding has been hypothesized [*Woodley et al.*, 1982] that includes: (1) pressure falls beneath the seeded cloud towers and convergence of unstable air in the cloud will as a result develop, (2) downdrafts are enhanced, (3) new towers will therefore form, (4) the cloud will widen, (5) the likelihood that the new cloud will merge with neighboring clouds will therefore increase, and (6) increased moist air is processed by the cloud to form rain.

In recent years the dynamic seeding strategy has been applied to Thailand and West Texas. Results from exploratory dynamic seeding experiments over west Texas have been reported by *Rosenfeld and Woodley* [1989; 1993]. Analysis of the seeding of 183 convective cells suggests that seeding increased the maximum height of the clouds by 7%, the areas of the cells by 43%, the durations by 36%, and the rain volumes of the cells by 130%. Overall the results are encouraging but such small increases in vertical development of the clouds are hardly consistent with earlier exploratory seeding experiments.

As a result of their experience in Texas, *Rosenfeld and Woodley* [1993] proposed an altered conceptual model of dynamic seeding in which explosive vertical development of seeded clouds is not emphasized. *Rosenfeld and Woodley* [1993] argue that the retention of the increased ice mass in the form of graupel is an important new aspect of their dynamic seeding conceptual model. This may delay the formation of a downdraft and allows more time for further growth of the cloud. The eventual unloading of the enhanced water mass, they argue, is favorable for subsequent regeneration of the cloud by the downdraft-induced gust fronts leading to larger, longer-lived cells. As pointed out by *Silverman* [2001], however, application of the revised hypothesis in Thailand [*Woodley et al.*, 2003a, 2003b] did not yield a statistically significant increase in rainfall, and the rainfall and enhanced downdraft presumably produced by it did not appear to be delayed [*Woodley et al.*, 1999b].

In summary, the concept of dynamic seeding is a physically plausible hypothesis that offers the opportunity to increase rainfall by much larger amounts than simply enhancing the precipitation efficiency of a cloud. It is a much more complex hypothesis, however, requiring greater quantitative understanding of the behavior of cumulus clouds and their interaction with each other, with the boundary layer, and with larger-scale weather systems. Fundamental research in dynamic seeding essentially terminated at the time that new cloud observing tools and multidimensional cloud models became available to the community. Systematic application of these tools to the study of dynamic seeding would help in evaluating if the hypothesized chain of events is possible and perhaps the conditions under which such responses are likely to occur.

8.3 HYGROSCOPIC RANDOMIZE SEEDING EXPERIMENTS

Hygroscopic seeding was mainly used in the past in warm clouds without any ice in them. However, more recently, this type of seeding methods have been tried in mixed-phase clouds. The aim in seeding warm clouds is to enhance drop growth by coalescence and thus improving the efficiency of rainfall formation. On the other hand, seeding mixed-phase clouds seems to affect both drop growth and ice formation, probably through the efficient formation of graupel particles. Appropriately sized salt particles, water droplets from sprays of either water or saline solution [*Bowen*, 1952; *Biswas and Dennis*, 1971; *Cotton*, 1982; *Murty et al.*, 2000;

Silverman and Sukarnjanasat, 2000], and hygroscopic flares [*Mather et al.*, 1997; *WMO*, 2000] have been used for seeding. Statistical results, observations and modeling results have provided some evidence that under certain conditions and with optimal seed drop size spectra, precipitation may be enhanced [*Farley and Chen*, 1975; *Rokicki and Young*, 1978; *Young*, 1996, *Reisin et al.*, 1996; *Yin et al.*, 2000a and b]. Hygroscopic flare particle seeding experiments have provided statistical support for rainfall increases (Figure 8-2) due to seeding based on single cloud analyses [*Mather et al.*, 1997; *Bigg*, 1997; *WMO*, 2000; *Silverman*, 2003], but the physical processes leading to these increases in precipitation are not well understood. Model simulations suggest that the increase in rainfall amounts stems from the increase in graupel numbers and masses, which are generated by the increased concentrations of large drops. Such increases could generate more rain but it is not clear how these procedures can affect the clouds for such a length of time as the measurements suggest.

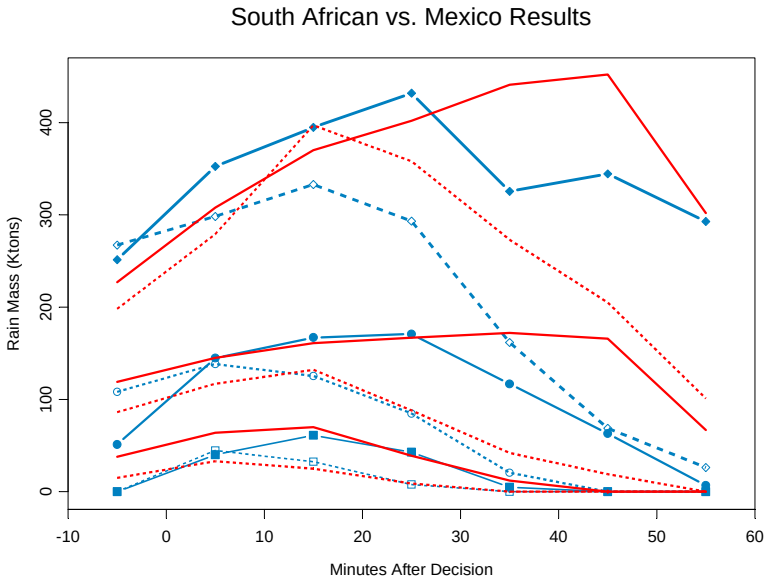

Figure 8-2. *Quartile values of Radar Derived Rain Mass (Precipitation Flux integrated over time) versus time after "decision time" for seeded and non-seeded cases for the South African (red lines) and Mexican (blue lines) experiments. Rain Mass is the Precipitation Flux integrated over 5-minute intervals. 1st quartile is the value of Rain Mass that is larger than the value for 25% of the storms; 2nd quartile value exceeds the value for 50% of the other storms; and 3rd quartile value exceeds the value for 75% of the storms.*

The development and use of the hygroscopic flares for rainfall enhancement was triggered by radar and airborne microphysical measurements of clouds downwind of

large paper mills, which indicated an apparent enhancement of the collision-coalescence mechanism for raindrop formation (see Chapter 5) in clouds affected by effluents from the mills [*Hobbs et al.*, 1970; *Mather*, 1991]. Observations by *Eagen et al.* [1974] and *Hindman et al.* [1977] suggested a similar connection between effluents from paper mills and enhanced precipitation.

The principle of enhancing the coalescence process via hygroscopic seeding is dependent on three important parameters: the chemistry (hygroscopicity), size and concentration of the particles (CCN) produced from the flares or large particle salt seeding. In addition, the effectiveness of seeding will depend on the natural background particles and their characteristics with regard to the same three parameters. The principle of flare seeding is to have the flares produce effective CCN (usually salts such as sodium chloride, potassium chloride, or calcium chloride) particles in larger sizes (large or giant nuclei) than occur in the natural environment.

The majority of the hygroscopic cloud seeding flares including the flares used in South Africa are based on the formula described by *Hindman* [1978] that was developed to initiate fog cover for military vessels. These flares incorporate sodium and calcium salts along with potassium perchlorate, magnesium powder and an organic binder as the fuel. The flares produce a plume of sodium, calcium and potassium salt particles along with magnesium oxide. The flares used in the South African experiment [*Mather et al.*, 1997] provide large CCN (>0.3 μm diameter) to a growing cloud, influencing the initial condensation process and allowing fewer CCN to activate to cloud droplets as shown by *Cooper et al.* [1997]. If the CCN that are introduced into the cloud from the flare are larger in size than the natural CCN, the introduced CCN will activate preferentially over the natural CCN and change the character of the cloud drop size distribution to favor the collision-coalescence process and the formation of rain. The larger artificial CCN inhibit the smaller natural CCN from nucleating, resulting in a broader droplet spectrum at cloud base. The fewer cloud droplets grow to larger sizes, and are often able to start growing by collision-coalescence with other cloud droplets within ~15 minutes, initiating the rain process earlier within a typical cumulus cloud lifetime of ~30 minutes.

Model simulations [*Reisin et al.*, 1996, *Yin et al.*, 2000a and b, *Caro et al.*, 2002, *Segal et al.*, 2005] suggest that in addition to the size of the hygroscopic particles the time of seeding is a crucial parameter. Seeding too early or too late can lead to reduced rain amounts or to be ineffective at all, respectively. The models suggest that the window of opportunity for effective hygroscopic seeding is small, although it is longer than that of glaciogenic seeding.

In both South Africa [*Mather et al.*, 1997] and Mexico [*WMO*, 2000], hygroscopic flares have been applied to mixed-phase convective cloud systems in limited physical and statistical experiments. Aircraft microphysical measurements were made to verify some of the processes involved. Radar-measured 30 dBZ volumes produced by the convective complexes were tracked by automated software and various storm and track properties were calculated. These two sets of experiments produced remarkably similar results in terms of the difference in radar-estimated rainfall between the seeded and non-seeded groups. The South African data have been re-evaluated independently by *Bigg* [1997] and *Silverman* [2000]; both concluded that there is statistically significant evidence of an increase in *radar-estimated* rainfall from seeded convective cloud systems. For instance, *Silverman's* [2000] re-evaluation showed an increase in rain mass ~30–60 minutes after seeding, significant at the 96 percent level (p=0.04) or higher. Silverman also found; 1) that adjusting for the "inadvertent bias" referred to by *Mather et al.* [1997] and "potentially compromising covariate" referred to by *Silverman* strengthened and sharpened the suggested effects of seeding; 2) the effects from larger cloud systems does not seem to have an effect on the results and that seeding apparently has no affect on these systems; and 3) cloud systems on the more continental Highveld-Bethlehem in South Africa responded much more favorably to seeding. The results from the initial randomized experiments were further supported by the results from a semi-operational experiment in South Africa [*Terblanche et al.*, 2002].

Mather et al. [1997], *Bigg* [1997], and *Silverman* [2000] all allude to apparent dynamic effects of seeding clouds, manifest in the seeded cloud systems being longer-lived. It was speculated that the relation between precipitation loading and evaporation, and the characteristics of the downdraft that is generated, and between the downdraft and the storm organization, evolution, and lifetime, determines the

dynamic effect of seeding on rainfall. Another factor not mentioned is the possible consequences of altered raindrop size distributions. If seeding shifts the raindrop size distribution to smaller raindrops, then greater sub-cloud evaporation would ensue, which would alter cold-pool dynamical effects. If seeding shifts the raindrop spectrum to larger drops the opposite response would be expected [*Yin et al.*, 2001].

Mather et al. [1997] conducted additional exploratory analyses in an attempt to gain additional insights into the differences in radar-detected storm properties between the randomly selected hygroscopic flare seeded and non-seeded storms. This after-the-fact analysis focused on the following questions:

Can any radar-measured differences between the seeded and control storms be sharpened by eliminating the larger storms from the data?

Are these differences congruent with the hygroscopic seeding hypothesis and do they occur in a physical plausible sequence?

Can any of these differences be used to develop a useful "seeding signature" algorithm?

The differences in overall storm properties produced the following results. The seeded storms lasted longer than the controls (p value < 0.01) and this had an enhancing effect on the time integrals of storm volume, mass, area and rain flux. The authors also showed that the seeded distribution of rain mass differs from the control at p values of < 0.01 [*Mather et al.*, 1997]. Most of the other properties that scored p values of ≤ 0.05 were related to radar-detected increases in reflectivity aloft and increases in storm densities but did not prove that more rain fell on the ground.

The individual storms selected for the experiment, almost without exception, extended well above the freezing level. For the exploratory analyses on the South African data, marked differences were found in storm properties above 6 km [*Mather et al.*, 1997]. The 6 km level generally corresponds to the –5° to –10°C level, which points to probable ice-phase processes being part of the apparent seeding effect. Some indication of how the microphysical changes of broadening the droplet spectrum can be brought about by hygroscopic flare particles, as well as supporting measurements, are given by *Cooper et al.* [1997], *Reisin et al.* [1996] and *Yin et al.* [2000b].

Although these effects on the ice processes are not well understood and need further research, they indicate the following:

- The natural contrast of high concentrations of ice particles in maritime clouds (in which collision-coalescence is active) that extend above the freezing level [*Koenig*, 1963; *Cotton*, 1972; *Koenig and Murray*, 1976; *Scott and Hobbs*, 1977], compared to the relatively low concentrations of ice particles found in continental clouds (in which coalescence is not active);
- Freezing temperatures that increases with an increase in droplet size, due to the higher probability that larger droplets will contain (or come in contact with) ice nuclei and the associated riming characteristics [*Johnson*, 1987]; and,
- The operation of various ice-multiplication processes, including the break-up of fragile ice crystals during melting and evaporation, ice splinter formation during riming, both of which are dependent on the presence of relatively large cloud droplets [*Hobbs*, 1969; *Hallet and Mossop*, 1974*; Vardiman*, 1978].

It appears that continental convective storms are remarkably sensitive to changes in the CCN ingested at cloud base. For example, both the South African and Mexican experiments with hygroscopic flares show very strong signals in terms of increased storm lifetime in seeded storms, increases in reflectivity aloft, and increases in storm densities. Thus, these hygroscopic flare seeding experiments suggest that it is possible, under appropriate conditions, to produce large differences in cloud properties by injection of hygroscopic particles into cloud bases. These properties need further investigation; further multi-parameter radar and in-situ airborne measurements of seeded and control clouds will be needed. One important measurement that needs to be included is an accurate record of precipitation on the ground. This is because errors in radar measurements could lead to the wrong conclusions about the effectiveness of seeding. Furthermore, if evaporation below cloud base is responsible for the enhanced development of the neighboring clouds, time resolved precipitation on the ground could help resolve this process.

The calculations of *Reisin et al.* [1996], *Cooper et al.* [1997], *Yin et al.* [2000a and b], *Caro et al.* [2002] and *Segal et al.* [2005] show that for clouds with maritime cloud droplet spectra, hygroscopic seeding should have no effect, since the collision-

coalescence acts very efficiently in such clouds. Relatively high concentrations of large natural CCN prevent the seeded particles from dominating the growth. Model calculations show that for clouds with natural CCN concentrations < 350 cm^{-3} should not respond favorably to hygroscopic seeding.

It has been postulated that the initial spreading of the seeding effect through a cloud occurs through the formation of drizzle drops. Modeling study by *Cooper et al.* [1997] indicate that the formation of drizzle is highly dependent on the particle size spectra produced by the flares and that the concentrations of drizzle drops produced can vary by several orders of magnitude depending on the particle size spectra. *Cooper et al.* found that the optimum particle size for seeding with hygroscopic flares in order to obtain higher concentrations of drizzle size drops is ~1 μm diameter. *Reisin et al.* [1996], *Yin et al.* [2000a and b] and *Segal et al.* [2005] showed that particles larger than 1 μm radius are the most effective for seeding. All these modeling studies also indicate that the role of the background CCN (size and concentrations) is crucial for determining the effectiveness of the seeded particles, because the seeded nuclei compete with the background aerosols for the available water vapor.

Among the interesting results yielded by the South African and Mexican hygroscopic seeding experiments we note the following:

Both experiments produced remarkably similar statistical results in terms of the differences in radar estimated rainfall for seeded versus non-seeded groups [*Bigg*, 1997; *Silverman*, 2000; *WMO*, 2000].

Reevaluation of the results for both experiments showed an increase in rain mass ~30–60 minutes after seeding, significant at the 96 percent level ($p = 0.04$) or higher.

Marked differences in concentrations of ice particles were found in natural maritime clouds (high) versus continental clouds (low), signifying the active role of the collision-coalescence in maritime clouds compared to continental clouds [cf., *Cotton*, 1972; *Koenig and Murray*, 1976; *Scott and Hobbs*, 1977].

Freezing temperatures increased with increasing drop size, presumably because larger droplets contain or have a higher probability of colliding with ice nuclei.

Relatively large droplets (diameter >24 μm) played a role in ice multiplication processes, including mechanical fracturing during melting and evaporation and ice splinter formation during riming [cf., *Hallett and Mossop*, 1974].
A delayed response in radar-derived storm properties was a possible function of seeding-induced dynamic processes beyond the classical cloud physics results that link CCN and droplet spectra to rain production [WMO, 2000].

The NRC (2003) in their assessment of weather modification research concluded that the South African and Mexican experiments have demonstrated responses in clouds to treatment in accordance with understanding of the chain of physical reactions leading to precipitation. But since the analyzed statistical results are for radar-defined floating targets, they still do not prove that rainfall can be increased by hygroscopic seeding on the ground for specific watersheds. Moreover, since seeding may alter the size-spectrum of raindrops which alters the radar return, uncertainties exist in the evaluation of actual rain amounts for seeded versus not-seeded floating targets. Finally, since the main response to seeding found in the South African, Mexican, and Thailand experiments is delayed in time for as much as 1 and 6h, respectively, following the cessation of seeding, we lack a clear understanding of the actual processes that can lead to such a physical response.

Thus while the results of the hygroscopic seeding experiments are quite promising they still do not constitute a "proof" that hygroscopic seeding can enhance rainfall on the ground over an extended area. The areas affected by cloud seeding remain an open question. In after-the-fact analyses several rain enhancement projects have reported evidence for physical effects outside the area or timing originally designated as the target, or beyond the time interval when seeding effects were anticipated. For example, in recent large particle hygroscopic and glaciogenic seeding trials involving warm-base convective clouds in Thailand and Texas, increases in rain were reported 3 to 12 hours after seeding was conducted, well beyond the time at which direct effects of seeding were expected and possibly outside the target area. In Project Whitetop the seeding appears to have decreased rain in the area immediately downwind of the seeding release line. This was followed by apparent rainfall increases well downwind in space and time. Does this mean that the scientists misjudged where seeding materials were actually reaching receptive cloud conditions or does it mean that the

primary effects of seeding were followed by secondary effects well beyond the original target? Such secondary effects could occur, for instance, if seeding materials become entrained in a downdraft and then are carried outward into the updraft of other clouds. In the case of the hygroscopic seeding experiments the postulated dynamic effects due to microphysical and dynamical interactions in the cloud and sub-cloud region and with the environment could result in longer-lived or progeny clouds. Another related uncertainty in seeding convective systems is whether a positive effect on some individual clouds (or cloud complexes) will aggregate to result in increased area rainfall. As more is learned about the global water balance and as new tools enable the cloud scientist to better understand clouds and their response to seeding, the question of extended area affects likely will become better defined and understood.

8.4 CONCLUSIONS

Over 50 years of experimentation have yielded the following results:

Experimentation with glaciogenic seeding materials have clearly indicated that ice crystal concentrations in clouds can be increased in a consistent and significant manner and modify ice and mixed phase processes.

There is evidence that seeding with hygroscopic materials can modify the cloud droplet size distribution and warm rain process in stratiform and convective clouds.

Randomized and operational glaciogenic seeding experiments of mixed-phase orographic and stratiform cloud has been shown, in some cases, to increase surface precipitation or to result in a redistribution of the precipitation.

Randomized controlled hygroscopic and glaciogenic seeding experiments of mixed phase convective clouds has shown radar derived increases in precipitation (storm lifetime) in some regions on single cloud systems. However, these experiments have not yet provided evidence of increases in area precipitation and the results did not conform to the original hypothesis indicating a lack of understanding of the physical cause and effect relationships.

Although it has been shown that for certain environmental and cloud conditions in some regions, precipitation could be increased by cloud seeding, the surprising result concerning deliberate seeding (injecting well characterized aerosols [CCN/GCCN and IN]) into clouds is that it has still not been established unambiguously that

precipitation on the ground can be increased in a consistent (temporal and spatial) and significant manner. This must be attributed in part to (1) lack of sufficient knowledge of the complex chain of physical and dynamical processes that lead to precipitation, (2) the poor design and inadequacies of crucial, adequate and appropriate measurements of background and modified processes in the majority of deliberate cloud seeding experiments, and in some cases, insufficient statistical evidence, (3) a lack of appreciation of the magnitude and importance of the natural variability of atmospheric (dynamic and thermodynamic) conditions, background aerosols, and cloud systems, (4) the difficulty to accurately measure precipitation on the ground at required spatial and temporal scales.

In view of these conclusions, it should not be surprising if evaluation of the effects of inadvertent seeding of clouds by pollution will in some respects be even more difficult than the evaluation of the effects of deliberate seeding. This is because:

At any specific location in the atmosphere the particles that may affect cloud structures and precipitation derive from both natural and anthropogenic sources (biomass burning, industrial, cities, agricultural practices and others). In most cases as opposed to cloud seeding experiments, it is difficult, if not impossible, to determine and differentiate the type of particles (Chapters 3, 4, 7).

A variety of particles, with different physical and chemical properties, are emitted by most pollutant sources (cf., the variety of emissions from a biomass burning, city, industrial, etc). These carious particles may affect clouds in different ways, some of which could be self-canceling (See Chapters 2, 3 and 5).

In addition to any cloud-active particles emitted directly by an anthropogenic source, various gases (e.g., SO_2, NO_x) emitted by the same source may be converted into cloud-active particles downwind (e.g., into sulfates and nitrates). One consequence of such gas-to-particle conversion is that an anthropogenic source may affect cloud structures and precipitation well downwind of the source (see Chapters 2 and 3). This is particularly true once the anthropogenic source material is processed through clouds downwind of the source.

In general, it is not possible to carry out controlled randomized experiments using anthropogenic emissions as a source of particles.

On the other hand, there are some advantages in utilizing anthropogenic sources to investigate the modification of clouds and precipitation by particles. For example:

In some cases concentrations of cloud-active particles emitted by certain industries (e.g., cloud condensation nuclei from paper mills) have been measured. Moreover, these particles are generally emitted continuously, day and night. Consequently, cloud structures and precipitation downwind of such sources may differ significantly from regions upwind of the source.

In those cases where a new industrial site is established in what was a previously pristine location, the structures of clouds and precipitation in the vicinity of the site can be compared before and after the establishment of the industry. Also, in the case of an isolated industry, it should be possible to characterize rather well the nature of the emissions. However, a complicating factor is the potential for climate variations during the period prior to and after the construction of the new industrial site.

Finally, the history of evaluating the effects of cloud seeding on precipitation has taught us a number of lessons that are useful for evaluating inadvertent modification of clouds and precipitation by aerosols. For that matter *Cotton and Pielke* [1995] also point out that cloud seeding evaluation has a number of implications to evaluating the effects of CO2 greenhouse gases on climate.
First, the scientific community has established a set of criteria for determining that there is "proof" that seeding has enhanced precipitation. For firm "proof" (see NRC, 2003; *Garstang et al.*, 2005) that seeding affects precipitation, *both* strong physical evidence of appropriate modifications to cloud structures and highly significant statistical evidence is required. Likewise, for firm "proof" that human production of aerosol in the atmosphere is altering precipitation, both strong physical evidence of appropriate modifications to cloud structures and significant statistical evidence is required. Unfortunately, as noted in *Cotton and Pielke* [1995] there is a human tendency to accept the results of assessments of inadvertent modification of clouds and precipitation even though those studies do not meet the standards of "proof" while at the same time requiring that cloud seeding evaluations meet such "proof" criteria.

Another lesson from evaluating cloud seeding experiments is that natural variability of clouds and precipitation can be quite large and thus can inhibit conclusive evaluation of even the best designed statistical experiments. The same can be said for

evaluating the effects of inadvertent introduction of aerosols into the climate system. To evaluate if human activity has produced some observed effect (cause and effect), one requires much longer time records than is available for most if not all data sets. Thus we often do not even have a measure of the natural variability of the climate effecting clouds and precipitation.

SUMMARY AND CONCLUSIONS

Lead Authors: IAPSAG lead authors

This WMO report reveals the difficulties in assessing the impact of aerosols on precipitation, despite a half-century of measurements ([e.g. early report of laboratory measurements by Gunn and Phillips, [1957]). In reviewing the literature we discovered that most publications deal with the effects of aerosols on clouds but very few actual measurements connect the effects on clouds with the effects on precipitation. Most references to precipitation are based on conceptual or numerical models.

The reason the connection between aerosols and precipitation is so difficult is because the lifetime of clouds and aerosols is short, the cloud properties are highly variable, and the variability in the aerosol chemical and physical properties, make it difficult to decipher the impact of aerosols on cloud properties and on the onset, rate and amounts of precipitation. In addition, once the precipitation process is altered the dynamics of the cloud systems is likewise altered and the entire system response can be quite nonlinear. In this report we illustrate these complexities by discussing in details the issues involved; namely, we discuss the role of precipitation in the hydrological cycle, the complexity of aerosol characteristics and their complex interactions with clouds and the processes that lead to precipitation development. We then reviewed the available observations and modeling work of the effects of aerosols on clouds and on precipitation. We devoted a chapter to the various methods available for aerosol, clouds and precipitation measurements using in situ and remote sensing methods. And finally we included a discussion on weather modification by cloud seeding as one example from which we may learn something about the potential effects of intentional interference in cloud processes aimed at modifying clouds and precipitation. In addition, since the response of clouds to seeding may have similarities to the effects of air pollution on cloud and precipitation development, we may want to adapt similar statistical methods in the latter study.

The overwhelming consensus of field measurements show that increasing CCN concentrations increases cloud droplet concentrations and decreases cloud drop sizes. However, the effect of particles on precipitation is much less certain. The growth of precipitation is a very non-linear process. Furthermore the dynamical response of clouds to variations in precipitation rates is even more nonlinear. Models show that a few giant CCN per liter of air may strongly affect precipitation development. Therefore, even for continental clouds, which have large concentrations of small CCN, it may be enough to have a few giant CCN to increase rainfall. To better understand the role of aerosols, and specifically giant aerosols on precipitation, instruments for measuring CCN from large volumes of air are needed.

The problem is even more complex when we deal with cold convective clouds. This is because precipitation in such clouds can grow in a number of ways: by the collision-coalescence process, by ice growth by deposition, by the riming of ice particles, or by all of the above. The simultaneous use of in situ and, remote sensing methods, supplemented by efficient and accurate numerical models, will be needed to more clearly delineate the roles of these various processes to the formation of precipitation and to the effects of aerosols on these processes. Likewise as precipitation falls from cumulus clouds into subcloud layers its evaporation can form cold pools which can control the subsequent propagation of the cloud systems. One cannot observe a single cloud and determine if aerosol variations lead to enhancement or reductions in precipitation, because the ultimate response of the clouds to aerosol changes may take place over periods of several hours and multiple cloud lifecycles. What may at first appear to be an appreciable enhancement of precipitation by aerosols may in the long run be a reduction in precipitation. The reverse sequence of events could also occur.

In the hydrological cycle water molecules evaporate from the oceans, seas, rivers, soils and plants and return to earth mainly by precipitation. The lifetime of a water molecule has been estimated to be about 9 days. Consequently, changes in cloud properties due to aerosols can modify the lifetime only slightly and thus modify only slightly the global amounts of rainfall. However, such small changes in cloud and precipitation properties may result in spatial and temporal redistribution of rainfall. This is not a small matter, because such changes could mean drought in some regions (especially in arid regions) or flooding in others.

It becomes clear that in order to evaluate the effects of aerosols from pollution or from natural sources on precipitation one has to rely on large amounts of data. Although case studies of individual storms can shed some light on the role of various processes, they cannot provide the answer to this complex question. At the same time, long term measurements also suffer from difficulties stemming from the changes that take place during the experiment. Researchers in weather modification have for years faced similar problems in their evaluation of experiments.

One important issue faced by all researchers in this field is the fact that often the expected changes in precipitation due to enhanced pollution could be smaller than the errors of the measurements. Therefore, in order to increase signal to noise ratio, the measurements of all variables must be accurate enough to be able to resolve the expected changes. Unfortunately, many of the instruments listed in Chapter 7 fall short of this requirement.

The methods to assess the effect of aerosol on precipitation can include direct measurements of the correlation between precipitation and aerosol concentration, whether from the surface, aircraft or satellites. Even though we clearly see in the measurements and in the model simulations the strong aerosol interference with cloud microphysics, we are not sure what is the magnitude or direction of the aerosol impact on precipitation and how it varies with meteorological conditions. The reasons behind this difficulty are the result of:

<u>The limited accuracy of the measurements:</u>

Radar measurements of precipitation can be off by up to 100%.

Measurements of the cloud droplet size from satellites are biased by up to 30% for convective clouds, due to departure of the clouds from the plane parallel model. However we can still measure the relative change of cloud properties with change in aerosol concentrations.

Aerosol column optical thicknesses measured from satellites are not yet accurate enough: accuracy is ±20% over the oceans, less accurate over vegetated land or over the deserts. Ground based remote sensing of aerosol can have a precision of ±0.02 in units of optical depth.

Translation of the optical thickness into the column aerosol concentration and into CCN is more difficult due to variation in the aerosol size distribution and chemical

composition and the vertical distribution of the aerosols. These are critical parameters needed for interpreting aerosols ingestion and effects on clouds.

In situ measurements from aircraft may influence the aerosol and cloud properties, and have limitations in correctly sampling all aerosol sizes. In addition, such measurements only represent small volumes that may not always correctly represent the processes that affect clouds. Surface based measurements may not always represent the total column or the cloud altitudes.

Small spatial and temporal coverage for highly variable parameters:

High spatial variability of precipitation makes it difficult to measure coincidental aerosol, clouds and precipitation. Therefore we are not aware of studies that include direct statistical correlations of aerosol and precipitation.

Cloud properties have a diurnal cycle not well represented by polar satellite observations. Geostationary satellite measure the diurnal cycle but with limited ability to derive the cloud droplet size.

Cause and effect: Once a statistical connection is established between the aerosol concentration, the cloud properties and precipitation, it is still difficult to assess whether the changes in the precipitation patterns are a results of the aerosols impact or whether it is changing of the precipitation patterns that affect the aerosol properties. Therefore the most informative measurements so far on the effect of aerosols on precipitation do not include simultaneous quantitative measurements of both aerosols and precipitation.

In summarizing this report it is valuable to list the type of studies that are required to help resolve the question of the effects of aerosols in general and pollution and biomass burning in particular on precipitation:

a) Better characterization of aerosols, such as:

To be useful in cloud and precipitation studies, size-resolved information about the numbers of particles emitted is required for the various primary aerosol sources, especially sea salt, mineral dust, pyrogenic aerosol and primary biogenic aerosol.

Emission information in the form of emission algorithms that permit calculation of an emission flux from model variables than a static array of emissions valid for one particular time.

The ability of mineral dust particles to act as CCN, GCCN, and IN as a function of aerosol size, origin, and airmass history needs to be determined.

The abundance and rate of production of submicron sea salt particles is still under dispute. Since these particles can play a significant role in cloud microphysics and precipitation in remote marine regions, observational constraints to their source parameterizations are urgently needed.

The characteristics, rate of emission and efficiency as CCN and IN of primary biogenic aerosols need to be investigated.

Due to the complexity of carbonaceous aerosol composition and emission processes, a critical concern is to define an adequate classification scheme for these aerosols based on observable characteristics.

There is a need to build a reliable inventory of emission parameterization of carbonaceous aerosols (BC, PPOC and SOA) that includes size distributions and number fluxes.

In building an inventory of emission the injection height should be included since changes in injection height due to shifts in agricultural or technical practices will have important consequences on the lifetime and fate of particles.

Accurate knowledge of the rates of the processes leading from SO_2 to sulfate aerosols is needed for clear and cloudy atmospheres.

Aerosol nitrate is expected to increase in climatic importance in the 21st century. Accurate measurement techniques and reliable modeling approaches for this component must be established.

In order to assess the human impact on cloud physics, we need to know the aerosol, CCN and IN distributions in the pre-anthropogenic atmosphere. Novel methods of inferring or backing-out pre-industrial cloud nucleating aerosol distributions are needed. The sources, characteristics, and fluxes of natural aerosol types must be investigated by carefully conducted field and laboratory studies.

New instruments should be developed and measurements should be carried out to determine CCN, GCCN and IN concentrations as a function of particle size, composition and supersaturation. Uncertainties are greatest for IN where multiple modes of particle activation are prevalent. These measurements should be conducted in the context of closure studies.

A program for validation and intercomparison of CCN observations should be carried out.

Global coordination of observational networks is needed for more complete coverage of global aerosols and precipitation chemistry related to aerosol removal.

Continuity of the observations and suitable locations of the observation sites (depending on the scale of phenomena) is very important. Aerosol type classification methods using depolarization ratio, wavelength dependence, and the lidar ratio (if available) are useful for the comparison.

More accurate assessment from satellites of the aerosol column concentration, vertical and size distribution, refractive index and single scattering albedo.

It is important to extend the measurements to small (100 nm particle diameter) particles in the retrievals, since many of these could be efficient CCN.

b) The effects on clouds and precipitation:

Long-term baseline measurements of CCN, GCCN and IN concentrations should be made at a number of locations throughout the world.

Vertical profiles of cloud microphysical processes, size, composition and phase of hydrometeors should be carried out by profiling from aircraft and from satellites and ground measurements. This is especially important in the tropics in areas affected by biomass burning and highly populated areas.

More accurate measurements of cloud droplet size through remote sensing (e.g. spectral polarized measurements of reflected sunlight).

Improved remote sensing measurements for liquid water path and total condensates.

Development of in situ instruments for measuring very small (5-30 micrometer diameter) ice crystals.

Development of new instruments to measure cloud droplets at high concentration and small sizes (50 - 100 micrometer diameter).

Experiments should be designed to better understand the role of ice in precipitation development and the connection between IN and ice crystals in clouds.

Multi year measurements from space of the precipitation patterns in missions coordinated with detailed clouds and aerosol measurements.

Improvements in instruments to measure snow rates water equivalent.

Long term statistical studies of the effects of pollution on precipitation in different types of conditions (e.g. orographic conditions, flat land, downwind effects of large cities on precipitation, in coastal areas where changes due to the transport of airmasses from sea to land and vise versa are prevalent, etc).

There is an urgent need for an improvement in the representation of cloud microphysical processes in models.

Modeling studies that extend beyond single-cloud responses but consider the cloud ensemble response to variations in cloud nucleating aerosols are needed.

Simulations of aerosol cloud interactions should be done in the context of observed structures of clouds and observed aerosol properties of the cloud environment.

Because of the coarse grid spacing of GCMs, clouds and cloud properties essentially have to be parameterized as sub-grid-scale processes. The challenge is to parameterize aerosol activation, the influence of aerosols on precipitation processes, the precipitation processes and their feedbacks on cloud and storm dynamics, and cloud processing of aerosols all in sub-grid-scale parameterizations! Clearly there is much room for improvement of existing parameterizations.

Models are particularly useful for providing quantified estimates of parameters such as precipitation amounts for a given simulation. However, the skill level of models in so doing should be quantified statistically.

Models could be used to isolate the role of aerosols from the influence of the meteorology and to give a quantitative answer as to the relative importance of each process.

It is important to extend the use of models to assess precipitation efficiency, and to consider the effect of changes of aerosol on precipitation efficiency.

Models are very effective tools for isolating *cause-and-effect* in a physical system. As models become more complex, it becomes increasingly difficult to isolate causal relations. Effort should be put into new methodologies for quantifying the sensitivity of a given parameter to a change in an input parameter or change in a combination of inputs.

Finally it is recommended that the WMO creates a web site to serve as central index to archives of public domain measurements of aerosol, cloud, and precipitation parameters. Individual agencies/countries to be encouraged to maintain long term web-accessible archives of research (including short-term field experiments) and operational measurements. Archives are encouraged to include key measured instrument parameters as well as retrieved parameters.

For example, for weather radar, reflectivity measurements are common to all radars while dual polarization is not. Rain rate is retrieved for most operational radar systems using a variety of methods. Both quality-controlled reflectivity and estimated rain rate would be archived. The data base would contain retrieved rain rate which are available from contributing sites. Additionally, the archived reflectivity will allow other methods of retrieval to be applied (e.g. different methodologies and future enhancements).

REFERENCES

Abdou, W.A., D.J. Diner, J.V. Martonchik, C.J. Bruegge, R.A. Kahn, B.J. Gaitley, K.A. Crean, L.A. Remer and B. Holben, Comparison of coincident Multiangle Imaging Spectroradiometer and Moderate Resolution Imaging Spectroradiometer aerosol optical depths over land and ocean scenes containing Aerosol Robotic Network sites, J. Geophys. Res., *Vol. 110, No. D10, D10S07* 10.1029/2004JD004693, 2005.

Abdul-Razzak, H., and S.J. Ghan, A parameterization of aerosol activation. Part 2: Multiple aerosol types, J. Geophys. Res., 105 (D5), 6837-6844, 2000.

Ackerman, A. S., M. P. Kirkpatrick, D. E. Stevens, and O. B. Toon The impact of humidity above stratiform clouds on indirect aerosol climate forcing, Nature 432, 1014 – 1017, 2004.

Ackerman, A. S., O.B. Toon, J.P.J. Taylor, W. Doug, P.V. Hobbs, R.J. Ferek, Effects of Aerosols on Cloud Albedo: Evaluation of Twomey's Parameterization of Cloud Susceptibility Using Measurements of Ship Tracks. J. of Atmos. Sci., 57, 2684-2695, 2000.

Ackerman, A.S., O.B. Toon, D.E. Stevens, A.J. Heymsfield, V. Ramanathan, and E.J. Welton, Reduction of tropical cloudiness by soot, *Sci.*, *288*, 1042-1047, 2000.

Ackerman, B., S.A. Changnon, G.L. Dzurisin, D.F. Gatz, R.C. Grosh, S.D. Hilberg, F.A. Huff, J.W. Mansell, H.T. Ochs III, M.E. Peden, P.T. Schickedanz, R.G. Semonin, and J.L. Vogel, Summary of METROMEX, Volume 2: Causes of Precipitation Anomalies, Illinois State Water Survey, Champaign, IL, pp 395, 1978.

Ackerman, A.S., P.V. Hobbs, and O.B. Toon, A model for particle microphysics, turbulent mixing, and radiative transfer in the stratocumulus-topped marine boundary layer and comparisons with measurements, *J. Atmos. Sci., 52*, 1204-1236, 1995.

Adams, P. J. and J. H. Seinfeld, Disproportionate impact of particulate emissions on global cloud condensation nuclei concentrations, *Geophys. Res. Lett.*, *30*, 1239, doi:10.1029/2002GL016303, 2003.

Adams, P. J., J. H. Seinfeld, and D. M. Koch, Global concentrations of tropospheric sulfate, nitrate, and ammonium aerosol simulated in a general circulation model, *J. Geophys. Res.*, *104*, 13,791-13,823, 1999.

Adams, P. J., J. H. Seinfeld, D. Koch, L. Mickley, and D. Jacob, General circulation model assessment of direct radiative forcing by the sulfate-nitrate-ammonium-water inorganic aerosol system, *J. Geophys. Res.*, *106*, 1097-1111, 2001.

Adler, R. F., J. Susskind, G. J. Huffman, D. Bolvin, E. Nelkin, A. Chang, R. Ferraro, A. Gruber, P. P. Xie, J. Janowiak, B. Rudolf, U. Schneider, S. Curtis, P. Arkin, The version-2 Global Precipitation Climatology Project (GPCP) monthly precipitation analysis (1979-present). J. Hydromet. **4**, 1147-1167, 2003.

Adler, R.F., C. Kidd, G. Petty, M. Morrissey, and H.M. Goodman, Intercomparison of global precipitation products: The third Precipitation Intercomparison Project (PIP-3), Bull. Amer. Meteor. Soc., 82, 1377-1396, 2001.

Adler, R.F., G.J. Huffman, A. Chang, R. Ferraro, P.-P. Xie, J. Janowiak, B. Rudolf, U. Schneider, S. Curtis, D. Bolvin, A. Gruber, J. Susskind, P. Arkin, and E. Nelkin, The version-2 Global Precipitation Climatology Project (GPCP) monthly precipitation analysis (1979–present), *J. Hydrometeorol. 4,* 1147–1167, 2003.

Afdermauer, A.N. and D.A. Johnson, Charge separation due to riming in an electric field. Quart. J. Roy. Meteor. Soc., 98, 369-382, 1972.

Albrecht, B.A., Aerosols, cloud microphysics, and fractional cloudiness, *Sci., 245*, 1227-1230, 1989.

Allison, L.J., E.B. Rogers, T.T. Wilheit and R.W. Fett, 1974: Tropical cyclone rainfall as measured by the Nimbus 5 electrically scanning microwave radiometer. Bul. Amer. Met. Soc., 55, 1074-1089.

American Meteorological Society, Statement on planned and inadvertent weather modification, *Bull. Amer. Meteorol. Soc.*, *66,* 447–448, 1984.

Amitai, E., D. B. Wolff, D. A. Marks, and D. S. Silberstein, Radar rainfall estimation, Lessons learned from the NASA/TRMM validation program. Second European Conference on Radar Meteorology (ERAD), Delft, The Netherlands. ERAD Publication Series, 1, 255-260 (Copernicus GmbH peer reviewed publication, ISBN 3-936586-04-7), 2002.

Andreae, M. O., and P. J. Crutzen, Atmospheric aerosols: Biogeochemical sources and role in atmospheric chemistry, *Science*, *276*, 1052-1056, 1997.

Andreae, M. O., and P. Merlet, Emission of trace gases and aerosols from biomass burning, *Global Biogeochem. Cycles*, *15*, 955-966, 2001.

Andreae, M. O., Climatic effects of changing atmospheric aerosol levels, in *World Survey of Climatology. Vol. 16: Future Climates of the World*, edited by A. Henderson-Sellers, pp. 341-392, Elsevier, Amsterdam, 1995.

Andreae, M. O., D. Rosenfeld, P. Artaxo, A. A. Costa, G. P. Frank, K. M. Longo, and M. A. F. Silva-Dias, Smoking rain clouds over the Amazon, *Science*, *303*, 1337-1342, 2004.

Andreae, M. O., E. Atlas, H. Cachier, W. R. Cofer, III, G. W. Harris, G. Helas, R. Koppmann, J.-P. Lacaux, and D. E. Ward, Trace gas and aerosol emissions from savanna fires, in *Biomass Burning and Global Change*, edited by J. S. Levine, pp. 278-295, MIT Press, Cambridge, Mass., 1996.

Andreae, M. O., H. Berresheim, T. W. Andreae, M. A. Kritz, T. S. Bates, and J. T. Merrill, Vertical distribution of dimethylsulfide, sulfur dioxide, aerosol ions, and radon over the northeast Pacific Ocean., *J. Atmos. Chem.*, *6*, 149-173, 1988.

Andreae, M. O., Ocean-atmosphere interactions in the global biogeochemical sulfur cycle, *Mar. Chem.*, *30*, 1-29, 1990.

Andreae, M. O., R. J. Charlson, F. Bruynseels, H. Storms, R. E. van Grieken, and W. Maenhaut, Internal mixture of sea salt, silicates and excess sulfate in marine aerosols, *Science*, *232*, 1620-1623, 1986.

Andreae, M. O., W. Elbert, R. Gabriel, D. W. Johnson, S. Osborne, and R. Wood, Soluble ion chemistry of the atmospheric aerosol and SO_2 concentrations over the eastern North Atlantic during ACE-2, *Tellus*, *52B*, 1066-1087, 2000.

Andreae, M. O., W. Elbert, Y. Cai, T. W. Andreae, and J. Gras, Non-seasalt sulfate, methanesulfonate, and nitrate aerosol concentrations and size distributions at Cape Grim, Tasmania, *J. Geophys. Res.*, *104*, 21,695-21,706, 1999.

Andreae, M.O., D. Rosenfeld, P. Artaxo, A.A. Costa, G.P. Frank, K.M. Longo, and M.A.F., Silvas-Dias, Smoking rain clouds over the Amazon, *Science, 303*, 1337-1342, 2004.

Andreae, M.O., E.V. Browell, , G.L. Gregory, R.C. Harriss, G.F. Hill, R.W. Talbot, G.W. Sachse, M. Garstang, D.J. Jacob, A.L. Torres, Biomass burning emissions and associated haze layers over Amazonia, *J. Geophys. Res., 93,* 1509–1527, 1988.

Andreae, M.O., J. Fishman, and J. Lindesay, The Southern Tropical Atlantic Region Experiment (STARE): Transport and Atmospheric Chemistry near the Equator - Atlantic (TRACE A) and Southern African Fire-Atmosphere Research Initiative (SAFARI): An introduction, J. Geophys. Res., 101 (D19), 23519-23520, 10.1029/96JD01786, 1996.

Andreae, M.O., R. Talbot, H. Berresheim, and K.M. Beecher, Precipitation chemistry of Central Amazonia, J. Geophy. Res., 95 (D10), 16,987-16999, 1990.

Andreae, T. W., M. O. Andreae, C. Ichoku, W. Maenhaut, J. Cafmeyer, A. Karnieli, and L. Orlovsky, Light scattering by dust and anthropogenic aerosol at a remote site in the Negev desert, Israel, *J. Geophys. Res.*, *107*, 4008, doi:10.1029/2001JD900252, 2002.

Andres, R. J., G. Marland, I. Fung, and E. Matthews, A 1°x1° distribution of carbon dioxide emissions from fossil fuel consumption and cement manufacture, 1950-1990, *Global Biogeochem. Cycles*, *10*, 419-429, 1996.

Andsager, K., K. V. Beard, and N. F. Laird, Laboratory measurements of axis ratios for large drops. J. Atmos. Sci., 56, 2673-2683, 1999.

Ansmann. A, M. Riebessell, U. Wandinger, C. Weitkamp, E. Voss, W. Lahman, and W. Michealis, Combined Raman elastic-backscatter LIDAR for vertical profiling of moisture, aerosol extinction, backscatter, and lidar ratio, Appl. Phys., B55, 18-28, 1992.

Anttila, T., and V. M. Kerminen, Influence of organic compounds on the cloud droplet activation: A model investigation considering the volatility, water solubility, and surface activity of organic matter, *J. Geophys. Res.*, *107*, 4662, doi:10.1029/2001JD001482, 2002.

Arimoto, R., B. J. Ray, N. F. Lewis, U. Tomza, and R. A. Duce, Mass-particle size distributions of atmospheric dust and the dry deposition of dust to the remote ocean, *J. Geophys. Res.*, *102*, 15,867-15,874, 1997.

Arimoto, R., Y.J. Kim, Y.P. Kim, P.K. Quinn, T.S. Bates, T.L. Anderson, S.L. Gong, M.C. I. Uno, B.J. Huebert, A.D. Clarke, Y. Shinozuka, R.J. Weber, J.R. Anderson, S.A. Guazzotti, R.C. Sullivan, D.A. Sodeman, K.A. Prather, and I. Sokolik, Characterization of Asian Dust during ACE-Asia, Global and Planetary Change, submitted.

Arkin, P.A., and B.M. Meisner, The relationship between large-scale convective rainfall and cold cloud over the western hemisphere during 1982-84, Mon. Wea. Rev., 115, 51-74, 1987.

Arkin, P.A., The relationship between fractional coverage of high cloud and rainfall accumulations during GATE over the B-scale array, Mon. Wea. Rev., 107, 1382-1387, 1979.

Artaxo, P., Aerosol sampling and analysis, in: Environmental Monitoring Handbook, Edited by Alex Guenther, McGraw-Hill Professional, New York, USA, ISBN: 0-07-135176-0, 2002.

Artaxo, P., F. Gerab, M. A. Yamasoe, and J. V. Martins, Fine mode aerosol composition at three long-term atmospheric monitoring sites in the Amazon Basin, *J. Geophys. Res.*, *99*, 22,857-22,868, 1994.

Artaxo, P., F. Gerab, M.L.C. Rabello, Elemental composition of aerosol particles from two background monitoring stations in the Amazon Basin, Nuclear Instruments and Methods in Physics Research, B75, 277-281, 1993.

Artaxo, P., H. Storms, F. Bruynseels, R. V. Grieken, and W. Maenhaut, Composition and sources of aerosols from the Amazon basin, *J. Geophys. Res.*, *93*, 1605-1615, 1988.

Artaxo, P., J. V. Martins, M. A. Yamasoe, A. S. Procópio, T. M. Pauliquevis, M. O. Andreae, P. Guyon, L. V. Gatti, and A. M. C. Leal, Physical and chemical properties of aerosols in the wet and dry season in Rondonia, Amazonia, *J. Geophys. Res.*, *107*, 8081, doi:10.1029/2001JD000666, 2002.

Artaxo, P., M. L. C. Rabello, W. Maenhaut, R. Van Grieken, Trace elements and individual particle analysis of aerosol particles from the Antarctic peninsula, Tellus, 44B, 318-334, 1992.

Artaxo, P., P. Oyola, R. Martinez, Aerosol composition and source apportionment in Santiago de Chile. Nuclear Instruments and Methods in Physics Research B, 150, 409-416, 1999.

Artaxo, P., W. Maenhaut, H. Storms, and R. Van. Grieken, Aerosol characteristics and sources for the Amazon Basin during the wet season, *J. Geophys. Res.*, *95*, 16,971-16,986, 1990.

Atlas, D., C. W. Ulbrich, F. D. Marks Jr., E. Amitai, and C. R. Williams, Systematic variation of drop size distribution and radar-rainfall relation, J. Geophys. Res., 104, 6155-6169, 1999.

Auer, A.H.Jr., D.L. Veal and J.D. Marwitz, Observations of Ice Crystal and Ice Nuclei Concentrations in Stable Cap Clouds. J. Atmos. Sci., 26, 1342-1343, 1969.

Austin, P., Y. Wang, R. Pincus, and V. Kujala, Precipitation in stratocumulus clouds: Observational and modeling results, *J. Atmos. Sci.*, *52*, 2329-2352, 1995.

Austin, P.H., S. Siems, and Y. Wang,Austin, Constraints on droplet growth in radiatively cooled stratocumulus clouds, *J. Geophys. Res., 100*, 14,231-14,242, 1995.

Austin, P.M., Relation between measured radar reflectivity and surface rainfall, Mon. Wea. Rev., 115, 1053–1070, 1987.

Ayers, G. P., J. P. Ivey, and R. W. Gillett, 1991: Coherence between seasonal cycle in dimethyl sulphide, methane-sulphonate and sulphates in marine air. *Nature*, **359**, 404-406.

Ayers, G.P., and J.L. Gras, Seasonal relationship between cloud condensation nuclei and aerosol methanesulfonate in marine air, *Nature, 351,* 834–835, 1991.

Ayers, G.P., J.P. Ivey, and R.W. Gillett, Coherence between seasonal cycles of dimethyl sulfide, methansulphonate and sulfate in marine air, *Nature, 349,* 404–406, 1991.

Ba, M. B., and A. Gruber, GOES Multispectral Rainfall Algorithm (GMSRA), J. Appl. Meteor., 40, 1500-1514, 2001.

Baker, B. A., On the nucleation of ice in highly supersaturated regions of clouds. *J. Atmos. Sci.*, **48**, 1904-1907, 1991.

Baker, B.A., Turbulent entrainment and mixing in clouds: A new observational approach, *J. Atmos. Sci*., *49*, 387-404, 1992.

Baker, M.B., and J. Latham, The evolution of droplet spectra and the rate of production of embryonic raindrops in small cumulus clouds, *J. Atmos. Sci*., *36*, 1612-1615, 1979.

Baker, M.B., R.G. Corbin, and J. Latham, The influence of entrainment on the evolution of cloud droplet spectra: I. A model of inhomogeneous mixing, *Quart. J. Roy. Meteorol. Soc., 106,* 581–598, 1980.

Baltensperger, U., E. Weingartner, H. Burtscher, J. Keskinen, Dynamic mass and surface area measurements, in: Aerosol Measurement, Principles, Techniques, and Applications, Wiley-Interscience, Second Edition, 387-418, 2001.

Baltensperger, U., M. Kalberer, J. Dommen, D. Paulsen, M. Alfarra, H. Coe, R. Fisseha, A. Gascho, M. Gysel, S. Nyeki, M. Sax, M. Steinbacher, A. Prevot, S. Sjoren, E. Weingartner, and R. Zenobi, Secondary organic aerosols from anthropogenic and biogenic precursors, Faraday Discussions, 130, 265-278, 2005.

Baltensperger, U., N. Streit, E. Weingartner, S. Nyeki, A. S. H. Prevot, R. Van Dingenen, A. Virkkula, J. P. Putaud, A. Even, H. ten Brink, A. Blatter, A. Neftel, and H. W. Gaggeler, Urban and rural aerosol characterization of summer smog events during the PIPAPO field campaign in Milan, Italy, *J. Geophys. Res.*, *107*, 8193, doi:10.1029/2001JD001292, 2002.

Barger, W. R., and W. D. Garrett, Surface-active organic material in air over Mediterranean and over eastern Equatorial Pacific, *J. Geophys. Res. -Oceans and Atmospheres*, *81*, 3151-3157, 1976.

Barkstrom, B.R., Some effects of 8-12 um radiant energy transfer on the mass and heat budgets of cloud droplets, *J. Atmos. Sci., 35*, 665-673, 1978.

Barnes W. L., T. S. Pagano, and V. V. Salomonson, Pre-launch characteristics of MODIS on EOS-AM1, IEEE Trans. Geosci. Remote Sens., **36**, 1088-1100, 1998.

Barrett, E.C., The estimation of monthly rainfall from satellite data. Mon. Weath. Rev, 101, 215-222, 1970.

Barrie, L. A., Y. Yi, et al., A comparison of large-scale atmospheric sulphate aerosol models (COSAM): overview and highlights, *Tellus*, *53B*, 615-645, 2001.

Barrie, L.A., and M.L. Barrie, Chemical components of lower tropospheric aerosols in the high Arctic: six years of observations, J. Atmos. Chem., 11, 211-266, 1990.

Barrie, L.A., Arctic air pollution: an overview of current knowledge, Atmos. Environ., 20, 643-663, 1986.

Barrie, L.A., Arctic air pollution: a case study of continent-to-ocean-to-continent transport, in The long-range atmospheric transport of natural and contaminant substances., edited by A.H. Knap, and M.-S. Kaiser, pp. 137-148, Kluwer Academic Publishers, Dordrecht, Holland, 1990.

Barrie, L.A., Y. Yi, W.R. Leaitch, U. Lohmann, P. Kasibhatla, G.J. Roelofs, J. Wilson, F. McGovern, C. Benkovitz, M.A. Melieres, K. Law, J. Prospero, M. Kritz, D. Bergmann, C. Bridgeman, M. Chin, J. Christensen, R. Easter, J. Feichter, C. Land, A. Jeuken, E. Kjellstrom, D. Koch, and P. Rasch, A comparison of large-scale atmospheric sulphate aerosol models (COSAM): overview and highlights, Tellus Series B Chemical and Physical Meteorology, 53 (5), 615-645, 2001.

Barth, M. C., and A. T. Church, Regional and global distributions and lifetimes of sulfate aerosols from Mexico city and southeast China, *J. Geophys. Res.*, *104*, 30,231-30,239, 1999.

Barth, M.C., D.A. Hegg, and P.V. Hobbs, Numerical modeling of cloud and precipitation chemistry associated with two rainbands and some comparisons with observations, *J. Geophys. Res., 97,* 5825-5845, 1992.

Bartlett, J.T., and P.R. Jonas, On the dispersion of the sizes of droplets growing by condensation in turbulent clouds, *Quart. J. Roy. Meteorol. Soc*., *98*, 150-164, 1972.

Bates, T. S., B. J. Huebert, J. L. Gras, F. B. Griffiths, and P. A. Durkee, The International Global Atmospheric Chemistry (IGAC) Project's First Aerosol Characterization Experiment (ACE-1) - Overview, *J. Geophys. Res*., *103*, 16,279-16,318, 1998.

Bates, T. S., D. J. Coffman, D. S. Covert, and P. K. Quinn, Regional marine boundary layer aerosol size distributions in the Indian, Atlantic, and Pacific Oceans: A comparison of INDOEX measurements with ACE-1, ACE-2, and Aerosols99, *J. Geophys. Res*., *107*, 8026, doi:10.1029/2001JD001174, 2002.

Bates, T. S., P. K. Quinn, D. J. Coffman, J. E. Johnson, T. L. Miller, D. S. Covert, A. Wiedensohler, S. Leinert, A. Nowak, and C. Neusuess, Regional physical and chemical properties of the marine boundary layer aerosol across the Atlantic during Aerosols99: An overview, *J. Geophys. Res.*, *106*, 20767-20782, 2001.

Bates, T. S., P. K. Quinn, D. S. Covert, D. J. Coffman, J. E. Johnson, and A. Wiedensohler, Aerosol physical properties and processes in the lower marine boundary layer: a comparison of shipboard sub-micron data from ACE-1 and ACE-2, *Tellus*, *52B*, 258-272, 2000.

Battan, L.J., Radar Observation of the Atmosphere, 324 pp., University of Chicago Press, Chicago, Ill, 1973.

Bauer, H., H. Giebl, R. Hitzenberger, A. Kasper-Giebl, G. Reischl, F. Zibuschka, and H. Puxbaum, Airborne bacteria as cloud condensation nuclei, *J. Geophys. Res.*, *108*, 4658, doi:10.1029/2003JD003545, 2003.

Bauer, P., J.P.V. Poiares Baptisa, and M. De Iulis, The effect of the melting layer on the microwave emission of clouds over the ocean, J. Atmos. Sci., 56, 852–867, 1999.

Bauer, P., Over-ocean rainfall retrieval from multisensor data of the Tropical Rainfall Measuring Mission. Part I: Design and evaluation of inversion databases, J. Atmos. Ocean. Tech., 18, 1315–1300, 2001.

Beard, K.V., and H.T. Ochs, III, Warm-rain initiation: an overview of microphysical mechanisms, *J. Appl. Meteorol*., *32*, 608-625, 1993.

Beard, K.V., D.B. Johnson, and D. Baumgardner, Aircraft observations of large raindrops in warm, shallow, convective clouds, *Geophys. Res. Lett., 13*, 991-994, 1986.

Beheng, K.D., A parameterization of warm cloud microphysical conversion processes, *Atmos. Res*., *33*, 193-206, 1994.

Beliaev, V.I., Size distribution of drops in a cloud during its condensation stage of development, *Akad. Nauk. SSSR, IZV*, Geofix. Ser., 8, 1209-1213, 1961.

Ben-Zvi, A., Comments on "A new look at the Israeli cloud seeding experiments, *J. Appl. Meteorol., 36,* 255–256, 1997.

Bergeron, T., On the physics of clouds and precipitation, in *Proc. 5th Assembly UGGI,* Vol. 2., Lisbon, 1933.

Bergeron, T., Über der mechanismus der ausgiebigan niederschläge, *Ber. Deut. Wetterd, 12,* 225–232, 1950.

Berglen, T. F., T. K. Berntsen, I. S. A. Isaksen, and J. K. Sundet, A global model of the coupled sulfur/oxidant chemistry in the troposphere: The sulfur cycle, *J. Geophys. Res*., *109*, D19310, doi:10.1029/2003JD003948, 2004.

Berry, E.X., and R.L. Reinhardt, An analysis of cloud drop growth by collection. Part I. Double distributions, *J. Atmos. Sci., 31*, 1814-1824, 1974.

Berry, E.X., Cloud droplet growth by coalescence*, J. Atmos. Sci., 24*, 688-701, 1967.

Bey, I., D.J. Jacob, J.A. Logan, and R.M. Yantosca, Asian chemical outflow to the Pacific: origins, pathways and budgets, J. Geophys. Res., 106, 23,097-23,114, 2001.

Bigg, E. K. Geographical differences in concentrations of ice nuclei. *Mon. Weather Rev*., 92:355- 356, 1964.

Bigg, E. K., Discrepancy between observation and prediction of concentrations of cloud condensation nuclei, *Atmos. Res*., *20*, 81-86, 1986.

Bigg, E.K. and C.M. Stevenson, Comparison of ice nuclei in different parts of the world. J. Rech. Atmos. 4, 41-58, 1970.

Bigg, E.K., An independent evaluation of a South African hygroscopic cloud seeding experiment, 1991-1995, *Atmos. Res., 43*, 111–127, 1997.

Bigg, E.K., Ice nucleus measurements in remote areas. J. Atmos. Sci., 30, 1153-1157, 1973.

Bigg, K. and S.C. Hopwood, Ice Nuclei in the Antarctic. J. Atmos. Sci., 20, 185-188, 1963.

Bilde M, and B. Svenningsson, CCN activation of slightly soluble organics: the importance of small amounts of inorganic salt and particle phase ,Tellus B-Chemical and physical meteorology 56 (2): 128-134, 2004

Bilde, M., and B. Svenningsson, CCN activation of slightly soluble organics: Importance of small amounts of inorganic salt and particle phase, Tellus, 56B, 128-134, 2004.

Birmili, W., A. Wiedensohler, J. Heintzenberg, and K. Lehmann, Atmospheric particle number size distribution in central Europe: Statistical relations to air masses and meteorology, *J. Geophys. Res*., *106*, 32005-32018, 2001.

Birmili, W., B. Yuskiewicz, A. Wiedensohler, F. Stratmann, T.W. Choularton, and K.N. Bower, Climate-relevant modification of the aerosol size distribution by processes associated with orographic clouds, *Atmos. Res., 50,* 241–263, 1999.

Bissonnette, L.R., and G. Roy, Lidar multiple scattering retrieval: Monte Carlo validation, field tests, and a case study, in 22nd International Laser Radar Conference, pp. 313-316, Matera, Italy, 2004.

Biswas, K.R., and A.S. Dennis, Formation of rain shower by salt seeding, *J. Appl. Meteorol., 10*, 780–784, 1971.

Bleck, R., A fast approximative method for integrating the stochastic coalescence equation, *J. Geophys. Res*., *75*, 5165-5171, 1970.

Boers, R., G. P. Ayers, and J. L. Gras, Coherence between seasonal cycles in satellite observed cloud optical depth ad boundary layer CCN concentration at a mid-latitude Southern Hemispheric site, Tellus, 46B, 123 – 131, 1994.

Boers, R., J. B. Jensen, P. B. Krummel, Microphysical and radiative structure of marine stratocumulus clouds over the Southern Ocean: Summer results and seasonal differences, Quart. J. Royal Meteor. Soc., 124, 151 – 168, 1998.

Boers, R., J. B. Jensen, P. B. Krummel, and H. Gerber, Microphysical and radiative structure of wintertime stratocumulus clouds over the Southern Ocean. Quart. J. Royal Meteor. Soc., 122, 1307 – 1339, 1996.

Boers, R., J.-R. Acarreta, J. Gras, Satellite monitoring of the droplet concentration of water clouds. Submitted to JGR, 2005.

Bond, T. C., D. G. Streets, K. F. Yarber, S. M. Nelson, J. H. Woo, and Z. Klimont, A technology-based global inventory of black and organic carbon emissions from combustion, *J. Geophys. Res.*, *109*, D14203, doi:10.1029/2003JD003697, 2004.

Bond, T. C., D. S. Covert, J. C. Kramlich, T. V. Larson, and R. J. Charlson, Primary particle emissions from residential coal burning: Optical properties and size distributions, *J. Geophys. Res.*, *107*, 8347, doi:10.1029/2001JD000571, 2002.

Borys R.D. and R.D. Duce, Relationships among lead, iodine, trace metals and ice nuclei in a coastal urban atmosphere. *J. Appl. Meteor.,* **18,** 1490–1494, 1979

Borys, R.D., D.H. Lowenthal, and D.L. Mitchel, The relationship among cloud physics, chemistry and precipitation rate in cold mountain clouds, *Atmos. Environ., 34,* 2593–2602, 2000.

Borys, R.D., D.H. Lowenthal, S.A. Cohn, and W.O.J. Brown, Mountaintop and radar measurements of anthropogenic aerosol effects on snow growth and snow rate, *Geophys. Res. Lett., 30(10),* 1538, doi:10.1029/2002GL016855, 2003.

Bott, A., A flux method for the numerical solution of the stochastic collection equation: extension to two dimensional particle distributions, *J. Atmos. Sci*., *57*, 284-294, 2000.

Bott, A., T. Trautmann, and W. Zdunkowski, A numerical model of the cloud-topped planetary boundary-layer: Radiation, turbulence and spectral microphysics in marine stratus, *Quart. J. Roy. Meteorol. Soc.*, *122*, 635-667, 1996.

Bott, A., U. Sievers, and W. Zdunkowski, A radiation fog model with a detailed treatment of the interaction between radiative transfer and fog microphysics, *J. Atmos. Sci., 47*, 2153-2166, 1990.

Boucher, O., and U. Lohmann, The sulfate-CCN-cloud albedo effect: A sensitivity study with two general circulation models, Tellus, B (47), 281-300, 1995.

Bowen, E.G., A new method of stimulating convective clouds to produce rain and hail, *Quart. J. Roy. Meteorol. Soc., 78*, 37–45, 1952.

Bower, K. N., and T. W. Choularton, Cloud processing of the cloud condensation nucleus spectrum and its climatological consequences, *Quart. J. R. Meteorol. Soc., 119*, 655-679, 1993.

Braham, R. R., and P. Spyers-Duran, Ice nucleus measurements in an urban atmosphere, *J. Appl. Meteor.*, *13*, 940-945, 1974.

Braham, R. R., Jr., What is the role of ice in summer rain-showers? *J. Atmos. Sci.*, **21**, 640-646, 1964.

Braham, R.R., Jr., Rainfall enhancement—a scientific challenge, in *Rainfall Enhancement—A Scientific Challenge*, *AMS Meteorol. Monogr., 21,* No. 43, 1–5, Amer. Meteorol. Soc., Boston, Mass., 1986.

Braham, R.R., The water and energy budgets of the thunderstorm and their relationship to thunderstorm development, *J. Atmos. Sci*., *9,* 227–242, 1952.

Brechtel, F. J., and S. M. Kreidenweis, Predicting particle critical supersaturation from hygroscopic growth measurements in the humidified TDMA. part I: Theory and sensitivity studies, *J. Atmos. Sci.*, *57*, 1854-1871, 2000a.

Brechtel, F. J., and S. M. Kreidenweis, Predicting particle critical supersaturation from hygroscopic growth measurements in the humidified TDMA. Part II: Laboratory and ambient studies, *J. Atmos. Sci.*, *57*, 1872-1887, 2000b.

Brechtel, F. J., S. M. Kreidenweis, and H. B. Swan, Air mass characteristics, aerosol particle number concentrations, and number size distributions at Macquarie Island during the First Aerosol Characterization Experiment (ACE 1), *J. Geophys. Res.*, *103*, 16351-16367, 1998.

Brenguier, J. L., and L. Chaumat: Droplet spectra broadening in cumulus clouds. Part I: Broadening in adiabatic cores. *J. Atmos. Sci.*, 58, 628-641, 2001.

Brenguier, J. L., H. Pawlowska, and L. J. Schüller, Cloud microphysical and radiative properties for parameterization and satellite monitoring of the indirect effect of aerosol on climate, *J. Geophys. Res*., **108**, 8632, doi:10.1029/2002JD002682, 2003.

Brenguier, J. L., H; Pawlowska, L. Schüller, R. Preusker, J. Fischer, and Y. Fouquart, Radiative properties of boundary layer clouds: droplet effective radius versus number concentration. J. Atmos. Sci. 57, 803-821, 2000b.

Brenguier, J. L., P. Y. Chuang, Y. Fouquart, D. W. Johnson, F. Parol, H. Pawlowska, J. Pelon, L. Schuller, F. Schroder, and J. Snider, An overview of the ACE-2 CLOUDYCOLUMN closure experiment, Tellus B, 52, 815–827, 2000a.

Bréon F. M., and S. Colzy, Global distribution of cloud droplet effective radius from POLDER polarization measurements, Geophys. Res. Lett., **27**, 4065-4068, 2000.

Bréon, F. M., and P. Goloub, Cloud droplet effective radius from spaceborne polarization measurements, Geophys. Res. Lett., **25**, 1879-1882, 1998.

Bréon, F.M. and M. Doutriaux-Boucher: A comparison of Cloud Droplet Radii measured from space, IEEE Trans. Geos. Rem. Sens., 43(8), 1796–1805, 2005.

Breon, F.-M., D. Tanre, and S. Generoso, Aerosol effect on cloud droplet size monitored from satellite, *Science, 295*, 834-838, 2002.

Brier, G.W., L.O. Grant, and P.W. Mielke, Jr., An evaluation of extended area effects from attempts to modify local clouds and cloud systems, *Proc. WMO/IAMAP Scientific Conf. on Weather Modification*, Tashkent, Uzbekistan, World Meteorol. Org., 439–447, 1973.

Bringi, V.N., and V. Chandrasekar, *Polarimetric Doppler Weather Radar: Principles and Applications*, 636 pp., Cambridge University Press, Cambridge, U.K., 2001.

Broekhuizen, K., Chang, R. Y.-W., Leatch, W. R., Li, S.-M., and Abbatt, J. P. D.: Closure between measured and modelled cloud condensation nuclei (CCN) using size-resolved aerosol compositions in downtown Toronto, Atmos. Chem. Phys. Discuss., 5, 6263–6293, SRef-ID: 1680-7375/acpd/2005-5-6263, 2005.

Broekhuizen, K., P. P. Kumar, and J. P. D. Abbatt, Partially soluble organics as cloud condensation nuclei: Role of trace soluble and surface active species, *Geophys. Res. Lett.*, *31*, 2004.

Broekhuizen, K., P.P. Kumar, and J.P.D. Abbatt, Partially soluble organics as cloud condensation nuclei: Role of trace soluble and surface active species - art. no. L01107, Geophysical Research Letters, 31 (1), 1107, 2004.

Broekhuizen, K., Pradeep Kumar, P., and Abbatt, J. P. D.: Partially soluble organics as cloud condensation nuclei: Role of trace soluble and surface active species, Geophys. Res. Lett., 31, L01107, doi:10.1029/2003GL018203, 2004.

Brook, J.R., T.F. Dann, and R.T. Burnett, The relationship among TSP, PM10, PM2.5, and Inorganic constituents of atmospheric particulate matter at multiple Canadian locations, J. Air & Waste Manage. Assoc., 47, 2-19, 1997.

Brooks, S. D., P. J. DeMott, and S. M. Kreidenweis, Water uptake by particles containing humic materials and mixtures of humic materials with ammonium sulfate, *Atmos. Environ.*, *38*, 1859-1868, 2004.

Browning, K.A., and F.H. Ludlam, Airflow in convective storms, *Quart. J. Roy. Meteorol. Soc., 88,* 117–135, 1962.

Brownscombe JL and N.S.C. Thorndike, Freezing and shattering of water droplets in free fall. *Nature, Lond.* **220** 687-689, 1968.

Bruintjes, R. T., T. L. Clark, and W. D. Hall. The dispersion of tracer plumes in mountainous regions in central Arizona: Comparisons between observations and modeling results. *J. Appl. Meteorol.* 34:971-988, 1995.

Bukowiecki, N., M. Hill, R. Gehrig, C.N. Zwicky, P. Lienemann, F. Hegedüs, G. Falkenberg, E. Weingartner, U. Baltensperger, Trace metals in ambient air: hourly size-segregated mass concentrations determined by Synchrotron-XRF, Environ. Sci. Technol., **39**, 5754-5762, 2005.

Buriez, J. C., M. Doutriaux-Boucher, F. Parol, and N. G. Loeb, Angular variability of the liquid water cloud optical thickness retrieved from ADEOS-POLDER, J. Atmos. Sci., **58**, 3007-3018, 2001.

Burnet, F., J. L. Brenguier, Experimental study of the entrainment-mixing process. Submitted to J. Atmos. Sci., 2006.

Cachier, H., C. Liousse, M.-H. Pertuisot, A. Gaudichet, F. Echalar, and J.-P. Lacaux, African fire particulate emission and atmospheric influence, in *Biomass Burning and Global Change*, edited by J. S. Levine, pp. 428-440, MIT Press, Cambridge, Mass., 1996.

Cachier, H., P. Buat-Ménard, M. Fontugne, and R. Chesselet, Long-range transport of continentally-derived particulate carbon in the marine atmosphere: Evidence from stable carbon isotope studies, *Tellus*, *35B*, 161-177, 1983.

Cairns, B., L. D. Travis, and E. E. Russell, 1997: Proc. SPIE, **3220**, London.

Cakmur, R.V., R.L. Miller, and I. Tegen, A comparison of seasonal and interannual variability of soil dust aerosols over the Atlantic Ocean as inferred by the TOMS AI and AVHRR AOT retrievals, J. Geophys. Res., 106 (D16), 18,287-18,304, 2001.

Calheiros, R. V., and I. Zawadzki, Reflectivity-rain rate relationships for radar hydrology in Brazil. J. Climate. Appl. Meteorol. 26, 118-132, 1987.

Campos, E., and I. Zawadzki, Instrument uncertainties in Z-R relations. J. Appl. Meteor., 39, 1088-1102, 2000.

Campuzano-Jost, P., C. D. Clark, H. Maring, D. S. Covert, S. Howell, V. Kapustin, K. A. Clarke, E. S. Saltzman, and A. J. Hynes, Near-real-time measurement of sea-salt aerosol during the SEAS campaign: Comparison of emission-based sodium detection with an aerosol volatility technique, *J. Atmos. Ocean. Technol.*, *20*, 1421-1430, 2003.

Cantrell, W., and A. Heymsfield, Production of ice in tropospheric clouds, Bulletin of the america Meteorological Society, 86 (6), 795-807, 2005.

Cantrell, W., G. Shaw, C. Leck, L. Granat, and H. Cachier, Relationships between cloud condensation nuclei spectra and aerosol particles on a south-north transect of the Indian Ocean, *J. Geophys. Res.*, *105*, 15313-15320, 2000.

Cantrell, W., G. Shaw, G. R. Cass, Z. Chowdhury, L. S. Hughes, K. A. Prather, S. A. Guazzotti, and K. R. Coffee, Closure between aerosol particles and cloud condensation nuclei at Kaashidhoo Climate Observatory, *J. Geophys. Res.*, *106*, 28,711-28,718, 2001.

Carlson, T. N., and J. M. Prospero, Large-scale movements of Saharan air impulses over western tropical Atlantic, BULL. AMER. MET. SOC. 52 (8): 779& 1971

Carmichael, G. R., D. G. Streets, G. Calori, M. Amann, M. Z. Jacobson, J. Hansen, and H. Ueda, Changing trends in sulfur emissions in Asia: Implications for acid deposition, air pollution, and climate, *Environ. Sci. Technol.*, *36*, 4707-4713, 2002.

Caro, D., W. Wobrock, and A.I. Flossmann, A numerical study on the impact of hygroscopic seeding on the development of cloud particle spectra, *J. Appl. Meteorol., 41*, 333–350, 2002.

Carrió, G.G., H. Jiang, and W.R. Cotton, Impact of aerosol intrusions on the Arctic boundary layer an on sea-ice melting rates. Part I: May 4, 1998 case, *J. Atmos. Sci*., *62*, doi: 10.1175/JAS3454.1, 3082-3093, 2005a.

Carrió, G.G., H. Jiang, and W.R. Cotton, Impact of aerosol intrusions on the Arctic boundary layer an on sea-ice melting rates. Part II: Multimonth simulations, *J. Atmos. Sci*., 62, doi: 10.1175/JAS3558.1**,** 2005b.

Carte, A**.** E. and S. C. Mossop, "Measurements of the Concentration of Atmospheric Ice Nuclei in Southern Africa, 1956 to 1960," *Bulletin de I'Ohservatoire du Puy de DGme, No. 4*, 137-149, 1960.

Castro, A., J. L. Marcos, J. Dessens, J. L. Sanchez, and R. Fraile, Concentration of ice nuclei in continental and maritime air masses in Leon (Spain), *Atmos. Res.*, *48*, 155-167, 1998.

Cavalli, F., M. C. Facchini, S. Decesari, M. Mircea, L. Emblico, S. Fuzzi, D. Ceburnis, Y. J. Yoon, C. D. O'Dowd, J. P. Putaud, and A. Dell'Acqua, Advances in characterization of size-resolved organic matter in marine aerosol over the North Atlantic, *J. Geophys. Res.*, *109*, D24215, doi:10.1029/2004JD005137, 2004.

Chahine, M.T., The hydrological cycle and its influence on climate, *Nature, 359*, 373–380, 1992.

Chan, M. N., and C. K. Chan, Hygroscopic properties of two model humic-like substances and their mixtures with inorganics of atmospheric importance, *Environ. Sci. Technol.*, *37*, 5109-5115, 2003.

Chan, M. N., M. Y. Choi, N. L. Ng, and C. K. Chan, Hygroscopicity of water-soluble organic compounds in atmospheric aerosols: Amino acids and biomass burning derived organic species, *Environ. Sci. Technol.*, *39*, 1555-1562, 2005.

Chand, D., O. Schmid, P. Gwaze, R. Parmar, G. Helas, K. Zeromskiene, A. Wiedensohler, A. Massling, and M. Andreae, Laboratory measurements of smoke optical properties from the burning of Indonesian peat and other types of biomass, Geophys. Res. Lett., 32 (12), Art. No. L12819, 2005.

Chapman, R. D., and M. J. Jose, The JHU/APL disdrometer, APL Technical Report SRO-97-03, 1997.

Chappell, C.F., L.O. Grant, and P.W. Mielke, Jr., Cloud seeding effects on precipitation intensity and duration of wintertime orographic clouds, *J. Appl. Meteorol., 10,* 1006–1010, 1971.

Charlson, R. J., J. E. Lovelock, M. O. Andreae, and S. G. Warren, Oceanic phytoplankton, atmospheric sulphur, cloud albedo, and climate, *Nature*, *326*, 655-661, 1987.

Charlson, R. J., J. H. Seinfeld, A. Nenes, M. Kulmala, A. Laaksonen, and M. C. Facchini, Reshaping the theory of cloud formation, *Science*, *292*, 2025-2026, 2001.

Charlson, R.J., J.E. Lovelock, M.O. Andreae, and S.G. Warren, Oceanic phytoplankton, atmospheric sulfur, cloud albedo and climate, *Nature, 326,* 655–661, 1987.

Chaumat , L., and J. L. Brenguier: Droplet spectra broadening in cumulus clouds. Part II: Micro-scale droplet concentration heterogeneities. *J. Atmos. Sci.*, 58, 642-654, 2001.

Che, H.Z., G.Y. Shi, X.Y. Zhang, R. Arimoto, J.Q. Zhao, L. Xu, B. Wang, and Z.H. Chen, Analysis of 40 years of solar radiation data from China, 1961?2000, Geophys. Res. Lett., 32, L06803, doi:10.1029/2004GL022322, 2005.

Chen, J.-P., and D. Lamb, Simulation of cloud microphysical and chemical processes using a multicomponent framework. Part I: Description of the microphysical model, *J. Atmos. Sci., 51*, 2613–2630, 1994**.**

Chen, Y. Z., N. Shah, F. E. Huggins, G. P. Huffman, W. P. Linak, and C. A. Miller, Investigation of primary fine particulate matter from coal combustion by computer-controlled scanning electron microscopy, *Fuel Processing Technology*, *85*, 743-761, 2004.

Chiapello, I., C. Moulin, and J.M. Prospero, Understanding the long-term variability of African dust transport across the Atlantic as recorded in both Barbados surface concentrations and large-scale Total Ozone Mapping Spectrometer (TOMS) optical thickness, J. Geophys. Res., 110, D18S10, doi:10.1029/2004JD005132, 2005.

Chin, M., P. Ginoux, S. Kinne, O. Torres, B. N. Holben, B. N. Duncan, R. V. Martin, J. A. Logan, A. Higurashi, and T.

Nakajima, 2002: Tropospheric aerosol optical thickness from the GOCART model and comparisons with satellite and sun photometer measurements, J. Atmos. Sci. **59**, 461-483.

Choi, M. Y., and C. K. Chan, Continuous measurements of the water activities of aqueous droplets of water-soluble organic compounds, *Journal of Physical Chemistry A*, *106*, 4566-4572, 2002.

Chosson, F., J. L. Brenguier, and L. Schüller, Entrainment-mixing and Radiative Transfer Simulation in Boundary-Layer Clouds. Submitted to J. Atmos. Sci., 2006

Chowdhary, J., B. Cairns, and L. D. Travis, Case studies of aerosol retrieval over the ocean from multiangle, multispectral photopolarimetric remote sensing data, J. Atmos. Sci., **59**, 383-397, 2002.

Chowdhary, J., B. Cairns, M. Mishchenko, and L. Travis, Retrieval of aerosol properties over the ocean using multispectral and multiangle photopolarimetric measurements from the Research Scanning Polarimeter, Geophys. Res. Lett., **28**, 243–246, 2001.

Chowdhary, J., B. Cairns, M. Mishchenko, P. Hobbs, G. Cota, J. Redemann, K. Rutledge, B. N. Holben, and E. Russell, Retrieval of Aerosol Scattering and Absorption Properties from Photopolarimetric Observations over the Ocean during the CLAMS Experiment. J. Atmos. Sci., 62, 1093-1118, 2005.

Chowdhury, Z., L. S. Hughes, and L. G. Salmon, Atmospheric particle size and composition measurements to support light extinction calculations over the Indian Ocean, *J. Geophys. Res.*, *106*, 28597-28605, 2001.

Christensen, J.H., The Danish Eulerian Hemispheric ModelAa three-dimensional air pollution model used for the Arctic, Atmospheric Environment,, 31 (24), 4169-4191, 1997.

Chuang, C.C., J.E. Penner, K.E. Taylor, A.S. Grossman, and J.J. Walton, An assessment of the radiative effects of anthropogenic sulfate, *J. Geophys. Res.*, *102*, 3761-3778, 1997.

Chuang, P. Y., D. R. Collins, H. Pawlowska, J. R. Snider, H. H. Jonsson, J. L. Brenguier, R. C. Flagan, and J. H. Seinfeld, CCN measurements during ACE-2 and their relationship to cloud microphysical properties, *Tellus Series B-Chemical and Physical Meteorology*, *52*, 843-867, 2000.

Chuang, P.Y., D.R. Collins, H. Pawlowska, J.R. Snider, H.H. Jonsson, J.L. Brenguier, R.L. Flagan, and J.H. Seinfeld, CCN measurements during ACE-2 and their relationship to cloud microphysical properties, *Tellus, 52B*, 843–867, 2000.

Chung, S. H., and J. H. Seinfeld, Global distribution and climate forcing of carbonaceous aerosols, *J. Geophys. Res.*, *107*, 4407, doi:10.1029/2001JD001397, 2002.

Chung, S. H., and J. H. Seinfeld: Climate response of direct radiative forcing of anthropogenic black carbon, *J. Geophys. Res.*, *110*, D11102, doi:10.1029/2004JD005441, 2005.

Ciach, G.J., and W. F. Krajewski, On the estimation of radar rainfall error variance. Adv. Water Resour., 22(6), 585-595, 1999.

Claeys, M., W. Wang, A. C. Ion, I. Kourtchev, A. Gelencser, and W. Maenhaut, Formation of secondary organic aerosols from isoprene and its gas-phase oxidation products through reaction with hydrogen peroxide, *Atmos. Environ.*, *38*, 4093-4098, 2004.

Clark, T.L., and W.D. Hall, A cloud physical parameterization method using movable basis functions: Stochastic coalescence parcel calculations, *J. Atmos. Sci*., *40*, 1709-1728, 1983.

Clark, T.L., Numerical modelling of the dynamics and microphysics of warm cumulus convection*, J. Atmos. Sci., 30,* 857-878, 1973.

Clark, T.L., On modeling nucleation and condensation theory in Eulerian spatial domain, *J. Atmos. Sci., 31,* 2099-2117, 1974.

Clark, T.L., Use of log-normal distributions for numerical calculations of condensation and collection, *J. Atmos. Sci., 33*, 810-821, 1976.

Clarke, A., V. Kapustin, S. Howell, K. Moore, B. Lienert, S. Masonis, T. Anderson, and D. Covert, Sea-salt size distributions from breaking waves: Implications for marine aerosol production and optical extinction measurements during SEAS, *J. Atmos. Ocean. Technol.*, *20*, 1362-1374, 2003.

Clarke, A.D., F. Eisele, V.N. Kapustin, K. Moore, D. Tanner, L. Mauldin, M. Litchy, B. Lienert, M.A. Carroll, and G. Albercook, Nucleation in the equatorial free troposphere: Favorable environments during PEM-Tropics, *J. Geophys. Res., 104*, 5735-5744, 10.1029/98JD02303, 1999.

Clarke, A.D., Y. Shinozuka, V.N. Kapustin, S. Howell, B. Huebert, S. Doherty, T. Anderson, D. Covert, J. Anderson, X. Hua, M.K.G. II, C. McNaughton, G. Carmichael, and R. Weber, Size distributions and mixtures of dust and black carbon aerosol in Asian outflow: Physiochemistry and optical properties. , . J. Geophys. Res., 109, D15S09, doi:10.1029/2003JD004378, 2004.

Clegg, S. L., J. H. Seinfeld, and P. Brimblecombe, Thermodynamic modelling of aqueous aerosols containing electrolytes and dissolved organic compounds, *J. Aerosol Sci.*, *32*, 713-738, 2001.

Clegg, S. L., P. Brimblecombe, and A. S. Wexler, Thermodynamic model of the system H^+-NH_4^+-SO_4^{2-}-NO_3^--H_2O at tropospheric temperatures, *Journal of Physical Chemistry A*, *102*, 2137-2154, 1998.

Clegg, S.L., and J.H. Seinfeld, Improvement of the Zdanovskii-Stokes-Robinson Model for Mixtures Containing Solutes of Different Charge Types, Journal of Physical Chemistry A, 108 (6), 1008-1017, 2004.

CNES, 2004: http://smsc.cnes.fr/POLDER/index.htm

Coakley, J.A. Jr., R.L. Bernstein, and P.A. Durkee, Effects of ship-track effluents on cloud reflectivity, *Science, 255*, 423–430, 1987.

Cofala, J., M. Amann, and R. Mechler, *Scenarios of world anthropogenic emissions of air pollutants and methane up to 2030.* International Institute for Applied Systems Analysis (IIASA), 2005.

Collins, D. R., H. H. Jonsson, J. H. Seinfeld, R. C. Flagan, S. Gasso, D. A. Hegg, P. B. Russell, B. Schmid, J. M. Livingston, E. Ostrom, K. J. Noone, L. M. Russell, and J. P. Putaud, In situ aerosol-size distributions and clear-column radiative closure during ACE-2, *Tellus*, *52B*, 498-525, 2000.

Comstock, K. K., C. S. Bretherton, and S. E. Yuter, Mesoscale variability and drizzle in southeast Pacific stratocumulus. *J. Atmos. Sci. 62*, 3792-3807, 2005.

Conant, W.C., A. Nenes, and J.H. Seinfeld, Black carbon radiative heating effects on cloud microphysics and implications for the aerosol indirect effect. 1. Extended Köhler theory, *J. Geophys. Res.*, *107*, D21, 4604, doi:10.1029/2002JD002094, 2002.

Conant, W.C., T.M. van Renken, T.A. Rissman, V. Varutbangkul, H.H. Jonsson, A. Nenes, J.L. Jimenez, A.E. Delia, R. Bahreini, G.C. Roberts, R.C. Flagan, and J.H. Seinfoled, Aerosol-cloud drop concentration closure in warm cumulus, *J. Geophys. Res.*, *109*, D13204, doi10:1029/2003JD004324, 2004.

Conover, J.H., Anomalous cloud lines, *J. Atmos. Sci., 23*, 778–785, 1966.

Cooke, W. F., C. Liousse, H. Cachier, and J. Feichter, Construction of a 1°x1° fossil fuel emission dataset for carbonaceous aerosol and implementation and radiative impact in the ECHAM-4 model, *J. Geophys. Res.*, *104*, 22,137-22,162, in press, 1999,.

Cooper, W.A., A method of detecting contact ice nuclei using filter samples. 8th Intl. Conf. on Cloud Physics, Clermont-Ferrand, France, 665- 668, 1980.

Cooper, W.A., and R.P. Lawson, Physical interpretation of results from the HIPLEX-1 experiment, *J. Clim. Appl. Meteorol., 23*, 523–540, 1984.

Cooper, W.A., Ice formation in wave clouds: Observed enhancement during evaporation, *Proc. Conf. Cloud Physics,* Dallas, Amer. Met. Soc., 147-152, 1995.

Cooper, W.A., R.T. Bruintjes, and G.K. Mather, Calculations pertaining to hygroscopic seeding with flares, *J. Appl. Meteorol., 36*, 1449-1469, 1997.

Corrigan, C. E., and T. Novakov, Cloud condensation nucleus activity of organic compounds: a laboratory study, *Atmos. Environ.*, *33*, 2661-2668, 1999.

Cotton, R.J., and P.R. Field, Ice nucleation characteristics of an isolated wave cloud, *Quart. J. Roy. Met. Soc., 128,* 2417-2437, 2002.

Cotton, W.R. and R.A. Anthes, Storm and Cloud Dynamics, Academic Press, 1989.

Cotton, W.R., and R.A. Pielke, *Human Impacts on Weather and Climate,* 288 pp., ASTeR Press, Ft. Collins, Colo., 1992.

Cotton, W.R., and R.A. Pielke, *Human Impacts on Weather and Climate*, 2nd edition, 288 pp., Cambridge University Press, New York, 1995.

Cotton, W.R., G. D. Alexander, R. Hertenstein, R.L. Walko, R.L. McAnelly, and M. Nicholls, Cloud venting--A review and some new global annual estimates, *Earth Sci. Rev.*, *39*, 169-206, 1995.

Cotton, W.R., G.J. Tripoli, R.M. Rauber, and E.A. Mulvihill, Numerical simulation of the effects of varying ice crystal nucleation rates and aggregation processes on orographic snowfall, *J. Clim. Appl. Meteorol.*, *25*, 1658-1680, 1986.

Cotton, W.R., M.S. Lin, R.L. McAnelly, and C.J. Tremback, A composite model of mesoscale convective complexes, *Mon. Wea. Rev., 117,* 765–783, 1989.

Cotton, W.R., Modification of precipitation from warm clouds—A review, *Bull. Amer. Meteorol. Soc., 63*, 146–160, 1982.

Cotton, W.R., Numerical simulation of precipitation development in supercooled cumuli. Part II, *Mon. Weather Rev., 11*, 764–784, 1972.

Cotton, W.R., R. McAnelly, G. Carrió, P. Mielke, and C. Hartzell, 2006: Simulations of Snowpack Augmentation in the Colorado Rocky Mountains. J. Weather Modification Association, In Press

Cotton, W.R., R.A. Pielke, Sr., R.L. Walko, G.E. Liston, C.J. Tremback, H. Jiang, R.L. McAnelly, J.Y. Harrington, M.E. Nicholls, G.G. Carrió, J.P. McFadden, RAMS 2001: Current status and future directions. *Meteor. Atmos Physics*, *82*, 5-29, 2003.

Cotton, W.R., Testing, implementation and evolution of seeding concepts—A review, *Meteorol. Monogr. 21*, 63–70, 1986a.

Cotton, W.R., Testing, implementation, and evolution of seeding concepts—a review, in *Precipitation Enhancement—A Scientific Challenge*, edited by R.R. Braham, Jr., *AMS Meteorol. Monogr. Ser., 43*, 139–149, Amer. Meteorol. Soc., Boston, Mass., 1986b.

Couch, R.H., C.W. Rowland, K.S. Ellis, M.P. Blythe, C.R. Regan, M.R. Koch, C.W. Antill, W.L. Kitchen, J.W. Cox, J.F. DeLorme, S.K. Crockett, R.W. Remus, J.C. Casas, and W.H. Hunt, lidar In-space Technology Experiment (LITE): NASA's first in-space lidar system for atmospheric research, Opt. Eng., 30, 88-95, 1991.

Covert, D. S., J. L. Gras, A. Wiedensohler, and F. Stratmann, Comparison of directly measured CCN with CCN modeled from the number-size distribution in the marine boundary layer during ACE 1 at Cape Grim, Tasmania, *J. Geophys. Res.*, *103*, 16597-16608, 1998.

Crutzen, P. J., and M. O. Andreae, Biomass burning in the tropics: Impact on atmospheric chemistry and biogeochemical cycles, *Science*, *250*, 1669-1678, 1990.

Cruz, C. N., and S. N. Pandis, A study of the ability of pure secondary organic aerosol to act as cloud condensation nuclei, *Atmos. Environ.*, *31*, 2205-2214, 1997.

Cruz, C. N., and S. N. Pandis, The effect of organic coatings on the cloud condensation nuclei activation of inorganic atmospheric aerosol, *J. Geophys. Res.*, *103*, 13111-13123, 1998.

Curry, J.A., C.A. Clayson, W.B. Rossow, R. Reeder, Y.-C. Zhang, P.J. Webster, G.Liu, and R.-S. Sheu, High resolution satellite-derived dataset of the surface fluxes of heat, freshwater, and momentum for the TOGA COARE IOP, Bull. Amer. Meteor. Soc., 80, 2059–2080, 1999.

Cziczo, D. J., D. M. Murphy, P. K. Hudson, and D. S. Thomson, Single particle measurements of the chemical composition of cirrus ice residue during CRYSTAL-FACE, *J. Geophys. Res.*, *109*, 2004.

Cziczo, D. J., P. J. DeMott, S. D. Brooks, A. J. Prenni, D. S. Thomson, D. Baumgardner, J. C. Wilson, S. M. Kreidenweis, and D. M. Murphy, Observations of organic species and atmospheric ice formation, *Geophys. Res. Lett.*, 31, doi: 10.1029/2004GL019822, 2004.

Cziczo, D.J., P.J. DeMott, S.D. Brooks, A.J. Prenni, D.S. Thomson, D. Baumgardner, J.C. Wilson, S.M. Kreidenweis, and D.M. Murphy, Observations of organic species and atmospheric ice formation - art. no. L12116, Geophysical Research Letters, 31 (12), 12116, 2004.

Davidson, C.I., J.M. Miller, and M.A. Pleskow, The influence of surface structure on predicted particle dry deposition to natural grass canopies, Water, Air, and Soil Pollution, 18 (1-3), 25-43, 1982.

Davison, P.S., D.L. Roberts, R.T. Arnold, and R.N. Colvile, Estimating the direct radiative forcing due to haze from the 1997 forest fires in Indonesia, Journal of Geophysical Research, 109, D10207, doi:10.1029/2003JD004264, 2004.

Decesari, S., S. Fuzzi, et al., Characterization of the organic composition of aerosols from Rondônia, Brazil, during the LBA-SMOCC 2002 experiment and its representation through model compounds, *Atmos. Chem. Phys. Discuss.*, *5*, 5687-5749, 2005.

DEH, Department of Environment and Heritage, Australian Government, in State of the Air: National Ambient Summary Report 1991-2001, 2004.

DeMott, P. J., K. Sassen, M. R. Poellet, D. Baumgardner, D. C. Rogers, S. D. Brooks, A. J. Prenni, and S. M. Kreidenweis, African dust aerosols as atmospheric ice nuclei, *Geophys. Res. Lett. 30* (14), 1732, doi:10.1029/2003GL017410, 2003.

DeMott, P.J., M.P. Meyers, W.R. Cotton, Parameterization and impact of ice initiation processes relevant to numerical model simulations of cirrus clouds. J. Atmos. Sci., 41, 77-90, 1994.

Dennis, A.S., and H.D. Orville, Comments on "A new look at the Israeli cloud seeding experiments," *J. Appl. Meteorol. 36,* 277–278, 1997.

Dennis, A.S., Editorial, *J. Appl. Meteorol., 28,* 1013, 1989.

Dennis, A.S., *Weather Modification by Cloud Seeding*, 267 pp., Academic Press, New York, 1980.

Dentener, F. J., G. R. Carmichael, Y. Zhang, J. Lelieveld, and P. J. Crutzen, Role of mineral aerosol as a reactive surface in the global troposphere, *J. Geophys. Res.*, *101*, 22,869-22,889, 1996.

Dentener, F., S. Kinne, T. Bond, O. Boucher, J. Cofala, S. Generoso, P. Ginoux, S. Gong, J. J. Hoelzemann, A. Ito, L. Marelli, J. Penner, J.-P. Putaud, C. Textor, M.Schulz, G. R. van der Werf, and J. Wilson, Emissions of primary aerosol and precursor gases for the years 2000 and 1750: Prescribed data-sets for AeroCom, *Atmos. Chem. Phys. Discuss.*, 2005, submitted.

Derwent, R. G., M. E. Jenkin, C. E. Johnson, and D. S. Stevenson, The global distribution of secondary particulate matter in a 3-D Lagrangian chemistry transport model, *J. Atmos. Chem.*, *44*, 57-95, 2003.

Deschamps, P. Y., F. M. Bréon, M. Leroy, A. Podaire, A. Bricaud, J. C. Buriez, and G. Seze, The POLDER mission: Instrument characteristics and scientific objectives, IEEE Trans. Geosci. Remote Sens., **32**, 598-615, 1994.

Deshler T., Contact ice nucleation by submicron atmospheric aerosols. PhD Dissertation, Department of Physics and Astronomy, University of Wyoming, Laramie, WY, 107 pp, 1982.

Deuzé, J. L., F. M. Bréon, C. Devaux, P. Goloub, M. Herman, B. Lafrance, F. Maignan, A. Marchand, F. Nadal, G. Perry, and D. Tanré, 2001: Remote sensing of aerosols over land surfaces from POLDER-ADEOS-1 polarized measurements, J Geophys. Res., **106**, 4913-4926.

Deuzé, J. L., M. Herman, P. Goloub, D. Tanré, and A. Marchand, 1999: Characterization of aerosols over ocean from POLDER/ADEOS-1, Geophys. Res. Lett. **26**, 1421-1424.

Deuzé, J. L., P. Goloub, M. Herman, A. Marchand, G. Perry, S. Susana, and D. Tanré, 2000: Estimate of the aerosol properties over the ocean with POLDER on ADEOS-1, J. Geophys. Res., **105** (D12), 15329-15346.

Diehl, K., C. Quick, S. Matthias-Maser, S.K. Mitra, and R. Jaenicke, The ice nucleating ability of pollen. Part I: Laboratory studies in deposition and condensation freezing modes, *Atmos. Res., 58*, 75–87, 2001.

Diehl, K., S. Matthias-Maser, S.K. Mitra, and R. Jaenicke, The ice nucleating ability of pollen. Part II: Laboratory studies in immersion and contact freezing modes. Atmos. Res. 61, 125–133, 2002.

Diem, J.E., and D.P. Brown, Anthropogenic impacts on summer precipitation in central Arizona, U.S.A., *The Prof. Geograph., 55,* 343–355, 2003.

Diner D. J., Ackerman TP, Anderson TL, et al., PARAGON - An integrated approach for characterizing aerosol climate impacts and environmental interactions Bullet. Amer. Meteor. Soc., 85, 1491-1501, 2004

Diner, D. J., J. C. Beckert, G. W. Bothwell, and J. I. Rodriguez, Performance of the MISR instrument during its first 20 months in Earth orbit, IEEE Trans. Geosci. Remote Sens., **40**, 1449-1466, 2002.

Diner, D. J., W. A. Abdou, C. J. Bruegge, et al., MISR aerosol retrievals over southern Africa during the SAFARI-2000 dry season campaign, Geophys. Res. Lett., **28**, 3127-3130, 2001.

Diner, D.J., J.C. Beckert, T.H. Reilly, et al., Multiangle Imaging SptectrRadiometer (MISR) description and experiment overview, IEEE Trans. Geosci. Remt. Sensing **36**, 1072-1087, 1998.

Dinger, J.E., H.B. Howell, and T.A. Wojciechowski, On the source and composition of cloud nuclei in a subsident air mass over the North Atlantic, *J. Atmos. Sci., 27,* 791–797, 1970.

Dong Y.Y., R.G. Oraltay, R.G. and J. Hallett, ice particle generation during evaporation. Atmos. Res. 32, 45-53, 1994

Donnadieu, G., Comparison of results obtained with the VIDIAZ spectropluviometer and the Joss-Waldvogel rainfall disdrometer in a "rain of thunder type". J. Appl. Meteor., 19, 593-597, 1978.

Doswell, C.A., H.E. Brooks, and R.A. Maddox, Flash flood forecasting: An ingredients-based methodology, *Wea. Forecasting*, *11,* 560–581, 1996.

Doviak, R.J., and D.S. Zrnic, Doppler Radar and Weather Observations, 562 pp., Academic Press, New York, N.Y., 1993.

Droessler, E.G. and K.J. Heffernan. Ice Nucleus Measurements in Hawaii. *Journal of Applied Meteorology*: Vol. 4, No. 4, pp. 442–445, 1965.

Dubovik, O., A. Smirnov, B. N. Holben, M. D. King, Y. J. Kaufman, T. F. Eck, and I. Slutsker, Accuracy assessments of aerosol optical properties retrieved from AERONET sun and sky-radiance measurements, J. Geophys. Res., **105**, 9791-9806, 2000.

Dubovik, O., B. N. Holben, T. F. Eck, A. Smirnov, Y. J. Kaufman, M. D. King, D. Tanré, and I. Slutsker, Climatology of aerosol absorption and optical properties in key worldwide locations, J. Atmos. Sci, **59**, 590-608, 2002.

Duce, R., Distributions and fluxes of mineral aerosol, in *Aerosol Forcing of Climate*, edited by R. J. Charlson & J. Heintzenberg, pp. 43-72, Wiley, Chichester, U.K., 1995.

Duchon, C.E., and G.R. Essenberg, Comparative rainfall observations from pit and aboveground raingauges with and without wind shields, Water Resour. Res., 37, 3253–3263, 2001.

Dulac, F., P. Buat-Ménard, D. Sutton, et al.,Assessment of the African airborne dust mass over the western Mediterranean Sea using Meteosat data, J. Geophys. Res., **97**, 2489-2506. 1992.

Durant, A.J. and R.A. Shaw. Evaporation freezing by contact nucleation inside-out, *Geophysical Research Letters, 32*, 2005.

Durkee, P. A., K. J. Noone, R. J. Ferek, D. W. Johnson, J. P. Taylor, T. J. Garrett, P. V. Hobbs, J. G. Hudson, C. S. Bretherton, G. Innis, G. M. Frick, W. A. Hoppel, C. D. O'Dowd, L. M. Russell, R. Gasparovic, K. E. Nielsen, S. A. Tessmer, E. Öström, S. R. Osborne, R. C. Flagan, J. H. Seinfeld and H. Rand, The Impact of Ship-Produced Aerosols on the Microstructure and Albedo of Warm Marine Stratocumulus Clouds: A Test of MAST Hypotheses 1i and 1ii. *J. Atmos. Sci.*, 57, 2554–2569, 2001.

Dusek, U., D. S. Covert, A. Wiedensohler, C. Neususs, D. Weise, and W. Cantrell, Cloud condensation nuclei spectra derived from size distributions and hygroscopic properties of the aerosol in coastal south-west Portugal during ACE-2, *Tellus Series B-Chemical and Physical Meteorology*, *55*, 35-53, 2003.

Dusek,U., G. P. Frank, L. Hildebrandt, J. Curtius, J. Schneider, S. Walter, D. Chand, F. Drewnick, S. Hings, D. Jung, S. Borrmann, M. O. Andreae, Size matters more than chemistry in controlling which aerosol particles can nucleate cloud droplets. Science, In Press, 2006

Dye J.E. and P.V. Hobbs, Effect of carbon dioxide on shattering of freezing water drops, Nature 209, 464, 1966.

Dye J.E. and P.V. Hobbs, Influence of environmental parameters on freezing and fragmentation of suspended water drops. J. Atmos. Sci. 25, 82, 1968

Eagan, R.C., P.V. Hobbs, and L.F. Radke, Measurements of cloud condensation nuclei and cloud droplet size distributions in the vicinity of forest fires, *J. Appl. Meteorol., 13*, 553–557, 1974b.

Eagan, R.C., P.V. Hobbs, and L.F. Radke, Particle emissions from a large Kraft paper mill and their effects on the microstructure of warm clouds, *J. Appl. Meteorol., 13*, 535–552, 1974a.

Easter, R. C., et al., MIRAGE: Model description and evaluation of aerosols and trace gases, *J. Geophys. Res.*, 109, doi:10.1029/2004JD004571, 2004.

Easter, R.C., and P.V. Hobbs, The formation of sulfates and the enhancement of cloud condensation nuclei in clouds, *J. Atmos. Sci., 31,* 1586–1594, 1974.

Ebert et al. upcoming BAMS article, I will get citation.

Ebert, E., Monitoring the quality of operational and semi-operational satellite precipitation estimates – the IPWG Validation/intercomparison study. 2nd International Precipitation Working Group (IPWG) Workshop, Monterey, CA, 25-28 October 2004, 9 pages, 2004.

Ebert, E.E., M.J. Manton, P.A. Arkin, R.J. Allam, G.E. Holpin, and A. Gruber, Results from the GPCP Algorithm Intercomparison Programme, Bull. Amer. Meteor. Soc., 77, 2875–2887, 1996.

Eleftheriadis, K., and I. Colbeck, Coarse atmospheric aerosol: size distributions of trace elements, *Atmos. Environ.*, *35*, 5321-5330, 2001.

Endresen, O., E. Sorgard, J. K. Sundet, S. B. Dalsoren, I. S. A. Isaksen, T. F. Berglen, and G. Gravir, Emission from international sea transportation and environmental impact, *J. Geophys. Res.*, *108*, 4560, doi:10.1029/2002JD002898, 2003.

Endresen, O., J. Bakke, E. Sorgard, T. F. Berglen, and P. Holmvang, Improved modelling of ship SO_2 emissions - a fuel-based approach, *Atmos. Environ.*, *39*, 3621-3628, 2005.

Ervens, B., G. Feingold, and S. M. Kreidenweis, The influence of water-soluble organic carbon on cloud drop number concentration. *J. Geophys. Res., 110,* D18211, doi:10.1029/2004JD005634, 2005.

Ervens, B., G. Feingold, S. L. Clegg, and S. M. Kreidenweis, Aqueous production of dicarboxylic acids. Part 2: Implications for cloud microphysics, J. Geophys. Res., **109**, D15206, doi:10.1029/2004JD004575, 2004.

Facchini, M. C., Fuzzi, S., Zappoli, S., Andracchio, A., Gelencser, A., Kiss, G., Krivacsy, Z., Meszaros, E., Hansson, H. C., Alsberg, T., and Zeb¨uhr, Y.: Partitioning of the organic aerosol component between fog droplets and interstitial aerosol, J. Geophys. Res., 104, 26 821–26 832, 1999a.

Facchini, M. C., M. Mircea, S. Fuzzi, and R. J. Charlson, Cloud albedo enhancement by surface-active organic solutes in growing droplets, *Nature*, *401*, 257-259, 1999.

Facchini, M. C., S. Decesari, M. Mircea, S. Fuzzi, and G. Loglio, Surface tension of atmospheric wet aerosol and cloud/fog droplets in relation to their organic carbon content and chemical composition, *Atmos. Environ.*, *34*, 4853-4857, 2000.

Falkovich, A., G. Schkolnik, E. Ganor, and Y. Rudich, Adsorption of organic compounds pertinent to urban environments onto mineral dust particles, J. Geophys. Res., 109 (D2), D02208, 2004.

Fankhauser, J.C., Estimates of thunderstorm precipitation efficiency from field measurements in LLOP, *Mon. Wea. Rev., 116,* 663–684, 1988.

Farley, R.D., and C.S. Chen, A detailed microphysical simulation of hygroscopic seeding on the warm process, *J. Appl. Meteorol., 14*, 718–733, 1975.

Feichter, J., E. Roeckner, U. Lohmann, and B. Liepert, Nonlinear aspects of the climate response to greenhouse gas and aerosol forcing. *J. Clim.,* 17(12), 2384-2398, 2004.

Feingold, G., 2003: Modeling of the first indirect effect: Analysis of measurement requirements, Geophys. Res. Lett., **30**, 1997, doi:10.1029/2003GL017967.

Feingold, G., and P. Y. Chuang, Analysis of the influence of film-forming compounds on droplet growth: Implications for cloud microphysical processes and climate, *J. Atmos. Sci.*, *59*, 2006-2018, 2002.

Feingold, G., and S.M. Kreidenweis, Cloud processing of aerosol as modeled by a large eddy simulation with coupled microphysics and aqueous chemistry, *J. Geophys. Res., 107,* 4687, doi:10.1029/2002JD002054, 2002.

Feingold, G., and S.M. Kreidenweis, Does heterogeneous processing of aerosol increase the number of cloud droplets? *J. Geophys. Res., 105*, 24,351-24,361, 2000.

Feingold, G., B. Stevens, W.R. Cotton, and R.L. Walko, An explicit cloud microphysics/LES model designed to simulate the Twomey effect, *Atmos. Res.*, *33*, 207-233, 1994.

Feingold, G., H. Jiang, and J. Y. Harrington, On smoke suppression of clouds in Amazonia, *Geophys. Res. Lett.*, *32*, No. 2,

L02804, 10.1029/2004GL021369, 2005.

Feingold, G., L. A. Remer, J. Ramaprasad, and Y. J. Kaufman, Analysis of smoke impact on clouds in Brazilian biomass burning regions: An extension of Twomey's approach, *J. Geophys. Res., 106(D19)*, 22,907–22,922, 2001.

Feingold, G., L.E. Wynn, D.E. Veron, and M. Previdi, First measurements of Twomey indirect effect using ground-based remote sensors, *Geophys. Res. Lett., 30*, 1287, 2003.

Feingold, G., R. Boers, B. Stevens, and W.R. Cotton, A modeling study of the effect of drizzle on cloud optical depth and susceptibility, *J. Geophys. Res.*, *102*, 13,527-13,534, 1997.

Feingold, G., R. L. Walko, B. Stevens, and W. R. Cotton, Simulations of marine stratocumulus using a new microphysical parameterization scheme, *Atmos. Res., 47–48*, 505-528, 1998.

Feingold, G., S. Kreidenweis, B. Stevens, and W. Cotton, Numerical Simulations of Stratocumulus Processing of Cloud Condensation Nuclei through Collision-Coalescence, *J. of Geophys. Res.*, 101 (D16), 21,391-21,402, 1996.

Feingold, G., W. L. Eberhard, D. E. Veron, and M. Previdi, 2003, First measurements of the Twomey indirect effect using ground-based remote sensors, Geophys. Res. Lett., **30**, 1287, doi:10.1029/2002GL016633.

Feingold, G., W. R. Cotton, S. M. Kreidenweis, and J. T. Davis, The impact of giant cloud condensation nuclei on drizzle formation in stratocumulus: Implications for cloud radiative properties, *J. Atmos. Sci.*, *56*, 4100-4117, 1999.

Feng, M., P. Hacker, R. Lukas, R. Weller, and S.P. Anderson, Upper ocean heat and salt balances in the western equatorial Pacific in response to the intraseasonal oscillation during TOGA COARE, J. Climate, 12, 2409–2427, 2000.

Ferek, R.J., D.A. Hegg, and P.V. Hobbs, Measurements of ship-induced tracks in clouds off the Washington coast, *J. Geophys. Res., 103*, 23199–23206, 1998.

Ferek, R.J., et al., Drizzle suppression in ship tracks, *J. Atmos. Sci., 57,* 2707–2728, 2000.

Ferraro, R.R., F. Weng, N.C. Grody, and A. Basist, An eight year (1987-94) climatology of rainfall, clouds, water vapor, snowcover, and sea-ice derived from SSM/I measurements. Bulletin American Meteorology Society, Vol. 77, 891-905, 1996.

Ferriday, J.G., and S.K. Avery, Passive microwave remote sensing of rainfall with SSM/I: Algorithm development and implementation, J. Appl. Meteor., 33, 1587–1596, 1994.

Ferrier, B.S., A double-moment multiple-phase four-class bulk ice scheme. Part I: description, *J. Atmos. Sci., 51*, 249- 280, 1994.

Field, P.R., R.J. Cotton, K. Noone, P. Glantz, P.H. Kaye, E. Hirst, R.S. Greenaway, C. Jost, R. Gabriel, T. Reiner, M. Andreae, C.P.R. Saunders, A. Archer, and T. Choularton, Ice nucleation in orographic wave clouds: Measurements made during INTACC, *Quart. J. Roy. Meteor. Soc., 127*, 575A, 1493-1512, 2001.

Findeisen, W., Die kolloidmeteorologisch Vorgänge bei der Niederschlagsbildung, *Met. Z., 55*, 121-132, 1938.

Fisch, G., J.Tota, L. A. T. Machado, M. A. F. Silva Dias, R. F. Da F. Lyra, C. A. Nobre, A. J. Dolman, and J. H. C. Gash, The convective boundary layer over pasture and forest in Amazonia, *Theor. Appl. Climatol.*, 78, 47-59, 2004.

Fiser O., Schoenhuber M, and Pesice P. "First results of DSD measurement by videodistrometer in the Czech Republic in 1998–1999" Studia Geophysica et Geodetica, 46, 3, 485–505, 2002.

Fisseha, R., J. Dommen, M. Sax, D. Paulsen, M. Kalberer, R. Maurer, F. Höfler, E. Weingartner, U. Baltensperger, Identification of organic acids in secondary organic aerosol and the corresponding gas phase from chamber experiments, Anal. Chem., **76**, 6535-6540, 2004.

Fitzgerald, J., Dependence of supersaturation spectrum of CCN on aerosol size distribution and composition, *J. Atmos. Sci.*, *30*, 628-634, 1973.

Fitzgerald, J.M., Marine aerosols: A review, Atmospheric Environment, 25A (No. 3/4), 533-545, 1991.

Fitzgerald, J.W., Effect of aerosol composition on cloud droplet size distribution: a numerical study, *J. Atmos. Sci., 31*, 1358-1367, 1974.

Fletcher, N.H., *The Phys. of Rainclouds,* 242 pp., Cambridge University Press, Cambridge, U.K., 1962.

Flossman, A.I., W.D. Hall, and H.R. Pruppacher, A theoretical study of the wet removal of atmospheric pollutants. Part I: The redistribution of aerosol particlescaptured through nucleation and impaction scavenging by cloud droplets, *J. Atmos. Sci., 42*, 582-606, 1985.

Flossmann, A. I., and W. Wobrock, Venting of gases by convective clouds, *J. Geophys. Res.*, 101, 18,639-18,650, 1996.

Flossmann, A.I., H.R. Pruppacher, and J.H. Topalian, A theoretical study of the wet removal of atmospheric pollutants. Part II. The uptake and redistribution of $(NH_4)_2SO_4$ gas simultaneously scavenged by growing cloud drops, *J. Atmos. Sci., 44,* 2912–2923, 1987.

Flossmann, A.I., W.D. Hall, and H.R. Pruppacher, A theoretical study of the wet removal of atmospheric pollutants. Part I. The redistribution of aerosol particles captured through nucleation and impaction scavenging by growing cloud drops, *J. Atmos. Sci., 42,* 583–606, 1985.

Flueck, J.A., W.L. Woodley, R.W. Burpee, and D.O. Stram, Comments on "FACE rainfall results: seeding effect or natural variability?," *J. Appl. Meteorol.*, *20*, 98–107, 1981.

Folland, C. K., Numerical models of the raingauge exposure problem, field experiments and an improved collector design, Quart. J. Roy. Meteor. Soc., 114, 1485-1516, 1988.

Follansbee, W.A., Estimation of averagae daily rainfall from satellite cloud photographs. NOAA Tech. Mem. NESS 44, Dept. of Commerce, Wash., DC, 39 pp, 1973.

Formenti, P., W. Elbert, W. Maenhaut, J. Haywood, and M. O. Andreae, Chemical composition of mineral dust during the Saharan Dust Experiment (SHADE) airborne campaign in the Cape Verde region, September 2000, *J. Geophys. Res.*, *108*, 8576, doi:10.1029/2002JD002408, 2003.

Franklin, B., Meteorological imaginations and conjectures, *Mem. Manchester Lit. and Phil. Soc., 2*, 374-381, 1789.

Fraser, R. S., Y. J. Kaufman & R. L. Mahoney, 1984: Satellite measurements of aerosol mass and transport, Atmos. Environ., **18**, 2577-2584.

Fridlind, A.M., A. S. Ackerman, E. J. Jensen, A. J. Heymsfield, M. R. Poellot, D. E. Stevens, D. Wang, L. M. Miloshevich, D. Baumgardner, R. P. Lawson, J. C. Wilson, R. C. Flagan, J. H. Seinfeld, H. H. Jonsson, T. M. VanReken, V.

Varutbangkul, and T. A. Rissman, Evidence for the predominance of mid-tropospheric aerosols as subtropical anvil cloud nuclei, *Science*, 304, 718 – 722, 2004.

Fuzzi, S., M. O. Andreae, B. J. Huebert, M. Kulmala, T. C. Bond, M. Boy, S. J. Doherty, A. Guenther, M. Kanakidou, K. Kawamura, V.-M. Kerminen, U. Lohmann, L. M. Russell, and U. Pöschl, Critical assessment of the current state of scientific knowledge, terminology, and research needs concerning the role of organic aerosols in the atmosphere, climate, and global change, *Atmos. Chem. Phys. Discuss.*, *5*, 11,729-11,780, 2005a.

Fuzzi, S., S. Decesari, et al., Overview of the inorganic and organic composition of size-segregated aerosol in Rondônia, Brazil, from the biomass burning period to the onset of the wet season, *J. Geophys. Res.*, 2005b, submitted.

Gabella, M., and E. Amitai, Radar rainfall estimates in an alpine environment using different gauge-adjustment techniques. Phys. Chem. Earth (B), 25, 927-931, 2000.

Gabric, A. J., R. Simo, R. A. Cropp, A. C. Hirst, and J. Dachs, Modeling estimates of the global emission of dimethylsulfide under enhanced greenhouse conditions, *Global Biogeochem. Cycles*, *18*, GB2014, doi:10.1029/2003GB002183, 2004.

Gabriel, K.R., and D. Rosenfeld, The second Israeli rainfall stimulation experiment: analysis of rainfall on both target area, *J. Appl. Meteorol., 29,* 1055–1067, 1990.

Gabriel, K.R., and J. Baras, The Israeli rainmaking experiment, 1961–1967: Final statistical tables and evaluation, *Tech. Rep., Dept. Meteorol., Hebrew University of Jerusalem*, Jerusalem, 47 pp., 1970.

Gabriel, K.R., and P. Feder, On the distribution of statistics suitable for evaluating rainfall stimulation experiments, *Technometrics, 11,* 149-160, 1969.

Gabriel, K.R., Recent results of the Israeli artificial rainfall stimulation experiment, *J. Appl. Meteorol., 6,* 437–438, 1967b.

Gabriel, K.R., The Israeli artificial rainfall stimulation experiment: statistical evaluation for the period 1961–1965, *Proc. 5th Berkeley Symp. on Mathematical Statistics and Probability*, *Vol. V., Weather Modifications*, edited by L.M. Le Cam and J. Neyman, 91–113, University of California Press, Berkeley, Calif., 1967a.

Gagin, A., and J. Neumann, Rain stimulation and cloud physics in Israel, in *Weather and Climate Modification*, edited by W.N. Hess, 454–494, John Wiley and Sons, New York, 1974.

Gagin, A., and J. Neumann, The second Israeli cloud seeding experiment—the effect of seeding on varying cloud populations, *Proc. 2nd WMO Scientific Conf. on Weather Modification*, Boulder, Colo., World Meteorol. Org., 195–204, 1976.

Gagin, A., and J. Neumann, The second Israeli randomized cloud seeding experiment: Evaluation of results, *J. Appl. Meteorol., 20*, 1301–1311, 1981.

Gagin, A., and K.R. Gabriel, Analysis of recording rain gauge data for the Israeli II experiment. Part I: Effects of cloud seeding on the components of daily rainfall, *J. Clim. Appl. Meteorol., 26*, 913–926, 1987.

Gagin, A., Evaluation of "static" and "dynamic" seeding concepts through analyses of Israeli II experiment and FACE-2 experiments, in *Rainfall Enhancement—A Scientific Challenge*, *AMS Meteorol. Monogr., 43*, 63–70, Amer. Meteorol. Soc., Boston, Mass., 1986.

Gagin, A., Ice nuclei, their physical characteristics and possible effect on precipitation initiation. Proc. Inter. Conf. Cloud Physics. Tokyo-Sapporo, 155, 1965.

Gagin, A., Studies of factors governing the colloidal stability of continental clouds. Preprint, Int. Confer. On Weather Mod. Canbara, Australia, AMer. Met. Soc., 5-11, 1971.

Gagin, A., Studies of the factors governing the colloidal stability of continental clouds, Preprints, *Intern. Conf. on Weather Modification,* Canberra, Amer. Meteor. Soc., 5–11, 1971.

Gagin, A., The ice phase in winter continental cumulus clouds, *J. Atmos. Sci., 32,* 1604–1614, 1975.

Gagin, A., The Israeli rainfall enhancement experiments. A physical overview, *J. Wea. Modif., 13,* 1–13, 1981.

Gagin, A., The relationship between the depth of cumuliform clouds and their raindrop characteristics, *J. Res. Atmos., 14,* 409–422, 1980.

Gagosian, R. B., O. C. Zafiriou, E. T. Peltzer, and J. B. Alford, Lipids in aerosols from the tropical North Pacific - Temporal variability, *Journal of Geophysical Research-Oceans and Atmospheres*, *87*, 1133-1144, 1982.

Gallagher, M.W., E. Nemitz, J.R. Dorsey, D. Fowler, M.A. Sutton, M. Flynn, and J. Duyzer, Measurements and parameterizations of small aerosol deposition velocities to grassland, arable crops, and forest: Influence of surface roughness length on deposition - art. no. 4154, Journal of Geophysical Research Atmospheres, 107 (D12), 4154, 2002.

Gallagher, M.W., K.M. Beswick, T.W. Choularton, J. Duyzer, H. Westrate, and P. Hummelsh?j, Measurements of aerosol fluxes to speulderforest using a micrometeorological technique, Atmospheric Environment, 31 (3), 359-373, 1997.

Gao, S., D. A. Hegg, P. V. Hobbs, T. W. Kirchstetter, B. I. Magi, and M. Sadilek, Water-soluble organic components in aerosols associated with savanna fires in southern Africa: Identification, evolution, and distribution, *J. Geophys. Res.*, *108*, 8491, doi:10.1029/2002/JD002324, 2003.

Gao, S., et al., Particle phase acidity and oligomer formation in secondary organic aerosol, *Environ. Sci. Technol.*, 38, 6582-6589, 2004.

Gao, S., N. L. Ng, M. Keywood, V. Varutbangkul, R. Bahreini, S. H. Chung, A. Nenes, J. He, K. Y. Yoo, J. L. Beauchamp, R. P. Hodyss, R. C. Flagan, and J. H. Seinfeld, Acid catalysis and oligomer formation lead to large increase in estimated atmospheric secondary organic aerosol, *Nature*, 2004, submitted 2004.

Gard, E. E., M. J. Kleeman, D. S. Gross, L. S. Hughes, J. O. Allen, B. D. Morrical, D. P. Fergenson, T. Dienes, M. E. Galli, R. J. Johnson, G. R. Cass, and K. A. Prather, Direct observation of heterogeneous chemistry in the atmosphere, *Science*, *279*, 1184-1187, 1998.

Garrett, T. J., C. Zhao, X. Dong, G. G. Mace, and P. V. Hobbs, Effects of varying aerosol regimes on low-level Arctic stratus, *Geophys. Res. Lett.*, *31*, L17105, doi:10.1029/2004GL019928, 2004.

Garrett, T. J., H. Gerber, D. G. Baumgardner, C. H. Twohy, and E. M. Weinstock, Small, highly reflective ice crystals in low-latitude cirrus, Geophys. Res. Lett., **30**, 2132-2135, 2003.

Garrett, T.J., and P.V. Hobbs, Long-range transport of continental aerosols over the Atlantic Ocean and their effects on cloud droplet size distributions, *J. Atmos. Sci., 52*, 2977–2984, 1995.

Garrett, T.J., P.V. Hobbs, and L.F. Radke, High Aitken nucleus concentrations above cloud tops in the Arctic, *J. Atmos. Sci., 59,* 779–783, 2002.

Garstang, M., R. Bruintjes, R. Serafin, H. Orville, B. Boe, W. Cotton and J. Warburton, Weather Modification: Finding common ground. Bulletin of American Meteorological Society, 86, 647-655, 2005.

Gaussiat, N. , H. Sauvageot, A. J. Illingworth, Cloud liquid water and ice content retrieval by multi-wavelength radar. J. Atmos. Oceanic Tech., 20, 1264-1275, 2003.

GAW, Proceedings of WMO/GAW Aerosol Measurement procedures guidelines and recommendations, GAW Report #153, available at http://www.wmo.ch/web/arep/gaw/gawreports.html, 2003.

GAW, Proceedings of WMO/GAW Experts Workshop on a Global Surface-based Network for Long Term Observations of Column Aerosol Optical Properties , Davos, Switzerland, 8-10 March 2004 GAW Report #162 available at http://www.wmo.ch/web/arep/gaw/gawreports.html., 2004.

Gelbard, F., Y. Tambour, and J.H. Seinfeld, Sectional representations for simulating aerosol dynamics, J. Colloid Interface Sci., 76, 541-556, 1980.

Gelencsér, A., A. Hoffer, Z. Krivácsy, G. Kiss, A. Molnár, and E. Mészáros, On the possible origin of humic matter in fine continental aerosol, *J. Geophys. Res.*, *107*, 4137, doi:10.1029/2001JD001299, 2002.

Gelencsér, A., *Carbonaceous aerosol*. Dordrecht, Netherlands: Springer, 350 pp. 350, 2004.

Generoso, S., F. M. Breon, Y. Balkanski, O. Boucher, and M. Schulz, Improving the seasonal cycle and interannual variations of biomass burning aerosol sources, *Atmos. Chem. Phys.*, *3*, 1211-1222, 2003.

Geogdzhayev IV, Mishchenko MI, Terez EI, et al., Regional advanced very high resolution radiometer-derived climatology of aerosol optical thickness and size, *J. Geoph. Res.110 (D23)*: Art. No. D23205 DEC 3, 2005.

Georgii, H. W., and E. Kleinjung, 1967: Relations between the chemical composition of atmospheric aerosol particles and the concentration of natural ice nuclei. *J. Rech. Atmos.,* **3,** 145–156, 1967.

Georgii, H.-W. amd R.S. Kaller, Ueber die Inaktivierung von Gefrierkernen durch Koagulation mit Aitkenkernen. ("On the deactivation of ice nuclei by coagulation with Aitken nuclei"). Berichte des Institutes fuer Meteorologie und Geophysik, Frakfurt/M, No. 21, 1970.

Gérard, B., J.-L. Deuzé, M. Herman, Y. J. Kaufman, P. Lallart, C. Oudard, L. A. Remer, B. Roger, B. Six, and D. Tanré, Comparisons between POLDER 2 and MODIS/Terra aerosol retrievals over ocean, J. Geophys. Res., 110, D24211, doi:10.1029/2005JD006218, 2005.

Gerber, H., Microphysics of marine stratocumulus clouds with two drizzle modes, *J. Atmos. Sci., 53,* 1649–1662, 1996.

Germann, U., and J. Joss, Operational Measurement of Precipitation in Mountainous Terrain, in Weather Radar: Principles and Advanced Applications, edited by P. Meischner, Springer-Verlag, Berlin, 52-77, 2004.

Germann, U., G. Galli, M. Boscacci, and M. Bolliger, Radar precipitation measurement in a mountainous region. *Quart. J. Roy. Meteor. Soc*., in press, 2006.

Ghan, A.J., L.R. Leung, R.C. Easter, and H. Abdul-Razzak, Prediction of droplet number in a general circulation model, *J. Geophys. Res*., *102*, 21,777-21,794, 1997.

Ghan, S. J., R. C. Easter, E. Chapman, H. Abdul-Razzak, Y. Zhang, R. Leung, N. Laulainen, R. Saylor, and R. Zaveri, A physically-based estimate of radiative forcing by anthropogenic sulfate aerosols, *J. Geophys. Res.*, 106, 5279-5293, 2001.

Giannini, A., R. Saravanan, and P. Chang, Oceanic forcing of Sahel rainfall on interannual to interdecadal time scales, *Science, 302*, 1027-1030, 2003.

Giebl, H., A. Berner, G. Reischl, H. Puxbaum, A. Kasper-Giebl, and R. Hitzenberger, CCN activation of oxalic and malonic acid test aerosols with the University of Vienna cloud condensation nuclei counter, *J. Aerosol Sci.*, *33*, 1623-1634, 2002.

Gill, P. S., T. E. Graedel, and C. J. Weschler, Organic films on atmospheric aerosol-particles, fog droplets, cloud droplets, raindrops, and snowflakes, *Rev. Geophys.*, *21*, 903-920, 1983.

Ginoux, P., M. Chin, I. Tegen, J. Prospero, B.N. Holben, O. Dubovik, and S.-J. Lin, Sources and distributions of dust aerosols simulated with the GOCART model, J. Geophys. Res., 106 (D17), 20,255-20,274, 2001.

Giorgi, F., A particle dry deposition parameterization scheme for use in tracer transport models, J. Geophysical Res., 91, 9794-9806, 1986.

Girard, E., and J.A. Curry, Simulation of arctic low-level clouds observed during the FIRE Arctic Clouds Experiment using a new bulk microphysics scheme, Journal of Geophysical Research Atmospheres, 106 (D14), 15139-15154, 2001.

Givati, A., and D. Rosenfeld, 2004: Quantifying precipitation suppression due to air pollution, *J. Appl. Meteorol., 43*, 1038–1056, 2004.

Gjertsen, U., M. Salek, and D. B. Michelson, Gauge adjustment of radar-based precipitation estimates in Europe, Proc. Third European Conf. on Radar in Meteorol. and Hydrol., Visby, Sweden, Copernicus GmbH, 7-11, 2004.

Gokhale, N.R., and J.D. Spengler, Freezing of freely suspended water droops by contact nucleation, *J. Appl. Meteorol., 11,* 157–160, 1972.

Golaz, J-C., V.E. Larson, and W.R. Cotton, A PDF-based model for boundary layer clouds. Part I: Method and model description, *J. Atmos. Sci*., *59*, 3540-3551, 2002a.

Golaz, J-C., V.E. Larson, and W.R. Cotton, A PDF-based model for boundary layer clouds. Part II: Model results. *J. Atmos. Sci*., *59*, 3552-3571, 2002b.

Goloub, P., and O. Arino, Verification of the consistency of POLDER aerosol index over land with ATSR-2/ERS-2 fire product. Geophys. Res. Lett., **27**, 899-902, 2000.

Goloub, P., J. L. Deuzé, M. Herman, and Y. Fouquart, Analysis of the POLDER polarization measurements performed over cloud covers, IEEE Trans. Geosci. Remote Sens., **32**, 78-88, 1994.

Gong, S. L., A parameterization of sea-salt aerosol source function for sub- and super-micron particles, *Global Biogeochem. Cycles*, *17*, 1097, doi:10.1029/2003GB002079, 2003.

Gong, S. L., and L. A. Barrie, Simulating the impact of sea salt on global nss sulphate aerosols, *J. Geophys. Res.*, *108*, 4516,

doi:1029/2002JD003181, 2003.

Gong, S. L., L. A. Barrie, and M. Lazare, Canadian Aerosol Module (CAM): A size-segregated simulation of atmospheric aerosol processes for climate and air quality models - 2. Global sea-salt aerosol and its budgets, *J. Geophys. Res.*, *107*, 4779, doi:10.1029/2001JD002004, 2002.

Gong, S.L., and L.A. Barrie, Simulating the Impact of Sea-salt on Global nss-Sulphate Aerosols, J. Geophys. Res., 108 (D16), 4516, doi:10.1029/2002JD003181, 2003.

Gong, S.L., L.A. Barrie, and M. Lazare, Canadian Aerosol Module: A size-segregated simulation of atmospheric aerosol processes for climate and air quality models 2. Global sea-salt aerosol and its budgets, J. Geophys. Res., 107 (D24), 4779, doi:10.1029/2001JD002004, 2002.

Gong, S.L., L.A. Barrie, J.-P. Blanchet, K.v. Salzen, U. Lohmann, G. Lesins, L. Spacek, L.M. Zhang, E. Girard, H. Lin, R. Leaitch, H. Leighton, P. Chylek, and P. Huang, Canadian Aerosol Module: A size-segregated simulation of atmospheric aerosol processes for climate and air quality models 1. Module development, J. Geophys. Res., 108 (D1), 4007, doi:10.1029/2001JD002002, 2003a.

Gong, S.L., X.Y. Zhang, T.L. Zhao, I.G. McKendry, D.A. Jaffe, and N.M. Lu, Characterization Of Soil Dust Distributions In China And Its Transport During ACE-ASIA 2. Model Simulation and Validation, Journal of Geophysical Research, 108 (D9), 4262, doi:10.1029/2002JD002633, 2003b.

Gong, S.L., X.Y. Zhang, T.L. Zhao, X.B. Zhang, L.A. Barrie, I.G. McKendry, and C.S. Zhao, A Simulated Climatology of Asian Dust Aerosol and its Trans-Pacific Transport 2. Interannual Variability and Climate Connections, Journal of Climate, 19 (1), 104-122, 2006.

Goodison, B. E., Accuracy of Canadian snow gauge measurements, J. Appl. Meteor., 17, 1542-1548, 1978.

Goodman, A., G. Underwood, and V. Grassian, A laboratory study of the heterogeneous reaction of nitric acid on calcium carbonate particles, Journal of Geophysical Research, 105 (D23), 29053-29064, 2000.

Gorbunov, B., A. Baklanov, N. Kakutkina, H.L. Windsor, and R. Toumi, Ice nucleation on soot particles, *J. Aerosol Sci*., *32*, 199-215, 2001.

Gorgucci, E., G. Scarchilli, and V. Chandrasekar, Sensitivity of multiparameter radar rainfall algorithms, J. Geophy. Res., 105(D2), 2215-2223, 2000.

Goudie, A.S., and N. J. Middleton, Saharan dust storms: nature and consequences, Earth-Science Reviews, 56, 179-204, 2001.

Grabowski, W. W., Indirect impact of atmospheric aerosols in idealized simulations of convective-radiative quasi-equilibrium, *J. Clim.*, submitted, 2006

Grabowski, W.W., X. Wu, and M.W. Moncrieff, Cloud resolving modeling of tropical cloud systems during Phase III of GATE. Part III: Effects of cloud microphysics, *J. Atmos. Sci*., *56*, 2384-2402, 1999.

Graf, H. F., J. Feichter, and B. Langmann, Volcanic sulfur emissions: Estimates of source strength and its contribution to the global sulfate distribution, *J. Geophys. Res.*, *102*, 10,727-10,738, 1997.

Graham, B., O. L. Mayol-Bracero, P. Guyon, G. C. Roberts, S. Decesari, M. C. Facchini, P. Artaxo, W. Maenhaut, P. Köll, and M. O. Andreae, Water-soluble organic compounds in biomass burning aerosols over Amazonia: 1. Characterization by NMR and GC-MS, *J. Geophys. Res.*, *107*, 8047, doi:10.1029/2001JD000336, 2002.

Graham, B., P. Guyon, P. Taylor, P. Artaxo, W. Maenhaut, M. M. Glovsky, R. C. Flagan, and M. O. Andreae, Organic compounds present in the natural Amazonian aerosol: Characterization by gas chromatography–mass spectrometry, *J. Geophys. Res.*, *108*, 4766, doi:10.1029/2003JD003990, 2003b.

Graham, B., P. Guyon, W. Maenhaut, P. E. Taylor, M. Ebert, S. Matthias-Maser, O. Mayol-Bracero, R. H. M. Godoi, P. Artaxo, F. Meixner, M. A. L. Moura, C. H. E. D. Rocha, R. van Grieken, M. M. Glovsky, R. C. Flagan, and M. O. Andreae, Composition and diurnal variability of the natural Amazonian aerosol, *J. Geophys. Res.*, *108*, 4765, doi:10.1029/2003JD004049, 2003a.

Grant, L.O., and A.M. Kahan, Weather modification for augmenting orographic precipitation, in *Weather and Climate Modification*, edited by W.N. Hess, 282–317, John Wiley and Sons, New York, 1974.

Grant, L.O., and P. W. Mielke, Jr., A randomized cloud seeding experiment at Climax, Colorado 1960-1965, *Proc. 5th Berkeley Symp. on Mathematical Statistics and Probability, Vol. V,* 115–131, University of California Press, Berkeley, Calif., 1967.

Grant, L.O., and R.D. Elliott, The cloud seeding temperature window, *J. Appl. Meteorol., 13,* 355–363, 1974.

Grant, L.O., The role of ice nuclei in the formation of precipitation, *Proc. Intern. Conf. Cloud Phys.*, Toronto, Ont., Amer. Meteorol. Soc., 305-310, 1968.

Gras, J.L., Cloud condensation nuclei over the southern-ocean, *Geophys. Res. Lett, 17,* 1565–1567, 1990.

Gras, J.L., CN, CCN, and particle size in Southern Ocean air at Cape Grim, Atmos. Res., 35, 233-251, 1995.

Grassl, H, Albedo reduction and radiative heating of clouds by absorbing aerosol particles. *Contribution to Atmos. Phys.*, Oxford. *48*, 199-210, 1975.

Greenfield, S., Rain scavenging of radioactive particulate matter from the atmosphere, J. Meteor., 14, 115-125, 1957.

Griffin, R. J., D. R. Cocker, III, J. H. Seinfeld, and D. Dabdub, Estimate of global atmospheric organic aerosols from oxidation of biogenic hydrocarbons, *Geophys. Res. Lett.*, *26*, 2721-2724, 1999.

Griffith, C.G., W.L. Woodley, P.G. Grube, D.W. martin, J. Stout and D.N. Sikdar, 1978: Rain estimates from geosynchronous satellite imagery: Visible and infrared studies. Mon. Wea. Rev., 106, 1153-1171.

Grini, A., G. Myhre, J. K. Sundet, and I. S. A. Isaksen, Modeling the annual cycle of sea salt in the global 3D model Oslo CTM2: Concentrations, fluxes, and radiative impact, *J. Clim.*, *15*, 1717-1730, 2002.

Groisman, P. V., V. V. Koknaeva, T. A. Belokrylova, and T. R. Karl, Overcoming biases in precipitation measurement: A history of the USSR experience, Bull. Amer. Meteor. Soc., 72, 1725-1733, 1991.

Groisman, P.V., and D.R. Legates, The accuracy of United States precipitation data, Bull. Amer. Meteor. Soc., 75, 215–227, 1994.

Grosch, M. and H-W. Georgii, Elemental composition of atmospheric aerosols and natural ice forming nuclei. J. Rech. Atmos.,

10, 227-232, 1976.

Guan, H., S.G. Cober, G.A. Isaac, A. Tremblay and A. Methot, Comparison of three cloud forecast schemes with in-situ aircraft measurements. *Wea. Forecasting*, ***17***, 1226-1235, 2002.

Guazzotti, S. A., K. R. Coffee, and K. A. Prather, Continuous measurements of size-resolved particle chemistry during INDOEX-Intensive Field Phase 99, *J. Geophys. Res.*, *106*, 28,607-28,627, 2001.

Guelle, W., M. Schulz, Y. Balkanski, and F. Dentener, Influence of the source formulation on modeling the atmospheric global distribution of sea salt aerosol, *J. Geophys. Res.*, *106*, 27,509-27,524, 2001.

Guibert, S., J. R. Snider, and J. L. Brenguier, 2003: Aerosol Activation in Marine Stratocumulus Clouds Part-I: Measurement Validation for a Closure Study PACE Topical Issue, J. Geophys. Res., 108, No. D15, 8628 10.1029.

Guibert, S., M. Schulz, S. Kinne, C. Textor, Y. Balkanski, S. Bauer, T. Berntsen, T. Berglen, O. Boucher, M. Chin, F. Dentener, T. Diehl, H. Feichter, D. Fillmore, S. Ghan, P. Ginoux, S. Gong, A. Grini, J. Hendricks, L. Horowitz, I. Isaksen, T. Iversen, S. Kloster, D. Koch, A. Kirkevåg, J. E. Kristjansson, M. Krol, A. Lauer, J.F. Lamarque, X. Liu, V. Montanaro, G. Myhre, J. Penner, G. Pitari, S. Reddy, Ø. Seland, P. Stier, T. Takemura, and X. Tie, Comparison of lidar data with model results from the aerocom intercomparison project, *in preparation*, 2005.

Gultepe, I., G. A. Isaac, W. R. Leaitch, and C. M. Banic, Parameterizations of marine stratus microphysics based on in situ observations: Implications for GCMs„*J. Clim., 9*, 345-357, 1996.

Gunn R. and B.B. Phillips, An experimental investigation of the effect of air pollution on the initiation of rain. J. Meteor., 14, 272-280, 1957.

Gunn, R., and G. D. Kinzer, The terminal velocity of fall for water drops in stagnant air. J. Meteor., 6, 243-248, 1949.

Guyon, P., B. Graham, G. C. Roberts, O. L. Mayol-Bracero, W. Maenhaut, P. Artaxo, and M. O. Andreae, In-canopy gradients, composition, sources, and optical properties of aerosol over the Amazon forest, *J. Geophys. Res.*, *108*, 4591, doi:10.1029/2003JD003465, 2003b.

Guyon, P., B. Graham, G.C. Roberts, O.L. MayolBracero, W. Maenhaut, P. Artaxo, and M.O. Andreae, In-canopy gradients, composition, sources, and optical properties of aerosol over the Amazon forest - art. no. 4591, Journal of Geophysical Research Atmospheres, 108 (D18), 4591, 2003.

Guyon, P., B. Graham, G.C. Roberts, O.L. MayolBracero, W. Maenhaut, P. Artaxo, and M.O. Andreae, Sources of optically active aerosol particles over the Amazon forest, Atmospheric Environment, 38 (7), 1039-1051, 2004.

Guyon, P., B. Graham, J. Beck, O. Boucher, E. Gerasopoulos, O. L. Mayol-Bracero, G. C. Roberts, P. Artaxo, and M. O. Andreae, Physical properties and concentration of aerosol particles over the Amazon tropical forest during background and biomass burning conditions, *Atmos. Chem. Phys.*, *3*, 951-967, 2003a.

Guyon, P., G. P. Frank, M. Welling, D. Chand, P. Artaxo, L. Rizzo, G. Nishioka, O. Kolle, H. Fritsch, M. A. F. Silva Dias, L. V. Gatti, A. M. Cordova, and M. O. Andreae, Airborne measurements of trace gases and aerosol particle emissions from biomass burning in Amazonia, *Atmos. Chem. Phys.*, *5*, 2989–3002, 2005.

Guzzi, R. and R. Rizzi, Effect of radiative exchange on the growth by condensation of a population of droplets, *Contributions to Atmospheric Physics*, Wiesbaden, W. Germany. *53*, No. 3, 351-365, 1980.

Guzzi, R., and R. Rizzi, The effect of radiative exchange on the growth of a population of droplets, *Contrib. Atmos. Phys., 53*, 351-365, 1980.

Gysel, M., E. Weingartner, and U. Baltensperger, Hygroscopicity of aerosol particles at low temperatures. 2. Theoretical and experimental hygroscopic properties of laboratory generated aerosols, *Environ. Sci. Technol.*, *36*, 63-68, 2002.

Habib, E., W.F. Krajewski, and A. Kruger, Sampling errors of tipping bucket raingauge measurements, J. Hydrol. Eng., 6, 159–166, 2001.

Habib, E., W.F. Krajewski, V. Nespor, and A. Kruger, Numerical simulation studies of raingauge data correction due to wind effect, J. Geophy. Res., 104(D16), 19,723-19,734, 1999.

Haddad, Z. S., J. P. Meagher, R. F. Adler, E. A. Smith, E. Im, and S. Durden, Global variability of precipitation according to the Tropical Rainfall Measuring Mission. *J. Geophys. Res.*, *109*, D17103, doi:10.1029/2004JD004607, 2004.

Hagen, D. E., J. Podzimek, and M. B. Trueblood, Upper-tropospheric aerosol sampled during project FIRE IFO II, *J. Atmos. Sci.*, *52*, 4196-4209, 1995.

Hallett, J., and S. C. Mossop, Production of secondary ice crystals during the riming process. *Nature*, **249**, 26-28, 1974.

Hallett, J., J. G. Hudson, and C. F. Rogers, Characterization of combustion aerosols for haze and cloud formation, *Aerosol Science and Technology*, *10*, 70-83, 1989.

Han, Q., W. B. Rossow, and A. A. Lacis, Near-global survey of effective droplet radii in liquid water clouds using ISCCP data. J. Climate, 7, 465-497, 1994.

Han, Q., W. B. Rossow, J. Chou, and R. M. Welch, Global survey of the relationship of cloud albedo and liquid water path with droplet size using ISCCP. J. Climate, 11, 1516-1528, 1998.

Han, Z., H. Ueda, K. Matsuda, R. Zhang, K. Arao, Y. Kanai, and H. Hasome, Model study on particle size segregation and deposition during Asian dust events in March 2002, Journal of Geophysical Research D: Atmospheres, 109 (19), D19205 1-22, 2004.

Hansen, A. R., and K. D. Beyer, Experimentally determined thermochemical properties of the malonic acid/water system: Implications for atmospheric aerosols, *Journal of Physical Chemistry A*, *108*, 3457-3466, 2004.

Hansen, J., M. Sato, and R. Ruedy, Radiative forcing and climate response, *J. Geophys. Res*., *102*, 6831-6864, 1997.

Hansen, K.M., J.H. Christensen, J. Brandt, L.M. Frohn, and C. Geels, Modelling atmospheric transport persistent organic pollutants in Northern Hemisphere with a 3-D dynamical model: DEHM-POP, Atmos. Chem. Phys., 4, 1339?1369, 2005.

Hao, W.-H., M.-H. Liu, M. Lorenzini, K. D. Singh, and D. E. Ward, Spatial distribution of tropical biomass burning in 1990 with 1°x1° resolution, in *Biomass Burning and Global Change*, edited by J. S. Levine, MIT Press, Cambridge, Mass., 1996.

Hao, W.-M., and M.-H. Liu, Spatial and temporal distribution of tropical biomass burning, *Global Biogeochem. Cycles*, *8*, 495-503, 1994.

Harrington, J.Y., G. Feingold, and W.R. Cotton, Radiative impacts on the growth of a population of drops within simulated summertime arctic stratus, *J. Atmos. Sci., 57,* 766–785, 2000.

Harris, D.H., and E. Foufoula-Georgiou, Subgrid variability and stochastic downscaling of modeled clouds: Effects on radiative transfer calculations for rainfall retrieval, J. Geophys. Res., 106, 10349–10362, 2001.

Harsvardhan, S. E. Schwartz, C. M. Benkovitz, and G. Guo, Aerosol influence on cloud microphysics examined by satellite measurements and chemical transport modeling. J. Atmos. Sci. 59, 714-725, 2002.

Hartmann, D. L., *Global Physical Climatology*. Academic Press, 408 pp., 1994.

Hartmann, D. L., M. E. Ockert-Bell, and M. L. Michelson, The effect of cloud type on the earth's energy balance: Global analysis. *J. Climate*, *5*, 1281-1304, 1992.

Hartz K.E.H, T. Rosenorn, S. R. Ferchak, T. M. Raymond, M. Bilde, N. M. Donahue, S. N. Pandis, Cloud condensation nuclei activation of monoterpene and sesquiterpene secondary organic aerosol, Journal of Geophysical Research-Atmospheres 110 (D14): Art. No. D14208, 2005.

Hasse, L., M. Grossklaus, K. Uhlig, and P. Timm, A ship rain gauge for use in high wind speeds, J. Oceanic. Atmos. Tech., 15, 380-386, 1998.

Hatzianastassiou, N., W. Wobrock, and A. I. Flossmann, The effect of cloud-processing of aerosol particles on clouds and radiation, *Tellus, 50B*, 478-490, 1998.

Hauser, D., P. Amayenc, B. Nutten, and P. Waldteufel, A new optical instrument for simultaneous measurements of raindrop diameter and fall distribution. J. Atmos. Oceanic Technol., 1, 256-269, 1984.

Haywood, J. M., S. R. Osborne, P. N. Francis, A. Keil, P. Formenti, M. O. Andreae, and P. H. Kaye, The mean physical and optical properties of regional haze dominated by biomass burning aerosol measured from the C-130 aircraft during SAFARI 2000, *J. Geophys. Res.*, *108*, 8473, doi:10.1029/2002JD002226, 2003b.

Haywood, J., P. Francis, O. Dubovik, M. Glew, and B. Holben, Comparison of aerosol size distributions, radiative properties, and optical depths determined by aircraft observations and Sun photometers during SAFARI 2000, *J. Geophys. Res.*, *108*, 8471, doi:10.1029/2002JD002250, 2003a.

Hegg D.A, Gao S, Hoppel W, Frick G, Caffrey P, Leaitch WR, Shantz N, Ambrusko J, Albrechcinski T, Laboratory studies of the efficiency of selected organic aerosols as CCN, Atmospheric Research 58 (3): 155-166, 2001.

Hegg, D. A., R. J. Ferek, and P. V. Hobbs, Cloud condensation nuclei over the Arctic Ocean in early spring, *J. Appl. Meteor.*, *34*, 2076-2082, 1995.

Hegg, D. A., S. Gao, W. Hoppel, G. Frick, P. Caffrey, W. R. Leaitch, N. Shantz, J. Ambrusko, and T. Albrechcinski, Laboratory studies of the efficiency of selected organic aerosols as CCN, *Atmos. Res.*, *58*, 155-166, 2001.

Hegg, D.A., and P.V. Hobbs, Cloud water chemistry and the production of sulfates in clouds, *Atmos. Environ., 15,* 1597–1604, 1981.

Hegg, D.A., and P.V. Hobbs, Comparisons of measured sulfate production due to ozone oxidation in clouds with a kinetic rate equation, *Geophys. Res. Lett., 14,* 719–721, 1987.

Hegg, D.A., and P.V. Hobbs, Comparisons of sulfate and nitrate production in clouds on the mid-Atlantic and Pacific Northwest Coasts of the United States, *J. Atmos. Chem., 7,* 325–333, 1988.

Hegg, D.A., and P.V. Hobbs, Measurements of sulfate production in natural clouds, *Atmos. Environ., 16,* 2663–2668, 1982.

Hegg, D.A., and P.V. Hobbs, Oxidation of sulfur dioxide in aqueous systems with particular reference to the atmosphere, *Atmos. Environ., 12*, 241–253, 1978.

Hegg, D.A., and P.V. Hobbs, Sulfate and nitrate chemistry in cumuliform clouds, *Atmos. Environ., 20,* 901–909, 1986.

Hegg, D.A., and P.V. Hobbs, The homogeneous oxidation of sulfur dioxide in cloud droplets, *Atmos. Environ., 13,* 981–987, 1979.

Hegg, D.A., and T.V. Larson, The effects of microphysical parameterization on model predictions of sulfate production in clouds, *Tellus, 42B,* 272-284, 1990.

Hegg, D.A., Heterogeneous production of cloud condensation nuclei in the marine atmosphere, *Geophys. Res. Lett., 17,* 2165-2168, 1990.

Hegg, D.A., L.F. Radke, and P.V. Hobbs, Measurements of Aitken nuclei and cloud condensation nuclei in the marine atmosphere and their relation to the DMS-cloud-climate hypothesis, *J. Geophys. Res., 96,* 18727–18,733, 1991b.

Hegg, D.A., L.F. Radke, and P.V. Hobbs, Particle production associated with marine clouds, *J. Geophys. Res., 95,* 13,917–13,926, 1990.

Hegg, D.A., P.-F. Yuen, and T.V. Larson, Modeling the effects of heterogeneous cloud chemistry on the marine particle size distribution, *J. Geophys. Res., 97,* 12,927–12,933, 1991.

Hegg, D.A., P.V. Hobbs, and L.F. Radke, Measurements of the scavenging of sulfate and nitrate in clouds, *Atmos. Environ., 18,* 1939–1946, 1984a.

Hegg, D.A., P.V. Hobbs, and L.F. Radke, Observations of the modification of cloud condensation nuclei in wave clouds, *J. Rech. Atmos., 14,* 217–222, 1980.

Hegg, D.A., Particle production in clouds, *Geophys. Res. Lett., 18,* 995-998, 1991.

Hegg, D.A., R. Majeed, P.-F. Yuen, M.B. Baker, and T.V. Larson, The impacts of SO_2 oxidation in cloud drops and in haze particles on aerosol light scattering and CCN activity, *Geophys. Res. Lett., 23,* 2613–2616, 1996.

Hegg, D.A., R.J. Ferek, P.V. Hobbs, and L.F. Radke, Dimethyl sulfide and cloud condensation nucleus correlations in the northeast Pacific Ocean, *J. Geophys. Res., 96,* 13189–13191, 1991a.

Hegg, D.A., S.A. Rutledge, and P.V. Hobbs, A numerical model for sulfur chemistry in warm-frontal rainbands, *J. Geophys. Res., 89,* 7133–7147, 1984b.

Hegg, D.A., S.A. Rutledge, and P.V. Hobbs, A numerical model for sulfur and nitrogen chemistry in narrow cold-frontal rainbands. II: Discussion of chemical fields, *J. Geophys. Res., 91,* 14403–14416, 1986.

Hegg, D.A., S.A. Rutledge, P.V. Hobbs, M.C. Barth, and O. Hertzman, The chemistry of a mesoscale rainband, *Quart. J. Roy. Meteorol. Soc., 115,* 867–886, 1989.

Hegg, D.A., The influence of liquid-phase oxidation of SO_2 in the troposphere, *J. Geophys. Res., 99,* 3773–3779, 1985.

Heintzenberg, J., and D. C. Covert, Size distribution and chemical composition of marine aerosols: A compilation and review, *Tellus*, *52B*, 1104-1122, 2000.

Heintzenberg, J., Fine particles in the global troposphere: a review, Tellus, 41B, 149-160, 1989.

Heintzenberg, J., K. Okada, and J. Strom, On the composition of non-volatile material in upper tropospheric aerosols and cirrus crystals, *Atmos. Res.*, *41*, 81-88, 1996.

Heisler, S. L., Friedlan.Sk, and R. B. Husar, Relationship of smog aerosol size and chemical element distributions to source characteristics, *Atmos. Environ.*, *7*, 633-649, 1973.

Henning S, Rosenorn T, D'Anna B, Gola AA, Svenningsson B, Bilde M, Cloud droplet activation and surface tension of mixtures of slightly soluble organics and inorganic salt, Atmospheric Chemistry and Physics 5: 575-582, 2005.

Henning, S., E. Weingartner, M. Schwikowski, H. W. Gaggeler, R. Gehrig, K. P. Hinz, A. Trimborn, B. Spengler, and U. Baltensperger, Seasonal variation of water-soluble ions of the aerosol at the high-alpine site Jungfraujoch (3580 m asl), *J. Geophys. Res.*, *108*, 4030, doi:10.1029/2002JD002439, 2003.

Hering, S., A. Eldering, and J. H. Seinfeld, Bimodal character of accumulation mode aerosol mass distributions in Southern California, *Atmos. Environ.*, *31*, 1-11, 1997.

Herman M., J.L. Deuzé, A. Marchand, B. Roger, and P. Lallart, Aerosol Remote Sensing from POLDER/ADEOS over the Ocean. Improved Retrieval using Non-Spherical Particle Model, , *J. Geophys. Res.- Atmos*., 110 (D10): Art. No. D10S02 MAR 9, 2005

Herman, J. R., P. K. Bhartia, O. Torres, C. Hsu, C. Seftor, and E. Celarier, Global distribution of UV-absorbing aerosol from Nimbus-7/TOMS data, *J. Geophys. Res.*, **102**, 16911-16922, 1997.

Herman, M., J. L. Deuzé, C. Devaux, P. Goloub, F. M. Bréon and D. Tanré, 1997: Remote sensing of aerosols over land surfaces including polarization measurements and application to POLDER measurements, J. Geophys. Res., **102**, 17039-17049, 1997.

Heymsfield, A. J., and R. G. Knollenberg, Properties of cirrus generating cells. *J. Atmos. Sci.,* **29,** 1358–1366, 1972.

Heymsfield, A.J., and K.M. Miller, Water vapor and ice mass transport into the anvils of CCOPE thunderstorms: Comparison with storm in flux and rainout, *J. Atmos. Sci., 45,* 3501–3514, 1988.

Heymsfield, A.J., Ice crystal terminal velocities. *J. Atmos. Sci.*, **26**, 1348-1351, 1972.

Heymsfield, G.M., and S. Schotz, Structure and evolution of a severe squall line over Oklahoma, *Mon. Wea. Rev., 113,* 1563–1589, 1985.

Hill, R. J., Geometric collision rates and trajectories of cloud droplets falling into a Burger's vortex, *Phys. of Fluids, 17*, 037103, 2005.

Hindman, E.E. II, P.V. Hobbs, and L.F. Radke, Airborne investigations of aerosol particles from a paper mill, *J. Air Poll. Cont. Assoc., 27,* 224–229, 1977.

Hindman, E.E., II, P.V. Hobbs, and L.F. Radke, Cloud condensation nucleus size distributions and their effects on cloud droplet size distributions, *J. Atmos. Sci., 34*, 951-955, 1977.

Hindman, E.E., II, The nature of aerosol particles from a paper mill and their effects on clouds and precipitation, *Ph.D. dissertation*, University of Washington, Seattle, 242 pp., 1975.

Hindman, E.E., II, Water droplet fogs formed from pyrotechnically generated condensation nuclei, *J. Wea. Modif.*, *10,* 77–96, 1978.

Hindman, E.E., M. Tag, B.A. Silverman, and P.V. Hobbs, Cloud condensation nuclei from a paper mill. Part II: Calculated effects on rainfall, *J. Appl. Meteorol., 16*, 753–755, 1977c.

Hindman, E.E., P.V. Hobbs, and L.F. Radke, Airborne investigations of aerosol particles from a paper mill, *J. Air Poll. Control Assoc., 27*, 224–229, 1977a.

Hindman, E.E., P.V. Hobbs, and L.F. Radke, Cloud condensation nuclei from a paper mill. Part I: Measured effects on clouds, *J. Appl. Meteorol., 16*, 745–252, 1977b.

Hinds, W.C., Aerosol Technology: Properties, Behavior, and Measurement of Airborne Particles, John Wiley & Sons, New York, 1982.

Hobbs, P. V., and J. D. Locatelli, Ice nuclei from a natural forest fire, *J. Appl. Meteor.*, *8*, 833-834, 1969.

Hobbs, P. V., and J. D. Locatelli, Ice nuclei from a natural forest fire. *J. Appl. Meteor.,* **8,** 833–834, 1969.

Hobbs, P. V., Simultaneous airborne measurements of cloud condensation nuclei and sodium-containing particles over the ocean, *Q. J. R. met. Soc.*, *97*, 263-271, 1971.

Hobbs, P.V. and A. J. Alkezweeny, The fragmentation of freezing water droplets in free fall**,** *J. Atmos. Sci., 25,* 881–888, 1968.

Hobbs, P.V., Aerosol-cloud interactions, in *Aerosol-Cloud-Clim. Interactions,* Ed. P. V. Hobbs, Academic Press, 33–73, 1993.

Hobbs, P.V., and A.L. Rangno, Comments on the Climax randomized cloud seeding experiments, *J. Appl. Meteorol., 18*, 1233–1237, 1979.

Hobbs, P.V., and A.L. Rangno, Ice particle concentrations in clouds, *J. Atmos. Sci., 42*, 2523-2549, 1985.

Hobbs, P.V., and A.L. Rangno, Ice particle concentrations in clouds, *J. Atmos. Sci., 42*, 2523–2549, 1985.

Hobbs, P.V., and A.L. Rangno, Microstructures of low and middle-level clouds over the Beaufort Sea, *Quart. J. Roy. Meteorol. Soc., 124*, 2035-2071, 1998.

Hobbs, P.V., and A.L. Rangno, Rapid development of high ice particle concentrations in small polar maritime cumuliform clouds. *J. Atmos. Sci.,* 47, 2710-2722, 1990.

Hobbs, P.V., and A.L. Rangno, Super-large raindrops, *Geophys. Res., Lett., 31*, L13102, doi:10.1029/2004GL020167, 2004.

Hobbs, P.V., and L.F. Radke, Cloud condensation nuclei from a simulated forest fire, *Sci.*, *163*, 279–280, 1969.

Hobbs, P.V., and L.F. Radke, Redistribution of snowfall across a mountain range by artificial seeding: A case study, *Science, 181*, 1043–1045, 1973.

Hobbs, P.V., and L.F. Radke, Redistribution of snowfall across a mountain range by artificial seeding: A case study, *Sci., 181*,

1043–1045, 1973.

Hobbs, P.V., and L.F. Radke, The nature of winter clouds and precipitation in the Cascade Mountains and their modification by artificial seeding. Part II: Techniques for the physical evaluation of seeding, *J. Appl. Meteorol., 14*, 805–818, 1975.

Hobbs, P.V., and R.J. Farber, Fragmentation of ice particles in clouds, *J. de Rech. Atmos., 6*, 245–258, 1973.

Hobbs, P.V., and Radke, L.F., Cloud condensation nuclei from a simulated forest fire, *Science, 163,* 279–280, 1969.

Hobbs, P.V., D.A. Bowdle, and L.F. Radke, Particles in the lower troposphere over the high plains of the United States. II: Cloud condensation nuclei, *J. Climate Appl. Meteorol., 24,* 1370–1376, 1985.

Hobbs, P.V., D.A. Bowdle, and L.F. Radke, Particles in the lower troposphere over the High Plains of the United States. I: Size distributions, elemental compositions and morphologies, *J. Clim. Appl. Meteorol., 24*, 1344–1356*,* 1985.

Hobbs, P.V., Ice multiplication in clouds, *J. Atmos. Sci., 26,* 315–318, 1969.

Hobbs, P.V., ***Ice Physics,*** Clarendon Press, Oxford: Clarendon, pp. 837, 1974.

Hobbs, P.V., L.F. Radke, and S.E. Shumway, Cloud condensation nuclei from industrial sources and their apparent influence on precipitation in Washington State, *J. Atmos. Sci., 27*, 81–89, 1970.

Hobbs, P.V., L.F. Radke, and S.E. Shumway, Cloud condensation nuclei from industrial sources and their apparent influences on precipitation in Washington State, *J. Atmos. Sci., 27*, 81–89, 1970.

Hobbs, P.V., M. Fullerton, and G. Bluhm, Ice nucleus "storms" in Hawaii. *Nature,* 230**,** 90–91, 1971.

Hobbs, P.V., Simultaneous airborne measurements of cloud condensation nuclei and sodium-containing particles over the ocean, *Quart. J. Roy. Meteorol. Soc., 97,* 263–271, 1971.

Hobbs, P.V., T.J. Garrett, Emissions from ships with respect to their effects on clouds, *J. Atmos. Sci., 57*, 2570–2590, 2000.

Hobbs, P.V., T.J. Matejka, P.H. Herzegh, J.D. Locatelli, and R.A. Houze, The mesoscale and microscale structure and organization of clouds and precipitation in midlatitude cycles. I: A case of a cold front, *J. Atmos. Sci., 37,* 1980.

Hobbs, P.V., The nature of winter clouds and precipitation in the Cascade Mountains and their modification by artificial seeding. Part I: Natural conditions, *J. Appl. Meteorol., 14*, 783–804, 1975a.

Hobbs, P.V., The nature of winter clouds and precipitation in the Cascade Mountains and their modification by artificial seeding. Part III: Case studies of the effects of seeding, *J. Appl. Meteorol., 14*, 819–858, 1975b.

Hobbs, PV, and DA Burrows, The Electrification of an Ice Sphere Moving through Natural Clouds. *J. Atmos. Sci.*, **23**, 757—763, 1966.

Hoelzemann, J. J., M. G. Schultz, G. P. Brasseur, C. Granier, and M. Simon, Global Wildland Fire Emission Model (GWEM): Evaluating the use of global area burnt satellite data, *J. Geophys. Res.*, *109*, D14S04, doi:10.1029/2003JD003666, 2004.

Hoff, R.M., A. Vandermeer, and L. Spacek., LITE/NARCM retrievals and implications for future missions, in Advances in Laser Remote Sensing, edited by C.L.a.J.P. A. Dabas, pp. 27-30, Editions de L'Ecole polytechnique, 91128 Palaiseux Cedex, France, 2001.

Hofschreuder, P., F.G. R?mer, N.F.M. Van Leeuwen, and B.G. Arends, Deposition of aerosol on Speulder Forest: Accumulation experiments, Atmospheric Environment, 31 (3), 351-357, 1997.

Hogan, R. J., A. J. Illingworth, E. J. O'Connor and J. P. V. Poiares Baptista, Characteristics of mixed-phase clouds: Part II: A climatology from ground-based lidar, Quart. J. Roy. Meteorol. Soc., 129, 2117-2134, 2003.

Holben, B. N., D. Tanré, A. Smirnov, T. F. Eck, I. Slutsker, N. Abuhassan, W. W. Newcomb, J. S. Schafer, B. Chatenet, F. Lavenu, Y. J. Kaufman, J. V. Castle, A. Setzer, B. Markham, D. Clark, R. Frouin, R. Halthore, A. Karneli, N. T. O'Neill, C. Pietras, R. T. Pinker, K. Voss, and G. Zibordi, An emerging ground-based aerosol climatology: Aerosol optical depth from AERONET, J. Geophys. Res, **106**, 12067-12097, 2001.

Holben, B. N., T. F. Eck, I. Slutsker, D. Tanré, J. P. Buis, A. Setzer, E. Vermote, J. A. Reagan, Y. J. Kaufman, T. Nakajima, F. Lavenu, I. Jankowiak and A. Smirnov, AERONET—A federated instrument network and data archive for aerosol characterization, Remote Sens. Environ., **66**, 1-16, 1998.

Hoppel, W. A., G. M. Frick, and R. E. Larson, Effect of nonprecipitating clouds on the aerosol size distribution in the marine boundary layer, *Geophys. Res. Lett.*, *13*, 125-128, 1986.

Hoppel, W. A., G. M. Frick, J. W. Fitzgerald, and B. J. Wattle, A cloud chamber study of the effect that nonprecipitating water clouds have on the aerosol size distribution, *Aerosol Science and Technology*, *20*, 1-30, 1994.

Hoppel, W. A., J. E. Dinger, and R. E. Ruskin, Vertical profiles of CCN at various geographical locations, *J. Atmos. Sci.*, *30*, 1410-1420, 1973.

Hoppel, W. A., J. W. Fitzgerald, G. M. Frick, R. E. Larson, and E. J. Mack, Aerosol size distributions and optical properties found in the marine boundary layer over the Atlantic Ocean, *J. Geophys. Res.*, *95*, 3659-3686, 1990.

Hoppel, W.A., J.W. Fitzgerald, G.M. Frick, and R.E. Larson, Aerosol size distributions and optical properties found in the marine boundary layer over the Atlantic Ocean, *J. Geophys. Res., 95*, 3659-3686, 1990.

Hoppel, W.A., Nucleation in the MSA-water vapor system, *Atmos. Environ., 21,* 2703-2709, 1987.

Hori M, Ohta S, Murao N, Yamagata S, Activation capability of water soluble organic substances as CCN, Journal of Aerosol Science 34 (4): 419-448, 2003.

Hori, M., S. Ohta, N. Murao, and S. Yamagata, Activation capability of water soluble organic substances as CCN, *J. Aerosol Sci.*, *34*, 419-448, 2003.

Houghton, H.G., Problems connected with the condensation and precipitation processes in the atmosphere, *Bull. Amer. Meteorol. Soc., 19,* 152-159, 1938.

Houghton, J. T., Y. Ding, D. J. Griggs, M. Noguer, P. J. van der Linden, X. Dai, K. Maskell, and C. A. Johnson (Ed.). *Climate Change 2001: The Scientific Basis. Contribution of Working Group I to the Third Assessment Report of the Intergovernmental Panel on Climate Change*. Cambridge, UK, and New York, NY, USA: Cambridge University Press, 881 p, 2001.

Hounslow, M.J., R.L. Ryall, and V.R. Marshall, A discretized population balance for nucleation, growth and aggregation, *AIChE J, 34*, 1821-1832, 1988.

Houze, R.A., Jr., S. Brodzik, C. Schumacher, S.E. Yuter, and C.R. Williams, Uncertainties in oceanic radar rain maps at

Kwajalein and implications for satellite validation, *J. Appl. Meteor*., *43*, 1114–1132, 2004.

Howell, W.E., The growth of cloud drops in uniformly cooled air, *J. Meteor., 6*, 134-149, 1949.

Hsu, K., X. Gao, S. Sorooshian, and H.V. Gupta, Precipitation estimation from remotely sensed information using artificial neural networks, Journal of Applied Meteorology, 36, 1176-1190, 1997.

Hudson, J. G. , Effects of CCN Concentrations on stratus Clouds, *J. Atmos. Sci.*, *40*, 480-486. 1983.

Hudson, J. G., and S. S. Yum, 1997: Droplet spectral broadening in marine stratus, J. Atmos. Sci., **54**, 2642-2654.

Hudson, J. G., and X. Da, Volatility and size of cloud condensation nuclei, *J. Geophys. Res.*, *101*, 4435-4442, 1996.

Hudson, J. G., J. Hallett, and C. F. Rogers, Field and laboratory measurements of cloud-forming properties of combustion aerosols, *J. Geophys. Res.*, *96*, 10,847-10,859, 1991.

Hudson, J.G..An instantaneous CCN spectrometer. *Atmos. and Ocean. Tech*., **6**, 1055-1065, 1989

Huebert, B.J., T. Bates, P.B. Russell, G. Shi, Y.J. Kim, K. Kawamura, G. Carmicheal, and T. Nakajima, An overview of ACE-Asia: Strateggies for quantifying the relationships between Asian aerosols and their climatic impacts, J. Geophys Res., 108 (D23), 8633,doi:1029/2003JD003550, 2003.

Huff, F.A., and W.L. Shipp, Spatial correlations of storm, monthly, and seasonal precipitation, J. App. Meteor., 8, 542–550, 1969.

Huffman, G. J., R. F. Adler, E. F. Stocker, D. T. Bolvin, and E. J. Nelkin, Analysis of TRMM 3-hourly multi-satellite precipitation estimates computed in both real and post-real time. Preprints, 12th Conf. on Sat. Meteor. and Oceanog., Long Beach, CA, Amer. Meteor. Soc., P4.11, 6 pp, 2003.

Huffman, G.J., and Coauthors, The Global Precipitation Climatology Project (GPCP) combined precipitation data set, Bull. Amer. Meteor. Soc., 78, 5–20, 1997.

Huffman, G.J., R.F. Adler, M.M. Morrissey, D.T. Bolvin, S. Curtis, R. Joyce, B. McGavock, and J. Susskind, Global precipitation at one-degree daily resolution from multisatellite observations, J. Hydrometeor., 2, 36-50, 2001.

Hughes, L. S., J. O. Allen, M. J. Kleeman, R. J. Johnson, G. R. Cass, D. S. Gross, E. E. Gard, M. E. Galli, B. D. Morrical, D. P. Fergenson, T. Dienes, C. A. Noble, P. J. Silva, and K. A. Prather, Size and composition distribution of atmospheric particles in southern California, *Environ. Sci. Technol.*, *33*, 3506-3515, 1999.

Hulme, M., T. J. Osborn, and T. C. Johns, Precipitation sensitivity to global warming: Comparison of observations with HadCM2 simulations, *Geophys. Res. Lett.*, 25, 3379-3382, 1998.

Hurrell, J. W., Decadal trends in the North Atlantic Oscillation: Regional temperatures and precipitation. *Science*, **269**, 676-679, 1995.

Husar, R. B., J. Prospero, and L. L. Stowe, Characterization of tropospheric aerosols over the oceans with the NOAA AVHRR optical thickness operational product. J. Geophys. Res., **102**, 16889-16909, 1997.

Husar, R.B., D.M. Tratt, B.A. Schichtel, S.R. Falke, F. Li, D. Jaffe, S. Gass¢, T. Gill, N.S. Laulainen, F. Lu, M.C. Reheis, Y. Chun, D. Westphal, B.N. Holben, C. Gueymard, I. McKendry, N. Kuring, G.C. Feldman, C. McClain, R.J. Frouin, J. Merrill, D. DuBois, F. Vignola, T. Murayama, S. Nickovic, W.E. Wilson, K. Sassen, N. Sugimoto, and W.C. Malm, Asian dust evens of April 1998, J. Geophys. Res., 106 (D16), 2001.

Iguchi, T., T. Kozu, R. Meneghini, J. Awaka, and K. Okamoto, Rain-profiling algorithm for TRMM precipitation radar, J. Appl. Meteor., 39, 2038–2052, 2000.

Illingworth, A., Improved Precipitation Rates and Data Quality Using Polarimetric Measurements, in Weather Radar: Principles and Advanced Applications, edited by P. Meischner, Springer-Verlag, Berlin, 130-166, 2004.

IPCC, Climate Change 2001: The Scientific Sasis, Contribution of working Group I to the Third Assessment Report of the Intergovernmental Panel on Climate Change, Cambridge University Press, 2001.

Isono, K., M Komabayashi, A Ono, Volcanoes as a Source of Atmospheric Ice Nuclci - Nature, 1959b.

Isono, K., M. Komabayashi, and A. Ono, The nature and origin of ice nuclei in the atmosphere, J. Meteor.. Soc. Japan, 37, 211-233, 1959a.

Israelevich, P. L., Z. Levin, J. H. Joseph, and E. Ganor, Desert aerosol transport in the Mediterranean region as inferred from the TOMS aerosol index, *J. Geophys. Res.*, *107*, 4572, doi:10.1029/2001JD002011, 2002.

Ito, A., and J. E. Penner, Global estimates of biomass burning emissions based on satellite imagery for the year 2000, *J. Geophys. Res.*, *109*, D14S05, doi:10.1029/2003JD004423., 2004.

Ito, A., and J. E. Penner, Historical emissions of carbonaceous aerosols from biomass and fossil fuel burning for the period 1870 - 2000, *Global Biogeochem. Cycles*, GB2028, doi:10.1029/2004GB002374, 2005.

Jacob, D.J., J.A. Logan, and P.P. Murti, Effect of rising Asian emissions on surface ozone in the United States, Geophysical Research Letters, 26 (14), 2175-2178, 1999.

Jacob, D.J., R. Avissar, G.C. Bond, S. Gaffin, J.T. Kiehl, J.L. Lean, U. Lohmann, M.E. Mann, R.A. Pielke, V. Ramanathan, and L.M. Russell, *Radiative forcing of climate change.* The National Acadamies Press, Washington, D.C., 207 pp, 2005.

Jacobson, M. Z., and J. H. Seinfeld, Evolution of nanoparticle size and mixing state near the point of emission, *Atmos. Environ.*, *38*, 1839-1850, 2004.

Jacobson, M. Z., Control of fossil-fuel particulate black carbon and organic matter, possibly the most effective method of slowing global warming, *J. Geophys. Res., 107,* doi:10.1029/2001JD001376, 2002.

Jacobson, M. Z., Strong radiative heating due to the mixing state of black carbon in atmospheric aerosols, *Nature*, 695-697, 2001.

Jacobson, M.Z., R.P. Turco, E.J. Jensen, and O.B. Toon, Modeling coagulation among particles of different composition and size, Atmospheric Environment, 28 (7), 1327-1338, 1994.

Jaeger, L., *Monatskarten des Niederschlags für die ganze Erde,* Bericht des Deutschen Wetterdienstes, Vol. 139, Offenbach a.M., 33 pp. and plates, 1976.

Jaenicke, R., Tropospheric Aerosols, in *Aerosol-Cloud-Climate Interactions*, edited by P. V. Hobbs, pp. 1-27, Academic Press, San Diego, 1993.

Jaffe, D., S. Tamura, and J. Harris, Seasonal cycle, composition and sources of background fine particles along the west coast of the U.S., Atmos. Environ., 39, 297- 306, 2005.

Jaffe, D.A., T. Anderson, D. Covert, R. Kotchenruther, B. Trost, J. Danielson, W. Simpson, T. Berntsen, S. Karlsdottir, D. Blake, J. Harris, G. Carmichael, and I. Uno, Transport of Asian air pollution to North America, Geophys.Res.Letts., 26, 711-714, 1999.

Jang, M., B. Carroll, B. Chandramouli, and M.K. Richard, Particle growth by acid-catalyzed heterogeneous reactions of organic carbonyls on preexisting aerosols, Environ. Sci.Technol., 37 (17), 3828-37, 2003.

Jang, M.S., and R.M. Kamens, Atmospheric secondary aerosol formation by heterogeneous reactions of aldehydes in the presence of a sulfuric acid aerosol catalyst, Environmental Science & Technology, 35 (24), 4758-4766, 2001a.

Jang, M.S., and R.M. Kamens, Characterization of secondary aerosol from the photooxidation of toluene in the presence of NOx and 1-propene, Environmental Science & Technology, 35 (18), 3626-3639, 2001b.

Jang, M.S., N.M. Czoschke, S. Lee, and R.M. Kamens, Heterogeneous atmospheric aerosol production by acid-catalyzed particle-phase reactions, Science, 298 (5594), 814-817, 2002.

Jankowiak, I., and D. Tanré, 1992: Satellite climatology of Saharan dust outbreaks: Method and preliminary results, J. Climate, **5**, 646-656.

Janowiak, J.E., and P. Xie, CAMS-OPI: A global satellite-rain gauge merged product for real-time precipitation monitoring applications, J. Climate, 12, 3335-3342, 1999.

Janowiak, J.E., R.J. Joyce, and Y. Yarosh, A real-time global half-hourly pixel resolution infrared dataset and its applications, Bulletin American Meteorology Society, Vol. 82, pp. 205-217, 2000.

Janowiak, J.E., Tropical rainfall: A comparison of satellite-derived rainfall estimates with model precipitation forecasts, climatologies, and observations, Mon. Wea. Rev., 120, 448-462, 1992.

Jaw, J.-J., Statisical theory of precipitation process, *Tellus*, *18*, 722-729, 1966.

Jennings, S.G., M. Geever, and T.C. O'Connor, Coastal CCN measurements at Mace Head with enhanced concentrations in strong winds, Atmos. Res., 46, 243-252, 1997.

Jennings, S.G., Wet Processes Affecting Atmospheric Aerosols, Chapter 14 in Atmospheric Particles, 476-507, 1998.

Jiang, H., and G. Feingold, Effect of aerosol on warm convective clouds: Aerosol-cloud-surface flux feedbacks in a new coupled large eddy model. *J. Geophys. Res., 111,* D01202, doi:10.1029/2005JD006138, 2006.

Jiang, H., G. Feingold, and W.R. Cotton, Simulations of aerosol-cloud-dynamical feedbacks resulting from entrainment of aerosol into the marine boundary layer during the Atlantic Stratocumulus Transition Experiment, *J. Geophys. Res*., *107*, 4813, doi:10.1029/2001JD001502, 2002.

Jiang, H., G. Feingold, W. R. Cotton, and P. Duynkerke. Large-eddy simulations of entrainment of cloud condensation nuclei into the Arctic boundary layer: May 18, 1999, FIRE/SHEBA case study, J. Geophys. Res, 106, 15,113-15,122. 2001.

Jiang, H.L., G. Feingold, W.R. Cotton, and P.G. Duynkerke, Large-eddy simulations of entrainment of cloud condensation nuclei into the Arctic boundary layer: May 18, 1998, FIRE/SHEBA case study, Journal of Geophysical Research Atmospheres, 106 (D14), 15113-15122, 2001.

Jickells, T.D., Z.S. An, K.K. Andersen, A.R. Baker, G. Bergametti, N. Brooks, P.W.B. J.J. Cao, R.A. Duce, K.A. Hunter, H. Kawahata, N. Kubilay, J. LaRoche, P.S. Liss, N. Mahowald, J.M. Prospero, A.J. Ridgwell, L. Tegen, and R. Torres, Global Iron Connections Between Desert Dust, Ocean Biogeochemistry, and Climate, Science, 308, 67-71, 2005.

Jimenez, J. L., J. T. Jayne, Q. Shi, C. E. Kolb, D. R. Worsnop, I. Yourshaw, J. H. Seinfeld, R. C. Flagan, X. F. Zhang, K. A. Smith, J. W. Morris, and P. Davidovits, Ambient aerosol sampling using the Aerodyne Aerosol Mass Spectrometer, *J. Geophys. Res*., *108*, 2003.

Jin, M., J.M. Shepherd, and M.D. King, Urban aerosols and their variations with clouds and rainfall: A case study for New York and Houston, *J. Geophys. Res., 110*, D10S20, 10.1029/2004JD005081, 2005.

Jiusto, J.E., Maritime concentration of condensation nuclei, *J. Rech. Atmos., 2,* 245-250, 1966.

John, W., S. M. Wall, J. L. Ondo, and W. Winklmayr, Modes in the size distributions of atmospheric inorganic aerosol, *Atmospheric Environment Part a-General Topics*, *24*, 2349-2359, 1990.

Johns, T. C., C. F. Durman, H. T. Banks, M. J. Roberts, A. J. McLaren, J. K. Ridley, C. A. Senior, K. D. Williams, A. Jones, G. J. Rickard, S. Cusack, W. J. Ingram, M. Crucifix, D. M. H. Sexton, M. M. Joshi, B.-W. Dong, H. Spencer, R. S. R. Hill, J. M. Gregory, A. B. Keen, A. K. Pardaens, J. A. Lowe, A. Bodas-Salcedo, S. Stark and Y. Searl, The new Hadley Centre climate model HadGEM1: Evaluation of coupled simulations. *J. Clim.* (in press), 2006.

Johnson, B.T., K.P. Shine and P.M. Forster, The semi-direct aerosol effect: Impact of absorbing aerosols on marine stratocumulus, *Quart. J. Roy. Meteorol. Soc.*, *30*, 1407-1422, 2004.

Johnson, D. B., The role of giant and ultragiant aerosol particles in warm rain initiation, *J. Atmos. Sci., 39*, 448-460, 1982.

Johnson, D. W., S. R. Osborne, R. Wood, K. Suhre, P. K. Quinn, T. Bates, M. O. Andreae, K. J. Noone, P. Glantz, B. Bandy, J. Rudolph, and C. O'Dowd, Observations of the evolution of the aerosol, cloud and boundary-layer characteristics during the 1st ACE-2 Lagrangian experiment, *Tellus*, *52B*, 348-374, 2000.

Johnson, D.B., On the relative efficiency of coalescence and riming, *J. Atmos. Sci., 44*, 1672–1680, 1987.

Johnson, D.B., The role of coalescence nuclei in warm rain initiation. *Ph.D. dissertation*, University of Chicago, 119 pp., 1979.

Johnson, D.B., Ultragiant urban aerosol particles*, Science, 194*, 941-942, 1976.

Johnson, R.H., and P.E. Ciesielski, Rainfall and radiative heating rates from TOGA COARE atmospheric budgets, J. Atmos. Sci., 57, 1497–1514, 2000.

Jones, A., D. L. Roberts, and M. J. Woodage, Indirect sulphate aerosol forcing in a climate model with an interactive sulphur cycle, J. Geophys. Res., 106, 20,293-230,310, 2001.

Jones, A., D.L. Roberts, and J. Slingo, A climate model study of indirect radiative forcing by anthropogenic sulphate aerosols, Nature, 370, 450-453, 1994.

Jordan, C.E., J. E. Dibb, B. E. Anderson, and H. E. Fuelberg, Uptake of nitrate and sulfate on dust aerosols during TRACE-P, J. Geophys. Res., 108 (D21), 8817, doi:10.1029/2002JD003101, 2003.

Joss, J., and A. Waldvogel, Ein Spectrograph fur Niedersclagstropfen mit automatisher Auswertung (A spectrograph for the automatic analysis of raindrops). Pure Appl. Geophys., 68, 240-246, 1967.

Joss, J., and A. Waldvogel, Raindrop size distribution and sampling size errors. J. Atmos. Sci., 566-569, 1969.

Joss, J., B. Schädler, G. Galli, R. Cavalli, M. Boscacci, E. Held, G. Della Bruna, G. Kappenberger, V. Nespor, and R. Spiess, Operational Use of Radar for Precipitation Measurements in Switzerland, vdf Hochschulverlag AG an der ETH Zürich, 108 pp., 1998.

Joyce, R. J.. J./ E. Janowiak, P. A. Arkin and P. Xie, CMORPH: A Method that Produces Global Precipitation Estimates from Passive Microwave and Infrared Date at High Spatial and Temporal Resolution. J. Hydrometeorology. 5, 487-503, 2004.

Jung, C.H., Y.P. Kim, and K.W. Lee, A moment model for simulating raindrop scavenging of aerosols, Journal of Aerosol Science, 34 (9), 1217-1233, 2003.

Junge, C. E. (1963). *Air Chemistry and Radioactivity*. New York: Academic Press, 382 p.

Junge, C., Die Rolle der Aerosole und der gasförmigen Beimengungen der Luft im Spurenstoffhaushalt der Troposphäre, *Tellus*, *V*, 1-26, 1953.

Junge, C.E., Fate of Pollutants in the Air and Water Environments, edited by I.H. Suffet, pp. 7-26, J. Wiley, New York, 1977.

Junker, C., and C. Liousse, A global emission inventory of carbonaceous aerosol including fossil fuel and biofuel sources for the period 1860 - 1997, *Atmos. Chem. Phys. Discuss.*, 2005, in press.

Kahn, R., B. Gaitley, J. Martonchik, D. Diner, K. Crean, and B. Holben, MISR global aerosol optical depth validation based on two years of coincident AERONET observations, J._Geophys. Res., *110, No. D10, D10S04*10.1029/2004JD004706, 2005.

Kahn, R., P. Banerjee, and D. McDonald, The sensitivity of multiangle imaging to natural mixtures of aerosols over ocean, *J. Geophys. Res*., **106**, 18219-18238, 2001.

Kahn, R., P. Banerjee, and D. McDonald, The sensitivity of multiangle imaging to natural mixtures of aerosols over ocean, J. Geophys. Res., **106**, 18219-18238, 2001.

Kahnert, M., and L. Tarrasøn, Transboundary particulate matter in Europe, in EMEP Report, 2003.

Kajii, Y., S. Kato, D. G. Streets, N. Y. Tsai, A. Shvidenko, S. Nilsson, I. McCallum, N. P. Minko, N. Abushenko, D. Altyntsev, and T. V. Khodzer, Boreal forest fires in Siberia in 1998: Estimation of area burned and emissions of pollutants by advanced very high resolution radiometer satellite data, *J. Geophys. Res.*, *107*, 4745, doi:10.1029/2001JD001078, 2002.

Kalashnikova, O. V., R. Kahn, I. N. Sokolik, and W. H. Li, The ability of multi-angle remote sensing observations to identify and distinguish mineral dust types: Optical models and retrievals of optically thick plumes. J. Geophys. Res., *110, No. D18, D18S14*10.1029/2004JD004550, 2005

Kalberer, M., D. Paulsen, M. Sax, M. Steinbacher, J. Dommen, A. S. H. Prevot, R. Fisseha, E. Weingartner, V. Frankevich, R. Zenobi, and U. Baltensperger, Identification of polymers as major components of atmospheric organic aerosols, *Science*, *303*, 1659-1662, 2004.

Kanakidou, M., J. H. Seinfeld, et al., Organic aerosol and global climate modelling: a review, *Atmos. Chem. Phys.*, *5*, 1053-1123, 2005.

Kanakidou, M., J.H. Seinfeld, S.N. Pandis, I. Barnes, F.J. Dentener, M.C. Facchini, R. van Dingenen, B. Ervens, A. Nenes, C.J. Nielsen, E. Swietlicki, J.P. Putaud, Y. Balkanski, S. Fuzzi, J. Horth, G.K. Moortgat, R. Winterhalter, C.E.L. Myhre, K. Tsigaridis, E. Vignati, E.G. Stephanou, and J. Wilson, Organic aerosol and global climate modelling: a review, Atmos. Chem. Phys., 5, 1053-1123, 2005.

Kanakidou, M., K. Tsigaridis, F. J. Dentener, and P. J. Crutzen, Human-activity-enhanced formation of organic aerosols by biogenic hydrocarbon oxidation, *J. Geophys. Res.*, *105*, 9243-9254, 2000.

Kapustin V. N., A. D. Clarke, Y. Shinozuka, S. Howell, V. Brekhovskikh, T. Nakajima, A. Higurashi, On the determination of a cloud condensation nuclei from satellite: Challenges and possibilities, *J. Geophys. Res.*, *111*, D04202, doi:10.1029/2004JD005527, 2006.

Karcher, B., T. Peter, U. M. Biermann, and U. Schumann, The initial composition of jet condensation trails, *J. Atmos. Sci.*, *53*, 3066-3083, 1996.

Kaufman Y.J. and T. Nakajima, Effects of Amazon smoke on cloud microphysics and albedo – Analysis from satellite imagery. *J. Appl. Meteor*. 32, 729 – 744, 1993.

Kaufman Y.J., D. Tanre, L. Remer, E. Vermote, A. Chu, and B. Holben, Operational remote sensing of tropospheric aerosol over land from EOS moderate resolution imaging spectroradiometer, *J. Geophys. Res., 102,* 17051–17067, 1997.

Kaufman, Y. J. and R. S. Fraser, The effect of smoke particles on clouds and climate forcing, Science, **277**, 1636-1639, 1997.

Kaufman, Y. J., D. Tanré, O. Dubovik, A. Karnieli, and L. A. Remer, Absorption of sunlight by dust as inferred from satellite and ground-based remote sensing, Geophys. Res. Lett., **28**, 1479-1483, 2001.

Kaufman, Y. J., I. Koren, L. A. Remer, D. Rosenfeld and Y. Rudich, The effect of smoke, dust, and pollution aerosol on shallow cloud development over the Atlantic Ocean, Proc. Nat. Acad. Scie., 102, 11207-11212, 2005b

Kaufman, Y. J., J. V. Martins, L. A. Remer, M. R. Schoeberl, and M. A. Yamasoe, 2002: Satellite retrieval of aerosol absorption over the oceans using sunglint, Geophys. Res. Lett., **29**, doi:10.1029/2002GL015403.

Kaufman, Y. J., O. Boucher, D. Tanré, M. Chin, L. A. Remer & T. Takemura**,** Aerosol anthropogenic component estimated from satellite data**,** Geoph. Res. Lett., VOL. 32, L17804, doi:10.1029/2005GL023125, 2005a

Kaufman, Y.J., I. Koren, L.A. Remer, D. Tanre, P. Ginoux, and S. Fan, Dust transport and deposition observed from the Terra-Moderate Resolution Imaging Spectroradiometer (MODIS) spacecraft over the Atlantic Ocean, J. Geophys. Res., 110, D10S12, doi:10.1029/2003JD004436, 2005c.

Kaufman, Y.J., J. M. Haywood, P. V. Hobbs, W. Hart, R. Kleidman & B. Schmid, Remote sensing of vertical distributions of smoke aerosol off the coast of Africa, Geophys. Res. Lett. 30, 16, 1831, 10.1029/2003GL017068, 2003.

Kautilya, *Arthasastra* translated by R. Shamasastry, *Government Oriental Library Series, Bibliotheca Sanskrita*, No. 37, Part 2, Bangalore, p. 64, 1915.

Kavouras, I. G., Mihalopoulos, N., and Stephanou, E. G.: Formation of atmospheric particles from organic acids produced by forests, Nature, 395, 683–686, 1998.

Keenan, T. D., and R. E. Carbone, A preliminary morphology of precipitation systems in tropical northern Australia, Quart J.

Roy. Meteor. Soc., 118, 283-326, 1992.

Kelvin, Lord, On the equilibrium of vapour at the curved surface of a liquid, *Proc. Roy. Soc. Edinb., 7,* 63–71, 1870.

Kerkweg, A., S. Wurzler, T. Reisin, and A. Bott, On the cloud processing of aerosol particles: an entraining air-parcel model with two dimensional spectral cloud microphysics and a new formulation of the collection kernel, *Quart. J. Roy. Meteorol. Soc., 129,* 1-18, 2003.

Kerminen, V. M., A. Virkkula, R. Hillamo, A. S. Wexler, and M. Kulmala, Secondary organics and atmospheric cloud condensation nuclei production, *J. Geophys. Res.*, *105*, 9255-9264, 2000.

Kerminen, V. M., Relative roles of secondary sulfate and organics in atmospheric cloud condensation nuclei production, *J. Geophys. Res.*, *106*, 17,321-17,333, 2001.

Kerr, R.A., Cloud seeding: One success in 35 years, *Sci., 217*, 519–522, 1982.

Kessler, E., *On the Distribution and Continuity of Water Substance in Atmospheric Circulation, Meteorol. Monogr., 10*, 84 pp, Amer. Meteor. Soc., Boston, Mass., 1969.

Khain, A. P., A. Pokrovsky, and I. Sednev, Some effects of cloud-aerosol interaction on cloud microphysics structure and precipitation formation: Numerical experiments with a spectral microphysics cloud ensemble model. *Atmos. Res., 52,* 195-220, 1999.

Khain, A.P., A. Pokrovsky, N. BenMoshe, and D. Rosenfeld , Simulating green-ocean-smoky and pyro-clouds observed in the Amazon region during the LBA-SMOCC campaign, *J. Atmos. Sci*, 61, 2963-2982, 2005.

Khain, A.P., and M.B. Pinsky, Turbulence effects on the collision kernel. II: Increase of the swept volume of colliding drops, *Quart.J.Roy. Meteor. Soc., 123*, 1543-1560, 1997.

Khain, A.P., D. Rosenfeld, A. Pokrovsky, Simulating convective clouds with sustained supercooled liquid water down to -37.5 deg C using a spectral microphysics model, Geophys. Res. Ltrs., 28, 3887-3890, 2001.

Khairoutdinov, M., and Y. Kogan, A new cloud physics parameterization in a large-eddy simulation model of marine stratocumulus, *Mon. Wea. Rev.*, *128*, 229-243, 2000.

Khairoutdinov, M.F., and Y.L. Kogan, A large eddy simulation model with explicit microphysics: Validation against aircraft observations of a stratocumulus-topped boundary layer, *J. Atmos.Sci., 56*, 2115-2131, 1999.

Khvorostyanov, V. I., and J. A. Curry, 1999: Toward the theory of stochastic condensation in clouds. Part II: Analytical solutions of the gamma-distribution type, J. Atmos. Sci., **56**, 3997-4013.

Kidder, S.Q. and T.H. Vonder Haar, Satellite Meteorology: An Introduction. Academic Press, New York, 466 pp, 1995.

Kiehl, J.T., T.L. Schneider, P.J. Rasch, M.C. Barth and J. Wong, Radiative forcing due to sulfate aerosols from simulations with the National Center for Atmospheric Research Community Climate Model, Version 3, *J. Geophys. Res*., *105*, 1441-1457, 2000.

Kim, B.-G., S. E. Schwartz, M. A. Miller, and Q. Min, Effective radius of cloud droplets by ground-based remote sensing: Relationship to aerosol, *J. Geophys. Res.*, *108*(D23), 4740, doi:10.1029/2003JD003721, 2003.

Kim, Y. J., J. F. Boatman, R. L. Gunter, D. L. Wellman, and S. W. Wilkison, Vertical distribution of atmospheric aerosol size distribution over South-Central New Mexico, *Atmos. Environ.*, *27A*, 1351-1362, 1993a.

Kim, Y. P., J. H. Seinfeld, and P. Saxena, Atmospheric gas-aerosol equilibrium. 1. Thermodynamic model, *Aerosol Science and Technology*, *19*, 157-181, 1993b.

Kim, Y., H. Sievering, J. Boatman, D. Wellman, and A. Pszenny, Aerosol size distribution and aerosol water content measurements during Atlantic Stratocumulus Transition Experiment/Marine Aerosol and Gas Exchange, *J. Geophys. Res.*, *100*, 23,027-23,038, 1995.

King, M. D., S. C. Tsay, and S. Platnick, 1995: In situ observations of the indirect effects of aerosol on clouds, Aerosol Forcing of Climate, R. J. Charlson and J. Heintzenberg, Eds., John Wiley and Sons, 227-248.

King, M. D., S. Platnick, P. Yang, G. T. Arnold, M. A. Gray, J. C. Riédi, S. A. Ackerman, and K. N. Liou, 2004: Remote sensing of liquid water and ice cloud optical thickness and effective radius in the arctic: Application of airborne multispectral MAS data. J. Atmos. Oceanic Technol., **21**, 857-875.

King, M. D., W. P. Menzel, Y. J. Kaufman, D. Tanré, B. C. Gao, S. Platnick, S. A. Ackerman, L. A. Remer, R. Pincus, and P. A. Hubanks, 2003: Cloud and aerosol properties, precipitable water, and profiles of temperature and humidity from MODIS. IEEE Trans. Geosci. Remote Sens., **41**, 442-458.

King, M. D., Y. J. Kaufman, D. Tanré, and T. Nakajima, 1999: Remote sensing of tropospheric aerosols from space: Past, present and future, Bull. Amer. Meteor. Soc., **80**, 2229-2259.

King, M.D., L.F. Radke, and P.V. Hobbs, Optical properties of marine stratocumulus clouds modified by ships, *J. Geophys. Res., 98*, 2729–2739, 1993.

King, M.D., W.P. Menzel, Y.J. Kaufman, D. Tanré, B.C. Gao, S. Platnick, S.A. Ackerman, L.A. Remer, R. Pincus, and P.A. Hubanks, Cloud and aerosol properties, precipitable water, and profiles of temperature and water vapor from MODIS, *IEEE Trans. Geosci. Remote Sens., 41*, 442–458, 2003.

Kinne, S., M. Schulz, C. Textor, S. Guibert, B. Y., S.E. Bauer, T. Berntsen, T. Berglen, O. Boucher, M. Chin, W. Collins, F. Dentener, T. Diehl, R. Easter, H. Feichter, D. Fillmore, S. Ghan, P. Ginoux, S. Gong, A. Grini, J. Hendricks, M. Herzog, L. Horowitz, P. Huang, I. Isaksen, T. Iversen, D. Koch, A. Kirkev?g, S. Kloster, M. Krol, E. Kristjansson, A. Lauer, J.F. Lamarque, G. Lesins, X. Liu, U. Lohmann, V. Montanaro, G. Myhre, J. Penner, G. Pitari, S. Reddy, ?. Seland, P. Stier, T. Takemura, and X. Tie, An AeroCom initial assessment ? optical properties in aerosol component modules of global models, Atmos. Chem. Phys. Disc., 5, 8285-8330, 2005.

Kirchstetter, T. W., T. Novakov, and P. V. Hobbs, Evidence that the spectral dependence of light absorption by aerosols is affected by organic carbon, *J. Geophys. Res.*, *109*, D21208, doi:10.1029/2004JD0004999, 2004.

Kiss, G., B. Varga, I. Galambos, and I. Ganszky, Characterization of water-soluble organic matter isolated from atmospheric fine aerosol, *J. Geophys. Res.*, *107*, 8339, doi:10.1029/2001JD000603, 2002.

Kittaka, C., R.B. Pierce, J.H. Crawford, M.H. Hitchman, D.R. Johnson, G.J. Tripoli, M. Chin, A.R. Bandy, R.J. Weber, R.W. Talbot, and B.E. Anderson, A three-dimensional regional modeling study of the impact of clouds on sulfate distributions during TRACE-P - art. no. D15S11, Journal of Geophysical Research Atmospheres, 109 (D15), S1511, 2004.

Kleeman, M. J., and G. R. Cass, Source contributions to the size and composition distribution of urban particulate air pollution, *Atmos. Environ.*, *32*, 2803-2816, 1998.

Kline, D.B., Evidence of geographical differences in ice nuclei concentrations. *Mon. Weather Rev., 91,* 681-686, 1963

Knight, C.A., A note on the action of hygroscopic cloud nuclei, *J. Atmos. Sci., 28,* 1296–1298, 1971.

Koehler, K. A., S. M. Kreidenweis, P. J. DeMott, A. J. Prenni, C. M. Carrico, B. Ervens, and G. Feingold, Water activity and activation diameters from hygroscopicity data – Part II: Application to organic species, *Atmos. Chem. Phys. Discuss.*, *5*, 10,881–10,924, 2005.

Koenig, L. R., The glaciating behavior of small cumulonimbus clouds. *J. Atmos Sci.*, **20**, 29-47, 1963..

Koenig, L.R., and F.W. Murray, Ice-bearing cumulus cloud evolution: Numerical simulations and general comparison against observations, *J. Appl. Meteorol.*, *15*, 747-762, 1976.

Koenig, L.R., and F.W. Murray, Ice-bearing cumulus cloud evolution: Numerical simulation and general comparison against observations, *J. Appl. Meteorol., 7*, 747–762, 1976.

Koenig, L.R., Some observations suggesting ice multiplication in the atmosphere, *J. Atmos. Sci., 25,* 460–463, 1968.

Kogan, Y.L., D.K. Lilly, Z.N. Kogan, and V.V. Filyushkin, The effect of CNN regeneration on the evolution of stratocumulus cloud layers, *Atmos. Res.*, *33*, 137-150, 1994.

Kogan, Y.L., M.P. Khairoutdinov, D.K. Lilly, Z.N. Kogan, and Q. Liu, Modeling of stratocumulus cloud layers in a large eddy simulation model with explicit microphysics, *J. Atmos. Sci., 52*, 2923-2940, 1995.

Köhler, H., Zur Thermodynamik der Kondensation on Hygrskopischen Kernen und Bermer Kungen über dos Zussammenfliessen der Tropfen, *Meddel. Met.-Hydr. Anst. Stockholm, 3,* No. 8, 1926.

Kojima, T., P.R. Buseck, J.C. Wilson, J.M. Reeves, and M.J. Mahoney, Aerosol particles from tropical convective systems: Cloud tops and cirrus anvils - art. no. D12201, Journal of Geophysical Research Atmospheres, 109 (D12), 12201, 2004.

Koren I., Y. J. Kaufman, D. Rosenfeld, L. A. Remer, Y. Rudich, Aerosol invigoration and restructuring of Atlantic convective clouds, *Geophys. Res. Lett., 32,* L14828, doi:10.1029/2005GL023187, 2005.

Koren, I., Y.J. Kaufman, L.A. Remer, and J.V. Martins, Measurements of the effect of Amazon smoke on inhibition of cloud formation, *Science, 303*, 1342–1345, 2004.

Korolev, A. V., M. P. Bailey, J. Hallett, and G. A. Isaac, and, Laboratory and in situ observation of deposition growth of frozen drops. *J. Appl. Meteor.*, **43**, 612-622, 2004.

Korolev, A.V., G.A. Isaac, S.G. Coper, J.W. Strapp, and J. Hallet, Microphysical characterization of mixed-phase clouds, *Quart. J. Roy. Meteorol. Soc., 129,* 39–65, 2003.

Kovetz A., and B. Olund, The effect of coalescence and condensation on rain formation in a cloud of finite vertical extent, *J. Atmos. Sci., 26*, 1060-1065, 1969.

Koziol, A.S., and H.G. Leighton, The effect of turbulence on the collision rates of small cloud drops, *J. Atmos. Sci*., *53*, 13, 1910-1920, 1996.

Krajewski, W. F., G. J. Ciach, and E. Habib, An analysis of small-scale rainfall variability in different climatological regimes, Hydrologic Sciences Journal, 48(2), 151-162, 2003.

Krajewski, W.F., and J. A. Smith, On the estimation of climatological Z-R relationships. J. Appl. Meteorol. 30, 1436-1445, 1991.

Krajewski, W.F., Cokriging radar-rainfall and rain gauge data. J. Geophys. Res. 92, 9571-9580, 1987.

Krajewski,W.F., and J.A. Smith, Radar hydrology: rainfall estimation, Adv. Water Res., 25, 1387–1394, 2002.

Krauss, E.B., and P. Squires, Experiments on the simulation of clouds to produce rain, *Nature, 159*, 489–491, 1947.

Kreidenweis, S. M., K. Koehler, P. J. DeMott, A. J. Prenni, C. Carrico, and B. Ervens, Water activity and activation diameters from hygroscopicity data - Part I: Theory and application to inorganic salts, *Atmos. Chem. Phys.*, *5*, 1357-1370, 2005.

Kreidenweis, S. M., L. M. McInnes, and F. J. Brechtel, Observations of aerosol volatility and elemental composition at Macquarie Island during the First Aerosol Characterization Experiment (ACE 1), *J. Geophys. Res.*, *103*, 16,511-16,524, 1998.

Krejci, R., J. Ström, M. de Reus, J. Williams, H. Fischer, M. O. Andreae, and H.-C. Hansson, Spatial and temporal distribution of atmospheric aerosols in the lowermost troposphere over the Amazonian tropical rainforest, *Atmos. Chem. Phys.*, *5*, 1527-1543, 2005.

Kristjánsson, J. E., Studies of the aerosol indirect effect from sulfate and black carbon aerosols, *J. Geophys. Res.*, 107, doi: 10.1029/2001JD000887, 2002.

Kristjánsson, J. E., T. Iversen, A. Kirkevåg, Ø. Seland, and J. Debernard, Response of the climate system to aerosol direct and indirect forcing: Role of cloud feedbacks, *J. Geophys. Res.*, *110*, D24206, doi:10.1029/2005JD006299, 2005.

Krivacsy, Z., A. Hoffer, Z. Sarvari, D. Temesi, U. Baltensperger, S. Nyeki, E. Weingartner, S. Kleefeld, and S. G. Jennings, Role of organic and black carbon in the chemical composition of atmospheric aerosol at European background sites, *Atmos. Environ.*, *35*, 6231-6244, 2001.

Krueger, B.J., V.H. Grassian, A. Laskin, and J.P. Cowin, The transformation of solid atmospheric particles into liquid droplets through heterogeneous chemistry: Laboratory insights into the processing of calcium containing mineral dust aerosol in the troposphere, Geophys.Res. Lett., 30, 10.1029/2002GL016563, 2003.

Kruger, A. and W.F. Krajewski, "Two-dimensional video disdrometer: A description" Journal of Atmospheric and Oceanic Technology, 19(5), pp. 602 - 617, 2002.

Kuligowski, R.J., A self-calibrating real-time GOES rainfall algorithm for short-term rainfall estimates, J. Hydrom., 3, 112–130, 2002.

Kulmala, M., A. Laaksonen, and L. Pirjola, Parameterizations for sulfuric acid/water nucleation rates, J. Geophys. Res., 103 (D7), 8301-8307, 1998.

Kulmala, M., A. Laaksonen, P. Korhonen, T. Vesala, T. Ahonen, and J. C. Barrett, The effect of atmospheric nitric acid vapor on cloud condensation nucleus activation, *J. Geophys. Res., 98*, 22949-22958, 1993.

Kulmala, M., A. Majerowicz, and P.E. Wagner, Condensational Growth at Large Vapor Concentration: Limits of Applicability

of the Mason Equation, J. Aerosol Sci., 20, 1023-1026, 1989.

Kulmala, M., Condensation growth and evaporation in the transition regime: an analytical expression, Aerosol Sci. Technol., 19, 381-388, 1993.

Kulmala, M., U. Pirjola, and J. M. Makela, Stable sulphate clusters as a source of new atmospheric particles, *Nature*, *404*, 66-69, 2000.

Kumai, M. and K.E. Francis, Nuclei in Snow and Ice Crystals on the Greenland Ice Cap under Natural and Artificially Stimulated Conditions, J. Atmos. Sci., 19, 474-481, 1962.

Kumai, M., Electron-microscope study of snow-crystal nuclei, *J. Met., 8,* 151–159, 1951.

Kumai, M., Identification of nuclei and concentrations of chemical species in snow crystals sampled at South Pole, *J. Atmos. Sci.*, *33*, 833-841, 1976.

Kumar, P. P., K. Broekhuizen, and J. P. D. Abbatt, Organic acids as cloud condensation nuclei: Laboratory studies of highly soluble and insoluble species, *Atmos. Chem. Phys.*, *3*, 509-520, 2003.

Kummerow, C, J. Simpson, O. Thiele, et al., The status of the Tropical Rainfall Measuring Mission (TRMM) after two years in orbit, J. Appl. Meteor., **39**, 1965-1982, 2000.

Kummerow, C, J. Simpson, O. Thiele, W. Barnes, A.T.C. Chang, E. Stocker, R.F. Adler, A. Hou, R. Kakar, F. Wentz, P. Ashcroft, T. Kozu, Y. Hong, K. Okamoto, T. Iguchi, H. Kuroiwa, E. Im, Z. Haddad, G. Huffman, B. Ferrier, W.S. Olson, E. Zipser, E.A. Smith, T.T. Wilheit, G. North, T. Krishnamurti, and K. Nakamura, The status of the Tropical Rainfall Measuring Mission (TRMM) after two years in orbit. J. Appl. Meteor., **39**, 1965-1982, 2000.

Kummerow, C., Beam filling errors in passive microwave rainfall retrievals, J. Appl. Meteorol., 37, 356–370, 1998.

Kummerow, C., W. Barnes, T. Kozu, J. Shiue, and J. Simpson, The Tropical Rainfall Measuring Mission (TRMM) sensor package, J. Atmos. Ocean. Tech., 15, 809–817, 1998.

Kurtyka, J. C., *Precipitation Measurements Study*, U. S. Army Signal Corps Engineering Laboratories, Fort Monmounth, New Jersey, Department of Army Project DA-3-3602-042, Signal Corps Project: 794C-0, 178 pages, 1953.

Laaksonen, A., A. Hamed, J. Joutsensaari, L. Hiltunen, F. Cavalli, W. Junkermann, A. Asmi, S. Fuzzi, and M.C. Facchini, Cloud condensation nucleus production from nucleation events at a highly polluted region, Geophys. Res. Lett., 32, L06812, doi:10.1029/2004GL022092, 2005.

Laaksonen, A., P. Korhonen, M. Kulmala, and R. J. Charlson, Modification of the Köhler equation to include soluble trace gases and slightly soluble substances, *J. Atmos. Sci.*, *55*, 853-862, 1998.

Langmann, B., and H.F. Graf, Indonesian smoke aerosols from peat fires and the contribution from volcanic sulfur emissions, Geophysical Research Letters, 30 (11), 1547, doi:10.1029/2002GL016646, 2003.

Larson, V.E., J.-C. Golaz, H. Jiang and W.R. Cotton, Supplying local microphysics parameterizations with information about subgrid variability: Latin hypercube sampling, *J. Atmos. Sci.*, *62*, 4010-4026, 2005.

Larson, V.E., R. Wood, P.R. Field, J.-C. Golaz, T.H. Vonder Haar, and W.R. Cotton, Small-scale and mesoscale variability of scalars in cloudy boundary layers: One-dimensional probability density functions, *J. Atmos. Sci*., *58*, 1978-1996, 2001.

Laskin, A., M. Iedema, A. Ichkovich, E. Graber, I. Taraniuk, and Y. Rudich, Direct observation of completely processed calcium carbonate dust particles, Faraday Discussions, 130, 453-468, 2005.

Latham, J., and R. L. Reed, Laboratory studies of the effects of mixing on the evolution of cloud droplet spectra. *Quart. J. Roy. Meteor. Soc.,* 103, 297-306. 1977.

Lau, K.-M., K.-M. Kim, and N.-C. Hsu, Observational Evidence Of Effects Of Absorbing Aerosols On Seasonal-to- Interannual Anomalies Of The Asian Monsoon, CLIVAR Exchanges, 10 (3), 2005.

Lavoué, D., C. Liousse, H. Cachier, B. J. Stocks, and J. G. Goldammer, Modeling of carbonaceous particles emitted by boreal and temperate wildfires at northern latitudes, *J. Geophys. Res.*, *105*, 26,871-26,890, 2000.

Le Canut, P., M. O. Andreae, G. W. Harris, F. G. Wienhold, and T. Zenker, Airborne studies of emissions from savanna fires in southern Africa, 1, Aerosol emissions measured with a laser optical particle counter, *J. Geophys. Res.*, *101*, 23,615-23,630, 1996.

Leaitch, W. R., and G. A. Isaac, Tropospheric aerosol size distributions from 1982 to 1988 over eastern north-america, *Atmospheric Environment Part a-General Topics*, *25*, 601-619, 1991.

Leaitch, W.R., J.W. Strapp, and G.A. Isaac, Cloud droplet nucleation and cloud scavenging of aerosol sulphaate in polluted atmospheres, *Tellus, 38B,* 328-344, 1986.

Leck, C., M. Norman, E. K. Bigg, and R. Hillamo, Chemical composition and sources of the high Arctic aerosol relevant for fog and cloud formation, *J. Geophys. Res.*, *107*, doi:10.1029/2001JD001463, 2002.

Leck, C., M. Tjernström, P. Matrai, E. Swietlicki, and K. Bigg, Can marine micro-organisms influence melting of the Arctic pack ice?, *Eos Trans. AGU*, *85*, 25-36, 2004.

Legates, D.R., and C.J. Willmott, Mean seasonal and spatial variability in gauge-corrected, global precipitation, *Int. J. Climatol., 10,* 111–127, 1990.

Legrand, M., and C. N'doumé, 2001: Satellite detection of dust using the IR imagery of Meteosat: 1. Infrared difference dust index, J. Geophys. Res., **106**, 18251-18274.

Lelieveld, J., G.-J. Roeloff, L. Ganzeveld, J. Feichter, and H. Rodhe, Terrestrial sources and distribution of atmospheric sulfur, *Phil. Trans. Roy. Soc. Lond., B352,* 149–158, 1997.

Lelieveld, J., H. Berresheim, S. Borrmann, P.J. Crutzen, F.J. Dentener, H. Fischer, J. Feichter, P.J. Flatau, J. Heland, R. Holzinger, R. Korrmann, M.G. Lawrence, Z. Levin, K.M. Markowicz, N. Mihalopoulos, A. Minikin, V. Ramanathan, M. deReus, G.J. Roelofs, H.A. Scheeren, J. Sciare, H. Schlager, M. Schultz, P. Siegmund, B. Steil, E.G. Stephanou, P. Stier, M. Traub, C. Warneke, J. Williams, and H. Ziereis, Global air pollution crossroads over the Mediterranean, Science, 298 (5594), 794-799, 2002.

Levin, L.M., and Y.S. Sedunov, Stochastic condensation of drops and kinetics of cloud spectrum formation, *J. Rech. Atmos*., *2*, 425–432, 1966.

Levin, Z., A. Teller, E. Ganor and Y. Yin, On the interactions of mineral dust, sea salt particles and clouds – A Measurement and

modeling study from the MEIDEX campaign, *J. Geophys. Res.* 110, D20202, doi:10.1029/2005JD005810, 2005.

Levin, Z., and S. A. Yankofsky, Contact versus immersion freezing of freely suspended droplets by bacterial ice nuclei, *Journal of Climate and Applied Meteorology*, *22*, 1964-1966, 1983.

Levin, Z., and S.A. Yankofsky, Ice nuclei of biological origin. In Lecture Notes in *Physics, Atmospheric Aerosols and Nucleation.* P.E. Wagner and G. Vali, Editors, Springer-Verlag Press, 620–633, 1988.

Levin, Z., E. Ganor, and V. Gladstein, The effects of desert particles coated with sulfate on rain formation in the eastern Mediterranean, *J. Appl. Meteor.*, *35*, 1511-1523, 1996.

Levin, Z., M. Neiburger and L. Rodriguez, Jr., Experimental evaluation of collection efficiencies and coalescence efficiencies of cloud drops, *J. Atmos. Sci., 30*, 944-946, 1973.

Levin, Z., S.A. Yankofsky, D. Pardess, and N. Magal, Possible application of bacterial condensation freezing to artificial rainfall enhancement, *J. Climate Appl. Meteorol., 26,* 1188–1197, 1987.

Levin, Z., S.O. Krichak, and T. Reisin, Numerical simulation of dispersal of inert seeding material in Israel using a three-dimensional mesoscale model, *J. Appl. Meteorol., 36*, 474–484, 1997.

Levine, J.S., W.R. Cofer, D.R. Cahoon, and E.L. Winstead, Biomass Burning: A Driver for Global Change, Environmental Science and Technology, 29 (3), 120A-125A, 1995.

Levkov, L., Congélation de gouttes d'eau au contact particules de CuS, *J. de Rech. Atmos., 5,* 133–136, 1971.

Li, Q.B., D.J. Jacob, I. Bey, P.I. Palmer, B.N. Duncan, B.D. Field, R.V. Martin, A.M. Fiore, R.M. Yantosca, D.D. Parrish, P.G. Simmonds, and S.J. Oltmans, Transatlantic transport of pollution and its effects on surface ozone in Europe and North America, J. Geophys. Res, 107(D13) doi:10.1029/2001JD001422, 2002.

Li, X., C.-H. Sui, and K.-N. Lau, Precipitation efficiency in the tropical deep convection: A 2-D cloud resolving model study, *J. Meteorol. Soc. Japan, 80,* 205–212, 2002.

Liepert, B.G., J. Feichter, U. Lohmann, and E. Roeckner, Can aerosols spin down the water cycle in a warmer and moister world, *Geophys. Res. Lett., 31*, doi: 10.1029/2003GL019060, 2004.

Liggio, J., S.-M. Li, and R. McLaren, Heterogeneous reactions of glyoxal on particulate matter: identification of acetals and sulfate esters, Environ. Sci. Tech., 39, 1532-1541, 2005a.

Liggio, J., S.-M. Li, and R. McLaren, Reactive uptake of glyoxyl on aerosols, J. Geophys. Res., 110, D10304, doi:10.1029/2004JD005113, 2005b.

Lihavainen, H., V. M. Kerminen, M. Komppula, J. Hatakka, V. Aaltonen, M. Kulmala, and Y. Viisanen, Production of "potential" cloud condensation nuclei associated with atmospheric new-particle formation in northern Finland, *J. Geophys. Res.*, *108*, 2003.

Li-Jones, X., and J. M. Prospero, Variations in the size distribution of non-sea-salt sulfate aerosol in the marine boundary layer at Barbados: Impact of African dust, *J. Geophys. Res.*, *103*, 16,073-16,084, 1998.

Limbeck, A., M. Kulmala, and H. Puxbaum, Secondary organic aerosol formation in the atmosphere via heterogeneous reaction of gaseous isoprene on acidic particles, *Geophys. Res. Lett.*, *30*, 1996, doi:10.1029/2003GL017738, 2003.

Liousse, C., J. E. Penner, C. Chuang, J. J. Walton, H. Eddleman, and H. Cachier, A global three-dimensional model study of carbonaceous aerosols, *J. Geophys. Res.*, *101*, 19,411-19,432, 1996a.

Liousse, C., J. E. Penner, J. J. Walton, H. Eddleman, C. Chuang, and H. Cachier, Modeling biomass burning aerosols, in *Biomass Burning and Global Change*, edited by J. S. Levine, pp. 492-508, MIT Press, Cambridge, Mass., 1996b.

Liousse, C., M. O. Andreae, P. Artaxo, P. Barbosa, H. Cachier, J. M. Grégoire, P. Hobbs, D. Lavoué, F. Mouillot, J. Penner, M. Scholes, and M. G. Schultz, Deriving global quantitative estimates for spatial and temporal distributions of biomass burning emissions, in *Emissions of Atmospheric Trace Compounds*, edited by C. Granier, P. Artaxo, & C. E. Reeves, pp. 71-113, Kluwer, Dordrecht, 2004.

List, R., A linear radar reflectivity-rainrate relationships for steady tropical rain, J. Atmos. Sci., 45, 3564-3572, 1988.

Liu, G., and J.A. Curry, Retrieval of precipitation from satellite microwave measurement using both emission and scattering, J. Geophys. Res., 97, 9959–9974, 1992.

Liu, P. S. K., W. R. Leaitch, C. M. Banic, and S.-M. Li, Aerosol observations at Chebogue Point during the 1993 North Atlantic Regional Experiment: Relationships among cloud condensation nuclei, size distribution, and chemistry, *J. Geophys. Res.*, *101*, 28,971-28,990, 1996.

Liu, Q., Y.L.. Kogan, D. K. Lilly, D. W. Johnson, G. E. Innis, P.A. Durkee and K.E. Nielsen, Modeling of Ship effluent transport and its sensitivity to boundary layer structure, *J. Atmos. Sci*., *57*, 2779-2791, 2000.

Liu, X.H., J.E. Penner, and M. Herzog, Model description, evaluation, and interactions between sulfate and nonsulfate aerosols, J. Geophys. Res., 110 (D18), 2005a.

Liu, Y., R. Fu, and R. Dickinson, Smoke aerosols altering South American monsoon, Bulletin of the American Meteorological Society, 86 (8), 1062-1063, 2005b.

Liu, Z., I. Matsui, N. Sugimoto, High-spectral-resolution lidar using an iodine absorption filter for atmospheric measurements, Opt. Eng. **38**, 1661-1670, 1999.

Lohmann, U. and G. Lesins, Stronger constraints on the anthropogenic indirect aerosol effect, *Science*, *298*, 1012-1016, 2002.

Lohmann, U. and J. Feichter, Can the direct and semi-direct aerosol effect compete with the indirect effect on a global scale? *Geophys. Res. Lett., 28*, 159-161, 2001.

Lohmann, U. and J. Feichter, Global indirect aerosol effects: A review, *Atmos. Chem. Phys. Disc*., *4*, *5*, 715-737, 2005.

Lohmann, U. and K. Diehl, Sensitivity studies of the importance of dust ice nuclei for the indirect aerosol effect on stratiform mixed-phase clouds, *J. Atmos. Sci.*, 63 968-982, 2006.

Lohmann, U. and Leck, C., Importance of submicron surface-active organic aerosols for pristine Arctic clouds, Tellus B, 57, 261-268, 2005.

Lohmann, U., A glaciation indirect aerosol effect caused by soot aerosols, *Geophys. Res. Lett., 29*, doi: 10.1029/2001GL014357, 2002.

Lohmann, U., and J. Feichter, Impact of sulfate aerosols on albedo and lifetime of clouds: A sensitivity study with the ECHAM4

GCM, *J. Geophys. Res. 102*, 13,685–13,700, 1997.

Lohmann, U., Can anthropogenic aerosols decrease the snowfall rate?, *J. Atmos. Sci.*, *61*, 2457-2468, 2004.

Lohmann, U., J. Feichter, C. Chuang, and J. Penner, Predicting the number of cloud droplets in the ECHAM GCM, J. Geophys. Res., 104 (D8), 9169-9198, 1999.

Lohmann, U., J. Feichter, J. E. Penner, and W. R. Leaitch, Indirect effect of sulfate and carbonaceous aerosols: A mechanistic treatment, *J. Geophys. Res.*, 105, 12,193-112,206, 2000.

Lohmann, U., J. Zhang, and J. Pi, Sensitivity studies of the effect of increased aerosol concentrations and snow crystal shape on the snowfall rate in the Arctic - art. no. 4341, Journal of Geophysical Research Atmospheres, 108 (D11), 4341, 2003.

Lohmann, U., K. Broekhuizen, R. Leaitch, N. Shantz, and J. Abbatt, How efficient is cloud droplet formation of organic aerosols? - art. no. L05108, Geophysical Research Letters, 31 (5), 5108, 2004.

Lohmann, U., W.R. Leaitch, L. Barrie, K. Law, Y. Yi, D. Bergmann, C. Bridgeman, M. Chin, J. Christensen, R. Easter, J. Feichter, A. Jeuken, E. Kjellstrom, D. Koch, P. Rasch, and G.J. Roelofs, Vertical distributions of sulfur species simulated by large scale atmospheric models in COSAM: Comparison with observations, Tellus Series B Chemical and Physical Meteorology, 53 (5), 646-672, 2001.

Low, T.B., and R. List, Collision, coalescence and breakup of raindrops. Part I: Experimentally established coalescence efficiencies and fragment size distributions in breakup, *J. Atmos. Sci., 39,* 1591–1606, 1982.

Lu, M.-L., and J. H. Seinfeld, Study of the aerosol indirect effect by LES of marine stratocumulus, *J. Atmos. Sci.*, in press. 2005

Luo, C., N. M. Mahowald, and J. del Corral, Sensitivity study of meteorological parameters on mineral aerosol mobilization, transport, and distribution, *J. Geophys. Res.*, *108*, 4447, doi:10.1029/2003JD003483, 2003.

Luo, Z., W.B. Rossow, T. Inoue, and C.J. Stubenrauch, Did the eruption of the Mt. Pinatubo volcano affect cirrus properties?, *J. Climate, 15*, 2806-2820, 2002.

Luria, M., C.C. Van Valin, J.N. Galloway, W.C. Keene, D.L. Wellman, H. Sievering, and J.F. Boatman, The relationship between dimethyl sulfide and particulate sulfate in the mid-Atlantic Ocean atmosphere, *Atmos. Environ., 23, 139–147,* 1989.

Maenhaut, W., J. Cafmeyer, S. Dubtsov, and X. G. Chi, Detailed mass size distributions of elements and species, and aerosol chemical mass closure during fall 1999 at Gent, Belgium, *Nuclear Instruments & Methods in Physics Research Section B-Beam Interactions With Materials and Atoms*, *189*, 238-242, 2002.

Magi, B. I., P. V. Hobbs, T. W. Kirchsetter, T. Novakov, D. E Hegg, S. Gao, J. Redemann, and B. Schmid, Aerosol Properties and Chemical Apportionment of Aerosol Optical Depth at Locations off the U.S. East Coast in July and August 2001 J. Atmos. Sci., 62,919-934, 2005..

Mahowald, N. M., and C. Luo, A less dusty future?, *Geophys. Res. Lett.*, *30*, 1903, doi:10.1029/2003GL017880, 2003.

Mahowald, N. M., C. S. Zender, C. Luo, D. Savoie, O. Torres, and J. del Corral, Understanding the 30-year Barbados desert dust record, *J. Geophys. Res.*, *107*, 4561, doi:10.1029/2002JD002097, 2002.

Malanichev, A., E. Mantseva, V. Shatalov, B. Strukov, and N. Vulykh, Numerical evaluation of the PCB transport over the Northern Hemisphere, Env. Poll., 128 (1?2), 279?289, 2004.

Malm, W. C., and S. M. Kreidenweis, The effects of models of aerosol hygroscopicity on the apportionment of extinction, *Atmos. Environ.*, *31*, 1965-1976, 1997.

Malm, W. C., L. T. Sisler, D. Kaufman, R. A. Eldred, and T. A. Cahill, Spatial and seasonal trends in particle concentrations and optical extinction in the United States, *J. Geophys. Res.*, *99*, 1347-1370, 1994.

Malm, W.C., B.A. Schichtel, M.L. Pitchford, L.L. Ashbaugh, and R.A. Eldred, Spatial and monthly trends in speciated fine particle concentration in the United States, J. Geophys. Res., 109, D03306, doi:10.1029/2003JD003739, 2004.

Malm, W.C., B.A. Schichtel, R.B. Ames, and K.A. Gebhart, A 10-year spatial and temporal trend of sulfate across the United States - art. no. 4627, Journal of Geophysical Research Atmospheres, 107 (D22), 4627, 2002.

Manton, M.J., and W.R. Cotton, Parameterization of the atmospheric surface layer, *J. Atmos. Sci., 34,* 331–334, 1977.

Marcolli, C., B. P. Luo, and T. Peter, Mixing of the organic aerosol fractions: Liquids as the thermodynamically stable phases, *Journal of Physical Chemistry A*, *108*, 2216-2224, 2004.

Marcolli, C., B.P. Luo, T. Peter, and F.G. Wienhold, Internal mixing of the organic aerosol by gas phase diffusion of semivolatile organic compounds, Atmospheric Chemistry And Physics, 4, 2593-2599, 2004.

Marecal, V., J. Mahfouf and P. Bauer, Comparison of TMI rainfall estimates and their impact on 4D-Var assimilation. Q.J. RMS, 128, 2737-2758, 2002.

Maria, S. F., L. M. Russell, M. K. Gilles, and S. C. B. Myneni, Organic aerosol growth mechanisms and their climate-forcing implications, *Science*, *306*, 1921-1924, 2004.

Marie, C., and J.M. Prospero, African Monsoon Multidisciplinary Analysis Atmospheric Chemistry (AMMA - AC): A new IGAC Task, in IGACtivities Newsletter, pp. 2-13, 2005.

Maring, H., D. L. Savoie, M. A. Izaguirre, L. Custals, and J. S. Reid, Mineral dust aerosol size distribution change during atmospheric transport, *J. Geophys. Res.*, *108*, 8592, doi:10.1029/2002JD002536, 2003.

Market, P., S. Allen, R. Scofield, R. Kuligowski, and A Gruber, Precipitation efficiency of warm season midwestern mesoscale convective systems, *Wea. Forecasting*, *18,* 1273–1285, 2003.

Marshak, A., Y. Knyazikhin, K. Evans, and W. Wiscombe, The "RED versus NIR" plane to retrieve broken-cloud optical depth from ground-based measurements, J. Atmos. Sci., **61**, 1911-1925, 2004.

Marshall, J. S., and W. Palmer, The distribution of raindrops with size. J. Meteorol. 5, 165-166, 1948.

Mårtensson, E. M., E. D. Nilsson, G. de Leeuw, L. H. Cohen, and H. C. Hansson, Laboratory simulations and parameterization of the primary marine aerosol production, *J. Geophys. Res.*, *108*, 4297, doi:10.1029/2002JD002263, 2003.

Martin, G.M., D.W. Johnson, and A. Spice, The measurement and parameterization of effective radius of droplets in warm stratocumulus clouds, J. Atmos. Sci., 51, 1823–1842, 1994.

Martin, G.M., D.W. Johnson, and A. Spice, The measurement and parameterization of effective radius of droplets in warm stratocumulus clouds, *J. Atmos. Sci.*, *51*, 1823-1842, 1994.

Martins, J. V., D. Tanré, L. A. Remer, Y. J. Kaufman, S. Mattoo, and R. Levy, MODIS Cloud screening for remote sensing of aerosol over oceans using spatial variability, Geophys. Res. Lett., **29**(12), doi:10.1029/2001GL013252, 2002.

Martonchik, J. V., D. J. Diner, K. A. Crean, and M. A. Bull, Regional aerosol retrieval results from MISR, IEEE Trans. Geosci. Remote Sens., **40**, 1520-1531, 2002.

Martonchik, J.V., D.J. Diner, R. Kahn, M.M. Verstraete, B. Pinty, H.R. Gordon, and T.P. Ackerman, Techniques for the Retrieval of aerosol properties over land ocean using multiangle data, IEEE Trans. Geosci. Remt. Sensing 36, 1212-1227, 1998.

Martonchik, J.V., D.J. Diner, R.A. Kahn, B.J. Gaitley, and B.N. Holben, Comparison of MISR and AERONET aerosol optical depths over desert sites, Geophys. Res. Let.,31, doi:10.1029/2004GL019807, 2004.

Marwitz, J.D., Precipitation efficiency of thunderstorms on the high plains, *J. Rech. Atmos.*, *6,* 367–370, 1972.

Marzano, F.S., M. Palmacci, D. Cimini, and J.F. Turk, Statistical integration of satellite passive microwave and infrared data for high-temporal sampling retrieval of rainfall, Proc. Int. Geosci. Rem. Sens. Symp, IEEE, 3 pp, 2002.

Mason, B.J. and J. Maybank, The fragmentation and electrification of freezing water drops. Quart. J. Roy. Meteor. Soc. 86, 176-186, 1960.

Mason, B.J., A review of 3 long-term cloud-seeding experiments, *Meteorol. Mag., 109*, 335–344, 1980.

Mason, B.J., and P.R. Jonas, The evolution of droplet spectra and large droplets by condensation in cumulus clouds, *Quart. J. Roy. Meteorol. Soc*., *100*, 23-38, 1974.

Mason, B.J., Personal reflections on 35 years of cloud seeding, *Contemp. Phys., 23*, 311-327, 1982.

Mason, B.J., The Physics of Coulds, Clarendon Press, Oxford, 1971.

Massie, S. T., O. Torres, and S. J. Smith, Total Ozone Mapping Spectrometer (TOMS) observations of increases in Asian aerosol in winter from 1979 to 2000, *J. Geophys. Res.*, *109*, D18211, doi:10.1029/2004JD004620, 2004.

Mather, G.K., Coalescence enhancement in large multicell storms caused by the emissions from a Kraft paper mill, *J. Appl. Meteorol., 30,* 1134–1146, 1991.

Mather, G.K., D.E. Terblanche, F.E. Steffens, and L. Fletcher, Results of the South African cloud seeding experiments using hygroscopic flares, *J. Appl. Meteorol., 36*, 1433–1447, 1997.

Matsui, T., H. Masunaga, R. Pielke, Sr., and W. K. Tao, Geophys. Res. Lett., **31**, L06109, doi:10.1029/2003GL019287, 2004.

Matsumoto, K., H. Tanaka, I. Nagao, and Y. Ishizaka, Contribution of particulate sulfate and organic carbon to cloud condensation nuclei in the marine atmosphere, *Geophys. Res. Lett.*, *24*, 655-658, 1997.

Matthias V., J. Boesenberg, S. Guibert, and M. Schultz, Comparison of EARLINET vertical extinction profiles and global aerosol modeling with LMDZT-INCA for the year 2000, 22nd International Laser Radar Conference (ILRC 2004), Matera, Italy, 12-16 July, ESA Publications Division, 2004.

Matthias, V., D. Balis, J. Bosenberg, R. Eixmann, M. Iarlori, L. Komguem, I. Mattis, A. Papayannis, G. Pappalardo, M.R. Perrone, and X. Wang, Vertical aerosol distribution over Europe: Statistical analysis of Raman lidar data from 10 European Aerosol Research Lidar Network (EARLINET) stations - art. no. D18201, Journal of Geophysical Research Atmospheres, 109 (D18), 18201, 2004.

Matthias-Maser, S., and R. Jaenicke, The size distribution of primary biological aerosol particles with radii >0.2 µm in an urban-rural influenced region, *Atmos. Res.*, *39*, 279-286, 1995.

Matthias-Maser, S., J. Brinkmann, and W. Schneider, The size distribution of marine atmospheric aerosol with regard to primary biological aerosol particles over the South Atlantic Ocean, *Atmos. Environ.*, *33*, 3569-3575, 1999.

Matthias-Maser, S., V. Obolkin, T. Khodzer, and R. Jaenicke, Seasonal variation of primary biological aerosol particles in the remote continental region of Lake Baikal/Siberia, *Atmos. Environ.*, *34*, 3805-3811, 2000.

Mayer, B., M. Schroder, R. Preusker, and L. Schuller, Remote sensing of water cloud droplet size distributions using the backscatter glory: a case study, Atmos. Chem. Phys., **4**, 1255-1263, 2004.

Mayol-Bracero, O. L., O. Rosario, C. E. Corrigan, R. Morales, I. Torres, and V. Perez, Chemical characterization of submicron organic aerosols in the tropical trade winds of the Caribbean using gas chromatography/mass spectrometry, *Atmos. Environ.*, *35*, 1735-1745, 2001.

Mayol-Bracero, O. L., P. Guyon, B. Graham, G. Roberts, M. O. Andreae, S. Decesari, M. C. Facchini, S. Fuzzi, and P. Artaxo, Water-soluble organic compounds in biomass burning aerosols over Amazonia: 2. Apportionment of the chemical composition and importance of the polyacidic fraction, *J. Geophys. Res.*, *107*, 8091, doi:10.1029/2001JD000522, 2002b.

Mayol-Bracero, O. L., R. Gabriel, M. O. Andreae, T. W. Kirchstetter, T. Novakov, J. Ogren, P. Sheridan, and D. G. Streets, Carbonaceous aerosols over the Indian Ocean during the Indian Ocean Experiment (INDOEX): Chemical characterization, optical properties and probable sources, *J. Geophys. Res.*, *107*, 8030, doi:10.1029/2000JD000039, 2002a.

Mazin, I.P., Toward a theory of the shaping of the particle size spectrum in clouds and precipitation, *Tsentral'naia Aerologischesk aia Observatoriia, 64*, 57-70, 1965.

Mazurek, M., M. C. Masonjones, H. D. Masonjones, L. G. Salmon, G. R. Cass, K. A. Hallock, and M. Leach, Visibility-reducing organic aerosols in the vicinity of Grand Canyon National Park: Properties observed by high resolution gas chromatography, *J. Geophys. Res.*, *102*, 3779-3793, 1997.

McArthur, B. L. J., D. H. Halliwell, O. J. Neibergall, N. T. O'Neill, J. R. Slusser, and C. Wehrli, Field comparison of network sunphotometers, J. Geophys. Res., 108, D19, 4596, 10.1029/2002JD002964, 2003.

McCormick, M.P., D.M. Winker, E.V. Browell, J.A. Coakley, C.S. Gardner, R.M. Hoff, G.S. Kent, S.H. Melfi, R.T. Menzies, C.M.R. Platt, D.A. Randall, and J.A. Reagan, Scientific investigations planned for the lidar In-space Technology Experiment (LITE), , , , , Feb., Bull. Amer. Meteorol. Soc., 74 (2), 205-214, 1993.

McFarquhar, G. M., and R. List, The effect of curve fits for the disdrometer calibration on raindrop spectra, rainfall rate, and radar reflectivity. J. Appl. Meteor., 32, 774-782, 1993.

McFiggans, G. , P. Artaxo, U. Baltensperger, H. Coe, M. C. Facchini, G. Feingold, S. Fuzzi, M. Gysel, A. Laaksonen, U. Lohmann, T. F. Mentel, D. M. Murphy, C. D. O'Dowd, J. R. Snider, E. Weingartner, The effect of physical and chemical aerosol properties on warm cloud droplet activation, Atmos. Chem. Phys. Discuss., 5, 8507-8647, 2005.

McGraw, R., Description of aerosol dynamics by the quadrature method of moments. *Aerosol Sci. and Technol., 27*, 255-265, 1997.

McInnes, L., D. Covert, and B. Baker, The number of sea-salt, sulfate, and carbonaceous particles in the marine atmosphere: EM measurements consistent with the ambient size distribution, *Tellus*, *49B*, 300-313, 1997.

McMurry, P. H., and M. R. Stolzenburg, On the sensitivity of particle-size to relative-humidity for Los Angeles aerosols. Atmos. Environ., 23, 497-507, 1989.

McNaughton, C.S., A.D. Clarke, S.G. Howell, K.G.M. II, V. Brekhovskikh, R.J. Weber, D.A. Orsini, D.S. Covert, G. Buzorius, F.J. Brechtel, G.R. Carmichael, Y. Tang, F.L. Eisele, R.L. Mauldin, A.R. Bandy, D.C. Thornton, and B. Blomquist, Spatial distribution and size evolution of particles in Asian outflow: Significance of primary and secondary aerosols during ACE-Asia and TRACE-P, J. Geophys. Res., 109, D19S06, doi:10.1029/2003JD003528, 2004.

Measures, R.M., Laser Remote Sensing, John Wiley, New York, 1984.

Meischner, P. (Ed.), Weather Radar: Principles and Advanced Applications, 337 pp., Springer-Verlag, Berlin, 2004.

Meischner, P., Weather Radar: Principles and Advanced Applications, editor, Springer-Verlag, Berlin, 337 pp. ISBN 3-540-00328-2, 2004.

Melfi, S.H., J.D. Spinhirne, S.-H. Chou, and P. S.P., Lidar observation of vertically organized convection in the planetary boundary layer over the ocean, J. Climate Appl. Meteor., 24, 806-821, 1985.

Meneghini, R., and T. Kozu, Spaceborne Weather Radar, 197 pp., Artech House, Boston, Mass., 1990.

Menon, S., A. D. DelGenio, D. Koch, and G. Tselioudis, GCM Simulations of the Aerosol Indirect Effect: Sensitivity to Cloud Parameterization and Aerosol Burden, *J. Atmos. Sci.*, 59, 692-713, 2002a.

Menon, S., and A. Del Genio, Evaluating the impacts of carbonaceous aerosols on clouds and climate. In: An Interdisciplinary Assessment: Human-Induced Climate Change, S.e. al. (ed.). Cambridge Univ. Press, Cambridge, UK, 2005.

Menon, S., et al., Evaluating aerosol/cloud/radiation process parameterizations with single-column models and Second Aerosol Characterization Experiment (ACE-2) cloudy column observations, *J. Geophys. Res.*, 108, doi:10.1029/2003JD003902, 2003.

Menon, S., J. Hansen, L. Nazarenko, and Y. Luo, Climate effects of black carbon aerosol in China and India, *Science*, *297*, 2250-2253, 2002b.

Menzies, R.T., D.M. Tratt, and W.H. Hunt, Lidar In-space Technology Experiment measurements of sea surface directional reflectance and the link to surface wind speed, Appl. Optics, 37 (n24), 5550-5559, 1998.

Methven, J., S.R. Arnold, A. Stohl, M.J. Evans, M. Avery, K. Law, A.C. Lewis, P.S. Monks, D. Parrish, C. Reeves, H. Schlager, E. Atlas, D. Blake, H. Coe, R.C. Cohen, J. Crosier, F. Flocke, J.S. Holloway, J.R. Hopkins, G. H?bler, J.D. Lee, R. Purvis, B. Rappengl?ck, T.B. Ryerson, G.W. Sachse, H. Singh, N. Watson, L. Whalley, and P. Williams, Establishing Lagrangian connections between observations within air masses crossing the Atlantic during the ICARTT experiment, J. Geophys. Res., submitted, 2006.

Metzger, S., F. Dentener, M. Krol, A. Jeuken, and J. Lelieveld, Gas/aerosol partitioning - 2. Global modeling results, *J. Geophys. Res.*, *107*, 2002a.

Metzger, S., F. Dentener, S. Pandis, and J. Lelieveld, Gas/aerosol partitioning: 1. A computationally efficient model, *J. Geophys. Res.*, *107*, 2002b.

Meyers, M.P., P.J. DeMott, and W.R. Cotton, New primary ice nucleation parameterizations in an explicit cloud model, *J. Appl. Meteorol.*, *31*, 708-721, 1992.

Meyers, M.P., R.L. Walko, J.Y. Harrington, and W.R. Cotton, New RAMS cloud microphysics prameterization. Part II: The two-moment scheme, *Atmos. Res.*, *45*, 3-39, 1997.

Michalsky, J. J., J. A. Schlemmer, W. E. Berkheiser, et al., Multiyear measurements of aerosol optical depth in the Atmospheric Radiation Measurement and Quantitative Links program, J. Geophys. Res., **106**,12099-12108, 2001.

Michel, C., C. Liousse, J.-M. Grégoire, K. Tansey, G. R. Carmichael, and J.-H. Woo, Biomass burning emission inventory from burnt area data given by SPOT-Vegetation satellite in the frame of TRACE-P and ACE-Asia campaigns, *J. Geophys. Res.*, 2005, in press.

Michelson, D. B., and J. Koistinen, Gauge-radar network adjustment for the Baltic Sea experiment. Phys. Chem. Earth (B), 25, 915-920, 2000.

Middlebrook, A. M., D. M. Murphy, and D. S. Thomson, Observations of organic material in individual marine particles at Cape Grim during the First Aerosol Characterization Experiment (ACE 1), *J. Geophys. Res.*, *103*, 16475-16483, 1998.

Mielke, P.W., Jr., Comments on the Climax I and II experiments including replies to Rangno and Hobbs, *J. Appl. Meteor., 34*, 1228-1232, 1995.

Mielke, P.W., Jr., G.W. Brier, L.O. Grant, G.J. Mulvey, and P.N. Rosenweig, A statistical reanalysis of the replicated Climax I and II wintertime orographic cloud seeding experiments, *J. Appl. Meteorol., 20*, 643–659, 1981.

Mielke, P.W., Jr., K. Berry, A.S. Dennis, P.L. Smith, J.R. Miller, Jr., and B.A. Silverman, HIPLEX-1: statistical evaluation, *J. Appl. Meteorol., 23*, 513–522, 1984.

Mielke, P.W., Jr., L.O. Grant, and C.F. Chappell, An independent replication of the Climax wintertime orographic cloud seeding experiment, *J. Appl. Meteorol., 10*, 1198–1212, 1971.

Mielke, P.W., Jr., L.O. Grant, and C.F. Chappell, Elevation and spatial variation effects of wintertime orographic cloud seeding, *J. Appl. Meteorol., 9*, 476–488, 1970; Corrigenda, *10,* 842, 1971; Corrigenda, *15,* 801, 1976.

Mikhailov, E., S. Vlasenko, R. Niessner, and U. Pöschl, Interaction of aerosol particles composed of protein and salts with water vapor: hygroscopic growth and microstructural rearrangement, *Atmos. Chem. Phys.*, *4*, 323-350, 2004.

Milbrandt, J., and M.K. Yau, A multi-moment bulk microphysics parameterization. Part I: Analysis of the role of the shape parameter. *J. Atmos. Sci*., *62*, doi: 10.1175/JAS3534.1, 3051-3064, 2005a.

Milbrandt, J., and M.K. Yau, A multimoment bulk microphysics parameterization. Part II: A proposed three-moment closure and scheme description, *J. Atmos. Sci*., 62, doi: 10.1175/JAS3535.1, 3065–3081, 2005b.

Milford, J.B., and C.I. Davidson, The sizes of particulate sulphate and nitrate in the atmosphere - a review, Journal of Air Pollution Control Association, 37, 125-134, 1987.

Miller, R. L., I. Tegen, and J. Perlwitz, Surface radiative forcing by soil dust aerosols and the hydrologic cycle, *J. Geophys. Res.*, *109*, D04203, doi:10.1029/2003JD004085, 2004.

Min, Q., and L.C. Harrison, Cloud properties derived from surface MFRSR measurements and comparison with GEOS results at the ARM SGP site, *Geophys. Res. Lett., 23*, 1641- 1644, 1996.

Ming, Y., V. Ramaswamy, P.A. Ginoux, L.W. Horowitz, and L.M. Russell, Geophysical Fluid Dynamics Laboratory general circulation model investigation of the indirect radiative effects of anthropogenic sulfate aerosol. *J. Geophy. Res.-Atmos.,* 110(D22), 2005.

Minnis, P., D. P. Garber, D. F. Young, and R. F. Arduini, Parameterizations of reflectance and effective emittance for satellite remote sensing of cloud properties, J. Atmos. Sci., **55**, 3313-3339, 1998.

Mircea, M. M.C.Facchini, S.Decesari, F.Cavalli, L.Emblico, S.Fuzzi, A.Vestin, J.Rissler, E.Swietlicki, G.Frank, M.O.Andreae, W.Maenhaut, Y.Rudich, P.Artaxo: Importance of the organic aerosol fraction for modeling aerosol hygroscopic growth and activation: a case study in the Amazon Basin, Atmos. Chem. Phys., 5, 3111-3126, 2005.

Mircea, M., M. C. Facchini, S. Decesari, F. Cavalli, L. Emblico, S. Fuzzi, A. Vestin, J. Rissler, E. Swietlicki, G. Frank, M. O. Andreae, W. Maenhaut, Y. Rudich, and P. Artaxo, Importance of the organic aerosol fraction for modeling aerosol hygroscopic growth and activation: a case study in the Amazon Basin, *Atmos. Chem. Phys.*, *5*, 3111–3126, 2005.

Mishchenko, M. I., and L. D. Travis, Satellite retrieval of aerosol properties over the ocean using polarization as well as intensity of reflected sunlight, J. Geophys. Res., **102**, 16989-17013, 1997.

Mishchenko, M. I., I. V. Geogdzhayev, L. Liu, J. A. Ogren, A. A. Lacis, W. B. Rossow, J. W. Hovenier, H. Volten, and O. Muñoz, Aerosol retrievals from AVHRR radiances: effects of particle nonsphericity and absorption and an updated long-term global climatology of aerosol properties, J. Quant. Spectrosc. Radiat. Transfer, **79**, 953-972, 2003.

Mishchenko, M. I., L. D. Travis, W. B. Rossow, B. Cairns, B. E. Carlson, and Q. Han, Retrieving CCN column density from single-channel measurements of reflected sunlight over the ocean: A sensitivity study, Geophys. Res. Lett., **24**, 2655–2658, 1997.

Mishchenko, M., B. Cairns, J. E. Hansen, L. D. Travis, R. Burg, Y. J. Kaufman, J. V. Martin, and E. P. Shettle, Monitoring of aerosol forcing of climate from space: Analysis of measurement requirements, J. Quant. Spectrosc. Radiat. Transfer, **88**, 149-161, 2004.

Mochida, M., Y. Kitamori, K. Kawamura, Y. Nojiri, and K. Suzuki, Fatty acids in the marine atmosphere: Factors governing their concentrations and evaluation of organic films on sea-salt particles, *J. Geophys. Res.*, *107*, 4325, doi:10.1029/2001JD001278, 2002.

Molders, N., and M.A. Olson, Impact of urban effects on precipitation in high latitudes, *J. Hydromet., 5,* 409–429, 2004.

Molina, M. J., A. V. Ivanov, S. Trakhtenberg, and L. T. Molina, Atmospheric evolution of organic aerosol, *Geophys. Res. Lett.*, *31*, L22104, doi:10.1029/2004GL020910, 2004.

Molnar, A., E. Meszaros, H. C. Hansson, H. Karlsson, A. Gelencser, G. Y. Kiss, and Z. Krivacsy, The importance of organic and elemental carbon in the fine atmospheric aerosol particles, *Atmos. Environ.*, *33*, 2745-2750, 1999.

Mooney, M. L. and G. W. Lunn. The Area of Maximum Effect Resulting from the Lake Almanor Randomized Cloud Seeding Experiment. *J. Appl. Meteorol.* 8(1):68–74, 1969.

Moore, K. G., A. D. Clarke, V. N. Kapustin, and S. G. Howell, Long-range transport of continental plumes over the Pacific Basin: Aerosol physiochemistry and optical properties during PEM-Tropics A and B, *J. Geophys. Res.*, *108*, 2003.

Mordy, W.A., Computations of the growth by condensation of a population of cloud droplets, *Tellus, 11*, 16-44, 1959

Morin, E., W.F. Krajewski, D.C. Goodrich, X. Gao, and S. Sorooshian, Estimating rainfall intensities from weather radar data: The scale-dependency problem, J. Hydrom., 4, 782–797, 2003.

Moroney, C., R. Davies, and J. P. Muller, 2002: Operational retrieval of cloud-top heights using MISR data, IEEE Trans. Geosci. Remote Sens., **40**, 1541.

Mossop, S.C., A. Ono and K. J. Heffernan, Studies of ice crystals in natural clouds. *J. Atmos. Res.*, **1**, 44-64, 1967.

Mossop, S.C., and J. Hallett, Ice crystal concentration in cumulus clouds: Influence of the drop spectrum, *Science*, *186*, 632-634, 1974.

Mossop, S.C., Concentrations of Ice Crystals in Clouds. Bull. of the Amer. Meteor. Soc., 51, 474-480, 1970.

Mossop, S.C., J. Hallett, Ice crystal concentration in cumulus clouds: Influence of the drop spectrum. Science, 186, 632-634. 1974.

Mossop, S.C., R. E. Ruskin, and J. K. Hefferman, Glaciation of a cumulus at -4 C. *J. Atmos. Sci.*, **25**, 889-899, 1968.

Mossop, S.C., R.E. Cottis and B. M. Bartlett, Ice crystal concentrations in cumulus and stratocumulus clouds. *Quart. J. Roy. Meteor. Soc.*, **98**, 105-123, 1972.

Mossop, S.C., Secondary ice particle production during rime growth: the effect of drop size distribution and rimer velocity, *Quar. J. Roy. Meteorol. Soc.*, *111*, 1113–1124, 1985.

Mossop, S.C., The influence of the drop size distribution in the production of secondary ice particles during graupel growth, *Quart. J. Roy. Meteorol. Soc., 104,* 323-330, 1978.

Moulin, C., C.E. Lambert, F. Dulac and U. Dayan, Control of atmospheric export of dust from North Africa by the North Atlantic oscillation. *Nature*, 387, 691-694, 1997.

Murakami, M., K. Kikuchi, and C. Magono, Experiments on aerosol scavenging by natural snow crystals. Part I: Collection efficiency of uncharged snow crystals for micron and sub-micron particles, Journal of the Meteorological Society of Japan, 63 (1), 119-128, 1985.

Murphy, D. M., and D. S. Thomson, Chemical composition of single aerosol particles at Idaho Hill: Negative Ion Measurements, *J. Geophys. Res.*, *102*, 6341-6352, 1997.

Murphy, D. M., D. S. Thomson, A. M. Middlebrook, and M. E. Schein, In situ single-particle characterization at Cape Grim, *J. Geophys. Res.*, *103*, 16,485-16,491, 1998b.

Murphy, D. M., J. R. Anderson, P. K. Quinn, L. M. McInnes, F. J. Brechtel, S. M. Kreidenweis, A. M. Middlebrook, M. Posfai, D. S. Thomson, and P. R. Buseck, Influence of sea-salt on aerosol radiative properties in the Southern Ocean marine boundary layer, *Nature*, *392*, 62-65, 1998a.

Murphy, D.M., and D.S. Thomson, Chemical composition of single aerosol particles at Idaho Hill, J. Geophys. Res., 102, 6341-6368, 1997.

Murty, A.S.R., et al., Eleven-year warm cloud seeding experiment in Maharashtra state, India, *J. Weather Modif., 32*, 10-20, 2000.

Nadal, F., and F. M. Bréon, 1999: Parameterization of surface polarized reflectance derived from POLDER spaceborne measurements, IEEE Trans Geosci. Remote Sens., **37**, 1709-1718.

Nakajima, T., A. Higurashi,, K. Kawamoto and J. Penner, A possible correlation between satellite-derived cloud and aerosol microphysical parameters. Geophys. Res. Lett. 28, 1171-1174, 2001.

Nakajima, T., and M. D. King, Determination of the optical thickness and effective particle radius of clouds from reflected solar radiation measurements. Part I: Theory. *J. Atmos. Sci., 47***,** 1878-1893, 1990.

Nat. Acad. Sci., 102, 11207-11212, 2005.

National Academy of Sciences-National Research Council, *Weather and Climate Modification: Progress and Problems*, 258 pp., Government Printing Office, Washington, D.C., 1973.

Neiburger, M., and C.W. Chien, Computations of the growth of cloud drops by condensation using an electronic digital computer. *Geophys. Monogr. Series*, *Vol. 5,* American Geophysical Union, 91-208, 1960.

Nelson, R.T., and N.R. Gokhale, Concentration of giant particles below cloud bases, Reprint, Proceedings of the First National Conf. on Weather Mod., April 28 to May 1, 1968.

Nenes, A., R. J. Charlson, M. C. Facchini, M. Kulmala, A. Laaksonen, and J. H. Seinfeld, Can chemical effects on cloud droplet number rival the first indirect effect? *Geophys. Res., Lett., 29*, 1848, doi:10.1029/2002GL015295, 2002a.

Nenes, A., S. N. Pandis, and C. Pilinis, ISORROPIA: A new thermodynamic equilibrium model for multiphase multicomponent inorganic aerosols, *Aquat. Geochem.*, *4*, 123-152, 1998.

Nenes, A., W.C. Conant, AND J.H. Seinfeld, Black carbon radiative heating effects on cloud microphysics and implications for the aerosol indirect effect 2. Cloud microphysics, *J. Geophys. Res*., *107*, D21, 4605, doi:10:1029/2002JD002101, 2002b.

Nešpor, V., and B. Sevruk, Estimation of wind-induced error of rainfall gauge measurements using a numerical simulation, J. Atmos. Ocean. Tech., 16, 450–464, 1999.

Nespor, V., W.F. Krajewski, and A. Kruger, Wind-induced error of rain drop size distribution measurement using a two-dimensional video disdrometer, J. Atmos and Oceanic Technol, 17, 1483-1492, 2000.

Neusüß, C., H. Wex, W. Birmili, A. Wiedensohler, C. Koziar, B. Busch, E. Bruggemann, T. Gnauk, M. Ebert, and D. S. Covert, Characterization and parameterization of atmospheric particle number-, mass-, and chemical-size distributions in central Europe during LACE 98 and MINT, *J. Geophys. Res.*, *107*, 2002.

Neusüß, C., M. Pelzing, A. Plewka, and H. Herrmann, A new analytical approach for size-resolved speciation of organic compounds in atmospheric aerosol particles: Methods and first results, *J. Geophys. Res.*, *105*, 4513-4527, 2000.

Newton, C.W., Circulations in large sheared cumulonimbus, *Tellus, 18,* 699–712, 1966.

Nho-Kim, E.-Y., M. Michou, and V.-H. Peuch, Parameterization of size-dependent particle dry deposition velocities for global modeling, Atmospheric Environment, 38 (13), 1933-1942, 2004.

Nicholson, K.W., The dry deposition of small particles: A review of experimental measurements, Atmospheric Environment, 22 (12), 2653-2666, 1988.

Nickerson, E.C., E. Richard, R. Rosset, and D.R. Smith, The numerical simulation of clouds, rain, and airflow over the Vosges and Black Forest Mountains: A meso-beta model with parameterized microphysics, *Mon. Wea. Rev*., *114*, 398-414, 1986.

Nickerson, E.C., FACE rainfall results: seeding effect or natural variability?, *J. Appl. Meteorol.*, *18*, 1097–1105, 1979.

Nickerson, E.C., Reply—The FACE-1 seeding effect revisited, *J. Appl. Meteorol.*, *20*, 108–114, 1981.

Nilsson, E. D., Ü. Rannik, E. Swietlicki, C. Leck, P. P. Aalto, J. Zhou, and M. Norman, Turbulent aerosol fluxes over the Arctic Ocean 2. Wind-driven sources from the sea, *J. Geophys. Res.*, *106*, 32,139-32,154, 2001.

Nober, F., H.-F. Graf and D. Rosenfeld, Sensitivity of the global circulation to the suppression of precipitation by anthropogenic aerosols, *Global Planet Change, 37,* 57–80, 2003.

Noble, C. A., and K. A. Prather, Real-time measurement of correlated size and composition profiles of individual atmospehric aerosol particles, *Environ. Sci. Tech.*, *30*, 2667-2680, 1996.

Noone, K., U. Baltensperger, A. Flossmann, S. Fuzzi, H. Hass, E. Nemitz, J.-P. Putaud, H. Puxbaum, U. Schurath, K. T?rseth, and H.t. Brink, Tropospheric Aerosols and Clouds, in Towards Cleaner Air for Europe - Science, Tools and Application, Part 1. Results from the EUROTRAC-2 Synthesis and Integration Project, edited by P.M. Midgley, P.J.H. Builtjes, and R.M.H. D. Fowler, C.N. Hewitt, N. Moussiopoulos, K. Noone, K. T?rseth and A. Volz-Thomas, Margraf Verlag, Weikersheim, 2003.

Novakov, T., and C. E. Corrigan, Cloud condensation nucleus activity of the organic component of biomass smoke particles, *Geophys. Res. Lett.*, *23*, 2141-2144, 1996.

Novakov, T., and J. E. Penner, Large contribution of organic aerosols to cloud-condensation-nuclei concentrations, *Nature*, *365*, 823-826, 1993.

Novakov, T., C. E. Corrigan, J. E. Penner, C. C. Chuang, O. Rosario, and O. L. M. Bracero, Organic aerosols in the Caribbean trade winds: A natural source?, *J. Geophys. Res.*, *102*, 21,307-21,313, 1997.

Noziere, B., and D.D. Riemer, The chemical processing of gas-phase carbonyl compounds by sulfuric acid aerosols: 2,4-pentandione, Atmos. Environ., 37, 841-851, 2003.

Ochs, H.T., K.V. Beard, R.R. Czys, N.F. Laird, D.E. Schaufelberger, and D.J. Holdridge, Collisions between small precipitation drops. Part I: Laboratory measurements of bounce, coalescence and temporary coalescence, *J. Atmos. Sci., 52,* 2258–2275, 1995.

O'Dowd, C. D., and M. H. Smith, Physicochemical properties of aerosols over the Northeast Atlantic: Evidence for wind-speed-related submicron sea-salt aerosol production, *J. Geophys. Res.*, *98*, 1137-1149, 1993.

O'Dowd, C. D., M. C. Facchini, F. Cavalli, D. Ceburnis, M. Mircea, S. Decesari, S. Fuzzi, Y. J. Yoon, and J.-P. Putaud, Biogenically driven organic contribution to marine aerosol, *Nature*, *431*, 676-680, 2004.

O'Dowd, C. D., M. H. Smith, I. E. Consterdine, and J. A. Lowe, Marine aerosol, sea-salt, and the marine sulphur cycle: A short review, *Atmos. Environ.*, *31*, 73-80, 1997.

O'Dowd, C. D., P. Aalto, K. Hameri, M. Kulmala, and T. Hoffmann, Aerosol formation - Atmospheric particles from organic vapours, *Nature*, *416*, 497-498, 2002.

O'Dowd, C.D., M.C.Facchini , F. Cavalli, D.Ceburnis, M. Mircea, Stefano Decesari, S.Fuzzi and Y.J.Yoon& J-P Putaud 2004: Biogenically-driven organic contribution to marine aerosol, *Nature*, 431, 676-680.

Oguchi, T., Electromagnetic wave propagation and scattering in rain and other hydrometeors, Proc. IEEE, 71, 1029-1078, 1983.

Okamoto, H., T. Nishizawa, S. Sato, A. Kamei, H. Kuroiwa, H. Kumagai, M. Yasui, N. Sugimoto, I. Matsui, and A. Shimizu, Study of clouds by shipborne radar and lidar measurements during R-V Mirai MR01-K02 cruise, in Proc. EarthCARE workshop (second international workshop on space-borne cloud profiling radar) CRL/ARS, Report 02-02, pp. 155-163, 2002.

Oke, T. R., Boundary Layer Climates, Cambridge University Press, Cambridge, 435 pages, 1987.

Oki, T., The global water cycle, in *Global Energy and Water Cycles*, edited by K.A. Browning and R.J. Gurney, 292 pp., Cambridge University Press, Cambridge, U.K., 1999.

Olson, T.M., and M.R. Hoffmann, Hydroxyalkylsulfonate formation: its role as a sulfur(IV) reservoir in atmospheric water droplets, Atmospheric Environment, 23 (5), 985-97, 1989.

Olson, W.S., P. Bauer, N.F. Viltard, D.E. Johnson, W.-K. Tao, R. Meneghini, and L. Liao, A melting-layer model for passive/active microwave remote sensing applications. Part I. Model formulation and comparison with observations, J. Appl. Meteor., 40, 1145–1163, 2001.

Omar, A.H., and C.S. Gardner, Observations by the lidar In-space Technology Experiment (LITE) of high altitude clouds over the Equator in regions exhibiting extremely cold temperatures, J. Geophys. Res., 106 (D1), 1227, 2001.

Oraltay, R.G., and J. Hallett, Evaporatioin and melting of ice crystals: A laboratory study. *Atmos. Res.,* 24, 169-189, 1989.

Oraltay, R.G., J. Hallett, Evaporation and melting of ice crystals: A laboratory study. Atmos. Res., 24, 169-189, 1989.

P. A. Durkee, R. E. Chartier, A. Brown, E. J. Trehubenko, S. D. Rogerson, C. Skupniewicz, and K. E. Nielsen, S. Platnick and M.D. King, Composite Ship Track Characteristics. *J. Atmos. Sci., 57*, 2542-2553, 2000.

Paluch, I.R., and D.H. Lenschow, Stratiform cloud formation in the marine boundary layer, *J. Atmos. Sci.*, *48*, 2141-2158, 1991.

Pandis, S.N., L.M. Russell, and J.H. Seinfeld, The relationship between DMS flux and CCN concentration in remote marine regions, *J. Geophys. Res., 99,* 16945–16957, 1994.

Pankow, J.F., An absorption model of the gas/aerosol partitioning involved in the formation of secondary organic aerosol, Atmos. Environ., 28 (2), 189-193, 1994a.

Pankow, J.F., An absortion model of gas/particle partitioning of organic compounds in the atmosphere, Atmos. Environ., 28 (2), 185-188, 1994b.

Pankow, J.F., and T.F. Bidleman, Effects of temperature, TSP and percent non-exchangeable material in determining the gas-particle partitioning of organic compounds, Atmos. Environ., 25A, 2241-2249, 1991.

Pankow, J.F., Review and Comparative Analysis of the Theories on Partitioning Between the Gas and Aerosol Particulate Phases in the Atmosphere, Atmospheric Environment, 21 (11), 2275-2283, 1987.

Park, S.H., and K.W. Lee, Condensational growth of polydisperse aerosol for the entire particle size range, Aerosol Sci. Technol., 33, 222-227, 2000.

Parol, F., J. C. Buriez, C. Vanbauce, P. Couvert, G. Seze, P. Goloub, and S. Cheinet, First results of the POLDER "Earth Radiation Budget and Clouds" operational algorithm, IEEE Trans Geosci. Remote Sens., **37**, 1597-1612, 1999.

Pawlowska, H. , and J. L. Brenguier, Microphysical properties of stratocumulus clouds during ACE-2. Tellus., 52B, 867-886, 2000.

Pawlowska, H., and J. L. Brenguier, An Observational Study of Drizzle Formation in Stratocumulus Clouds during ACE-2 for GCM parameterizations PACE Topical Issue, J. Geophys. Res., 108, No. D19, 8587 10.1029, 2003.

Peng, C. G., A. H. L. Chow, and C. K. Chan, Hygroscopic study of glucose, citric acid, and sorbitol using an electrodynamic balance: Comparison with UNIFAC predictions, *Aerosol Science and Technology*, *35*, 753-758, 2001b.

Peng, C., M. N. Chan, and C. K. Chan, The hygroscopic properties of dicarboxylic and multifunctional acids: Measurements and UNIFAC predictions, *Environ. Sci. Technol.*, *35*, 4495-4501, 2001a.

Penner, J. E., M. O. Andreae, H. Annegarn, L. Barrie, J. Feichter, D. Hegg, A. Jayaraman, R. Leaitch, D. Murphy, J. Nganga, and G. Pitari, Aerosols, their Direct and Indirect Effects, in *Climate Change 2001: The Scientific Basis. Contribution of Working Group I to the Third Assessment Report of the Intergovernmental Panel on Climate Change*, edited by J. T. Houghton, Y. Ding, D. J. Griggs, M. Noguer, P. J. van der Linden, X. Dai, K. Maskell, & C. A. Johnson, pp. 289-348, Cambridge University Press, Cambridge, UK, and New York, NY, USA, 2001.

Perry, K.D., and P.V. Hobbs, Further evidence for particle nucleation in clear air adjacent to marine cumulus clouds, *J. Geophys. Res., 99,* 22,803–22,818, 1994.

Perry, K.D., and P.V. Hobbs, Influences of isolated cumulus clouds on the humidity of their surroundings, *J. Atmos. Sci., 53,* 159–174, 1996.

Peters, K., and R. Eiden, Modelling the dry deposition velocity of aerosol particles to a spruce forest, Atmospheric Environment - Part A General Topics, 26 A (14), 2555-2564, 1992.

Petzold, A., and M. Schönlinner, Multi-angle absorption photometry—a new method for the measurement of aerosol light absorption and atmospheric black carbon, J. Aerosol Sci., **35**, 421-441, 2004.

Petzold, A., J. Strom, S. Ohlsson, and F. P. Schroder, Elemental composition and morphology of ice-crystal residual particles in cirrus clouds and contrails, *Atmos. Res.*, *49*, 21-34, 1998.

Petzold, A., M. Fiebig, H. Flentje, A. Keil, U. Leiterer, F. Schroder, A. Stifter, M. Wendisch, and P. Wendling, Vertical variability of aerosol properties observed at a continental site during the Lindenberg Aerosol Characterization Experiment (LACE 98), *J. Geophys. Res.*, *107*, 2002.

Pezold, A, Gysel M, Vancassel X, Hitzenberger R, Puxbaum H, Vrochticky S, Weingartner E, Baltensperger U, Mirabel P, On the effects of organic matter and sulphur-containing compounds on the CCN activation of combustion particles, Atmospheric Chemistry and Physics, 5, 3187-3203, 2005.

Philander, S. G. H., D. Gu, D. Halpern, G. Lambert, N.-G. Lau, T. Li, and R. C. Pacanowski, Why the ITCZ is mostly north of the equator. *J. Climate, 9*, 2958-2972, 1996.

Phillips, V.T.J., T.W. Choularton, A.M. Blyth, and J. Latham, The influence of aerosol concentrations on the glaciation and precipitation of a cumulus cloud, Quarterly Journal of the Royal Meteorological Society, 128 (581), 951-971, 2002.

Piironen, A.K., and E.W. Eloranta, Convective boundary layer mean depths, cloud base altitudes, cloud top altitudes, cloud coverages, and cloud shadows obtained from Volume Imaging Lidar data, J. Geophys. Res., 100 (D12), 25569-25576, 1995.

Pilinis, C., and J.H. Seinfeld, Continued development of a general equilibrium model for inorganic multicomponent atmospheric aerosols, Atmos. Environ., 21, 2453-2466, 1987.

Pilinis, C., K. P. Capaldo, A. Nenes, and S. N. Pandis, MADM - A new multicomponent aerosol dynamics model, *Aerosol Science and Technology*, *32*, 482-502, 2000.

Pincus, R., and S.A. Klein, Unresolved spatial variability and microphysical process rates in large-scale models, *J. Geophys. Res.*, *105*, 27,059-27,065, 2000.

Pinsky, M., and A. Khain, Formation of inhomogeneity in drop concentration induced by the inertia of drops falling in a turbulent flow, and the influence of the inhomogeneity on the drop-spectrum broadening, *Quart. J. Roy. Meteorol. Soc.*, *123*, 165-186, 1997.

Pinsky, M.B., A. Khain and Z. Levin, The role of the inertia of cloud drops in the evolution of the spectra during drop growth by diffusion. *Quart. J. Roy. Meteorol. Soc.*, *125*, 553- 581, 1999.

Pinsky, M.B., and A.P. Khain, Turbulence effects on droplet growth and size distributions in clouds—a review, *J. Aerosol Sci., 28,* 1127–1214, 1997.

Pirjola, L., C. D. O'Dowd, I. M. Brooks, and M. Kulmala, Can new particle formation occur in the clean marine boundary layer?, *J. Geophys. Res.*, *105*, 26,531-26,546, 2000.

Pitter, R.L., and H.R. Pruppacher, A wind tunnel investigation of freezing of small water drops falling at terminal velocity in air, *Quart. J. Roy. Meteorol. Soc., 99,* 540–550, 1973.

Platnick, S., Vertical photon transport in cloud remote sensing problems, J. Geophys. Res., **105**, 22919-22935, 2000.

Platnick, S., M.D. King, S.A. Ackerman, W.P. Menzel, B.A. Baum, J.C. Riédi, and R.A. Frey, The MODIS cloud products: Algorithms and examples from Terra, *IEEE Trans. Geosci. Remote Sens.*, *41*, 459–473, 2003.

Popovitcheva, O.B., M.E. Trukhin, N.M. Persiantseva, and N.K. Shonija, Water adsorption on aircraft-combustor soot under young plume conditions, Atmospheric Environment, 35, 1673-1676, 2001.

Porch, W.M., C.-Y.J. Kao, and R.G. Kelley, Jr., Ship trails and ship induced cloud dynamics, *Atmos. Environ., 24A*, 1051–1059, 1990.

Posfai, M., J. Li, J. R. Anderson, and P. R. Buseck, Aerosol bacteria over the Southern Ocean during ACE-1, *Atmos. Res.*, *66*, 231-240, 2003.

Powell, K.A., C.R. Trepte, and G.S.Kent, Observations of Saharan Dust by LITE, in Advances in Atmospheric Remote Sensing with Lidar, Selected Papers of the 18th ILRC, pp. 149-152, Berlin, 1996.

Prenni, A. J., P. J. De Mott, and S. M. Kreidenweis, Water uptake of internally mixed particles containing ammonium sulfate and dicarboxylic acids, *Atmos. Environ.*, *37*, 4243-4251, 2003.

Prenni, A. J., P. J. DeMott, S. M. Kreidenweis, D. E. Sherman, L. M. Russell, and Y. Ming, The effects of low molecular weight dicarboxylic acids on cloud formation, *Journal of Physical Chemistry a*, *105*, 11,240-11,248, 2001.

Prospero, J. M., P. Ginoux, O. Torres, S. E. Nicholson, and T. E. Gill, Environmental characterization of global sources of atmospheric soil dust identified with the Nimbus 7 Total Ozone Mapping Spectrometer (TOMS) absorbing aerosol product, *Rev. Geophys.*, *40*, 1002, doi:10.1029/2000RG000095, 2002.

Prospero, J.M., Long-term measurements of the transport of African mineral dust to the southeastern United States: Implications for regional air quality, *J. of Geophys. Res. D*: Atmospheres, 104 (D13), 15917-15927, 1999.

Prospero, J.M., M. Uematsu, and D.L. Savoie, Mineral aerosol transport to the Pacific Ocean, in Chemical Oceanograph, edited by J.P. Riley, pp. 187-218, Academic Press, New York, 1989.

Pruppacher H. and R.J. Schlamp, A wind tunnel investigation on ice multiplication by freezing of waterdrops falling at termional velocity in air. *J. Geophys. Res., 80*, 380-386, 1975.

Pruppacher, H. R., and J. D. Klett, *Microphysics of Clouds and Precipitation*. Dordrecht: Reidel, pp. 954 , 1997.

Pueschel, R. F., and G. Langer, Sugar cane fires as a source of ice nuclei in Hawaii. *J. Appl. Meteor.,* **12,** 549–551, 1973.

Putaud, J. P., R. van Dingenen, M. Mangoni, A. Virkkula, F. Raes, H. Maring, J. M. Prospero, E. Swietlicki, O. H. Berg, H. Hillamo, and T. Mäkelä, Chemical mass closure and origin assessment of the submicron aerosol in the marine boundary layer and the free troposphere at Tenerife during ACE-2, *Tellus*, *52B*, 141-168, 2000.

Putaud, J.-P., F. Raes, R. Van Dingenen, J.P.U. Baltensperger, E. Brüggemann, M.C. Facchini, S. Decesari, S. Fuzzi, R. Gehrig, H.C. Hansson, C. Hüglin, P. Laj, G. Lorbeer, W. Maenhaut, N. Mihalopoulos, K. Müller, X. Querol, S. Rodriguez, J. Schneider, G. Spindler, H. ten Brink, K. Tørseth, B. Wehner and A. Wiedensohler: A European Aerosol Phenomenology. 2: chemical characteristics of particulate matter at kerbside, urban, rural and background sites in Europe, Atmos. Environ., 38, 2579-2595, 2004.

Putaud, J.-P., R.V. Dingenen, U. Baltensperger, E. Br?ggemann, A. Charron, M.-C. Facchini, S. Decesari, S. Fuzzi, R. Gehrig, H.-C. Hansson, R.M. Harrison, A.M. Jones, P. Laj, G. Lorbeer, W. Maenhaut, N. Mihalopoulos, K. M?ller, F. Palmgren, X. Querol, S. Rodriguez, J. Schneider, G. Spindler, H.t. Brink, P. Tunved, K. T?rseth, B. Wehner, E. Weingartner, A. Wiedensohler, P. W?hlin, and F. Raes, A European aerosol phenomenology. Physical and chemical characteristics of

particulate matter at kerbside, urban, rural and background sites in Europe, Joint Research Centre, European Commission, EUR 20411 EN, 2003.

Quaas, J., O. Boucher and U. Lohmann, Constraining the total aerosol indirect effect in the LMDZ and ECHAM4 GCMs using MODIS satellite data, *Atmos. Chem. Phys. Disc.*, 5, 9669-9690, 2005.

Quaas, J., O. Boucher, and F.-M. Bréon, Aerosol indirect effects in POLDER satellite data and the Laboratoire de Météorologie Dynamique-Zoom (LMDZ) general circulation model, *J. Geophys. Res.*, 109, doi: 10.1029/2003JD004317, 2004.

Quinn, P. K., D. J. Coffman, V. N. Kapustin, T. S. Bates, and D. S. Covert, Aerosol optical properties in the marine boundary layer during the First Aerosol Characterization Experiment (ACE 1) and the underlying chemical and physical aerosol properties, *J. Geophys. Res.*, *103*, 16,547-16,563, 1998.

Quinn, P. K., S. F. Marshall, T. S. Bates, D. S. Covert, and V. N. Kapustin, Comparison of measured and calculated aerosol properties relevant to the direct radiative forcing of tropospheric sulfate aerosol on climate, *J. Geophys. Res.*, *100*, 8977-8991, 1995.

Radke, L. F., D. A. Hegg, J. H. Lyons, C. A. Brock, P. V. Hobbs, R. Weiss, and R. Rasmussen, Airborne measurements on smokes from biomass burning, in *Aerosols and Climate*, edited by P. V. Hobbs & M. P. McCormick, pp. 411-422, A. Deepak Publishing, Hampton, VA, 1988.

Radke, L. F., D. A. Hegg, P. V. Hobbs, J. D. Nance, J. H. Lyons, K. K. Laursen, R. E. Weiss, P. J. Riggan, and D. E. Ward, Particulate and trace gas emissions from large biomass fires in North America, in *Global Biomass Burning: Atmospheric, Climatic and Biospheric Implications*, edited by J. S. Levine, pp. 209-224, MIT Press, Cambridge, Mass., 1991.

Radke, L.F., and P.V. Hobbs, An automatic cloud condensation nuclei counter, *J. Appl. Meteorol., 8,* 105–109, 1969.

Radke, L.F., and P.V. Hobbs, Cloud condensation nuclei on the Atlantic seaboard of the United States, *Science, 193*, 999–1002, 1976.

Radke, L.F., and P.V. Hobbs, Humidity and particle fields around some small cumulus clouds, *J. Atmos. Sci., 48,* 1190-1193, 1991.

Radke, L.F., and P.V. Hobbs, Measurement of cloud condensation nuclei, light scattering coefficient, sodium-containing particles, and Aitken nuclei in the Olympic Mountains of Washington, *J. Atmos. Sci., 26,* 281-288, 1969.

Radke, L.F., J.A. Coakley Jr., and M.D. King, Direct and remote sensing observations of the effects of ship tracks on clouds, *Science, 246*, 1146–1149, 1989.

Raemdonck, H., W. Maenhaut, and M. O. Andreae, Chemistry of marine aerosol over the tropical equatorial Pacific, *J. Geophys. Res.*, *91*, 8623-8636, 1986.

Raes, F., T. Bates, F. McGovern, and M. van Liedekerke, The 2nd Aerosol Characterization Experiment (ACE-2): general overview and main results, *Tellus*, *52B*, 111-125, 2000.

Ramanathan, V., P. J. Crutzen, J. Lelieveld, A. P. Mitra, D. Althausen, J. Anderson, M. O. Andreae, W. Cantrell, G. R. Cass, C. E. Chung, A. D. Clarke, J. A. Coakley, W. D. Collins, W. C. Conant, F. Dulac, J. Heintzenberg, A. J. Heymsfield, B. Holben, S. Howell, J. Hudson, A. Jayaraman, J. T. Kiehl, T. N. Krishnamurti, D. Lubin, G. McFarquhar, T. Novakov, J. A. Ogren, I. A. Podgorny, K. Prather, K. Priestley, J. M. Prospero, P. K. Quinn, K. Rajeev, P. Rasch, S. Rupert, R. Sadourny, S. K. Satheesh, G. E. Shaw, P. Sheridan, and F. P. J. Valero, Indian Ocean Experiment: An integrated analysis of the climate forcing and effects of the great Indo-Asian haze, *J. Geophys. Res., 106*, 28371–28398, 2001a.

Ramanathan, V., C. Chung, D. Kim, T. Bettge, L. Buja, J.T. Kiehl, W.M. Washington, Q. Fu, D.R. Sikka, and M. Wild, Atmospheric Brown Clouds: Impacts on South Asian Climate and Hydrological Cycle, PNAS, 102 (15), 5326-5333, 2005.

Ramanathan, V., P. Crutzen, J. Kiehl, and D. Rosenfeld, 2001: Aerosols, Climate, and the Hydrological Cycle, *Science*, 294: 2119-2124.

Randall, D., M. Khairoutdinov, A. Arakawa, and W. Grabowski, Breaking the cloud parameterization deadlock, *Bull. Amer. Meteorol. Soc.*, *84*, 1547-1564, 2003.

Rangno A.L. and P. V. Hobbs: Microstructures and precipitation development in cumulus and small cumulonimbus clouds over the warm pool of the tropical Pacific Ocean. *Q. J. Roy. Meteor. Soc., 131*, 639-673, 2005.

Rangno, A.L., and P.V. Hobbs, A new look at the Israeli cloud seeding experiments, *J. Appl. Meteorol., 34*, 1169–1193, 1995a.

Rangno, A.L., and P.V. Hobbs, A re-evaluation of the Climax cloud seeding experiments using NOAA published data, *J. Clim. Appl. Meteorol., 26*, 757–762, 1987.

Rangno, A.L., and P.V. Hobbs, *Comprehensive Reply to Rosenfeld*, Cloud and Aerosol Research Group, Dept. Atmospheric Sciences, University of Washington, Seattle, 25 pp., 1997b <http://cargsun2.atmos.washington.edu/sys/research/archive/1997_comments_seeding.pdf>.

Rangno, A.L., and P.V. Hobbs, Criteria for the development of significant concentrations of ice particles in cumulus clouds, *Atmos. Res., 21*, 1–13, 1988.

Rangno, A.L., and P.V. Hobbs, Further analyses of the Climax cloud-seeding experiments, *J. Appl. Meteorol., 32*, 1837–1847, 1993.

Rangno, A.L., and P.V. Hobbs, Ice particle concentrations and precipitation development in small polar maritime continental clouds, *Quart. J. Roy. Meteorol. Soc., 117*, 207-241, 1991.

Rangno, A.L., and P.V. Hobbs, Ice particle concentrations and precipitation development in small continental cumuliform clouds, *Quart. J. Roy. Meteorol. Soc., 120*, 573-601, 1994.

Rangno, A.L., and P.V. Hobbs, Ice particles in stratiform clouds in the Arctic and possible mechanisms for the production of high ice concentrations, *J. Geophys. Res., 106*, 15065-15075, 2001.

Rangno, A.L., and P.V. Hobbs, Reply to Ben-Zvi, *J. Appl. Meteorol., 36*, 257–259, 1997d.

Rangno, A.L., and P.V. Hobbs, Reply to Dennis and Orville, *J. Appl. Meteorol., 36*, 279–279, 1997c.

Rangno, A.L., and P.V. Hobbs, Reply to Rosenfeld, *J. Appl. Meteorol., 36*, 272–276, 1997a.

Rangno, A.L., and P.V. Hobbs, Reply to Woodley, *J. Appl. Meteorol., 36*, 253–254, 1997e.

Rangno, A.L., Rain from clouds with tops warmer than –10°C in Israel, *Quart. J. Roy. Meteorol. Soc., 114*, 495–513, 1988.

Rasch, P.J., J. Feichter, K. Law, N. Mahowald, J. Penner, C. Benkovitz, C. Genthon, C. Giannakopoulos, P. Kasibhatla, D. Koch, H. Levy, T. Maki, M. Prather, D.L. Roberts, G.J. Roelofs, D. Stevenson, Z. Stockwell, S. Taguchi, M. Kritz, M. Chipperfield, D. Baldocchi, P. McMurry, L. Barrie, Y. Balkansi, R. Chatfield, E. Kjellstrom, M. Lawrence, H.N. Lee, J. Lelieveld, K.J. Noone, J. Seinfeld, G. Stenchikov, S. Schwartz, C. Walcek, and D. Williamson, A comparison of scavenging and deposition processes in global models: results from the WCRP Cambridge Workshop of 1995, Tellus Series B Chemical and Physical Meteorology, 52 (4), 1025-1056, 2000.

Rau, J. A., and M. A. K. Khalil, Anthropogenic contributions to the carbonaceous content of aerosols over the Pacific Ocean, *Atmos. Environ.*, *27A*, 1297-1307, 1993.

Ravishankara, A.R., and C.A. Longfellow, Reactions on tropospheric condensed matter, Phys. Chem. Chem. Phys., 1, 5433-5441, 1999.

Raymond, T. M., and S. N. Pandis, Cloud activation of single-component organic aerosol particles, *J. Geophys. Res.*, *107*, 4787, doi:10.1029/2002JD002159, 2002.

Raymond, T. M., and S. N. Pandis, Formation of cloud droplets by multicomponent organic particles, *J. Geophys. Res.*, *108*, 2003.

Reddy, M. S., and C. Venkataraman, Inventory of aerosol and sulphur dioxide emissions from India. Part II - biomass combustion, *Atmos. Environ.*, *36*, 699-712, 2002.

Reffernan, K.J. and R.N. Bracewell, Comparison of florida and california freezing-nucleus measurements, January 1957. *J. of the Atmos. Sci.* 16, 337–339, 1959.

Reid, J. S., and P. V. Hobbs, Physical and optical properties of young smoke from individual biomass fires in Brazil, *J. Geophys. Res.*, *103*, 32,013-32,030, 1998.

Reid, J. S., H. H. Jonsson, H. B. Maring, A. Smirnov, D. L. Savoie, S. S. Cliff, E. A. Reid, J. M. Livingston, M. M. Meier, O. Dubovik, and S. C. Tsay, Comparison of size and morphological measurements of coarse mode dust particles from Africa, *J. Geophys. Res.*, *108*, 8593, doi:10.1029/2002JD002485, 2003.

Reid, J. S., P. V. Hobbs, R. J. Ferek, D. R. Blake, J. V. Martins, M. R. Dunlap, and C. Liousse, Physical, chemical, and optical properties of regional hazes dominated by smoke in Brazil, *J. Geophys. Res.*, *103*, 32,059-32,080, 1998.

Reid, J. S., R. Koppmann, T. F. Eck, and D. P. Eleuterio, A review of biomass burning emissions part II: intensive physical properties of biomass burning particles, *Atmos. Chem. Phys.*, *5*, 799-825, 2005.

Reid, J.S., P.V. Hobbs, A.L. Rangno, and D.A. Hegg, Relationships between cloud droplet effective radius, liquid water content, and droplet concentration for warm clouds in Brazil embedded in biomass smoke, *J. Geophys. Res., 104,* 6145–6153, 1999.

Reisin, T., S. Tzivion, and Z. Levin, Seeding convective clouds with ice nuclei or hygroscopic particles: A numerical study using a model with detailed microphysics, *J. Appl. Meteorol., 35*, 1416–1434, 1996.

Reisin, T., Z. Levin, and S. Tzivion, Rain production in convective clouds as simulated in an axisymmetric model with detailed microphysics. Part II: effects of varying drops and ice nucleation, *J. Atmos. Sci., 53*, 1815-1837, 1996b.

Reisin, T., Z. Levin, and S. Tzivion, Rain production in convective clouds as simulated in an axisymmetric model with detailed microphysics. Part I: description of the model, *J. Atmos. Sci., 53*, 497-519, 1996a.

Reisner, J., R. M. Rasmussen, and R. T. Bruintjes, Explicit forecasting of supercooled water in winter storms using the MM5 mesoscale model, *Quart. J. Roy. Meteorol. Soc., 124*, 1071-1107, 1998.

Remer, L. A., Y. J. Kaufman, D. Tanré, S. Mattoo, D. A. Chu, J. V. Martins, R. R. Li, C. Ichoku, R. C. Levy, R. G. Kleidman, T. F. Eck, E. Vermote, and B. N. Holben, The MODIS aerosol algorithm, products and validation, J Atmos Sci., **62**, 947-972, 2005.

Remer, L.A, D. Tanre´, Y. J. Kaufman, C. Ichoku, S. Mattoo, R. Levy, D. A. Chu, B. Holben, O. Dubovik, A. Smirnov, J. V. Martins,5 R.-R. Li, and Z. Ahmad. Validation of MODIS aerosol retrieval over ocean, *Geophys. Res. Lett., 29*, 8008, doi: 10.1029/2001GL013204, 2002.

Respondek, P. S., A. I. Flossmann, R. R. Alheit, and H. R. Pruppacher, A theoretical study of the wet removal of atmospheric pollutants. Part V: the uptake, redistribution and deposition of $(NH_4)_2SO_4$ by a convective cloud containing ice, *J. Atmos. Sci., 52*, 2121-2132, 1995.

Reynolds, O., On the manner in which raindrops (snowflakes) and hailstones are formed, *Proc. Manchester Lit. Phil. Soc., 16,* 23–33, 1877. (Also, *17*, 15–24, 1878; *6*, 48–60, and 161–170, 1879; also *Nature, 15*, 163–165, 1877 and *17*, 207–209, 1878.)

Riédi, J., M. Doutriaux-Boucher, P. Goloub, and P. Couvert, Global distribution of cloud top phase from POLDER/ADEOS I, Geophys. Res. Lett.,, **27**, 1707-1710, 2000.

Riemer, N., H. Vogel, and B. Vogel, Soot aging time scales in polluted regions during day and night, *Atmos. Chem. Phys.*, *4*, 1885-1893, 2004.

Rinehart, R., Radar For Meteorologists, 4th edition, Rinehart Publication, Columbia, MO, USA, ISBN 0-9658002-1-0,pp 482, 2004.

Rissler, J., A. Vestin, E. Swietlicki, G. Fisch, J. Zhou, P. Artaxo, and M. O. Andreae, Size distribution and hygroscopic properties of aerosol particles from dry-season biomass burning in Amazonia, *Atmos. Chem. Phys. Discuss.*, *5*, 8149-8207, 2005.

Rissler, J., E. Swietlicki, J. Zhou, G. Roberts, M. O. Andreae, L. V. Gatti, and P. Artaxo, Physical properties of the sub-micrometer aerosol over the Amazon rain forest during the wet-to-dry season transition - Comparison of modeled and measured CCN concentrations, *Atmos. Chem. Phys.*, *4*, 2119-2143, 2004.

Rivera-Carpio, C. A., C. E. Corrigan, T. Novakov, J. E. Penner, C. F. Rogers, and J. C. Chow, Derivation of contributions of sulfate and carbonaceous aerosols to cloud condensation nuclei from mass size distributions, *J. Geophys. Res.*, *101*, 19,483-19,493, 1996.

Roach, W.T., On the effect of radiative exchange on the growth by condensation of a cloud or fog droplet, *Quart. J. Roy. Meteor. Soc., 102*, 361-372 1976.

Roach, W.T., On the effect of radiative exchange on the growth by condensation of a cloud or fog droplet, *Quart. J. Roy. Meteorol. Soc*., *102*, 361-372, 1976.

Roberts, G. C., Andreae, M. O., Zhou, J., and Artaxo, P.: Cloud condensation nuclei in the Amazon Basin: "Marine" conditions over a continent?, Geophys. Res. Lett., 28(14), 2807–2810, 2001.

Roberts, G. C., M. O. Andreae, J. Zhou, and P. Artaxo, Cloud condensation nuclei in the Amazon Basin: "Marine" conditions over a continent?, *Geophys. Res. Lett.*, *28*, 2807-2810, 2001.

Roberts, G., P. Artaxo, J. Zhou, E. Swietlicki, and M. O. Andreae, Sensitivity of CCN spectra on chemical and physical properties of aerosol: A case study from the Amazon Basin, *J. Geophys. Res.*, *107*, 8070, doi:10.1029/2001JD000583, 2002.

Roberts, G.C., A. Nenes, J.H. Seinfeld, and M.O. Andreae, Impact of biomass burning on cloud properties in the Amazon Basin, J. Geophys. Res., 108 (D2), 4062, doi:10.1029/2001JD000985, 2003.

Roberts, G.C., and A. Nenes, A continuous-flow streamwise thermal-gradient CCN chamber for atmospheric measurements, Aerosol Sci. Technol., **39**, 206-221, 2005.

Roberts, P., and J. Hallett, A laboratory study of the ice nucleating properties of some mineral particulates, *Quart. J. Roy. Meteorol. Soc., 94,* 25–34, 1968.

Roderick, M.L., and G.D. Farquhar, The cause of decreased pan evaporation over the past 50 years, *Sci., 298,* 1410–1411, 2002.

Rodriguez, M.A., and D. Dabdub, IMAGES-SCAPE2: A modeling study of size- and chemically resolved aerosol thermodynamics in a global chemical transport model, J. Geophys. Res., 109, D02203, doi:10.1029/2003JD003639, 2004.

Roeckner, E., P. Stier, J. Feichter, S. Kloster, M. Esch, and I. Fischer-Bruns, Impact of carbonaceous aerosol emissions on regional climate change. *Climate Dynamics, in press, 2006.*

Roelofs, G. J., P. Kasibhatla, L. Barrie, D. Bergmann, C. Bridgeman, M. Chin, J. Christensen, R. Easter, J. Feichter, A. Jeuken, E. Kjellstrom, D. Koch, C. Land, U. Lohmann, and P. Rasch, Analysis of regional budgets of sulfur species modeled for the COSAM exercise, *Tellus*, *53B*, 673-694, 2001.

Roelofs, G.-J., P. Kasibhatla, L. Barrie, D. Bergmann, C. Bridgeman, M. Chin, J. Christensen, R. Easter, J. Feichter, A. Jeuken, E. Kjellstr?m, D. Koch, C. Land, U. Lohmann, P. Rasch, and Y. Yi, Analysis of regional budgets of sulfur species modelled for the COSAM exercise, Tellus Series A Dynamic Meteorology and Oceanography, 53 (B), 673-694, 2001.

Rogers, C. F., J. G. Hudson, B. Zielinska, R. L. Tanner, J. Hallett, and J. G. Watson, Cloud condensation nuclei from biomass burning, in *Global Biomass Burning: Atmospheric, Climatic and Biospheric Implications*, edited by J. S. Levine, pp. 431-438, MIT Press, Cambridge, Mass., 1991.

Rogers, D.C., P.J. DeMott, and S.M. Kreidenweis, Airborne measurements of tropospheric ice-nucleating aerosol particles in the Arctic spring, *J. Geophys. Res., 106,* 15,053–15,063, 2001.

Rogers, J. C., and H. van Loon, The seesaw in winter temperatures between Greenland and northern Europe. Part II: Some oceanic and atmospheric effects in middle and high latitudes. *Mon. Wea. Rev.*, *107*, 509-519, 1979.

Rogers, R.R., and M.K. Yau, *A Short Course in Cloud Physics*, 304 pp., Pergamon, Tarrytown, N.Y., 1989.

Rokicki, M.L., and K.C. Young, The initiation of precipitation in updrafts, *J. Appl. Meteorol., 17*, 745–754, 1978.

Rolland, P., K. N. Liou, M. D. King, S. C. Tsay, and G. M. McFarquhar, 2000: Remote sensing of optical and microphysical properties of cirrus clouds using MODIS channels: Methodology and sensitivity to assumptions, J. Geophys. Res., **105**, 11,721-11,738.

Rosenfeld D., and I.M. Lensky, Satellite-based insights into precipitation formation processes in continental and maritime convective clouds, Bull. Amer. Meteor. Soc., 79, 2457–2476, 1998.

Rosenfeld D., Y. Rudich, and R. Lahav, Desert dust suppressing precipitation: A possible desertification feedback loop, Proc. Nat. Acad. Sci., 98, 5975–5980, 2001.

Rosenfeld, D., TRMM observed first direct evidence of smoke from forest fires inhibiting rainfall, Geophys. Res. Lett., **26**, 3105-3108, 1999.

Rosenfeld, D., Suppression of rain and snow by urban and industrial air pollution, Science, **287**, 1793-1796, 2000.

Rosenfeld, D., and E. Amitai, Comparison of WPMM versus regression for evaluating Z-R relationships. J. Appl. Meteorol. 37, 1241-1249, 1998.

Rosenfeld, D., and G. Feingold, Explanation of discrepancies among satellite observations of the aerosol indirect effects, *Geophys. Res. Lett., 30*, doi: 10.1029/2003GL017684, 2003.

Rosenfeld, D., and H. Farbstein, Possible influence of desert dust on seedability of clouds in Israel, *J. Appl. Meteorol., 31*, 722–731, 1992.

Rosenfeld, D., and R. Nirel, Seeding effectiveness—The interaction of desert dust and the southern margins of rain cloud systems in Israel, *J. Appl. Meteorol., 35,* 1502–1510, 1996.

Rosenfeld, D., and W. L. Woodley. Effects of cloud seeding in West Texas: Additional results and new insights. *J. Appl. Meteorol.* 32:1848-66, 1993.

Rosenfeld, D., and W.L. Woodley, Effects of cloud seeding in West Texas. *J. Appl. Meteor.*, *28*, 1050-1080, 1989.

Rosenfeld, D., and W.L. Woodley, Closing the 50-year circle: From cloud seeding to space and back to climate change through precipitation physics, *Meteorol. Monogr., 51,* 59–80, 2003.

Rosenfeld, D., and W.L. Woodley, Deep convective clouds withs ustaine highly supercooled liquid water until -37.5 C, *Nature*, *405*, 440-442, 2000.

Rosenfeld, D., and W.L. Woodley, Effects of cloud seeding in west Texas, *J. Appl. Meteorol., 28*, 1050-1080, 1989.

Rosenfeld, D., and W.L. Woodley, Effects of cloud seeding in west Texas: Additional results and new insights, *J. Appl. Meteorol.*, *32*, 1848-1866, 1993.

Rosenfeld, D., Comment on "A new look at the Israeli cloud seeding experiments," *J. Appl. Meteorol., 36*, 260–271, 1997.

Rosenfeld, D., R. Lahav, A. Khain, and M. Pinsky, The role of sea spray in cleansing air pollution over ocean via cloud processes, *Sci., 297*, 1667–1670, 2002.

Rosenfeld, D., R. Lahav, A. Khain, and M. Pinsky, The role of sea spray in cleansing air pollution over ocean via cloud processes, *Science, 297*, 1667-1670, 2002.

Rosenfeld, D., Suppression of rain and snow by urban air pollution. Science., 287, 1793–1796, 2000.

Rosenfeld, D., The third Israeli randomized cloud seeding experiment in the south: evaluation of the results and review of all three experiments, *Preprints, 14th Conf. on Planned and Inadvertent Wea. Modif.*, Everett, Wash., 17–21 August 1998, Amer. Meteorol. Soc., 565–568, 1998.

Rosenfeld, D., TRMM observed first direct evidence of smoke from forest fires inhibiting rainfall, *Geophys. Res. Lett., 26*, 3105–3108, 1999.

Ross, K. E., S. J. Piketh, R. T. Bruintjes, R. P. Burger, R. J. Swap, and H. J. Annegarn, Spatial and seasonal variations in CCN distribution and the aerosol-CCN relationship over southern Africa, *J. Geophys. Res.*, *108*, 8481, doi:10.1029/2002JD002384, 2003.

Rossow, W.B., A.W. Walker, and L.C. Gardner, Comparisons of ISCCP and other cloud amounts, *J. Climate, 6*, 2394–2418, 1993.

Rossow, W.B., and R.A. Schiffer, ISCCP cloud data products, *Bull. Amer. Meteorol. Soc., 72,* 2–20, 1991.

Rotstayn, L. D., and J. E. Penner, Indirect aerosol forcing, quasi-forcing, and climate response, *J. Climate*, 14, 2001.

Rotstayn, L. D., and Y. G. Liu, A smaller global estimate of the second indirect aerosol effect, *Geophys. Res. Lett., 32*, L05708, doi:10.1029/2004GL021922, 2005**.**

Rotstayn, L.D., and U. Lohmann, Tropical rainfall trends and the indirect aerosol effect, *J. Clim., 15*, 2103–2116, 2002.

Rotstayn, L.D., B.F. Ryan, and J.E. Penner, Precipitation changes in a GCM resulting from the indirect effects of anthropogenic aerosols, *Geophys. Res. Lett.*, *27*, 3045-3048, 2000.

Rudich, Y., O. Khersonsky, and D. Rosenfeld, Treating clouds with a grain of salt, *Geophys. Res. Lett.*, *29*, 2060, doi:10.1029/2002GL016055, 2002.

Rudolf, B., H. Hauschild, W. Rueth, and U. Schneider, Terrestrial Precipitation Analysis: Operational Method and Required Density of Point Measurements, in *Global Precipitations and Climate Change,* edited by M. Desbois and G. Desalmond, NATO ASI Series I, 26, Springer-Verlag, 173-186, 1994.

Ruijgrok, W., C.I. Davidson, and K.W. Nicholson, Dry deposition of particles: Implications and recommendations for mapping of deposition over Europe, Tellus, 47B, 587-601, 1995.

Russell, L. M., Aerosol organic-mass-to-organic-carbon ratio measurements, *Environ. Sci. Technol.*, *37*, 2982-2987, 2003.

Russo, F., D.N. Whiteman, B. Demoz, I. Veselovskii, S.H. Melfi, and R.M. Hoff, Development of Raman lidar techniques to address the indirect aerosol effect: Retrieving the liquid water content of clouds, in 22nd International Laser Radar Conference, pp. 411-414, Matera, Italy, 2004.

Ryan, B. F., and W. D. King. A critical review of the Australian experience in cloud seeding. *Bull. Am. Meteorol. Soc.* 78:239-354, 1997.

Ryzhkov, A. V., and D. S. Zrnic, Comparison of dual-polarization radar estimators of rain. J. Atmos. Oceanic. Technol., 12, 249-256, 1995.

Sachidananda, M., and D. S. Zrnic, Rain-rate estimates from differential polarization measurements, J. Atmos. Oceanic Technol., 4, 588-598, 1987.

Saleeby, S.M., and W.R. Cotton, A large-droplet mode and prognostic number concentration of cloud droplets in the Colorado State University Regional Atmospheric Modeling System (RAMS). Part I: Module descriptions and supercell test simulations, *J. Appl. Meteorol*., *43*, 182-195, 2004.

Saleeby, S.M., and W.R. Cotton, A large-droplet mode and prognostic number concentration of cloud droplets in the Colorado State University Regional Atmospheric Modeling System (RAMS). Part II: Sensitivity to a Colorado winter snowfall event. *J. Appl. Meteorol*., 44, 1912-1929, 2005.

Sassen, K., Dusty ice clouds over Alaska, *Nature*, 434, 456, 2005.

Satake, S., I. Uno, T. Takemura, G.R. Carmichael, Y. Tang, D. Streets, N. Sugimoto, A. Shimizu, M. Uematsu, J.-S. Han, and S. Ohta, Characteristics of Asian aerosol transport simulated with a regional-scale chemical transport model during the ACE-Asia observation, *Journal of Geophysical Research D: Atmospheres,* 109 (19), D19S22 1-16, 2004.

Sauvageot, H., J-P. Lacaux, The shape of averaged drop size distributions. *J. Atmos. Sci.*, 52, 1070-1083, 1995.

Sax, R.I., J. Thomas, M. Bonebrake and J. Hallett, Ice evolution within seeded and nonseeded Florida cumuli. *J. Appl. Meteorol*., *18*, 203-214, 1979.

Sax, R.I., S.A. Changnon, L.O. Grant, W.F. Hitchfield, P.V. Hobbs, A.M. Kahan, and J.S. Simpson, Weather modification: Where are we now and where are we going? An editorial overview, *J. Appl. Meteorol., 14*, 652–672, 1975.

Saxena, P. and Hildemann, L. M.: Water-Soluble Organics in Atmospheric Particles: A Critical Review of the Literature and Application of Thermodynamics to Identify Candidate Compounds, *J. Atmos. Chem.*, 24, 57–109, 1996.

Saxena, P., L.M. Hildemann, P.H. McMurry, and J.H. Seinfeld, Organics alter hygroscopic behavior of atmospheric particles, Journal of Geophysical Research, 100 (D9), 18,755?18,770, 1995.

Schaap, M., H. Van Der Gon, F. J. Dentener, A. J. H. Visschedijk, M. Van Loon, H. M. ten Brink, J. P. Putaud, B. Guillaume, C. Liousse, and P. J. H. Builtjes, Anthropogenic black carbon and fine aerosol distribution over Europe, *J. Geophys. Res.*, *109*, D18207, doi:10.1029/2003JD004330, 2004.

Schaefer, V.J., The natural and artificial formation of snow in the atmosphere. *Trans. Amer. Geophys.* 29, 492. 1948

Schemenauer, R.S., and A.A. Tsonis, Comments on "Physical Interpretation of Results from the HIPLEX-1 Experiment," *J. Appl. Meteorol.*, *24*, 1269–1274, 1985.

Schemenauer, R.S., and G.A. Isaac, The importance of cloud top lifetime in the description of natural cloud characteristics, *J. Appl. Meteorol.*, *23*, 267–279, 1984.

Schery, S.D., and S. Whittlestone, Evidence of high deposition of ultrafine particles at Mauna Loa Observatory, Atmospheric Environment, 29 (22), 3319-3324, 1995.

Schmid, O., P. Artaxo, W. P. Arnott, D. Chand, L. V. Gatti, G. P. Frank, A. Hoffer, M. Schnaiter, and M. O. Andreae, Spectral

light absorption by ambient aerosols influenced by biomass burning in the Amazon Basin. I: Comparison and field calibration of absorption measurement techniques, *Atmos. Chem. Phys. Discuss.*, *5*, 9355-9404, 2005.

Schnell, R. C., and G. Vali, Biogenic ice nuclei 1. Terrestrial and marine sources, *J. Atmos. Sci.*, *33*, 1554-1564, 1976.

Schnell, R.C and A. C. Delany, 1976: Airborne ice nuclei near an active volcano. *Nature,* **264,** 535–536, 1976.

Schnell, R.C. and G. Vali, Biogenic ice nuclei, Part I: Terrestrial and marine sources. J. Atmos . Sci., 33, 1554-1564, 1976a.

Schnell, R.C. and G. Vali, Biogenic ice nuclei, Part II: Bacterial sources. J. Atmos. Sci., 33, 1565-1570, 1976b.

Schönhuber, M., H. Urban, J.P.V. Poiares Baptista, W.L. Randeu and W. Riedler, Measurements of Precipitation Characteristics by a New Distrometer, Proceedings of Atmospheric Physics and Dynamics in the Analysis and Prognosis of Precipitation Fields, November 15 - 18, 1994, Rome, Italy, 1994.

Schüller, L., J. L. Brenguier, and H. Pawlowska, 2003: Retrieval of Microphysical, Geometrical and Radiative Properties of Marine Stratocumulus from Remote Sensing, PACE Topical Issue, J. Geophys. Res., 108, No. D15, 8631 10.1029.

Schüller, L., R. Bennartz, J.-L. Brenguier, and J. Fischer: An algorithm for the retrieval of droplet number concentration and geometrical thickness of stratiform marine boundary layer clouds applied to MODIS Radiometric Observations, J. Appl. Met., 44, 28-38, 2005.

Schultz, P., An explicit cloud physics parameterization for operational numerical weather prediction, *Mon. Wea. Rev., 123,* 3331–3343, 1995.

Schulz, M., G. de Leeuw, and Y. Balkanski, Sea-salt aerosol source functions and emissions, in *Emissions of Atmospheric Trace Compounds*, edited by C. Granier, P. Artaxo, & C. E. Reeves, pp. 333-359, Kluwer, Dordrecht, 2004.

Schwartz, S. E., F. Arnold, J. P. Blanchet, P. A. Durkee, D. J. Hofmann, W. A. Hoppel, M. D. King, A. A. Lacis, T. Nakajima, J. A. Ogren, and O. B. Toon, Group report: Connections between aerosol properties and forcing of climate. Aerosol Forcing of Climate, R. J. Charlson and J. Heintzenberg, Eds., John Wiley and Sons, 251-280, 1995.

Schwartz, S. E., Harsvardhan, and C. M. Benkovitz, Influence of anthropogenic aerosol on cloud optical depth and albedo shown by satellite measurements and chemical transport modeling. Proc. Natl. Acad. Sci. USA, 99, 1784-1789, 2002.

Scofield, R.A. and V.J. Oliver, A scheme for estimating convective rainfall from satellite imagery. NOAA Tech. Mem. NESS 86, Dept. of Commerce, Wash., DC, 47 pp, 1977.

Scott, B.C., and P.V. Hobbs, A theoretical study of the evolution of mixed-phase cumulus clouds, *J. Atmos. Sci.*, *34*, 812-826, 1977.

Scott, W.D., and P.V. Hobbs, The formation of sulfate in water droplets, *J. Atmos. Sci., 24,* 54-57, 1967.

Segal, Y., A. Khain, M. Pinsky and D. Rosenfeld, Effects of hygroscopic seeding on raindrop formation as seen from simulations using a 2000-bin spectral cloud parcel model, Atmospheric Research, 71, 3-34, 2004

Sehmel, G.A., Particle and gas dry deposition: A review, Atmospheric Environment - Part A General Topics, 14 (9), 983-1011, 1980.

Seifert, A. and K.D. Beheng, (2001): A double-moment parameterization for simulating autoconversion, accretion and self collection. *Atmos.~ Res*. **59-60**, 265-281, 2005.

Seifert, A. and K.D.Beheng, (2005a):A two-moment cloud microphysics parameterization for mixed-phase clouds. Part I: Model Description, *Meteorol. and Atmos. Phys.*, in press, 2005a.

Seifert, A. and K.D.Beheng, (2005b): A two-moment cloud microphysics parameterization for mixed-phase clouds. Part II: Maritime vs. continental deep convective storms, *Meteorol. and Atmos. Phys.*, in press, 2005b.

Seinfeld JH, Kahn RA, Anderson TL, et al., Scientific objectives, measurement needs, and challenges motivating the PARAGON aerosol initiative, Bullet. Amer. Meteor. Soc., 85, 1501-1508, 2004.

Seinfeld, J. H., and J. F. Pankow, Organic atmospheric particulate material, *Annual Review of Physical Chemistry*, *54*, 121-140, 2003.

Seinfeld, J. H., and S. N. Pandis (1998). *Atmospheric chemistry and physics: From air pollution to climate change*. New York: John Wiley, 1326 p.

Seinfeld, J.H., G.R. Carmichael, R. Arimoto, W.C. Conant, F.J. Brechtel, T.S. Bates, T.A. Cahill, A.D. Clarke, S.J. Doherty, P.J. Flatau, B.J. Huebert, J. Kim, K.M. Markowicz, P.K. Quinn, L.M. Russell, P.B. Russell, A. Shimizu, Y. Shinozuka, Y.T. C. H. Song, I. Uno, A.M. Vogelmann, R.J. Weber, J.-H. Woo, and X.Y. Zhang, ACE-ASIA: Regional Climatic and Atmospheric Chemical Effects of Asian Dust and Pollution, Bulletin of the American Meteorological Society, 85, 367-380, 2004.

Sekiguchi, M., T. Nakajima, K. Suzuki, K. Kawamoto, A. Higurashi, D. Rosenfeld, I. Sano, and S. Mukai, A study of the direct and indirect effects of aerosols using global satellite data sets of aerosol and cloud parameters, J. Geophys. Res., **108**, 4699, doi:10.1029/2002JD003359, 2003

Seliga, T. A., and V. N. Bringi, Potential use of the radar reflectivity at orthogonal polarizations for measuring precipitation, J. Appl. Meteor., 15, 69-76, 1976.

Semeena, V.S., and G. Lammel, The significance of the grasshopper effect on the atmospheric distribution of president organic substances, Geophys. Res. Lett., 32 (doi:10.1029/2004GL022229), 2005.

Seo, D.-J., J. P. Breidenbach, and E. R. Johnson, Real-time estimation of mean field bias in radar rainfall data. J. Hydrol. 223, 131-147, 1999.

Sevruk, B., *Methods of Correction for Systematic Error in Point Precipitation Measurement for Operational Use*. Operational Hydrology Report No. 21, WMO - No. 589, Secretariat of the WMO, Geneva, 35 pp, 1982.

Shantz, N. C., W. R. Leaitch, and P. F. Caffrey, Effect of organics of low solubility on the growth rate of cloud droplets, *J. Geophys. Res.*, *108*, 4168, doi:10.1029/2002JD002540, 2003.

Shaw, R.A., W. C. Reade, L.R. Collins, and J. Verlinde, Preferential concentration of cloud droplets by turbulence: Effects on the early evolution of cumulus cloud droplet spectra, *J. Atmos. Sci.*, *55*, 1965-1976, 1998.

Shepherd, J.M., and S.J. Burian, Detection of urban-induced rainfall anomalies in a major coastal city. *Earth Interactions, 7*, 1-17, 2003.

Sheppard, B. E., and P. I. Joe, Comparison of raindrop size distribution measurements by a Joss-Waldvogel disdrometer, a PMS

2DG spectrometer, and a POSS Doppler radar. J. Atmos. Oceanic Technol., 11, 874-887, 1994.

Sheppard, B. E., Effect of irregularities in the diameter classification of raindrops by Joss-Waldvogel disdrometer. J. Atmos. Oceanic Technol., 7, 180-183, 1990.

Sherwood, S. A microphysical connection among biomass burning, cumulus clouds, and stratospheric moisture, *Science*, *295*, 1272-1275, 2002.

Shimizu, A., N. Sugimoto, and I. Matsui, Lidar observations of aerosol vertical profiles in Thailand, in Autumn Meeting, Meteorological society of Japan, 2005.

Shinozuka, Y., A. D. Clarke, S. G. Howell, V. N. Kapustin, and B. J. Huebert, Sea-salt vertical profiles over the Southern and tropical Pacific oceans: Microphysics, optical properties, spatial variability, and variations with wind speed, *J. Geophys. Res.*, *109*, D24201, doi:10.1029/2004JD004975, 2004.

Shrestha, A. B., C. P. Wake, and J. E. Dibb, Chemical composition of aerosol and snow in the high Himalaya during the summer monsoon season, *Atmos. Environ.*, *31*, 2815-2826, 1997.

Shulman, M. L., M. C. Jacobson, R. J. Charlson, R. E. Synovec, and T. E. Young, Dissolution behavior and surface tension effects of organic compounds in nucleating cloud droplets, *Geophys. Res. Lett.*, *23*, 277-280, 1996.

Sicre, M. A., J. C. Marty, and A. Saliot, N-alkanes, fatty-acid esters, and fatty-acid salts in size fractionated aerosols collected over the Mediterranean Sea, *J. Geophys. Res.*, *95*, 3649-3657, 1990.

Sievering, H., The dry deposition of small particles: A review of experimental measurement, Atmospheric Environment, 23 (12), 2863-2864, 1989.

Sikdar, D.N., ATS-3 observed cloud brightness field related to a meso-to-subsynoptic scale rainfall pattern. Tellus, 22, 521-532, 1972.

Silverman, B. A., and M. Glass, A numerical simulation of warm cumulus clouds: Part I. parameterized vs. non-parameterized microphysics, *J. Atmos. Sci, 30,* 1620-1637, 1973.

Silverman, B.A., A critical assessment of glaciogenic seeding of convective clouds for rain enhancement, *Bull. Amer. Meteorol. Soc., 82*, 903–924, 2001.

Silverman, B.A., A critical assessment of hygroscopic seeding of convective clouds for rainfall enhancement, *Bull. Amer. Meteorol. Soc., 84,* 1219–1230, 2003.

Silverman, B.A., An independent statistical reevaluation of the South African hygroscopic flare seeding experiment, *J. Appl. Meteorol., 39*, 1373–1378, 2000.

Silverman, B.A., and W. Sukarnjanasat, Results of the Thailand warm-cloud hygroscopic particle seeding experiment, *J. Appl. Meteorol., 39*,1160–1175, 2000.

Silverman, B.A., Static mode seeding of summer cumuli-a review, in *Rainfall Enhancement—A Scientific Challenge, AMS Meteorol. Monogr., 21*, 7–24, Amer. Meteorol. Soc., Boston, Mass., 1986.

Simoneit, B. R. T., J. N. Cardoso, and N. Robinson, An assessment of the origin and composition of higher molecular weight organic matter in aerosols over Amazonia, *Chemosphere*, *21*, 1285-1301, 1990.

Simpson, J., and W.L. Woodley, Florida Area Cumulus Experiments 1970–1973 rainfall results, *Appl. Meteorol., 14*, 734–744, 1975.

Simpson, J., C. Kummerow, W.-K. Tao, and R.F. Adler, On the Tropical Rainfall Measuring Mission (TRMM) satellite. Meteorol. Atmos. Phys., **60**, 19-36, 1996.

Simpson, J., G.W. Brier, and R.H. Simpson, STORMFURY cumulus seeding experiment 1965: Statistical analysis and main results, *J. Atmos. Sci*., *24*, 508-521, 1967.

Simpson, J.S., Comment on "Field experimentation in weather modification," *J. Amer. Statist. Assoc., 74*, 95–97, 1979.

Singh, N., N.A. Sontakke, H.N. Singh, and A.K. Pandey, Recent trend in spatiotemporal variation of rainfall over India-an investigation into basin-scale rainfall fluctuations, in "Regional Hydrological Impacts of Climatic Change-Hydroclimatic Variability", IAHS Publ., 296, 273-282, 2005.

Sinha, P., P. V. Hobbs, R. J. Yokelson, D. R. Blake, S. Gao, and T. W. Kirchstetter, Distributions of trace gases and aerosols during the dry biomass burning season in southern Africa, *J. Geophys. Res.*, *108*, 4536, doi:10.1029/2003JD003691, 2003.

Sirois, A., and L.A. Barrie, Arctic lower tropospheric aerosol trends and composition at Alert, Canada: 1980-1995, Journal of Geophysical Research, 104 (D9), 11599-11618, 1999.

Slanina, J., H.M. ten Brink, R.P. Otjes, A. Even, P. Jongejan, A. Khlystov, A. Waijers-Ijpelaan, and M. Hu, The continuous analysis of nitrate and ammonium in aerosols by the steam jet aerosol collector (SJAC): extension and validation of the methodology, Atmos. Environ., 35, 2319-2330, 2001.

Slingo, A. and H. M. Schrecker, On the shortwave radiative properties of stratiform water clouds. *Quart. J. Roy. Meteor. Soc.*, *108*, 407-426, 1982.

Slinn, W.G.N., Precipitation scavenging, in Atmospheric Science and Power Production, edited by D. Randerson, pp. 466-532, Document DOE/TIC-27601, Technical Information Center, Office of Scientific and Technical Information, U.S. Department Of Energy, 1984.

Smith, D. M., M. S. Akhter, J. A. Jassim, C. A. Sergides, W. F. Welch, and A. R. Chughtai, Studies of the structure and reactivity of soot, *Aerosol Science and Technology*, *10*, 311-325, 1989.

Smith, E. A., J. Adams, P. Baptista, et al, Optimizing orbit-instrument configuration for the Global Precipitation Mission (GPM) satellite fleet, Proc. Int. Geosci. Remote Sens. Symp., 2001.

Smith, E.A, J.E. Lamm, R. Adler, J. Alishouse, K. Aonashi, E. Barrett, P. Bauer, W. Berg, A. Chang, R. Ferraro, J. Ferriday, S. Goodman, N. Grody, C. Kidd, D. Kniveton, C. Kummerow, G. Liu, F. Marano, A. Mugnai, W. Olson, G. Petty, A. Shibata, R. Spencer, F. Wentz, T. Wilheit, and E. Zipser, Results of the WetNet PIP-2 project, J. Atmos. Sci., 55, 1483–1536, 1998.

Smith, P.L., A.S. Dennis, B.A. Silverman, A.B. Super, E.W. Holroyd, W.A. Cooper, P.W. Mielke, K.J. Berry, H.D. Orville, and J.R. Miller, HIPLEX-1: Experimental design and response variables, *J. Clim. Appl. Meteorol., 23*, 497–512, 1984.

Smith, R. B., Q. Jiang, M. G. Fearon, P. Tabary, M. Dorninger, J. D. Doyle, and R. Beniot, Orographic precipitation and air mass transformation: An Alpine example. *Quart. J. Roy. Meteor. Soc*., *129*, 433-454, 2003.

Smith, R. B., Q. Jiang, M. G. Fearon, P. Tabary, M. Dorninger, J. D. Doyle, and R. Beniot, Orographic precipitation and air mass transformation: An Alpine example. *Quart. J. Roy. Meteorol. Soc*., *129*, 433-454, 2003.

Smith, S. J., H. Pitcher, and T. M. L. Wigley, Global and regional anthropogenic sulfur dioxide emissions, *Global Planet. Change*, *29*, 99-119, 2001.

Snider, J. R., and J. L. Brenguier, Cloud condensation nuclei and cloud droplet measurements during ACE-2, *Tellus*, *52B*, 828-842, 2000.

Snider, J. R., S. Guibert, and J. L. Brenguier, Aerosol Activation in Marine Stratocumulus Clouds, Part-II: Köhler and Parcel Theory Closure Studies, PACE Topical Issue, *J. Geophys. Res., 108*, No. D15, 862910.1029, 2003.

Snider, J.R., and J.L. Brenguier, Cloud condensation nuclei and cloud droplet measurements during ACE-2, *Tellus, 52B*, 828–842, 2000.

Sorooshian, S., K. Hsu, X. Gao, H.V. Gupta, B. Imam, and D. Braithwaite, Evaluation of PERSIANN system satellite-based estimates of tropical rainfall, Bulletin American Meteorology Society, 81, 2035-2046, 2000.

Soulage, G., Methods of measurement of ice nuclei concentrations. *Nubila, 6*, 43-47, 1964.

Spencer, R. W., D. W. Martin, B. Hinton, and J. A, Weinman, Satellite microwave radiances correlated with radar rain rates over land, Nature, 304, 141-143, 1983.

Spencer, R.W., D.W. Martin, B. Hinton and J.A. Weinman, Satellite microwave radiances coorelated with radar rain rates over land. Nature, 304, 141-143, 1983.

Squires, P., and S. Twomey, A comparison of cloud nucleus measurements over central North America and the Caribbean Sea, *J. Atmos. Sci., 23,* 401–404, 1966.

Squires, P., and T. Twomey, The relation between cloud drop numbers and the spectrum of cloud nuclei, In *Physics of Precipitation, Monograph. No. 5*, Amer. Geophys. Union., Washington, DC, 1961, 211–219.

Squires, P., The microstructure and colloidal stability of warm clouds. I. The relation between structure and stability, *Tellus, 10*, 256-271, 1958.

Stein, U. and P. Alpert, Factor separation in numerical simulations, *J. Atmos. Sci., 50*, 2107-2115, 1993.

Steiner, M., J.A. Smith, S.J. Burges, C.V. Alonso, and R.W. Darden, Effect of bias adjustment and raingauge data quality control on radar rainfall estimation, *Water Resour. Res.*, *35*, 2487–2503, 1999.

Steiner, M., T.L. Bell, Y. Zhang, and E.F. Wood, Comparison of two methods for estimating the sampling-related uncertainty of satellite rainfall averages based on a large radar dataset, *J. Climate*, *16*, 3759–3778, 2003.

Stepanov, A.S., Condensational growth of cloud droplets in a turbulent medium taking into account diabatic effects in the approximation of the smallness of the water content, *Akademiza Nauk SSSR, 11*, 267-277, 1975.

Stephens, G. L., Radiation profiles in extended water clouds. II: Parameterization schemes, J. Atmos. Sci., **35**, 2123-2132, 1978.

Stephens, G. L., et al., The Cloud-SAT mission and the A-Train. A new dimension of space-based observations of clouds and precipitation. *Bull. Amer. Meteorol. Soc.*, doi:10.1175/BAMS-83-12-1771, 1771-1790, 2002.

Stevens, B. and coauthors, Dynamics and chemistry of marine stratocumulus -DYCOMS-II, 2003, *Bull. Amer. Meteorol. Soc.*, *84***,** 579-593, 2003.

Stevens, B., G. Feingold, W.R. Cotton, and R.L. Walko, Elements of the microphysical structure of numerically simulated stratocumulus, *J. Atmos. Sci.*, *53***,** 980-1006, 1996.

Stevens, B., G. Vali, K. Comstock, R. Wood, M. C. vanZanten, P. H. Austin, C. S. Bretherton, and D. H. Lenschow, Pockets of open cells (POC) and drizzle in marine stratocumulus. *Bull. Amer. Meteor. Soc*., **86**, 51-57, 2005.

Stevens, B., W.R. Cotton, and G. Feingold, A critique of one- and two-dimensional models of boundary layer clouds with a binned representations of drop microphysics, *Atmos. Res*., *47-48*, 529-553, 1998.

Stevenson, C.M., An improved Millipore filter technique for measuring the concentrations of freezing nuclei in the atmosphere. Quart. J. Roy. Meteor. Soc. 94, 35-43, 1968.

Stier, P., J. Feichter, S. Kinne, S. Kloster, E. Vignati, J. Wilson, L. Ganzeveld, I. Tegen, M. Werner, Y. Balkanski, M. Schulz, O. Boucher, A. Minikin, and A. Petzold, The aerosol-climate model ECHAM5-HAM, *Atmos. Chem. Phys.*, *5*, 1125-1156, 2005a.

Stier, P., J. Feichter, S. Kloster, E. Vignati, and J. Wilson, Emission-induced nonlinearities in the global aerosol system: Results from the ECHAM5-HAM aerosol-climate model, *J. Clim.*, 2005b, submitted.

Stith, J. L., J. A. Haggerty, A. Heymsfield and C. A. Grainger: Microphysical characteristics of tropical updrafts in clean conditions. *J. Appl. Meteor.,* **43**, 779–794, 2004.

Stith, J.L., D.A. Burrows, P.J. DeMott, Initiation of ice: Comparison of numerical model results with observations of ice development in a cumulu cloud. *Atmos. Environ., 32,* 13-30, 1994.

Stith, J.L., L.F. Radke, and P.V. Hobbs, Particle emissions and the production of ozone and nitrogen oxides from the burning of forest slash, *Atmos. Environ., 15,* 73–82, 1981.

Stow, C. D., and K. Jones, A self evaluating disdrometer for the measurement of raindrop size and charge at the ground. J. Appl. Meteor., 20, 1160-1176, 1981.

Strangeways, I.C., Back to basics: the 'met. enclosure': Part 2(b)–Raingauges, their errors, Weather, 51, 298–303, 1996.

Strawbridge, K.B., and B.J. Snyder, Planetary boundary layer height determination during Pacific 2001 using the advantage of a scanning lidar instrument, Atmos Environ., 38 (34), 5861-5871, 2004.

Strawbridge, K.B., and R.M. Hoff, LITE validation experiment along California's coast: preliminary results, Geophysical Research Letters, 23 (1), 73-76, 1996.

Streets, D. G., and S. T. Waldhoff, Present and future emissions of air pollutants in China: SO_2, NO_x, and CO, *Atmos. Environ.*, *34*, 363-374, 2000.

Streets, D. G., K. F. Yarber, J.-H. Woo, and G. R. Carmichael, Biomass burning in Asia: Annual and seasonal estimates and atmospheric emissions, *Global Biogeochem. Cycles*, *17*, 1099, doi:10.1029/2003GB002040, 2003.

Streets, D. G., N. Y. Tsai, H. Akimoto, and K. Oka, Sulfur dioxide emissions in Asia in the period 1985-1997, *Atmos. Environ.*, *34*, 4413-4424, 2000.

Streets, D. G., S. Gupta, S. T. Waldhoff, M. Q. Wang, T. C. Bond, and B. Yiyun, Black carbon emissions in China, *Atmos. Environ.*, *35*, 4281-4296, 2001.

Streets, D. G., T. C. Bond, T. Lee, and C. Jang, On the future of carbonaceous aerosol emissions, *J. Geophys. Res.*, *109*, D24212, doi:10.1029/2004JD004902, 2004.

Strom, J., and S. Ohlsson, In situ measurements of enhanced crystal number densities in cirrus clouds caused by aircraft exhaust, *J. Geophys. Res.*, *103*, 11,355-11,361, 1998.

Sugimoto, I.M. N., and A. Shimizu, Measurement of water-cloud particle size with a dual-polarization pulsed bistatic lidar, Optical Review, 8 (6), 476-479, 2001.

Sullivan R. C., and K.A. Prather, Recent advances in our understanding of atmospheric chemistry and climate made possible by on-line aerosol analysis instrumentation Anal. Chem., **77**, 3861-3885, 2005.

Super, A. B. Further Exploratory Analysis of the Bridger Range Winter Cloud Seeding Experiment. *J. Appl. Meteorol.* 25(12),1926–1933, 1986.

Super, A. B., and J. A. Heimbach. Evaluation of the Bridger Range Winter Cloud Seeding Experiment Using Control Gages. *J. Appl. Meteorol*. 22(12):1989–2011, 1983.

Super, A. B., and J. A. Heimbach. Microphysical effects of wintertime cloud seeding with silver iodide over the Rocky Mountains. Part II: Observations over the Bridger Range, Montana. *J. Appl. Meteorol.* 27,1152-1165, 1988.

Svenningsson, B., J. Rissler, E. Swietlicki, M. M., M. Bilde, M. C. Facchini, S. Decesari, S. Fuzzi, J. Zhou, J. Monster, and T. Rosenorn, Hygroscopic growth and critical supersaturations for mixed aerosol particles of inorganic and organic compounds of atmospheric relevance, *Atmos. Chem. Phys. Discuss.*, *5*, 2833–2877, 2005.

Sverdrup, G. M., K. T. Whitby, and W. E. Clark, Characterization of California aerosols .2. Aerosol size distribution measurements in Mojave Desert, *Atmos. Environ.*, *9*, 483-494, 1975.

Swap, R.J., H.J. Annegarn, J.T. Suttles, M.D. King, S. Platnick, J.L. Privette, and R.J. Scholes, Africa burning: A thematic analysis of the Southern African Regional Science Initiative (SAFARI 2000), J. Geophys. Res., 108 (D13), 8465, doi:10.1029/2003JD003747, 2003.

Swap, R.J., M. Garstang, S.A. Macko, P.D. Tyson, W. Maenhaut, P. Artaxo, P. Kallberg, and R. Talbot., The Long Range Transport of Southern African Aerosols to the Tropical South Atlantic, Journal of Geophysical Research, 101, 23,777-23,791, 1996.

Szidat, S., T. M. Jenk, H.-A. Synal, M. Kalberer, L. Wacker, I. Hajdas, A. Kasper-Giebl, and U. Baltensperger, Contributions of fossil fuel, biomass burning, and biogenic emissions to carbonaceous aerosols in Zürich as traced by ^{14}C, *J. Geophys. Res.*, 2006, in press.

Szyrmer, W. and I. Zawadzki, Biogenic and Anthropogenic Sources of Ice-Forming Nuclei: A Review, Bull. Amer. Met. Soc., 78, 209-228, 1997.

Szyrmer, W., and I. Zawadzki, Biogenic and anthropogenic sources of ice-forming nuclei: A review, *Bull. Am. Meteorol. Soc.*, *78*, 209-228, 1997.

Tabazadeh, A., R.J. Yokelson, H.B. Singh, P.V. Hobbs, J.H. Crawford, and L.T. Iraci, 2004; Heterogeneous chemistry involving methanol in tropospheric clouds, *Geophys. Res. Lett., 31,* L06114, doi:10.1029/2003GL018775, 2004.

Takahashi, T., Hail in an axisymmetric cloud model, *J. Atmos. Sci*., *33*, 1579-1601, 1976.

Takemura, T., T. Nozawa, S. Emori, T. Y. Nakajima, and T. Nakajima, Simulation of climate response to aerosol direct and indirect effects with aerosol transport-radiation model, *J. Geophys. Res.*, 110, doi:10.1029/2004JD00502, 2005.

Talbot, R. W., M. O. Andreae, H. Berresheim, P. Artaxo, M. Garstang, R. C. Harriss, K. M. Beecher, and S. M. Li, Aerosol chemistry during the wet season in Central Amazonia: The influence of long-range transport, *J. Geophys. Res.*, *95*, 16,955-16,969, 1990.

Talbot, R. W., M. O. Andreae, T. W. Andreae, and R. C. Harriss, Regional aerosol chemistry of the Amazon Basin during the dry season, *J. Geophys. Res.*, *93*, 1499-1508, 1988.

Talbot, R.W., Andreae, M. O., Berresheim, H., Artaxo, P., Garstang, M., Harriss, R. C., Beecher, K. M., and Li, S. M.: Aerosols chemistry during the wet season in Central Amazonia: The influence of long-range transport, J. Geophys. Res., 95, 16 955–16 969, 1990.

Tang, I. N., and H. R. Munkelwitz, Water activities, densities, and refractive indices of aqueous sulfates and sodium nitrate droplets of atmospheric importance, *J. Geophys. Res.*, *99*, 18,801-18,808, 1994.

Tang, I. N., Thermodynamic and optical properties of mixed-salt aerosols of atmospheric importance, *J. Geophys. Res.*, *102*, 1883-1893, 1997.

Tanré, D., F. M. Bréon, J. L. Deuzé, et al., Global observation of anthropogenic aerosols from satellite, Geophys. Res. Lett**., 28**, 4555-4558, 2001.

Tanré, D., Y.J. Kaufman, M. Herman, and S. Mattoo, Remote sensing of aerosol over oceans from EOS-MODIS, *J. Geophys. Res., 102*, 16971–16988, 1997.

Taylor, J.P., and A. McHaffie, Measurements of cloud susceptibility, *J. Atmos. Sci., 51*, 1298–1306, 1994.

Tegen, I., M. Werner, S. P. Harrison, and K. E. Kohfeld, Relative importance of climate and land use in determining present and future global soil dust emission, *Geophys. Res. Lett.*, *31*, L05105, doi:10.1029/2003GL019216, 2004.

Tegen, I., Modeling the mineral dust aerosol cycle in the climate system, *Quaternary Science Reviews*, *22*, 1821-1834, 2003.

Tegen, I., P. Hollrig, M. Chin, I. Fung, D. Jacob, and J. Penner, Contribution of different aerosol species to the global aerosol extinction optical thickness: Estimates from model results, *J. Geophys. Res.*, *102*, 23,895-23,915, 1997.

Tegen, I., S. P. Harrison, K. Kohfeld, I. C. Prentice, M. Coe, and M. Heimann, Impact of vegetation and preferential source areas on global dust aerosol: Results from a model study, *J. Geophys. Res.*, *107*, 4576, doi:10.1029/2001JD000963, 2002.

Telford, J. W., A new aspect of coalescence theory. *J. Meteorol., 12*, 436-444, 1955.

Telford, J.W., and S.K. Chai, A new aspect of condensation theory, *Pageoph*, *118*, 720-742, 1980.

Telford, J.W., T.S. Keck, and S.K. Chai, Entrainment at cloud tops and the droplet spectra, *J. Atmos. Sci*., *41*, 3170-3179, 1984.

Teller, A. and Z. Levin, The effects of aerosols on precipitation and dimensions of subtropical clouds; a sensitivity study using a numerical cloud model, *Atmos. Chemistry and Phys.*, 6, 67-80, 2006.

ten Brink, H., W. Maenhaut, R. Hitzenberger, T. Gnauk, G. Spindler, A. Even, X. G. Chi, H. Bauer, H. Puxbaum, J. P. Putaud, J. Tursic, and A. Berner, INTERCOMP2000: the comparability of methods in use in Europe for measuring the carbon content of aerosol, *Atmos. Environ.*, *38*, 6507-6519, 2004.

Terblanche, D.E., F.E. Steffens, L. Fletcher, M.P. Mittermaier, and R.C. Parsons, Towards the operational application of hygroscopic flares for rainfall enhancement in South Africa, *J. Appl. Meteorol., 39,* 1811–1821, 2002.

Tervahattu, H., J. Juhanoja, and K. Kupiainen, Identification of an organic coating on marine aerosol particles by TOF-SIMS, *J. Geophys. Res.*, *107*, 4319, doi:10.1029/2001JD001403, 2002b.

Tervahattu, H., K. Hartonen, V. M. Kerminen, K. Kupiainen, P. Aarnio, T. Koskentalo, A. F. Tuck, and V. Vaida, New evidence of an organic layer on marine aerosols, *J. Geophys. Res.*, *107*, 4053, doi:10.1029/2000JD000282, 2002a.

Tesmer, J.R., and T.T. Wilheit, An improved microwave radiative transfer model for tropical oceanic precipitation, J. Atmos. Sci., 55, 1674–1688, 1998.

Textor, C., H.-F. Graf, C. Timmreck, and A. Robock, Emissions from volcanoes, in *Emissions of Atmospheric Trace Compounds*, edited by C. Granier, P. Artaxo, & C. E. Reeves, Kluwer, Dordrecht, 2004.

Textor, C., M. Schulz, et al., Analysis and quantification of the diversities of aerosol life cycles within AeroCom, *Atmos. Chem. Phys. Discuss.*, *5*, 8331-8420, 2005.

Textor, C., M. Schulz, S. Kinne, S. Guibert, B. Y., S.E. Bauer, T. Berntsen, T. Berglen, O. Boucher, M. Chin, F. Dentener, T. Diehl, R. Easter, H. Feichter, D. Fillmore, S. Ghan, P. Ginoux, S. Gong, A. Grini, J. Hendricks, L. Horowitz, P. Huang, I. Isaksen, T. Iversen, A. Kirkev?g, S. Kloster, D. Koch, E. Kristjansson, M. Krol, A. Lauer, J.F. Lamarque, X. Liu, V. Montanaro, G. Myhre, J. Penner, G. Pitari, S. Reddy, ?. Seland, P. Stier, T. Takemura, and X. Tie, Analysis and quantification of the diversities of aerosol life cycles within AeroCom, Atmos. Chem. Phys. Discuss., 5, 8331-8420, 2005.

Thiessen, A.H., Precipitation averages for large areas, *Mon. Wea. Rev*., *39*, 1082–1084, 1911.

Timothy M. VanReken, T.M., Cloud condensation nucleus activation properties of biogenic secondary organic aerosol. *J. Geophys. Res.* 110, D07206, doi:10.1029/2004JD005465, 2005.

Tobias, H.J., and P.J. Ziemann, Thermal Desorption Mass Spectrometric Analysis of Organic Aerosol Formed from Reactions of 1-Tetradecene and O3 in the Presence of Alcohols and Carboxylic Acids, Environmental Science and Technology, 34 (11), 2105-2115, 2000.

Tokay, A., A. Kruger, and W. Krajewski, Comparison of drop-size distribution measurements by impact and optical disdrometers, J. Appl. Meteor., 40, 2083-2097, 2001.

Tokay, A., and D. A. Short, Evidence from tropical raindrop spectra of the origin of rain from stratiform versus convective clouds. J. Appl. Meteor., 35, 355-371. 1996.

Tompkins, A.M., C. Cardinali, J.-J. Morcrette, and M. Rodwell, Influence of aerosol climatology on forecasts of the African Easterly Jet, Geophysical Research Letters, 32, L10801, doi:10.1029/2004GL022189, 2005.

Toon, O. B., R.P. Turco, D. Westphal, R. Malone, and M. Liu, A multidimensional model for aerosols: description of computational analogs, *J. Atmos. Sci., 45*, 2123-2144, 1988.

Torres, O., P.K. Bhartia, J.R. Herman, A. Sinyuk, P. Ginoux, and B. Holben, A Long-term record of aerosol optical depth from TOMS observations and comparison to AERONET measurements. *J. Atmos. Sci., 59*, 398-413, 2002.

Tørseth, K., L. Tarrasǿn, and M. Amann, Transboundary Particulate Matter in Europe:, in EMEP Report 5/2002, 2002.

Tørseth, K., Transboundary Particulate Matter in Europe, in EMEP Report, 2004.

Trenberth, K. E., D. P. Stepaniak, and J. M. Caron, The global monsoon as seen through the divergent atmosphere circulation. *J. Climate*, **13**, 3969-3993, 2000.

Trochkine, D., Y. Iwasaka, A. Matsuki, M. Yamada, Y. S. Kim, T. Nagatani, D. Zhang, G. Y. Shi, and Z. Shen, Mineral aerosol particles collected in Dunhuang, China, and their comparison with chemically modified particles collected over Japan, *J. Geophys. Res.*, *108*, 8642, doi:10.1029/2002JD003268, 2003.

Tsai, F., T.-H. Liu, S.C. Liu, T.-Y. Chen, T.L. Anderson, and S.J. Masonis, Model simulation and analysis of coarse and fine particle distributions during ACE-Asia, J. Geophys. Res., 109, D19S20, doi:10.1029/2003JD003665, 2004.

Tsigaridis, K., and M. Kanakidou, Global modelling of secondary organic aerosol in the troposphere: a sensitivity analysis, *Atmos. Chem. Phys.*, *3*, 1849-1869, 2003.

Tsigaridis, K., J. Lathière, M. Kanakidou, and D. A. Hauglustaine, Naturally driven variability in the global secondary organic aerosol over a decade, *Atmos. Chem. Phys. Discuss.*, *5*, 1255-1283, 2005.

Tukey, J.W., D.R. Brillinger, and L. V. Jones, *Report of the Statistical Task Force to the Weather Modification Advisory Board, Vol. II*, U.S. Government Printing Office, pE-3, 1978b.

Tukey, J.W., L.V. Jones, and D.R. Brillinger, *The Management of Weather Resources, Vol. I, Proposals for a National Policy and Program*, Report of the Statistical Task Force to the Weather Modification Advisory Board, Government Printing Office, 118 pp., 1978a.

Turekian, V. C., S. A. Macko, and W. C. Keene, Concentrations, isotopic compositions, and sources of size-resolved, particulate organic carbon and oxalate in near-surface marine air at Bermuda during spring, *J. Geophys. Res.*, *108*, 4157, doi:10.1029/2002JD002053, 2003.

Turk, F. J., E. E. Ebert, H. J. Oh, B. J. Sohn, V. Levizzani, E. A. Smith, and R. R. Ferraro, Validation of an operational global precipitation analysis at short time scales. 12th AMS Conf. Satellite Meteorology and Oceanography, 9-13 February, Long Beach, CA, 2003.

Turpin, B. J., and H.-J. Lim, Species contributions to PM2.5 mass concentrations: Revisiting common assumptions for estimating organic mass, *Aerosol Science and Technology*, *35*, 602-610, 2001.

Turpin, B.J., P. Saxena, and E. Andrews, Measuring and simulating particulate organics in the atmosphere: problems and

prospects, Atmospheric Environment, 34 (18), 2983?3013, 2000.

Tustison, B., D. Harris, and E. Foufoula-Georgiou, Scale issues in verification of precipitation forecasts, *J. Geophys. Res*., *106*, 11,775-11,784, 2001.

Tustison, B., D. Harris, and E. Foufoula-Georgiou, Scale issues in verification of precipitation forecasts, J. Geophys. Res., 106, 11,775-11,784, 2001.

Twomey S. and T.A. Wojciechowski, Observations of the geographical variation of cloud nuclei. J. Atmos. Sci., 26, 648-651, 1969.

Twomey S., and T. Cocks, Remote sensing of cloud parameters from spectral reflectance measurements in the near-infrared. Beitr. Phys. Atmos., 62, 172-179, 1989.

Twomey S., The influence of pollution on the shortwave albedo of clouds. *J. Atmos. Sci., 34*, 1149-1152, 1977.

Twomey, S., Pollution and the planetary albedo, *Atmos. Environ*., **8**, 1251-1256, 1974.

Twomey, S., Aerosols, clouds and radiation, *Atmos. Environ*., *25A*, 2435-2442, 1991.

Twomey, S., and J. Warner, Comparison of measurements of cloud droplets and cloud nuclei, *J. Atmos. Sci., 24,* 702–703, 1967.

Twomey, S., and K.A. Davidson, Automatic observations of cloud nucleus concentration, *J. Atmos. Sci., 27,* 1056–1059, 1970.

Twomey, S., and K.A. Davidson, Automatic observations of cloud nuclei, September 1969–August 1970, *J. Atmos. Sci., 28,* 1295–1296, 1972.

Twomey, S., and T.A. Wocjiechowski, Observations of the geographical variation of cloud nuclei, *J. Atmos. Sci., 26,* 684–688, 1969.

Twomey, S., Composition of cloud nuclei, *J. Atmos. Sci.*, *28*, 377-381, 1971.

Twomey, S., On the composition of cloud nuclei in the northeastern United States, *J. de Rech. Atmos., 3*, 281-285, 1968.

Twomey, S., On the nature and origin of natural cloud nuclei, *Bull. Obs. de Puy de Dome, 1,* 1–5, 1960.

Twomey, S., Pollution and the planetary albedo, *Atmos. Environ., 8,* 1251–1256, 1974.

Twomey, S., The composition of cloud nuclei, *Journal of the Atmospheric Sciences*: *28*, 377–381, 1971.

Tzivion, S., G. Feingold and Z. Levin, An efficient numerical solution to the stochastic collection equation, *J. Atmos. Sci., 44*, 3139-3149, 1987.

U.S. CLIVAR Pan American Implementation Panel, *U.S. CLIVAR Pan American Research: A Scientific Prospectus and Implementation Plan,* U.S. CLIVAR Office, Washington, DC, 58 pp., 2002.

Ulbrich, C. W., Natural variations in the analytical form of the raindrop size distribution. *J. Climate Appl. Meteor*., 22, 1764-1775, 1983.

Usher, C.R., C.A. Cleveland Jr., D.R. Strongin, and M.A. Schoonen, Reactions on Mineral Dust, *Chemical Reviews,* 103 (12), 4883-4939, 2003.

Vali, G., Atmospheric ice nucleation -- a review. *J. Rech. Atmos.*, 19, 105-115, 1985.

Vali, G., Nucleation terminology, *Bull. Amer. Meteorol. Soc., 66,* 1426–1427, 1985.

Van den Heever, S.C., and W.R. Cotton, The impact of hail size on simulated supercell storms. *J. Atmos. Sci*., *61*, 1596-1609, 2004.

Van den Heever, S.C., G. G. Carrio, W.R. Cotton, P. J. DeMott and A. J. Prenni, Impacts of nucleating aerosol on Florida convection. Part I: Mesoscale simulations, *J. Atmos. Sci.,* in press, 2005.

Van der Werf, G. R., J. T. Randerson, J. Collatz, and L. Giglio, Carbon emissions from fires in tropical and subtropical ecosystems, *Global Change Biology*, *9*, 547-562, 2003.

Van Dingenen, R., F. Raes, et al., A European aerosol phenomenology-1: physical characteristics of particulate matter at kerbside, urban, rural and background sites in Europe, *Atmos. Environ.*, *38*, 2561-2577, 2004.

Van Grieken, R., C. Xhoffer, L. Wouters, P. Artaxo, Micro-analysis techniques for the characterization of individual environmental particles. *Analytical Sciences*, 7, 1117-1122, 1991.

van Loon, H., and J.C. Rogers, The seesaw in winter temperatures between Greenland and northern Europe. Part I: General Description. *Mon. Wea. Rev.*, *106*, 296-310, 1978.

Vanbauce, C., B. Cadet, and R. T. Marchand, Comparison of POLDER apparent and corrected oxygen pressure to ARM/MMCR cloud boundary pressures, *Geophys. Res. Lett.*, **30**, 1212, 2003.

Vanbauce, C., J. C. Buriez, F. Parol, B. Bonnel, G. Seze G, and P. Couvert, Apparent pressure derived from ADEOS-POLDER observations in the oxygen A-band over ocean, Geophys. Res. Lett., **25**, 3159-3162, 1998.

VanReken, T. M., T. A. Rissman, G. C. Roberts, V. Varutbangkul, H. H. Jonsson, R. C. Flagan, and J. H. Seinfeld, Toward aerosol/cloud condensation nuclei (CCN) closure during CRYSTAL-FACE, *J. Geophys. Res.*, *108*, 2003.

Vardiman, L., The generation of secondary ice particles in cloud crystal-crystal collisions, *J. Atmos. Sci., 35*, 2168–2180, 1978.

Veefkind, J. P., G. de Leeuw, and P. A. Durkee, Retrieval of aerosol optical depth over land using two-angle view satellite radiometry during TARFOX, *Geophys. Res. Lett*., **25**, 3135-3138, 1998.

Venkataraman, C., C.K. Reddy, S. Josson, and M.S. Reddy, Aerosol size and chemical characteristics at Mumbai, India, during the INDOEX-IFP (1999), *Atmospheric Environment,* 36 (12), 1979-1991, 2002.

Verlinde, J., P.J. Flatau, and W.R. Cotton, Analytical solutions to the collection growth equation: Comparison with approximate methods and application to cloud microphysics parameterization schemes, *J. Atmos. Sci.*, *47*, 2871-2880, 1990.

Vermote, E. and Y.J. Kaufman, 1995: Absolute Calibration of AVHRR Visible and Near Infrared Channels Using Ocean and Cloud Views. *Int. J. Rem. Sens.* , **16**, 2317-2340.

Vet, R.J., J.R. Brook, T.F. Dann, and J. Dion, The Nature of PM2.5 Mass, Composition and Precursors in Canada, in Precursor Contributions to Ambient Fine aprticulate Matter in Canada, Meteorogical Service of Canada, Toronto, 2001.

Vignati, E., G. de Leeuw, and R. Berkowicz, Modeling coastal aerosol transport and effects of surf-produced aerosols on processes in the marine atmospheric boundary layer, *J. Geophys. Res.*, *106*, 20,225-20,238, 2001.

Wadhams, P., Ice thickness in the Arctic Ocean: The statistical reliability of experimental data, *J. Geophys. Res. -Oceans,* 102

(C13), 27951-27959, 1997.

Waldvogel, A., The N_0 jump of raindrop spectra. *J. Atmos. Sci.*, 31, 1068-1078, 1974.

Walko, R.L, W.R. Cotton, J.L. Harrington, and M.P. Meyers, New RAMS cloud microphysics parameterization. Part I: The single-moment scheme, *Atmos. Res.*, *38*, 29-62, 1995.

Wallace, J.M., and P.V. Hobbs, *Atmospheric Science: An Introductory Survey,* 2nd Edition, Academic Press, 2006.

Wang, C., A modeling study on the climate impacts of black carbon aerosols, *J. Geophys. Res., 109*, D03106, doi:10.1029/2003JD004084, 2004.

Wang, M.Y., and J.E. Overland, Detecting arctic climate change using Koppen climate classification, Climatic Change, 67 (1), 43-62, 2004.

Warburton, J. A., S. K. Chai, and L. G. Young. A new concept for assessing silver iodide cloud seeding effects in snow by physical and chemical methods. *Atmos. Res.* 36:171-176, 1995.

Warner, J., A reduction in rainfall associated with smoke from sugarcane fires-An inadvertent weather modification?, *J. Appl. Meteor., 7*, 247–251, 1968.

Warner, J., A reduction of rain associated with smoke from sugar-cane fires—An inadvertent weather modification, *J. App. Meteorol., 7,* 247–251, 1968.

Warner, J., and S. Twomey, The production of cloud nuclei by cane fires and the effect on cloud droplet concentration, *J. Atmos. Sci., 24*, 704–706, 1967.

Warner, J., The micro-structure of cumulus clouds. I. General features of the droplet spectrum. *J. Atmos. Sci*., *26*, 1049-1059, 1969.

Warren, S.G., C.J. Hahn, J. London, R.M. Chervine and R.L. Jenne, Global distribution of total cloud cover and cloud type amounts over land. *NCAR Technical Note*, NCAR/TN-273+STR, 29 pp, 1986a.

Warren, S.G., C.J. Hahn, J. London, R.M. Chervine and R.L. Jenne, Global distribution of total cloud cover and cloud type amounts over ocean. *NCAR Technical Note*, NCAR/TN-317+STR, 42 pp, 1986b.

National Research Council of the National Academy of Sciences, *Critical Issues in Weather Modification Research*, Board on Atmospheric Sciences and Climate, Division on Earth and Life Studies, National Research Council of the National Academy of Sciences, The National Academy Press, 123pp., 2003.

Weber, R. J., P. H. McMurry, L. Mauldin, D. J. Tanner, F. L. Eisele, F. J. Brechtel, S. M. Kreidenweis, G. L. Kok, R. D. Schillawski, and D. Baumgardner, A study of new particle formation and growth involving biogenic and trace gas species measured during ACE 1, *J. Geophys. Res.*, *103*, 16385-16396, 1998.

Wegener, A., *Thermodynamik der Atmosphäre,* J. A. Barth, Leipzig, 1911.

Wehrli, C., Calibration of filter radiometers for determination of atmospheric optical depth, Metrologia, 37, 419-422, 2000

Weingartner, E., H. Burtscher, and U. Baltensperger, Hygroscopic properties of carbon and diesel soot particles, *Atmos. Environ.*, *31*, 2311-2327, 1997.

Weingartner, E., M. Gysel, and U. Baltensperger, Hygroscopicity of aerosol particles at low temperatures. 1. New low-temperature H-TDMA instrument: Setup and first applications, *Environ. Sci. Technol.*, *36*, 55-62, 2002.

Weingartner, E., S. Nyeki, and U. Baltensperger, Seasonal and diurnal variation of aerosol size distributions ($10 < D < 750$ nm) at a high-alpine site (Jungfraujoch 3580 m asl), *J. Geophys. Res.*, *104*, 26,809-26,820, 1999.

Welch, H.E., D.C.G. Muir, B.N. Billeck, W.L. Lockhart, G.J. Brunskill, H.J. Kling, M.P. Olson, and R. M. Lemoine, Brown snow: A long range transport event in the Canadian Arctic, Environ. Sci. Technol., 25, 280?286, 1991.

Weller, R.A., F. Bradley, and R. Lukas, The interface or air-sea flux component of the TOGA Coupled Ocean-Atmosphere Response Experiment and its impact on subsequent air-sea interaction studies, J. Atmos. Ocean. Tech., 21, 223–257, 2004.

Wen, C.-S., Effects of the correlative time of the fluctuating force field on the random growth of cloud droplets, *Scientia Senica*, *15*, 870-879, 1966.

Werner, M., I. Tegen, S. P. Harrison, K. E. Kohfeld, I. C. Prentice, Y. Balkanski, H. Rodhe, and C. Roelandt, Seasonal and interannual variability of the mineral dust cycle under present and glacial climate conditions, *J. Geophys. Res.*, *107*, 4744, doi:10.1029/2002JD002365, 2002.

Wesely, M.L., and B.B. Hicks, A review of the current status of knowledge on dry deposition, Atmospheric Environment, 34 (12-14), 2261-2282, 2000.

Wetzel M.A, L.L. Stowe LL, Satellite-observed patterns in stratus microphysics, aerosol optical thickness, and shortwave radiative forcing. J. Geophys. Res. –Atmos. 104 (D24): 31287-31299, 1999.

Wexler, A. S., and J. H. Seinfeld, Second-generation inorganic aerosol model, *Atmos. Environ.*, *25A*, 2731-2748, 1991.

Weymouth, G., G. A. Mills, D. Jones, E. E. Ebert, and M. J. Manton, A continental-scale daily rainfall analysis system, Aust. Met. Mag., 48, 169-179, 1999.

Whelpdale, D.M. and R. List, The coalescence process of raindrop growth, *J. Geophys. Res., 76*, 2836-2856, 1971.

Whitby, E.R., and P.H. McMurry, Modal aerosol dynamics modeling, Aerosol Sci. Technol, 27, 673-688, 1997.

Whitby, K. T., B. Y. H. Liu, and R. B. Husar, Aerosol size distribution of Los Angeles smog, *Journal of Colloid and Interface Science*, *39*, 177-204, 1972.

Whitby, K. T., Physical characteristics of sulfur aerosols, *Atmos. Environ.*, *12*, 135-159, 1978.

Whitby, K. T., W. E. Clark, V. A. Marple, G. M. Sverdrup, G. J. Sem, K. Willeke, B. Y. H. Liu, and D. Y. H. Pui, Characterization of California aerosols .1. Size distributions of freeway aerosol, *Atmos. Environ.*, *9*, 463-482, 1975.

Whitby, K.T., The physical characteristics of sulfur aerosols, Atmos. Environ., 12, 135-159, 1978.

Whiteaker, J., D. Suess, and K. Prather, Effects of meteorological conditions on aerosol composition and mixing state in Bakersfield, CA, Env. Sci. & Tech., 36 (11), 2345-2353, 2002.

Whiteman, D. N., Examination of the traditional Raman lidar technique. I. Evaluating the temperature-dependent lidar equations, Appl. Opt., 42, 2571-2593, 2003.

Wiedensohler, A., and D. S. Covert, Number concentrations and size distributions of atmospheric aerosol under baseline condition at Cape Grim, *J. Aerosol Sci.*, *27*, S99-S100, 1996.

Wieland, W., Die Wasserdampfkondensation an naturlichen Aerosol bei geingen Übersaffigungen, *Z. Angew. Math. Physics, 7,* 428–436, 1956.

Wilheit, T.T., Some comments on passive microwave measurement of rain, Bull. Amer. Meteor. Soc., 67, 1226–1232, 1986.

Williams, K.D., A. Jones, D.L. Roberts, C.A. Senior, and M.J. Woodage, The response of the climate system to the indirect effects of anthropogenic sulfate aerosol, *Clim. Dyn*., *17*, 845-856, 2001.

Williams, R.M., A model for the dry deposition of particles to natural water surfaces, Atmospheric Environment - Part A General Topics, 16 (8), 1933-1938, 1982.

Wilson, J.W., and E. A. Brandes, Radar measurement of rainfall -a summary. Bull. Amer. Meteor. Soc. 60, 1048-1058, 1979.

Winker, D. M., et al., "The CALIPSO mission: Spaceborne lidar for observation of aerosols and clouds," Proc. SPIE, vol. 4893, pp. 1-11, 2003.

Winker, D. M., Hunt, W. H. and Hostetler, C. A., Status and Performance of the CALIOP Lidar. Proc. SPIE, 5575, pp. 8-15, 2004.

Winker, D.M., and C.R. Trepte, Laminar cirrus observed near the tropical tropopause by LITE, Geophys. Res. Lett., 25, 3351-3354, 1998.

Winker, D.M., J. Pelon, and M.P. McCormick, The CALIPSO mission: Spaceborne lidar for observation of aerosols and clouds, in SPIE Asia-Pacific Sym. On Rem. Sen. Of the Atmosphere, Environment and Space, Hangzhou, China, 2002.

Wise, M. E., J. D. Surratt, D. B. Curtis, J. E. Shilling, and M. A. Tolbert, Hygroscopic growth of ammonium sulfate/dicarboxylic acids, *J. Geophys. Res.*, *108*, 4638, doi:10.1029/2003JD003775, 2003.

WMO (World Meteorological Organization), *Statement on Planned and Inadvertent Weather Modification*, World Meteorological Organization, Geneva, 1992.

WMO, GAW Aerosol Measurement Procedures, Guidelines and Recommendations, GAW Report No. 153, Geneva, 2003

WMO, WMO/GAW Experts Workshop on a Global Surface Based Network for Long Term Observations of Column Aerosol Optical Properties, U. Baltensperger, L. Barrie, C. Wehrli, eds, GAW Report No. 162, Geneva, 2005.

Wolf, M. E., and G. M. Hidy, Aerosols and climate: Anthropogenic emissions and trends for 50 years, *J. Geophys. Res.*, *102*, 11,113-11,121, 1997.

Woodcock, A.H., and R.H. Jones, Rainfall trends in Hawaii, *J. Appl. Meteorol., 9,* 690–695, 1970.

Woodcock, A.H., R.A. Duce, and J.L. Moyers, Salt particles and raindrops in Hawaii, *J. Atmos. Sci.*, *28*, 1252-1257. 1971.

Woodcock, A.H., Salt nuclei in marine air as a function of altitude and wind force, *J. Meteorol.*, *10*, 362-371, 1953.

Woodley W. L., D. Rosenfeld, and B. A. Silverman. Results of on-top glaciogenic cloud seeding in Thailand. Part I: The demonstration experiment, *J. Appl. Meteorol.* 42:920-938, 2003a.

Woodley W. L., D. Rosenfeld, and B. A. Silverman. Results of on-top glaciogenic cloud seeding in Thailand. Part II: Exploratory analyses. *J. Appl. Meteorol.* 42:939-951, 2003b.

Woodley, W.L., A. Barnston, J.A. Flueck, and R. Biondini, The Florida Area Cumulus Experiment's second phase (FACE-2). Part II: replicated and confirmatory analyses, *J. Appl. Meteorol.*, *22*, 1529–1540, 1983.

Woodley, W.L., and D. Rosenfeld, The development and testing of a new method to evaluate the operational cloud-seeding programs in Texas, *J. Appl. Meteorol.*, *43,* 249–263, 2004.

Woodley, W.L., B. Jordan, A. Barnston, J. Simpson, R. Biondini, and J.A. Flueck, Rainfall results of the Florida Area Cumulus Experiment, 1970–76, *J. Appl. Meteorol., 21*, 139–164, 1982.

Woodley, W.L., Comments on "A new look at the Israeli cloud seeding experiments," *J. Appl. Meteorol., 36*, 250–252, 1997.

World Meteorological Organization (WMO), Report of the WMO workshop on hygroscopic seeding, *WMP Report No. 35, World Meteorological Organization*, WMO/TD No. 1006, Geneva, Switzerland, 68pp, 2000.

Wurtele, Z., Analysis of the Israeli cloud seeding experiment by means of concomitant meteorological variables, *J. Appl. Meteorol., 10*, 1185–1192, 1971.

Wurzler, S., T. G. Reisin, and Z. Levin, Modification of mineral dust particles by cloud processing and subsequent effects on drop size distributions, *J. Geophys. Res., 105*, 4501-4512, 2000.

Xie, P., and P.A. Arkin, Global precipitation: A 17-year monthly analysis based on gauge observations, satellite estimates, and numerical model outputs, Bull. Amer. Meteor. Soc., 78, 2539–2558, 1997.

Xue, H., and G. Feingold, Large eddy simulations of trade-wind cumuli: Investigation of aerosol indirect effects. *J. Atmos. Sci.*, in press, 2006.

Yang, D., B. E. Goodison, J. R. Metcalfe, V. S. Golubev, R. Bates, T. Pangburn, and C. L. Hanson, Accuracy of NWS 8" Standard Nonrecording Precipitation Gauge: Results and Application of WMO Intercomparison, *J. Oceanic Atmos. Tech*., *15*, 54-68, 1998.

Yankofsky, S., Z. Levin, T. Bertold, and N. Sandlerman, Some basic characteristics of bacterial freezing nuclei, *J. Appl. Meteorol., 20,* 1013–1019, 1981.

Yevich, R., and J. A. Logan, An assessment of biofuel use and burning of agricultural waste in the developing world, *Global Biogeochem. Cycles*, *17*, 1095, doi:10.1029/2002GB001952, 2003.

Yienger, J.J., M. Galanter, T.A. Holloway, M.J. Phandnis, S.K. Guttikunda, G.R. Carmichael, W.J. Moxim, and H.L. II, The episodic nature of air pollution transport from Asia to North America, J. Geophys. Res., 105, 26,931- 26,945, 2000.

Yin, Y., K.S. Carslaw, and G. Feingold, Vertical transport and processing of aerosols in a mixed-phase convective cloud and the feedback on cloud development, *Quart. J. Roy. Meteorol. Soc.*, *131*, no. 605, 221-245, 2005.

Yin, Y., S. Wurzler, Z. Levin, and T. G. Reisin, Interactions of mineral dust particles and clouds: Effects on precipitation and cloud optical properties, *J. Geophys. Res.*, *107*, 4724, doi:10.1029/2001JD001544, 2002.

Yin, Y., Z. Levin, T. G. Reisin and S. Tzivion: Seeding convective clouds with hygroscopic flares; Numerical simulations using a cloud model with detailed microphysics. *J. Appl. Meteorol.*, 39, 1460-1472, 2000b.

Yin, Y., Z. Levin, T. G. Reisin, and S. Tzivion, The effects of giant condensation nuclei on the development of precipitation in convective clouds – a numerical study. *Atmos. Res., 53*, 91-116, 2000a.

Yin, Y., Z. Levin, T. G. Reisin, and S. Tzivion. On the response of radar-derived properties to hygroscopic flare seeding. *J. Appl. Meteorol.* 40:1654-1661, 2001.

Young, K.C., *Microphysical Processes in Clouds*, Oxford University Press, New York, 335–336, 1993.

Young, K.C., Weather modification—A theoretician's viewpoint, *Bull. Amer. Meteorol. Soc., 77*, 2701–2710, 1996.

Yuter, S. E., and R. A. Houze, Jr., The natural variability of precipitating clouds over the western Pacific warm pool, *Quart. J. Roy. Met. Soc., 124*, 53-99, 1998.

Yuter, S. E., and W. S. Parker, Rain measurement on ship revisited: the 1997 PACS TEPPS cruise, J. Appl. Meteor., 40, 1003-1018, 2001.

Yuter, S.E., Precipitation Radar, in Encycl. Atmos. Sci., edited by J. Holton, J. Pyle, and J. Curry, Academic Press, London, U.K., 1833-1852, 2002.

Zappoli, S., A. Andracchio, S. Fuzzi, M. C. Facchini, A. Gelencser, G. Kiss, Z. Krivacsy, A. Molnar, E. Meszaros, H.-C. Hansson, K. Rosman, and Y. Zebühr, Inorganic, organic and macromolecular components of fine aerosol in different areas of Europe in relation to their water solubility, *Atmos. Environ.*, *33*, 2733-2743, 1999.

Zawadzki, I., and A. Bellon, Error statistics of VPR correction in stratiform precipitation, Preprints, 31st Conf. Radar Meteor., Seattle, Wash., Amer. Meteor. Soc., 225–228, 2003.

Zender, C. S., H. S. Bian, and D. Newman, Mineral Dust Entrainment and Deposition (DEAD) model: Description and 1990s dust climatology, *J. Geophys. Res.*, *108*, 4416, doi:10.1029/2002JD002775, 2003.

Zender, C. S., R. L. Miller, and I. Tegen, Quantifying mineral dust mass budgets: Terminology, constraints, and current estimates, *Eos Trans. AGU*, *85*, 509&512, 2004.

Zhai, P., X. Zhang, H. Wan, and Z. Pan, Trends in Total Precipitation and Frequency of Daily Precipitation Extremes over China, J. of Climate, 18, 10961108, 2005.

Zhang, J., U. Lohmann, and P. Stier, A microphysical parameterization for convective clouds in the ECHAM5 Climate Model: 1. Single column model results evaluated at the Oklahoma RM site. *J. Geophys. Res*., *110*, D15S07, doi:10.1029/2004JD005128., 2005.

Zhang, L., D.V. Michelangeli, and P.A. Taylor, Numerical studies of aerosol scavenging by low-level, warm stratiform clouds and precipitation, Atmospheric Environment, 38 (28), 4653-4665, 2004.

Zhang, L., S.-L. Gong, J. Padro, and L. Barrie, A Size-segregated Particle Dry Deposition Scheme for an Atmospheric Aerosol Module, Atmos. Environ., 35 (3), 549-560, 2001.

Zhang, Q., C. O. Stanier, M. R. Canagaratna, J. T. Jayne, D. R. Worsnop, S. N. Pandis, and J. L. Jimenez, Insights into the chemistry of new particle formation and growth events in Pittsburgh based on aerosol mass spectrometry, *Environ. Sci. Technol.*, *38*, 4797-4809, 2004a.

Zhang, X.Y., Y.Q. Wang, D. Wang, S.L. Gong, R. Arimoto, L.J. Mao, and J. Li, Characterization and Sources of Regional-scale Transported Carbonaceous and Dust aerosols from different pathways in costal and sandy land areas of China, J. Geophys. Res., 110 (D15), doi: 10.1029/2004JD005457, 2005.

Zhang, Y. H., X. L. Zhu, S. Slanina, M. Shao, L. M. Zeng, M. Hu, M. Bergin, and L. Salmon, Aerosol pollution in some Chinese cities (IUPAC Technical Report), *Pure and Applied Chemistry*, *76*, 1227-1239, 2004b.

Zhao, T.L., S.L. Gong, X.Y. Zhang, and I.G. McKendry, Modelled size-segregated wet and dry deposition budgets of soil dust aerosol during ACE-Asia, 2001: Implications for Trans-Pacific Transport, Journal of Geophysical Research, 108 (D23), 8665, doi:10.1029/2002JD003363, 2003.

Zhao, T.L., S.L. Gong, X.Y. Zhang, J.-P. Blanchet, I.G. McKendry, and Z.J. Zhou, A Simulated Climatology of Asian Dust Aerosol and its Trans-Pacific Transport 1. Mean climate and validation, Journal of Climate, 19 (1), 88-103, 2006.

Zhou, J. C., E. Swietlicki, O. H. Berg, P. P. Aalto, K. Hameri, E. D. Nilsson, and C. Leck, Hygroscopic properties of aerosol particles over the central Arctic Ocean during summer, *J. Geophys. Res.*, *106*, 32111-32123, 2001.

Zuberi, B., K. S. Johnson, G. K. Aleks, L. T. Molina, and A. Laskin, Hydrophilic properties of aged soot, *Geophys. Res. Lett.*, *32*, doi:10.1029/2004GL021496, 2005.

Zuberi, B., K.S. Johnson, G.K. Aleks, L.T. Molina, and M.J. Molina, Hydrophilic properties of aged soot, Geophys. Res. Lett., 32, L01807, doi: 10.1029/2004GL021496, 2005.

Zufall, M.J., and C.I. Davidson, Dry deposition of particles, Atmospheric Particles, 425-473, 1998.